Constraints on the formation of mineralization and volatile activity in the layered mafic-ultramafic Caribou Lake Gabbro, Northwest Territories, Canada

By

Kevin John Neyedley

A thesis submitted to Saint Mary's University, Halifax, Nova Scotia in partial fulfillment of the requirements for the degree of Master of Science in Applied Science

August, 2016, Halifax, Nova Scotia

Approved: Dr. Jacob Hanley
Supervisor
Department of Geology
Saint Mary's University

Approved: Mr. Hendrik Falck
Supervisory Committee
Northwest Territories Geological Survey

Approved: Dr. Yana Fedortchouk
Supervisory Committee
Department of Earth Sciences
Dalhousie University

Approved: Dr. Linda Campbell
Supervisory Committee
Department of Environmental Science
Saint Mary's University

Approved: Dr. Iain Samson
External Examiner
Department of Earth and Environmental Sciences
University of Windsor

Date: August 29, 2016

Abstract

Constraints on the formation of mineralization and volatile activity in the layered mafic-ultramafic Caribou Lake Gabbro, Northwest Territories, Canada

By: Kevin John Neyedley

The Caribou Lake Gabbro, NT, Canada is a small layered mafic-ultramafic intrusion hosting minor Ni-Cu-PGE sulphide mineralization. Sulphide mineralization is described in detail and directly compared to early magmatic sulphide melt inclusions. Constraints on the initial silicate melt and R factors to produce the sulphide mineralization are determined. As well, it is demonstrated that sulphide melt inclusion compositions provide a reasonable estimate for metal tenor in sulphide mineralization. Melt and fluid inclusions present in mafic pegmatites and gabbros allow for a study of the volatile history and fluid and melt evolution of the system. Melt inclusion compositions indicate the system formed from an evolved metal-depleted melt. Fluid inclusions preserve the trapping of immiscible carbonic-aqueous brine fluids that may have been exsolved from different parts of the intrusion. This process has been described in economic Ni-Cu-PGE deposits, suggesting the presence of these fluids is not directly related to mineralization potential.

August 29, 2016

Acknowledgements

I would like to thank Dr. Jacob Hanley for his willingness to take me on and providing his time, assistance, and guidance over the years to provide me with everything I needed to succeed. As well as giving me time and space to work independently on this project to make my own thoughts and models for the study area. I would also like to thank my committee members Hendrik Falck (Northwest Territories Geological Survey), Dr. Yana Fedortchouk (Dalhousie University), and Dr. Linda Campbell (Saint Mary's University) for their continued support. Hendrik's enthusiasm and interest in the project was evident from the beginning during the field work, where we spent many nights contemplating geology problems around the campfire. Thank you to Dr. Iain Samson from the University of Windsor for his helpful comments and suggestions to improve this thesis. The Hanley group of students over the years here have all contributed to this project in one way or another. I would like to thank the Northwest Territories Geological Survey for funding this project and the support lent by many of the staff there (Scott Cairns, John Ketchum, Luke Ootes, Valerie Jackson, Barrett Elliot, Kelly Pierce, and Susan Sample). My high school geography teach, Mr. Richard Humphrey, sparked my interest in geology way back in grade 10 at Glenlawn Collegiate and I could not have asked for a better introduction to what is now my career. Finally, of course, my parents and brother, thank you for your endless support through the years and letting me do whatever I wanted in life.

Table of Contents

List of Figures

In Chapter 1

In Chapter 2

In Chapter 3

List of Tables

In Chapter 1

In Chapter 2

In Chapter 3

Chapter 1: Introduction

1.0 Structure of thesis

This thesis consists of four chapters. Chapter 1 contains a brief outline of the thesis structure, highlights the main objectives, and provides a general background on the geology of the Caribou Lake Gabbro. Chapter 2 provides a detailed description of the sulphide mineralization present in the Caribou Lake Gabbro and directly compares the mineralization to early magmatic sulphide melt inclusions. Chapter 2 represents a stand-alone manuscript for submission to *Ore Geology Reviews*. Chapter 3 focuses on the melt and fluid inclusion systematics of the Caribou Lake Gabbro and this chapter represents a stand-alone manuscript to be submitted to *Mineralium Deposita*. Chapter 4 suggests future work and studies that would aid in the understanding of the formation of the Caribou Lake Gabbro.

1.1 Primary objectives of thesis

The primary objectives of this thesis were to provide a comprehensive mineralogical characterization of the different styles of sulphide mineralization hosted within the Caribou Lake Gabbro, Northwest Territories, Canada. The sulphide mineralization would then be directly compared to early magmatic sulphide melt inclusions to determine if the initial sulphide liquid of the system had been influenced by fractional crystallization or alteration. The results of this thesis identify genetic relationships between the preserved sulphide melt inclusions and mineralization. This

relationship could be usefull to predict the metal fertility of other layered mafic-ultramafic systems.

1.2 Secondary objectives of thesis

Mafic pegmatites in the Caribou Lake Gabbro contain early coarse-grained apatite which host abundant secondary fluid inclusions and minor primary fluid inclusions. By examining fluid inclusions within the Caribou Lake Gabbro, the fluid history of the system can be traced and therefore they can help us understand if/when metals were either mobilized or brought into the system. Silicate melt inclusions also preserved in apatite provide a unique opportunity to investigate the starting liquid composition of the system.

1.3 List of abbreviations

The following table summarizes commonly used abbreviations and acronyms used in this thesis (following page):

Table 1.1: List of acronyms and abbreviations used throughout this thesis

Abbreviation	Meaning
at %	atomic percent
BLIS	Blatchford Lake Intrusive Suite
BMS	base metal sulfide
BSE	back scattered electron
C°_{sil}	initial concentration of an element in the silicate liquid
C°_{sul}	initial concentration of an element in the sulfide liquid
C^{f}_{sil}	concentration of an element in the fractionated silicate magma
C^{f}_{sul}	concentration of an element in the fractionated sulfide liquid
CLG	Caribou Lake Gabbro
D	partition coefficient
DDH	diamond drill hole
$D^{sul/sil}$	partition coefficient of an element between sulphide and silicate liquid
EMP	electron microprobe
F	fraction of sulphide liquid remaining
FIA	fluid inclusion assemblage
Fo#	forsterite number of olivine
FT	Fischer-Tropsch synthesis
GC	gas chromatography
HFSE	high field Strength elements
ISS	intermediate solid solution
LA-ICP-MS	laser ablation inductively-coupled plasma mass spectrometry
L_{aq}	liquid aqueous phase
L_{CO2}	liquid carbonic phase
MORB	mid ocean ridge basalt
MSS	monosulphide solid solution
NLS	Nechalacho Layered Suite
P	pressure
PGE	platinum group element
PGM	platinum group mineral
ppb	parts per billion
ppm	parts per million
R	ratio of silicate to sulphide liquid
REE	rare earth element
SEM-EDS	scanning electron microscope-energy dispersive X-ray spectroscopy
SIMS	secondary ion mass spectrometry
SMI	silicate melt inclusion
SUL	sulphide melt inclusion
T	temperature
T_{Cla}	temperature of clathrate melting
Th_{CH4}	temperature of CH_4-dominant phase homogenization
Th_{CO2}	temperature of carbonic phase homogenization
Tm_{CO2}	temperature of carbonic phase melting
$T_m^{liquidus}$	minimum liquidus temperature
V_{CH4}	vapor CH_4-dominant phase
V_{CO2}	vapor carbonic phase
vol %	volume percent
wt%	weight percent
wt% $NaCl_{equiv}$	weight percent NaCl equivalent

1.4 Overview of geology and geochemistry

1.4.1 Regional geology

The Caribou Lake Gabbro (CLG) is located approximately 90 km southeast of Yellowknife, Northwest Territories along the Hearne Channel, Great Slave Lake and lies at the southern margin in the Slave Province of the Canadian Shield (Figure 1.1). The CLG comprises the western suite of the alkaline to peralkaline Blatchford Lake Intrusive Suite (BLIS), which is thought to be related to the formation of the Authapuscow Aulacogen and the associated failed rift (Bowring et al, 1984; Hoffman, 1980) that could have promoted crustal thinning, decompressional melting and provided conduits for mantle derived magmas (Mumford, 2013 unpublished PhD thesis). The BLIS intrudes sedimentary rocks of the Archean Yellowknife Supergroup, Morose granite, and the Defeat granodiorite (Davidson, 1972, 1978). Geophysical gravity studies by Birkett et al (1994) and Pilkington (2012) suggested that the BLIS is a relatively thin tabular body, approximately 1 km thick with deep mafic (CLG) roots at the western contacts. The CLG also appears to extend underneath the Grace Lake granite for almost half of the BLIS.

The first detailed mapping of the BLIS was undertaken by Davidson (1972). His subsequent work (Davidson, 1978, 1981, 1982) identified six distinct units based on field relationships and geochronology: (i) Caribou Lake gabbro ranging to leucoferrodiorite (2184 ± 2 Ma, Mumford, 2013 unpublished PhD thesis); (ii) Whiteman Lake quartz syenite (2185 ± 2 Ma, Bowring et al, 1984); (iii) Hearne Channel granite (2175 ± 5 Ma, Bowring et al, 1984); (iv) Mad Lake granite (2166 ± 47 Ma, Wanless et al, 1979); (v) Grace Lake granite (2176.2 ± 1.3 Ma, Sinclair et al, 1994); vi) Thor Lake syenite (2164 ± 11 Ma, Mumford, 2013 unpublished PhD thesis). Based on geochemistry (Davidson,

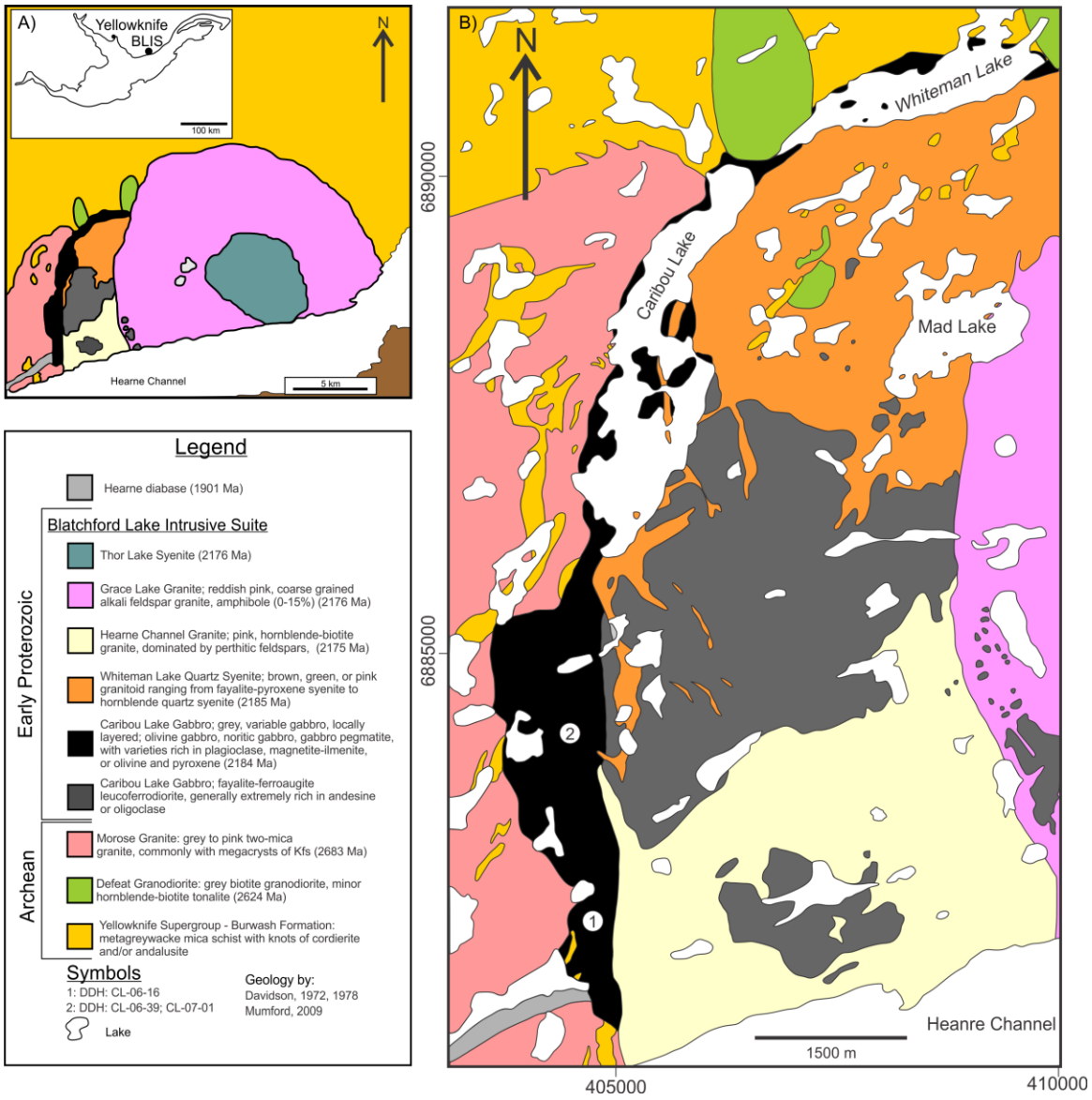

Figure 1.1: Regional and local geological maps of the Blatchford Lake Intrusive Suite. A) Location map and regional geological map of the Blatchford Lake Intrusive Suite, modified after Davidson (1982) and Mumford (2013, unpublished PhD Thesis). B) Detailed geologic map of the western portion of the Blatchford Lake Intrusive suite, modified after Davidson (1982) and Mumford (2013, unpublished PhD Thesis). Locations of diamond drill holes (DDH) used in this study are shown as well.

1981), the BLIS could be broken into two distinct portions; an older sub-alkaline western lobe (Units i-iv) and a younger peralkaline eastern lobe (Units v-vi). Mumford (2013, unpublished PhD thesis) has described units ii to vi as coeval multi-phase intrusions, (based on contacts and variations within the granitic intrusions), that show large scale changes from north to south; therefore, these units (ii, iii, iv) are transitional and the Mad Lake granite can be distributed between the northern Whiteman Lake and southern Hearne Channel, eliminating the Mad Lake granite from the intrusive suite.

1.4.2 Exploration History

The Earl Jack Syndicate investigated aeromagnetic anomalies during 1963 in the Caribou Lake area. They discovered Fe-Ti occurrences with up to 15 % oxide corresponding to aeromagnetic highs within an anorthositic gabbro in the higher mineralized grade zones, assays returned values of 30 % Fe and 10 % TiO_2. No claims were staked because zones of titanium and iron mineralization were deemed too small to be considered economic at the time (Curry et al, 1963). Shield Resources performed magnetic surveys during the 1960's and discovered sulphide occurrences associated with magnetic lows. Numerous trenches were also blasted during the time Shield held claims in the area, several of which contained niccolite hosted in carbonate veins (Curry, 1969).

Airborne magnetic and EM survey were conducted by New Caledonia Mining in 1994 and collected till samples looking for diamond indicator minerals. A few magnetic anomalies were identified, with a follow-up ground magnetic survey suggested for one anomally. They also stated that no significant concentrations of base metals were recognized in the gabbroic units (Warman and Gelo, 1995).

In 2004, Kodiak Exploration performed reconnaissance prospecting of the Caribou Lake gabbro. They sampled previously known niccolite showings with one sample returned assay values of 38.2 % Ni and 3.8 % Co. One sample of gabbro within the Whiteman Lake syenite was collected and had values of 19.7 % Cu and 0.3 % Ni. A total of 130 samples were analyzed (Marmont, 2006). During the summer of 2005 Kodiak Exploration hired Aurora Geoscience to perform a prospecting and sampling program as well as to investigate the areas around the magnetic anomalies discovered by New Caledonia Mining. Aurora Geosciences' program resulted in 714 samples being submitted for assay. Of all the 2004 and 2005 samples submitted for assay (n=844), 91 came back with values greater than 0.1 % Cu and 41 with greater than 0.1 % Ni. Because of these assay results, an airborne VTEM electromagnetic and magnetic survey over the Caribou Lake intrusion were conducted. From these surveys thirteen strong EM anomalies were identified and twelve of them occurred in the mafic-ultramafic units of the Caribou Lake intrusion (Marmont, 2006).

Kodiak's prospecting work continued into 2006 and focused on areas located around the anomalies from the EM and magnetic surveys. This program identified new anomalies that contained modest amounts of PGE (30 ppb Pt-Pd) and one sample with Pt and Pd values of 97 and 25 ppb, respectively. Some mineralized carbonate veins were also found during this program, which returned assay values of 8.4 % Ni and 1.25 % Co (Marmont, 2006).

In 2006, Kodiak also undertook a drilling program that was designed to test the EM anomalies, explore the contact of the CLG, test the depth of surface showings, as well as to determine the stratigraphy of the CLG. The first, third and fifth drill holes produced

the best results of the program, encountering massive sulphides with grades ~0.53 % Ni and ~0.7 % Cu (Marmont, 2006). Kodiak continued its drill program in 2007 with an additional fifteen drill holes to explore the basal contact of the CLG, re-test some VTEM anomalies and to improve their understanding of the stratigraphy. No significant sulphide intersections were encountered during the 2007 drill program (Marmont, 2007).

1.4.3 Study Area

The oldest part of the Blatchford Lake Intrusive Suite is the CLG (2184 ± 2 Ma; Mumford, 2013 unpublished PhD thesis) which intrudes into the Archean sedimentary rocks of the Yellowknife Supergroup, the Morose granite, and the Defeat granodiorite (Figure 1.1; Davidson, 1982). Contacts between the CLG and its Archean host rocks are commonly obscured by vegetation, swamps, or lakes. Davidson (1978) described a chilled margin along the western contact and also observed progressive changes from west to east across the gabbro starting with pegmatitic patches in massive olivine gabbro along the west and north shores of Caribou and Whiteman Lakes transitioning into a massive to faintly layered noritic gabbro with plagioclase defining a weak foliation, with the most eastern portion of the gabbro described as a leucoferrodiorite.

1.4.4 Diamond drill hole summaries

1.4.4.1 Drill hole CL-06-16

Drill hole CL-06-16 is a 170.6 m long vertical drill hole that was drilled into the southern portion of the CLG (Figure 1.1). This hole was chosen for the study based on its moderate disseminated sulphide mineralization. The hole is predominately composed of a gabbroic unit that varies from fine- to coarse-grained. Plagioclase and clinopyroxene modal proportions are relatively consistent throughout the unit, ranging from 30-50 %

plagioclase and 20-35 % clinopyroxene. Orthopyroxene and olivine vary significantly through the gabbroic unit, ranging from 0-10 % for both minerals. Alteration intensity varies throughout the gabbro as well. Short intervals of a melagabbro were observed at 34.7-36.1 m in the core, which will be referred to as a clinopyroxenite. The upper and lower contacts with the surrounding gabbro are gradational. Clinopyroxenite consists of 5-10 % plagioclase, 50-75 % clinopyroxene, 0-15 % olivine, Fe-Ti oxides 10-15 %, and 3-5 % pyrrhotite with trace chalcopyrite. From 51.8 m to 64.5 m, weak to moderate disseminated sulphides are present, primarily pyrrhotite with minor amounts of chalcopyrite. A small anorthosite unit occurs at 90 m within the gabbro and is only ~10 cm in length. From 87.5-88.1 m and 92.2-108.9 m alteration zones contain abundant calcite-quartz veinlets and stringers composed of epidote, pyrite, serpentine and chlorite. Minor amounts of bleaching are present within the zone as well as minor amounts of hematite alteration. Below the alteration zone is a thick interval of quartz syenite (108.9-139.05 m) and then a plagioclase-rich diabase (139.05-151.5 m). A small interval of gabbro is present from 151.5-153.3 m. The hole ends in plagioclase rich diabase. A stratigraphic column showing differences in mineralogy and alteration is illustrated in Figures 1.2, 1.3 and 1.4.

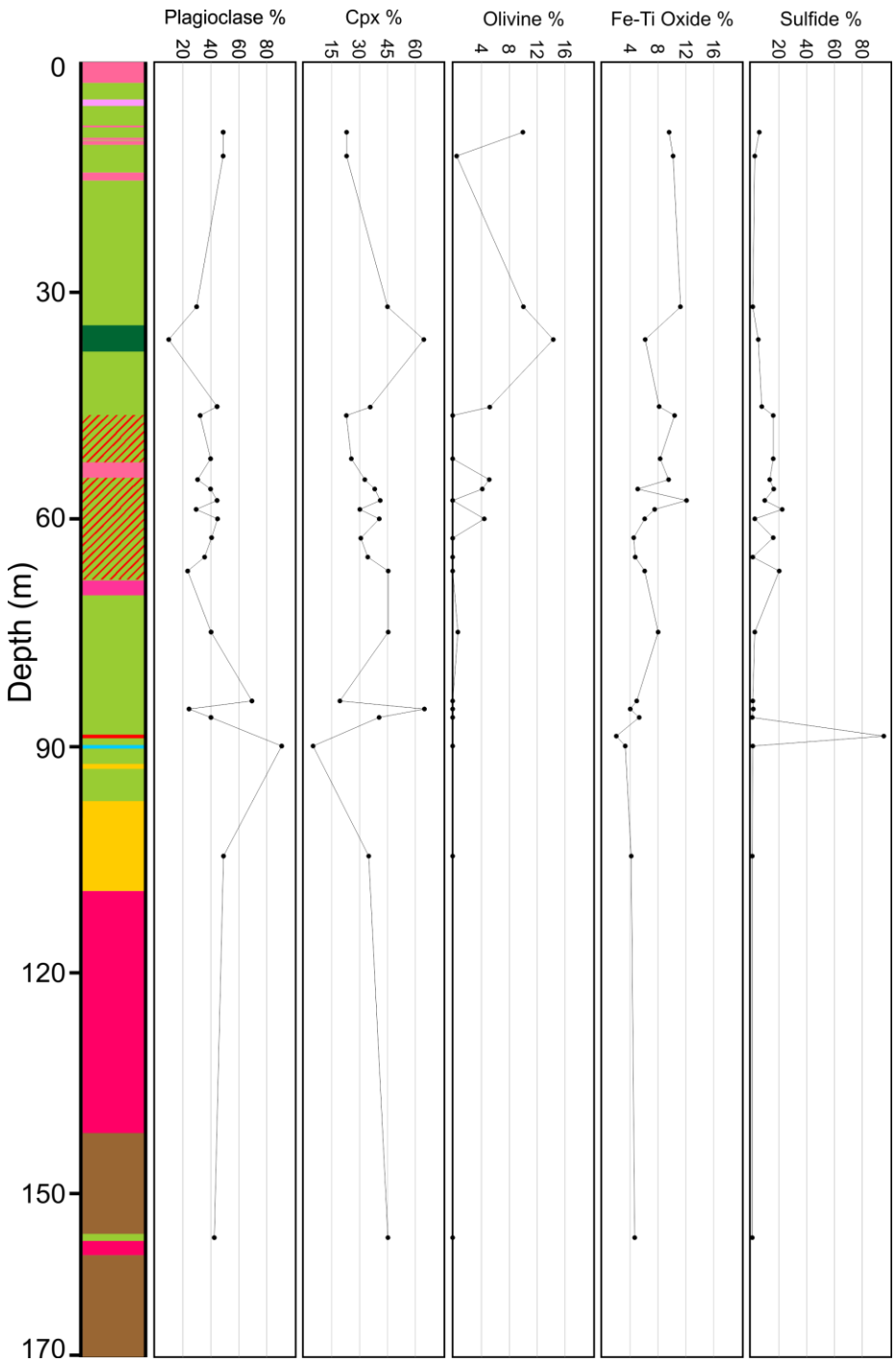

Figure 1.2: Stratigraphic column of CL-06-16 showing variations in mineral proportions.

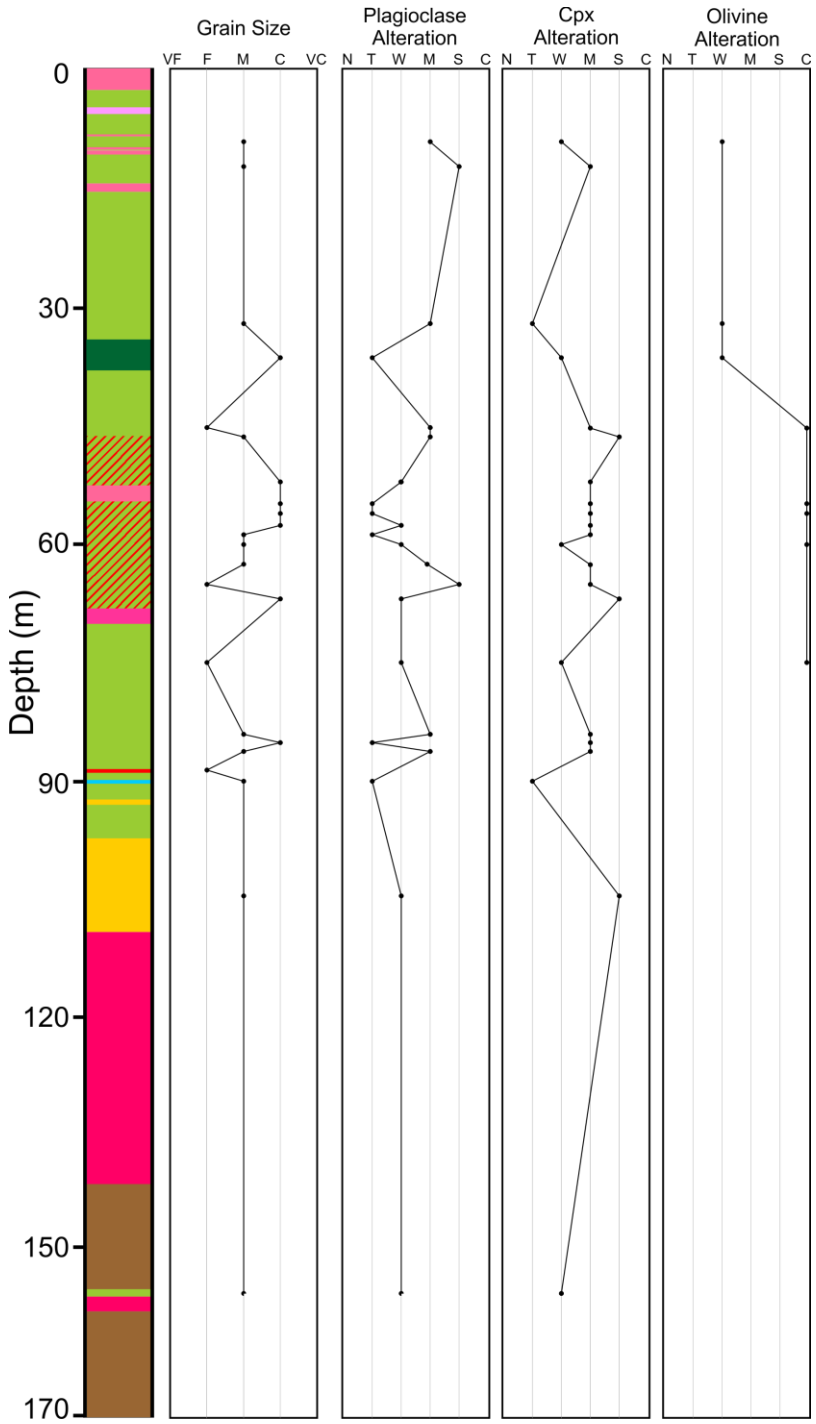

Figure 1.3: Stratigraphic column of CL-06-16 showing variations in alteration. Grain sizes: very fine (VF) = <0.8mm; fine (F) = 0.8-1.5; medium (M) = 1.5-3mm; coarse (C) 3-7mm; very coarse = 7-12mm. Alteration intensity: none (N), trace (T), weak (W), moderate (M), strong (S), complete (C).

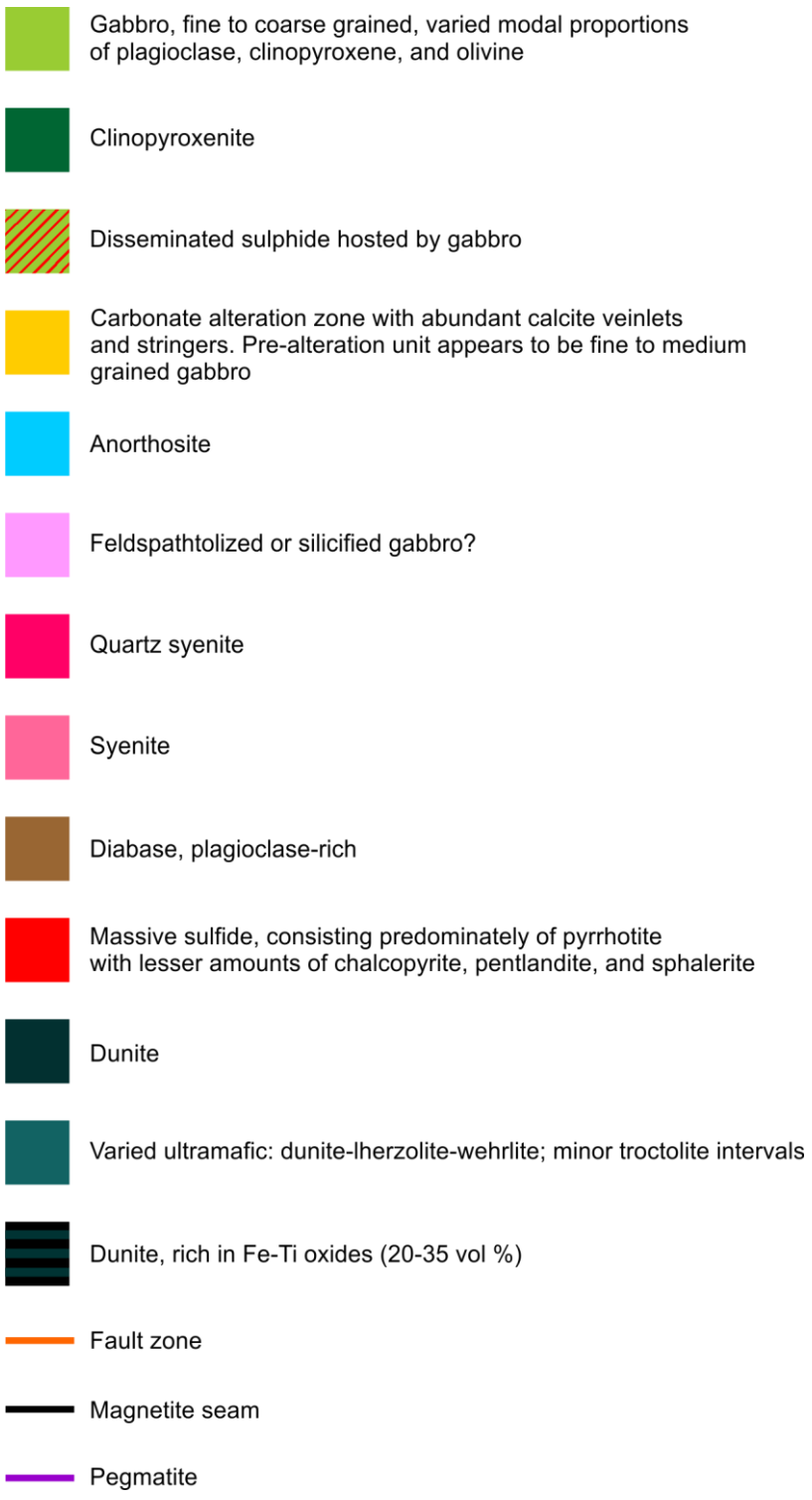

Figure 1.4: Legend for stratigraphic columns in Figures 1.2, 1.3, 1.5 and 1.6.

1.4.4.2 Drill hole CL-06-39

Drill hole CL-06-39 is a 163.1 m long vertical drill hole that was drilled approximately 2000 m north of CL-06-16 (Figure 1.1). The significance of this hole is that it contains a ~70 m thick interval of ultramafic rocks, the thickest ultramafic succession identified by Kodiak's drill program. The upper ~27 m of the hole is primarily composed of a gabbro with grain sizes ranging from medium- to coarse-grained and relatively consistent modal proportions of plagioclase (45-50 %), clinopyroxene (40-45 %,) and Fe-Ti oxides (2-7 %). A few pegmatitic gabbros were also encountered within the first 27 m, one at 4.1 m and the other at 6.85 m. These pegmatites are different from the host gabbro in modal mineral abundances, with the pegmatite at 4.1 m being composed of primarily of clinopyroxene (~65 %) and plagioclase (~35 %) and the pegmatite at 6.9 m being composed of primarily of plagioclase (~65 %) and clinopyroxene (30 %). A small 60 cm interval of dunite is present at 20.3 m within the gabbro and is strongly altered. The gabbros upper contact with the dunite is slightly chilled for 2 cm downhole, where grain sizes change from < 1 mm at the contact to 2-8 mm after the contact. A thick ultramafic interval was encountered from 27.7 m to 97.45 m and is primarily composed of olivine (60-90 %), clinopyroxene (10-20 %) and plagioclase (0-5 %), varying between dunite, lherzolite and wehrlite. Rarely, plagioclase modal abundances reach ~10-15 %, as such, some short intervals can be classified as troctolite (e.g., 83.9 m). Iron-titanium oxides concentrations range considerably throughout the ultramafic interval, with modal abundances anywhere from trace amounts to 35 % of a given interval. A short (40 cm) interval of gabbro occurs within the ultramafics, with sharp contacts and abrupt differences in modal proportions, but magnetite appears to be focused around the

contacts. From 82.1-84.8 m, a carbonate alteration zone is present, which is adjacent to a small fault surface at 85.7 m. From 97.45-118.45 m, the lithology is composed primarily of varied gabbros that can be rich in plagioclase, clinopyroxene, or Fe-Ti oxides. Each type of gabbro is generally restricted to a short interval (< 20 cm) and contacts appear to be gradational. Rare, thin ultramafic and oxide-rich ultramafic sections are also present within this interval. Two pegmatites occur, one at 100 m, which is an anorthosite and another at 103.9 m, which is an olivine gabbro. A magnetite rich (~70 % Fe-Ti oxides) interval is present at 103.7 m shortly before the pegmatite. After the varied gabbro interval, a uniform gabbro occurs from 118.45 to 122.95 m, where an anorthosite is intersected from 122.95-125.9 m, which appears to be highly altered. The lower contact of the anorthosite is gradational with a gabbro below at 125.9 m, while the top contact of the anorthosite is sharp. The gabbro from 125.9-152.9 m is similar to the uniform gabbro present above the anorthosite. At 152.9 m, the lithology transitions into an oxide-rich dunite, with Fe-Ti oxides composing 20-35 % of the interval. This oxide-rich dunite extends to 156.9 m where it has a sharp contact with a gabbroic pegmatite. The narrow pegmatite is only present for 20 cm before the lithology returns to a gabbro at 157.2 m. The gabbro occurs for 3 m and then the unit changes into a syenite at 160.3 m, which then ends the length of the drill hole at 163.05 m. Stratigraphic column showing variations in mineralogy and alteration is illustrated in Figures 1.5 and 1.6.

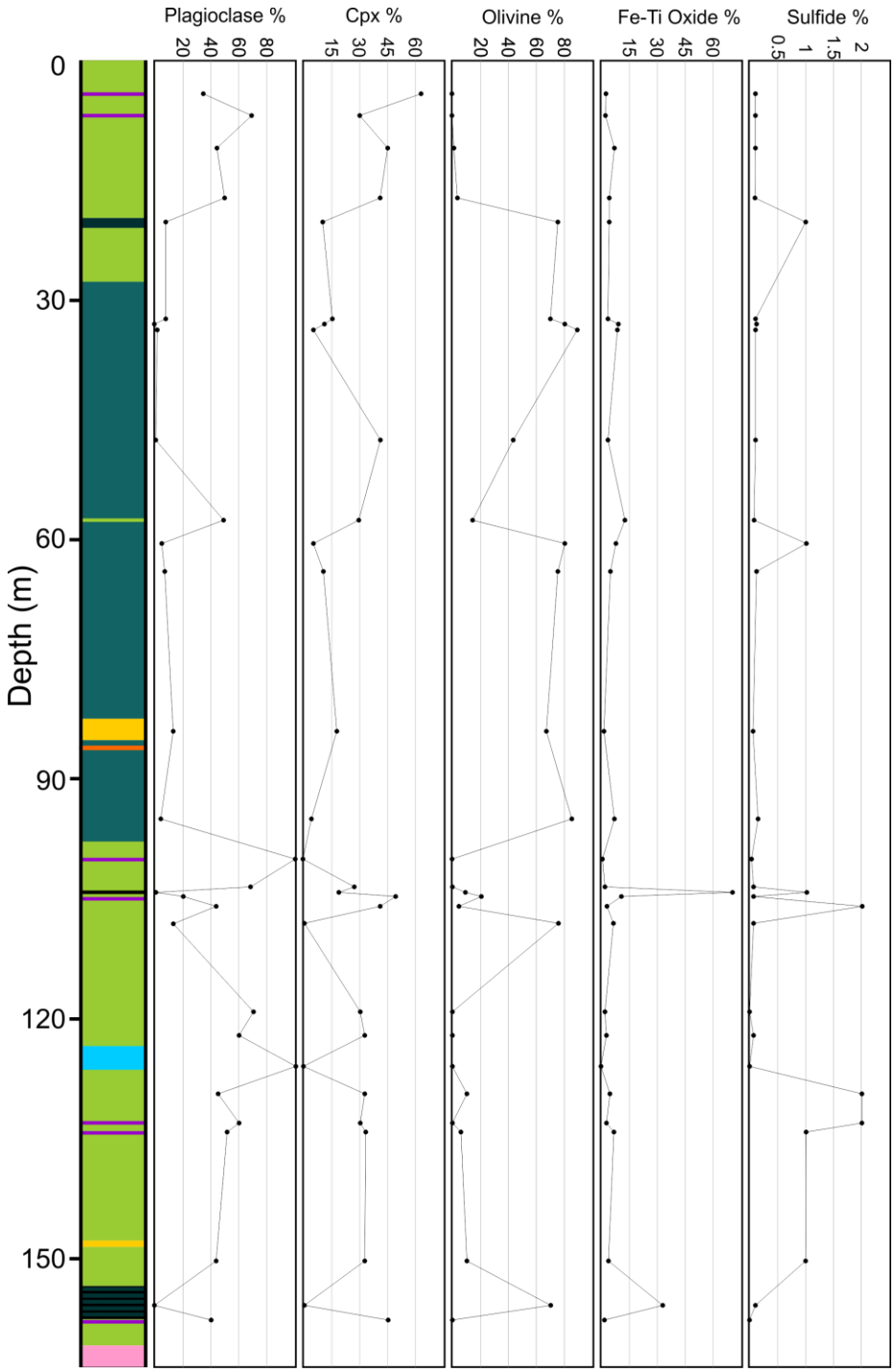

Figure 1.5: Stratigraphic column of CL-06-39 showing variations in mineral proportions.

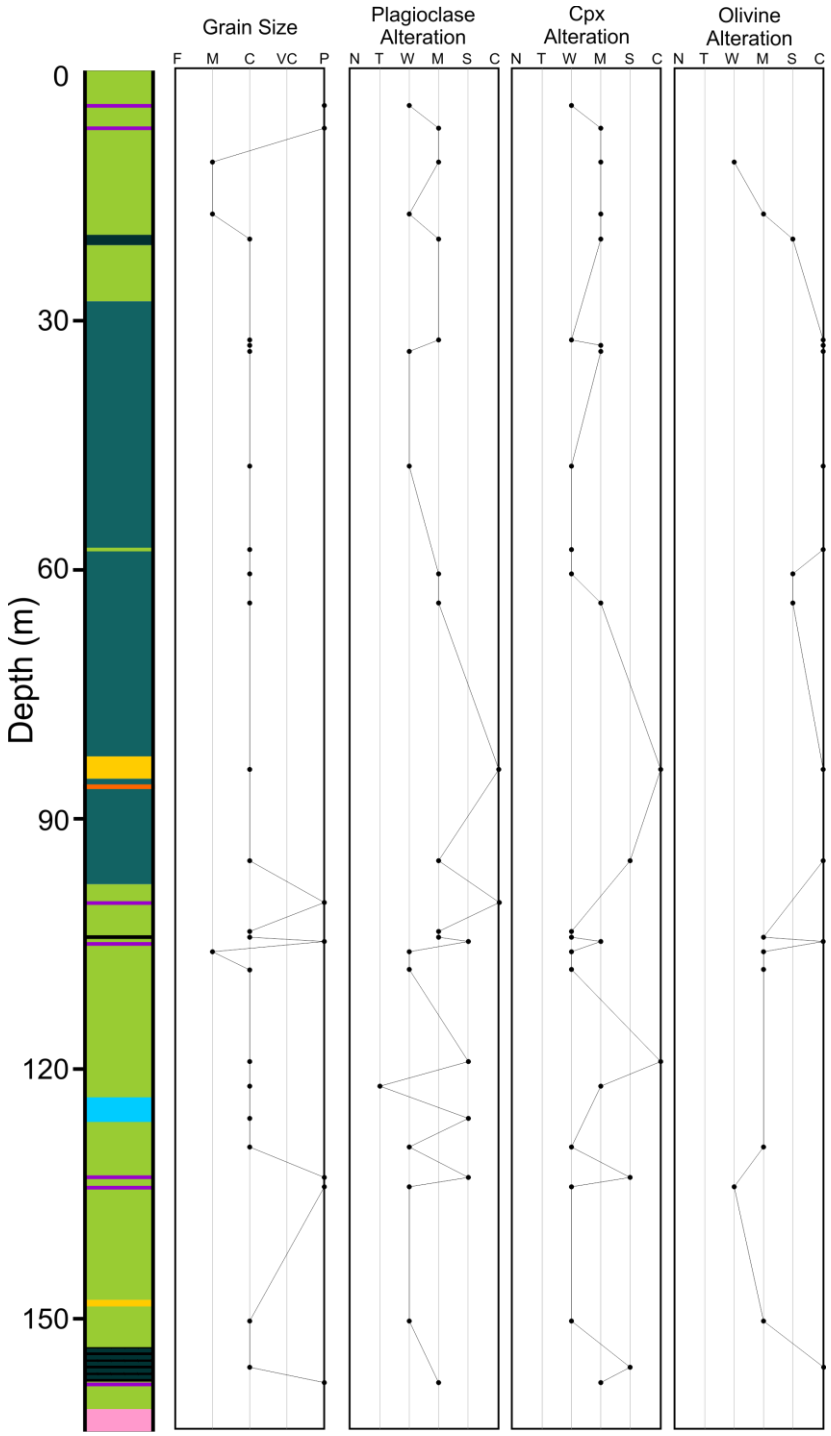

Figure 1.6: Stratigraphic column of CL-06-39 showing variations in alteration. Grain sizes: fine (F) = 0.8-1.5 mm; medium (M) = 1.5-3 mm; coarse (C) 3-7 mm; very coarse = 7-12 mm; pegmatitic (P) = >12 mm. Alteration intensity: none (N), trace (T), weak (W), moderate (M), strong (S), complete (C).

1.4.5 Geochemistry

Rocks of the CLG are of alkaline to sub-alkaline affinity and follow a tholeiitic trend (Figure 1.7). Chondrite-normalized REE plots of unaltered fine-grained gabbros within the CLG display a negative slope, with a moderate enrichment in the light rare-earth elements (LREE) over the heavy rare-earth elements (HREE); (Figure 1.8A). Both the unaltered and altered fine-grained gabbros both have similar LREE enriched profiles with a positive Eu anomaly (Figure 1.8A). Primitive mantle normalized plots of the unaltered fine-grained gabbros show a slight enrichment in Sr and Ti relative to altered fine-grained gabbros (Figure 1.8B). Both altered and unaltered gabbros show depletions in Th, U, and HREE relative to primitive mantle. Altered fine-grained gabbros are highly enriched in Pb compared to unaltered gabbros, and show moderate enrichments in Cs and Rb, while being slightly depleted in some LREE (Figure 1.8B).

Gabbroic rocks in the intrusion show similar SiO_2 contents (39-45 wt %) with each other regardless of their relative position in drill core. Typically, the gabbros with greater amounts of SiO_2 are a function of higher alteration present in the sample and Al_2O_3 also follows this trend. Magnetite and ilmenite are a direct control on the FeO and TiO_2 content of gabbros. As units with more FeO and TiO_2 (15-18 and 2.6-4.2 wt %, respectively) contain 5-12 % Fe-Ti oxides, while gabbros with lesser amounts of Fe-Ti oxides (2-3 %) have FeO and TiO_2 contents of ~11 and ~1.5 wt %, respectively. Ultramafic rocks (dunite, clinopyroxenite) have MgO concentrations of 13-18 wt % and a wide range of FeO and TiO_2 concentrations (22-51 and 2-8 wt % respectively) contents controlled by magnetite and ilmenite. Vanadium concentrations are highly variable, ranging from 50 ppm up to 2.3 wt % averaging ~500 ppm.

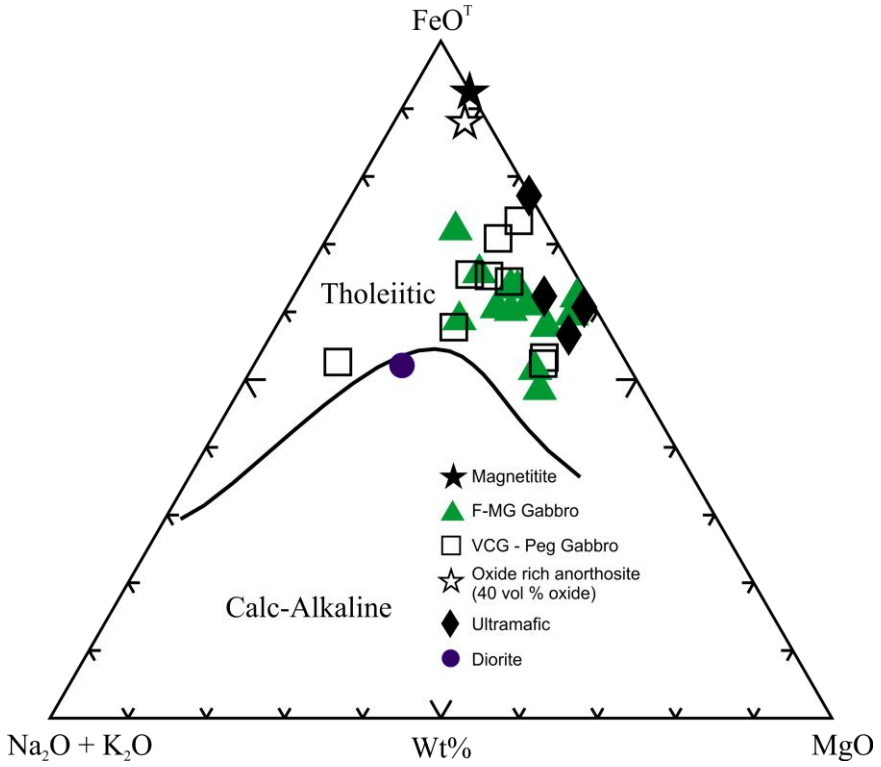

Figure 1.7: AFM diagram (after Irvine and Barager, 1971) of rocks from the Caribou Lake Intrusion show that they are of a tholeiitic composition and as the melt evolved, rocks move away from the FeO-MgO tie line. F-MG Gabbro = fine- to medium-grained gabbro. VCG-pegmatitic gabbro = very coarse grained – pegmatitic gabbro. FeO^T = total Fe.

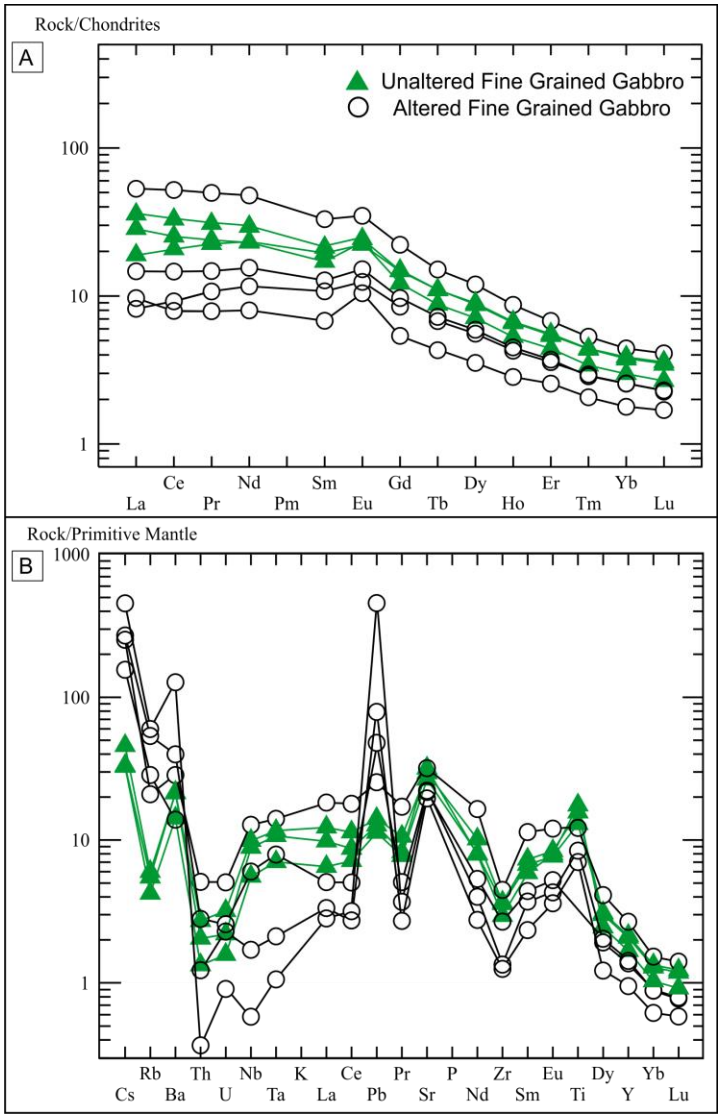

Figure 1.8: A) Chondrite normalized plot comparing unaltered and moderately to highly altered fine-grained gabbros. Both show the same negative slope and a positive Eu anomaly. B) Normalized primitive mantle plot comparing same unaltered and altered fine-grained gabbros as in A. Both show similar trends in trace elements, except for Pb, which is highly enriched in the altered samples. After Sun and McDonough, 1989.

1.5 References

Birkett, T.C., Richardson, D.G. and Sinclair, W.D., 1994, Gravity modeling of the Blachford Lake Intrusive Suite, Northwest Territories. *In* Studies of rare-metal deposits in the Northwest Territories. *Edited by* W.D. Sinclair and D.G. Richardson. Geological Survey of Canada, p. 5-16.

Bowring, S. A., Van Schmus, W. R. & Hoffman, P. F., 1984, U-Pb zircon ages from Authapascow Aulacogen, East Arm of Great Slave Lake, NWT, Canada: Canadian Journal of Earth Sciences, v. 21, p. 1315-1324.

Davidson, A., 1972, Granite Studies in the Slave Province: *Report of Activities*: Geological Survey of Canada, p. 109-115.

Davidson, A., 1978, The Blachford Lake Intrusive Suite: An Aphebian alkaline plutonic complex in the Slave Province, Northwest Territories: *Current Research*: Geological Survey of Canada, p. 119-127.

Davidson, A., 1981, Petrochemistry of the Blachford Lake Complex, District of Mackenzie: *Geological Survey of Canada Open File 764*, 24 p.

Davidson, A., 1982, Petrochemistry of the Blachford Lake complex near Yellowknife, Northwest Territories. In: Maurice, Y. T. (ed.) *Uranium in Granites*: Geological Survey of Canada, 71-79.

Curry, J.D., Lee, W.K., and Overveld, R., 1963, Earl-Jack Syndicate exploration report: submitted by Earl Jack Syndicate, Department of Indian and Northern Affairs, Activities Report 015065, 2 p.

Curry, J.D., 1969, Electromagnetic and magnetic geophysical surveys for parts of the NC claim group: submitted by Shield Resources Ltd, Department of Indian Affairs and Northern Development, Activities Report 018838, 6 p.

Hoffman, P.F., 1980, Wopmay Orogen: a Wilson cycle of early Proterozoic age in 99 the Northwest of the Canadian Shield. *In* The continental crust and its mineral deposits. *Edited by* D.W. Strangway. Geological Association of Canada, Special Paper 20, p. 523-549.

Irvine, T.N., and Baragar, W.R.A., 1971, A guide to the chemical classification of the common volcanic rocks: Canadian Journal of Earth Sciences, v. 8, p. 523-548.

Marmont, C., 2006, Report on Diamond Drilling, Airborne and Ground Geophysical Surveys, Lithogeochemical Sampling and Prospecting; submitted by Kodiak Exploration, Northwest Territories Geoscience Office, Activities Report 085101, p. 123.

Marmont, C., 2007, Report on diamond drilling; submitted by Kodiak Exploration, Northwest Territories Geoscience Office, Activities Report 085317, p. 283.

Mumford, T., 2013, Petrology of the Blatchford Lake Intrusive Suite, Northwest Territories Canada. *Unpublished* Ph.D. thesis, Carleton University. 240 p.

Pilkington, M., Thomas, M.D, and Mumford, T.R., 2012, Geological significance of a new high resolution gravity gradiometric and magnetic survey over the Blatchford Lake Complex, Northwest Territories: Geological Survey of Canada, Open File 7084, Poster.

Sinclair, W. D., Hunt, P. A. & Birkett, T. C., 1994, U-Pb zircon and monazite ages of the Grace Lake Granite, Blatchford Lake Intrusive Suite, Slave Province, Northwest Territories. *Radiogenic Age and Isotopic Studies: Report 8; Geological Survey of Canada, Current Research 1994-F,* 15-20.

Sun, S., and McDonough, W.F., 1989, Chemical and isotopic systematics of oceanic basalts: implications for mantle composition and processes. In Saunders, A.D., and Norry, M.J., (eds.) Magmatism in the Ocean Basins: Geological Society Special Publication No. 42, p. 313-345.

Wanless, R. K., Stevens, R. D., Lachance, G. R. & Delabio, R. N., 1979, District of Mackenzie. In: Geological Survey of Canada - Radiogenic age and isotopic studies, R. (ed.), p. 34-38.

Warman, T.A, and Gelo, K.K., 1995, Assessment report on the geological and geophysical programs conducted of the Bagpipe claims, Mackenzie Mining District, Northwest Territories; submitted by Caledonia Mining Corporation, Department of Indian and Northern Affairs, Activities Report 083658, 122 p.

Chapter 2: Ore-forming processes in the Caribou Lake Gabbro, Northwest Territories, Canada

Kevin Neyedley [a,+], Jacob J. Hanley [a], Hendrik Falck [b], Robert J. Bodnar [c], Luca Fedele [c], Mostafa Fayek [d], and Ryan Sharpe [d]

[a] *Department of Geology, Saint Mary's University, 923 Robie Street, Halifax, Nova Scotia, Canada B3H 3C3*

[b] *Northwest Territories Geological Survey, 4601-B 52nd Ave, Yellowknife, NT, X1A 2R3*

[c] *Fluids Research Group, Department of Geosciences, Virginia Tech, 1405 Perry St, Blacksburg, VA, 24061*

[d] *Department of Geological Sciences, University of Manitoba, Winnipeg, Manitoba, Canada, R3T 2N2*

[+] Corresponding Author: kevinneyedley@gmail.com

Number of pages: 90

Number of figures: 11

Number of tables: 6

For submission to *Ore Geology Reviews*

Abstract

Magmatic Ni-Cu-Co-Fe sulphide melt inclusions and associated sulphide mineralization hosted in cumulate rocks of the Caribou Lake Gabbro (CLG), Blatchford Lake Intrusive Suite, Northwest Territories, Canada, present an opportunity to study ore forming processes in a sub-economic system. Three distinct styles of sulphide mineralization occur in the CLG; (i) disseminated sulphides, (ii) semi-massive to massive sulphides, and (iii) trace sulphide "PGE-enriched" mineralization. Within all mineralization styles, the mineral assemblage consists of pyrrhotite + chalcopyrite + pentlandite + magnetite + ilmenite. Trace metal phases identified consist of sphalerite, galena, glaucodot-gersdorffite [(Co,Fe)AsS-NiAsS], molybdenite, tellurobismuthite (Bi_2Te_3), altaite (PbTe), electrum, nickeline, melonite ($NiTe_2$), empressite (AgTe), and unidentified Se-Te-Pb, Bi-Te, and Pb-Te minerals. No platinum-group minerals were

observed in any mineralization styles. Within coarse-grained olivine gabbro, sulphide melt inclusions occur along healed fractures in olivine and plagioclase, and as primary inclusions in ilmenite. Secondary sulphide melt inclusions co-entrapped with silicate melt also occur in cumulus apatite in an altered mafic pegmatite. Sulphide melt inclusions consist predominately of pyrrhotite, with lesser amounts and variable proportions of chalcopyrite, cobaltian-pentlandite, sphalerite, magnetite, and glaucodot-gersdorffite. No platinum-group minerals are observed in the sulphide melt inclusions.

The metal tenors of sulphide melt inclusions and sulphide mineralization are comparable with respect to Cu concentration, with sulphide melt inclusions between 0.06 and 2.7 wt %, and mineralization between 0.54 and 2.9 wt % (recalculated to 100% sulphide). Cobalt is also similar between sulphide melt inclusions (950-4,400 ppm) and mineralization (1,350-3,500 ppm). In contrast to Cu and Co, Ni is much more enriched in mineralization (0.94-2.1 wt %) than in sulphide melt inclusions (0.13-0.59 wt %). The difference in Ni concentration is the result of the sulphide melt having undergone minor fractional crystallization of monosulphide solid solution (MSS) prior to sulphide melt inclusion entrapment. This affected the Ni tenor more because Ni is more compatible in MSS than Co and Cu.

Modeling shows it is not possible to produce the disseminated, semi-massive, and massive sulphide mineralization from an S-undepleted tholeiitic liquid containing 120 ppm Cu and 12 ppb Pd. The best approximation for the formation of these three mineralization styles requires a silicate liquid with 44 ppm Cu and 0.08 ppb Pd, that likely resulted from an initial S-undepleted tholeiitic melt that lost sulphide melt multiple times, possibly as the melt ascended to the current depth of the CLG. The dominance of

MSS products (pyrrhotite and pentlandite) in the mineralization would suggest that fractional crystallization of the sulphide liquid with an R factor ≤ 3000 gave rise to all styles of mineralization except the trace sulphide "PGE-enriched" mineralization. The trace sulphide "PGE-enriched" mineralization may have been formed from a S-undepleted tholeiitic liquid that experienced sulphide liquid saturation followed by equilibrium sulphide liquid crystallization at an R factor between 7,500 and 100,000. Factors that can explain the low metal tenors of sulphide mineralization within the CLG include, low R-factors and low degrees of mantle partial melting.

Sulphide melt inclusions can give an estimate of the sulphide liquid compostion at a specific stage in a mineralizing systems history. Composition of sulphide melt inclusions in the CLG confirms that the system was initially PGE-poor and predict Co and Cu concentrations in sulphide mineralization, suggesting sulphide melt inclusions can be used to predict the metal tenor of a mafic-ultramafic system where potential sulphide mineralization has not yet been intersected. This ablility to predict metal tenor, has application to surfical mineral exploration programs where sulphide melt inclusions may be present in highly resistive minerals (e.g., apatite) in soils and tills derived from weathering of an intrusion.

2.0 Introduction

Numerous processes can affect the sulphide liquid once it has separated from a silicate liquid prior to sulphide minerals crystallizing, settling, and accumulating to form a Ni-Cu-PGE deposit. A sulphide liquid undergoing fractional crystallization will produce a Fe-Ni rich monosulphide solid solution (MSS), leaving behind a Cu-rich residue, which in time will crystallize to form an intermediate solid solution (ISS) (Ebel and Naldrett, 1997; Barnes et al., 1997, 2005). Upon cooling, the MSS exsolves pyrrhotite and pentlandite, while the ISS exsolves Cu-rich minerals such as chalcopyrite and cubanite. Metamorphic and hydrothermal events can also play a major role in modifying Ni-Cu-PGE ores after crystallization from a sulphide liquid (Sudbury: Molnar et al., 1997, Molnar et al., 1999, Hanley et al., 2005; Coldwell Complex: Watkinson and Ohnensterrer, 1992; Salt Chuck: Alaska, Watkinson and Melling, 1992; Ferguson Lake, Nunavut: Campos-Alvarez, et al., 2012; Stillwater Complex, Montana: Polovina et al., 2004, Hanley et al., 2008; South Kawishiwi Intrusion, Duluth Complex: Gál et al., 2013).

Studying sulphide melt inclusions (SUL) can help determine the composition of the initial (unmodified) sulphide liquid that led to the formation of sulphide mineralization. Sulphide inclusions have been documented in magmatic Ni-Cu-PGE settings previously (Platreef, Bushveld Complex: Holwell et al., 2011; Platinova reef, Skaergaard Intrusion: Holwell, et al., 2015; Uruguayan dike swarm: Prichard et al., 2004; Noril’sk: Czamanske et al., 1992; Stillwater complex: Barnes and Naldrett, 1985). Since SUL will behave as a closed system once trapped, the composition of the trapped liquid is not likely to be modified, unlike the sulphide mineralization, which may have been influenced by fractional crystallization and/or hydrothermal activity. Sulphide melt

inclusion metal tenors are likely representative of the initial sulphide liquid and knowing the initial metal tenor will determine if the liquid was initially depleted or enriched in base and precious metals and can possibly allow for prediction of the metal tenor of sulphide mineralization (Holwell et al., 2011). Sulphide melt inclusion isotopic ratios are also likely representative of the initial sulphide liquid and can help aid in determining if external sulfur was added to the system and the timing of sulfur saturation in a magma. Comparing sulphide mineralization and SUL metal tenor and isotopic compositions can help understand processes that may have occurred during the cooling history of the sulphide liquid.

In this paper we examine the sulphide mineralization and sulphide melt inclusions in the Caribou Lake Gabbro (CLG) in the Northwest Territories, Canada. We describe the sulphide mineralization mineralogy and metal tenor of the system and directly compare them to sulphide melt inclusions. Sulfur isotopes of the mineralization and sulphide melt inclusions are also presented. This comparison is essential in order to understand the processes that have occurred during the history of the CLG to lead to the formation of magmatic sulphide Ni-Cu-PGE accumulations and the processes that may have modified the metal tenors of the initial sulphide liquid to the metal tenors present in sulphide mineralization.

2.1 Geological setting

2.1.1 Regional geology and tectonic setting

The CLG comprises the western suite of the Blatchford Lake intrusive suite (BLIS) and is located approximately 90 km southeast of Yellowknife, Northwest

Territories along the Hearne Channel, Great Slave Lake (Figure 2.1A). The BLIS occurs at the southern margin of the Slave Province and is adjacent to the Athapuscow Aulacogen (Hoffman, 1973; Bowring et al, 1984). Evidence for deformation of the BLIS is minimal with only a weak sub-vertical, northwest trending foliation that is highly localized and minor Proterozoic sub-vertical faults that trend north-south (Mumford, 2013, unpublished PhD Thesis). The intrusive suite intrudes the Archean metasedimentary rocks of the Burwash Formation (Yellowknife Supergroup), Morose granite, and the Defeat granodiorite. In the region surrounding the BLIS, there are no reported volcanic rocks of a comparable age or similar composition, implying that the magma responsible for the formation of the BLIS never made it to surface or the volcanic equivalents have been eroded away (Mumford, 2013, unpublished PhD Thesis). The parental melt for the BLIS is likely a metasomatized depleted mantle source (Mumford, 2013, unpublished PhD Thesis) and through tectonic reconstructions during the Paleoproterozoic, deformation along the southern Slave craton was influenced by either; i) a failed rift (Bowring et al, 1984; Hoffman, 1973), or ii) transpressional forces extending the length of an oblique crustal-scale boundary (Hoffman, 1987; Hammer et al, 1992; Bleeker & Hall, 2007). These scenarios could result in crustal thinning invoking decompressional melting and the establishment of deep-seated structures (i.e., conduits) for a mantle derived melt (Mumford, 2013, unpublished PhD Thesis).

2.2. Local geology

The oldest intrusive phase of the BLIS is the CLG (2184 ± 2 Ma, Mumford, 2012) which intrudes into the Archean sedimentary rocks of the Yellowknife Supergroup, the Morose granite, and the Defeat granodiorite (Figure. 2.1B) (Davidson, 1982). Davidson

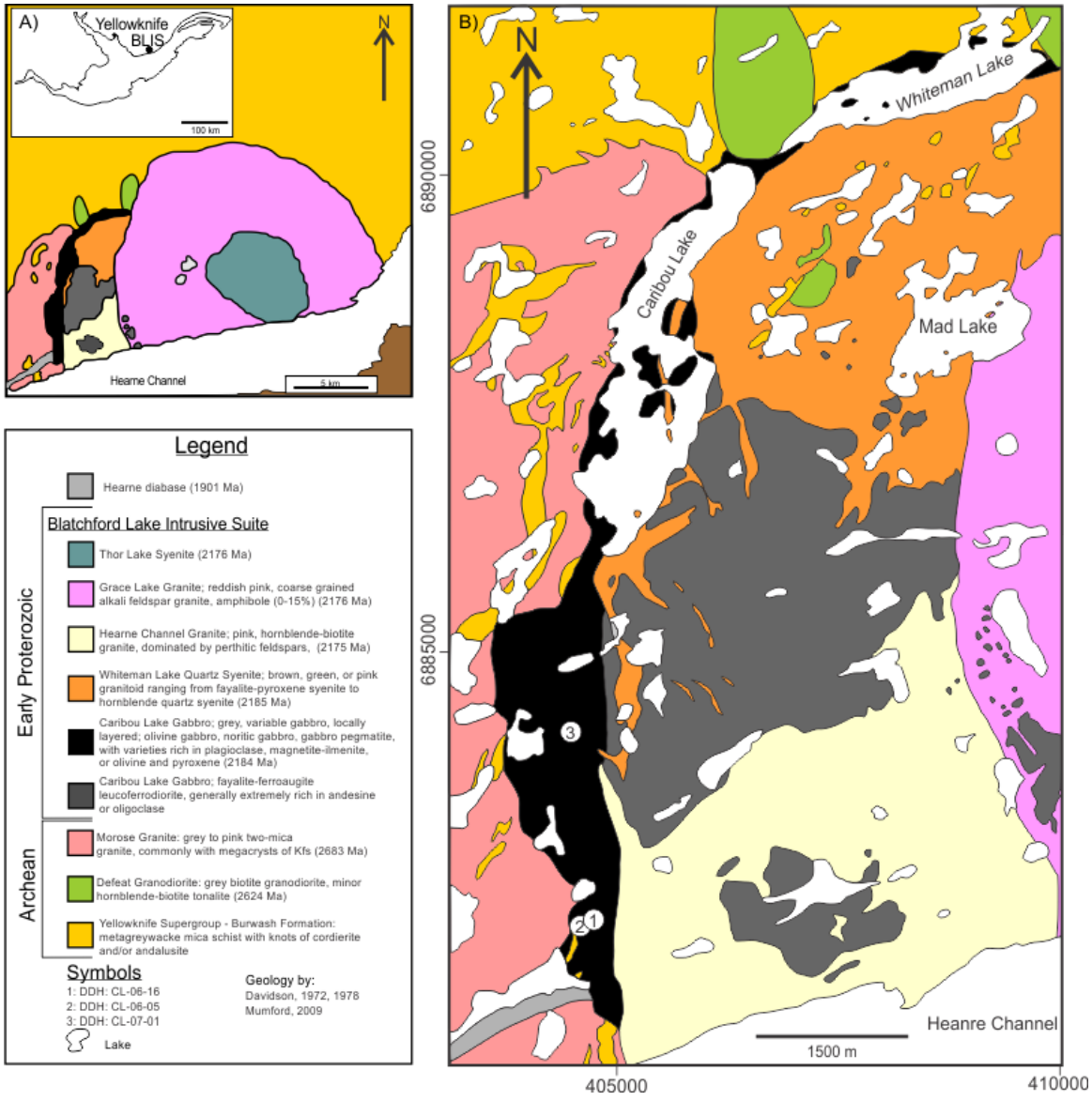

Figure 2.1: Regional and local geological maps of the Blatchford Lake Intrusive Suite. A) Location map and regional geological map of the Blatchford Lake Intrusive Suite, modified after Davidson (1982) and Mumford (2013, unpublished PhD Thesis). B) Detailed geologic map of the western portion of the Blatchford Lake Intrusive suite, modified after Davidson (1982) and Mumford (2013, unpublished PhD Thesis). Locations of diamond drill holes (DDH) used in this study are shown as well.

(1972) and his subsequent work (Davidson, 1978, 1981, 1982) and further work by Mumford (2013, unpublished PhD Thesis) identified five distinct units based on field relationships and geochronology: i) Caribou Lake gabbro grading in to leucoferrodiorite (2184 ± 2 Ma, Mumford, 2012); ii) Whiteman Lake quartz syenite (2185 ± 2 Ma, Bowring et al., 1984); iii) Hearne Channel granite (2175 ± 5 Ma, Bowring et al., 1984); iv) Grace Lake granite (2176.2 ± 1.3 Ma, Sinclair et al., 1994); v) Thor Lake syenite (2164 ± 11 Ma, Mumford, 2013 unpublished PhD Thesis).

Based on geochemistry (Davidson, 1981), the BLIS is divided into two distinct portions; an older sub-alkaline western lobe (Units i-iii) and a younger peralkaline eastern lobe (Units iv-v). Geophysical gravity surveys reported by Birkett et al. (1994) and Pilkington (2012) suggest that the BLIS is a relatively thin tabular body, approximately 1 km thick with deep mafic (CLG) roots at the western contacts. The CLG also appears to extend under the Grace Lake granite for almost half the width of the complex.

Contacts between the CLG and its Archean host rocks are commonly obscured by vegetation, swamps, and/or lakes. Davidson (1972, 1978) and Mumford (unpublished, 2013 PhD Thesis) described a chilled margin along the western contact that dips steeply (70-85°) away from the centre of the BLIS. Progressive lithological changes from west to east across the CLG were also observed by Davidson (1972, 1978) and Mumford (2013, unpublished PhD Thesis), with pegmatitic patches along the west and north shores of Caribou and Whiteman lakes, transitioning into a massive to faintly layered gabbro with plagioclase defining a weak foliation, and grading to a leucoferrodiorite in the most eastern portion of the CLG.

The CLG is a crudely layered mafic-ultramafic intrusion that is composed of a variety of units. Diamond drilling in 2006 and 2007 by Kodiak Exploration Limited identified multiple phases that were not recognized during the regional surface mapping. The dominant lithology of the CLG is a fine- to medium-grained gabbro but locally it can be rich in olivine, clinopyroxene, plagioclase, and/or Fe-Ti oxides. Ultramafic lithologies include dunite, clinopyroxenite, olivine clinopyroxenite, wehrlite and troctolite. Other phases observed include anorthosites and magnetitite. As Marmont (2006, 2007) and Mumford (unpublished, 2013 PhD Thesis) described and as observed during field work for this study, there is evidence that the CLG was of a cumulate origin. Correlation of individual units between closely spaced drill holes is extremely difficult and the ultramafic cumulate section (that should be the lowest portion of the CLG) has upper and lower with massive gabbro, providing evidence that the CLG was likely formed from numerous small batches of melt rather than from a single batch.

Diamond drilling results by Kodiak Exploration Limited in 2006 were notable with massive to moderate (10-25 vol %) disseminated sulphide encountered in four drill holes, including an intersection of 0.53 % Ni and 0.7 % Cu over 3.18m (Marmont, 2006). Sulphides are hosted in a fine- to medium-grained gabbro and are primarily composed of pyrrhotite with lesser amounts of chalcopyrite, pentlandite, and pyrite (Marmont, 2006). The stratigraphic position of sulphide mineralization is variable, with semi-massive to massive sulphide being encountered at ~20 m depth in diamond drill hole (DDH) CL-06-01, ~35 m in DDH CL-06-03, and ~80 m in DDH CL-07-05. All massive sulphide intersections were only 1.5-3 m thick with ~2 m of disseminated sulphide occurring above and below massive sulphides. Approximately 10 m of disseminated sulphide

mineralization occurred in one DDH (CL-06-16) occurring over an interval of 53 to 63 m. Disseminated and massive sulphide mineralizations contain minimal platinum group elements (PGE) (< 30 ppb Pd+Pt). Relatively higher PGE grades (~100-200 ppb Pt+Pd) were intersected (DDH CL-07-09) in a fine-grained gabbro that contained minimal amounts of sulphide (< 3 vol %, Marmont, 2007).

2.2 Methodology

All samples collected for this study were collected during the 2013 summer field season, which involved surface mapping of the CLG and detailed logging of drill core from Kodiak Exploration Limited. Representative samples of sulphide mineralization and associated lithologies were collected from a variety of drill holes. Nine samples were collected from DDH CL-06-16, from a 10 m interval of disseminated sulphide and two additional samples of semi-massive and massive sulphide intersections approximately 15 and 20 m below the disseminated sulphides, respectively (Figure 1.3). Three samples of semi-massive to massive mineralization were collected from DDH CL-06-01 and four samples were collected from DDH CL-06-05, with two representing disseminated mineralization above massive mineralization, while the other two samples were of massive sulphide. Two additional samples from DDH CL-07-09 were collected representing trace sulphide "PGE-enriched" mineralization at depths of 59 and 63 m. Sulphide melt inclusion samples came from DDH CL-07-01 from depths of 127 and 373 m.

Drill core samples were sent to the Ontario Geological Survey (GeoLabs) in Sudbury, Ontario for whole rock analyses. Major element and loss of ignition (LOI)

determined by X-ray fluorescence spectrometry (XRF). The sample powders underwent LOI determinations, and were then fused with a borate flux to produce a glass disk. Trace elements were analyzed by inductively-coupled plasma mass spectrometry (ICP-MS) after closed vessel, four acid (HF-HCl-HNO_3-$HClO_4$) digestion. Relative analytical uncertainties are within ± 5 % for all major elements and ± 3 % for most trace elements. Nickel sulphide fire assay was conducted on mineralized samples for PGE (Pt, Pd, Ru, Rh, Ir) and Au determination. The sample is powdered and mixed with a Ni and S mixture and heated to produce a Ni sulphide disk. The Ni sulphide disk is then dissolved in aqua regia to produce a concentrate containing all six precious metals and then analyzed by ICP-MS.

Sulphide mineralization and sulphide melt inclusion samples were characterized petrographically using a Nikon Eclipse H550L microscope, using transmitted and reflected light. The composition and textural settings of base metal sulphides and discrete metal phases was conducted using a LEO1450VP scanning electron microscope (SEM) at Saint Mary's University, equipped with an energy dispersive X-ray (EDS) Oxford INCA 80 mm^2 silicon drift detector (SDD) capable of quantitative analysis. Measurements were conducted at a working distance of ~20 mm, with a beam current of 40 µA and accelerating voltage of 25-30 kV. Raw data were reduced using the software package INCA.

Electron microprobe analyses of olivine were performed using a Cameca SX-50 electron microprobe (EMP) at the University of Toronto. The instrument was operating at 20 kV accelerating voltage with a 30 nA beam current and beam diameter of 1 µm. Raw

microprobe data count rates were converted to concentrations using the ZAF data reduction scheme using the software Probe for EMPA (Advanced Microbeam Inc.).

Trace element concentrations of sulphide melt inclusions and associated host minerals (apatite, plagioclase, olivine) were measured by laser ablation inductively coupled plasma mass spectrometery (LA-ICP-MS) at Virginia Tech, Blacksburg, Virginia, using an Agilent 7500ce quadrupole ICP-MS and a Lambda Physik GeoLas 193 nm Excimer laser ablation system. The laser is linked to an Olympus petrographic microscope equipped with a 25x UV-VIS Schwarzschild objective for analyses as well as 5x and 10x objectives for transmitted light viewing of the sample. A He carrier gas flow of ~1 L/min was passes through the ablation cell with a volume of ~1 cm^3. Dwell times for all elements were 10 ms, except for ^{105}Pd, ^{106}Pd, ^{108}Pd, ^{195}Pt, and ^{197}Au, (50 ms) to improve detection limits. Oxide production rates were maintained below 1 %. Calibration of analyte sensitivities utilized the standard reference material 610 from NIST (National Institute of Standards and Technology) and the PGE-bearing pyrrhotite standard PO724 distributed by Memorial University (Sylvester et al., 2005). Each standard was analyzed twice before and twice after each analytical session that included 15-25 inclusion and host phase ablations, and the standards were used for data reduction and drift correction. Sulphide melt inclusion acquisition included 40-60 s of gas blank (laser off) before the laser shutter was opened to begin ablation of the host. The sites of interest were ablated using a beam diameter slightly larger than the inclusion (16-90 μm) and host phases were ablated with a spot size of 24 μm, which was the most common spot size used to ablate inclusions. Aerosols were generated using a pulsed beam with a repetition rate of 5 Hz and an output energy of 150 mJ. Since a majority of inclusions were not exposed at the

surface, the ablation process consisted of ablating the host before encountering the inclusion and continuing ablation until the entire inclusion was ablated. For complete operating conditions of the LA-ICP-MS system see Appendix 2.

Trace element quantification of sulphide melt inclusions was performed using the software SILLS (Guillong et al., 2008). This involved deconvoluting the mixed sulphide inclusion plus host signal from the host only signal after calculation of background corrected count rates for each isotope and quantification of inclusion and host compositions. Since inclusions are polyphase, complete inclusions present below the minerals surface needed to be analyzed because if the inclusions were exposed at surface, all mineral phases may not be present within a single inclusion due to plucking during the grinding and polishing process of the thick section production. Analysis of exposed sulphide inclusions by SEM revealed consistent phases and slight variations in phase proportions in olivine and ilmenite hosted inclusions. Exposed sulphide inclusions in apatite and plagioclase were predominately single phase consisting of pyrrhotite, with minor chalcopyrite present in apatite hosted inclusions. Unopened inclusions hosted in apatite and plagioclase, were assumed to have the same bulk Fe as pyrrhotite. Since inclusions in olivine are polyphase, an estimate of the bulk Fe needed to be calculated by a weighted average of the Fe content of each phase within the inclusions, which required an accurate estimate of the vol % of each phase by calculating the area each mineral phase occupied within a single exposed sulphide melt inclusion (91-99 vol % pyrrhotite, 0-6 vol % chalcopyrite, 0-3 vol % cobaltian-pentlandite) obtained by back scattered electron image analysis of cross sectional areas of individual inclusions. The relative

uncertainty associated with this method of calculation vol % estimation is ± 5 % (relative).

Trace element concentrations in individual sulphide minerals in mineralization were measured by LA-ICP-MS at Laurentian University, Sudbury, Ontario using a Thermo X Series II quadrupole ICP-MS coupled to a Resonetics RESOlution M50 laser ablation system containing a 193 nm, 20 ns pulsed ArF Excimer laser. Ablation occurred in He carrier gas (650 mL/min), which was combined with a small amount of high purity N_2 (6 mL/min) and Ar (800 mL/min) before being fed into the plasma. Dwell time for all elements was 10 ms, and oxide production rates were maintained below 0.3 % (ThO/Th checked on NIST 612). Calibration of analyte sensitivities utilized the standard reference material 610 from NIST and a PGE-bearing pyrrhotite standard PO725 distributed by Memorial University (Sylvester et al., 2005). A chalcopyrite PGE "blank" was used to evaluate the $^{63}Cu^{40}Ar$ and $^{65}Cu^{40}Ar$ interferences on ^{103}Rh and ^{105}Pd, respectively and allow for manual correction. Unknowns were bracketed with standards between every ten analyses. The sulphide acquisition consisted of 30s of a gas blank followed by ~10-15s of sample ablation. The laser conditions used were: repetition rate of 5 Hz, spot size between 36 and 66 μm, and a fluence of 6 J/cm^2. Trace element quantification of sulphide time-signal intensity data was performed using the software SILLS (Guillong et al, 2008). For complete operation conditions of the LA-ICP-MS system see Appendix 2. Internal standardization utilized the Fe content of the sulphide minerals determined separately by SEM.

Samples that contained large (>2 mm) sulphide grains were drilled out with a ~2 mm diamond drill bit to produce a sulphide powder. This powder was sent to the Queens

Facility for Isotope Research (QFIR) in Kingston, Ontario. Stable sulfur isotope measurements were completed on pyrrhotite, chalcopyrite, and pyrite using a Carlo Erba NCS 2500 elemental analyzer coupled to a Finnigan MAT 252 mass spectrometer with a Finnigan MAT Conflo 11. Values are reported in the δ notation in units of per mil (‰) relative to standard Vienna Canyon Diablo Troilite (V-CDT). Replicate $\delta^{34}S$ analyses are reproducible to within ±0.3‰.

Sulfur isotope compositions of sulphide mineralization, secondary sulphides (e.g., along fracture planes in core) , and sedimentary pyrrhotite were determined *in situ* using a CAMECA IMS 7f secondary ion mass spectrometer (SIMS) at the University of Manitoba, Winnipeg, Manitoba. A cesium (Cs^+) primary beam with a 2 nA current, was accelerated (+10 kV) onto the sample surface with a sputtering diameter of 15 μm; the instrument operated at a 200 V sample offset, -9 kV secondary accelerating voltage and at mass resolving power of 347. During the measurement process by SIMS, an intrinsic mass dependent bias is introduced, which is referred to as instrumental mass fractionation (IMF) and typically favors the low mass isotope. The greatest contributor to the IMF is the ionization process, which depends most strongly upon sample characteristics (i.e., chemical composition). This is referred to as compositionally dependent fractionation or "matrix effects" (e.g., Riciputi *et al.* 1998). Therefore, accurate isotopic SIMS analysis requires that IMF be corrected for by standardizing the IMF using mineral standards that are compositionally similar to the unknown. SIMS results from the standard are compared to its accepted isotopic composition in order to calculate a correction factor that is applied to the unknowns measured during the same analysis session (e.g., Holliger, 1988). A grain of Anderson pyrrhotite with an accepted $\delta^{34}S$ value of 1.4 ± 0.3‰ from the

Anderson Lake Mine, Manitoba, Canada was used as the sulfur isotope standard (Crowe and Vaughn, 1996). Spot-to-spot reproducibility for Anderson pyrrhotite was 0.3 ‰ and precision for individual analysis was 0.3 ‰ for $\delta^{34}S$ values. Therefore, 2σ errors for sulfur isotope analyses are 0.3 ‰. Isotopic data are reported in standard δ-notation relative to the appropriate standard, Canyon Diablo Troilite (CDT) for $^{34}S/^{32}S$. The equation for calculating δ values in units of per mil (‰) is:

$$\delta_{sample} = (R_{sample}/R_{std}-1)x10^3 \quad [1]$$

where R_{sample} and R_{std} are the absolute isotope ratios in sample and standard, respectively. Isotope ratios measured by SIMS were compared to the accepted ratios (calculated from δ values determined by conventional analyses and gas source mass spectrometry) for each mineral using equation [2]:

$$R_{sample}=[(\delta_{sample}/10^3)+1]R_{std} \quad [2]$$

where R_{std} ($^{34}S/^{32}S$) for CDT is 4.450045 x 10^{-2} (Jenson & Nakai, 1962). These data can be used to calculate isotope mass fractionation that occurs during SIMS analysis by using equation [3]:

$$\alpha SIMS=R_{SIMS}/R_{conv.} \quad [3]$$

where R_{SIMS} is the ratio measured by SIMS and R_{conv} is the accepted ratio measured by conventional gas source mass spectrometry. These ratios can be converted to ‰ notation by:

$$\delta_{bias}= [(R_{SIMS}/R_{conv.})-1] \times 10^3 \quad [4]$$

2.3 Results

2.3.1 Sulphide mineralization petrography

Two main types of sulphide mineralization occur in the CLG: (i) fine- to coarse-grained disseminated sulphides, comprising the longest interval of sulphide mineralization (~10 m) encountered in diamond drilling by Kodiak Exploration (Marmont, 2006, 2007); and (ii) Massive to semi-massive sulphide mineralization is represented comprising relatively short intervals of drill core (~1.5-3 m). Disseminated mineralization is hosted in fine- to medium-grained gabbros, that has gradational upper contacts with lesser mineralized (≤ 5 % sulphide) fine-grained gabbro that increases in its sulphide content and sulphide grain size into disseminated mineralization (~10-25 % sulphide). The lower contact of disseminated mineralization is defined by a ~1 cm thick pyrrhotite seam separating mineralization from barren, fine- to medium-grained gabbro below. Upper and lower contacts of massive sulphide are sharp with fine- to medium-grained gabbros that contain ≤ 5 % sulphide. Occasionally, a short interval (≤ 2 m) of disseminated sulphides occurs above and below massive sulphide mineralization with occasional sulphide stringers crosscutting the weakly foliated gabbro. A minor trace sulphide mineralization style is present within fine-grained gabbro and shows with local enrichment in PGE, determined through assay analyses (Marmont, 2007). These samples contain only trace amounts of sulphides and through detailed SEM work, no platinum group minerals (PGM) were observed.

Massive and semi-massive sulphide mineralization is primarily composed of pyrrhotite (~80 %), with lesser amounts of chalcopyrite (2-9 %), magnetite (5 %), pentlandite (1-3 %), pyrite (≤ 2 %), ilmenite (trace), and sphalerite (trace). Pyrrhotite is

massive and hosts all other sulphides and oxides as inclusions. Chalcopyrite primarily occurs as anhedral inclusions within pyrrhotite and is ≤ 2 mm in size (Figure 2.2A). Very fine-grained (< 0.05 mm) inclusions of sphalerite and pyrrhotite occur in chalcopyrite. Pentlandite occurs as flame lamella in pyrrhotite and in a blocky form (Figure 2.2B, C). Individual grains of blocky pentlandite are ≤ 0.1 mm and are generally concentrated around chalcopyrite; as well, blocky pentlandite occurs as chains (i.e., linked network of grains) in pyrrhotite. The pentlandite chains are up to 600 μm in length. Unlike blocky pentlandite, flame pentlandite has no strong association with chalcopyrite and individual lamella are ≤ 80 μm. Flame pentlandite does show a strong correlation to fractures in pyrrhotite, as lamellas are most common perpendicular to these fractures. Blocky pentlandite comprises the majority volume of pentlandite present in massive and semi-massive sulphides. Sphalerite grains have irregular to blebby form, are ≤ 0.1 mm, and occur as inclusions within chalcopyrite and pyrrhotite or on the edges of chalcopyrite (Figure 2.2A). Pyrite is not observed as a primary sulphide mineral but as an alteration of pyrrhotite and magnetite. Grains of pyrite are typically concentrated along fractures, occur in a blocky form, and are ≤ 0.2 mm (Figure 2.2B). Magnetite occurs as 1-2.5 mm inclusions within pyrrhotite, typically blebby, and moderately fractured (Figure 2.2A). Pyrrhotite can occur as ≤ 0.5 mm inclusions at the centre of magnetite grains. These small inclusions of pyrrhotite usually have a thin rim or small inclusions of chalcopyrite associated with them, suggesting they may be sulphide melt inclusions. All magnetite grains display a very thin exsolution texture of ilmenite. Very fine-grained pyrrhotite and chalcopyrite is observed in fractures and along the edges of magnetite grains.

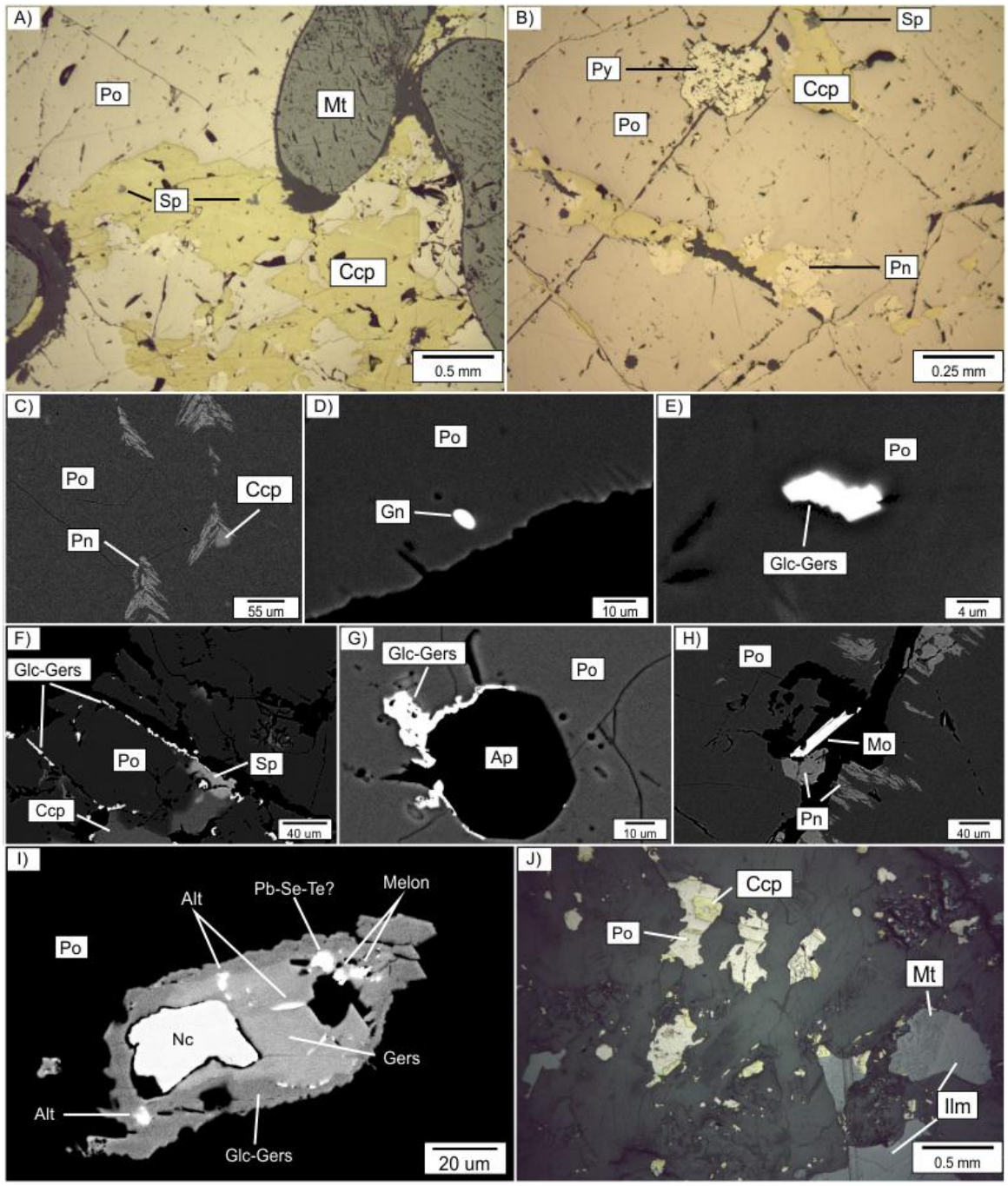
A)
Po
Mt
Sp
Ccp
0.5 mm
B)
Sp
Py
Ccp
Po
Pn
0.25 mm
C)
Po
Ccp
Pn
55 um
D)
Po
Gn
10 um
E)
Po
Glc-Gers
4 um
F)
Glc-Gers
Po
Sp
Ccp
40 um
G)
Glc-Gers
Po
Ap
10 um
H)
Po
Mo
Pn
40 um
I)
Alt
Pb-Se-Te?
Melon
Po
Nc
Gers
Alt
Glc-Gers
20 um
J)
Ccp
Po
Mt
Ilm
0.5 mm

Figure 2.2 (previous page): Representative petrography of sulphide mineralization. A) Massive pyrrhotite with anhedral inclusions of chalcopyrite and blebs of magnetite displaying fine-grained ilmenite exsolution. Very fine-grained anhedral inclusions of sphalerite occur in chalcopyrite. CL-06-05-81.6, massive sulphide mineralization. Reflected Light (RL). B) Massive pyrrhotite with anhedral inclusions of chalcopyrite, and blocky pentlandite occurs around the edges of chalcopyrite. Fine-grained sphalerite occurs on the edge of chalcopyrite and anhedral pyrite occurs along a fracture in pyrrhotite. CL-06-05-81.6, massive sulphide mineralization. RL. C) Fine-grained pentlandite flame lamella in pyrrhotite with a small bleb of chalcopyrite. CL-06-16-84.6, massive sulphide mineralization. Back scattered electron image (BSE). D) Anhedral bleb of galena in pyrrhotite. CL-06-16-56.3, disseminated sulphide mineralization. BSE. E) Anhedral bleb of glaucodot-gersdorffite in pyrrhotite. CL-06-16-56.3, disseminated sulphide mineralization. BSE. F) Anhedral blebs of glaucodot-gersdorffite occur along the grain margin and as inclusions in pyrrhotite. Fine-grained sphalerite and chalcopyrite are also present along the grain margins of pyrrhotite. CL-06-05-81.6, massive sulphide mineralization. BSE. G) Anhedral glaucodot-gersdorffite occurs along the contact of pyrrhotite and apatite. CL-06-16-84.6, massive sulphide mineralization. BSE. H) Molybdenite occurs along a fracture in pyrrhotite. Flame lamella and blocky pentlandite are also present along the margin of the fracture. CL-06-16-84.6, massive sulphide mineralization. BSE. I) Composite sulfarsenide inclusion in pyrrhotite where end-member gersdorffite forms the core and an intermediate composition of glaucodot-gersdorffite forms the rim. A large nickeline inclusion occurs within the composite grain as well as very fine inclusions of melonite, altaite, and unknown Pb-Se-Te grains. CL-06-16-84.6, massive sulphide mineralization. BSE. J) Representative microphotograph of trace sulphide "PGE-enriched" mineralization composed of fine-grained pyrrhotite and chalcopyrite with composite grains of ilmenite and magnetite. CL-07-09-60. RL. Alt = Altaite; Ap = Apatite; Ccp = Chalcopyrite; Gn = Galena; Gers = Gersdorffite; Glc-Gers = Glaucodot-gersdorffite solid solution; Ilm = Ilmenite; Mt = Magnetite; Melon = Melonite; Mo = Molybdenite; Nc = Nickeline; Pn = Pentlandite; Py = Pyrite; Po = Pyrrhotite; Sp = Sphalerite.

Trace metal phases present in massive sulphide mineralization include galena, glaucodot-gersdorffite [(Co,Fe)AsS-NiAsS], molybdenite, tellurobismuthite (Bi_2Te_3), altaite (PbTe), electrum (Au:Ag ratio ~70:30 at %), nickeline, melonite ($NiTe_2$), and unidentified Se-Te-Pb, Bi-Te, and Pb-Te minerals. Galena primarily occurs as blebby to anhedral inclusions within pyrrhotite (Figure 2.2D) (64.4 % of grains analyzed, n=149), but is also present as inclusions within chalcopyrite (13.4 %), glaucodot-gersdorffite (18.5 %), pentlandite (2 %), sphalerite (0.7 %), or along fractures in pyrrhotite (1 %). Grains of galena are ≤ 37 μm in their maximum dimension and occasionally, galena contains SEM-EDS detectable Se, up to 5.8 atomic % (n=3). Glaucodot-gersdorffite occurs as anhedral blebs to tabular inclusions within pyrrhotite (Figure 2.2E) (36 % of grains analyzed, n=45) and pentlandite (4 %), along fractures in pyrrhotite (9 %), or along the edges of pyrrhotite at the contact with silicates or apatite (51 %; Figure 2.2F, G). Grains of glaucodot-gersdorffite are ≤ 91 μm in their maximum dimension and have Co:Ni ratios ranging from 0.2-2.0 (average = 0.7±0.4; n=45). The range in Co:Ni ratio of glaucodot-gersdorffite is consistent among all its different textures and occurrences. Molybdenite tends to occur within and near fractures in pyrrhotite that have been infilled by quartz, grains are tabular, and are ≤ 71 μm in their maximum dimension (Figure 2.2H). In one example, molybdenite is observed as an inclusion within glaucodot-gersdorffite. Tellurobismuthite and altaite occur as ≤ 4 μm anhedral inclusions within approximately 12 % of the glaucodot-gersdorffite grains analyzed. Nickeline, melonite, and unidentified Se-Te-Pb and Te-Pb minerals are observed as inclusions within a single grain composed of glaucodot-gersdorffite. The host glaucodot-gersdorffite grain has an intermediate member of glaucodot-gersdorffite solid solution forming the rim and a core composed of

gersdorffite (Figure 2.2I). Grains of electrum are present as anhedral inclusions within 4 % of glaucodot-gersdorffite grains that are inclusions in pyrrhotite, and electrum grains are ≤ 6 μm. No PGM are observed in the massive sulphide.

Disseminated sulphides comprise 10-25 vol % of a fine- to medium-grained gabbro over a length of ~10.4 m in drill core. The mineral mode of sulphides present was determined using the program ImageJ to calculate the area each mineral phase occupies based on several representative micorphotographs of sulphide mineralization. The vol % each mineral comprises is as follows: pyrrhotite represents 75-85 %, chalcopyrite 2-8 %, pyrite trace-3 %, pentlandite trace-3 %, magnetite 5-10 %, ilmenite 5-10 %, and sphalerite trace. Sulphide textures present in the disseminated sulphide mineralization are the same as those observed in semi-massive to massive sulphide mineralization. Pyrrhotite grains are angular, ≤ 4 mm (~1 mm), and occur interstitial to silicates. Plagioclase is a common euhedral inclusion within pyrrhotite and inclusions range from 0.1-2 mm. Magnetite and ilmenite are also present as 0.01-0.2 mm inclusions within pyrrhotite. Chalcopyrite generally occurs as anhedral to tabular inclusions within pyrrhotite or along the edges of pyrrhotite and grains are ≤ 1 mm (ave. ~0.1 mm). Chalcopyrite also occurs as smaller (≤ 0.05 mm) grains interstitial to silicates. Rarely, chalcopyrite occurs spatially associated with actinolite and biotite alteration after clinopyroxene. As in the massive sulphides, pentlandite shows both blocky and flame lamella forms. Pentlandite blocks and flames are ≤ 100 μm, and individual chains of blocky pentlandite are up to 500 μm in length. Sphalerite occurs as anhedral blebs that are ≤ 100 μm, are typically concentrated around chalcopyrite and in some cases sphalerite displays chalcopyrite disease. Pyrite occurs primarily as an alteration product of

pyrrhotite and is concentrated along fractures, with grains ≤ 500 μm. Very fine-grained pyrite also occurs on the edges of, and infilling fractures of plagioclase. Composite grains of magnetite and ilmenite are present thought the disseminated sulphide mineralization, featuring blebby and trellis exsolution of ilmenite from original titanomagnetite grains. Composite oxide grain sizes are ≤ 4 mm (~1 mm), while individual grains of magnetite and ilmenite are typically ≤ 1.5 mm. Inclusions of pyrrhotite, ≤ 0.2 mm, occur in ilmenite/magnetite and commonly have a thin rim of chalcopyrite.

Only minor amounts of trace metal phases are present in the disseminated sulphides, primarily glaucodot-gersdorffite inclusions occurring within pyrrhotite that are tabular to anhedral and are ≤ 60 μm. Altaite and melonite occur as ≤ 2 μm, anhedral inclusions within glaucodot-gersdorffite. Empressite (AgTe), which is not observed in the massive sulphides, also occurs as an inclusion in glaucodot-gersdorffite as anhedral, ≤ 2 μm blebs. Galena (≤ 7 μm) and tellurobismuthite (≤ 2 μm) are observed as blebby inclusions within pyrrhotite. No PGM are observed in the disseminated sulphide samples.

Trace sulphide "PGE-enriched" mineralization occurs within a fine-grained gabbro. Sulphides occur in only trace amounts and pyrrhotite comprises the majority of sulphides with minor chalcopyrite, ilmenite, magnetite, and traces of pyrite and pentlandite (Figure 2.2J). Pyrrhotite grains are ≤ 1.8 mm (~0.5 mm), anhedral blebs that occur interstitially to silicates. Chalcopyrite grains are ≤ 0.4 mm (~0.1 mm) and predominantly occur as tabular to anhedral inclusions within or on the edges of pyrrhotite. Rarely chalcopyrite is observed associated with alteration of clinopyroxene and is very fine-grained (< 0.1 mm). Ilmenite and magnetite composite grains are ≤ 1.5 mm and occur interstitial to silicates. The overall proportion of ilmenite:magnetite is ~9:1 and

when magnetite is present it is always associated with ilmenite, whereas ilmenite primarily occurs on its own. In spite of detailed SEM work, no discrete metal phases or PGM were observed.

2.3.2 Bulk rock base metal and platinum-group element chemistry

Disseminated sulphide mineralization contains minor amounts of PGE (~2 to 62 ppb; combined Pd+Pt+Ir+Rh+Ru), where Pd and Pt are the major PGE and comprise 28 to 94 % and 0.4 to 69 %, respectively (Pt\Pd = 0.004-2.5). In semi-massive to massive sulphide mineralization, total PGE content ranges from 6 to 31 ppb, with Pd comprising 49 to 72 % of total PGE and Pt comprising 1 to 32 % (Pt\Pd = 0.017-0.67). Gold is also low, ranging from 2 to 11 ppb in disseminated sulphides and from 13 to 39 ppb in semi-massive to massive sulphide mineralization. Base metal concentrations in bulk rock are relatively low with Ni ranging from 0.12 to 0.41 wt % in disseminated sulphide mineralization and from 0.48 to 1.72 wt % in semi-massive and massive sulphide mineralization. Cobalt concentrations range from 0.02 to 0.04 wt % and 0.04 to 0.13 wt % and Cu ranges from 0.06 to 0.72 wt % and 0.14 to 1.04 wt % in disseminated and semi-massive to massive sulphide mineralization, respectively. Base metals (Ni, Co, Cu) and PGE in all of these mineralization styles have a positive correlation with S content, indicating base metal sulphides are the primary control on these metals. Nickel and Co have a positive correlation, suggesting pentlandite abundance or its Co content is the primary control on bulk Co. Base and precious metal assays are presented in Table 2.1. Two samples were collected from the trace sulphide “PGE-enriched” mineralization style as indentified in drilling by Kodiak Exploration (Marmont, 2007). The base metal concentrations in this mineralization style are very low compared to the other

Table 2.1: Whole rock base and precious metal assay results and results recalculated to 100% for sulphide mineralization in the CLG

mineralization style	disseminated sulphide												semi-massive sulphide			massive sulphide			trace sulphide	
drill hole	CL-06-16								CL-06-01		CL-06-05		CL-06-16		CL-06-01	CL-06-16	CL-06-05		CL-07-09	
depth (m)	52.5	55.0	56.3	57.5	58.6	59.9	61.7	63.8	18.8	22.5	75.1	77.7	47.6	78.7	22.0	84.6	81.2	81.6	57.0	60.0
Ni (wt%)	0.25	0.25	0.27	0.41	0.23	0.07	0.29	0.38	0.04	0.30	0.12	0.05	0.89	0.48	0.63	1.72	1.25	1.17	0.02	0.02
Cu	0.40	0.38	0.37	0.55	0.35	0.09	0.32	0.72	0.19	0.06	0.47	0.63	0.48	0.14	1.04	0.57	0.48	0.94	0.02	0.06
Co	0.03	0.03	0.03	0.04	0.03	0.01	0.03	0.04	0.01	0.04	0.02	0.01	0.10	0.04	0.08	0.11	0.13	0.12	0.01	0.01
Au (ppb)	6.59	9.72	8.19	12	8.23	4.53	7.44	9.51	1.58	11.4	4.43	6.84	13.2	2.65	9.48	13.3	16.8	38.9	8.91	14.3
Ir	1.22	0.21	0.72	0.92	0.45	0.06	0.32	0.48	0.03	0.8	0.11	0.08	0.93	0.27	2.74	0.27	1.16	1.14	0.07	0.08
Pd	3.55	4.96	6.15	7.41	5.63	1.85	6.89	8.66	1.35	58	3.14	2.93	9.73	4.31	15.5	21.6	12.6	10.3	113	117
Pt	0.23	0.33	0.37	<0.17	0.28	0.69	2.47	0.43	0.68	0.25	2.75	7.33	4.23	0.58	0.3	7.7	8.42	<0.17	29.6	37.2
Rh	1.26	0.66	0.82	1.14	0.56	0.08	0.52	0.82	0.05	1.13	0.16	0.16	1.32	0.58	3.25	0.97	2.5	2.45	3.18	4.36
Ru	2.64	0.2	1.19	1.67	0.6	<0.08	0.54	0.39	<0.08	1.26	0.16	0.14	1.13	0.23	5.56	0.09	1.31	1.21	0.42	0.53
recalculated to 100% sulphide																				
Ni (wt%)	1.49	1.40	1.43	1.41	1.53	1.95	1.33	1.50	1.39	1.05	1.45	0.94	1.46	1.93	1.12	2.07	1.41	1.39	2.59	1.86
Cu	2.35	2.11	1.94	1.86	2.38	2.37	1.60	2.90	1.96	2.44	1.87	12.09	0.79	0.86	0.84	1.25	0.54	1.12	3.76	5.28
Co	0.16	0.16	0.16	0.14	0.17	0.24	0.14	0.15	0.35	0.14	0.23	0.15	0.16	0.16	0.14	0.13	0.15	0.15	0.86	0.58
Au (ppb)	38.6	54.0	43.4	40.9	55.8	128	37.5	38.2	54.7	44.1	62.6	145	21.7	10.6	17.0	15.9	18.9	46.0	1538	1464
Ir	7.15	1.17	3.81	3.13	3.05	1.69	1.61	1.93	1.04	3.10	1.56	1.70	1.53	1.08	4.91	0.32	1.31	1.35	12.08	8.19
Pd	20.8	27.5	32.6	25.2	38.2	52.1	34.7	34.8	46.8	225	44.4	62.3	16.0	17.2	27.7	25.9	14.2	12.2	19507	11976
Pt	1.35	1.83	1.96	0.58	1.90	19.4	12.5	1.73	23.6	0.97	38.9	156	6.95	2.32	0.54	9.22	9.49	<0.20	5110	3808
Rh	7.38	3.67	4.34	<3.88	3.80	2.25	2.62	3.30	1.73	4.37	2.26	3.40	2.17	2.32	5.82	1.16	2.82	2.90	549	446
Ru	15.5	1.11	6.30	5.69	4.07	<2.25	2.72	1.57	<2.77	4.88	2.26	2.98	1.86	0.92	9.95	0.11	1.48	1.43	72.5	54.2

mineralization styles (Co = 50-57 ppm; Cu = 218-516 ppm; Ni = 150-182 ppm), however the total PGE contents are significantly higher (146-159 ppb; combined Pd+Pt+Ir+Rh+Ru). Palladium and Pt comprise ~97 % of the PGE in the trace sulphide mineralization, with Pd ranging from 113 to 117 ppb and Pt from 29 to 37 ppb (Pt\Pd = 0.26-0.32), while the IPGE (Ir+Rh+Ru) are present in abundances of 4 to 5 ppb. Gold has similar concentration in the trace sulphide mineralization (9-14 ppb) as was observed in the massive and disseminated mineralization styles. Unlike the massive and disseminated sulphide mineralization styles, the trace sulphide style does not show a strong positive correlation with increasing sulfur content, indicating that PGM may be present in these samples (but not observed) or the PGE are in solid solution within base metal sulphides in varying concentrations.

Recalculation of Ni, Cu, Co, Au, and PGE whole rock assay values to 100 % sulphide has been completed using the average compositions of pyrrhotite, chalcopyrite, and pentlandite based on the observation these minerals are the primary three phases present in sulphide mineralization. Error in this calculation, introduced by minor amounts of pyrite in the samples, is negligible. No olivine is present within mineralized intervals, therefore no significant Ni or Co within olivine structure needs to be accounted for in the calculation. Recalculated base and precious metal values are present in Table 2.1.

Disseminated and semi-massive to massive mineralization have similar profiles when normalized to primitive mantle and show Co and Ni enrichment relative to primitive mantle (Figure 2.3 A, B). Disseminated sulphides have relatively higher IPGE (Ir, Ru, Rh) values (1-15 ppb) when compared to semi-massive and massive sulphides (≤ 3 ppb) and are similar to or depleted relative to primitive mantle. Platinum and Pd

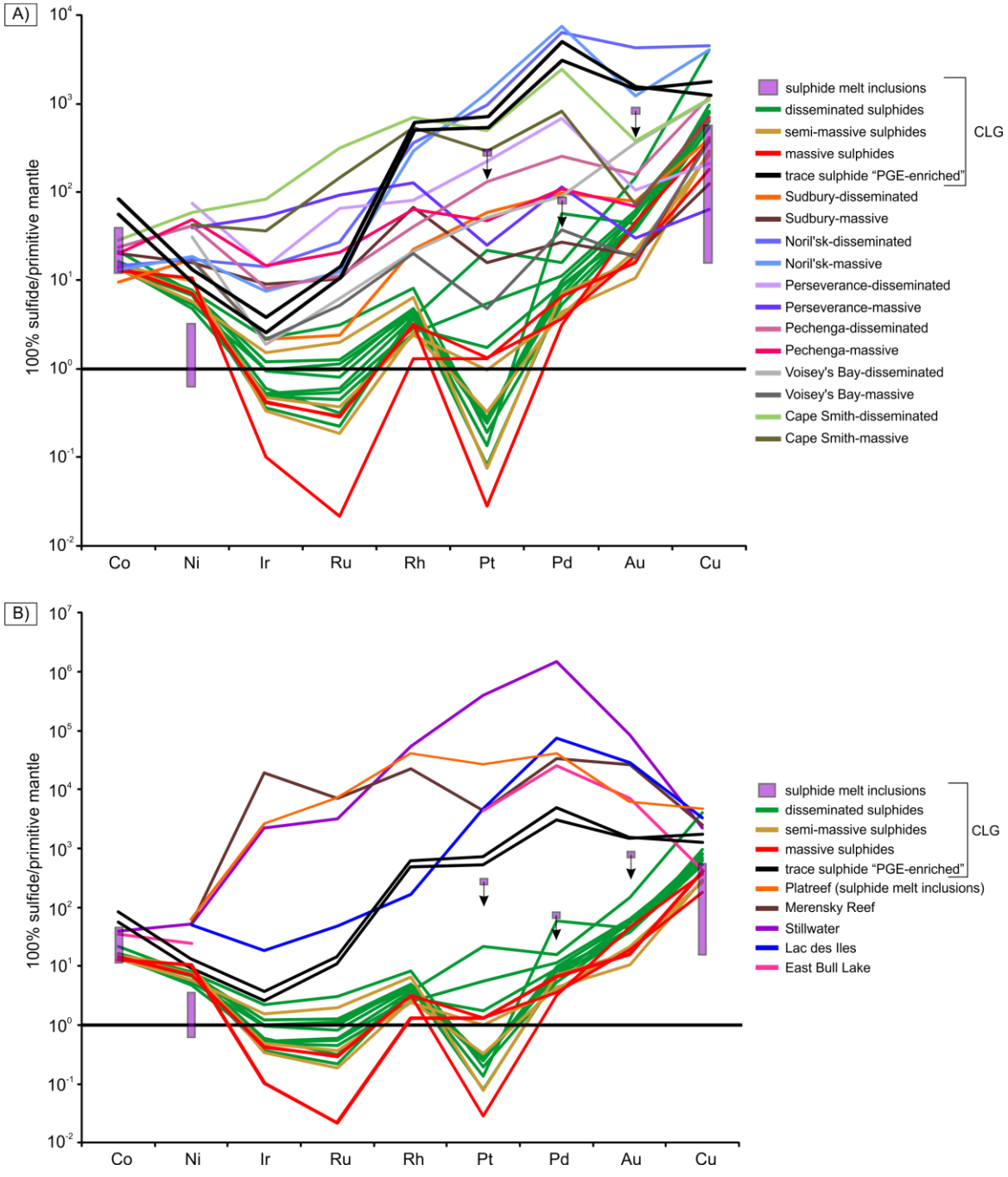
A)
100% sulfide/primitive mantle
Co
Ni
Ir
Ru
Rh
Pt
Pd
Au
Cu
sulphide melt inclusions
disseminated sulphides
semi-massive sulphides
massive sulphides
trace sulphide "PGE-enriched"
CLG
Sudbury-disseminated
Sudbury-massive
Noril'sk-disseminated
Noril'sk-massive
Perseverance-disseminated
Perseverance-massive
Pechenga-disseminated
Pechenga-massive
Voisey's Bay-disseminated
Voisey's Bay-massive
Cape Smith-disseminated
Cape Smith-massive
B)
100% sulfide/primitive mantle
Co
Ni
Ir
Ru
Rh
Pt
Pd
Au
Cu
sulphide melt inclusions
disseminated sulphides
semi-massive sulphides
massive sulphides
trace sulphide "PGE-enriched"
CLG
Platreef (sulphide melt inclusions)
Merensky Reef
Stillwater
Lac des Iles
East Bull Lake

Figure 2.3 (previous page): Caribou Lake Gabbro (CLG) mineralization recalculated to 100 % sulphide and normalized to primitive mantle. Sulphide melt inclusion compositions are also plotted. Note, Pt, Pd, and Au compositions for sulphide melt inclusions are based on minimum detection limits for inclusions hosted in plagioclase and apatite and arrows indicate that these elements real concentrations are lower than the concentration plotted. A) Comparison of CLG mineralization to large Ni-Cu-PGE deposits globally. Only Co and some Cu values from other deposits are similar to the CLG. All PGE, except Ir, in disseminated, semi-massive, and massive sulphide mineralization are more enriched in the other Ni-Cu-PGE deposits compared to the CLG. Trace sulphide "PGE-enriched" mineralization in the CLG shares a similar profile to Noril'sk. Sudbury: Naldrett (1984); Noril'sk: Barnes et al., 1997b; Perseverance: Barnes et al., 1988; Pechenga: Barnes et al., 2001; Voisey's Bay: Naldrett et al., 2000; Cape Smith: Barnes et al., 1997b B) Comparison of the CLG mineralization to PGE deposits globally. Trace sulphide "PGE-enriched" mineralization in the CLG shares a similar pattern to these PGE deposits, but overall concentrations are significantly lower in the CLG. Stillwater Complex: Godel and Barnes, 2008; Merensky Reef: Naldrett, 1981; Platreef: Holwell et al., 2011; Lac des Iles: Hinchey (2005); East Bull Lake: Peck et al., 2001.

concentrations are relatively consistent between the three mineralization styles (12-52 ppb Pd; 0.2-23 ppb Pt), with a few higher values occurring in disseminated mineralization (224 ppb Pd; 39 ppb Pt) (Figure 2.3A, B). Palladium is moderately enriched compared to primitive mantle where as Pt is commonly depleted and the Pd:Pt ratio is highly variable, ranging from 0.4 to 232 in disseminated and semi-massive to massive sulphide. The ratio between IPGE and PPGE is also highly variable as well ranging from 0.7-22. Gold tends to have higher concentrations in disseminated sulphides (38-128 ppb) than in semi-massive and massive mineralization (10-46 ppb) and is also enriched compared to primitive mantle. Copper is the only base metal that is highly enriched compared to primitive mantle and disseminated sulphides contain slightly higher concentrations (Figure 2.3A, B). One sample from a pyrrhotite rich stringer occurring ~4 m above massive sulphide mineralization is enriched in Pt relative to all other samples (156 ppb) and moderately enriched in Au (145 ppb). Copper in this stringer is also highly enriched relative to all other samples with 12.1 wt % Cu. After recalculation to 100 % sulphide for trace sulphide "PGE-enriched" mineralization samples, PGE are significantly enriched (except Ir) compared to the other styles of mineralization while, base metal (Ni ,Cu, Co) are only moderately higher (Figure 2.3A, B). Palladium and Pt are 12-20 ppm and 4-5 ppm, respectively with IPGE between 500-630 ppb. The Pd:Pt ratio is generally lower in the trace sulphide mineralization (~3-4) compared to the disseminated and massive mineralization styles (~1-60), while the PPGE:IPGE ratio is higher ~31-39 in trace sulphide mineralization than other mineralization styles (~0.7-27).

2.3.3 Trace element distribution between sulphide minerals

In massive sulphides, As (2-50 ppm), Se (36-67 ppm), and Ta (13-30 ppb) concentrations are comparable between pyrite, chalcopyrite, pyrrhotite, and pentlandite. Pentlandite has higher concentrations of Co (1.8-7.6 wt %), V (3-17 ppm), Ag (13-80 ppm), Te (2-5 ppm), Tl (13-22 ppm), and Bi (9-25 ppm) relative to all sulphide phases analyzed and Pd (40-150 ppb) is comparable between pentlandite and chalcopyrite. Antimony is comparable in pyrite and pentlandite (100-400 ppb). Chalcopyrite contains more Zn (230-980 ppm), Cd (1-5 ppm), and Rh (15-20 ppm) than the other sulphides and Pt (20-36 ppb), Au (40-8600 ppb), Re (183-410 ppb), and Sn (37-150 ppm) are comparable in chalcopyrite and pyrrhotite, while Pt is below detection limits (< 43 ppb) in pyrite and pentlandite. Trace elements that concentrate into pyrite over other sulphides are Cr (< 13 ppm) and Pb (120-250 ppm) and only Ir concentrates into pyrrhotite (30-70 ppb). Osmium is below detection limits in all sulphide phases (< 50 ppb). Pyrrhotite contains (on average) 0.8 wt % Ni. Complete LA-ICP-MS results for trace elements in sulphide mineral analyses are presented in Table 2.2.

In disseminated sulphides, the distribution of trace elements between sulphide minerals is similar to that of the massive sulphides with the exception of Cr (< 2 ppm), Ta (< 5 ppb), Ir (<16 ppb), and Pt (< 54 ppb) are all below detection limits. Gold is not similar in chalcopyrite and pyrrhotite but is concentrated into pentlandite (28-300 ppb), Sb is only concentrated in pyrite (600-2300 ppb) and not evenly between pyrite and pentlandite as in the massive sulphide. The main hosts for Sn (234-1200 ppb) are pentlandite and chalcopyrite in disseminated sulphides, whereas pyrrhotite and chalcopyrite host Sn in the massive sulphide. Rhenium (50-500 ppb) is partitioned

Table 2.2: LA-ICP-MS analyses of sulphide minerals from massive and disseminated sulphide mineralization

analyte	^{60}Ni (wt%)	^{65}Cu	^{51}V (ppm)	^{53}Cr	^{59}Co	^{66}Zn	^{75}As	^{82}Se	^{99}Ru	^{101}Ru	^{103}Rh	^{105}Pd	^{106}Pd	^{107}Ag	^{108}Pd	^{111}Cd	^{118}Sn	^{121}Sb	^{125}Te	^{181}Ta	^{185}Re	^{189}Os	^{193}Ir	^{195}Pt	^{197}Au	^{205}Tl	^{208}Pb	^{209}Bi
massive sulphide (>80% sulphide); CL-06-05-81.6																												
12 - Py	0.53	0.001	b.d.l	b.d.l	1589	0.80	2.35	60.8	0.00	b.d.l	0.04	b.d.l	b.d.l	1.56	b.d.l	b.d.l	49.0	0.43	0.35	b.d.l	0.18	b.d.l	b.d.l	b.d.l	0.03	0.49	200	0.71
13 - Py	0.23	0.01	b.d.l	b.d.l	641	6.56	1.90	52.6	0.00	b.d.l	0.02	b.d.l	b.d.l	3.40	0.05	0.58	15.8	0.31	b.d.l	b.d.l	0.06	b.d.l	b.d.l	b.d.l	b.d.l	0.39	249	1.02
21 - Py	0.099	0.03	2.79	b.d.l	339	97.0	30.4	46.9	b.d.l	b.d.l	0.02	b.d.l	b.d.l	1.06	b.d.l	0.39	26.3	0.26	1.34	b.d.l	0.06	b.d.l	b.d.l	b.d.l	0.05	0.07	143	4.49
22 - Py	0.072	0.01	6.73	13.9	617	7.05	11.3	47.4	0.00	b.d.l	b.d.l	b.d.l	b.d.l	0.65	0.05	0.21	10.3	1.54	2.35	0.01	0.06	b.d.l	0.05	b.d.l	0.06	0.04	122	4.85
24 - Py	0.15	1.60	1.67	b.d.l	315	11.5	18.3	43.5	0.04	b.d.l	0.64	0.00	b.d.l	3.00	b.d.l	b.d.l	116	0.51	0.97	0.01	0.13	b.d.l	b.d.l	b.d.l	0.71	0.46	204	3.54
4 - Pn	35.0	0.01	17.1	b.d.l	38179	3.96	8.51	42.9	0.00	0.00	b.d.l	b.d.l	0.13	31.1	b.d.l	b.d.l	119	0.33	4.67	0.03	b.d.l	b.d.l	b.d.l	b.d.l	0.08	21.8	115	13.2
5 - Pn	19.0	0.003	15.9	b.d.l	18774	44.5	2.99	36.9	0.00	0.00	b.d.l	b.d.l	0.05	12.8	b.d.l	b.d.l	26.1	0.21	1.88	b.d.l	0.29	b.d.l	b.d.l	b.d.l	b.d.l	17.6	61.8	9.43
7 - Pn	15.1	0.002	3.51	b.d.l	22469	4.59	4.71	37.7	0.00	0.00	0.01	0.05	0.11	22.7	0.05	b.d.l	11.5	0.10	2.63	0.02	0.08	b.d.l	0.30	b.d.l	0.07	16.3	114	15.8
8 - Pn	37.0	0.03	b.d.l	b.d.l	76079	45.7	2.28	66.9	0.00	0.00	0.04	0.03	0.15	81.4	0.06	0.35	27.0	0.35	2.66	0.02	0.20	b.d.l	b.d.l	b.d.l	0.74	12.9	183	24.9
9 - Ccp	0.091	39.6	b.d.l	b.d.l	13.7	239	3.89	47.4	0.34	b.d.l	15.5	0.00	0.09	18.1	b.d.l	1.59	47.0	0.19	2.23	b.d.l	b.d.l	b.d.l	b.d.l	b.d.l	0.10	0.38	18.1	5.24
10 - Ccp	0.003	40.3	b.d.l	b.d.l	2.07	978	52.9	48.9	0.65	0.63	15.3	0.00	0.13	15.9	b.d.l	4.46	146.3	0.13	b.d.l	b.d.l	b.d.l	b.d.l	b.d.l	0.36	0.24	0.07	9.25	0.94
19 - Ccp	0.032	35.3	1.47	b.d.l	78.3	227	3.44	48.7	b.d.l	b.d.l	14.5	0.00	0.07	14.7	b.d.l	0.53	44.4	b.d.l	2.15	b.d.l	0.41	b.d.l	b.d.l	b.d.l	b.d.l	0.20	7.15	2.05
23 - Ccp	0.001	34.4	b.d.l	b.d.l	0.89	617	13.4	48.6	0.41	b.d.l	16.3	0.00	0.10	9.76	0.11	2.30	37.0	0.24	1.65	b.d.l	0.18	b.d.l	b.d.l	0.13	8.64	1.00	33.7	2.73
26 - Ccp	0.005	40.3	b.d.l	b.d.l	3.29	232	1.97	64.4	0.83	b.d.l	20.2	0.00	b.d.l	21.3	b.d.l	2.97	345	b.d.l	1.35	b.d.l	0.42	b.d.l	b.d.l	b.d.l	b.d.l	0.39	15.2	1.72
6 - Po	0.84	0.002	2.27	b.d.l	575	2.66	1.83	46.6	b.d.l	b.d.l	b.d.l	b.d.l	b.d.l	1.29	0.07	b.d.l	26.4	b.d.l	b.d.l	b.d.l	0.21	b.d.l	b.d.l	b.d.l	b.d.l	0.05	14.6	3.99
11 - Po	0.80	0.11	6.43	6.25	470	105	30.1	43.9	0.00	0.00	b.d.l	b.d.l	0.08	0.45	b.d.l	b.d.l	69.7	0.09	b.d.l	b.d.l	0.30	b.d.l	0.03	b.d.l	1.30	0.67	1.93	0.56
17 - Po	0.85	0.08	1.28	b.d.l	532	58.0	5.23	49.4	b.d.l	b.d.l	b.d.l	b.d.l	b.d.l	0.77	b.d.l	b.d.l	57.2	0.08	b.d.l	b.d.l	0.24	b.d.l	0.04	b.d.l	0.04	b.d.l	36.9	1.19
25 - Po	0.60	0.01	1.66	b.d.l	264	209	11.7	41.9	b.d.l	b.d.l	b.d.l	b.d.l	b.d.l	0.64	b.d.l	0.68	151	0.20	b.d.l	b.d.l	0.38	b.d.l	0.07	0.20	2.44	b.d.l	5.55	1.23
disseminated/net-textured sulphide; CL-06-16-56.3																												
8 - Py	0.15	0.002	b.d.l	b.d.l	455	2.42	1.25	44.0	0.00	b.d.l	b.d.l	b.d.l	b.d.l	0.39	b.d.l	b.d.l	b.d.l	0.67	0.41	b.d.l	0.13	b.d.l	b.d.l	b.d.l	b.d.l	0.16	212	1.42
11 - Py	0.24	0.10	b.d.l	b.d.l	781	2.40	0.65	40.5	0.00	b.d.l	b.d.l	b.d.l	b.d.l	2.43	b.d.l	b.d.l	0.06	2.29	b.d.l	b.d.l	0.38	b.d.l	b.d.l	b.d.l	0.05	0.30	243	0.98
21 - Py	0.12	0.001	b.d.l	b.d.l	315	1.18	0.58	39.3	b.d.l	b.d.l	b.d.l	b.d.l	b.d.l	0.36	b.d.l	b.d.l	b.d.l	0.94	b.d.l	b.d.l	2.19	b.d.l	b.d.l	b.d.l	b.d.l	0.10	121	0.99
23 - Py	0.13	0.001	b.d.l	b.d.l	473	1.33	b.d.l	42.9	0.00	b.d.l	0.02	b.d.l	b.d.l	0.77	b.d.l	b.d.l	0.08	0.61	0.34	b.d.l	0.49	b.d.l	b.d.l	b.d.l	b.d.l	0.22	139	0.88
26 - Py	0.26	0.002	b.d.l	b.d.l	1151	4.29	0.97	38.3	0.00	b.d.l	b.d.l	b.d.l	b.d.l	1.51	b.d.l	b.d.l	0.29	0.71	b.d.l	b.d.l	0.19	b.d.l	b.d.l	b.d.l	b.d.l	0.12	156	0.53
10 - Pn	23.0	3.14	1.17	b.d.l	55868	77.1	1.62	42.3	0.00	0.00	1.31	0.42	0.37	116	0.41	0.64	0.14	0.09	6.21	b.d.l	0.19	b.d.l	b.d.l	b.d.l	41.1	38.1	359	69.5
18 - Pn	30.1	0.44	10.8	b.d.l	79772	118	2.18	41.3	0.00	0.00	0.15	0.27	0.44	138	0.38	0.49	1.26	0.12	b.d.l	b.d.l	0.07	b.d.l	b.d.l	b.d.l	11.1	9.06	154	15.5
19 - Pn	26.0	0.60	63.9	b.d.l	57205	131	2.75	50.8	0.00	0.00	0.31	0.23	0.46	88.7	0.38	0.89	0.38	0.07	4.97	b.d.l	0.18	b.d.l	b.d.l	b.d.l	0.24	67.3	137	43.2
25 - Pn	26.1	0.16	1.15	b.d.l	51461	8.23	1.15	36.1	0.00	0.12	0.08	0.21	0.18	79.9	0.28	b.d.l	0.36	0.07	1.25	b.d.l	b.d.l	b.d.l	b.d.l	b.d.l	0.03	110	105	18.4
4 - Ccp	0.04	37.5	b.d.l	b.d.l	44.2	564	b.d.l	42.8	0.25	0.16	15.6	0.00	0.12	20.6	0.08	3.66	0.07	b.d.l	0.74	b.d.l	0.15	b.d.l	b.d.l	b.d.l	b.d.l	0.53	24.6	4.72
9 - Ccp	0.11	25.6	b.d.l	b.d.l	18.4	282	0.52	31.4	0.21	0.03	10.6	0.00	0.08	24.3	0.04	1.89	0.45	b.d.l	2.11	b.d.l	0.11	b.d.l	b.d.l	b.d.l	0.10	0.64	23.1	10.5
13 - Ccp	0.00	35.4	b.d.l	b.d.l	b.d.l	672	b.d.l	36.7	0.84	b.d.l	16.9	2.61	0.33	20.8	b.d.l	4.39	1.23	0.05	1.26	b.d.l	b.d.l	b.d.l	b.d.l	b.d.l	b.d.l	b.d.l	4.19	1.07
17 - Ccp	b.d.l	32.6	b.d.l	b.d.l	36.7	312	2.34	33.1	0.27	b.d.l	14.3	0.00	0.11	20.4	0.11	1.74	0.80	b.d.l	1.68	b.d.l	b.d.l	b.d.l	b.d.l	b.d.l	b.d.l	0.29	8.47	1.78
24 - Ccp	0.09	34.1	6.03	b.d.l	31.6	147	1.57	37.1	0.27	0.00	15.5	0.00	0.06	24.5	0.06	1.22	0.23	0.04	0.88	b.d.l	b.d.l	b.d.l	b.d.l	b.d.l	b.d.l	2.42	18.8	1.96
6 - Po	1.24	0.65	0.77	b.d.l	694	8.80	0.92	44.1	0.00	0.00	0.24	0.00	b.d.l	3.12	b.d.l	b.d.l	0.12	b.d.l	b.d.l	b.d.l	0.30	b.d.l	b.d.l	b.d.l	b.d.l	2.63	61.0	2.87
7 - Po	0.94	b.d.l	0.59	b.d.l	421	1.80	0.60	39.5	0.00	0.00	b.d.l	b.d.l	b.d.l	0.23	b.d.l	b.d.l	0.18	b.d.l	0.25	b.d.l	0.14	b.d.l	b.d.l	b.d.l	b.d.l	0.02	4.22	1.43
12 - Po	0.93	0.001	b.d.l	b.d.l	752	2.10	0.78	37.3	0.00	0.00	b.d.l	b.d.l	b.d.l	0.07	b.d.l	b.d.l	0.22	b.d.l	b.d.l	b.d.l	0.05	b.d.l	b.d.l	b.d.l	b.d.l	b.d.l	0.56	0.19
20 - Po	0.95	b.d.l	0.38	b.d.l	657	0.68	0.83	42.9	0.00	0.00	0.01	b.d.l	b.d.l	0.07	b.d.l	b.d.l	0.32	b.d.l	b.d.l	b.d.l	0.46	b.d.l	b.d.l	b.d.l	b.d.l	0.01	1.44	0.62
22 - Po	0.91	0.001	b.d.l	b.d.l	759	1.27	b.d.l	37.6	0.00	0.00	b.d.l	b.d.l	b.d.l	0.22	b.d.l	b.d.l	0.12	b.d.l	b.d.l	b.d.l	0.16	b.d.l	b.d.l	b.d.l	b.d.l	b.d.l	2.66	1.20

b.d.l = below detection limits; Py = pyrite; Pn = pentlandite; Ccp = chalcopyrite; Po = pyrrhotite; ^{xx} = element concentrations based on listed isotope measured

between pyrite and pyrrhotite in disseminated sulphides. Pyrrhotite on average contains 1.0 wt % Ni.

As shown in Figure 2.4, trace metals in pyrrhotite, chalcopyrite, and pyrite tend to be higher in concentrations in massive sulphide relative to disseminated sulphide mineralization, and pentlandite has higher concentrations for most trace elements in disseminated sulphide mineralization. The most notable enrichments in massive sulphide relative to disseminated sulphides are for Sn, Au, Zn, and As, while only Rh and Tl are consistently concentrated in the disseminated sulphides.

2.3.4 Sulphide melt inclusion petrography and paragenesis

Sulphide melt inclusions were identified in two different lithologies; a coarse-grained olivine gabbro, where SUL are hosted in olivine, plagioclase, and ilmenite, and a highly altered gabbroic pegmatite, where SUL are hosted in apatite.

Olivine grains hosting SUL are 6-15 mm in size, subhedral, and moderately fractured. Sulphide melt inclusions in olivine occur as circular to oval blebs in secondary trails along healed fracture planes (Figure 2.5A). The size of the inclusions range from 25 to 160 µm (avg. 55 µm). Based on petrographic observations, the olivine-hosted SUL are polyphase and consist of pyrrhotite, chalcopyrite, pentlandite, sphalerite and magnetite. Ilmenite grains hosting SUL occur interstitially to olivine and plagioclase and are 4-5 mm in size. Sulphide melt inclusions in ilmenite have a larger size range than olivine hosted SUL (40 to 230 µm, avg. ~65 µm) and are circular to tubular in shape (Figure 2.5B). Unlike olivine-hosted SUL, ilmenite hosted SUL appear to be primary in origin as they are randomly orientated and do not have a planar alignment as SUL in olivine, which is consistent with ilmenite being an interstitial phase while olivine is a primary cumulate

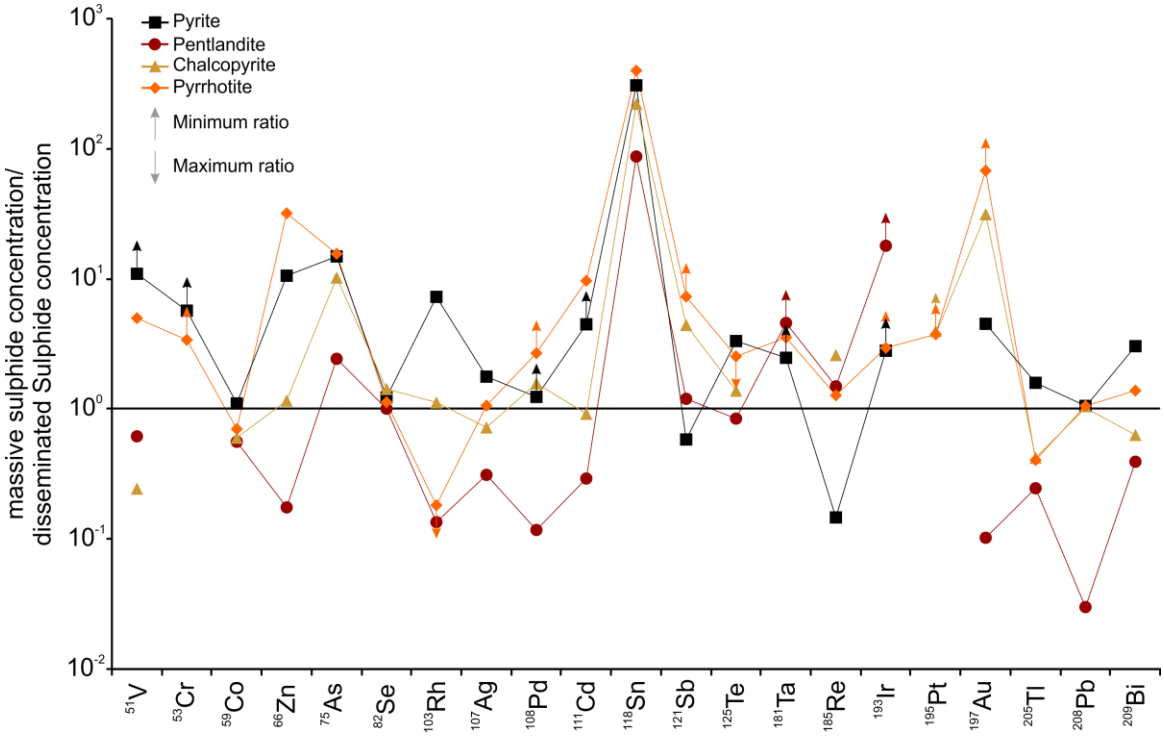

Figure 2.4: Log graph of average massive sulphide/disseminated sulphide ratios for trace element concentrations in sulphide minerals analyzed by LA-ICP-MS. Pyrite (massive, n=5 analyses; disseminated, n=5 analyses), pentlandite (massive, n= 4 analyses; disseminated, n=4 analyses), chalcopyrite (massive, n=5 analyses; disseminated, n=5 analyses) and pyrrhotite (massive, n=4 analyses; disseminated, n=5 analyses). Complete sulphide LA-ICP-MS analysis results are presented in Table 2.3. Arrows indicating a minimum ratio specify a certain element was below detection limits in a sulphide mineral from the disseminated sulphides and arrows indicating a maximum ratio indicate that a certain element was below detection in a sulphide mineral analyzed from the massive sulphides. No data point above an element indicates that it was below detection limits in both disseminated and massive sulphide.

A)
SUL Trail
Ol
0.25 mm
B)
Mt
Ilm
SUL
0.25 mm
C)
Ap
SUL-SIL Trail
D)
E)
0.25 mm
D)
SIL
SUL
60 um
E)
Ap
SIL
SUL
30 um
F)
Ap
Po
Po
Ccp
30 um
G)
Apatite
H)
S Kα
I)
Mg Kα
J)
Si Kα
K)
Cpx
SUL Trail
Plag
0.25 mm
L)
Po
Plag
30 um
M)
Ilm
Po
Mt
Co-Pn
Ccp
Sp
60 um
N)
Mt
Ol
Po
Glc-Gers
Ccp
14 um

Figure 2.5 (previous page): Representative sulphide melt inclusion petrography and inclusion mineralogy. A) Secondary sulphide melt inclusion trail occurring in olivine. B) A composite Fe-Ti oxide grain composed of ilmenite and magnetite with primary sulphide melt inclusions hosted in the Ilm phase. C) Secondary trail of sulphide and silicate melt inclusions hosted within apatite. D) Enlarged section of the inclusion trail in C, showing an interconnected network of tube shaped sulphide-silicate melt inclusions. E-F) Enlarged section of inclusion trail in C, showing silicate melt connecting two sulphide inclusions. One sulphide inclusion consists of pyrrhotite and chalcopyrite, while the other inclusion is only pyrrhotite. G-J) Scanning electron microscopy element maps of a sulphide melt inclusion that is surrounding an inclusion of silicate melt. K) Secondary sulphide melt inclusion trail occurring within plagioclase. L) Sulphide melt inclusions hosted in plagioclase consisting only of pyrrhotite. M) Representative sulphide melt inclusions occurring within ilmenite. Mineralogy of the sulphide inclusions consists predominantly of pyrrhotite, with lesser amounts of chalcopyrite, cobaltian pentlandite, and sphalerite. N) Representative sulphide melt inclusion hosted in olivine. Mineralogy of the inclusion consists of pyrrhotite, chalcopyrite, magnetite, and glaucodot-gersdorffite. Ap = Apatite; Ccp = Chalcopyrite; Cpx = Clinopyroxene; Co-Pn = Cobaltian-pentlandite; Glc-Gers = Glaucodot-Gersdorffite; Ilm = Ilmenite; Mt = Magnetite; Ol = Olivine; Plag = Plagioclase; Po = Pyrrhotite; SIL = Silicate melt inclusion; Sp = Sphalerite; SUL = Sulphide melt inclusion.

mineral. Sulphide melt inclusions occurring within ilmenite contain the same mineral assemblage as olivine hosted SUL. Olivine and ilmenite SUL are contained within a single ilmenite or olivine grain and never crosscut grain boundaries.

Apatite grains hosting SUL are very coarse-grained (≤ 20 mm), subhedral to euhedral cumulate grains and are highly fractured. Sulphide melt inclusions in apatite occur in secondary trails and are subspherical or tube shaped in appearance (Figure 2.5C, D). Sulphide melt inclusions range in size from 5 to 25 μm (avg. 10 μm). Within SUL trails, small (≤ 8 μm) quantities of suspected silicate glass are present, creating an interconnected network of tube shaped sulphide-silicate melt inclusions. As shown in Figure 2.5E, F and G, single inclusions can be composed of a silicate glass and sulphide melt, where the silicate glass fills the inclusion in between two distinct SUL. Elemental SEM-EDS mapping of a mixed silicate-sulphide inclusion shows that in between two sulphide inclusions, a small amount of silicate glass is trapped, indicated by the elevated SiO_2 and MgO (Figure 2.5H, I, and J). The proportion of sulphide to silicate glass within a single trail is highly variable from inclusion to inclusion, which indicates coeval entrapment of the two melt phases and the textures are representative of a liquid rather than a solid mineral being entrapped. Plagioclase grains hosting SUL are 1-15 mm euhedral, cumulate grains that show weak to moderate sericitic alteration throughout. Plagioclase-hosted SUL from secondary trails and are circular to oval in shape, ranging in size from 5 to 15 μm (avg. ~8 μm; Figure 2.5K, L). Apatite and plagioclase hosted SUL are composed of pyrrhotite and minor chalcopyrite. Sulphide melt inclusion trails are contained within a single apatite or plagioclase grain and never crosscut grain boundaries, indicating they did not get trapped after the solidus was reached.

2.3.5 Sulphide melt inclusion mineralogy and chemistry

Based on reflected light and SEM-EDS, five different sulphide and sulfarsenide phases are observed in SUL: pyrrhotite, chalcopyrite, cobaltian-pentlandite, sphalerite, and one occurrence of glaucodot-gersdorffite (Figure 2.5M and N). The volumetric proportions of SUL described below are only an estimate because during cutting and polishing to expose SULs at the surface, sulphide phases may have been partially or completely removed.

Pyrrhotite is the dominant sulphide phase in all SUL and comprises 91-100 vol % of individual inclusions. Chalcopyrite typically occurs as subangular to rounded phases near the edges of the inclusions and occurs in 56 % of inclusions hosted in olivine, 59 % of inclusions in ilmenite, 11 % of inclusions in apatite, and 6 % of inclusions in plagioclase. The chalcopyrite volumetric proportion of the total sulphide melt inclusion is very similar between each host phase (0-8 % in olivine, 0-8 % in ilmenite, 0-9 % in apatite, and 0-3 % in plagioclase). Cobaltian-pentlandite typically occurs as flame lamella and/or in a blocky form on the edges of inclusions (Figure 2.5M). In olivine, cobaltian-pentlandite occurs in 44 % of inclusions, comprising 0-5 vol % of individual inclusions. Cobaltian-pentlandite occurs more often in ilmenite hosted inclusions (64 %) but occupies a lesser proportion of individual inclusions (0-3 vol %). Petrographically, no cobaltian-pentlandite is observed in apatite or plagioclase hosted SUL. Sphalerite occurs as a subrounded phase near the edge of inclusions and occurs in 6 % of olivine hosted inclusions, 5 % of ilmenite hosted inclusions and is not observed in apatite or plagioclase hosted inclusions (Figure 2.5M). Volumetrically, sphalerite comprises 0-0.2 % of olivine hosted inclusions and significantly more of ilmenite hosted inclusions (0-1.5 vol %). Only

one SUL (hosted by olivine) contained glaucodot-gersdorffite, which occurs as a rounded bleb on the the inner inclusion wall or edge of the inclusion in the host, and comprises 0.007 vol % of the inclusion (Figure 2.5M).

Representative SEM-EDS analyses of sulphide phases within SUL are summarized in Table 2.3. The Fe content of pyrrhotite is consistent for all inclusions hosted all four host minerals, ranging between 59.5-62.2 wt %. No Ni in pyrrhotite was detected using SEM-EDS. The average Cu in chalcopyrite is 32.0 wt %, which is slightly (~2 %) less than ideal composition. Cobaltian pentlandite is Fe-deficient, with 13.6 to 19.8 wt % Fe (Fe poor compared to stoichiometric pentlandite). The Fe deficiency is accounted for by the large amounts of Co (31.3-40.9 wt %).

2.3.6 Sulphide melt inclusions bulk chemistry

Sulphide melt inclusion compositions were determined by LA-ICP-MS for inclusions hosted in apatite, plagioclase, and olivine. Representative laser signals are shown in Figure 2.6. Bulk compositions in olivine are semi-quantitative because SUL are exposed at surface and is unlikely that the entire inclusion was ablated, since a portion of the inclusion was removed during sample polishing. Therefore only trace element compositions of SUL in apatite and plagioclase will be presented from inclusions buried below the mineral surface which represent complete polyphase inclusions.

Plagioclase-hosted SUL have Cu concentrations ranging from 640-27,200 ppm (avg. 7,800 ± 4,400 ppm; 1σ, n=29), Ni concentrations of 1,300-5,940 ppm (avg.1,900 ± 980 ppm; 1σ, n=24), and Co concentrations from 950-4,430 ppm (avg. 1,780 ± 820 ppm; 1σ, n=29). The Co:Ni ratio of plagioclase-hosted SUL ranges from 0.7-1.4 (avg. 0.9 ± 0.2; 1σ, n=24) and Cu:Ni ratios of 0.2-6.6 (avg. 4.2 ± 1.3; 1σ, n=24) (Figure 2.7A, B).

Table 2.3: Representative SEM-EDS analyses of individual phases present within sulphide melt inclusions

sample/inclusion	CL-07-01-373/37				CL-07-01-373/36	
host mineral	ilmenite				ilmenite	
mineral phase	Po	Ccp	Sp	Co-Pn	Po	Ccp
S (wt%)	39.8	34.6	37.3	33.4	39.8	35.2
Fe	60.2	32.1	0.00	20.9	60.2	32.0
Cu	0.00	33.3	0.00	0.00	0.00	32.8
Co	0.00	0.00	0.00	31.3	0.00	0.00
Ni	0.00	0.00	0.00	14.3	0.00	0.00
Zn	0.00	0.00	62.73	0.00	0.00	0.00
Total	100	100	100	100	100	100
Volume %	93.2	4.4	1.6	0.8	91.8	8.2
sample/inclusion	CL-07-01-373/34		CL-07-01-373/1			CL-07-01-373/25
host mineral	olivine		olivine			olivine
mineral phase	Po	Pn	Po	Ccp	Co-Pn	Po
S (wt%)	36.8	32.1	38.8	36.2	32.6	38.2
Fe	63.2	13.7	61.2	32.0	16.3	61.8
Cu	0	0.00	0.00	31.8	0.00	0.00
Co	0	40.9	0.00	0.00	38.1	0.00
Ni	0	13.3	0.00	0.00	13.1	0.00
Zn	0	0.00	0.00	0.00	0.00	0.00
Total	100	100	100	100	100	100
Volume %	97.1	2.90	91.7	4.80	3.50	100
sample/inclusion	CL-07-01-127/5	CL-07-01-127/7	CL-07-01-127/17	CL-07-01-373/1	CL-07-01-373/6	CL-07-01-373/8
host mineral	apatite	apatite	apatite	plagioclase	plagioclase	plagioclase
mineral phase	Po	Po	Po	Po	Po	Po
S (wt%)	40.2	39.0	39.5	40.5	39.8	54.4
Fe	59.8	61.0	60.5	59.5	60.3	44.5
Cu	0.00	0.00	0.00	0.00	0.00	0.00
Co	0.00	0.00	0.00	0.00	0.00	0.00
Ni	0.00	0.00	0.00	0.00	0.00	1.14
Zn	0.00	0.00	0.00	0.00	0.00	0.00
Total	100	100	100	100	100	100
Volume %	100	100	100	100	100	100

Po = pyrrhotite; Ccp = chalcopyrite; Sp = sphalerite; Co-Pn = cobaltian pentlandite

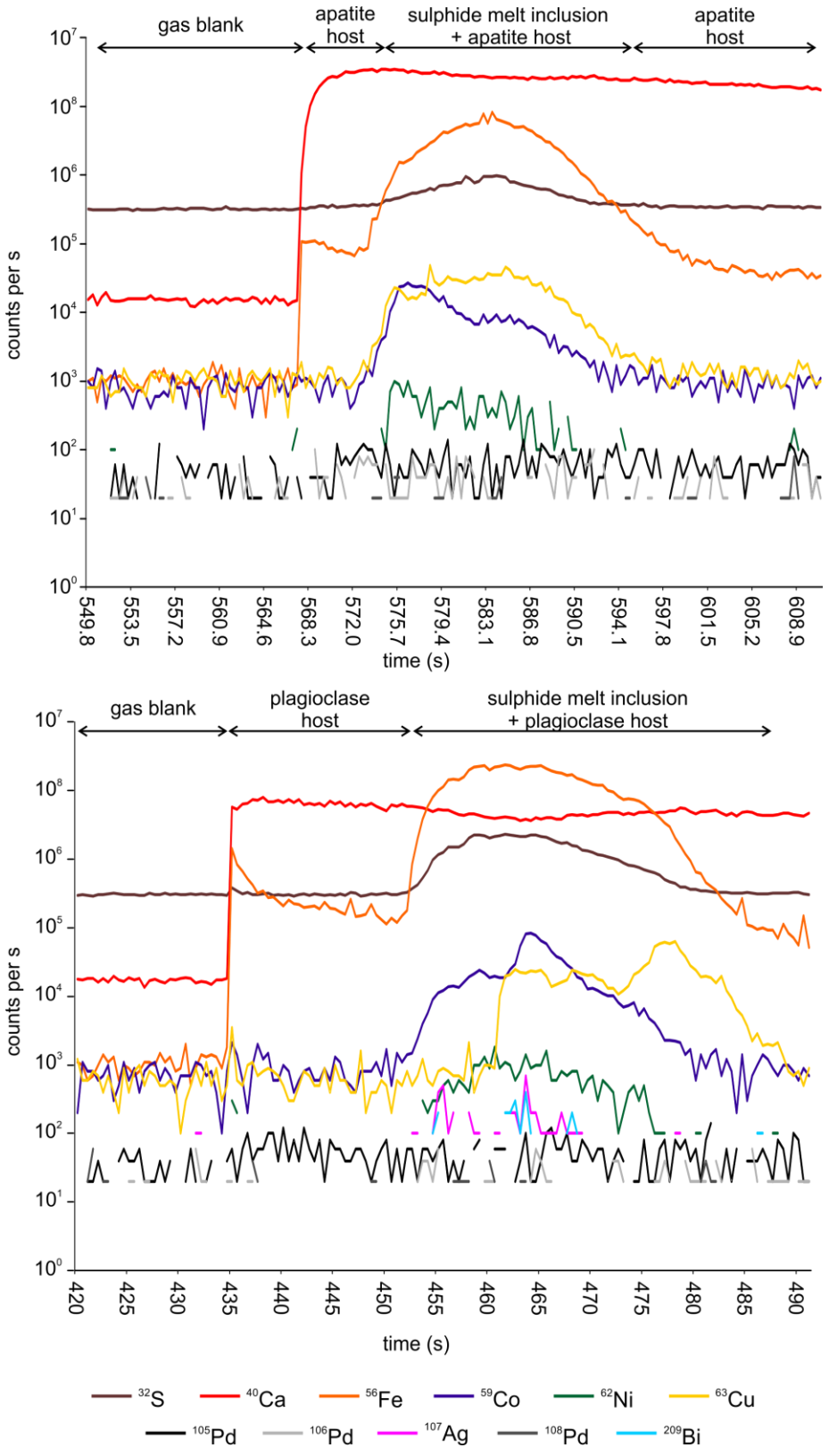
gas blank
apatite host
sulphide melt inclusion + apatite host
apatite host
counts per s
time (s)
gas blank
plagioclase host
sulphide melt inclusion + plagioclase host
counts per s
time (s)
32S
40Ca
56Fe
59Co
62Ni
63Cu
105Pd
106Pd
107Ag
108Pd
209Bi

Figure 2.6 (previous page): Example LA-ICP-MS profile (signal intensity in counts per second vs. time) showing the ablation of sulphide melt inclusions in apatite and plagioclase. A) Apatite hosted sulphide melt inclusion LA-ICP-MS signal. A gas blank is collected for ~20 s, at which point the laser is turned on and a representative apatite host composition is collected. At time ~573 s, the sulphide melt inclusion is encountered (note increased count rates for Fe, Cu, Co, Ni) and a mixed signal of apatite and sulphide is collected. B) Plagioclase hosted sulphide melt inclusion LA-ICP-MS signal. Inclusion is encountered at ~452 s, note increased count rates of Co, Ni, Cu, Ag, and Bi. In both the apatite and plagioclase signals, all Pd isotopes (105, 106, and 108) are consistent throughout the gas blank, inclusion host collection, and when the sulphide inclusion is intersected, indicating Pd is below detection limits. Note the correlation between Co and Ni, as both elements are concentrated into cobaltian pentlandite in the inclusions. Also, the offset between Co+Ni and Cu indicates that cobaltian-pentlandite and chalcopyrite are present within the inclusion and Ni, Co, and Cu are not in solid solution in pyrrhotite; these are recognizable phases in the transient signals.

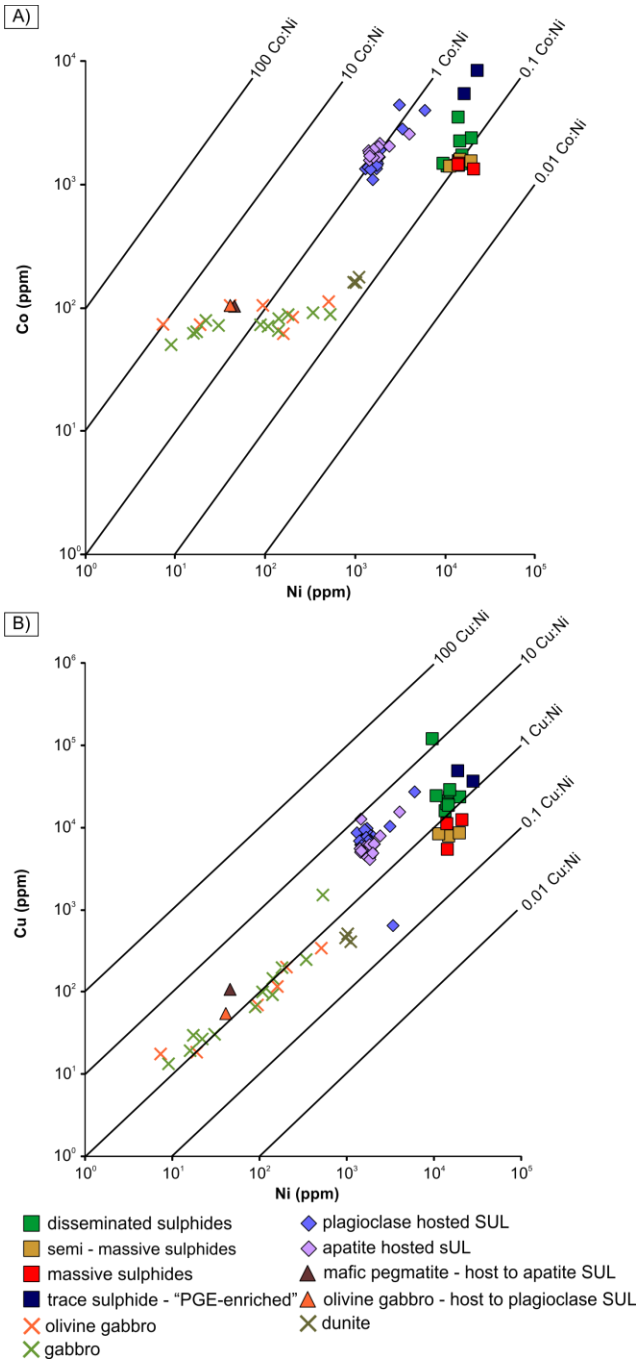

Figure 2.7: Ratios of sulphide melt inclusions plotted against sulphide mineralization that has been recalculated to 100 % sulphide. A) Cobalt plotted against Ni. Note how sulphide melt inclusions plot at approximately Co:Ni ratios of ~1, while sulphide mineralization plots at ratios of ~0.1. B) Copper plotted against Ni. Note how sulphide melt inclusions plots at approximately Cu:Ni ratios of ~5-10, while sulphide mineralization falls around 1.

The Cu:Co ratios of plagioclase-hosted SUL ranges from 0.2 to 6.8 (avg. 4.6 ± 1.4; 1σ, n=29). Trace elements that occur in plagioclase hosted SUL include Ti (320-21,000 ppm; avg. 5,200 ± 3,740 ppm; 1σ, n=25), Zn (100-3,870 ppm; avg. 200 ± 140 ppm; 1σ, n=6), Ag (6.9-69.9 ppm; avg. 15.6 ± 18.5 ppm, 1σ, n=11), Pb (4.0-420 ppm; avg. 121 ± 145 ppm, 1σ, n=16), and Bi (0.9-6.9 ppm; avg. 3.3 ± 2.7 ppm, 1σ, n=6).

Apatite-hosted SUL have Cu concentrations of 4,000-15,500 ppm (avg. 6,500 ± 2,600 ppm; 1σ, n=30), Ni ranging from 1,400-3,400 ppm (avg. 1,900 ± 630 ppm; 1σ, n=16), and Co from 1,100-2,700 (avg. 2,000 ± 430 ppm; 1σ, n=33). The Co:Ni ratio of apatite-hosted SUL ranges from 0.64-1.3 (avg. 1.1 ±0.1; 1σ, n=16) and Cu:Ni ratio is 2.2-8.8 (avg. 3.5 ±1.6; 1σ, n=15; Figure 2.7A, B). The Cu:Co ratios of apatite hosted SUL range from 1.5-8.1 (avg. 3.0 ± 1.3; 1σ, n=30). Other than Cu, Co, and Ni, the only trace elements above detection limits in apatite-hosted SUL are Pb (63.5-161 ppm; avg. 105 ± 55.8 ppm, 1σ, n=7) and Bi (avg. 3.3 ± 0.02 ppm, 1σ, n=2). Palladium, Pt, and Au were always below detection limits in all SUL analyzed in apatite, plagioclase, and in olivine. The minimum detection limits in apatite and plagioclase hosted SUL for Pd, Pt, and Au were very high (330 ppb, 2,000 ppb, and 833 ppb, respectively) owing to the relatively small inclusion size. Although olivine hosted SUL may have been partially removed during polishing, their much larger inclusion size (and therefore mass) allows for lower detection limits for PGE and Au. Minimum detections limits for olivine-hosted SUL for Pd, Pt, and Au were 9 ppb, 50 ppb, and 42 ppb, respectively. Complete LA-ICP-MS results for SUL are presented in Table 2.4.

Table 2.4: LA-ICP-MS analyses of plagioclase and apatite hosted sulphide melt inclusions

Sample/Inclusion	^{59}Co (ppm)	^{62}Ni	^{65}Cu	^{49}Ti	^{66}Zn	^{105}Pd	^{106}Pd	^{107}Ag	^{108}Pd	^{195}Pt	^{197}Au	^{208}Pb	^{209}Bi
Plag_373_12_1	1538	1678	8195	317	b.d.l	b.d.l	b.d.l	b.d.l	b.d.l	b.d.l	b.d.l	5.4	b.d.l
Plag_373_12_2	1628	1678	4463	3098	b.d.l	b.d.l	b.d.l	b.d.l	b.d.l	b.d.l	b.d.l	b.d.l	b.d.l
Plag_373_12_3	2825	3359	641	4899	3873	b.d.l	b.d.l	b.d.l	b.d.l	b.d.l	b.d.l	214	6.9
Plag_373_12_4	1673	1856	8289	4581	448	b.d.l	b.d.l	17.9	b.d.l	b.d.l	b.d.l	422	b.d.l
Plag_373_12_5	1344	1725	6638	5518	b.d.l	b.d.l	b.d.l	b.d.l	b.d.l	b.d.l	b.d.l	b.d.l	b.d.l
Plag_373_12_6	1541	1729	7535	8627	b.d.l	b.d.l	b.d.l	b.d.l	b.d.l	b.d.l	b.d.l	6.9	b.d.l
Plag_373_12_7	1471	1481	5036	1964	b.d.l	b.d.l	b.d.l	6.9	b.d.l	b.d.l	b.d.l	b.d.l	1.1
Plag_373_12_11	1341	1299	8621	4186	119	b.d.l	b.d.l	7.8	b.d.l	b.d.l	b.d.l	12.5	0.9
Plag_373_12_12	2743	b.d.l	13872	1315	b.d.l	b.d.l	b.d.l	b.d.l	b.d.l	b.d.l	b.d.l	b.d.l	b.d.l
Plag_373_12_13	1413	1430	6173	b.d.l	b.d.l	b.d.l	b.d.l	b.d.l	b.d.l	b.d.l	b.d.l	b.d.l	b.d.l
Plag_373_12_14	1414	1470	7127	2246	b.d.l	b.d.l	b.d.l	9.5	b.d.l	b.d.l	b.d.l	10.7	b.d.l
Plag_373_12_15	1968	1692	9781	4254	150	b.d.l	b.d.l	7.0	b.d.l	b.d.l	b.d.l	6.2	b.d.l
Plag_373_12_16	1660	1673	8933	2901	101	b.d.l	b.d.l	7.1	b.d.l	b.d.l	b.d.l	4.4	1.1
Plag_373_12_17	1481	1774	4247	3953	b.d.l	b.d.l	b.d.l	b.d.l	b.d.l	b.d.l	b.d.l	29.2	b.d.l
Plag_373_12_18	1456	1589	9398	4183	b.d.l	b.d.l	b.d.l	b.d.l	b.d.l	b.d.l	b.d.l	b.d.l	b.d.l
Plag_373_12_19	1417	1515	6814	3304	b.d.l	b.d.l	b.d.l	b.d.l	b.d.l	b.d.l	b.d.l	7.1	b.d.l
Plag_373_12_20	1404	1504	7028	2138	b.d.l	b.d.l	b.d.l	11.1	b.d.l	b.d.l	b.d.l	11.8	b.d.l
Plag_373_12_21	1096	1569	6695	2909	b.d.l	b.d.l	b.d.l	b.d.l	b.d.l	b.d.l	b.d.l	b.d.l	b.d.l
Plag_373_12_22	1433	1656	7586	2381	b.d.l	b.d.l	b.d.l	8.1	b.d.l	b.d.l	b.d.l	4.0	b.d.l
Plag_373_12_23	1429	1744	6903	3275	181	b.d.l	b.d.l	7.4	b.d.l	b.d.l	b.d.l	38804	6.1
Plag_373_12_24	3998	5937	27165	9303	b.d.l	b.d.l	b.d.l	69.9	b.d.l	b.d.l	b.d.l	525	b.d.l
Plag_373_12_25	4431	3096	10335	b.d.l	256	b.d.l	b.d.l	19.2	b.d.l	b.d.l	b.d.l	424	3.6
Plag_373_9_2	949	b.d.l	5127	20789	b.d.l	b.d.l	b.d.l	b.d.l	b.d.l	b.d.l	b.d.l	b.d.l	b.d.l
Plag_373_9_3	1079	b.d.l	5975	12696	b.d.l	b.d.l	b.d.l	b.d.l	b.d.l	b.d.l	b.d.l	b.d.l	b.d.l
Plag_373_9_4	1379	1387	6862	9223	b.d.l	b.d.l	b.d.l	b.d.l	b.d.l	b.d.l	b.d.l	b.d.l	b.d.l
Plag_373_9_5	1412	b.d.l	5801	11795	b.d.l	b.d.l	b.d.l	b.d.l	b.d.l	b.d.l	b.d.l	b.d.l	b.d.l
Plag_373_9_6	1326	1478	6056	6589	b.d.l	b.d.l	b.d.l	b.d.l	b.d.l	b.d.l	b.d.l	b.d.l	b.d.l
Plag_373_9_7	2839	b.d.l	9599	b.d.l	b.d.l	b.d.l	b.d.l	b.d.l	b.d.l	b.d.l	b.d.l	233	b.d.l
Plag_373_9_8	1906	1896	5158	14532	b.d.l	b.d.l	b.d.l	b.d.l	b.d.l	b.d.l	b.d.l	19.2	b.d.l
Ap_127-4-1	2436	2048	6291	178	b.d.l	b.d.l	n.m	b.d.l	b.d.l	b.d.l	b.d.l	143	3.3
Ap_127-4-2	2601	b.d.l	4117	b.d.l	b.d.l	b.d.l	n.m	b.d.l	b.d.l	b.d.l	b.d.l	161	b.d.l
Ap_127-4-3	1067	b.d.l	b.d.l	1910	b.d.l	b.d.l	n.m	b.d.l	b.d.l	b.d.l	b.d.l	63.5	b.d.l
Ap_127-4-4	2441	2037	6310	178	b.d.l	b.d.l	n.m	b.d.l	b.d.l	b.d.l	b.d.l	143	3.3
Ap_127-4-5	2599	b.d.l	4023	b.d.l	b.d.l	b.d.l	n.m	b.d.l	b.d.l	b.d.l	b.d.l	143	b.d.l
Ap_127-4-6	1130	b.d.l	b.d.l	2047	b.d.l	b.d.l	n.m	b.d.l	b.d.l	b.d.l	b.d.l	64.3	b.d.l
Ap_127-4-7	2703	b.d.l	10036	b.d.l	b.d.l	b.d.l	n.m	b.d.l	b.d.l	b.d.l	b.d.l	b.d.l	b.d.l
Ap_127-4-8	2131	b.d.l	5272	b.d.l	b.d.l	b.d.l	n.m	b.d.l	b.d.l	b.d.l	b.d.l	b.d.l	b.d.l
Ap_127-4-9	2259	1823	4087	b.d.l	b.d.l	b.d.l	n.m	b.d.l	b.d.l	b.d.l	b.d.l	b.d.l	b.d.l
Ap_127-4-10	1890	b.d.l	4273	b.d.l	b.d.l	b.d.l	n.m	b.d.l	b.d.l	b.d.l	b.d.l	b.d.l	b.d.l
Ap_127-4-11	2164	b.d.l	4519	b.d.l	b.d.l	b.d.l	n.m	b.d.l	b.d.l	b.d.l	b.d.l	b.d.l	b.d.l
Ap_127-4-14	2319	1968	4886	184	b.d.l	b.d.l	n.m	b.d.l	b.d.l	b.d.l	b.d.l	16.0	b.d.l
Ap_127-4-1	2158	1875	4621	n.m	n.m	b.d.l	b.d.l	n.m	b.d.l	b.d.l	b.d.l	n.m	n.m
Ap_127-4-3	1688	1822	4383	n.m	n.m	b.d.l	b.d.l	n.m	b.d.l	b.d.l	b.d.l	n.m	n.m
Ap_127-4-4	2568	3994	15483	n.m	n.m	b.d.l	b.d.l	n.m	b.d.l	b.d.l	b.d.l	n.m	n.m
Ap_127-4-5	2907	b.d.l	8738	n.m	n.m	b.d.l	b.d.l	n.m	b.d.l	b.d.l	b.d.l	n.m	n.m
Ap_127-3-1	2048	2393	7913	n.m	n.m	b.d.l	b.d.l	n.m	b.d.l	b.d.l	b.d.l	n.m	n.m
Ap_127-3-3	1794	1589	b.d.l	n.m	n.m	b.d.l	b.d.l	n.m	b.d.l	b.d.l	b.d.l	n.m	n.m
Ap_127-3-4	1573	1438	12692	n.m	n.m	b.d.l	b.d.l	n.m	b.d.l	b.d.l	b.d.l	n.m	n.m
Ap_127-3-5	1860	b.d.l	5249	n.m	n.m	b.d.l	b.d.l	n.m	b.d.l	b.d.l	b.d.l	n.m	n.m
Ap_127-3-6	1660	1594	5824	n.m	n.m	b.d.l	b.d.l	n.m	b.d.l	b.d.l	b.d.l	n.m	n.m
Ap_127-3-7	2031	1809	6193	n.m	n.m	b.d.l	b.d.l	n.m	b.d.l	b.d.l	b.d.l	n.m	n.m
Ap_127-3-8	1786	b.d.l	5053	n.m	n.m	b.d.l	b.d.l	n.m	b.d.l	b.d.l	b.d.l	n.m	n.m
Ap_127-3-10	1548	b.d.l	4353	n.m	n.m	b.d.l	b.d.l	n.m	b.d.l	b.d.l	b.d.l	n.m	n.m
Ap_127-3-14	1883	1409	5536	n.m	n.m	b.d.l	b.d.l	n.m	b.d.l	b.d.l	b.d.l	n.m	n.m
Ap_127-3-15	1932	1606	4628	n.m	n.m	b.d.l	b.d.l	n.m	b.d.l	b.d.l	b.d.l	n.m	n.m
Ap_127-3-16	1794	b.d.l	5385	n.m	n.m	b.d.l	b.d.l	n.m	b.d.l	b.d.l	b.d.l	n.m	n.m
Ap_127-3-17	1974	b.d.l	5964	n.m	n.m	b.d.l	b.d.l	n.m	b.d.l	b.d.l	b.d.l	n.m	n.m
Ap_127-3-18	1800	1429	5005	n.m	n.m	b.d.l	b.d.l	n.m	b.d.l	b.d.l	b.d.l	n.m	n.m
Ap_127-3-24	1701	1450	5214	n.m	n.m	b.d.l	b.d.l	n.m	b.d.l	b.d.l	b.d.l	n.m	n.m
Ap_127-3-25	1561	b.d.l	4326	n.m	n.m	b.d.l	b.d.l	n.m	b.d.l	b.d.l	b.d.l	n.m	n.m
Ap_127-3-26	1839	b.d.l	5750	n.m	n.m	b.d.l	b.d.l	n.m	b.d.l	b.d.l	b.d.l	n.m	n.m
Ap_127-3-27	2374	b.d.l	7555	n.m	n.m	b.d.l	b.d.l	n.m	b.d.l	b.d.l	b.d.l	n.m	n.m

n.m = not measured; b.d.l = below detection limits; ^{XX} represent measured isotopes and data is not only for the indicated isotope but for the element

2.3.7 Sulfur isotopes

The sulfur isotope composition ($\delta^{34}S$) of the volumetrically dominant pyrrhotite phase of SUL hosted in olivine and ilmenite (determined *in situ* by SIMS) was -0.6 to +1.0‰ (avg. +0.3 ± 0.5 ‰; 1σ, n=8) and -0.3 to +1.4 ‰ (avg. +0.2 ± 0.6 ‰; 1σ, n=7), respectively; both of which are typical of a mantle source ($\delta^{34}S$ = 0 ± 2 ‰, Ohmoto & Rye, 1979). Bulk sulfur isotope analyses for $\delta^{34}S$ in disseminated and massive pyrrhotite from mineralized intervals have consistent values ($\delta^{34}S$ ranging from +1.0 to +1.4 ‰; avg. +1.2 ± 0.1 ‰; 1σ, n=14) and chalcopyrite from mineralization has a value of $\delta^{34}S$ of +1.0 ± 0.2 ‰ (n=1). Interstitial pyrrhotite not associated with mineralization has bulk $\delta^{34}S$ values ranging from -0.4 to +0.9 ‰ (avg. +0.3 ± 0.5 ‰; 1σ, n=7) and *in situ* $\delta^{34}S$ range from +0.5 to +1.4 ‰ (avg. +0.8 ± 0.3 ‰; 1σ, n=14). Secondary pyrite that is exposed along fracture planes in drill core have bulk $\delta^{34}S$ values of +0.7 ± 0.1 ‰ (n=2) and a secondary pyrrhotite stringer analyzed *in situ* has values between -1.3 and +2.5 ‰ (avg. +0.6 ± 1.0 ‰; 1σ, n=7). The Archean sedimentary Burwash Formation contains minor amounts of pyrrhotite and *in situ* analyses of these sulphides have $\delta^{34}S$ values ranging from -0.3 to +0.8 ‰ (avg. +0.2 ± 0.4 ‰; 1σ, n=10). No distinct differences in $\delta^{34}S$ values are present between the different sulphide minerals, *in situ* and bulk analyses of mineralization, and between SUL, sulphide mineralization, and barren units. A summary for sulfur isotope results are presented in Table 2.5.

2.3.8 Olivine petrography and chemistry

Olivine occurs in a variety of different rock types within the studied drill holes. Olivine is present as an early cumulate phase (e.g., in dunite, magnetitite) or as a relatively late cumulus phase in some lithologies (e.g., in gabbro). Early cumulate olivine

Table 2.5: Summarized sulphur isotope results of by conventional (bulk) and *in situ* methods

lithology	mineral	sulphide texture/occurrence	generation	$\delta^{34}S$ (‰ VCDT)	method
olivine gabbro	Po	ilmenite hosted SUL	primary	0.2 ± 0.6 (n=7)	I
olivine gabbro	Po	olivine hosted SUL	primary	0.3 ± 0.5 (n=8)	I
olivine gabbro	Po	interstitial	primary	0.8 ± 0.3 (n=14)	I
gabbro	Po	stringer	secondary	0.8 ± 1.1 (n=8)	I
Burwash sediments	Po	matrix	-	0.2 ± 0.4 (n=10)	I
massive sulphide	Po	massive	primary	1.2 ± 0.1 (n=4)	C
massive sulphide	Ccp	massive	primary	1.0 (n=1)	C
semi-massive sulphide	Po	semi-massive	primary	1.2 ± 0.1 (n=2)	C
gabbro	Po	disseminated	primary	1.2 ± 0.1 (n=8)	C
gabbro	Py	fracture	secondary	0.7 ± 0.1 (n=2)	C
rocks not associated with mineralization	Po	interstitial	primary	0.3 ± 0.5 (n=7)	C

Py=pyrite; Po=pyrrhotite; Ccp=chalcopyrite; SUL = sulphide melt inclusion; C = Conventional Analysis; I = *In Situ* by SIMS

ranges in size from 0.25-3 mm (avg. 1 mm) with euhedral grain form, and have an average forsterite content (Fo#) of 59.5 in clinopyroxenite 71.7 in dunite (Figure 2.8A). Late cumulus olivine is 0.2-2.5 mm in size (ave. 0.75 mm) and has sub-anhedral habit containing occasional inclusions of plagioclase. Late cumulus olivine has an average Fo# of 47.9 in olivine gabbros and 59.3 in gabbros. Serpentinization intensity is highly variable within each textural style of olivine present, ranging from rare to pervasive replacement. Early cumulate olivine is also present within very coarse-grained olivine gabbro. Grains are 6-15 mm in size and sub-euhedral showing rare serpentinization. The olivine gabbro hosts SUL and olivine grains have an average Fo# of 55. No variation in Fo content occurs with proximity to SUL (Figure 2.8B). Representative EMP analyses of olivine are presented in Table 2.6.

Nickel content in olivine is low within all grains analyzed, with late cumulate olivine containing 60 ppm in olivine gabbro to 675 ppm in magnetite-ilmenite-rich clinopyroxenite (Figure 2.8A). Early cumulus olivine has a range in Ni content from 40 ppm in olivine clinopyroxenite to 1140 ppm in dunite. The olivine gabbro hosting SUL has no detectable concentrations of Ni in its olivine (by SEM-EDS).

2.4 Discussion

2.4.1 Fractionation of a sulphide liquid and formation of sulphide mineralization

Once sulphide saturation occurs in a melt, an immiscible sulphide liquid will form. The first phase to crystallize from this sulphide liquid at temperatures around 1000°C is the Fe-rich MSS, which leaves the remaining sulphide liquid enriched in Ni, Cu, Zn, precious (Pt, Pd, Au, Ag) and semi-metals (As, Te, Se, Bi, Sb, Pb) as their

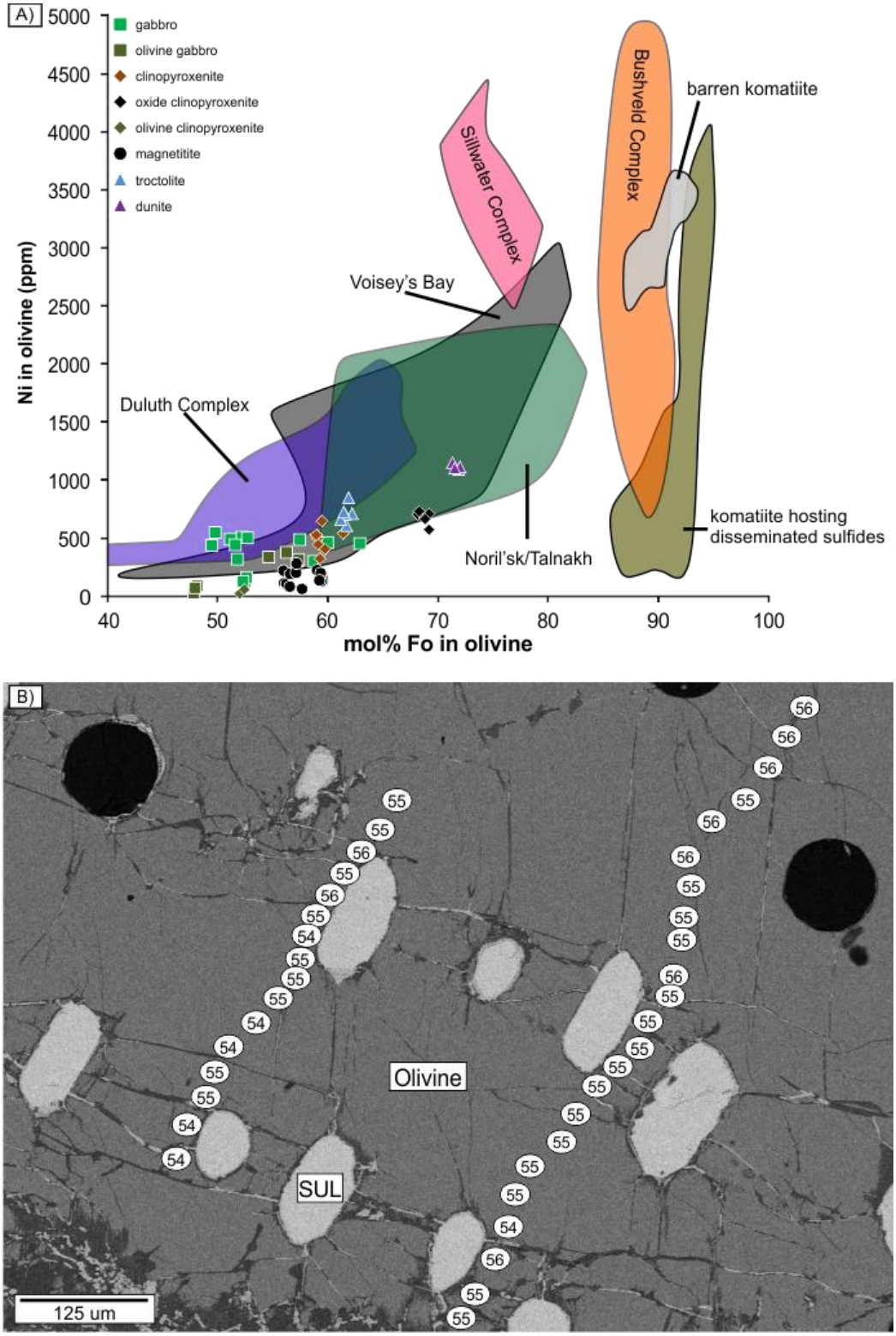
A)
gabbro
olivine gabbro
clinopyroxenite
oxide clinopyroxenite
olivine clinopyroxenite
magnetitite
troctolite
dunite
Ni in olivine (ppm)
mol% Fo in olivine
Duluth Complex
Voisey's Bay
Stillwater Complex
Bushveld Complex
barren komatiite
komatiite hosting disseminated sulfides
Noril'sk/Talnakh
B)
Olivine
SUL
125 um

Figure 2.8 (previous page): Nickel and calculated Fo content of olivines in the Caribou Lake Gabbro. A) Plot of Ni content in olivine against forsterite content of olivine for the CLG and various Ni-Cu-PGE deposits. Data for barren komatiite and komatiites hosting disseminated sulphides came from Barnes and Fiorentini (2012) and references therein. Olivine data for the Bushveld Complex is for olivine-rich cumulates occurring beneath the Platreef from the northern limb of the complex at Turfspruit and Sandsloot (Yudovskaya et al., 2013). Data for the Stillwater Complex is from Barnes and Naldrett (1985) for olivine cumulate rocks within the J-M reef. Voisey's Bay olivine data is from Li and Naldrett (1999) and Li et al. (2007) for all major rock types in the intrusion. Data for Noril'sk and Talnakh intrusions is for various gabbroic rocks from Li et al. (2003). Duluth Complex olivine data is from Ripley et al. (2007) from the basal zone of the Partridge River intrusion. B) SEM-BSE image of olivine hosted sulphide melt inclusions (SUL). Numbers on the image represent Fo content of olivine. Note, how Fo content does not change regardless of analysis location relative to location of SUL.

Table 2.6: Representative olivine EMP analysis from various units within the Caribou Lake Gabbro

drillhole	CL-06-16			CL-06-39				CL-07-01				
depth (m)	8.9	33.7	35.7	20.35	60.23	103	128	140	249	308	329	354
rock type	gabbro	olivine gabbro	clinopyroxenite	troctolite	dunite	oxide clinopyroxenite	gabbro	olivine clinopyroxenite	olivine gabbro	magnetitite	magnetitite	gabbro
analysis #	1	3	2	2	1	1	6	4	8	1	1	2
SiO_2	36.2	35.5	36.4	36.8	37.4	37.1	35.3	35.5	34.5	36.2	35.5	35.5
Al_2O_3	0.00	b.d.l	0.02	0.00	0.01	0.01	0.00	0.01	0.02	b.d.l	0.01	b.d.l
FeO	35.1	37.0	35.0	32.7	25.1	27.4	41.2	38.4	42.1	34.4	37.1	39.1
MgO	28.5	27.1	29.1	30.7	35.6	33.4	23.3	25.3	22.1	28.4	27.0	24.7
MnO	0.49	0.53	0.54	0.46	0.37	0.43	0.66	0.66	0.61	0.56	0.55	0.66
CaO	0.05	0.06	0.04	0.07	0.09	0.10	0.05	0.08	0.05	0.12	0.08	0.06
NiO	0.04	0.05	0.07	0.09	0.15	0.09	0.07	0.01	0.01	0.03	0.01	0.04
TiO_2	b.d.l	0.01	0.02	0.05	0.01	0.02	b.d.l	b.d.l	b.d.l	0.02	0.02	b.d.l
Cr_2O_3	b.d.l	b.d.l	b.d.l	b.d.l	0.00	b.d.l	b.d.l	b.d.l	b.d.l	0.00	0.00	b.d.l
V_2O_3	b.d.l	0.01	b.d.l	b.d.l	b.d.l	0.00	b.d.l	0.01	b.d.l	b.d.l	b.d.l	0.01
Na_2O	n.m.	b.d.l	n.m.	n.m.	b.d.l	b.d.l	0.00	b.d.l	0.04	0.06	b.d.l	b.d.l
K_2O	n.m.	b.d.l	n.m.	n.m.	0.00	b.d.l	0.00	0.00	b.d.l	0.00	b.d.l	b.d.l
Total	100.4	100.3	101.2	100.8	98.7	98.6	100.6	99.9	99.5	99.7	100.2	100.1
Fo#	58.8	56.2	59.3	62.2	71.3	68.1	49.8	53.5	48.0	59.0	56.0	52.5
Ni (ppm)	300	377	526	710	1151	703	548	58.0	47.9	225	111	319
Cation Numbers Based on 4 Oxygens												
Si	1.00	0.99	1.00	1.00	1.00	1.01	1.01	1.01	0.00	1.01	0.99	1.01
Ti	0.00	0.00	0.00	0.00	0.00	0.00	0.00	0.00	0.00	0.00	0.00	0.00
Al	0.00	0.00	0.00	0.00	0.00	0.00	0.00	0.00	0.00	0.00	0.00	0.00
Cr	0.00	0.00	0.00	0.00	0.00	0.00	0.00	0.00	1.02	0.00	0.00	0.00
Fe	0.81	0.86	0.80	0.74	0.56	0.62	0.98	0.91	0.02	0.80	0.87	0.93
Mn	0.01	0.01	0.01	0.01	0.01	0.01	0.02	0.02	0.96	0.01	0.01	0.02
Mg	1.18	1.13	1.19	1.24	1.42	1.35	0.99	1.07	0.00	1.18	1.12	1.05
Ca	0.00	0.00	0.00	0.00	0.00	0.00	0.00	0.00	0.00	0.00	0.00	0.00
Total	3.00	3.00	3.00	3.00	3.00	3.00	3.00	3.00	3.00	3.00	3.00	3.00

b.d.l = below detection limits; n.m. = not measured; Fo# = forsterite content

partition coefficients (K_D) between MSS and residual sulphide liquid are generally < 1, except for IPGE (Ir, Os, and Ru), Rh and Re, which partition into MSS (Kullerud et al., 1969; Fleet et al., 1993; Barnes et al., 1997a; Ballhaus et al., 2001; Brenan, 2002; Mungall et al., 2005; Helmy et al., 2007; Helmy et al., 2010; Holwell and McDonald, 2010; Liu and Brenan, 2015). Initially, Ni is slightly incompatible with MSS at high temperatures and high metal/S ratios with K_D ~0.6 but becomes more compatible with MSS at lower temperatures and lower metal/S ratios with K_D slightly > 2 (Barnes et al., 1997a; Ballhaus et al., 2001). As the temperature falls to ≤ 900°C, the Cu-rich residual liquid crystallizes to form ISS, which will be rich in Pt, Pd, and Au (Fleet et al., 1993; Barnes et al., 1997a; Ballhaus et al., 2001; Barnes and Lightfoot, 2005; Mungall et al., 2005; Holwell and McDonald, 2010). As the temperature of the system falls to < 650°C, MSS and ISS become unstable and start to exsolve sulphide mineral phases. Pyrrhotite and pentlandite are the two dominant minerals to be exsolved from MSS and chalcopyrite is the primary mineral exsolved from ISS. While the exsolution of base metal sulphides occurs from MSS and ISS, PGE and precious and semimetals that were present as solid solution within MSS and ISS may exsolve to form discrete PGM along the grain margins and boundaries of sulphide grains (Holwell and McDonald, 2010). This fractionation of sulphide minerals can result in the zonation of Ni-Cu-PGE deposits with Ni-rich pyrrhotite-pentlandite assemblages forming one ore zone and a second ore zone dominated by chalcopyrite (e.g., Sudbury and Noril'sk; Li et al., 1992; Distler 1994; Naldrett et al., 1994; Zientek et al., 1994; Naldrett et al., 1997; Naldrett et al., 1999; Barnes et al., 2006).

Experiments by Helmy et al. (2007) indicate that if a sulphide melt contains a modest enrichment in Te relative to Pd and Pt, then MSS and ISS will essentially be PGE free, and Pd and Pt will be partitioned into a telluride melt. They also observed that as temperatures decreased and MSS crystallization continued, the sulphide melt shifted to higher Te/S ratios until a separate telluride melt exsolved, however their experiments contained higher (Pt+Pd)/semimetal ratios than observed in natural systems. Helmy et al. (2013) also performed experiments with As-rich melts and determined that if a sulphide melt reaches As saturation, a Ni-PGE-rich melt will form. With the tendency of Pt and Pd to form stable PGM with Te, As, Sb, and Bi, a low (Pt+Pd)/(Te+Sb+Bi) ratio should prevent Pt and Pd portioning into sulphide phases and would keep Pt and Pd in the sulphide melt until a Bi-Sb-Te and/or As-rich melt can exsolve (Helmy et al., 2007, 2013). Liu and Brenan (2015) experimentally determined K_D for PGE, Se, Te, As, Sb and Bi between MSS-ISS, MSS-sulphide liquid, and ISS-sulphide liquid and determined Se is near unity for partitioning between ISS-sulphide liquid, while Te, As, Sb, and Bi are weakly to moderately incompatible in ISS, suggesting they would be concentrated into the sulphide liquid as Helmy et al. (2007) experiments implicated for Te. All observed telluride minerals in massive sulphide mineralization from the CLG occur as inclusions within glaucodot-gersdorffite. It is consistent that Te, As, and Bi to be concentrated together with experiments of Liu and Brenan (2015).

An important comment from Helmy et al. (2007) in regards to the CLG mineralization is if Ni-tellurides occur in abundance, the (Pt+Pd)/semimetal ratio and absolute Pt and Pd contents in the sulphide melt were most likely low when tellurides crystallized. This would suggest the possibility for extensive Pt-Pd mineralization is low.

As Ni-tellurides are present in the CLG and no Pt- or Pd-telluride phases observed, combined with low Pt and Pd in solid solution in base metal sulphides, one can conclude that Pt and Pd concentrations were low in the sulphide melt. In addition, Ni-tellurides are sparse, suggesting that the Te content of the sulphide liquid was likely low as well.

The results of Helmy et al. (2007, 2013) experiments may have implications for the formation of arsenides, sulfarsenides, and tellurides within the CLG. The concentration of As in a sulphide melt needs to be between 0.5 and 2.0 wt %, for As saturation and the subsequent formation of an As-rich liquid (Helmy et al., 2013). If an As-rich melt separated early from a sulphide liquid, then euhedral grains of sulfarsenides and/or arsenides should be present as inclusions within base metal sulphides, because the As-rich liquid would have crystallized at high temperatures prior to crystallization of MSS (e.g., Creighton, Dare et al., 2010; Spotted Quoll, Prichard et al., 2013). Mineralization in the CLG does not contain any euhedral sulfarsenide or arsenide grains, suggesting that sulfarsenides and arsenides did not crystallize from an early As-rich liquid. The occurrence of sulfarsenides and arsenides in the CLG as inclusions and along edges of base metal sulphides, combined with their small grain size and sparse population, it is most likely that sulfarsenides and arsenides formed by exsolution from base metal sulphides during cooling rather than crystallization from an early As-rich liquid.

The occurrence of galena in the CLG predominantly as inclusions in base metal sulphides, suggests galena formed as an exsolution product during cooling of sulphides. However with little known about the formation of galena in magmatic sulphides and more experimental work needs to be completed (Dare et al., 2014). Molybdenite most likely

was introduced as a hydrothermal phase as it is associated with fractures containing quartz. The electrum formation mechanism is unclear but it occurs as inclusions within glaucodot-gersdorffite, suggesting it may have exsolved from base metal sulphides during cooling along with the sulfarsenides.

Zonation of sulphide mineralization resulting from fractional crystallization of a sulphide liquid is not present in the CLG in contrast to large Ni-Cu-PGE deposits (i.e., Sudbury and Noril'sk; Li et al., 1992; Distler 1994; Naldrett et al., 1994; Zientek et al., 1994; Naldrett et al., 1997; Naldrett et al., 1999; Barnes et al., 2006). Extremely low concentrations of PGE are observed in sulphide minerals in the CLG, making it difficult to determine the relative partitioning of PGE between MSS products (pyrrhotite and pentlandite) and ISS products (chalcopyrite). As described above, IPGE, Rh, and Re are compatible in MSS over a sulphide liquid, therefore should concentrate into pyrrhotite and pentlandite. While Pyrrhotite and pentlandite in the CLG show a minor preference of Ir and Rh over chalcopyrite, but Re is distributed evenly between pyrrhotite and chalcopyrite and Ru is concentrated in chalcopyrite.Osmium is below detection limits in all sulphide minerals. Li et al. (1996) and Barnes et al. (1997a) experimentally have shown that as the sulfur content of the sulphide liquid or of MSS decreases, the K_D for IPGE and Rh become closer to and can be less than 1. Ballhaus et al. (2001) experiments show that as the metal/S ratio of the MSS (metal/$S_{(MSS}$)) increases Rh and Ir have similar K_D over the range of 0.85-1, whereas Li et al. (1996) data show a decrease in K_D as the metal/$S_{(MSS}$) ratio increases. Li et al. (1996) used wt % concentrations of Ir and Rh which Ballhaus et al. (2001) suggest this resulted in a miscalculation of the partitioning of PGE. Ruthenium's partition coefficient has a positive correlation with the metal/$S_{(MSS)}$ ratio

(Ballhaus et al., 2001), which Li et al. (1996) and Barnes et al. (1997a) did not conduct experiments on. The preference of Ru to be concentrated into chalcopyrite over pyrrhotite and pentlandite in the CLG could therefore be related to a low metal/$S_{(MSS)}$ ratio of the sulphide liquid.

If semimetals (As, Se, Te, Sb, Bi) were not in high enough concentrations to form a separate semimetal-rich liquid, then they should be present in solid solution within base metal sulphides, as discrete grains occurring as inclusions, or along the edges of base metal sulphides formed as exsolution products during cooling (Helmy et al., 2007, 2010, 2013; Holwell and McDonald, 2010; Liu and Brenan, 2015). As Helmy et al. (2007) and Liu and Brenan (2015) show that Pd and Pt tend to be concentrated into a semimetal-rich liquid over ISS, given that semimetals are in enough concentration to form a separate liquid. With no PGM observed in the CLG mineralization, it would suggest the concentration of semimetals (As, Sb, Bi, Te, Se) were relatively low in the sulphide liquid (see SUL compositions; Table 2.4) and that Pt and Pd would stay in solution with ISS and be present in their crystallized products (chalcopyrite) (Helmy et al., 2007). The concentrations of Pd and Pt in pyrrhotite, pentlandite, and chalcopyrite are extremely low (Pt < 250 ppb; Pd < 900 ppb), combined with no PGM observed in mineralization and the low concentrations of PGE and semimetals in SUL. This would suggest that the sulphide liquid responsible for forming mineralization in the CLG was low in PGE and semimetals.

2.4.2 Formation of sulphide melt inclusions

The polyphase mineralogy (pyrrhotite, pentlandite, chalcopyrite, sphalerite, magnetite, sulfarsenide) of the SUL within the CLG is consistent with the mineral

assemblage expected to be produced through fractional crystallization of a sulphide melt as described above. Chalcopyrite, sphalerite, and sulfarsenides should be located near the paleo-top or along the margins of the inclusions as is expected from fractionation and crystallization of a sulphide liquid (Prichard et al., 2004) as is observed in SUL of the CLG (Figure 2.5M, N). The presence of magnetite on the margins could be attributed to by the crystallization of pyrrhotite because as pyrrhotite begins to form, Fe_2O_3 will diffuse outward from the immiscible sulphide due to an increase of fO_2 (Naldrett, 1969; Prichard et al., 2004). The Fe_2O_3 will then react with FeO and TiO_2 of the silicate liquid and form titaniferous magnetite at the sulphide-silicate boundary (Naldrett, 1969; Prichard et al., 2004). Where silicate melt was observed coentrapped with sulphide melt (Figure 2.5E-J), it provided evidence of the migration of interstitial melts in non-cotectic proportions indicating that the migrating sulphide liquid were not primary droplets but samples of accumulating liquid that was migrating.

As previously mentioned, the composition of a trapped sulphide liquid should be representative of the mineralization barring any processes altering the composition (i.e., fractionation, hydrothermal alteration) (Holwell et al., 2011). Sulphide melt inclusion compositions normalized to Ni+Co-Cu-Fe are displayed in Figure 2.9, and are compositionally similar to those experimentally determined MSS by Kullerud et al. (1969). As shown in Figure 2.7B, the Cu:Ni ratios of SUL are between ~2 and 6, with few outliers (9 and 0.2), and the Cu:Ni ratios of mineralization range from ~0.5 to 1.5, with one outlier of 12. The Cu concentrations are fairly consistent between SUL (0.06-2.7 wt %) and mineralization (0.54-2.9 wt %, outlier of 12.1 wt %), but the Ni contents are enriched in the mineralization (0.94-2.1 wt %) compared to SUL (0.13-0.59 wt %; Figure

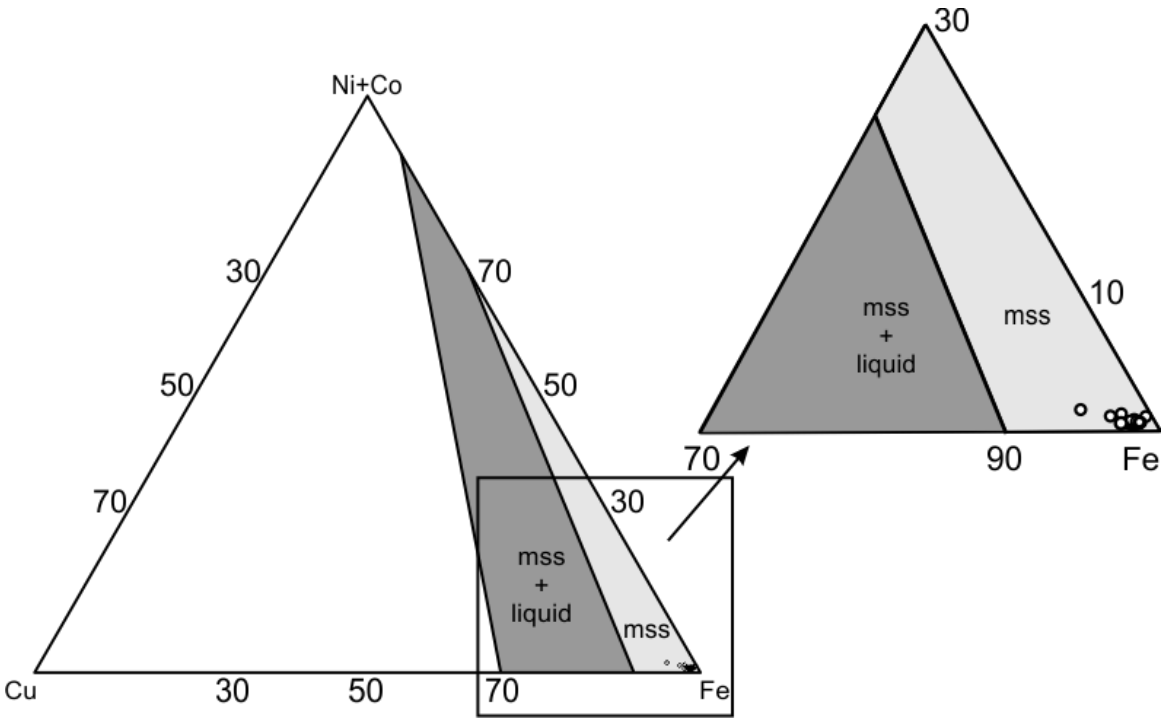

Figure 2.9: Bulk sulphide melt inclusion compositions plotted in the Fe-(Ni+Co)-Cu field. Monosulphide solid solution (mss) and mss + liquid stability fields are based on the experiments of Kullerud et al. (1969) performed at 1100°C.

7B). Keeping in mind that Ni becomes more compatible into MSS as temperature falls (Barnes et al., 1997a; Ballhaus et al., 2001), it would appear that the sulphide liquid likely underwent a minor degree of fractionation before entrapment, for the Ni concentration to be lower in SUL than in mineralization. The Co:Ni ratio is also different between SUL and mineralization (~1 in SUL and ~0.1 in mineralization) but the Co concentrations are relatively constant (949-4,431 ppm in SUL and 1,339-3,534 ppm in mineralization) (Figure 2.7A). The K_D of Co between MSS and residual sulphide liquid is less than that of Ni but greater than that of Cu (L.A. Rose, 1998 unpublished thesis). This could explain the high Co:Ni ratio of the SUL compared to mineralization. If the sulphide liquid crystallized a small amount of MSS prior to the trapping of SUL, this would increase the Co:Ni ratio of the remaining sulphide liquid. Crystallization of olivine prior to the segregation of a sulphide liquid can cause the Co:Ni ratio of the sulphide liquid to be high because of the higher K_D of Ni into olivine than Co into olivine (Duke, 1976; Seifert et al., 1988). However, the high Co:Ni ratio of SUL cannot be explained by this process because of the relatively depleted nature of Ni in olivine within the CLG (Figure 2.8A). Also, if olivine was responsible for removing Ni from the system, pentlandite present in mineralization should have a higher Co concentration than is present (e.g., Upper Zone of the Bushveld complex; Merkle and Von Gruenewaldt, 1986). Since Ni has a higher K_D between sulphide and silicate liquid than Co, the removal of a small batch of sulphide liquid from the magma prior to the formation of the sulphide liquid responsible for the formation of SUL, would increase the bulk Co:Ni ratio of the magma and would result in the high Co:Ni ratios observed in the SUL (MacLean and Shamazaki, 1976; Rajamani

and Naldrett, 1978; Merkle and Von Gruenewaldt, 1986; Li and Audetat, 2012; Patten et al., 2013).

The Cu:Co ratios of SUL and mineralization are fairly consistent (unlike Cu:Ni and Co:Ni) with both ratios ranging from 1-20. However, SUL Cu:Co ratios plot slightly lower than mineralization ratios (~1-8), which could indicate a small amount of Co was partitioned into the crystallizing MSS phase prior to entrapment of SUL, as Co has a slightly higher D into MSS than Cu (L.A. Rose, 1998 unpublished thesis; Barnes et al., 1997a; Ballhaus et al., 2001; Mungall et al., 2005).

2.4.3 Other occurrences of sulphide melt inclusions in Ni-Cu-PGE deposits

As described by Holwell et al. (2011) SUL from the Platreef of the Bushveld Complex, South Africa have been trapped very early in the crystallization history as inclusions within chromite. The SUL in chromite are polyphase consisting primarily of pyrrhotite, pentlandite, and chalcopyrite, which is similar to the SUL of CLG. The most notable mineralogical difference between the Platreef and CLG SUL is the presence of PGM in the Platreef SUL, where cooperite (PtS), laurite (RuS_2), moncheite ($PtTe_2$), and sperrylite ($PtAs_2$) occur along the edge of SUL (Holwell et al., 2011). The occurrence of chalcopyrite and PGM along the SUL margins could be related to the fractionation of the sulphide liquid during cooling. Pyrrhotite and pentlandite form from MSS with chalcopyrite forming from the relatively later ISS and PGM forming from a residual semi-metal rich melt, which would result in chalcopyrite and PGM located on the margins of SUL (Holwell and McDonald, 2010; Holwell et al., 2011).

In the study carried out by Holwell et al. (2011) with SUL hosted in an opaque mineral (chromite), the inclusions had to be exposed at surface, which would have

resulted in partial or complete loss of a mineral within the inclusion. To overcome this issue, they homogenized sections of the host rock to 1195°C completely homogenizing the SUL and followed by rapid quenching. After the the heating treatment, they then polished the sections to expose the inclusions and then were analyzed by LA-ICP-MS to ensure that all contents were analyzed. Fortunately, SUL in the CLG are hosted in translucent minerals (apatite and plagioclase) so there is no need to homogenize the inclusions as they are visible through the microscope objectives attached to the LA-ICP-MS and inclusions present below surface can be analyzed. All PGE, semi-metals (As, Sb, Te, Bi) and Au were all present in ppm concentrations for homogenized SUL in the Platreef, with average Pt and Pd contents of 190.2 and 160.5 ppm, respectively (Holwell et al., 2011). Nickel (12.3 wt %) and Cu (14.1 wt %) concentrations are ~60x greater in the Platreef than in the CLG (Ni=~0.2 wt %; Cu=~0.8 wt %). Also, Holwell et al. (2011) noted that the compositions of SUL are similar to bulk rock when recalculated to 100 % sulphide by Holwell and McDonald (2007). The presence of PGM and the higher concentrations of PGE in SUL of the Platreef would imply that the initial sulphide liquid was PGE-rich and is supportive of a model where PGE were concentrated in the sulphide liquid prior to intrusion (Holwell et al., 2011).

Prichard et al. (2004) describe sulphide blebs occurring within a mafic dike belonging to the Uruguayan dike swarm. The formation of sulphide blebs was early relative to the crystallization of silicate minerals and the occurrence of interstitial sulphides immediately below the blebs may implied that the sulphide liquid was sinking and migrating prior to solidification of the silicate melt (Prichard et al., 2004). The blebs do not occur enclosed within a single mineral as SUL CLG or the Platreef, but are

enclosed by the silicate groundmass, with a sharp lower margin and an irregular upper margin consisting of a mixture of silicate and sulphide minerals (Prichard et al., 2004). The sulphide blebs are composed predominately of magnetite, pyrrhotite, pentlandite, chalcopyrite, and cubanite, as well as some PGM that occur in chalcopyrite rich veinlets that crosscut magnetite and terminate at the blebs grain boundary (Prichard et al., 2004). The sulphide blebs could be divided into two distinct zones representing sulphide liquid evolution and segregation of MSS and ISS. The lower zones of the blebs are composed of pyrrhotite and pentlandite (representing MSS) and the upper zone is composed largely of chalcopyrite intergrown with cubanite laths, representative of ISS (Prichard et al., 2004). The presence of the "late" chalcopyrite-rich veinlets that crosscut magnetite and terminate at the blebs margins are representative of a highly fractionated sulphide liquid, which was enriched in Cu, Pb, Sn, Ag, Mo, Pd, Bi, Te, and Sb (Prichard et al., 2004). Titaniferous magnetite is present within the blebs along their margins and the marginsare typically fractured and filled by chalcopyrite. Sulphide droplets similar to the ones described by Prichard et al. (2004) have also been described in the Noril'sk-Talnakh district, where Czamanske et al. (1992) documented sulphide droplets with a pyrrhotite and pentlandite base with chalcopyrite comprising the uppermost portion of the droplet. Prichard et al. (2004) also examined similar sulphide droplets from Noril'sk and observed Pt- and Pd-tellurides, bismuthides, and arsenides within the sulphide droplets.

The SUL of the Platreef and the sulphide droplets from Uruguay and Noril'sk have similar mineralogy with respect to their major mineral assemblage to the CLG (pyrrhotite, pentlandite, chalcopyrite, magnetite), but the CLG lacks the presence of PGM compared to these other occurrences. Possible explanations for the lack of PGM in SUL

could be that the sulphide liquid was depleted with respect to PGE or a semi-metal liquid had separated before SUL became trapped leaving the sulphide liquid depleted in PGE (Ballhaus et al., 2001; Helmy et al., 2007). As there is no evidence for an early semi-metal rich liquid in sulphide mineralization of the CLG, the latter scenario seems unlikely.

2.4.4 Comparison of the Caribou Lake Gabbro mineralization to Ni-Cu-PGE deposits globally

Metal tenor (metal content in 100 % sulphide) of sulphide mineralization has been calculated because a majority of metals are assumed to reside in base metal sulphides and would give an estimate of the sulphide liquid that lead to the formation of mineralization. Since sulphide contents vary between mineralization intervals within a deposit and between various deposits, mineralization is recalculated to 100 % sulphide to compare the various styles. Tenor calculations used the whole rock S, Cu, and Ni concentrations as well as Ni in pyrrhotite obtained through LA-ICP-MS analysis.

Comparing the CLG mineralization styles to major PGE deposits globally (e.g., Stillwater Complex, Bushveld Complex, Lac des Iles, East Bull Lake), it is evident that the CLG is extremely depleted in PGE and Au (Figure 2.3B). Massive, semi-massive, and disseminated sulphide mineralization exhibit a concave pattern while the PGE deposits show a convex pattern. The trace sulphide mineralization is depleted in PGE relative to the other deposits but does have a similar convex pattern, except for the relative Ir depletion (Figure 2.3B). The base metals in the CLG (Co, Ni, Cu) are also relatively depleted compared to the PGE deposits. Comparison of CLG mineralization to major Ni-Cu deposits globally (e.g., Sudbury, Noril'sk, Perseverance, Pechanga, Voisey's Bay,

Cape Smith) shows that the CLG is depleted in Ni but has similar Co ratios relative to primitive mantle. Copper in the CLG is similar to a majority of the deposits except for Noril'sk (Figure 2.3A). The CLG is depleted in PGE compared to Ni-Cu deposits but has similar Au ratios relative to primitive mantle compared to Perseverance, Voisey's Bay, Sudbury, and Cape Smith (Figure 2.3A).

2.4.5 Sulfur isotopes and inducing sulphide saturation

Assimilation of externally derived sulphur is believed to be a crucial process in the formation of a magmatic Ni-Cu-PGE deposit by invoking S-saturation in the system (Ripley and Li, 2003, 2013). Other mechanisms have been proposed to promote sulfur saturation such as: (i) the assimilation of felsic country rocks (i.e., addition of SiO_2), which decreases the solubility of S, promoting sulfur saturation (Irvine, 1975; Li and Naldrett, 1993) and has been suggested at the Nebo-Babel deposit, Western Australia (Seat et al., 2009); and (ii) an increase in fO_2 in the melt, lowers the amount of S required to reach sulfur saturation (Buchanan et al., 1981), as suggested by Lehmann et al. (2007) at the Jinchaun Ni-Cu-PGE deposit, China. However, Ripley and Li (2013) point out that it is still uncertain if silica contamination or an increase in fO_2 can account for the large amount of sulphide observed in Ni-Cu-PGE deposits (e.g., Jinchaun).

Sulfur isotopes are the most common technique used to assess the role that externally derived sulfur may have played in the formation of a magmatic Ni-Cu-PGE deposit and can provide an indication of the amount of S assimilated (Ripley and Li, 2003, 2013). Studies on Ni-Cu-PGE deposits such as Voisey's Bay (Ripley et al., 1999), Duluth (Ripley, 1981), Noril'sk (Li et al., 2003), and Uitkomst (Li et al., 2002) have all used sulfur isotopes as evidence for the incorporation of external S to invoke sulfur

saturation. However, the use of sulfur isotopes is only effective if the $\delta^{34}S$ signature of the contaminant(s) is different than the $\delta^{34}S$ signature of the sulphide liquid. Mixing may result in the homogenization of $\delta^{34}S$ values, or if contamination of S-poor country rocks occurred then the $\delta^{34}S$ values may remain consistent with mantle values and sulfur isotopes would not provide an indication of externally derived sulfur (Ripley and Li, 2003, 2013).

Sulfur isotopes of pyrrhotite in the Archean sedimentary Burwash Formation have $\delta^{34}S$ within mantle range (-0.3 to +0.8 ‰). *In situ* isotope analysis of SUL and disseminated sulphides, as well as mineral separate isotope analysis of pyrrhotite and chalcopyrite within mineralization and pyrite along fracture planes all have $\delta^{34}S$ values consistent with a mantle source as well (-1.3 to +2.5‰). Therefore, the use of sulfur isotopes to document the effect of sulfur contamination from the Burwash Formation is not an effective method.

One issue with a model that requires sulfur contamination from the Burwash Formation to induce sulphide saturation in the CLG is the difficulty of liberating sulfur from pyrrhotite (Ripley et al., 1999). A fluid at temperatures < 700°C and in equilibrium with pyrrhotite, graphite, and ilmenite or magnetite would have only minor X_{H2S} (< 0.01), therefore only minor amounts of sulphide would be added to a melt through advection or diffusion (Andrews and Ripley, 1989; Ripley et al., 1999). Also, as Ripley et al. (1999) noted for Voisey's Bay, directly melting pyrrhotite in the sediments and transferring the liberated sulfur to a melt is not likely to occur in a tholeiitic melt, due to the relatively high melting point for pyrrhotite varieties (~1000°C; Naldrett, 1969). Thus it would difficult to derive external sulfur from the Burwash Formation and invoke sulphide

saturation in the CLG melt. Contamination of the BLIS has been modeled by Mumford (unpublished, 2013 PhD Thesis) by plotting ƐNd vs Th/Yb to track crustal contamination. The results demonstrate the most likely lithology to contaminate the BLIS was the Morose Granite and possibly lower crustal rocks of similar composition to the Kam group of the Yellowknife Greenstone Belt. With the narrow range in $\delta^{34}S$ values from the CLG and the difficulty to liberate sulfur from pyrrhotite, combined with the modeling by Mumford, it would appear that sulphide saturation may have be induced by the addition of SiO_2 from the Morose Granite to the CLG melt and not by contamination from the Burwash sediments.

2.4.6 Olivine chemistry as an indicator of early sulphide segregation

The amount of Ni in olivine displays a positive correlation with the mole % Fo of olivine, generally as Fo decreases, Ni decreases as seen in Figure 2.8A. This trend is expected for olivine formed through fractionation crystallization. Since MgO and Ni are highly compatible in olivine, as crystallization proceeds, olivine progressively removes MgO and Ni from the melt and as Ni is removed, initially, it shows a sharp decrease with respect to Fo but becomes more gradual at lower Fo contents (Simkin and Smith, 1970; Li et al., 2007). For Fo values in the range of Fo_{50} to Fo_{60}, variable Ni contents are present (Figure 2.8A). This scatter in Ni concentrations could be due to the "trapped liquid shift" as described by Barnes (1986). This "shift" occurs when olivine crystallizing from an intercumulus liquid nucleates on a core of early cumulus olivine. The olivine crystallizing from the intercumulus liquid will be much richer in FeO and with the diffusion rates of Fe and Mg within the olivine structure being relatively fast, the resulting olivine will be of a homogeneous Fo composition and be much richer in Fe (lower Fo) than the original

cumulus olivine. Li and Naldrett (1999) also state that the Ni content will be lower as well because the intercumulus liquid will be Ni poor. The "trapped liquid effect" is a good possibility for the relatively low Fo overall, because olivine is rarely seen as massive cumulate rocks formed by equilibrium crystallization in the CLG but is generally a relatively late cumulate mineral and likely formed via gravitational settling or flow differentiation likely allowing interaction with intercumulus liquid (Ripley et al., 2007).

The scatter in Ni contents may also be due to interaction with a sulphide liquid. The exchange partition coefficient (K_D) for the interaction of olivine with a sulphide liquid is defined as:

$$K_D = (NiS/FeS)_{sulphide}/(NiO/FeO)_{olivine} \quad [5]$$

As described by Brenan (2003), the K_D is a function of the Ni+Cu content and the fO_2 of the sulphide liquid. If these two parameters are kept constant, then the K_D will be constant, so if olivine with variable FeO content is immersed into a sulphide liquid, an olivine with a higher FeO content will contain more Ni than an olivine with lower FeO, producing a relationship opposite to normal crystallization (Brenan, 2003; Li et al., 2007). This relationship has been shown at the Stillwater Complex (Barnes and Naldrett, 1985), Voisey's Bay (Li and Naldrett, 1999), Noril'sk and Talnakh intrusions (Li et al., 2003), and Jinchaun deposit (Li et al., 2004). Comparing Fo content of olivine adjacent to SUL and Fo content of olivine distal to SUL, no variation in Fo is present and SEM-EDS did not detect any Ni (Figure 2.8B). This observation would imply that local Fe-Ni exchange did not occur between SUL and olivine.

Comparing the Ni and Fo contents of olivine in the CLG to other Ni-Cu-PGE deposits globally (Figure 2.8A), the CLG has relatively low Fo and extremely low Ni.

The most notable difference would be for the olivine-rich ultramafic rocks of the Bushveld Complex beneath the Platreef (Yudovskaya et al., 2013). The Fo content is relatively consistent between 84 and 92, which is much higher than dunites from the CLG (Fo_{71-72}). The Ni contents of olivine from the Bushveld are highly variable ranging from ~700-5,000 ppm, while olivine from the CLG dunite is relatively poor in Ni (~1,100 ppm) (Figure 2.8A). Olivine rich cumulates from the J-M Reef of the Stillwater Complex (Barnes and Naldrett, 1985) have olivine compositions that are much more enriched in Ni than the CLG and have relatively higher Fo contents. The same relative Ni and Fo enrichments are also present for a majority of gabbroic rocks from the Noril'sk and Talnakh intrusions (Li et al., 2003) and from the basal zone of the Partridge River intrusion, Duluth Complex (Ripley et al., 2007) (Figure 2.8A). Olivine from Voisey's Bay are generally more Fo and Ni rich, until Fo_{62} where the Ni-Fo trend between the CLG and Voisey's Bay are similar (Figure 2.8A). The most plausibly explanation(s) for the relatively low Fo and Ni contents of olivine from the CLG would be the parental magma(s) had relatively low Ni concentrations or that the sulphide liquid had already separated before olivine crystallized. However, with the presence of SUL as secondary inclusion trails in olivine, it would imply that olivine was crystallizing prior to a sulphide liquid separating and therefore the segregation of a sulphide liquid may not be responsible for the Ni depletion in olivine. As well, the scatter in Ni content in olivine could simply be due to different parental magmas with variable Ni concentration. If sulphide mineralization in the CLG formed at high R factors and/or the parental magma was sufficiently rich in Ni, then there would be no appreciable depletion of Ni in olivine due

to competition with sulphide liquid (e.g., Betheno and Mirabela komatiite deposits, Barnes et al., 2013).

2.4.7 Magmatic mineralizing processes in the Caribou Lake Gabbro

To model the magmatic processes responsible for the studied magmatic sulphide mineralization, mineralization was plotted on a Cu versus Pd diagram (e.g., Barnes et al., 1993) and modeled sulphide compositions segregated from a basaltic liquid by varying R factors were calculated using the equation of Campbell and Naldrett (1979),

$$C°_{sul}/C°_{sil} = D^{sul/sil}(R+1)/(R+D), \quad [6]$$

where $C°_{sul}$ = the initial concentration of an element in the sulphide liquid, $C°_{sil}$ = the initial concentration of an element in the silicate liquid, $D^{sul/sil}$ = the partition coefficient of an element between sulphide and silicate liquid, and R = the ratio of silicate to sulphide liquid (R factor). Partition coefficients used for Cu between sulphide and silicate liquid are 1,380 (Peach et al., 1990; Patten et al., 2013) and 33,000 for Pd (Peach et al., 1994).

Three stages are suggested for the formation of disseminated and semi- to massive sulfide mineralization: i) initial loss of 0.1 to 0.2 wt % sulphide at depth during ascent; ii) a secondary stage of sulphide loss prior to formation of sulphide mineralization; and iii) formation of sulphide liquid responsible for forming sulphide mineralization. Modeling of the system has been done for using an initial silicate melt composition with concentrations of 120 ppm Cu and 12 ppb Pd was used because these values are representative of S-undepleted tholeiites and picrites (Lightfoot and Keays, 2005; Keays and Lightfoot, 2007). However, this composition would not produce the disseminated, semi-massive, or massive sulphide mineralization present in the CLG. The trace sulphide

"PGE-enriched" mineralization may be produced from such a liquid at an R factor of ~970, but the compositional evolution line falls slightly above where mineralization plots.

In order for a silicate liquid to produce the observed sulphide mineralization at different R factors, the Cu/Pd ratio needs to be increased, which can be accomplished by the melt losing sulphide at depth prior to intrusion at its present location (stage i), because Pd will be removed at a greater rate than Cu due to their respectively D's between sulphide and silicate liquid. This can be modeled by using the following equation of Barnes et al. (1993) for determining the composition of a silicate liquid after sulphide segregation:

$$C^{f}_{sil}/C°_{sil} = 1/[1+X(D^{sul/sil}-1)\backslash 100], \qquad [7]$$

Where C^{f}_{sil} = concentration of an element in the fractionated silicate magma, $C°_{sil}$ = the initial concentration of an element in the silicate liquid, X = weight percent sulphide that has segregated, and $D^{sul/sil}$ = the partition coefficient of the element between the sulphide and silicate liquid. Using equation [7] for an initially S-undepleted silicate source melt with a Cu and Pd concentrations of 120 ppm and 12 ppb, respectively, the silicate melt would have to lose > 0.3 wt % sulphide to produce the disseminated, semi-massive, and massive sulphide mineralization of the CLG (stage i). This is unlikely because a basaltic magma can typically only carry ~1000-2000 ppm (depending on fO_2, pressure, silicate melt composition) sulfur before sulfur saturation occurs and sulphides start to precipitate (Mavrogenes and O'Neil, 1999; O'Neil and Mavrogenes, 2002). A scenario that seems most plausible is that the silicate liquid lost sulphide multiple times upon its ascent to its present location.

Starting with an initial silicate melt with a Cu concentration of 120 ppm and Pd of 12 ppm, if 0.1 to 0.2 wt % sulphide liquid was lost as the silicate melt ascended (stage i; prior to emplacement), this would result in a silicate melt with Cu and Pd contents of 50 to 39 ppm and 0.35 to 0.24 ppb, respectively. The Cu values are in good agreement with the Cu concentration (59 ppm) of the chilled margin in the CLG (Mumford, 2013 unpublished PhD Thesis). The values for Cu and Pd are also in good agreement with S-depleted tholeiites and picrites (Lightfoot and Keays, 2005; Keays and Lightfoot, 2007). Using equation [6], it is still not possible to produce the disseminated, semi-massive, or massive sulphide mineralization present in the CLG from these new silictae compositions after losing 0.1-0.2 wt % sulphide. This would suggest that even after the initial silicate melt lost a large amount of sulphide prior to magma emplacement (stage i), additional sulphide loss was required (stage ii). Considering an initial loss of sulphide and using equation [7], revised values of 50 ppm Cu and 0.35 ppm Pd were calculated for , 0.005 to 0.01 wt % sulphide would have to be lost for compositional trend lines for R factors of 150-1680 to produce the mineralization of the CLG (stage ii; Figure 2.10). This would result in new silicate melt compositions of 47 ppm Cu and 0.13 ppb Pd (0.005 wt % sulphide lost) and 44 ppm Cu and 0.08 ppb Pd (0.01 wt % sulphide lost). If a silicate melt with Cu and Pd concentrations of 39 ppm and 0.24 ppb lost 0.005 wt % sulphide, it would contain 36 ppm Cu and 0.09 ppb Pd, and if it lost 0.01 wt % sulphide it would have Cu = 34 ppm and Pd = 0.06 ppb. Losing 0.01 wt % sulphide from either starting composition gives the best approximation for R factors passing through mineralization. A silicate melt with 50 ppm Cu and 0.35 ppb Pd and 0.01 wt % sulphide lost (stage iii), R factors that would give rise to the disseminated, semi-massive, and massive sulphide mineralization

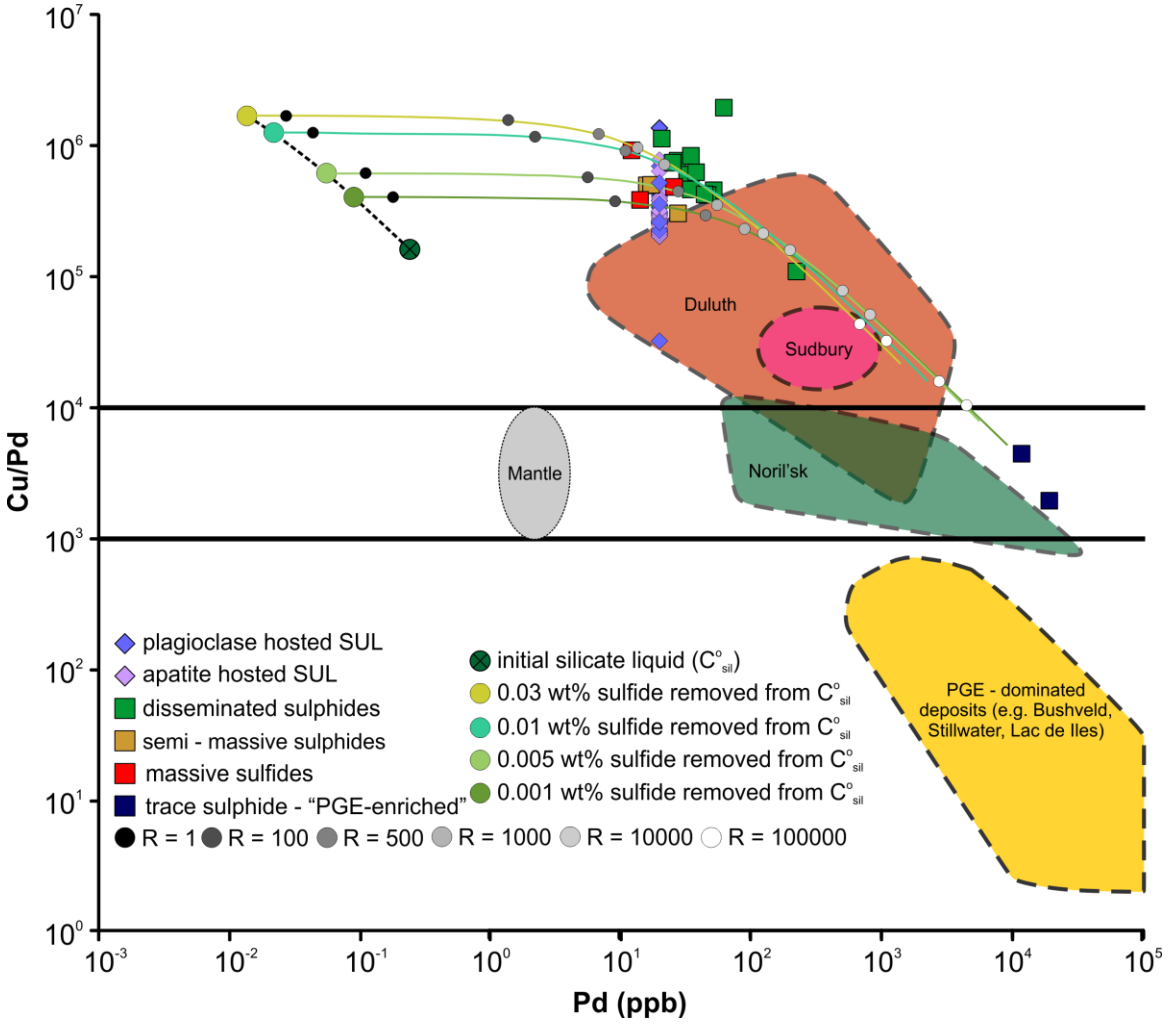

Figure 2.10: Plot of Cu/Pd against Pd showing the composition sulphide mineralization in the Caribou Lake Gabbro and results of modeling. Values for Mantle and PGE-dominated deposits are from Barnes et al., 1993, Duluth: Thériault et al., 2000, Noril'sk: Barnes and Maier, 1999, Sudbury: Naldrett, 1981.

would range from 470 up to 1,680 (Figure 2.10). If the silicate melt had 39 ppm Cu and 0.24 ppb Pd (stage iii), R factors range from 500 to 2,420 (Figure 2.10).

To model fractional crystallization of the sulphide liquid, the following equation is used (Mungall, 2002):

$$C^{f}_{sul} = C°_{sul}F^{(Dmss/sul-1)}, \quad [8]$$

where C^{f}_{sul} = concentration of an element in the fractionated sulphide liquid, $C°_{sil}$ = the initial concentration of an element in the sulphide liquid, $D^{mss/sul}$ = the partition coefficient of the element between the MSS and sulphide liquid, and F = fraction of sulphide liquid remaining. For a silicate melt with a Cu content of 44 ppm and 0.08 ppb Pd, an R factor of 500 could be responsible for crystallizing the disseminated sulphide mineralization if > 90 % of the sulphide liquid crystallized as MSS; ~80 % crystallization could produce the semi-massive and massive sulphide mineralization. At an R factor of 2,500, semi-massive and massive sulphide mineralization could be produce by crystallizing up to 50 % of the sulphide liquid as MSS; between 60 and 80 % sulphide liquid crystallizing as MSS could produce the disseminated sulphide mineralization. For a silicate melt containing only 34 ppm Cu and 0.06 ppb Pd, at an R factor of 1,500, 50 to 70 % of the sulphide liquid would need to crystallize as MSS to produce semi-massive and massive sulphide mineralization, while 80 to 90 % crystallization of the sulphide liquid as MSS would produce the disseminated sulphides (Figure 2.11A). At an R factor of 3,000, 0.001 to 55 % of the sulphide liquid would need to crystallize as MSS to produce semi-massive and massive sulphides and 70 to 80 % sulphide liquid crystallization as MSS could produce the disseminated sulphides (Figure 2.11A). Since sulphide mineralization within the CLG is predominately composed of MSS products (pyrrhotite and pentlandite), with only minor

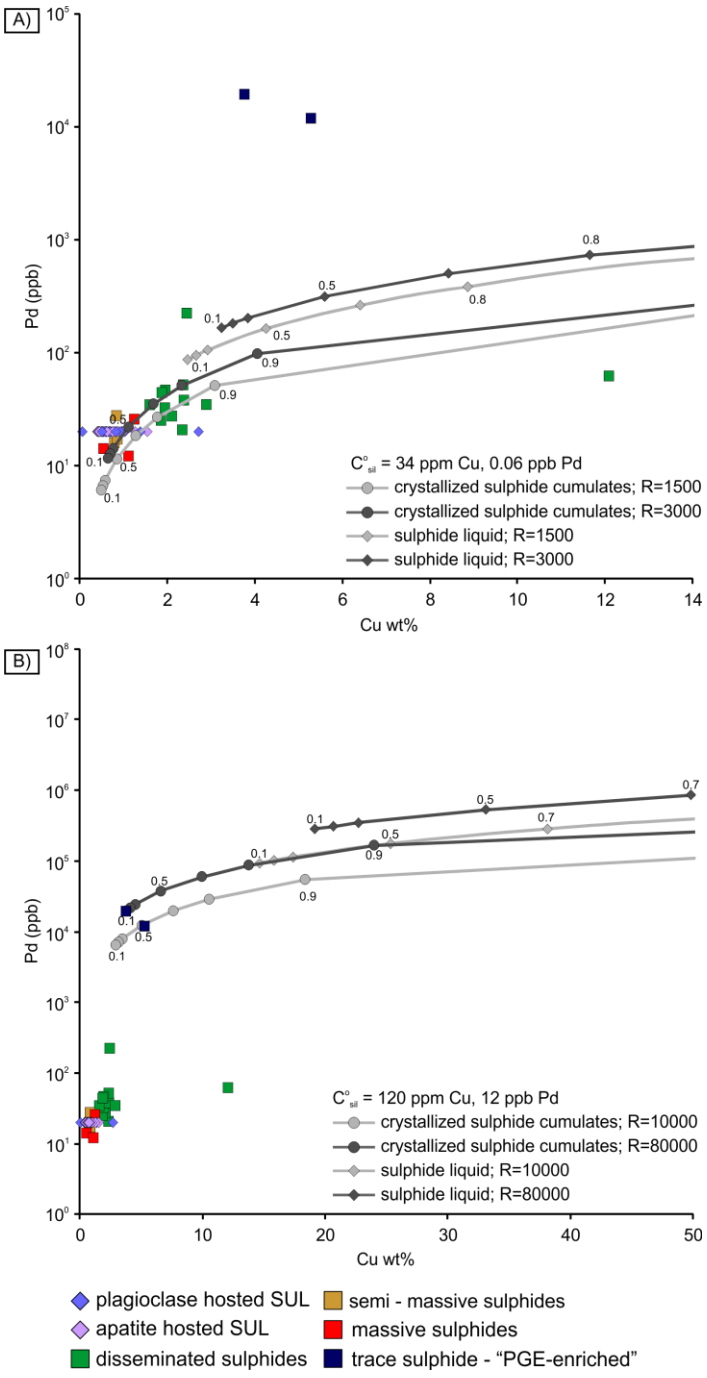

Figure 2.11: Modelling results for fractional crystallization of a sulphide liquid. Liquid and cumulate trends are calculated using equation [8] for fractional crystallization. Numbers along liquid and cumulate lines represent fraction of MSS that has crystallized. A) Cu vs Pd compositions formed under fractional crystallization from a S-depleted silicate melt (Cu=34 ppm; Pd=0.06 ppb). B) Cu vs. Pd compositions formed under fractional crystallization from a S-undepleted silicate melt (Cu=120 ppm; Pd=12 ppb).

ISS products (chalcopyrite), it would suggest that fractional crystallization of the sulphide liquid with an R factor ≤ 3,000 likely gave rise to the CLG mineralization. If the trace sulphide "PGE-enriched" mineralization formed under fractional crystallization, then it would have formed at an R factor of 10,000 with ~50 % of the sulphide liquid crystallizing as MSS or over a range of R factors of 70,000 to 150,000 with ≤ 10 % of the sulphide liquid crystallizaing as MSS from an initial silicate liquid with a composition similar to S-undepleted tholeiites and picrites (Figure 2.11B).

To assess the amount of sulphide liquid that would need to crystallize as MSS, under equilibrium crystallization, to produce the mineralization observed in the CLG, the following equation is used (*c.f.* Li et al., 1992: Fleet et al., 1993; Barnes et al., 1997a)

$$C^{f}_{sul} = C°_{sil}[D^{mss/sul}/((1-F)+FD^{mss/sul})], \quad [9]$$

where C^{f}_{sul} = concentration of an element in the fractionated sulphide liquid, $C°_{sil}$ = the initial concentration of an element in the silicate liquid, $D^{mss/sul}$ = the partition coefficient of the element between the MSS and sulphide liquid, and F = fraction of sulphide liquid remaining. Partition coefficients used for Cu between MSS and sulphide liquid are 0.2 (Ballhaus et al., 2001; Mungall et al., 2005) and 0.07 for Pd (Mungall et al., 2005; Liu and Brenan, 2015). Under MSS equilibrium crystallization for a silicate melt with Cu and Pd concentrations of 44 ppm and 0.08 ppb, respectively, no range of R factors can produce MSS crystallization products that are similar to disseminated to massive sulphide mineralization of the CLG. As well, if the silicate melt contained only 34 ppm Cu and 0.06 ppb Pd, no range of R factors can produce the CLG mineralization. If the CLG mineralization did form under equilibrium sulphide crystallization, then the silicate melt would need to contain ~120 ppm Cu, similar to S-undepleted tholeiites and picrites, but

only ~0.08 ppb Pd, which is similar to S-depleted tholeiite. In order for a silicate liquid of a S-undepleted tholeiitic composition to have a concentration of 0.08 ppb Pd, it must have lost a significant proportion of sulphide at depth prior to sulphide crystallization. However, to have a Cu concentration of 120 ppm, little to no sulphide would have been lost from a S-undepleted tholeiitic liquid, therefore the composition of the silicate liquid to produce the CLG mineralization under MSS equilibrium crystallization seems unreasonable. As well, the R factors that would produce the CLG disseminated to massive sulphide mineralization from a silicate liquid composition of 120 ppm Cu and 0.08 ppb Pd range from 20,000 up to 5,000,000, which also seem unreasonable. Trace sulphide "PGE-enriched" mineralization does not also seem reasonable to have been produced through MSS equilibrium crystallization, as R factors ranging from 30,000 to 5,000,000 could produce the trace sulphide "PGE-enriched" mineralization from an initial silicate liquid with 220 ppm Cu and 15 ppb Pd.

Through modeling estimations of the sulphide liquid and R factors responsible for the evolution of mineralization in the CLG, it appears that two different mineralization events took place: 1) trace sulphide “PGE-enriched” sulphide mineralization that evolved at high R factors under fractional crystallization from a S-undepleted silicate liquid and, 2) disseminated to massive sulphide mineralization that formed from a S-depleted silicate melt under relatively low R factors through fractional crystallization.

2.4.8 Reasons for the low metal tenor of the Caribou Lake Gabbro

Depletion of Ni in olivine combined with the relatively low Ni tenor in sulphide mineralization, would suggest that a sulphide liquid was lost early on in the magmas history, prior to olivine crystallization and segregation of a sulphide liquid. If a sulphide

liquid did not separate prior to olivine crystallization and/or segregation of a sulphide liquid, then mineralization and SUL should contain more Ni than what is present. As discussed above, modeling of sulphide crystallization suggests that sulphide was lost prior to formation of sulphide mineralization as the silicate melt would have only contained ~44 ppm Cu and ~0.08 ppb Pd to produce the disseminated, semi-massive, and massive sulphide mineralization, which is significantly depleted compared to tholeiites and picrites that have not experienced sulphide saturation (Keays and Lightfoot, 2005; Lightfoot and Keays, 2007). However, trace sulphide "PGE-enriched" mineralization may have formed from a S-undepleted tholeiite with Cu and Pd concentrations of 120 ppm and 12 ppb and this style of mineralization in the CLG could be representative of the sulphide liquid that was lost prior to crystallization of the other sulphide mineralization styles.

It is evident through modeling that the majority of mineralization in the CLG was formed through low R factors (≤ 3,000) and would explain the overall low metal tenor of the system and relatively short intervals of mineralization. Through observation of drill core throughout the CLG, lithologies are not overly continuous and are relatively short in length, which could imply that multiple small injections of magma formed the CLG (Mumford, 2013, unpublished PhD Thesis) and therefore, indicate the sulphide liquid did not interact significantly with silicate liquids, resulting in a low R factor.

Another explanation for the poor metal tenor in the CLG could be explained by low degrees of partial melting of the mantle. Since sulphide minerals have relatively lower melting temperatures than silicates in the upper mantle, they would primarily melt during the first stages of partial melting of the upper mantle (Li et al., 2001). As well, with Ni, Cu, and PGE prefering to reside in a sulphide liquid, they will be concentrated

into an initial sulphide liquid during partial melting (Li et al., 2001). As Barnes and Maier (1999) explain, molten sulphide will become completely dissolved in a silicate melt only when approximately 30 % partial melting of the upper mantle occurs. If a smaller degree of partial melting occurs, then not all of the sulphide liquid may be dissolved into the silicate liquid, therefore leaving behind the sulphide liquid in the upper mantle and the Ni, Cu, and PGE that reside in the sulphide liquid (Li et al., 2001). Magmas resulting from high degrees of partial melting (e.g., komatiites) can dissolve all sulphide liquid and therefore should be rich in Ni, Cu, and PGE (Keays, 1995; Li et al., 2001). A low degree of partial melting for the CLG could explain the poor metal tenors in the system as well as the relatively low Fo content of olivine compared to other economic Ni-Cu-PGE deposits.

2.5 Conclusion

Through modeling, estimations of R factors responsible for the formation of sulphide mineralization in the were made and appears CLG, it appears that two distinct mineralizating events occurred: (i) the formation of the trace sulphide "PGE-enriched" sulphide mineralization by fractional crystallization of sulphide melt, involving high R factors (70,000-150,000), from a S-undepleted silicate liquid resulted and; (ii) the formation of disseminated to massive sulphide mineralization from a S-depleted silicate magma that underwent fractional sulphide crystallization involving relatively low R factors ($\leq$ 3,000) forming the disseminated to massive sulphide mineralization.

Depletions in PGE and similar Cu and Co concentrations in both SUL and disseminated-massive sulphide mineralization, suggest these inclusions contain the

parental sulphide liquid responsible for the formation of the disseminated to massive sulphide mineralization. However, Ni concentrations in SUL are significantly lower compared to sulphide mineralization, implying that prior to SUL entrapment, minor fractional crystallization of MSS occurred, removing Ni from the sulphide liquid. ThereforeSUL in the Caribou Lake Gabbro represent a snapshot of the parental sulphide liquid composition, confirming the PGE-poor nature of the system, and can predict the base metal sulphide metal tenor mineralization. For highly chemically-resistive minerals (e.g., apatite) present in soils and tills, SUL preserved in these minerals may provide a potential tool for locating and assessing metal tenor in hidden potentially mineralized mafic-ultramafic intrusions during greenfields exploration.

In the absence of any evidence for Fe-Ni exchange of olivine with sulphide melt in the CLG, olivine is depleted in Ni (≤ 1138 ppm) compared to economic Ni-Cu-PGE deposits, suggesting olivine crystallized from a Ni-depleted melt. As well, with SUL occurring as secondary inclusions in olivine, it would suggest that olivine began to crystallize prior to sulfide liquid formation and likely not be responsible for the Ni depletion in olivine

Overall, sulphide mineralization in the CLG is depleted in PGE and semi-metals. This could be the result of a combination of a several processes: (i) a large amount of sulphide was lost at depth prior to the intrusions present location resulting in poor metal contents in the silicate liquid (e.g., Ni-poor olivine); (ii) as shown through modeling, low R factors likely limited the metal grades in mineralization, and/or (iii) a low degree of partial melting of a source region.

2.6 Acknowledgements

Financial support for this project came from the Northwest Territories Geological Survey, an NSERC DG to JH, and Nova Scotia Research and Innovation Scholarship and SEG Fellowship to KN. We would like to thank Dr. Joe Petrus for LA-ICP-MS analyses of sulphide minerals at Laurentian University, Yanan Liu for assistance with EMP analyses at the University of Toronto, Xiang Yang and Connor Dalzell for SEM-EDS assistance at Saint Mary's University, and the staff at Queen's Facility for Isotope Research for sulfur isotope analysis. Jim Mungall provided helpful comments for the modeling discussion and Aldona Wiacek provided assistance with MATLab. Scott Cairns, John Ketchum, Luke Ootes, Valerie Jackson, and Thomas Mumford are thanked for their helpful discussions about the local and regional geology of the BLIS.

2.7 References

Andrews, M.S., and Ripley, E.M., 1989, Mass transfer and sulfur fixation in the contact aureole of the Duluth intrusion, Dunka Road Cu-Ni deposit, Minnesota: The Canadian Mineralogist, v. 27, p. 293-310.

Ballhaus, C., Tredoux, M., and Späth, A., 2001, Phase relations in the Fe-Ni-Cu-PGE-S system at magmatic temperature and application to massive sulphide ores of the Sudbury Igneous Complex: Journal of Petrology, v. 42, p. 1911-1926.

Barnes, S.-J., and Maier, W.D., 1999, The fractionation of Ni, Cu and the noble metals in silicate and sulphide liquids. *In* Dynamic processes in magmatic ore deposits and their application to mineral exploration. *Edited by* R.R. Keays, C.M. Lesher, P.C. Lightfoot and C.E.G. Farrow. Geological Association of Canada Short Course Series, v. 13.

Barnes, S-J., and Lightfoot, P.C., 2005, Formation of Magmatic Nickel Sulphide Deposits and Processes Affecting Their Copper and Platinum Group Element Contents: Economic Geology, 100th Anniversary Volume, p. 179-214.

Barnes, S.-J., Couture, J.-F., Sawyer, E.W., and Bouchaib, C., 1993, Nickel-copper sulphide occurrences in Belleterre-Angliers belt of the Pontiac Subprovince and the use of Cu/Pd ratios in interpreting platinum group element distributions: Economic Geology, v. 88, p. 1402-1418.

Barnes, S-J., Makovicky, E., Makovicky, M., Rose-Hansen, J., and Karup-Moller, S., 1997a, Partition coefficients for Ni, Cu, Pd, Pt, Rh, and Ir between monosulphide solid solution and sulphide liquid and the formation of compositionally zoned Ni-Cu sulphide bodies by fractional crystallization of sulphide liquid: Canadian Journal of Earth Sciences, v. 34, p. 366-374.

Barnes, S.-J., Zientek, M., and Severson, M.J., 1997b, Ni, Cu, Au and platinum group element contents of sulphides associated with intraplate magmatism: a synthesis: Canadian Journal of Earth Sciences, v. 34, p. 337–351

Barnes, S.-J., Melehik, V., and Sokolov, S. V., 2001, The composition and mode of formation of the Pechenga nickel deposits, Kola peninsula, northwestern Russia: Canadian Mineralogist, v. 39, p. 447-472.

Barnes, S-J., Cox, R.A., and Zientek, M.L., 2006, Platinum-group element, gold, silver, and base metal distribution in compositionally zoned sulphide droplets from the Medvezky Creek Mine, Noril'sk, Russia: Contributions to Mineralogy and Petrology, v. 152, v. 187-200.

Barnes, S.J., 1986, The effect of trapped liquid crystallization on cumulus mineral compositions in layered intrusions: Contributions to Mineralogy and petrology, v. 93, p. 524-531.

Barnes, S.J., and Naldrett, A.J., 1985, Geochemistry of the J-M (Howland) Reef of the Stillwater Complex, Minneapolis Adit area. I. Sulphide chemistry and sulphide-olivine equilibrium: Economic Geology, v. 80, p. 627-645.

Barnes, S.J., Gole, M.J., and Hill, R.E.T., 1988, The Agnew nickel deposit, Western Australia. Part II. Sulphide geochemistry, with emphasis on the platinum group elements: Economic Geology, v. 83, p. 537-550

Barnes, S.J., Fiorentini, M.L., Duuring, P., Grguric, B.A., and Perring, C.S., 2011, The Perseverance and Mount Keith nickel deposits of the Agnes-Wiluna Belt, Yilgarn Craton, western Australia: Reviews in Economic Geology, v. 17, p. 52-88.

Barnes, S.J., Godel, B., Gürer, G., Brenan, J.M., Robertson, J., and Paterson, D., 2013, Sulphide-olivine Fe-Ni exchange and the origin of anomalously Ni rich magmatic sulphides: Economic Geology, v. 108, v. 1971-1982.

Birkett, T.C., Richardson, D.G., and Sinclair, W.D., 1994, Gravity modeling of the Blachford Lake Intrusive Suite, Northwest Territories. *In* Studies of rare-metal deposits in the Northwest Territories. *Edited by* W.D. Sinclair and D.G. Richardson. Geological Survey of Canada, p. 5-16.

Bleeker, W., and Hall, B., 2007, The Slave Craton: Geology and metallogenic evolution. *In* Mineral Deposits of Canada: A Synthesis of Major Deposit-Types, District Metallogeny, the Evolution of Geological Provinces, and Exploration Methods. *Edited by* W.D. Goodfellow. Geological Association of Canada, Mineral Deposits Division, Special Publication, p. 849-879.

Bowring, S. A., Van Schmus, W. R., & Hoffman, P. F., 1984, U-Pb zircon ages from Authapascow Aulacogen, East Arm of Great Slave Lake, NWT, Canada: Canadian Journal of Earth Sciences, v. 21, p. 1315-1324.

Brenan, J.M., 2002, Re-Os fractionation in magmatic sulphide melt by monosulphide solid solution: Earth and Planetary Science Letters, v. 199, p. 257-268.

Brenan, J.M., 2003, Effects of fO_2, fS_2, temperature, and melt composition on Fe-Ni exchange between olivine and sulphide liquid: implications for natural olivine-sulphide assemblages: Geochimica et Cosmochimica Acta, v. 67, p. 2663-2681.

Buchanan, D.L., Nolan, J., Suddaby, P., Rouse, J.E., Viljoen, M.J., and Davenport, J.W.J., 1981, The genesis of sulphide mineralization in a portion of the Potgietersrus Limb of the Bushveld Complex: Economic Geology, v. 76, p. 568-579.

Campbell, I.H., and Naldrett, A.J., 1979, The influence of silicate:sulphide ratios on the geochemistry of magmatic sulphides: Economic Geology, v. 74, p. 1503-1505.

Campos-Alvarez, N.O., Samson, I.M., and Fryer, B.J., 2012, The roles of magmatic and hydrothermal processes in PGE mineralization, Ferguson Lake deposit, Nunavut, Canada: Mineralium Deposita, v. 47, p. 441-465.

Crowe, D.E., and Vaughn, R.G., 1996, Characterization and use of isotopically homogeneous standards for in situ laser microprobe analysis of $^{34}S/^{32}S$ ratios: American Mineralogist, v. 81, p. 187-193.

Czamanske, G.K., Kunilov, V.Y., Zientek, M.L., Cabri, L.J., Likhachev, A.P., Calk, L.C., and Oscarson, R.L., 1992, A proton-microprobe study of magmatic sulphide ores from the Noril'sk-Talnakh district, Siberia: The Canadian Mineralogist, v. 30, p. 249-287.

Dare, S.A.S., Barnes, S-J., Prichard, H.M., and Fisher, P.C., 2010, The timing and formation of platinum-group minerals from the Creighton Ni-Cu-platinum-group element sulphide deposit, Sudbury, Canada: early crystallization of PGE-rich sulfarsenides: Economic Geology, v. 105, p. 1071-1096.

Dare, S.A.S., Barnes, S-J., Prichard, H.M., and Fisher, P.C., 2014, Mineralogy and geochemistry of Cu-rich ores from the McCreedy East Ni-Cu-PGE deposit (Sudbury, Canada): implications for the behavior of platinum group and chalcophile elements at the end of crystallization of a sulphide liquid: Economic Geology, v. 109, p. 343-366.

Davidson, A., 1972, Granite Studies in the Slave Province. *Report of Activities*: Geological Survey of Canada, p. 109-115.

Davidson, A., 1978, The Blachford Lake Intrusive Suite: An Aphebian alkaline plutonic complex in the Slave Province, Northwest Territories. *Current Research*: Geological Survey of Canada, p. 119-127.

Davidson, A., 1981, Petrochemistry of the Blachford Lake Complex, District of Mackenzie. *Geological Survey of Canada Open File 764*, 24 p.

Davidson, A., 1982, Petrochemistry of the Blachford Lake complex near Yellowknife, Northwest Territories. In: Maurice, Y. T. (ed.) *Uranium in Granites*: Geological Survey of Canada, 71-79.

Distler, V.V., 1994, Platinum mineralization of the Noril'sk deposits: *In* Lightfoot, P.C., Naldrett, A.,J., (*eds*) Proceedings of Sudbury-Noril'sk symposium, Ontario Geological Survey Special Publication 5, p. 243-260.

Duke, J.M., 1976, Distribution of the period four transition elements among olivine, calcic clinopyroxene and mafic silicate liquid; experimental results: Journal of Petrology, v. 17, p. 499-521.

Ebel, D.S., and Naldrett, A.J., 1997, Crystallization of sulphide liquids and the interpretation of ore composition: Canadian Journal of Earth Sciences, v. 34, p. 352-365.

Fleet, M.E., Chryssoulis, S.L., Stone, W.E., and Weisener, C.G., 1993, Partitioning of platinum-group elements and Au in the Fe-Ni-Cu-S system: experiments on the fractional crystallization of sulphide melt: Contributions to Mineralogy and Petrology, v. 115, p. 36-44.

Gál, B., Molnár, F., Guzmics, T., Mogessie, A., Szabó, C., and Peterson, D., 2013, Segregation of magmatic fluids and their potential in the mobilization of platinum group elements in the South Kawishiwi Intrusion, Duluth Complex, Minnesota-Evidence from petrography, apatite geochemistry, and coexisting fluid and melt inclusions: Ore Geology Reviews, v. 54, p. 59-80.

Godel, B., and Barnes, S-J., 2008, Platinum-group elements in sulphide minerals and the whole rocks of the J-M Reef (Stillwater Complex): implications for the formation of the reef: Chemical Geology, v. 248, p. 272-294.

Guillong, M. M., Maier, D.L., Allan, M.M., Heinrich, C.A., and Yardley, B.W.D., 2008, Appendix A6: SILLS: a MATLAB based program for the reduction of laser ablation ICP-MS data of homogeneous materials and inclusions. *In* Laser Ablation ICP-MS in the Earth Sciences: Current Practices and Outstanding Issues. *Edited by* P. Sylvester. Mineralogical Association of Canada Short Course Series, v. 40.

Hammer, S., Bowring, S., Vanbreemen, O., and Parrish, R., 1992, Great Slave Lake Shear Zone, NW Canada-Mylonitic record of early Protoerzoic continental convergence, collision and indentation: Journal of Petrology, v. 14, p. 757-773.

Hanley, J.J., Mungall, J.E., Pettke, T., Spooner, E.T.C, and Bray, C.J., 2005, Ore metal redistribution by hydrocarbon-brine and hydrocarbon-halide melt phases, North Range footwall of the Sudbury Igneous Complex, Ontario, Canada: Mineralium Deposita, v. 40, p. 237-258.

Hanley, J.J., Mungall, J.E., Pettke, T., Spooner, E.T.C., and Bray, C.J., 2008, Fluid and halide melt inclusions of magmatic origin in the Ultramafic and Lower Banded series, Stillwater Complex, Montana, USA: Journal of Petrology, v. 49, p. 1133-1160.

Helmy, H. H., Ballhaus, C., Berndt, J., Bockrath, C., and Wohlgemuth-Ueberwasser, C., 2007, Formation of Pt, Pd and Ni tellurides: experiments in sulphide-telluride systems: Contributions to Mineralogy and Petrology, v. 153, p. 577-591.

Helmy, H. H., Ballhaus, C., Wohlgemuth-Ueberwasser, C., Fonseca, R.O.C., and Laurenz, V., 2010, Partitioning of Se, As, Sb, Te and Bi between monosulphide solid solution and sulphide melt-application to magmatic sulphide deposits: Geochimica et Cosmochimica Acta, v. 74, p. 6174-6179.

Helmy, H.M., Ballhaus, C., Fonseca, R.O.C., and Nagel, T.J., 2013, Fractionation of platinum, palladium, nickel, and copper in sulphide-arsenide systems at magmatic temperature: Contributions to Mineralogy and petrology, v. 166, p. 1725-1737.

Hinchey, J.G., Hattori, K.H., and Lavigne, M.J., 2005, Geology, petrology, and controls on PGE mineralization of the Southern Roby and Twlight Zones, Lac des Iles mine, Canada: Economic Geology, v. 100, p. 43-61.

Hoffman, P.F., 1987, Continental transform tectonics-Great Slave Lake shear zone (Ca-1.9 Ga), northwest Canada: Geology, v. 15, p. 785-788.

Hoffman, P., 1973, Evolution of an early Proterozoic continental margin – Coronation geosynclines and associated aulacogens of northwest Canadian Shield. Philosophical Transactions of the Royal Society of London a-Mathematical Physical and Engineering Sciences, v. 273, p. 547-581.

Holliger, P., 1988, Ages U/Pb defines in situ sur oxides d'uranium a l'analyseu ionique: methodologie et consequences geochemiques. Comptes rendus de l'Académie des Sciences Paris, v. 307, p. 367-373.

Holwell, D.A., and McDonald, I., 2007, Distribution of platinum-group elements in the Platreef at Overysel, northern Bushveld Complex: a combined PGM and LA-ICP-MS study: Contributions to Mineralogy and Petrology, v. 154, p. 171-190.

Holwell, D.A., and McDonald, I., 2010, A review of the behavior of platinum group elements within natural magmatic sulphide ore systems: Platinum Metals Review, v. 54, p. 26-36.

Holwell, D.A., McDonald, I., and Butler, I.B., 2011, Precious metal enrichment in the Platreef, Bushveld Complex, South Africa: evidence from homogenized magmatic sulphide melt inclusions: Contributions to Mineralogy and Petrology, v. 161, p. 1011-1026.

Holwell, D.A., Keays, R.R., McDonald, I., and Williams, M.R., 2015, Extreme enrichment of Se, Te, PGE and Au in Cu sulphide microdroplets: evidence from LA-ICP-MS analysis of sulphides in the Skaergaard Intrusion, east Greenland: Contributions to Mineralogy and Petrology, v. 170, DOI 10.1007/s00410-015-1203-y.

Irvine, T. N., 1975, Crystallization sequence of the Muskox intrusion and other layered intrusions-II. Origin of chromitite layers and similar deposits of other magmatic ores: Geochimica et Cosmochimica Acta, v. 39, p. 991-1020.

Jensen M. L. and Nakai N., 1962, Sulfur isotope meteorite standards, results and recommendations. In *Biogeochemistry of Sulfur Isotopes*, NSF Symposium, p. 30-35.

Keays, R.R., 1995, The role of komatiitic and picritic magmatism and S-saturation in the formation of ore deposits: Lithos, v. 34, p. 1-18.

Keays, R.R., and Lightfoot, P.C., 2007, Siderophile and chalcophile metal variations in Tertiary picrites and basalts from West Greenland with implications for the sulphide saturation history of continental flood basalt magmas: Mineralium Deposita, v. 42, p. 319-336.

Kullerud, G., Yund, R.A., Moh, G., 1969, Phase relations in the Cu–Fe–S and Cu–Ni –S systems. *In* Wilson, H.D.B. (Ed.), Magmatic Ore Deposits: Economic Geology Monograph, v. 4, p. 323-343.

Lehmann, J., Arndt, N., Windley, B., Zhou, M.-F., Wang, C.Y., and Harris, C., 2007, Field relationships and geochemical constraints on the emplacement of the Jinchuan intrusion and its Ni-Cu-PGE sulphide deposit, Gansu, China: Economic Geology, v. 102, p. 75-94.

Li, C., and Naldrett, A.J., 1993, Sulphide capacity of magma: a quantitative model and its application to the formation of sulphide ores at Sudbury, Ontario: Economic Geology, v. 88, p. 1253-1260.

Li, C., and Naldrett, A.J., 1999, Geology and petrology of the Voisey's Bay intrusion: reaction of olivine with sulphide and silicate liquids: Lithos, v. 47, p. 1-31.

Li, C., Naldrett, A.J., Coats, C.J.A., and Johannessen, P., 1992, Platinum, palladium, gold, and copper-rich stringers at the Strathcona Mine, Sudbury: their enrichment by fractionation of a sulphide liquid: Economic Geology, v. 87, p. 1584-1598.

Li, C., Barnes, S-J., Makovicky, E., Rose-Hansen, J.R., and Makovicky, M., 1996, Partitioning of nickel, copper, iridium, rhenium, platinum, and palladium between monosulphide solid solution and sulphide liquid: effects of composition and temperature: Geochimica et Cosmochimica Acta, v. 60, p. 1231-1238.

Li, C., Maier, W.D., and de Waal, S.A., 2001, Magmatic Ni-Cu versus PGE deposits: contrasting genetic controls and exploration implications: South African Journal of Geology, v. 104, p. 309-318.

Li, C., Ripley, E.M., Maier, W.D., and Gomwe, T.E.S., 2002, Olivine and sulfur isotopic compositions of the Uitkomst Ni-Cu sulphide ore-bearing complex, South Africa: evidence for sulfur contamination and multiple magma emplacements: Chemical Geology, v. 188, p. 149-159.

Li, C., Ripley, E.M., and Naldrett, A.J., 2003, Compositional variations of olivine and sulfur isotopes in the Noril'sk and Talnakh intrusions, Siberia: implications for ore-forming processes in dynamic magma conduits: Economic Geology, v. 98, p. 69-86.

Li, C., Xu, Z., de Waal, S.A., Ripley, E.M., and Maier, W.D., 2004, Compositional variations of olivine from the Jinchuan Ni-Cu sulphide deposit, western China: implications for ore genesis: Mineralium Deposita, v. 39, p. 159-172.

Li, C., Naldrett, A.J., and Ripley, E.M., 2007, Controls on the Fo and Ni contents of olivine in sulphide-bearing mafic/ultramafic intrusions: principles, modeling, and examples from Voisey's Bay: Earth Science Frontiers, v. 14, p. 177-185.

Li, Y., and Audétat, A., 2012, Partitioning of V, Mn, Co, Ni, Cu, Zn, As, Mo, Ag, Sn, Sb, W, Au, Pb, and Bi between sulphide phases and hydrous basanite melt at upper mantle conditions: Earth and Planetary Science Letters, v. 355-356, p. 327-340.

Lightfoot, P.C., and Keays, R.R., 2005, Siderophile and chalcophile metal variations in flood basalts from the Siberian Trap, Noril'sk region: implications for the origin of the Ni-Cu-PGE sulphide ores: Economic Geology, v. 100, p. 439-462.

Liu, Y., and Brenan, J., 2015, Partitioning of platinum-group elements (PGE) and chalcogens (Se, Te, As, Sb, Bi) between monosulphide-solid solution (MSS), intermediate solid solution (ISS) and sulphide liquid at controlled fO_2-fS_2 conditions: Geochimica et Cosmochimica Acta, v. 159, p. 139-161.

MacLean, W. H., and Shimazaki, H., 1976, The partition of Co, Ni, Cu, and Zn between sulphide and silicate liquids: Economic Geology, v. 71, p. 1049-1057.

Marmont, C., 2006, Report on Diamond Drilling, Airborne and Ground Geophysical Surveys, Lithogeochemical Sampling and Prospecting; submitted by Kodiak Exploration, Northwest Territories Geoscience Office, Activities Report 085101, p. 123.

Marmont, C., 2007, Report on Diamond Drilling; submitted by Kodiak Exploration, Northwest Territories Geoscience Office, Activities Report 085317, p. 283.

Mavrogenes, J.A., and O'Neil, H.St.C., 1999, The relative effects of pressure, temperature, and oxygen fugacity on the solubility of sulphide in mafic magmas: Geochimica et Cosmochimica Acta, v. 63, p. 1173-1180.

Merkle, R.K.W., and Von Gruenewaldt, G., 1986, Compositional variation of Co-rich pentlandite: relation to the evolution of the Upper Zone of the western Bushveld Complex, South Africa: The Canadian Mineralogist, v. 24, p. 529-546.

Molnár, F., Watkinson, D.H., Jones, P.C., and Gatter, I., 1997, Fluid inclusion evidence for hydrothermal enrichment of magmatic ore at the Contact Zone of the Ni-Cu-Platinum group element 4b deposit, Lindsley mine, Sudbury, Canada: Economic Geology, v. 92, p. 674-685.

Molnár, F., Watkinson, D.H., and Everest, J.O., 1999, Fluid-inclusion characteristics of hydrothermal Cu-Ni-PGE veins in granitic and metavolcanic rocks at the contact of the Little Stobie deposit, Sudbury, Canada: Chemical Geology, v. 154, p. 279-301.

Mumford, T.R., Ketchum, J., Falck, H., and Heaman, L., 2012, New geochemical, geochronologicial, and isotopic data for the Blatchford Lake Intrusive Suite and the Simpson Island dyke: Northwest Territories Geoscience Office, NWT Open File Report, 2012-005, 41 p.

Mumford, T.R., 2013, Petrology of the Blatchford Lake Intrusive Suite, Northwest Territories, Canada, Unpublished PhD thesis, Ottawa, Canada, Carleton University, 240 p.

Mungall, J.E., 2002, Late-stage sulphide liquid mobility in the main mass of the Sudbury Igneous Complex: Examples from the Victor Deep, McCreedy East, and Trillabelle deposits: Economic Geology, v.97, p. 1563-1576.

Mungall, J.E., Andrews, D.R.A., Cabri, L.J., Sylvester, P.J., and Turbrett, M., 2005, Partitioning of Cu, Ni, Au, and platinum-group elements between monosulphide solid solution and sulphide melt under controlled oxygen and sulfur fugacities: Geochimica et Cosmochimica Acta, v. 69, p. 4349-4360.

Naldrett, A.J., 1969, A portion of the Fe-S-O and its application to sulphide magmas: Journal of Petrology, v. 10, p. 171-201.

Naldrett, A.J., 1981, Platinum-group element deposits: Canadian Inst of Mining Metallurgy, Special Volume 23, p. 197-232.

Naldrett, A.J., 1984, Ni-Cu ores of the Sudbury Igneous Complex: Ontario Geological Survey, Special Volume 1, p. 302–308.

Naldrett, A.J., Asif, M., Gorbachev, N.S., Kunilov, V.Ye., Stekhin, A.I., Fedorenko, V.A., Lightfoot, P.C., 1994, The composition of the Ni-Cu ores of the Oktyabr'sky deposit, Noril'sk region. In: Lightfoot, P.C., and Naldrett, A.J., (eds) Proceedings of Sudbury- Noril'sk symposium, Ontario Geological Survey, Special Publication, v. 5, p. 357-373.

Naldrett, A.J., Ebel, D.S., Asif, M., Morrison, G., and Moore, C.M., 1997, Fractional crystallization of sulphide melts as illustrated at Noril'sk and Sudbury: European Journal of Mineralogy, v. 9, p. 365-377.

Naldrett, A.J., Asif, M., Schandl, E., Searcy, T., Morrison, G.G., Binney, W.P., and Moore, C., 1999, Platinum-group elements in the Sudbury ores: Significance with respect to the origin of different ore zones and to the exploration for footwall orebodies: Economic Geology, v. 94, p. 185-210.

Naldrett, A.J., Asif, M., and Kristic, S., 2000, The composition of mineralization of the Voisey's Bay Ni-Cu sulphide deposit, with special reference to platinum group elements: Economic Geology, v. 95, p. 845–865.

O'Neil, H.St.C., and Mavrogenes, J.A., 2002, The sulphide capacity and the sulfur content at sulphide saturation of silicate melts at 1400°C and 1 bar: Journal of Petrology, v. 43, p. 1049-1087.

Patten, C., Barnes, S-J., Mathez, E.A., and Jenner, F.E., 2013, Partition coefficients of chalcophile elements between sulphide and silicate melts and the early crystallization history of sulphide liquid: LA-ICP-MS analysis of MORB sulphide droplets: Chemical Geology, v. 358, p. 170-188.

Peach, C.L., Mathez, E.A., and Keays, R.R., 1990, Sulphide melt-silicate melt distribution coefficients for noble metals and other chalcophile elements as deduced from MORB: implications for partial melting: Geochimica et Cosmochimica Acta, v. 54, p. 3379-3389.

Peach, C.L., Mathez, E.A., Keays, R.R., and Reeves, S.J., 1994, Experimentally determined sulphide melt-silicate melt partition coefficients for iridium and palladium: Chemical Geology, v. 117, p. 361-377.

Peck, D.C., Keays, R.R., James, R.S., Chubb, P.T., and Reeves. S.J., 2001, Controls on the formation of contact-type platinum-group element mineralization in the East Bull Lake Intrusion: Economic Geology, v. 96, p. 559-581.

Pilkington, M., Thomas, M.D, and Mumford, T.R., 2012, Geological significance of a new high resolution gravity gradiometric and magnetic survey over the Blatchford Lake Complex, Northwest Territories; Geological Survey of Canada, Open File 7084, Poster.

Polovina, J.S., Hudson, D.M., Jones, R.E., 2004, Petrographic and geochemical characteristics of Postmagmatic hydrothermal alteration and mineralization in the J-M Reef, Stillwater Complex, Montana: The Canadian Mineralogist, v. 42, p. 261-277.

Prichard, H.M., Hutchinson, D., and Fisher, P.C., 2004, Petrology and crystallization history of multiphase sulphide droplets in a mafic dyke from Uruguay: implications for the origin of Cu-Ni-PGE sulphide deposits: Economic Geology, v. 99, p. 365-376.

Prichard, H.M., Fisher, P.C., McDonald, I., Knight, R.D., Sharp, D.R., and Williams, J.P., 2013, The distribution of PGE and the role of arsenic as a collector of PGE in the Spotted Quoll nickel ore deposit in the Forrestania Greenstone Belt, Western Australia: Economic Geology, v. 108, p. 1903-1921.

Rajamani, V., and Naldrett, A.J., 1978, Partitioning of Fe, Co, Ni, and Cu between sulphide liquid and basaltic melts and the composition of Ni-Cu sulphide deposits: Economic Geology, v. 73, p. 82-93.

Riciputi, L.R., Paterson, B.A. and Ripperdan, R.L., 1998, Measurement of light stable isotope ratios by SIMS: Matrix effects for oxygen, carbon, and sulfur isotopes in minerals: International Journal of Mass Spectrometry, v. 178, p. 81-112.

Ripley, E.M., 1981, Sulfur isotope studies of the Dunka Road Cu-Ni deposit, Duluth Complex, Minnesota: Economic Geology, v. 76, p. 610-620.

Ripley, E.M., and Li, C., 2003, Sulfur isotope exchange and metal enrichment in the formation of magmatic Cu-Ni-(PGE) deposits: Economic Geology, v. 98, p. 635-641.

Ripley, E.M., and Li, C., 2013, Sulphide saturation in mafic magmas: Is external sulfur required for magmatic Ni-Cu-(PGE) ore genesis?: Economic Geology, v. 108, p. 45-58.

Ripley, E.M., Park, Y-R., Li, C., and Naldrett, A.J., 1999, Sulfur and oxygen isotopic evidence of country rock contamination in the Voisey's Bay Ni-Cu-Co deposit, Labrador, Canada: Lithos, v. 47, p. 53-68.

Ripley, E.M., Taib, N.I., Li, C., and Moore, C.H., 2007, Chemical and mineralogical heterogeneity in the basal zone of the Partridge River intrusion: implications for the origin of Cu-Ni sulphide mineralization in the Duluth Complex, midcontinent rift system: Contributions to Mineralogy and Petrology, v. 154, p. 35-54.

Rose, L.A., 1998, The partitioning of cobalt between monosulphide solid solution and sulphide liquid in the Fe-S system, Unpublished B.Sc. thesis, London, Canada, University of Western Ontario, 32 p.

Seat, Z., Beresford, S.W., Grguric, B.A., Mary Gee, M.A., and Grassineau, N.V., 2009, Reevaluation of the role of external sulfur addition in the genesis of Ni-Cu-PGE deposits: evidence from the Nebo-Babel Ni-Cu-PGE deposit, west Musgrave, Western Australia: Economic Geology, v. 104, p. 521-538.

Seifert, S., O'Neill, and Brey, G., 1988, The partitioning of Fe, Ni and Co between olivine, metal, and basaltic liquid: an experimental and thermodynamic investigation, with application to the composition of the lunar core: Geochimica et Cosmochimica Acta, v. 52, p. 603-616.

Simkin, T., and Smith, J.V., 1970, Minor element distribution in olivine: Journal of Geology, v. 78, p. 304-325.

Sinclair, W. D., Hunt, P. A. and Birkett, T. C., 1994, U-Pb zircon and monazite ages of the Grace Lake Granite, Blatchford Lake Intrusive Suite, Slave Province, Northwest Territories. Radiogenic Age and Isotopic Studies: Report 8; Geological Survey of Canada, Current Research 1994-F, p. 15-20.

Sylvester, P. J., Cabri, L. J., Tubrett, M. N., McMahon, G., Laflamme, J. H. G., and Peregoedova, A., 2005, Synthesis and evaluation of a fused pyrrhotite standard reference material for platinum group element and gold analysis by laser ablation-ICPMS: International Platinum Symposium, Extended Abstracts, v. 10, p. 16-20.

Watkinson, D.H., and Melling, D.R., 1992, Hydrothermal origin of platinum-group mineralization in low-temperature copper sulphide-rich assemblages, Salt Chuck intrusion, Alaska: Economic Geology, v. 87, p. 175-184.

Watkinson, D., and Ohnenstetter, D., 1992, Hydrothermal origin of platinum-group mineralization in the Two Duck Lake intrusion, Coldwell Complex, northwestern Ontario: The Canadian Mineralogist, v. 30, p. 121-136.

Yudovskaya, M.A., Kinnard, J.A., Sobolev, A.V., Kuzmin, D.V., McDonald, I., and Wilson, A.H., 2013, Petrogenesis of the Lower Zone olivine-rich cumulates beneath the Platreef and their correlation with recognized occurrences in the Bushveld Complex: Economic Geology, v. 108, p. 1923-1952.

Zientek, M.L., Likhachev, A.P., Kunilov, V.Y., Barnes, S-J., Meier, A.L., Carlson, R.R., Briggs, P.H., Fries, T.L., and Adrian, B.M., 1994, Cumulus processes and the composition of the magmatic ore deposits: examples from the Talnakh district Russia: Ontario Geological Survey Special Volume 5, p. 373-392.

Chapter 3: Volatile activity in the Caribou Lake Gabbro, Northwest Territories, Canada - recorded by melt and fluid inclusions in mafic pegmatites

Kevin Neyedley [a,+], Jacob J. Hanley [a], Hendrik Falck [b], Robert J. Bodnar [c], Luca Fedele [c]

[a] *Department of Geology, Saint Mary's University, 923 Robie Street, Halifax, Nova Scotia, Canada B3H 3C3*

[b] *Northwest Territories Geological Survey, 4601-B 52nd Ave, Yellowknife, NT, X1A 2R3*

[c] *Fluids Research Group, Department of Geosciences, Virginia Tech, 1405 Perry St, Blacksburg, VA, 24061*

[+] Corresponding Author: kevinneyedley@gmail.com

Number of pages: 100

Number of figures: 25

Number of tables: 12

For submission to *Contributions to Mineralogy and Petrology*

Abstract

Mafic pegmatites in the Caribou Lake Gabbro (CLG), Northwest Territories, Canada, comprise irregular pods and patches consisting of coarse-grained clinopyroxene, plagioclase, apatite, Fe-Ti oxides, with minor orthopyroxene, biotite, and sulphides. Apatite in these pegmatites hosts a variety of primary and secondary fluid inclusions: (i) type P2 primary polyphase (i.e., containing > two phase at room temperature) brine-carbonic fluid inclusions, (ii) type S1 secondary polyphase CO_2-dominant carbonic fluid inclusions, (iii) type S2 secondary polyphase CH_4-dominant carbonic-brine fluid inclusions, (iv) type S3 secondary polyphase mixed (i.e., heterogeneously entrapped) brine-carbonic fluid inclusions, and (v) type S4 secondary mixed silicate-sulphide melt inclusions. Type S3 inclusions preserve assemblages of two immiscible fluids being co-entrapped, a carbonic-dominant fluid and an aqueous brine and S1 inclusions are likely

the end-member carbonic-dominant fluid while the end-member aqueous-brine fluid was not observed in the samples. A fine- to medium-grained gabbro hosts primary silicate melt inclusions (type P1 inclusions) within cumulus apatite. Apatite in the mafic pegmatites and apatite hosting P1 inclusions are all F-rich with X_F (mol fraction of F in the Cl-F-OH site) ranging from 0.73 to 1.0 and all have similar trace element patterns, but apatite in the mafic pegmatites contain higher concentrations of trace elements.

Major and trace element concentrations in P1 inclusions determined by SEM-EDS and LA-ICP-MS show the melt is of a gabbroic to syeno-dioritic composition. However, the trace elements show a more enriched melt signature with metals (Ni, Cu, Co) being relatively depleted compared to MORB and primitive mantle, while high field strength elements (HFSE) are highly enriched, likely indicating a low degree of partial melting of the mantle was the source for the CLG melt, the melt was crustally contaminated, or sulphide had already separted from the melt causing the low Ni, Cu, and Co. Trace elements such as Zr, Nb, Ta, W, Hf, and Cs were detected in S3 inclusions by SEM-EDS and LA-ICP-MS, and are likely sourced from a late-stage intercumulus liquid, that was enriched in these elements, and was squeezed upwards during crystal settling.

Entrapment conditions for P1 melt inclusions can be constrained by the minimum liquidus temperature ($T_m^{liquidus}$), determined by microthermometry and combined with an estimated pressure of entrapment determined by the Al- and Ti-in-amphibole thermobarometer. These yield P-T conditions of 1130° to 1200°C and 1.6 to 4.5 kbar, for melt entrapment indicating the emplacement depth of the CLG was between 5.9 and 16.6 km. The $T_m^{liquidus}$ can also be used as the maximum T for entrapment of P2 and S1 inclusions. The minimum temperature for P2 inclusions can be constrained by the lower

limit of the Al-in-hornblende thermometer, therefore P2 isochores intersection with $T_m^{liquidus}$ and Al-in-hornblende thermometer give P-T entrapment conditions ranging from 910°-1200°C and 3.2-4.4 kbar (11.8-16.3 km depth). Since S1 inclusions are the end-member fluid for the immiscible S3 inclusions, they can be used to estimate S3 fluid inclusion entrapment as well. The minimum T for S1/S3 inclusions can be constrained by the apatite-biotite halogen exchange thermometer that represents final equilibrium in the unit. The intersection of S1 isochores with $T_m^{liquidus}$ and the apatite-biotite thermometer give P-T conditions of 455° to 1200°C and 1.5 to 4.05 kbar (5.6-15 km depth). The high temperature of entrapment for fluid inclusions suggest that volatile activity is magmatic in origin and not related to a later hydrothermal event. Fluids similar to those reported in this study have previously been documented in economic Ni-Cu-PGE deposits. Since the CLG is only weakly mineralized (low PGE and base metal tenor), this may suggest the presence of these fluid types in layered mafic-ultramafic systems are not related to mineralization potential and primary PGE-bearing sulphide concentrations need to be present for PGE remobilization by fluid to occur.

3.0 Introduction

Fluid and melt inclusion studies of mineralized Ni-Cu-PGE layered mafic-ultramafic intrusions are uncommon in the literature (Table 3.1; Ballhaus and Stumpfl, 1986; Frost and Touret, 1989; Larsen et al., 1992; Glebovitsky et al., 2001; Hanley et al., 2008; Somarin et al., 2009; Hanley and Gladney, 2011; Gál et al., 2013) and there are no reported fluid and melt inclusion data for barren layered-mafic ultramafic intrusions. Characterizing fluid and melt evolution is important in understanding the genesis of mineralized systems, notably if fluids have had an effect on metal mobility in the system at postcumulus conditions. It is also important to document fluid related processes in barren systems as well in order to understand how these processes alter the mineralogy and geochemistry of the rocks. A major challenge that needs to be addressed when comparing mineralized and barren systems, is to distinguish magmatic-hydrothermal events that are common to both settings from events that are unique to the mineralized setting.

A series of studies of layered mafic-ultramafic intrusions involving direct analyses of fluid inclusions or through mineral chemistry have documented volatile activity in primarily mineralized systems (Bushveld: Ballhaus and Stumpfl, 1986; Schiffries, 1990; Boudreau and Kruger, 1990; Mathez, 1995; Willmore et al., 2000; Stillwater: Boudreau and McCallum, 1989, 1992; Meurer et al., 1999; Polovina et al., 2004; Hanley et al., 2008; Lac des Iles: Somarin et al., 2009; Hanley and Gladney, 2011; Schisa et al., 2014; Skaergaard: Larsen et al., 1992; Duluth: Gál et al., 2013; Laramie: Frost and Touret, 1989; Lukkulaisvaara: Glebovitsky et al., 2001; Munni Munni: Boudreau et al., 1993; Great Dyke: Boudreau et al., 1995) and are supported by experimental studies

Table 3.1: Summary of relevant fluid and melt inclusion studies of layered mafic-ultramafic intrusions

Intrusion	Inclusion types and host mineral	Inclusion characteristics	Entrapment conditions	Reference
South Kawishiwi Intrusion, Duluth	Primary fluid and silictae melt inclusions hosted in quartz from a gabbroic pegmatite.	CO_2-H_2O-CH_4-N_2 fluid inclusions (95 mol% CO_2, 4.5 mol% H_2O, 0.4 mol% CH_4); silicate melt inclusions	T_t = 850° - 950°C; P_t ~1.7 kbar	Gál et al., 2013
North Roby Zone, Lac des Iles, Ontario	Primary carbonic fluid inclusions hosted in quartz, apatite, and magnesiohornblende from a gabbroic pegmatite	$CO_2 \pm CH_4 \pm H_2O \pm N_2$ (upto 10 mol% CH_4)	T_t (qtz)= 535° - 650°C; P_t (qtz)= 0.4 - 3.2 kbar	Hanley & Gladney, 2011
North Roby Zone, Lac des Iles, Ontario	Suspected primary fluid inclusions in plagioclase from a gabbroic pegmatite	CO_2-H_2O, CO_2-H_2O-NaCl (15-25 wt% $NaCl_{equiv.}$); H_2O-NaCl (21.6-48.5 wt% $NaCl_{equiv.}$); H_2O (13.18-25.5 wt% $NaCl_{equiv.}$)	T_t= ~707°C	Somarin et al., 2009
Stillwater Complex, Montana	Primary fluid and melt inclusions hosted in quartz from a gabbroic pegmatite and in olivine from an orthopyroxenite.	Polyphase brines (47-79 wt% $NaCl_{equiv.}$); Mixed polyphase brine-CO_2; CO_2; H_2O (6-29 wt% $NaCl_{equiv.}$); Halide melt inclusions (> 83 wt% $NaCl_{equiv.}$); silicate melt inclusions	Polyphase brine + Mixed polyphase brine-CO_2 + CO_2: $T_{t\ (graphic\ qtz)}$ = 700 - 715°C, $P_{t\ (graphic\ qtz)}$ = 4.3 - 5.6 kbar. Halide melt inclusions: T_t = 660 - 800°C	Hanley et al., 2008
Bushveld, South Africa	Secondary inclusions hosted within postcumulus quartz	NaCl-H_2O (>80 wt% $NaCl_{equiv.}$); Immiscible NaCl-H_2O-CO_2 (15-70 wt% $NaCl_{equiv.}$); Polyphase inclusions; CO_2; CH_4 , hydrated $CaCl_2$	T_t = 650° - 750°C; P_t = 4 - 5 kbar	Ballhaus & Stumpfl, 1986; Schiffries, 1990
Skaergaard Intrusion, Greenland	Primary inclusions hosted in apatite and granophyric quartz from gabbroic pegmatites	H_2O-NaCl-CH_4 (17.5-22.8 wt% $NaCl_{equiv.}$, < 6 mol% CH_4); immiscbile Fe- and Si-rich melt inclusions	T_t = 655° - 770°C; $T_m^{Liquidus}$= 1080°-1120 °C	Larsen et al., 1992; Jakobsen et al., 2011
Lukkulaisvaara Intrusion, Russia	Secondary inclusions hosted in quartz from gabbroic pegmatites, quartz veins, and alteration assemblages with sulfide minerals	H_2O-rich; CO_2-rich; H_2O-salt; CO_2-H_2O; H_2O-$NaCl_{(solid)}$-vapor; CH_4-N_2; CO_2-CH_4-N_2	T_t = 290° - 370°C; P_t = 1.5 - 2.5 kbar	Glebovitsky et al., 2001
Laramie Anorthosite Complex, Wyoming	Primary and secondary inclusions hosted in quartz from the Sybille Monzosyenite	CO_2-CH_4; H_2O; H_2O-NaCl fluid inclusions; carbonate-chloride-silicate-oxide melt inclusions.	Primary CO_2: T_t = 950° - 1000°C; P_t = 2.5 - 3.5 kbar	Frost & Touret, 1989

(e.g., Mathez and Webster, 2005). In these studies, volatile compositions range from high salinity aqueous-dominant brines, hydrosaline melts, and immiscible brine-carbonic fluids in the system NaCl-$CaCl_2$-H_2O-CO_2-CH_4 to more rarely documented H_2O-poor carbonic fluids ($CO_2 \pm CH_4$). Apatite mineral chemistry (i.e., halogen chemistry) in these systems provides evidence for the saturation of a high salinity brine at specific stages of melt evolution. Evidence for volatiles of variable composition exsolving from different parts of the cumulate pile, and the remobilization of ore metals by volatiles is abundant. For example, PGE grades may be positively correlated with hydrothermal alteration intensity but negatively correlated with sulphide content (Polovina et al., 2004). Direct measurements of ore metals in fluid inclusions show that the fluids were metal-bearing at the time of entrapment (Hanley, 2006 unpublished PhD thesis; Hanley and Gladney, 2011). However, these observations are heavily criticized by ore deposit geologists as being secondary in nature to primary metal enrichment by magmatic processes. Examining fluid and melt inclusions in robust mineral hosts in a barren system, such as the Caribou Lake Gabbro (CLG), can provide a better understanding whether these observations are common to all layered intrusions and allow the only method to see through the alteration of the system, notably alteration that occurred after magmatic-hydrothermal events occurred.

In this study, mafic pegmatites from the CLG hosting fluid and melt inclusions were studied using a variety of micro-analytical techniques [scanning electron microscopy-back scattered electron (SEM-BSE), scanning electron microscopy-energy dispersive X-ray (SEM-EDS), electron microprobe (EMP), Raman spectroscopy, laser ablation inductively coupled plasma mass spectrometery (LA-ICP-MS),

microthermometry, gas chromatography (GC)] were used to characterize these inclusions and provide the first detailed fluid inclusion study of the CLG. Collectively, the data gathered place first constraints on the P-T conditions of pegmatite crystallization and hydrothermal activity, and allow fluid sources to be considered.

3.1 Geological setting

3.1.1 Regional geology and tectonic setting

The CLG comprises the most western unit of the Blatchford Lake Intrusive Suite (BLIS), located ~90 km southeast of Yellowknife, NT along the Hearne Channel of Great Slave Lake (Figure 3.1A). The BLIS is situated at the southern margin of the Slave Province adjacent to the Athapuscow Aulacogen (Hoffman, 1973; Bowring et al., 1984). The BLIS is only weakly deformed, indicated by a weak, highly localized sub-vertical, northwest trending foliation and minor Proterozoic sub-vertical faults that trend north-south (Mumford, 2013 unpublished PhD Thesis). The BLIS intrudes into Archean metasedimentary rocks of the Burwash Formation (Yellowknife Supergroup), Morose granite, and Defeat granodiorite. In the region surrounding the BLIS, no reported volcanic rocks of a similar age or composition have been reported, implying that either the magma source responsible for the formation of the BLIS was restricted in its extent to the subsurface, or the volcanic equivalents were eroded away (Mumford, 2013 unpublished PhD Thesis). Tectonic reconstructions during the Paleoproterozoic suggest deformation along the southern Slave craton was influenced by: i) a failed rift (Bowring et al., 1984; Hoffman, 1973) or ii) transpressional forces extending the length of an oblique crustal-scale boundary (Hoffman, 1987; Hammer et al., 1992; Bleeker and Hall, 2007). Either of

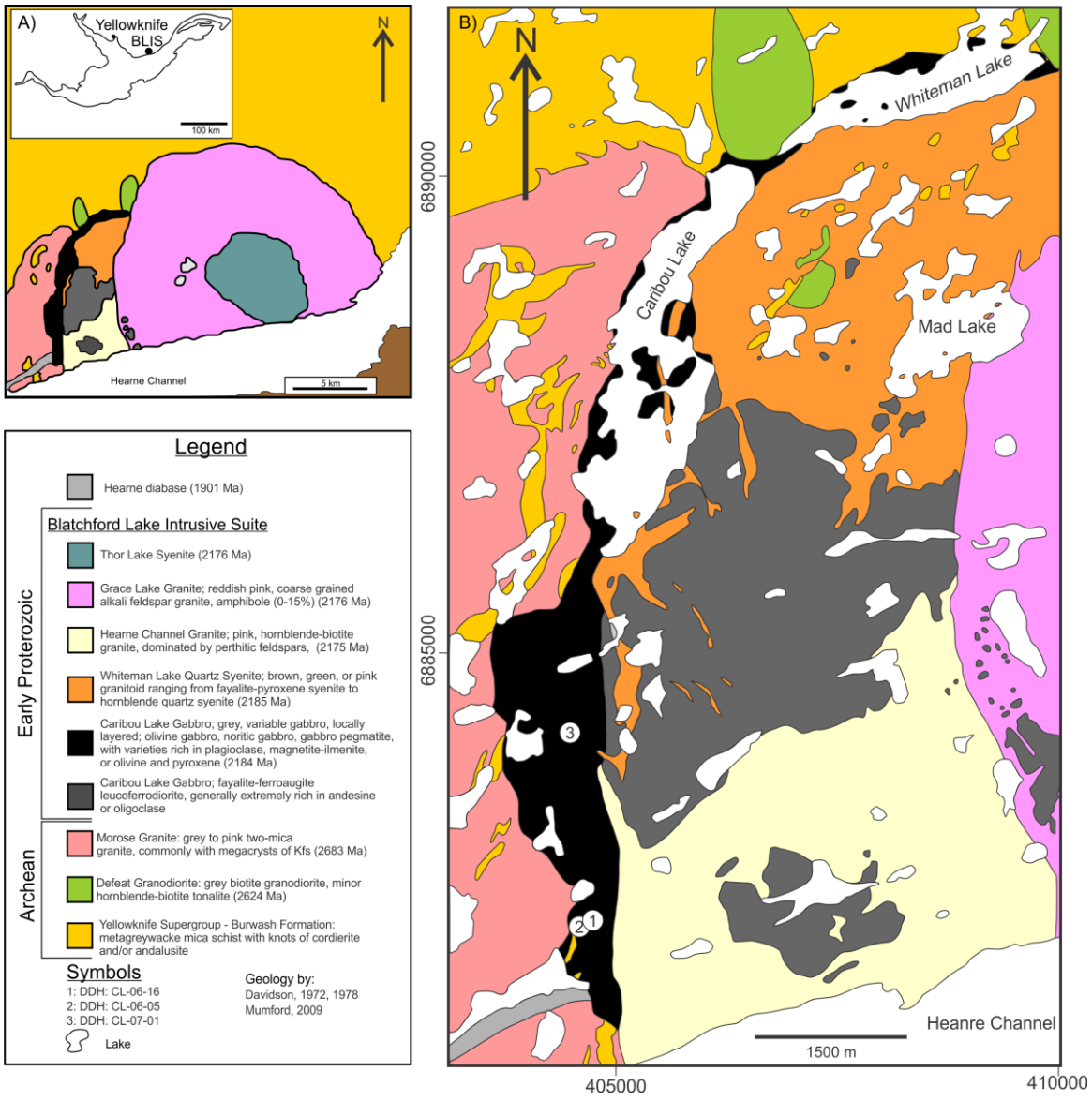

Figure 3.1: Regional and local geological maps of the Blatchford Lake Intrusive Suite. A) Location map and regional geological map of the Blatchford Lake Intrusive Suite, modified after Davidson (1982) and Mumford (2013, unpublished PhD Thesis). B) Detailed geological map of the western portion of the Blatchford Lake Intrusive suite, modified after Davidson (1982) and Mumford (2013, unpublished PhD Thesis). Locations of diamond drill holes (DDH) used in this study are shown as well.

these scenarios could result in crustal thinning, promoting decompressional melting and the establishment of deep seated structures (i.e., conduits) for migration of a mantle derived melt (Mumford, 2013 unpublished PhD Thesis) that acted as the parental melt for the BLIS. A metasomatized, depleted mantle source is suggested for the BLIS (Mumford, 2013 unpublished PhD Thesis).

3.1.2 Local geology

The CLG (2184 ± 2 Ma, Mumford, 2013 unpublished PhD Thesis) is the oldest and first magmatic phase of the BLIS which intrudes into the Archean sedimentary rocks of the Yellowknife Supergroup, the Morose granite, and the Defeat granodiorite (Figure 3.1B; Davidson, 1982). Davidson (1972, 1978, 1981, 1982) and Mumford (2013 unpublished PhD Thesis) identified five distinct units based on field relationships and geochronology: i) Caribou Lake Gabbro evolving from dunite to leucoferrodiorite (2184 ± 2 Ma, Mumford, 2013 unpublished PhD Thesis); ii) Whiteman Lake quartz syenite (2185 ± 2 Ma, Bowring et al., 1984); iii) Hearne Channel granite (2175 ± 5 Ma, Bowring et al., 1984); iv) Grace Lake granite (2176.2 ± 1.3 Ma, Sinclair et al., 1994); v) Thor Lake syenite (2164 ± 11 Ma, Mumford, 2013 unpublished PhD Thesis).

Geochemically, the BLIS can be broken into two distinct portions; an older sub-alkaline western lobe (Units i-iii) and a younger peralkaline eastern lobe (Units iv-v) (Davidson, 1981). Geophysical gravity studies by Birkett et al. (1994) and Pilkington (2012) suggests the BLIS is a relatively thin tabular body (~1 km thick) with a deep mafic (CLG) root at its western contact. The CLG also appears to extend under the Grace Lake granite for almost half of the entire surface area expression of the complex. Contacts between the CLG and its Archean host rocks are rarely observed due to cover by

vegetation, swamps, and/or lakes. However, a chilled margin occurs along the western contact and dips steeply (70-85°) away from the centre of the BLIS (Davidson 1972, 1978; Mumford, 2013 unpublished PhD Thesis). Progressive changes in rock texture and composition occur from west to east across the CLG beginning with pegmatitic patches along the west and north shores of Caribou and Whiteman Lakes, transitioning into a massive to poorly layered gabbro with a weak foliation defined by plagioclase, and progressing into a leucoferrodiorite as the most eastern portion of the CLG (Davidson 1972, 1978; Mumford, 2013 unpublished PhD Thesis).

The CLG is a crudely layered mafic-ultramafic intrusion that is composed of a variety of units. Diamond drilling in 2006 and 2007 by Kodiak Exploration Limited allowed for identification of multiple new lithologies that were not previously identified through surficial mapping by Davidson (1972, 1978). The dominant lithology throughout the CLG is a fine- to medium-grained gabbro that is comprised of olivine, clinopyroxene, plagioclase, and Fe-Ti oxides, with minor orthopyroxene and apatite. Ultramafic lithologies observed in drill core include dunite, clinopyroxenite, olivine clinopyroxenite, wehrlite, and troctolite. Other rock types observed include anorthosites and magnetitites and locally, pegmatitic gabbros occur. The CLG was predominantly formed through cumulate processes and is a very complex system (Mumford, 2013 unpublished PhD thesis). Correlation of individual units between closely spaced drill holes is extremely difficult due to lateral variability in texture and unit thickness. With the upper and lower contacts of ultramafic cumulate sections commonly bounded by massive gabbro, preserving the tops and bottoms of typical layered sequences, suggesting that the CLG

was formed from numerous small batches of magma instead of from a single batch of magma (Mumford, 2013 unpublished PhD Thesis).

Diamond drilling by Kodiak Exploration Limited in 2006 encountered massive to heavily disseminated sulphide in four drill holes, including 0.53 % Ni and 0.7 % Cu over 3.18 m (Marmont, 2006). Disseminated sulphides are hosted by a fine- to medium-grained gabbro and are composed of pyrrhotite with lesser amounts of chalcopyrite, pentlandite, and pyrite (Marmont, 2006). The relative stratigraphic position of sulphide mineralization in drill holes is variable, with semi-massive to massive sulphide encountered at a depth of ~20 m in diamond drill hole (DDH) CL-06-01, ~35 m in DDH CL-06-03, and ~80 m in DDH CL-07-05. All massive sulphide intersections were only 1.5 to 3 m thick with ~2 m of disseminated sulphide above and below and consist of the same mineralogy as the disseminated sulphides. Disseminated sulphide mineralization occurs in DDH CL-06-16 with a thickness of ~10 m over a depth of 53 to 63 m. Disseminated and massive sulphides show marginal enrichment in platinum group elements (PGE) (< 30 ppb Pd+Pt). Relatively high PGE (~100-200 ppb Pt+Pd) were intersected (DDH CL-07-09) in a fine-grained gabbro that contained minimal amounts of sulphide (< 3 vol %; Marmont, 2007). A detailed description of sulphide mineralization is presented in Chapter 2.

3.2 Methodology

Samples collected for this study were obtained during the 2013 summer field season. This field work involved detailed core logging and surface mapping of the CLG. Fluid and melt inclusions were observed in two different settings: i) in fine- to very

coarse-grained apatite hosted in highly altered mafic pegmatites (CL-07-01-127, -167, -173.9, CL-07-05-499); and ii) in fine- to medium- grained apatite hosted in a medium-grained gabbro (CL-07-01-29.1).

Petrographic characteristics (from thin and thick sections) were completed using an Olympus BX51 microscope, in transmitted and reflected light. The characterization of solid phases in exposed fluid and melt inclusions present at the surface of samples was conducted using a LEO1450VP scanning electron microscope (SEM) at Saint Mary's University, equipped with an energy dispersive X-ray (EDS) Oxford INCA 80mm^2 silicon drift detector (SDD) capable of quantitative analysis. All analyses were conducted at a working distance of ~20mm, with a beam current of 40 µA and accelerating voltage of 25-30 kV. Raw data were reduced using the software package INCA.

Drill core samples were sent to the Ontario Geological Survey GeoLabs in Sudbury, Ontario, for whole rock analyses. Major elements were determined by X-ray fluorescence spectrometry (XRF) on a borate flux-fused glass disk after loss of ignition (LOI) determination. Trace elements were analyzed by inductively-coupled plasma mass spectrometry (ICP-MS) after closed vessel, four acid (HF-HCl-HNO_3-$HClO_4$) digestion. Relative analytical uncertainties are within ± 5 % for all major elements and ± 3 % for most trace elements. Standards used were MRB-29, AGV-2, NPD-1, BHVO-2, LDI-2, SY-4, and GSP-2.

Fluid inclusion microthermometric measurements were performed on a Linkam FTIR600 heating-freezing stage mounted on an Olympus BX51 microscope at Saint Mary's University, Halifax, Canada. Calibration of the stage was completed using synthetic fluid inclusion standards of pure H_2O (melting at 0^{o}C and homogenization at

374.1°C) and pure CO_2 (melting at -56.6°C). Uncertainties for the microthermometric measurements are ± 0.2°C at a heating rate of 1°C/min, based on repeated analyses of these standards. For type S1 inclusions, the software of BULK and ISOC [Bakker, 2003; equations of state from Bowers & Helgeson (1983) and Bakker (1999)] were used to calculate molar volumes (cc/mol) and isochores, and utilized the mode of CO_2 homogenization (i.e., to liquid, to vapor, to supercritical fluid) and the temperature of CO_2 homogenization (Th_{CO2}). The presence of CO_2 clathrates were noted in type P2 and S3 inclusions ($Th_{CO2} > Tm_{CLA}$) and bulk salinities (wt % NaCl equivalent) were calculated using measured values of Tm_{CLA} following methods from Darling (1991) and Diamond (1992).

Microthermometry of melt inclusions were performed using a Linkam TS1500 equipped-heating stage with sapphire heating plates mounted on an Olympus BX53 microscope with a Q imaging colour video camera. Heating rates varied between 10°C/min and 100°C/min, and a flow rate of 40 mL/min of Ar gas was used to try and prevent oxidation of melt inclusions and their apatite host during heating. The error associated with the absolute temperature is ±2°C based on monitoring of fixed temperature stability. Pure Ag (961.8°C), Au (1064°C), and Cu (1085°C) metals were used as standards to calibrate the stage by measuring their melting points and comparing them against accepted values to create a linear calibration curve to correct observed temperatures to actual temperatures.

Qualitative Raman spectroscopy was performed on polished thick sections containing fluid inclusions at Saint Mary's University, Halifax. The instrument used was a Jobin-Yvon Horiba LabRam HR confocal Raman microscope with an 800 mm

spectrograph and Synapse 1024 x 256 pixel CCD detector. A 1800 groves/mm grating and 25 µm confocal hole size were used during spectrum collection, with a 532 nm (green) Nd-YAG laser (105 mW laser power at objective) was used for excitation, directed through a 100x objective. Pure silicon was used as a frequency calibration standard. Spectrum collection over the range 100-4000 cm^{-1} was done at an acquisition of 0.5s per accumulation with 60 accumulations obtained per inclusion analysis. Using the empirical quantification parameters and methodologies summarized by Wopenka and Pasteris (1986, 1987), Dubessy et al. (1989), Burke (2001), and Beeskow et al. (2005), semi-quantitative determination of gas species relative abundances (in mol %) were calculated. Wavelength-dependant relative Raman scattering cross-sections ($\sigma_{532\ nm}$) for each gas species were determined by interpolation from Table 2 in Burke (2001). Instrument efficiencies (ζ) for CO_2 and CH_4 were determined by comparing microthermometrically-determined CO_2 and CH_4 contents to those determined by Raman spectroscopy for quartz-hosted CO_2-CH_4 standard inclusions from the South Wales Coal Field (Beeskow et al., 2005). Uncertainties in calculated mole fractions of species present in the carbonic phase of the inclusions are within 20 % relative.

Gas chromatographic (GC) analysis was performed on samples of fragmented apatite extracted from a mafic pegmatite (CL-07-01-127). All samples were fragmented and hand-picked for GC analysis (1-3 mm in maximum dimension). Fragments were washed twice in deionized water, treated with a 1M HCl solution overnight to remove any carbonates present, and re-washed and sonicated in deionized water to remove any remaining residue. Samples were then dried on a hot plate in a sterile glass vial and

weighed prior to analysis. Gas chromatographic analysis of bulk fluid inclusion volatiles was conducted at Saint Mary's University using an Agilent 7890 series gas chromatograph equipped with a micro-thermal conductivity detector (TCD) and $2H_2$-flame ionization detectors (FID), one installed in tandem with the TCD and the other on an independent valve-flow path. For determination of trace hydrocarbon phases (Method 2), an alumina-PLOT capillary analytical column (50 m × 0.53 mm × 10 μm) was used in series with a flame ionization detector (FID) capable of analyzing combustible compounds (e.g., alkanes, alkenes/alkynes, thiols). For the analysis of non-combustible volatile species (e.g., H_2O, CO_2; Method 1) an alumina-PLOT analytical column (30m x 0.53 mm x 10 μm) was using in series with a thermal conductivity detector (TCD) and FID. Raw data was compiled by the software package Agilent Chromatographic Chemstation® and then, by using the calibration curves composed of standard gas mixtures (Matheson Tri-Standards), the sample data was converted to moles/g of rock. For detailed analytical procedure and quality control evaluation for routine analyses at Saint Mary's University (Department of Geology), see Kerr et al. (2015).

Electron microprobe analyses of apatite, biotite, amphibole, and plagioclase were performed using a Cameca SX-50 electron microprobe (EMP) at the University of Toronto. The instrument was operating at 15 kV accelerating voltage with a 20 nA beam current for all mineral analyses. The beam diameter was 15 μm for apatite and 10 μm for biotite, amphibole, and plagioclase analyses. Raw microprobe data count rates were converted to concentrations using the ZAF data reduction scheme using the software Probe for $EMPA_{TM}$ (Advanced Microbeam Inc.).

Trace element concentrations from individual apatite grains were determined by LA-ICP-MS at Laurentian University, Sudbury, Ontario using a Thermo X Series II quadrupole ICP-MS coupled to a Resonetics RESOlution M50 laser ablation system using a 193 nm, 20 ns pulse ArF Excimer laser. Ablation occurred in He (650 mL/min), which was combined with a small amount of high purity N_2 (6 mL/min) and Ar (800 mL/min) before being fed into the plasma. Dwell time for all elements was 10 ms and oxide production rates were maintained below 0.3 % (ThO/Th checked on NIST 612). Calibration of analyte sensitivities utilized the standard reference material 610 from NIST. Standards were bracketed between every ten analyses to correct for instrumental drift. Apatite measurements consisted of 30 seconds of a gas blank (laser off) followed by ~25-35 seconds of sample ablation. The laser conditions used were: repetition rate of 5 Hz, a spot size of 66 µm, and a fluence of 6 J/cm^2. Trace element quantification of apatite analyses was performed using the software SILLS (Guillong et al, 2008). For complete operation conditions of the LA-ICPMS system see Appendix 2. Internal standardization utilized the Ca content of the apatite determined independently by EMP.

Trace element concentrations of fluid and silicate melt inclusions and the apatite host mineral were measured by LA-ICP-MS at Virginia Tech, Blacksburg, Virginia, using an Agilent 7500ce quadrupole ICP-MS and a Lambda Physik GeoLas 193 nm excimer laser ablation system. The laser is attached to an Olympus petrographic microscope equipped with a 25x UV-VIS Schwarzschild objective for analyses, and 5x and 10x objectives for transmitted light viewing of the sample. The He carrier gas flow was ~1 L/min through an ablation cell with a volume of ~1 cm^3. Dwell time for all isotopes was 10 ms, except for Pd^{108}, Pt^{195}, and Au^{197} (50 ms) and Ni^{62}, As^{75}, Ta^{181}, and W^{182} (30 ms)

to improve detection limits. For silicate melt inclusions all dwell times for all isotopes was 10 ms. Oxide production rates were maintained below 1 %. Calibration of analyte sensitivities utilized the standard glass reference material 610 from NIST (National Institute of Standards and Technology) for both fluid and silicate melt inclusions and the PGE-bearing pyrrhotite standard PO724 from by Memorial University (Sylvester et al., 2005) additionally for fluid inclusions. Each standard was ablated twice before and after each analytical session containing a total of 15-25 analyses (for fluid inclusions and host analyses) and 12 analyses (silicate melt inclusions and host analyses) for drift correction prior to data reduction. Fluid inclusion measurements each consisted of 40-60 seconds of gas blank before the laser was turned on. A beam diameter slightly larger than fluid inclusions ranging from 16-32 µm was used, host ablations were done with a spot size of 24 µm, which was the most common spot size used to ablate inclusions. Silicate melt inclusions used a beam diameter of 32-120 µm and 44-60 µm for the apatite host. Aerosols were generated using a pulsed beam at a repetition rate of 5 Hz for fluid inclusions and 10 Hz for silicate melt inclusions and both had an output energy of 150 mJ. Since the majority of inclusions were not exposed at surface the host phase was ablated before opening the inclusion and ablation was stopped once the entire inclusion was ablated. For complete operation conditions of the LA-ICP-MS system see Appendix 2.

Trace element quantification of the fluid and silicate melt inclusions was performed using the software SILLS (Guillong et al., 2008). This involved deconvoluting the mixed fluid/silicate melt inclusion + host signal from the host only signal after calculation of background corrected count rates for each isotope, and quantification of

inclusion and host compositions. Absolute trace element concentrations could not be quantified because of the lack of internal standard (bulk inclusion salinity), since carbonic inclusions lacked a visible aqueous phase, no salinity estimate of the aqueous component could be determined. Under normal circumstances, brine-carbonic fluid inclusion trace element concentrations can be quantified by using wt % NaCl equiv. as an internal standard and determining the bulk salinity of the inclusion. However, due to the presence of silicates in these inclusions (see results below), this method cannot be applied because it is not known how much Na is being contributed by the silicates. Therefore, fluid inclusions were quantified by assuming 100 % total oxides in the inclusions and using La as a matrix (i.e., apatite) only tracer. Values obtained from this method are only maximum values because they do not take into account Cl, H_2O, and CO_2 and therefore the data are only semi-quantitative allow for general correlations to be explored. Quantification of silicate melt inclusions and host compositions utilized SiO_2 as internal standard of the melt inclusions determined separately by SEM. With the inclusions being polyphase, complete inclusions buried below the mineral surface needed to be analyzed because if the inclusions were exposed at surface, all phases may not be present within a single inclusion due to grinding and polishing during sample preparation.

3.3 Results

3.3.1 Petrography of fluid and melt inclusion bearing rocks and mineral compositions

Silicate melt inclusions are hosted in cumulus apatite grains within a fine- to medium-grained gabbro (CL-07-01-29.1; Figure 3.2A-C). Apatite (5-7 vol %) occurs as ≤ 0.5 mm, anhedral-subhedral equant inclusions within plagioclase, clinopyroxene, olivine,

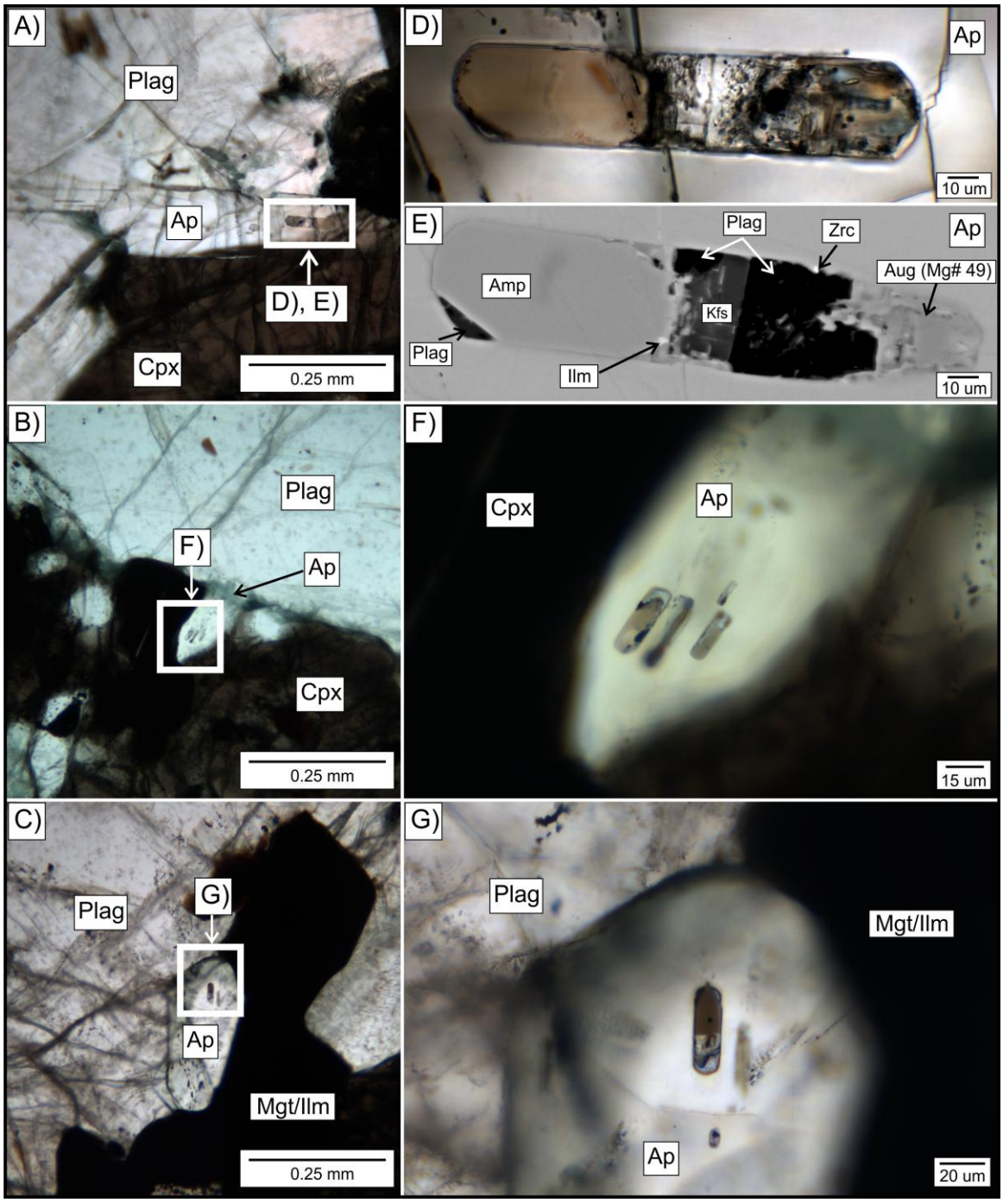
A)
Plag
Ap
D), E)
Cpx
0.25 mm
D)
Ap
10 um
E)
Plag
Zrc
Ap
Amp
Aug (Mg# 49)
Kfs
Plag
Ilm
10 um
B)
Plag
F)
Ap
Cpx
0.25 mm
F)
Cpx
Ap
15 um
C)
Plag
G)
Ap
Mgt/Ilm
0.25 mm
G)
Plag
Mgt/Ilm
Ap
20 um

Figure 3.2 (previous page): Petrographic characteristics of apatite and silicate melt inclusion in a fine- to medium-grained gabbro (CL-07-01-29.1). A) Photomicrograph of apatite hosting a large silicate melt inclusion. Plane polarized light (PPL). B) Apatite partially included in clinopyroxene hosting fine-grained melt inclusions that are elongated in the same direction as the apatite grain. PPL. C) Photomicrograph of apatite hosting small melt inclusions that also parallel the elongation axis of the apatite grains as in the grains in D and A. PPL. D) Magnified view of the melt inclusion outlined in A). PPL. E) SEM-EDS image of the melt inclusion outlined in A). Minerals identified in the inclusion include: Aug, Plag, Kfs, Ilm, and Zrc. F) Magnified view photomicrograph of melt inclusions outlined in D). PPL. G) Magnified view photomicrograph of melt inclusions outlined in F. PPL. Note that the phases in melt inclusions present in E and G could not be identified through SEM-EDS because they were not exposed at surface. Amp = amphibole; Ap = apatite; Aug = augite; Cpx = clinopyroxene; Kfs = K-feldspar; Ilm = ilmenite; Mgt/Ilm = magnetite/ilmenite composite grain; Plag = plagioclase; Zrc = zircon.

ilmenite, magnetite, and biotite. Apatite is also a common interstitial matrix phase as well, where grains are ≤ 1.5 mm, anhedral-subhedral, and equant to tabular in form. Apatite is has higher concentrations of F compared to Cl, containing up to 3.6 wt % F (3.22 ± 0.26 wt %; n=10), with Cl up to 0.14 wt % (0.09 ± 0.04 wt %; n=10). Mole fraction chlorapatite (X_{Cl}) ranges from 0.002 to 0.02 and mole fraction fluorapatite (X_F) from 0.79 to 0.98, thus approaching end-member fluorapatite (Figure 3.3). Plagioclase (An_{37-40}; 60-65 vol %) grains are 0.5-8 mm (~1.7 mm), tabular, and euhedral-subhedral. Clinopyroxene (20-25 vol %) occurs interstitial to plagioclase and grains are ≤ 3 mm (~1.2 mm), subhedral-anhedral, and contains < 0.5 mm inclusions of magnetite/ilmenite composite grains. Minor amounts of olivine are present (3-5 vol %) and is generally alterd to serpentine, with only a few grains unaltered. Grains are ≤ 2.5 mm (~1.5 mm), highly fractured with magnetite commonly infilling the fractures, and occurring interstitial to plagioclase. Interstitial biotite (2-3 vol %) grains are ≤ 2 mm (~1 mm), euhedral and tabular. Biotite in CL-07-01-29.1 (Figure 3.4A) also contains more F than Cl, with up to 0.09 wt % F (0.07 ± 0.02 wt %; n=2) and up to 0.06 wt % Cl (0.05 ± 0.01 wt %; n=2). Biotite is also common as rims on magnetite-ilmenite grains. Trace amounts of primary amphibole (grains are < 0.5 mm) are present as an interstitial phase. Magnetite-ilmenite (5 vol %) grains are ≤ 2 mm (~0.9 mm), anhedral, occur interstitial to plagioclase, and display blebby and trellis style exsolution of ilmenite from an original titanomagnetite grain.

Primary and secondary fluid inclusions are hosted in early coarse-grained apatite (i.e., is not interstitial) in moderate to highly pervasively altered mafic pegmatites and is enclosed by altered clinopyroxene and plagioclase (CL-07-01-127, 167, 173.9; CL-07-05-

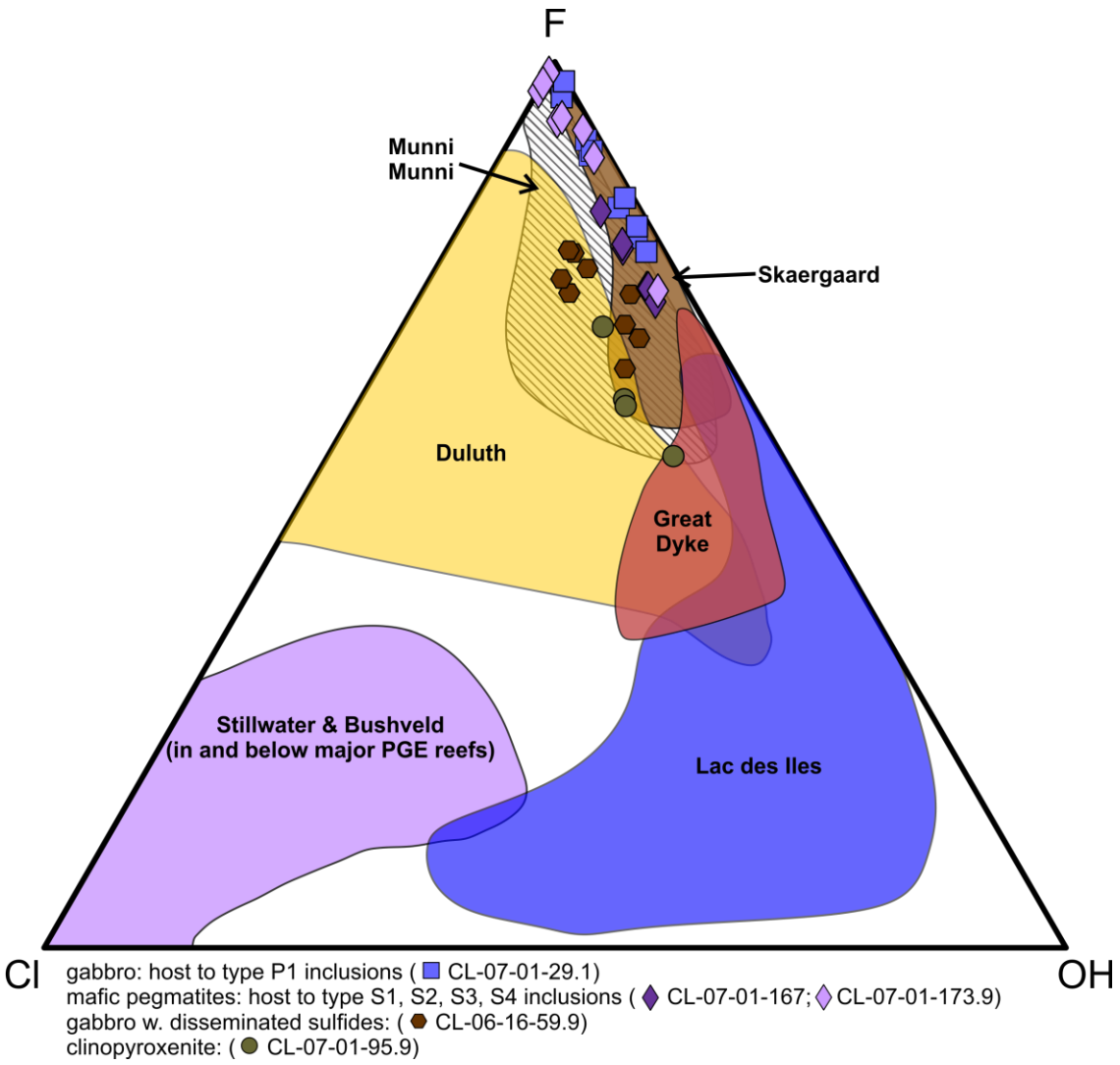

Figure 3.3: Triangular plot of mole proportions of F-Cl-OH of apatite from fluid and melt inclusion bearing lithologies, clinopyroxenite, and a gabbro hosting disseminated sulphides from the CLG compared to apatite compositions from other Ni-Cu-PGE deposits globally (Stillwater, Bushveld, and Skaergaard complexes, Great Dyke: Boudreau, 1995; Lac Des Iles: Schisa et al., 2014; Duluth: Gál et al., 2014).

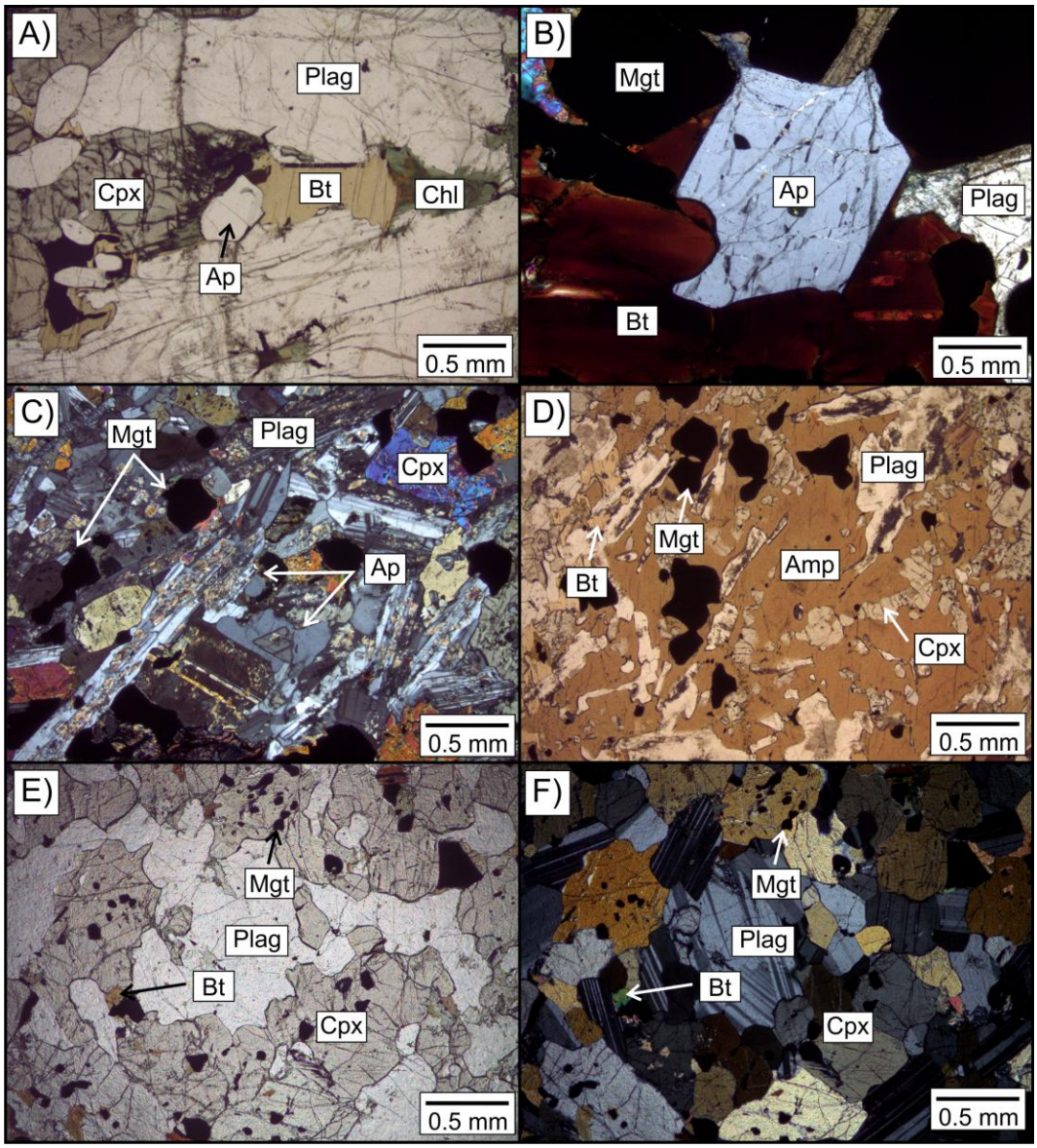

Figure 3.4: Representative microphotographs of various minerals in the CLG. A) Cumulate apatite and interstitial biotite used for the apatite-biotite thermometer for CL-07-01-29.1. PPL. B) Interstitial apatite and biotite in a clinopyroxenite (CL-07-01-95.9). XPL. C) Fine-grained interstitial apatite hosted in a fine-grained gabbro (CL-06-16-59.9). XPL. D) Amphibole phenocryst with inclusions of plagioclase, clinopyroxene, and magnetite. This amphibole was used for amphibole-plagioclase thermometer and Al-in-hornblende barometer. PPL. E) Representative microphotograph of an unaltered fine-grained gabbro used for geochemistry comparisons to fluid and melt inclusion bearing samples. PPL. F) Same as E but in XPL. Amp = amphibole; Ap = apatite; Bt = biotite; Chl = chlorite; Cpx = clinopyroxene; Mgt = magnetite; Plag = plagioclase.

499; Figure 3.5 A, B). Coarse-grained apatite in the mafic pegmatites is 5 to 20 mm in length (avg. 10 mm), weakly to highly fractured, and is anhedral to euhedral (Figure 3.5 C-F). Apatite in the mafic pegmatites have higher concentrations of F (up to 3.77 wt %; 3.19 ± 0.4 wt %; n=15) compared to Cl (up to 0.27 wt %; 0.20 ± 0.07 wt %; n=15). Mole fraction X_{Cl} ranges from 0.01 to 0.04 and X_F from 0.73 and 1.0 (Figure 3.3). Minor amounts of euhedral ~1 mm apatite are present as inclusions within clinopyroxene and composite magnetite-ilmenite grains. Primary silicate minerals in the mafic pegmatites are clinopyroxene, plagioclase, minor orthopyroxene and biotite. Biotite from CL-07-01-173.9 generally has higher concentrations of Cl compared to F, with up to 0.62 wt % Cl (0.42 ± 0.16 wt %; n=8) and up to 0.36 wt % F (0.15 ± 0.12 wt %; n=8). Clinopyroxene is moderately to completely altered to amphibole and plagioclase is typically highly sericitized and alteration for both minerals is pervasive throughout all examined pegmatites. Amphibole is also commonly altered along its edges to biotite and/or chlorite. A minor amount of spotty calcite alteration is present in the pegmatites as well. Minor amounts of sulphides and oxides are present in the mafic pegmatites (pyrrhotite, chalcopyrite, sphalerite, pentlandite, magnetite, and ilmenite).

Coarse-grained, an-subhedral interstitial apatite occurs in a clinopyroxenite (CL-07-01-95.9; Figure 3.4A) where it occurs interstitial to biotite, plagioclase, and magnetite (Figure 3.4A). Apatite in the clinopyroxenite is also F-rich but contains slightly more Cl than the fluid and melt inclusion bearing samples (2.68 ± 0.18 wt % F, 0.62 ± 0.13 wt % Cl, n=9) with X_{Cl} between 0.06 and 0.12 and X_F between 0.65 and 0.79. Biotite from the clinopyroxenite (Figure 3.4A) also has higher concentrations of F compared to Cl (0.26 ± 0.08 wt % F, 0.12 ± 0.02 wt % Cl, n=5).

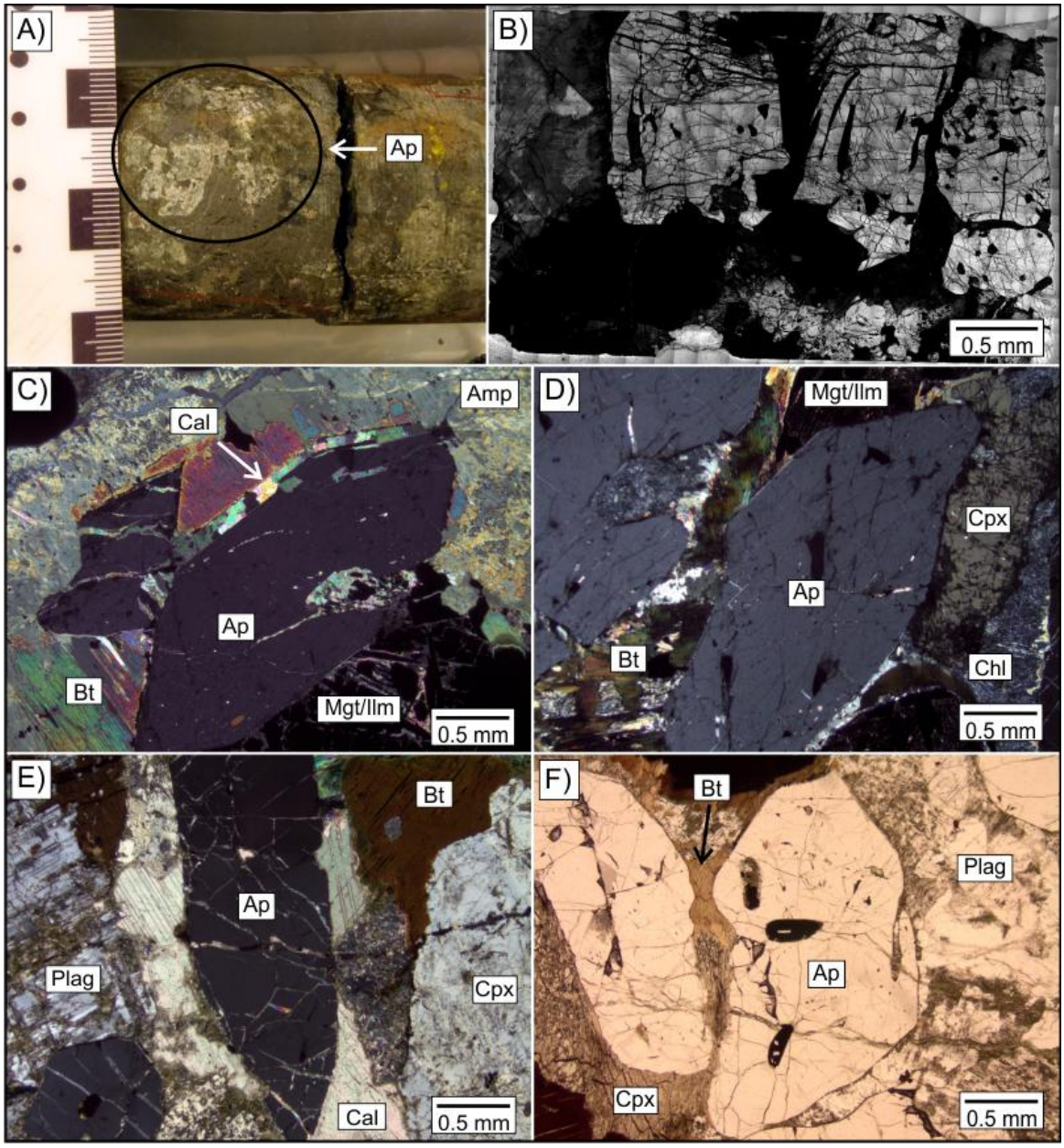
A)
Ap
B)
0.5 mm
C)
Amp
Cal
Ap
Bt
Mgt/Ilm
0.5 mm
D)
Mgt/Ilm
Cpx
Ap
Bt
Chl
0.5 mm
E)
Bt
Ap
Plag
Cpx
Cal
0.5 mm
F)
Bt
Plag
Ap
Cpx
0.5 mm

Figure 3.5 (previous page): Drill core and thin section photographs of fluid inclusion-bearing apatite in the CLG. A) Photograph of drill core from diamond drill hole CL-07-01 at a depth of 127 m showing extremely coarse-grained apatite (circled) hosted in a highly altered mafic-ultramafic pegmatite. B) Scanned image of CL-07-01-127 thin section showing the extremely coarse-grained nature of apatite. C) Photomicrograph of coarse-grained apatite from CL-07-01-127 and the various alteration minerals present in the unit. Cross polarized light (XPL). D) Photomicrograph of coarse-grained apatite in CL-07-01-167 and various alteration and minor primary minerals. XPL. E) Photomicrograph of coarse-grained apatite in CL-07-01-173.9 and various alteration and primary igneous minerals. XPL. F) Photomicrograph of coarse-grained apatite from CL-07-01-173.9 and primary igneous minerals present in the sample. Plane polarized light. Alt = alteration pod of chlorite + amphibole; Amp = amphibole; Ap = apatite; Bt = biotite; Cal = calcite; Chl = chlorite; Cpx = clinopyroxene; Mgt/Ilm = magnetite and ilmenite composite grain; Plag = plagioclase.

Anhedral apatite is also present as a fine-grained interstitial phase in fine-grained gabbros and contains the most Cl-rich apatite analyzed in the CLG (0.77 ± 0.08 wt % Cl, 2.25 ± 0.22 wt % F; n=4) with X_{Cl} from 0.1 up to 0.12 and X_F is between 0.55 and 0.70. (CL-06-16-59.9; Figure 3.4B). Amphibole phenocrysts occur in CL-06-16-59.9 as well and contain abundant inclusions of plagioclase, clinopyroxene, and magnetite (Figure 3.4C). Amphibole and plagioclase compositions from a fine-grained gabbro with minor disseminated sulphides were also analyzed by EMP. Amphibole (*var*. magnesio-hastingsite; Figure 3.4C) has variable F and Cl contents ranging from below detection limits (b.d.l) to 0.14 wt % F (~0.07 ± 0.04 wt % F, n=7) and from 0.05 to 0.12 wt % Cl (~0.09 ± 0.02 wt % Cl, n=10). Plagioclase (*var*. labradorite; Figure 3.4C) has a range in anorthite content from 50 to 61. Representative apatite and biotite and amphibole and plagioclase analyses are presented in Table 3.2 and Table 3.3, respectively. For comparison purposes, Figure 3.4D and E, show microphotographs of unaltered fine-grained gabbros, which consist of plagioclase, clinopyroxene, and minor biotite and magnetite.

Melt and fluid inclusion bearing apatite analyzed by LA-ICP-MS show enrichment in LREE compared to HREE when normalized to chondrite and have enriched trace element patterns compared to primitive mantle (Figure 3.6A, B). As well, based on the fields of Belousova et al., (2002), apatite from the CLG predominately falls in the mafic rocks and iron ore fields (Figure 3.6C).

3.3.2 Whole rock geochemistry

The major and trace element data of the fluid and melt inclusion bearing rocks are summarized in Table 3.4 and major (Figure 3.7A) and selected incompatible trace

Table 3.2: Representative apatite and biotite EMP analyses and calculated temperatures based on the apatite-halogen exchange thermometer

diamond drill hole	CL-07-01	CL-07-01	CL-07-01	CL-07-01	CL-07-01	CL-07-01	CL-07-01	CL-07-01	CL-07-01	CL-06-16	CL-06-16
depth (m)	29.1	29.1	167	167	173.9	173.9	173.9	95.9	95.9	59.9	59.9
apatite analyses											
apatite number	Ap-5-Area 1	Ap-7-Area 1	Ap-5-Rim	Ap-6	Ap-2	Ap-3	Ap-6	Ap-3	Ap-5	Ap-1	Ap-2
CaO	54.7	54.9	54.2	54.9	54.0	53.9	54.5	54.6	54.6	54.1	53.3
P_2O_5	41.0	41.4	40.9	41.2	40.8	41.1	40.8	41.0	41.1	40.9	40.5
F	2.94	3.00	2.89	3.06	3.43	3.45	3.28	2.89	2.52	2.00	2.54
Cl	0.13	0.09	0.27	0.27	0.21	0.17	0.11	0.63	0.50	0.71	0.69
La_2O_3	0.04	0.08	0.05	0.11	0.20	0.29	0.14	0.08	0.13	0.08	0.01
Ce_2O_3	0.13	0.17	0.16	0.25	0.48	0.51	0.65	0.28	0.18	0.17	0.24
Nd_2O_3	b.d.l	0.13	0.03	b.d.l	0.13	0.12	0.14	0.04	0.07	b.d.l	b.d.l
Total	98.1	98.7	98.5	98.8	98.7	98.7	98.8	98.4	98.4	97.2	98.0
thermobarometric parameters from apatite recalculation [1]											
X_F	0.80	0.81	0.79	0.83	0.93	0.94	0.89	0.79	0.69	0.55	0.70
X_{Cl}	0.02	0.01	0.04	0.04	0.03	0.02	0.02	0.09	0.07	0.11	0.10
X_{OH}	0.18	0.17	0.17	0.13	0.04	0.04	0.09	0.12	0.24	0.34	0.20
X_F/X_{OH}	4.44	4.69	4.58	6.40	25.8	24.1	9.58	6.53	2.87	1.61	3.50

biotite analyses								
biotite number	Ap-Bt-5	Ap-Bt-7		Ap-Bt-2	Ap-Bt-3	Ap-Bt-6	Ap-Bt-3	Ap-Bt-5
SiO_2	35.0	35.1		34.8	35.2	35.4	36.5	36.0
TiO_2	6.41	6.32		4.99	4.69	4.08	5.91	5.69
Al_2O_3	13.4	13.3		11.2	11.5	12.6	13.6	13.5
FeO	23.0	23.0		30.8	29.9	24.7	15.6	16.8
MnO	0.16	0.13		0.20	0.22	0.21	0.11	0.05
MgO	8.77	8.76		5.06	5.18	8.92	14.6	14.7
CaO	b.d.l	0.03		0.07	0.02	0.04	0.06	0.04
Na_2O	0.16	0.18		0.23	0.18	0.50	0.71	0.69
K_2O	9.71	9.60		8.95	9.07	9.36	8.97	9.05
F	0.09	0.06		0.19	0.13	0.27	0.21	0.39
Cl	0.06	0.04		0.53	0.62	0.33	0.13	0.14
H_2O	3.71	3.67		3.43	3.47	3.58	3.43	3.46
Oxide Totals	100.4	100.1		100.3	100.1	99.8	99.8	100.4
thermobarometric parameters from coexisting biotite recalculation [2]								
X_F	0.01	0.01		0.02	0.02	0.03	0.02	0.05
X_{Cl}	0.00	0.00		0.04	0.04	0.02	0.01	0.01
X_{OH}	0.98	0.99		0.94	0.94	0.94	0.97	0.94
X_{Fe}	0.73	0.73		0.84	0.83	0.73	0.57	0.58
X_F/X_{OH}	0.01	0.01		0.03	0.02	0.04	0.03	0.05
thermobarometric calculations								
$K_{D,F}$ [3]	5.98	6.49		6.92	7.24	5.59	5.54	4.07
T (°C)[4]	545	494		487	459	588	540	749

[1] Determined from apatite compositions recalculated assuming 2OH and 12 (OH, O, F, Cl)

[2] Determined from biotite compositions recalculated assuming 2OH and 24 (OH, O, F, Cl)

[3] Calculated F-OH exchange coefficient for coexisting apatite-biotite using formulation of Zhu and Sverjensky (1992)

[4] Calculated temperature of final equilibrium using F-OH exchange thermometer expression of Zhu and Sverjensky (1992)

Table 3.3: Representative EMP analyses of amphibole and plagioclase from CL-06-16-59.9 and calculated temperatures and pressures from the amphibole-plagioclase thermometer and Al- and Ti-in-hornblende thermobarometer

amphibole EMP data					
SiO_2 (wt %)	41.3	41.1	40.9	41.4	41.3
TiO_2	4.10	3.27	3.82	4.15	4.09
Al_2O_3	12.1	11.9	12.4	11.9	12.0
FeO	14.6	16.0	15.4	15.0	14.6
MgO	11.5	11.5	11.4	11.4	11.7
MnO	0.16	0.18	0.17	0.14	0.16
CaO	11.7	11.1	11.3	11.6	11.8
Na_2O	2.54	2.26	2.43	2.41	2.38
K_2O	1.21	1.05	1.06	1.21	1.20
F	0.07	0.06	0.07	b.d.l.	0.14
Cl	0.10	0.06	0.11	0.08	0.12
NiO	b.d.l.	0.04	0.03	0.04	0.02
Cr_2O_3	b.d.l.	0.01	0.01	0.00	0.02
V_2O_3	0.07	0.04	0.08	0.09	0.07
H_2O	0.94	0.94	0.94	0.94	0.94
Total	100.31	99.46	99.99	100.38	100.44
plagioclase EMP data					
SiO_2 (wt %)	55.0	55.0	55.1	54.7	53.7
TiO_2	0.11	0.06	0.00	0.05	0.02
Al_2O_3	29.2	28.9	29.2	29.0	28.3
FeO	0.24	0.50	0.22	0.18	2.05
MgO	0.00	0.08	0.01	0.02	0.98
MnO	b.d.l.	0.02	0.00	b.d.l.	0.05
CaO	10.7	10.3	10.4	10.5	9.82
Na_2O	5.38	5.65	5.47	5.55	5.15
K_2O	0.12	0.07	0.09	0.14	0.18
Total	100.8	100.5	100.5	100.1	100.2
thermobarometric and classification parameters from amphibole recalculation [1]					
Si p.f.u.	6.07	6.08	6.03	6.09	6.08
Al^{IV}	1.93	1.92	1.97	1.91	1.92
Al^{VI}	0.18	0.16	0.18	0.16	0.16
Al_{TOT}	2.10	2.08	2.15	2.07	2.08
Mg	2.52	2.53	2.50	2.51	2.56
Fe^{2+}	1.55	1.37	1.44	1.54	1.51
thermobarometric and classification parameters from plagioclase recalculation [2]					
Ab	47.3	49.7	48.4	48.4	48.1
An	52.0	49.9	51.0	50.8	50.8
thermobarometric calculations					
T (°C)[3]	915	909	918	914	907
T (°C)[4]	1075	925	990	1010	995
P (kbar)[4]	2.65	1.60	3.50	2.61	2.65

[1]Cations calculated on the basis of 23 (O, F, Cl) p.f.u.

[2]Cations calculated on the basis of 32O

[3]Calculated using the hornblende-plagioclase thermometer of Holland and Blundy (1990) assuming a constant P of 2 kbar; change in P of 0.5 kbar results in 7°C change on calculated temperature

[4]Calculated using the Al- and Ti-in-hornblende barometer of Ernst and Liu (1998)

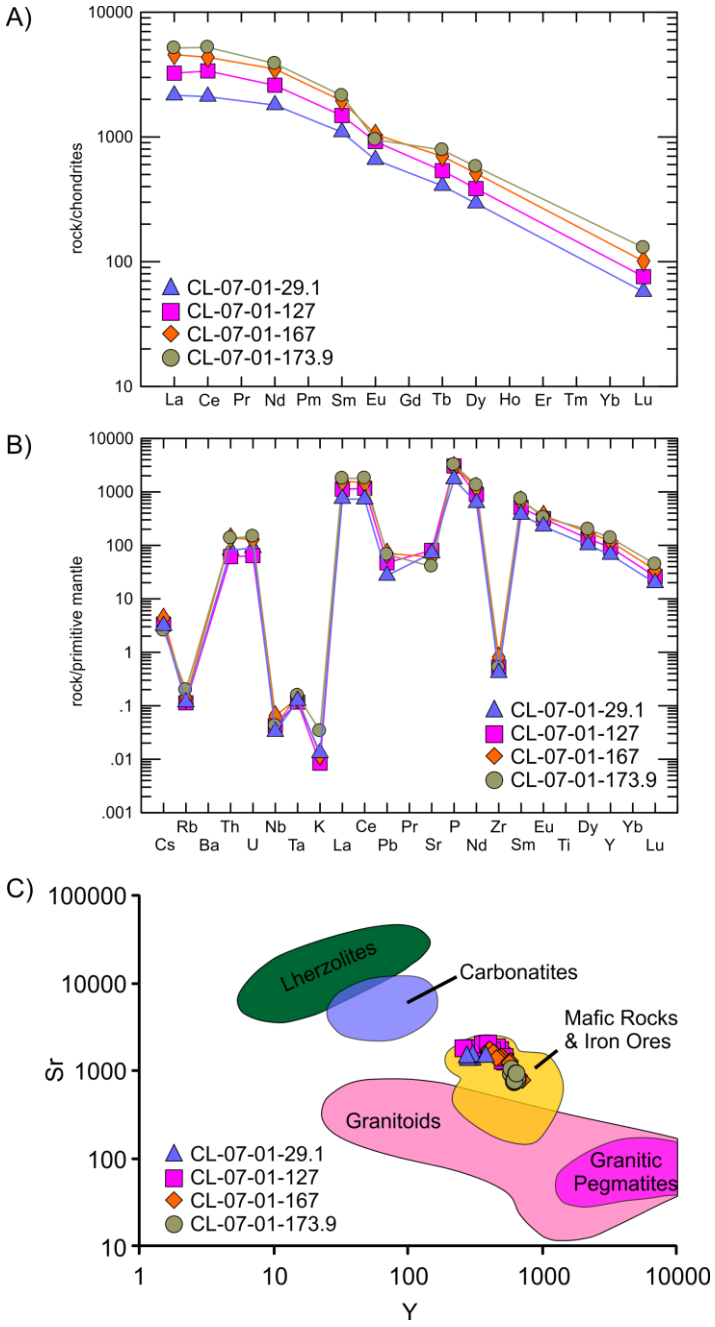

Figure 3.6: Apatite trace element geochemistry. A) Average apatite trace element compositions normalized to chondrite, note the steep LREE:HREE slope. B) Average apatite trace element compositions normalized to primitive mantle. C) Plot of Sr against Y content in apatite. Different rock type fields are from Belousova et al. (2012). Note how the CLG apatites plot in the mafic rocks and iron ore compositional field.

Table 3.4: Major and trace element geochemistry of fluid and melt inclusion bearing rocks and an unaltered fine grained gabbro

lithology	gabbro	mafic peg[1]	mafic peg[1]	mafic peg[1]	mafic peg[1]	gabbro[2]
diamond drill hole	CL-07-01	CL-07-01	CL-07-01	CL-07-01	CL-07-05	CL-07-01
depth (m)	29.1	127	167	173.9	499	354.2
SiO_2 (wt%)	39.3	28.7	39.1	39.0	40.2	41.3
TiO_2	4.55	6.56	2.61	4.62	4.43	3.25
Al_2O_3	11.0	4.1	13.3	10.3	11.9	12.5
Fe_2O_3	22.5	33.8	18.4	24.4	19.2	20.0
MnO	0.33	0.42	0.19	0.32	0.28	0.22
MgO	5.11	6.84	8.31	4.14	5.53	7.97
CaO	10.6	12.7	10.2	11.2	10.9	10.5
Na_2O	2.69	0.94	1.86	3.06	2.26	2.16
K_2O	0.43	0.44	0.44	0.59	1.32	0.24
P_2O_5	2.53	4.09	0.35	1.97	0.85	0.17
LOI	0.39	0.30	4.15	0.02	1.26	0.48
Total	99.5	98.9	98.9	99.6	98.1	98.7
Ba (ppm)	376	147	199	429	503	151
Be	0.50	1.18	0.57	1.21	17.54	0.54
Bi	b.d.l	b.d.l	b.d.l	b.d.l	0.37	b.d.l
Cd	0.14	0.65	0.21	0.31	0.55	0.12
Ce	92.6	287	31.8	145	271	20.1
Co	47.8	103	59.5	47.4	71.7	88.0
Cr	21.0	21.0	71.0	32.0	29.0	321
Cs	0.32	0.45	2.00	0.59	4.90	0.26
Cu	12.9	107	142	62.5	113	197
Dy	6.42	18.1	3.03	9.75	27.9	2.21
Er	2.23	6.49	1.12	3.62	13.7	0.89
Eu	4.83	8.44	2.02	5.52	4.79	1.41
Ga	18.8	23.2	22.6	27.1	23.4	20.6
Gd	11.7	31.2	4.56	16.3	31.9	3.06
Hf	1.60	3.87	1.54	3.40	25.2	1.28
Ho	1.02	2.88	0.49	1.59	5.17	0.37
In	0.08	0.18	0.08	0.16	0.19	0.07
La	37.2	118	12.6	60.6	109	8.43
Li	5.10	4.00	18.90	6.10	25.7	8.50
Lu	0.17	0.48	0.10	0.29	1.33	0.09
Mo	1.82	2.80	0.73	2.51	1.66	0.83
Nb	17.7	41.6	9.10	39.9	88.5	7.05
Nd	63.5	186	22.3	94.7	147	13.7
Ni	4.90	45.6	190	47.2	77.0	180
Pb	1.10	10.3	1.80	1.80	88.8	1.00
Pr	13.4	40.9	4.72	20.9	35.9	2.92
Rb	5.59	10.7	13.3	16.1	79.2	3.48
Sb	b.d.l	b.d.l	b.d.l	0.04	0.08	b.d.l
Sc	14.7	17.8	13.2	15.9	22.3	26.1
Sm	13.2	36.8	5.05	19.2	34.6	3.25
Sn	0.50	2.35	1.51	2.43	>14	0.52
Sr	1021	224	673	741	478	623
Ta	1.25	2.54	0.57	2.47	5.89	0.47
Tb	1.34	3.64	0.56	1.95	4.87	0.41
Th	0.78	2.35	0.43	2.38	26.7	0.23
Tl	0.04	0.06	0.17	0.08	0.4	0.02
Tm	0.24	0.71	0.14	0.41	1.80	0.11
U	0.20	0.57	0.11	0.52	3.65	0.07
V	25.8	244	342	211	438	449
W	0.08	0.30	0.20	0.35	3.24	0.09
Y	26.4	73.3	12.2	40.2	135	9.45
Yb	1.31	3.70	0.75	2.20	10.4	0.63
Zn	168	394	98.0	178	407	131
Zr	57.0	132	50.0	118	1109	41.0

[1] mafic peg = mafic pegmatite; [2] relataively unaltered fine grained gabbro; b.d.l = below detection limits

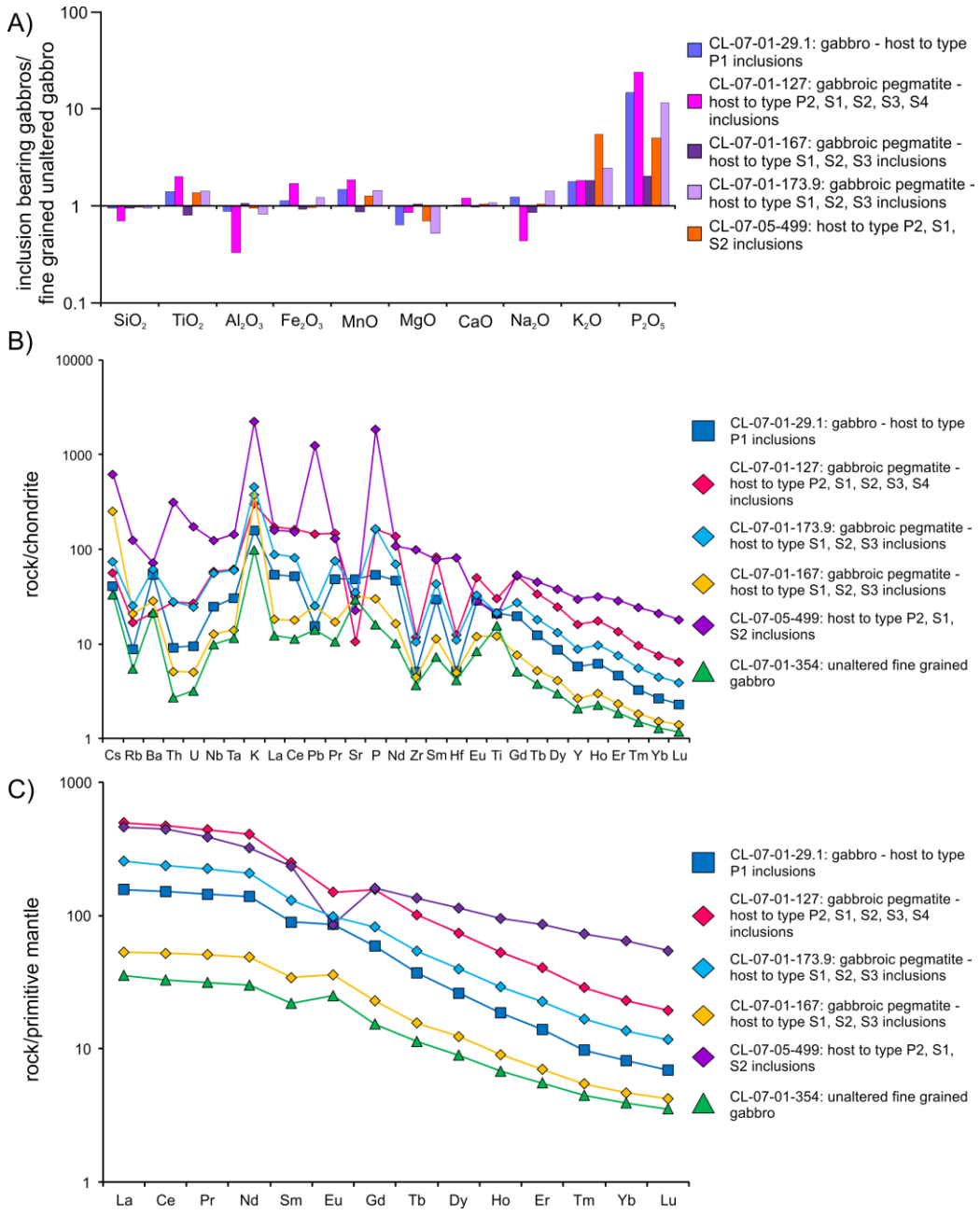

Figure 3.7: Major and trace element geochemistry plots of fluid and melt inclusion bearing rocks and a fine-grained relatively unaltered gabbro from the CLG. A) Major element plot of fluid and melt inclusion bearing rocks normalized to a fine-grained gabbro to determine relative enrichments of elements in the inclusion bearing rocks. B) Trace element plot of inclusion bearing rocks and fine-grained gabbro normalized to chondrite. C) Trace element plot of inclusion bearing rocks and fine-grained gabbro normalized to primitive mantle.

elements are plotted in Figure 3.7 (normalized to primitive mantle, Figure 3.7B; normalized to chondrite, Figure 3.7C; Sun and McDonough, 1989) along with relatively unaltered fine-grained gabbros from the CLG. Compositionally, the mafic pegmatitic are typically enriched in P, K, Ti, Mn, Fe, and Ca compared to their host gabbros and are depleted in Si, Al, Mg, and Na (Figure 3.7A). These differences can be accounted for by the higher abundances of apatite, ilmenite, magnetite, and biotite and lesser amounts of plagioclase and pyroxene present in the mafic pegmatites compared to the host gabbros. The gabbro hosting type P1 inclusions is enriched in P, K, Mn, and Ti and has similar Si, Al, Fe and Ca to the host gabbros (Figure 3.7A). This can be accounted for mineralogically by greater amounts of apatite, biotite, and ilmenite in the melt inclusion bearing rock. Representative photos of the unaltered fine-grained gabbro are shown in Figure 3.4E, F. Fluid and melt inclusion bearing samples show relatively parallel trace element patterns to those of the unaltered fine-grained gabbros when normalized to primitive mantle, but are generally much more enriched in trace elements (Figure 3.7B). Generally only Sr, K, and Zr, in the fluid and melt inclusion samples are in similar concentration to the fine-grained gabbros. The enrichment in REE and other trace elements in the fluid and melt inclusion bearing samples is most likely controlled by the high amounts of apatite present in these samples. All samples normalized to chondrite (Figure 3.7C) display a negative slope (enriched in LREE compared to HREE) and have a positive Eu anomaly with the exception of CL-07-01-127 and CL-07-05-499, which both display a negative Eu anomaly. With the exception of CL-07-05-499, fluid and melt inclusion bearing samples are much more enriched in LREE over HREE compared to the unaltered fine-grained gabbros (Figure 3.7C).

3.3.4 Fluid and melt inclusion descriptions

Two varieties of primary melt and fluid inclusions were observed; type P1) silicate melt inclusions (SMI) and type P2) polyphase brine-carbonic fluid inclusions. As well, four varieties of secondary melt and fluid inclusions were observed: type S1) polyphase (i.e., containing > two phase at room temperature) CO_2-dominant carbonic fluid inclusions, type S2) polyphase CH_4-dominant carbonic-brine fluid inclusions, type S3) polyphase mixed (i.e., heterogeneously entrapped) brine-carbonic fluid inclusions, and type S4) mixed silicate-sulphide melt inclusions. Inclusions were grouped using the fluid inclusion assemblage (FIA) method, whereby single FIA represent groups of temporally coeval inclusions (i.e., trapped at the same time) present in clusters, along healed fractures, or along grain boundaries.

3.3.4.1 Type P1, SMI

Type P1 inclusions occur as SMI assemblages consisting of two to four inclusions and are hosted in cumulus apatite in a medium-grained gabbro (CL-07-01-29.1; petrography described above) where they occur either parallel to the elongation axis or at the center of an individual apatite grain (i.e., in an inclusion rich zone), providing strong evidence for a primary origin (Figure 3.2 A-C). Type P1 inclusions range in size from < 8 µm up to 100 µm and vary in shape from elliptical to spherical (Figure 3.2 D-F). At room temperature (24°C), type P1 inclusions do not contain a vapor bubble and all type P1 inclusions observed appear to contain multiple crystalline phases. Typically, type P1 inclusions consist of variable proportions of light to medium brown and clear phases with rare opaque grains, indicating the melt has crystallized after entrapment (Figure 3.2 D-F). An SEM-EDS map showing major element compositional variations of the inclusion in

Figure 3.2 D,E is shown in Figure 3.8 and shows the variation in element X-ray intensities in the inclusion. Examining exposed unhomogenized type P1 inclusions by SEM-EDS, numerous crystalline phases were identified in the melt inclusions based on SEM-EDS analyses: plagioclase (Ab_{93-98}), K-feldspar, clinopyroxene (*var*. augite; X_{Mg}=49), amphibole (*var*. ferrokaersutite?), biotite, magnetite, ilmenite, and zircon (Figure 3.2 D,E).

3.3.4.2 Type P2, polyphase brine-carbonic fluid inclusions

Type P2 fluid inclusions occur throughout coarse-grained apatite in mafic pegmatites, where they are parallel to the elongation axis of apatite, again suggesting that they are primary in origin (Figure 3.9 A, B). Inclusions are up to 20 µm, but are very thin and tubular in shape making it difficult to identify liquid and vapor phases, phase proportions, and if solids are present within the inclusions. At room temperature (24°C) P2 inclusion trails rarely contain halite daughter minerals (Figure 3.9C) and these trails have V_{CO2} vol % ranging from 25 to 45. More commonly P2 inclusions do not contain daughter minerals and consist of a liquid aqueous phase (L_{aq}) and a liquid carbonic phase (L_{CO2}) or a vapor carbonic phase (V_{CO2}) with V_{CO2} vol % between 45 and 70 (Figure 3.9 D-G).

3.3.4.3 Type S1, polyphase CO_2-dominant carbonic fluid inclusions

Type S1 fluid inclusions occur as secondary trails in apatite where they occur in various orientations throughout their host grain (e.g., parallel fractures, crosscutting fractures) (Figure 3.9 H). Inclusions consist of L_{CO2}, V_{CO2}, and occasionally a solid phase at room temperature (24°C). Inclusions show highly variable V_{CO2} vol %, ranging from 40 up to 95, but ratios are relatively similar within a single FIA (±15 vol %) with rare

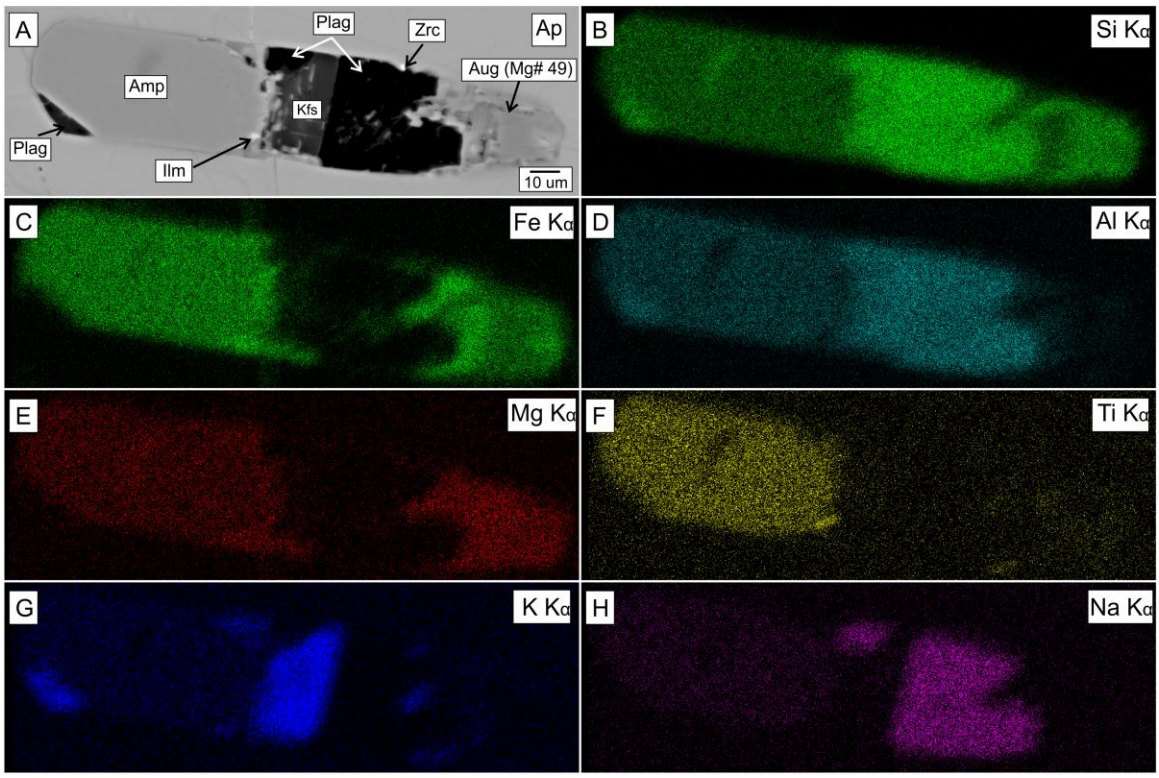

Figure 3.8: SEM-EDS element map of exposed unhomogenized silicate melt inclusion in CL-07-01-29.1 showing relative intensity of X-rays. A) BSE image of exposed melt inclusions. Amp = amphibole; Ap = apatite; Aug = augite; Ilm = ilmenite; Kfs = K-feldspar; Plag = plagioclase; Zrc = zircon, B) Kα intensity of Si, C) Kα intensity of Fe, D) Kα intensity of Al, E) Kα intensity of Mg, F) Kα intensity of Ti, G) Kα intensity of K, H) Kα intensity of Na. Note the variation in Mg# of augite and the difference in Mg Kα.

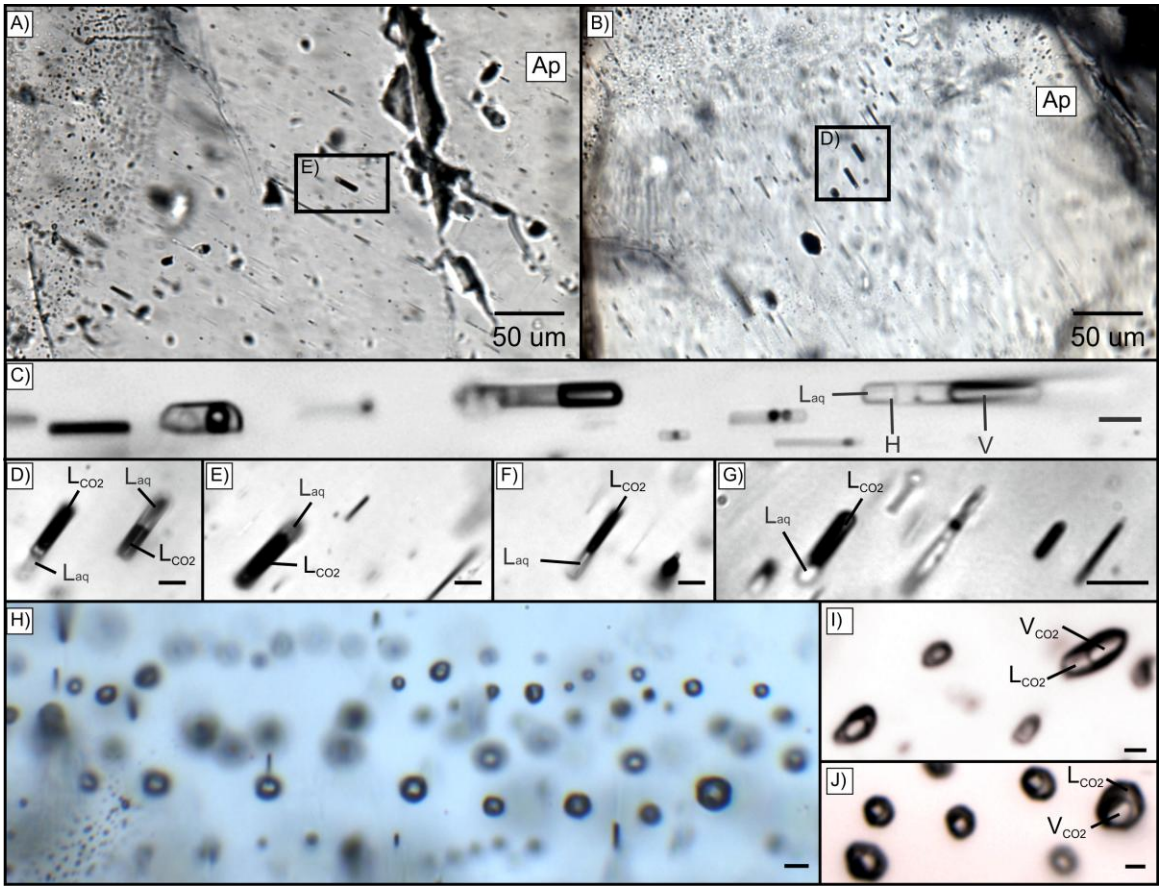

Figure 3.9: Primary and secondary type P2 and S1 fluid inclusions hosted in apatite. All scale bars in the figure are 5 µm unless otherwise indicated. All fluid inclusions images taken at room temperature (24°C). A-B) Fluid inclusion microphotographs of primary fluid inclusions hosted in apatite. C) Primary inclusions containing rare halite daughter mineral. Note the variation in vapor bubble proportions between inclusions. D-G) Primary inclusions showing variable V:L ratios. H) Trail of secondary type S1 carbonic fluid inclusions. I-J) Note the variation in V:L ratios between secondary type S1 carbonic fluid inclusions. L_{aq} = liquid aqueous phase; L_{CO2} = liquid carbonic phase; V_{CO2} = vapor carbonic phase; H = halite.

exceptions with variations of V_{CO2} vol %, up to 30 vol % (Figure 3.9 I, J). Type S1 inclusions typically display negative crystal shape, have spherical to tabular morphologies, and range in size from 8-40 µm (~15 µm). Small (3-8 µm) birefringent calcite crystals are rarely present in type S1 inclusions and have variable phase proportions within a single FIA, suggesting accidental entrapment.

3.3.4.4 Type S2, polyphase CH_4-dominant carbonic-brine fluid inclusions

Type S3 fluid inclusions occur as secondary trails in apatite where they generally occur parallel to fractures. Inclusions consist of a liquid CH_4-dominant phase (L_{CH4}), and L_{aq} with solids at room temperature (24°C). Inclusions show variable V_{CO2} vol % within a given assemblage ranging from 10 to 100 (Figure 3.10). Type S3 inclusions typically display negative crystal shape, have spherical to tabular morphologies, and range in size from 8-20 µm (~12 µm). Small (2-10 µm) birefringent calcite crystals are commonly present in type S2 inclusions and have variable phase proportions within a single FIA, suggesting accidental entrapment (Figure 3.10).

3.3.4.5 Type S3, polyphase mixed brine-carbonic fluid inclusions

Type S3 fluid inclusions occur in secondary trails (i.e., healed fractures) in apatite where they generally parallel open fractures and occur in various trail orientations throughout the host grains (Figure 3.11 A,B). Inclusions contain a L_{CO2}, L_{aq} with solids and rarely a V_{CO2} at room temperature (24°C). Inclusions show variable V_{CO2} vol % within a single assemblage (35-70) and overall V_{CO2} vol % of type S3 inclusions range from 15 to 80 (Figure 3.11 A-J). Type S3 inclusions have sub-spherical to tabular morphologies, and range in size from 4-25 µm (~12 µm). Large birefringent calcite crystals (2-12 µm) are the most common solid phases present (Figure 3.12A) and display

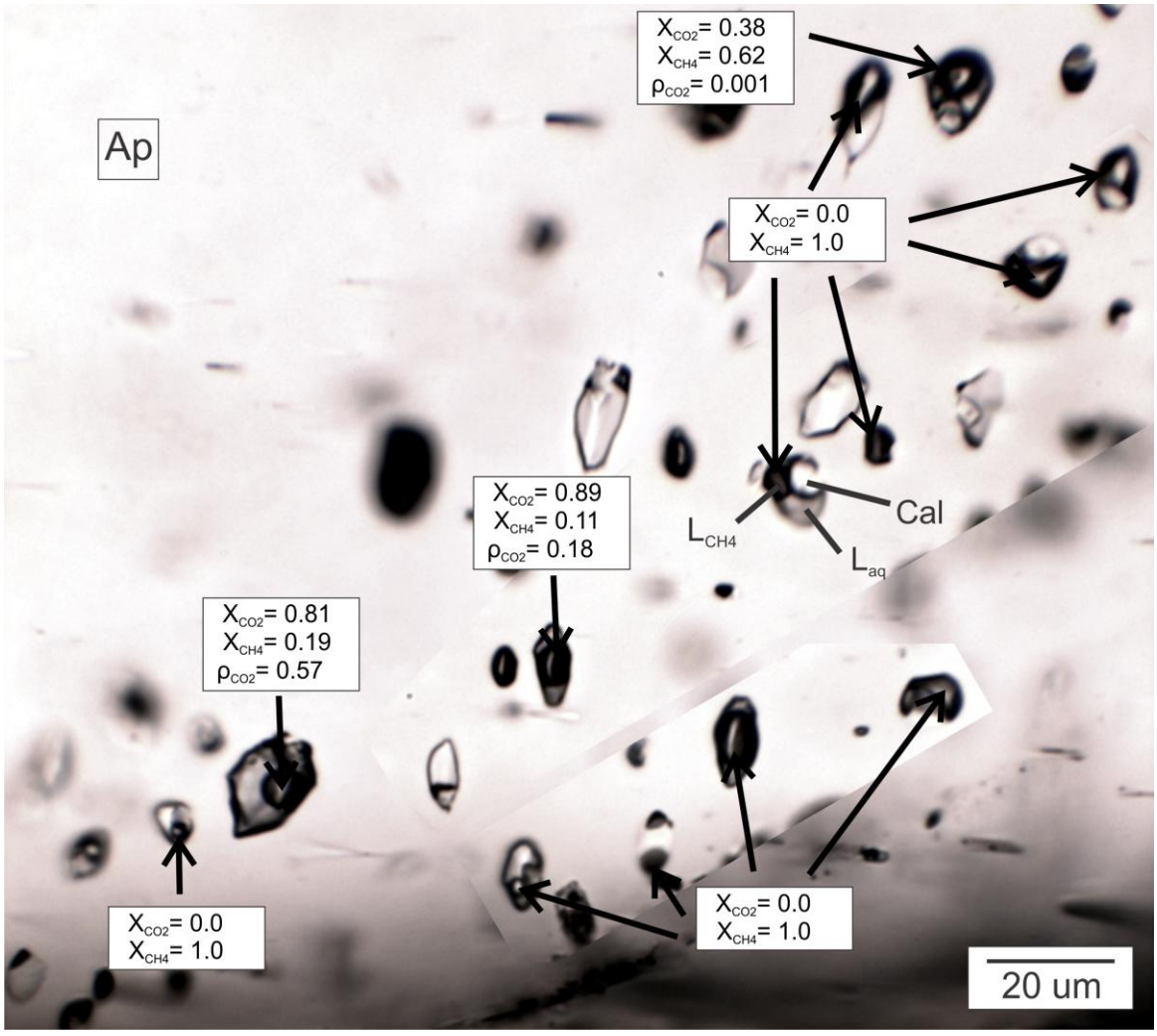

Figure 3.10: Representative FIA of S2-S3$_{CH4}$ inclusions with CO_2:CH_4 proportions determined by Raman spectroscopy. All carbonic phases were homogenous at room temperature (24°C) and therefore CO_2:CH_4 proportions are determined for the bulk carbonic phase. Note the various V:L ratios and variations in calcite crystal sizes. As discussed in the results section for S2 inclusions, Raman spectroscopy was conducted on these inclusions that showed Th_{CH4} >-82.3°C, but no CO_2 was detected, indicating other dissolved species are present but due to the fluorescent nature of the apatite Raman spectra, any other volatile species could not be identified. L_{aq} = liquid aqueous phase; L_{CH4} = liquid CH_4-rich carbonic phase; Cal = calcite.

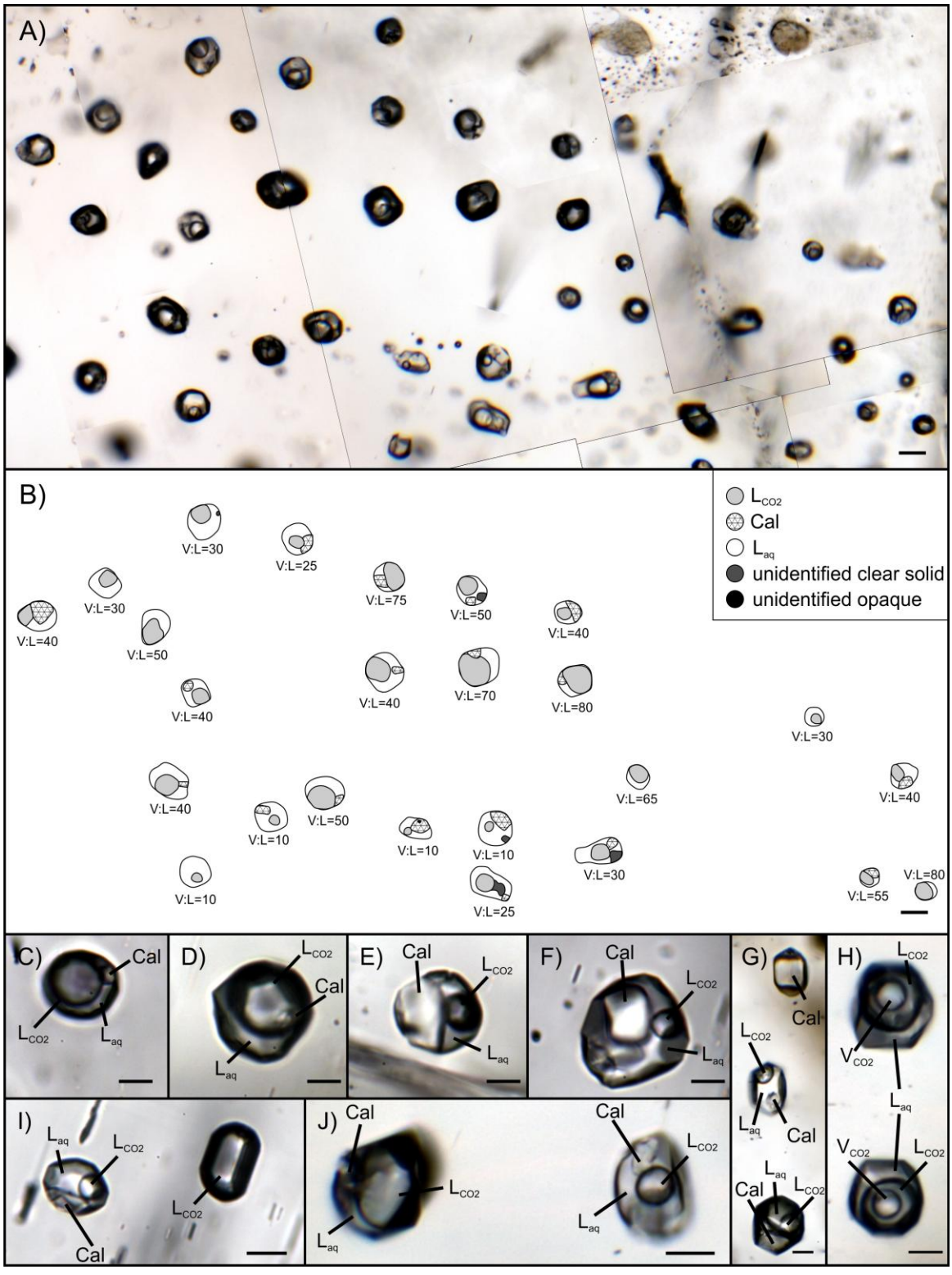
A)
B)
L_{CO2}
Cal
L_{aq}
unidentified clear solid
unidentified opaque
V:L=30
V:L=25
V:L=75
V:L=50
V:L=40
V:L=30
V:L=40
V:L=50
V:L=40
V:L=70
V:L=80
V:L=30
V:L=40
V:L=65
V:L=40
V:L=10
V:L=50
V:L=10
V:L=10
V:L=30
V:L=10
V:L=25
V:L=55
V:L=80
C)
D)
E)
F)
G)
H)
I)
J)
Cal
L_{CO2}
L_{aq}
V_{CO2}

Figure 3.11 (previous page): Photomicrographs of type S3 fluid inclusions hosted in apatite. All scale bars in the figure are 5 μm. All fluid inclusions images taken at room temperature (24°C). A-B) Fluid inclusion photomicrograph (PPL) and interpretive line map showing distribution of type S3 inclusions in apatite. Note the highly variable V:L ratios present in this assemblage as well as the highly variable calcite phase proportions between fluid inclusions. C-F) Type S3 fluid inclusions showing various V:L ratios and various sizes of accidentally entrapped calcite crystals. G) Fluid inclusion trail of S3 inclusions showing variable V:L ratios and various sizes of accidentally entrapped calcite. H) Rare S3 inclusions showing L_{CO2}+V_{CO2} and no accidentally entrapped calcite. I) Type S3 inclusion coexisting in the same FIA with a type S1 fluid inclusion. J) Fluid inclusion trail of S3 inclusions showing variable V:L ratios and various sizes of accidentally entrapped calcite. L_{aq} = liquid aqueous phase; L_{CO2} = liquid carbonic phase; V_{CO2} = vapor carbonic phase; Cal = calcite.

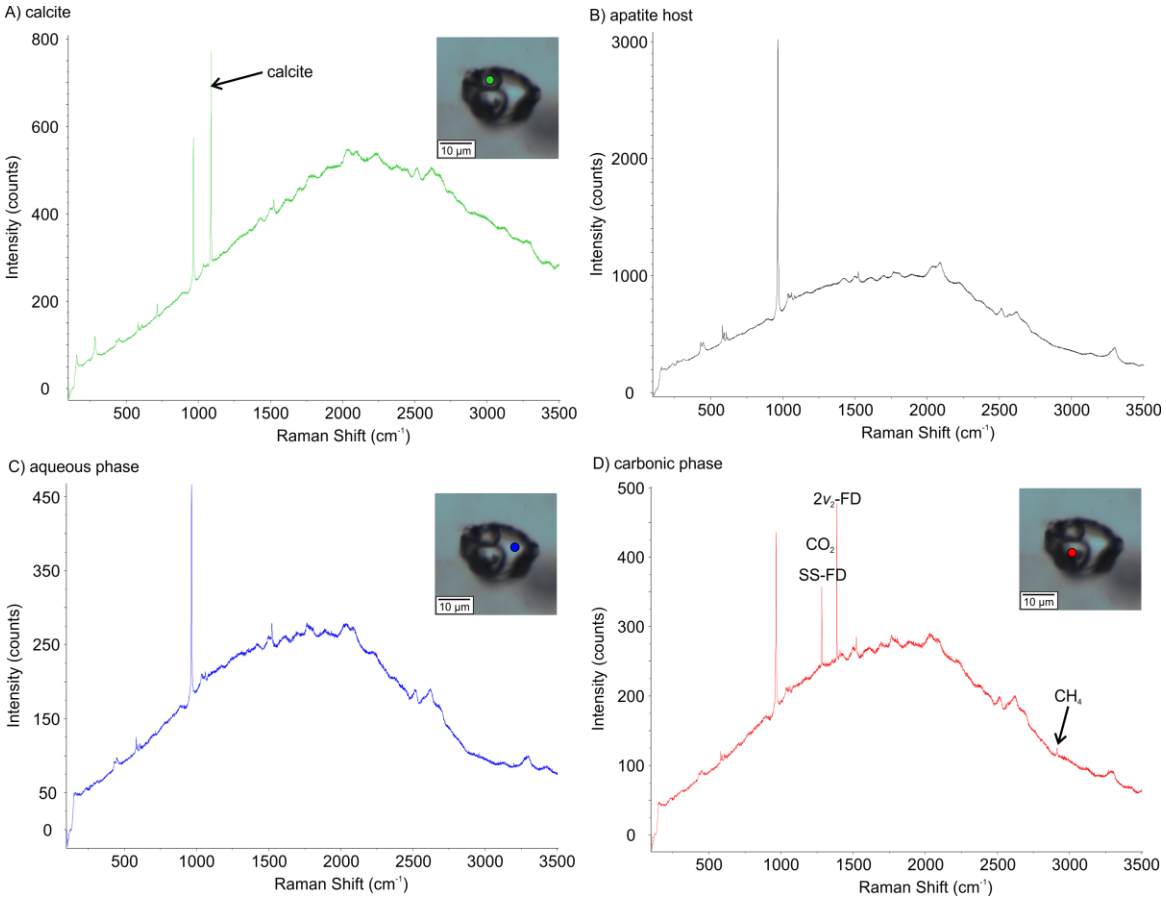

Figure 3.12: Raman spectroscopy analysis of an S3 fluid inclusion. Spot analysis for each spectrum is indicated by the dot in the fluid inclusion image. A) Raman spectra of an accidentally trapped calcite grain in the inclusion. B) Representative apatite analysis by Raman. C) Raman spectra for the aqueous phase in a type S3 inclusion. Note in comparison to B, the overlap of the H_2O spectral range (3000-3600 cm^{-1}) with the apatite host. D) Carbonic phase in a type S3 inclusion composed primarily of CO_2 (peaks at 1285 and 1388 cm^{-1}) and minor CH_4 (peak at 2917cm^{-1}).

variable phase ratios within inclusions of a given assemblage, suggesting they were accidentally trapped (i.e., a saturated phase at time of entrapment). As well, calcite commonly occurs as solid inclusions within the host apatite consistent with accidental entrapment.

Thick sections of CL-07-01-127 were examined by SEM-EDS to identify solid phases that occur within type S1 and S3 fluid inclusions by examining exposed fluid inclusions. Up to 9 solid phases were observed in exposed fluid inclusions determined by SEM-EDS and include: magnetite, monazite, arsenopyrite, an unidentified Ta-bearing mineral, unidentified W-Si-bearing mineral, and an unidentified Si-Fe-Mg-Ti-Al phase (silicate melt?). One grain of each chalcopyrite and sphalerite were found within separate inclusions. Tantalum and W-Si bearing phases are typically found in association with the Si-Fe-Mg-Ti-Al phase and calcite (Figure 3.13 A, B). Monazite was never found alone in fluid inclusions, but with calcite, magnetite, and/or the Si-Fe-Mg phase and was present in 78 of several hundred inclusions analyzed (Table 3.5; Figure 3.13 C,D). Magnetite was observed in 25 inclusions and the Si-Fe-Mg phase was present in 99 of the several hundred inclusions analyzed (Table 3.5). Along with these phases identified within fluid inclusions, magnetite and monazite were also identified as solid inclusions within the host apatite. All of these solids are considered to be accidentally trapped phases because the distribution of each type of solid in a given FIA is inconsistent and the volumetric proportion of each solid in an inclusion is highly variable. Summary of solid phases identified in exposed fluid inclusions is presented in Table 3.5.

Type S3 inclusions coexist with Type S1 inclusions within a given FIA (Figure 3.11I), however it is difficult to tell if the inclusions are truly Type S1 or if they are Type

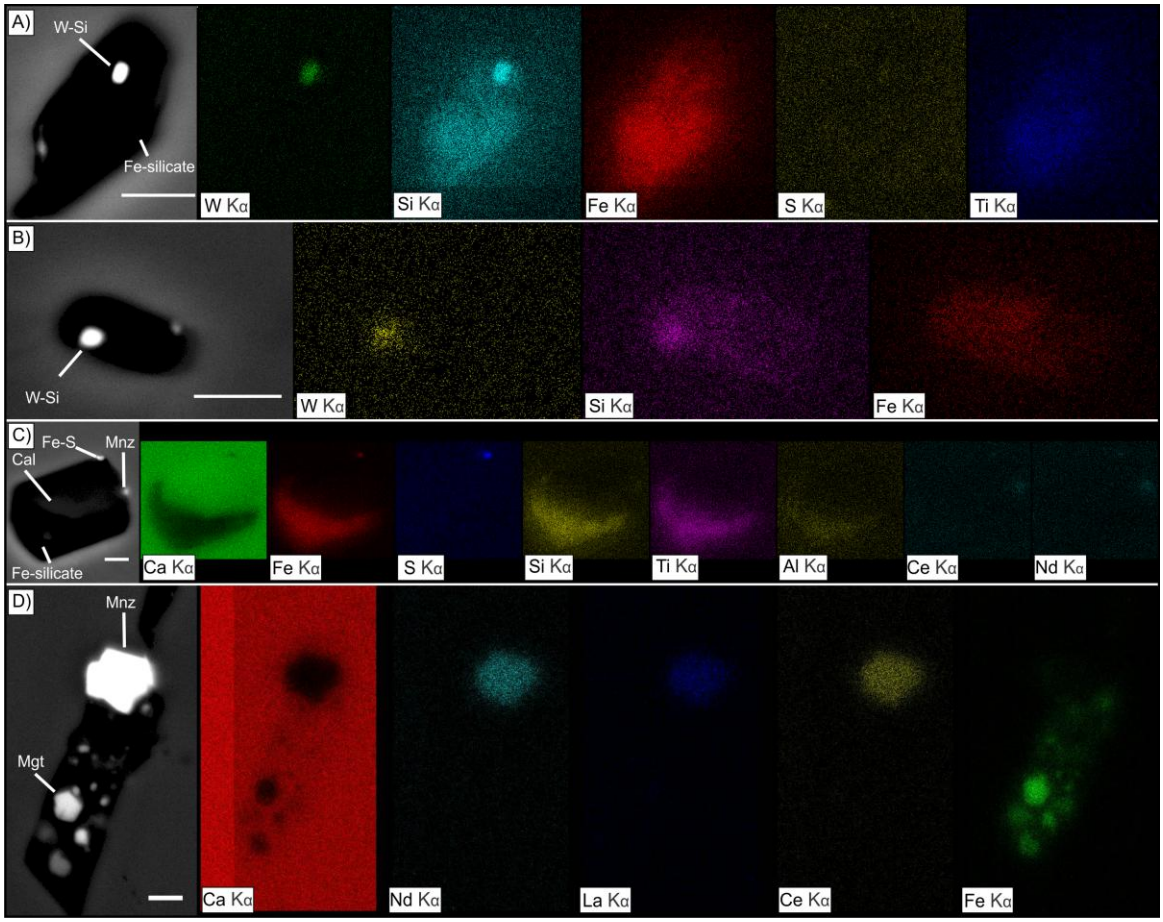

Figure 3.13: SEM-EDS X-ray intensity element maps of exposed type S3 fluid inclusions. All scale bars are 5 µm A) Note the elevated W in the centre of the inclusion as well as the elevated Si and Fe throughout (melt?). B) Note the elevated W occurring in the centre of the inclusion and the elevated S on the bottom of the inclusion. C) Note the presence of elevated Fe and S in the top right of the inclusion, Ce and Nd (not shown) appear on the right side of the inclusion (monazite). Calcite comprises the majority of the volume of this particular inclusion and note the elevated Fe, Si, Ti, and Al present in the lower left portion of the inclusion (melt?). D) Large grain of monazite and numerous grains of magnetite are present in the inclusion. Cal = calcite; Fe-silicate = Si-Fe-Mg-Ti-Al phase; Mgt = magnetite; Mnz = monazite; Fe-S = Fe-sulphide (pyrite or pyrrhotite); W-Si = W-Si phase.

Table 3.5: Breakdown of solid phases idenified in S3 fluid inclusions by SEM-EDS

solid phases in inclusions	magnetite + silicate melt	magnetite + calcite	magnetite + calcite + silicate melt	monazite + silicate melt	monazite + calcite + silicate melt	monazite + calcite	Fe-S + calcite + silicate melt	Ta + silicate melt	Ta	W-Si + silicate melt	Fe-Cu-Zn-S Inclusion + silicate melt	Total number of inclusions with solids analyzed
Number of inclusions	18	3	4	51	18	9	2	2	1	3	1	112

Ta = unidentified Ta-phase; W-Si = unidentified W-Si phase

S3 with an extremely large vapor phase making the aqueous phase difficult to observe. Raman spectroscopy was attempted to determine if an aqueous phase was present in S1 inclusions, but due to the fluorescent nature of the host apatite, the spectral range at which H_2O characteristic Raman peaks occur is obstructed by the apatite fluorescence and therefore could not determine if an aquoues phase is present in S1 inclusions (Figure 3.13 B, C). Type 3 inclusions also coexist with type S2 inclusions within a given FIA (Figure 3.10). The highly variable carbonic:brine ratios present in type S3 inclusions, combined with the occurrence of S1 or S2 inclusions occurring within a single assemblage with type S3 inclusions, would suggest heterogeneous entrapment of two immiscible fluids. From here forward, type S3 inclusions coexisting with S2 inclusions will be referred to as type $S3_{CH4}$.

3.3.4.6 Type S4, mixed silicate-sulphide melt inclusions

Secondary trails composed of mixed silicate and sulphide melt inclusions occur in apatite and are subspherical and tube shaped (Figure 2.5). Sulphide and silicate inclusions range in size from 5 to 25 μm, with an average size of 10 μm and create an interconnected network of tube shaped mixed silicate-sulphide melt inclusions. Single inclusions within a given trail can be composed of a silicate glass and/or sulphide melt. In instances where the silicate and sulphide melt occur together as a single inclusion, the silicate glass fills the inclusion in between two distinct sulphide melt inclusions (Figure 2.5). Elemental mapping by SEM-EDS of a mixed silicate-sulphide inclusion shows that the silicate glass in between two distinct sulphide inclusions contains up to 26 wt % SiO_2 and 16 wt % MgO (Figure 2.5). Coeval entrapment of the silicate and sulphide melt is indicated by the variable proportions of each phase within individual inclusions from a single trail and the

interconnected, tubular shapes and textures of inclusions and trails is representative of a liquid being entrapped rather than a solid. Petrographically, pyrrhotite is the dominant phase observed in the sulphide inclusions with rare chalcopyrite and no distinct mineral phases could be identified in the silicate inclusions. These mixed trails of Type S3 inclusions are contained within a single apatite grain and never crosscut grain boundaries. For a detailed characterization of the sulphide melt inclusions, see Chapter 2. Microthermometry was not conducted on these inclusions.

3.3.5 Microthermometry and Raman spectroscopy

3.3.5.1 Type P1, silicate melt inclusions

Microthermometry was conducted on 18 type P1 SMI from CL-07-01-29.1. These inclusions did not contain vapor bubbles at room temperature (24°C) and are not glassy. First melting of solids in SMI was reliably observed in 12 inclusions occurring between 557° and 701°C (652°C ± 40; n=12) and first melting of the SMI is an approximation of final crystallization temperature of the melt. The first appearance of a vapor bubble during heating was obtained in only 3 inclusions and occurred between 988° and 1171°C. The difficulty in reliably obtaining first melting and vapor bubble appearance in SMI relates to internal oxidation, which occurs at temperatures as low as 630°C during heating despite the attempt to depress this by the use of Ar externally. The inclusions would become very dark on the edges or throughout the entire inclusion, obscuring the transparency of the SMI. The minimum liquidus temperature ($T_m^{liquidus}$) is determined when the solid phases present in a SMI have completely melted; this was observed in 11 inclusions. Complete melting of solids in 10 inclusions occurred between 1119° and 1231°C (1164°C ± 35; n=10) with one outlier of 1015°C. Five SMI decrepitated between

1000° and 1175°C before $T_m^{liquidus}$ was observed, and 2 of these inclusion decrepitated in the same range as $T_m^{liquidus}$ was observed, indicated these inclusions were likely close to their $T_m^{liquidus}$. Two of the inclusions completely oxidized and did not provide any reliable microthermometric measurements. Figure 3.14 shows the progressive melt changes with increasing temperature during microthermometry. Table 3.6 presents a summary of melt inclusion microthermometry results.

3.3.5.2 Type P2, polyphase brine-carbonic fluid inclusions

Owing to the small size and thin tubular shape of P2 inclusions and the rarity of inclusions large enough to observe microthermometric changes in, on, only a few measurements were obtained. P2 inclusions show melting of the carbonic phase (Tm_{CO2}) between -57.3° and -57.1°C. Homogenization of the carbonic phase (Th_{CO2}) was observed in two inclusions and occurred at 21.3°C to the liquid state ($L_{CO2}+V_{CO2} \rightarrow L_{CO2}$) and at 25.5°C to the vapor state ($L_{CO2}+V_{CO2} \rightarrow V_{CO2}$), respectively. Clathrate melting (Tm_{CLA}) was confidently identified in only one P2 inclusion, at -16.9°C equating to a salinity of 28.3 wt % NaCl. In one inclusion, a solid appeared to form during cooling and this solid did not melt until 17°C. This solid may be antarcticite, if so then the melting of it at ~17°C would equate to aqueous phase salinity of approximately 40 wt % $CaCl_2$ (Oakes et al., 1990). Fluid inclusion microthermometry data is presented in Table 3.7.

3.3.5.3 Type S1, polyphase CO_2-dominant carbonic fluid inclusions

Type S1 inclusions show Tm_{CO2} between -58.8° and -56.7°C (Figure 3.15A) and Th_{CO2} between 26.9° to 30.9°C (Figure 3.15B). The depression of Tm_{CO2} below -56.6°C (pure CO_2) indicates that additional volatile species (e.g., CH_4) are present in the carbonic

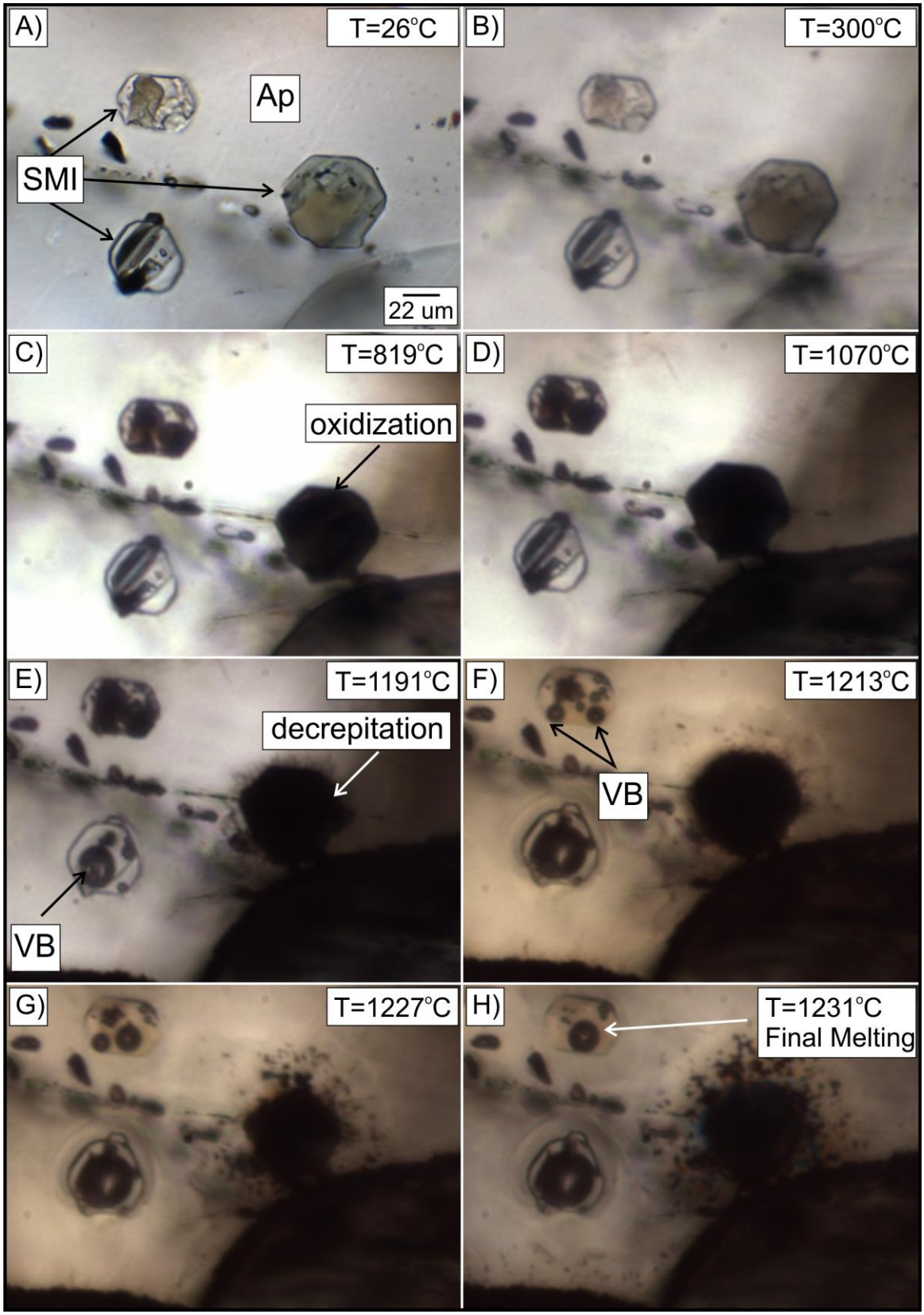
A)
T=26°C
Ap
SMI
22 um
B)
T=300°C
C)
T=819°C
oxidization
D)
T=1070°C
E)
T=1191°C
decrepitation
VB
F)
T=1213°C
VB
G)
T=1227°C
H)
T=1231°C
Final Melting

Figure 3.14: Photomicrographs of silicate melt inclusion during microthermometry heating from 26°C to 1231°C. A) Room temperature image of SMI. B) At 300°C no melting has occurred yet, but the inclusion appearance has changed and phases have shifted color. C) Melt inclusions have already begun to melt at 819°C. D) Increased presence of melt inside SMI. E) Vapor bubbles became visible at ~1171°C and in the inclusion in the top left. F) Increased melt proportions in one SMI and the vapor bubble in the other expanded. G) Vapor bubbles increase in size in one SMI and the melt on the right hand side of the image has decrepitated. H) Slightly above 1230°C all mineral phases in the inclusion in the top left were completely melted and the vapor bubble disappeared at ~1265°C.

Table 3.6: Silicate melt inclusion microthermometric results

inclusion	1st Melt (°C)[1]	B_{App} (°C)[2]	B_{Dapp} (°C)[3]	$T_m^{liquidus}$(°C)[4]
29.1_A	659	n.o.	n.o.	1114[a]
29.1_D_9	638	n.o.	n.o.	1136
29.1_D_12	691	n.o.	n.o.	1101[a]
29.1_B_3	691	n.o.	n.o.	1139
29.1_B_12	n.o.	n.o.	n.o.	1119
29.1_B_6	n.o.	1105	1152	1161
29.1_B_1a	n.o.	988	n.o.	1161
29.1_B_1b	n.o.	n.o.	n.o.	1074[a]
29.1_C_5	n.o.	n.o.	n.o.	1154
29.1_D_14	701	n.o.	n.o.	1034[a]
29.1_D_11	670	n.o.	n.o.	1157
29.1_D_R	670	n.o.	n.o.	1166
29.1_D_Q	638	n.o.	n.o.	1135[b]
29.1_C_9	627	1171	1265	1231
29.1_B_8	622	n.o.	n.o.	1216
29.1_D_6	665	n.o.	n.o.	1220[b]
29.1C-1	557	n.o.	n.o.	1015
29.1C-3	n.o.	n.o.	n.o.	1039[a]
Ave	652	1088	1208	1164[c]
Max	701	1171	1265	1231[c]
Min	557	988	1152	1119[c]
STD	40	93	80	35[c]
n	12	3	2	10[c]

[1] 1st Melting = first melting of solid phases in SMI observed; [2] B_{app} = vapor bubble appeared in SMI; [3] B_{dapp} = vapor bubble disappearance; [4] $T_m^{liquidus}$ = minimum liquidus temperature; [a] SMI decrepitated; [b] SMI became too dark to observe melting; [c] = does not include outlier of 1015°C; n.o. = phase change not observed

Table 3.7: Summary of fluid inclusion microthermometric data

inclusion type	assemblage	inclusion #	Th_{CH4}(°C)	mode	Tm_{CO2} (°C)	Th_{CO2}(°C)	mode	Tm_{CLA} (°C)	Wt% NaCl equiv.	T_{hTOT} (°C)	mode	V:L	size (µm)
P2	SI	1	-	-	-57.3	25.5	V	-16.9	28.3	n.o.	n.o.	60	15
P2	A	1	-	-	n.o.	n.o.	n.o.	n.o.	n.o.	428[1]	V	55	15
P2	A	2	-	-	-57.1	21.3	L	n.o.	n.o.	428[1]	V	50	15
P2	SI	1	-	-	-57.3	n.o.	n.o.	n.o.	n.o.	428[1]	V	55	20
S1	B	1	-	-	-57.1	30.3	V	-	-	-	-	95	11
S1	B	2	-	-	-57.3	30.0	V	-	-	-	-	90	13
S1	B	3	-	-	-57.0	29.7	V	-	-	-	-	90	12
S1	B	4	-	-	-57.0	29.8	V	-	-	-	-	85	11
S1	C	1	-	-	-57.6	29.4	V	-	-	-	-	65	22
S1	C	2	-	-	-57.8	29.2	V	-	-	-	-	65	11
S1	C	3	-	-	-57.8	29.6	V	-	-	-	-	60	22
S1	C	4	-	-	-57.7	29.6	V	-	-	-	-	55	12
S1	C	5	-	-	-57.5	29.4	V	-	-	-	-	65	11
S1	C	6	-	-	-57.7	29.8	V	-	-	-	-	55	19
S1	D	1	-	-	-57.1	30.2	V	-	-	-	-	50	22
S1	D	2	-	-	-57.1	30.3	V	-	-	-	-	55	19
S1	D	3	-	-	-57.1	30.3	V	-	-	-	-	50	27
S1	D	4	-	-	-57.2	30.2	V	-	-	-	-	45	39
S1	D	5	-	-	-57.0	30.4	V	-	-	-	-	70	34
S1	E	1	-	-	-57.3	29.7	V	-	-	-	-	60	7
S1	E	2	-	-	-57.4	29.6	V	-	-	-	-	50	10
S1	E	3	-	-	-57.4	28.9	V	-	-	-	-	60	9
S1	E	4	-	-	-57.4	28.9	V	-	-	-	-	55	11
S1	F	1	-	-	-57.1	29.2	V	-	-	-	-	60	7
S1	F	2	-	-	-57.1	28.9	V	-	-	-	-	55	10
S1	F	3	-	-	-57.3	29.5	V	-	-	-	-	60	10
S1	F	4	-	-	-57.3	29.5	V	-	-	-	-	60	8
S1	F	5	-	-	-57.2	29.6	V	-	-	-	-	55	13
S1	F	6	-	-	-57.1	29.8	V	-	-	-	-	40	10
S1	F	7	-	-	-57.1	29.8	V	-	-	-	-	50	8
S1	F	8	-	-	-57.0	29.6	V	-	-	-	-	45	12
S1	F	9	-	-	-57.1	29.3	V	-	-	-	-	50	10
S1	SI	1	-	-	-57.2	29.9	V	-	-	-	-	60	20
S1	SI	1	-	-	-57.7	29.9	V	-	-	-	-	65	22
S1	SI	1	-	-	-57.6	30.2	V	-	-	-	-	80	15
S1	SI	1	-	-	-57.3	30.2	L	-	-	-	-	50	16
S1	SI	1	-	-	-57.1	30.7	L	-	-	-	-	65	22
S1	SI	1	-	-	-57.3	29.5	V	-	-	-	-	65	13
S1	G	1	-	-	-57.8	28.9	V	-	-	-	-	65	10
S1	G	2	-	-	-57.8	29.3	V	-	-	-	-	70	12
S1	G	3	-	-	-57.6	29.9	V	-	-	-	-	80	10
S1	G	4	-	-	-57.8	29.2	V	-	-	-	-	80	10
S1	G	5	-	-	-57.8	27.9	V	-	-	-	-	75	12
S1	G	6	-	-	-57.5	27.1	V	-	-	-	-	70	10
S1	G	7	-	-	-57.3	26.9	V	-	-	-	-	70	10
S1	H	1	-	-	-57.1	27.9	V	-	-	-	-	80	15
S1	H	2	-	-	-57.2	28.2	V	-	-	-	-	80	10
S1	H	3	-	-	-57.3	29.9	V	-	-	-	-	75	15
S1	H	4	-	-	-57.1	27.3	V	-	-	-	-	75	10
S1	H	5	-	-	-57.2	28.9	V	-	-	-	-	75	10
S1	I	1	-	-	-57.0	30.2	V	-	-	-	-	65	20
S1	I	2	-	-	-56.9	30.5	V	-	-	-	-	60	20
S1	I	3	-	-	-56.9	30.1	V	-	-	-	-	65	20

Table 3.7: Continued

inclusion type	assemblage	inclusion #	Th_{CH4} (°C)	mode	Tm_{CO2} (°C)	Th_{CO2} (°C)	mode	Tm_{CLA} (°C)	Wt% NaCl equiv.	T_{hTOT} (°C)	mode	V:L	size (μm)
S1	I	4	-	-	-56.9	30.7	V	-	-	-	-	50	30
S1	I	5	-	-	-56.8	30.2	V	-	-	-	-	65	12
S1	I	6	-	-	-56.8	30.2	V	-	-	-	-	70	20
S1	I	7	-	-	-57.1	30.8	V	-	-	-	-	70	15
S1	I	8	-	-	-56.9	30.4	V	-	-	-	-	65	20
S1	I	9	-	-	-56.7	27.6	V	-	-	-	-	75	15
S1	J	1	-	-	-57.3	30.9	V	-	-	-	-	65	12
S1	J	2	-	-	-57.5	28.4	V	-	-	-	-	70	10
S1	J	3	-	-	-57.4	28.4	V	-	-	-	-	60	12
S1	SI	1	-	-	-57.3	29.9	V	-	-	-	-	70	15
S1	K	1	-	-	-57.4	29.4	V	-	-	-	-	70	18
S1	K	2	-	-	-58.1	27.1	V	-	-	-	-	85	10
S1	K	3	-	-	-57.4	28.9	V	-	-	-	-	90	10
S1	L	1	-	-	-58.8	27.9	V	-	-	-	-	80	13
S1	L	2	-	-	-58.6	29.3	V	-	-	-	-	70	10
S1	L	3	-	-	-58.7	29.1	V	-	-	-	-	85	12
S3	M	1	-	-	-57.0	30.2	L	-10.3	24.4	n.o.	n.o.	50	20
S3	M	2	-	-	-57.2	1.2	L	-9.2	23.7	286[1]	-	35	20
S3	M	3	-	-	-57.0	11.2	L	-10.7	24.7	n.o.	n.o.	60	15
S3	M	4	-	-	-56.8	30.6	V	-10.0	24.2	n.o.	n.o.	50	20
S3	N	1	-	-	-58.2	6.0	L	-9.2	23.7	n.o.	n.o.	40	20
S3	N	2	-	-	-57.6	26.1	L	-10.1	24.3	n.o.	n.o.	60	20
S3	N	3	-	-	-57.6	17.1	L	-3.0	18.7	n.o.	n.o.	30	20
S3	N	4	-	-	-57.6	18.0	L	-2.1	17.9	n.o.	n.o.	35	15
S3	O	1	-	-	-58.1	10.2	L	-9.8	24.1	n.o.	n.o.	65	12
S3	O	2	-	-	-57.5	-7.9	L	-8.4	23.2	252[1]	L	15	12
S3	SI	1	-	-	-58.7	6.9	L	-8.5	23.2	294[1]	L	20	12
S3	P	1	-	-	-57.2	0.8	L	-11.3	25.1	284[1]	-	35	20
S3	P	2	-	-	-57.2	28.6	V	-8.8	23.4	n.o.	n.o.	60	22
S3	P	3	-	-	-57.1	-0.1	L	-9.0	23.6	284[1]	-	45	12
S3	P	4	-	-	-56.9	n.o.	n.o.	n.o.	n.o.	n.o.	n.o.	70	15
S3	Q	1	-	-	-56.7	26.6	V	-9.1	23.7	n.o.	n.o.	80	22
S3	Q	2	-	-	-56.6	n.o.	n.o.	-8.8	23.4	n.o.	n.o.	80	20
S3	SI	1	-	-	-64.9	-5.5	L	-6.4	21.6	n.o.	n.o.	15	18
S3	R	1	-	-	-57.4	7.9	L	-8.6	23.3	n.o.	n.o.	40	15
S3	R	2	-	-	-56.7	24.0	L	-6.7	21.9	n.o.	n.o.	30	15
S2	S	1	-68.0	L	-	-	-	n.o.	n.o.	n.o.	n.o.	90	18
S2	S	2	-68.0	L	-	-	-	n.o.	n.o.	n.o.	n.o.	90	12
S2	T	1	-90.6	L	-	-	L	2.0	13.2	n.o.	n.o.	25	15
$S3_{CH4}$	T	2	-	-	-57.9	25.5	V	3.4	11.3	n.o.	n.o.	50	25
$S3_{CH4}$	T	3	-	-	-58.7	22.7	L	0.6	14.9	n.o.	n.o.	30	10
$S3_{CH4}$	T	4	-	-	-59.1	21.8	L	0.3	15.3	n.o.	n.o.	25	22
S2	U	1	-96.1	L	-	-		-13.3	26.2	n.o.	n.o.	35	14
$S3_{CH4}$	U	2		L	-61.4	10.5	L	3.2	11.7	n.o.	n.o.	28	18
S2	U	3	-72.4	L	-	-	-	n.o.	n.o.	n.o.	n.o.	75	10
$S3_{CH4}$	U	4		L	-65.6	7.5	L	2.3	12.8	n.o.	n.o.	15	12
S2	U	5	-71.0	L	-	-	-					100	15
S2	U	6	-74.3	L	-	-	-					75	10
$S3_{CH4}$	V	1	-	-	-58.9	19.2	L	3.4	11.2	n.o.	n.o.	35	18
$S3_{CH4}$	V	2	-	-	-58.8	n.o.	n.o.	4.7	9.4	n.o.	n.o.	25	16
S2	V	3	-73.2	L	-	-	-	n.o.	n.o.	n.o.	n.o.	70	10
S2	V	4	-83.6	V	-	-	-					100	12
$S3_{CH4}$	V	5	-	-	-57.8	4.1	L	2.6	12.5	n.o.	n.o.	45	16

Th_{CH4}= homogenization temperature of CH_4; Tm_{CO2}= final melting temperature of CO_2; Th_{CO2}= homogenization temperature of CO_2; Tm_{CLA}= clathrate melting temperature; Th_{TOT} = total homogenization temperature; Mode = homogenization mode to vapor (V) or to liquid (L);[1] Decrepitated; n.o. = phase change not observed; SI = single inclusion

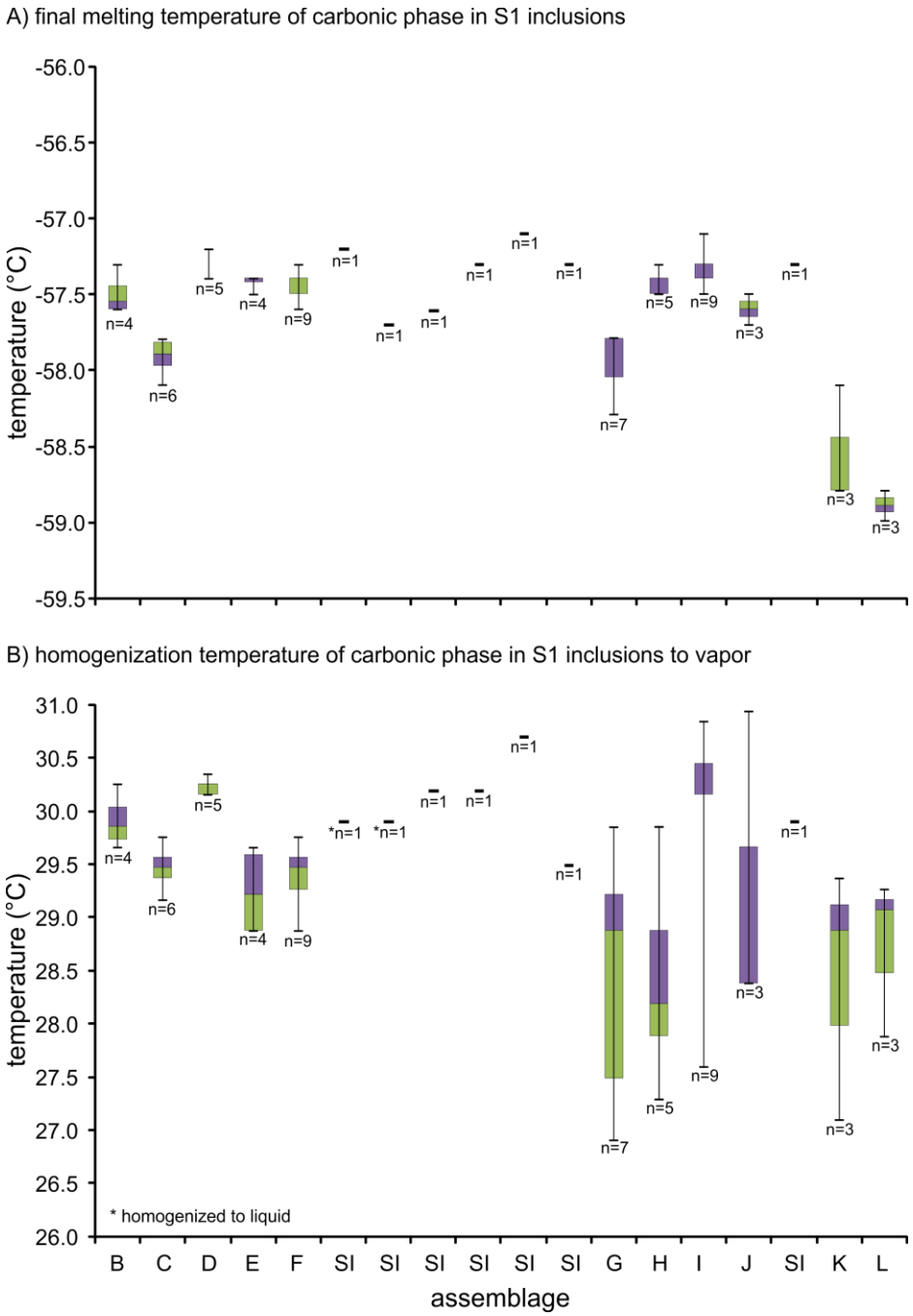

Figure 3.15: Box-whisker plots for microthermometric data type S1 carbonic fluid inclusion assemblages. Data for single assemblages (letters along x-axis) and individual inclusions (solid bars, labeled along x-axis as "SI") are shown. A) Variation in carbonic phase melting temperature (Tm_{CO2}) for individual assemblages and inclusions. Note that measurements of fluid inclusion Tm_{CO2} are slightly depressed below that for pure CO_2 (-56.6°C); see text for explanation. B) Range in carbonic phase homogenization temperature for individual assemblages and inclusions.

phase. The presence of CH_4 was confirmed by Raman spectroscopy (up to 5 % CH_4) (Table 3.8). Homogenization of the carbonic phase mainly occurred to vapor ($L_{CO2}+V_{CO2} \rightarrow V_{CO2}$) with only 2 inclusions homogenizing to liquid ($L_{CO2}+V_{CO2} \rightarrow L_{CO2}$). Estimated densities of the V_{CO2} phase determined by Raman (CO_2 fermi diad spacing) range from 0.33 to 0.69 g/cm^3, based on the equation of Rosso and Bodnar (1995). The bulk densities of type S1 inclusions range from 0.706 to 0.731 g/cm^3, were determined using the program BULK and expressions from Bowers and Helgeson (1983) and Bakker (1999).

3.3.5.4 Type S2, polyphase CH_4-dominant carbonic-brine fluid inclusions

Homogenization of the CH_4-dominant phase (Th_{CH4}) in type S2 inclusions occurs between -96.1° and -68.0°C. Homogenization of the methane phase occurred to the liquid state ($L_{CH4}+V_{CH4} \rightarrow L_{CH4}$). Values of Th_{CH4} occurring above the CH_4 critical point (-82.3°C) indicates that there are minor amounts of other dissolved volatiles (e.g., CO_2) present within bulk carbonic fluid. However, Raman spectroscopy was conducted on inclusions that showed Th_{CH4} >-82.3°C, and no CO_2 was detected, indicating other dissolved species are present but due to the fluorescent nature of the apatite Raman spectra, any other volatile species could not be identified. Clathrate melting was identified in only two S2 inclusions at -13.3° and 2.0°C, equating to salinities of 26.2 and 13.2 wt % NaCl equiv.

3.3.5.5 Type S3, polyphase mixed brine-carbonic fluid inclusions

Type S3 inclusions show Tm_{CO2} between -64.9° and -56.6°C (Figure 3.16A) and Th_{CO2} occurs between -7.9° and 30.6°C (Figure 3.16B). As with type S1 inclusions Tm_{CO2} is typically below -56.6°C and the presence of CH_4 was confirmed by Raman

Table 3.8: CO_2 and CH_4 proportions in the carbonic phase in fluid inclusions determined by Raman spectroscopy

sample/area	inclusion type	xCO_2	xCH_4	CO_2 density (g/cm^3)[a]	sample/area	inclusion type	xCO_2	xCH_4	CO_2 density (g/cm^3)[a]
127-C Area 1	S3	0.92	0.08	0.71	127-D Area 2	S2	0.00	1.00	-
	S3	0.98	0.02	0.06		S2	0.00	1.00	-
	S3	0.95	0.05	0.61		S2	0.00	1.00	-
	S3	0.98	0.02	0.30		S2	0.00	1.00	-
						$S3_{CH4}$	0.81	0.19	0.17
127-C Area 2	S3	1.00	0.00	0.16		S2	0.00	1.00	-
	S3	0.98	0.02	0.34		S2	0.00	1.00	-
	S3	0.98	0.02	0.43		$S3_{CH4}$	0.54	0.46	0.20
	S3	0.98	0.02	0.49					
	S3	0.96	0.04	0.27	127-D Area 3	S1	1.00	0.00	0.33
						S1	0.98	0.02	0.51
127-C Area 3	S2	0.00	1.00	-		S1	0.97	0.03	0.33
	$S3_{CH4}$	0.97	0.03	0.48		S2	0.00	1.00	-
	S2	0.00	1.00	-		S1	0.96	0.04	0.52
	$S3_{CH4}$	0.98	0.02	0.74		S1	0.98	0.02	0.34
						S1	0.97	0.03	0.35
127-C Area 3b	S3	0.97	0.03	0.32		S1	0.97	0.03	0.52
	S3	0.97	0.03	0.35		S1	0.97	0.03	0.36
	S3	0.97	0.03	0.51		S1	0.97	0.03	0.50
	S3	0.97	0.03	0.37		S1	0.96	0.04	0.51
	S3	0.98	0.02	0.32		S1	0.98	0.02	0.49
	S3	0.98	0.02	0.32		S1	0.97	0.03	0.69
						S1	0.95	0.05	0.48
127-C Area 4	S3	0.98	0.02	0.68		S1	0.98	0.02	0.34
	S3	1.00	0.00	0.51		S1	0.97	0.03	0.39
	S3	0.95	0.05	0.71		S1	0.98	0.02	0.53
	S3	0.99	0.01	0.34		S1	1.00	0.00	0.53
	S3	0.95	0.05	0.71		S1	1.00	0.00	0.52
	S3	0.97	0.03	0.16		S1	0.97	0.03	0.34
	S3	0.94	0.06	0.89		S1	0.98	0.02	0.52
						S1	0.98	0.02	0.52
127-D Area 1	S3	0.98	0.02	0.71		S1	0.97	0.03	0.35
	S3	0.98	0.02	0.16		S1	0.97	0.03	0.52
	S3	0.98	0.02	0.71		S1	0.97	0.03	0.54
	S3	0.96	0.04	0.71					
	S3	0.97	0.03	0.53	127-D Area 5	$S3_{CH4}$	0.97	0.03	0.33
	S3	0.99	0.01	0.70		S2	0.00	1.00	-
						$S3_{CH4}$	0.82	0.18	0.53
127-D Area 2	S2	0.00	1.00	-		$S3_{CH4}$	0.87	0.13	0.52
	$S3_{CH4}$	0.81	0.19	0.53		$S3_{CH4}$	0.49	0.51	0.37
	S2	0.00	1.00	-		$S3_{CH4}$	0.96	0.04	0.34
	$S3_{CH4}$	0.89	0.11	0.17		$S3_{CH4}$	0.96	0.04	0.35
	S2	0.00	1.00	-		$S3_{CH4}$	0.96	0.04	0.52
	S2	0.00	1.00	-		$S3_{CH4}$	0.99	0.01	0.53
	S2	0.00	1.00	-		$S3_{CH4}$	0.98	0.02	0.52
	S2	0.00	1.00	-		$S3_{CH4}$	0.97	0.03	0.18

a = density determined by the CO_2 fermi diad spacing and calculated based on the calibration of Rosso and Bodnar (1995)

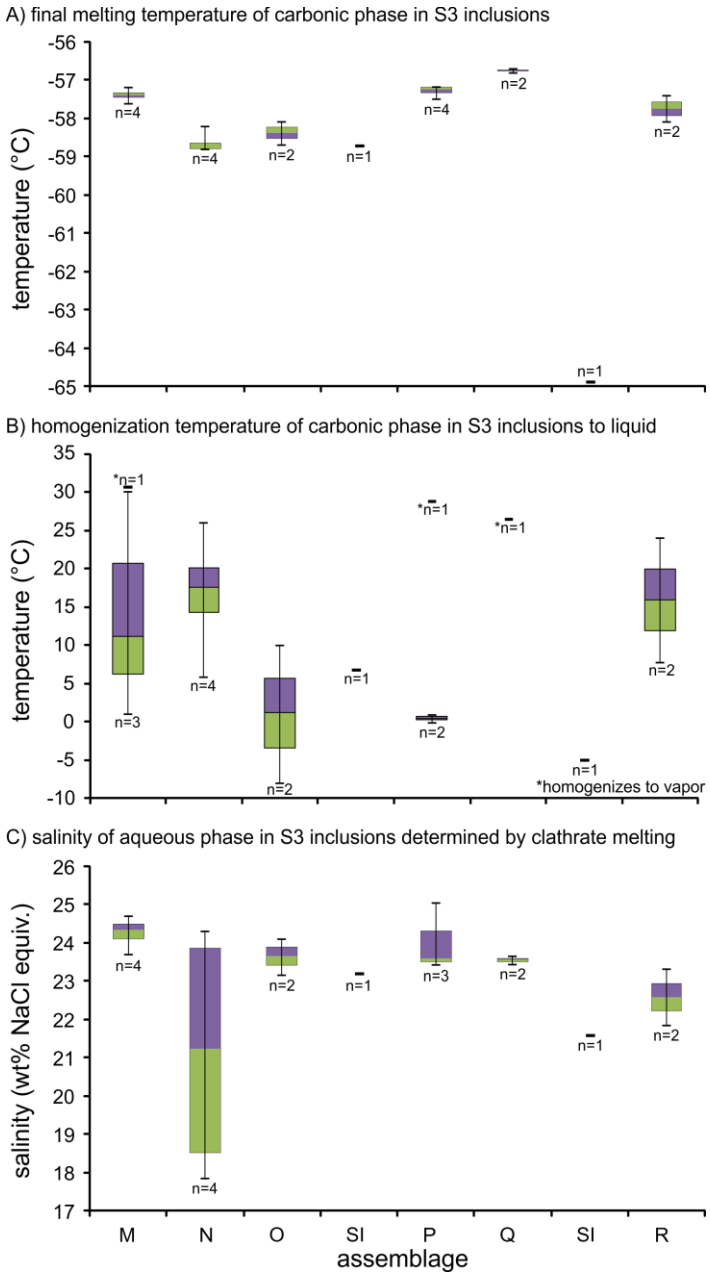

Figure 3.16 (previous page): Box-whisker plots for microthermometric data for type S3 brine-carbonic fluid inclusion assemblages. Data for single assemblages (letters along x-axis) and individual inclusions (solid bars, labeled along x-axis as "SI") are shown. A) Variation in CO_2 melting temperature (Tm_{CO2}) for individual assemblages and inclusions. Note that measurements of fluid inclusion Tm_{CO2} are slightly depressed below that for pure CO_2 (-56.6°C); see text for explanation. B) Range in CO_2 homogenization temperature for individual assemblages and inclusions. C) Range in salinity (wt % NaCl equiv.) for the aqueous component of individual assemblages and inclusions determined by clathrate melting.

spectroscopy, with up to 8 % CH_4 (Table 3.8; Figure 3.12D). Homogenization of the carbonic phase primarily occurred to the liquid state ($L_{CO2}+V_{CO2} \rightarrow L_{CO2}$), while homogenization to the vapor state was rarely observed ($L_{CO2}+V_{CO2} \rightarrow V_{CO2}$). First ice melting in type S3 inclusions was noted to occur at approximately -31°C, indicating other dissolved cations besides Na^+ are present within the brine portion of the inclusion. Clathrate melting (Tm_{CLA}) occurred between -11.3° and -2.1°C, equating to salinities between 17.9 and 25.1 wt % NaCl equiv. (Figure 3.16C). Estimated densities of the V_{CO2} phase based on the CO_2 fermi diad spacing determined by Raman spectroscopy conducted on the homogenized V_{CO2} phase in S3 inclusions, range from 0.06 to 0.89 g/cm^3 (avg 0.47 ± 0.22, n=28).

3.3.5.6 Type $S3_{CH4}$, polyphase mixed brine-carbonic fluid inclusions

Type $S3_{CH4}$ inclusions show Tm_{CO2} between -65.6° and -57.8°C and Th_{CO2} between 4.1° and 25.5°C. As with type S3 inclusions Tm_{CO2} is typically below -56.6°C and the presence of CH_4 was confirmed by Raman spectroscopy, with up to 51 % CH_4 present in the carbonic phase. Homogenization of the carbonic phase primarily occurred to the liquid state ($L_{CO2}+V_{CO2} \rightarrow L_{CO2}$), while homogenization to the vapor state was rarely observed ($L_{CO2}+V_{CO2} \rightarrow V_{CO2}$). First ice melting in type $S3_{CH4}$ inclusions occurred at approximately -29°C, indicating other dissolved cations besides Na^+ are present within the brine portion of the inclusion. Clathrate melting (Tm_{CLA}) occurred between 0.3° and 4.7°C, equating to salinities between 9.4 and 15.3 wt % NaCl equiv. Estimated densities of the V_{CO2} phase based on the CO_2 fermi diad spacing determined by Raman range from 0.17 to 0.74 g/cm^3 (avg. 0.40 ± 0.17, n=17).

3.3.6 Gas chromatography

Apatite from CL-07-01-127 was separated and crushed to determine bulk fluid hydrocarbon content by gas chromatography (GC). This method takes into account all fluid inclusion generations representing a bulk analysis of volatile species present in fluid inclusions. A wide variety of hydrocarbons were detected in the analysis and in summary, the hydrocarbon content of the sample contains up to 79.59 mol % C1 hydrocarbons (CH_4), 15.69 mol % C2 hydrocarbons, 2.56 mol % C3 hydrocarbons, 1.21 mol % C4 hydrocarbons, 0.60 mol % C5 hydrocarbons, and 0.35 mol % C6 hydrocarbons (Figure 3.17).

3.3.7 Silicate melt inclusion chemistry

Due to challenges associated with homogenizing type P1 inclusions and their rarity, the major element compositions were not determined on homogenous (i.e., glassy) inclusions. However, major element compositions of unhomogenized P1 inclusions were estimated using a defined area analysis of exposed P1 inclusions by SEM-EDS. Results of SEM-EDS defined area analyses are presented in Table 3.9. Based on the abundances of P in the major element data, the host contribution (contamination) associated with this method is no more than 2 wt % of the total analyzed elements. Defined area analyses gave ranges of 49.7-53.7 wt % SiO_2, 1.4-7.6 wt % Na_2O, 0.9-5.4 wt % K_2O, 1.95-4.96 wt % MgO, and 14.6-17.0 wt % FeO. Melt inclusion compositions determined by this method range from gabbroic to syeno-dioritic (Figure 3.18A). Using trace element discrimination diagrams SMI compositions primarily plot in the arc-basalt compositional field. Unaltered fine-grained gabbros plot in the E-MORB field and the chilled margin

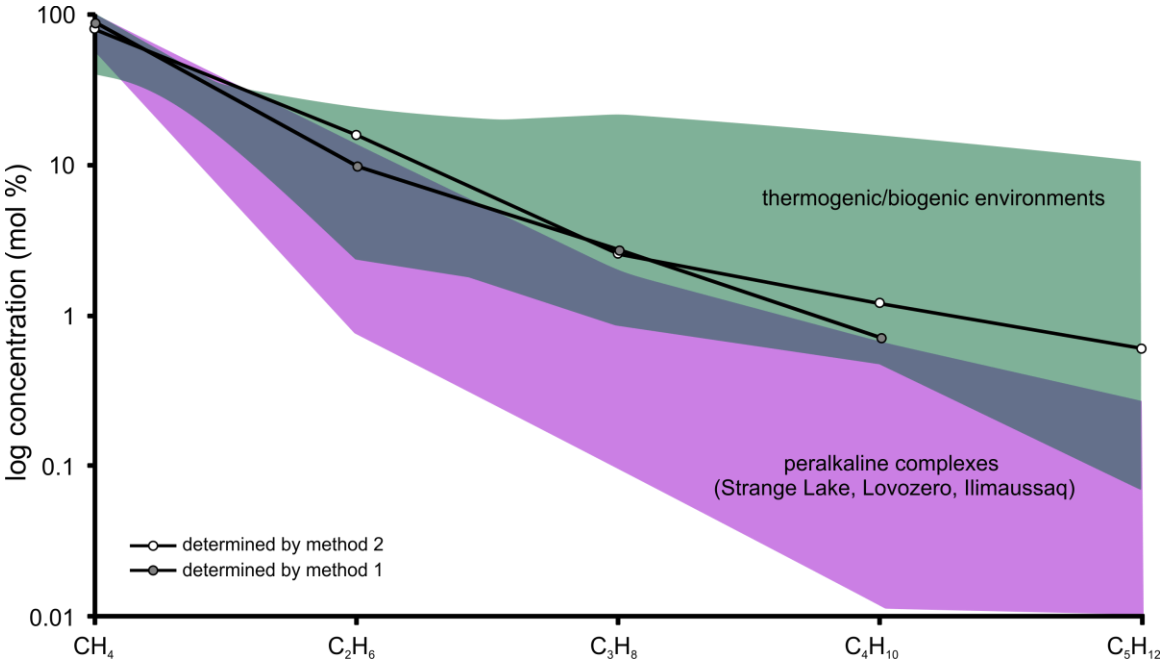

Figure 3.17: Saturated hydrocarbon abundances versus carbon number for the bulk fluid in apatite from two separate aliquots from mafic pegmatite CL-07-01-127. Note the relatively flat slope with increasing carbon number and the CLG data plot slightly above the peralkaline field and in the thermogenic/biogenic environments. The thermogenic/biogenic field is compiled data from the China oil fields (Chen et al., 2000), the Ula Formation in Norway (Potter and Konnerup-Madsen, 2003, and references therein), and the Green Tuff Basin in Japan (Sakata et al., 1997). Peralkaline field is compiled data from Strange Lake (Salvi and Williams-Jones, 1997), Lovozero (Potter et al., 2004), Ilimaussaq (Petersilie and Sørensen, 1970, Konnerup-Madsen et al., 1979, and Konnerup-Madsen and Rose-Hansen, 1982).

Table 3.9: Summary of SEM-EDS defined area analyses on exposed silicate melt inclusions in apatite from CL-07-01-29.1

	silictae melt inclusion analyses											
inclusion #	29.1-1a	29.1-1b	29.1-1c	29.1-6a	29.1-6b	29.1-9a	29.1-9b	29.1-9c	Min	Max	Ave	STD
SiO_2	49.7	49.9	49.6	53.4	53.8	54.6	53.3	53.4	49.6	54.6	52.2	2.1
TiO_2	2.24	2.23	2.29	1.19	1.19	0.00	0.25	0.24	0.00	2.29	1.20	0.97
Al_2O_3	13.3	13.3	13.2	14.6	14.6	13.9	13.8	13.9	13.2	14.6	13.8	0.56
FeO	14.7	14.7	14.6	14.8	14.8	16.9	17.2	17.2	14.6	17.2	15.6	1.22
MgO	3.66	3.56	3.71	1.97	1.95	4.78	4.96	4.76	1.95	4.96	3.67	1.19
MnO	0.25	0.30	0.30	0.20	0.18	0.00	0.21	0.21	0.00	0.30	0.21	0.09
CaO	8.68	8.55	8.74	3.85	3.75	1.98	2.23	2.36	1.98	8.74	5.02	3.09
Na_2O	4.51	4.77	4.68	7.58	7.54	1.40	1.26	1.42	1.26	7.58	4.15	2.60
K_2O	2.25	2.17	2.16	0.92	0.93	5.58	5.38	5.36	0.92	5.58	3.09	2.01
P_2O_5	0.81	0.59	0.74	1.28	1.10	0.93	1.23	1.03	0.59	1.28	0.96	0.24
Total	100.00	100.00	100.00	100.00	100.00	100.00	100.00	100.00	100.00	100.00	100.00	0.00

a,b,c = multiple rasters condcuted on same melt inclusion

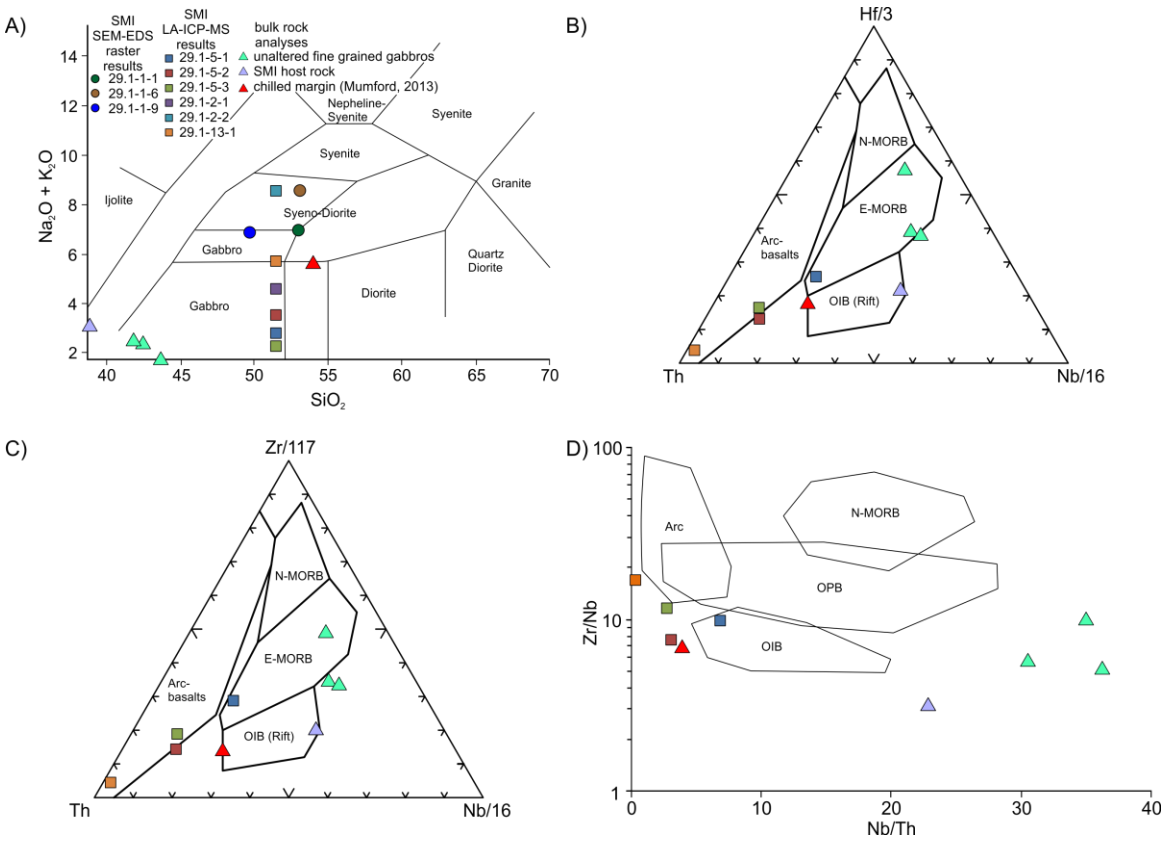

Figure 3.18: Major and trace element discrimination diagrams for silicate melt inclusions. A) Total alkalis vs. silica diagram for plutonic rocks. SEM-EDS defined area analyses data and LA-ICP-MS data are both plotted and both methods show the melt composition ranging from gabbroic to syeno-dioritic. B) Ternary plot of Th-Hf/3-Nb/16 of silicate melt inclusions, unaltered fine-grained gabbros, gabbro hosting silicate melt inclusions, and the chilled margin of the CLG (Mumford, 2013, unpublished PhD thesis). Note the silicate melt inclusions plot primarily in the arc-basalt field, while the fine-grained gabbros plot in the E-MORB field. C) Ternary plot of Th-Zr/117-Nb/16 of silicate melt inclusions, unaltered fine-grained gabbros, gabbro hosting silicate melt inclusions, and the chilled margin of the CLG (Mumford, 2013, unpublished PhD thesis). Note the silicate melt inclusions plot primarily in the arc-basalt field, while the fine-grained gabbros plot in the E-MORB field. D) Plot of Nb/Th vs. Zr/Nb of of silicate melt inclusions, unaltered fine-grained gabbros, gabbro hosting silicate melt inclusions, and the chilled margin of the CLG (Mumford, 2013, unpublished PhD thesis). Note how silicate melts and the chilled margin plot near the arc field, while the gabbros have high Nb/Th ratios and do not plot in any field.

sample collected by Mumford (2013, unpublished PhD thesis) plots in the oceanic island basalt field (Figure 3.18B,C,D).

Major and trace elements of SMI were also determined simultaneously by LA-ICP-MS. An example LA-ICP-MS signal of a P1 inclusion is shown in Figure 3.19; an increase count rates in major and trace elements (e.g., Si, K, Al, Na, Fe, Mg) relative to the apatite host indicate the opening of the inclusion (Figure 3.19). Trace elements in type P1 inclusions determined by LA-ICP-MS show enrichments in B, Rb, Zr, Nb, Sn, Cs, Ba Hf, Ta, Th, and U when compared to MORB, while V, Cr, Ni, and Cu are all below detection limits and have a maximum melt:MORB ratio of ~1 when using their detection limits as a maximum value (Figure 3.20A). Cobalt is above detection limits in the inclusions and has concentrations between 14 and 66 ppm; Co has a melt:MORB ratio of ~1 (Figure 3.20A). Comparing the compositions to primitive mantle, a similar pattern to the comparison to MORB is observed. Metals are typically below detection limits or have a ratio around 1 while HFSE are highly enriched in the inclusions (Figure 3.20B). Complete LA-ICP-MS results of type P1 inclusions are presented in Table 3.10. Comparing major element compositions by SEM-EDS defined area analyses and LA-ICP-MS, FeO and MgO are higher in LA-ICP-MS results, otherwise all other major elements correlate well between the two techniques.

3.3.8 LA-ICP-MS of fluid inclusions

Trace element concentrations of secondary type S3 inclusions were obtained by LA-ICP-MS for several FIAs in mafic pegmatites from the CLG. As the laser intersected the inclusions, increases in count rates occurred commonly for measured isotopes of Na, K, Fe, Si, Mg, Al, Ti, V, Mn, Zr, W, Nb, Ta, Cs, and Hf (Figure 3.21). Cobalt, Ni, and Cu

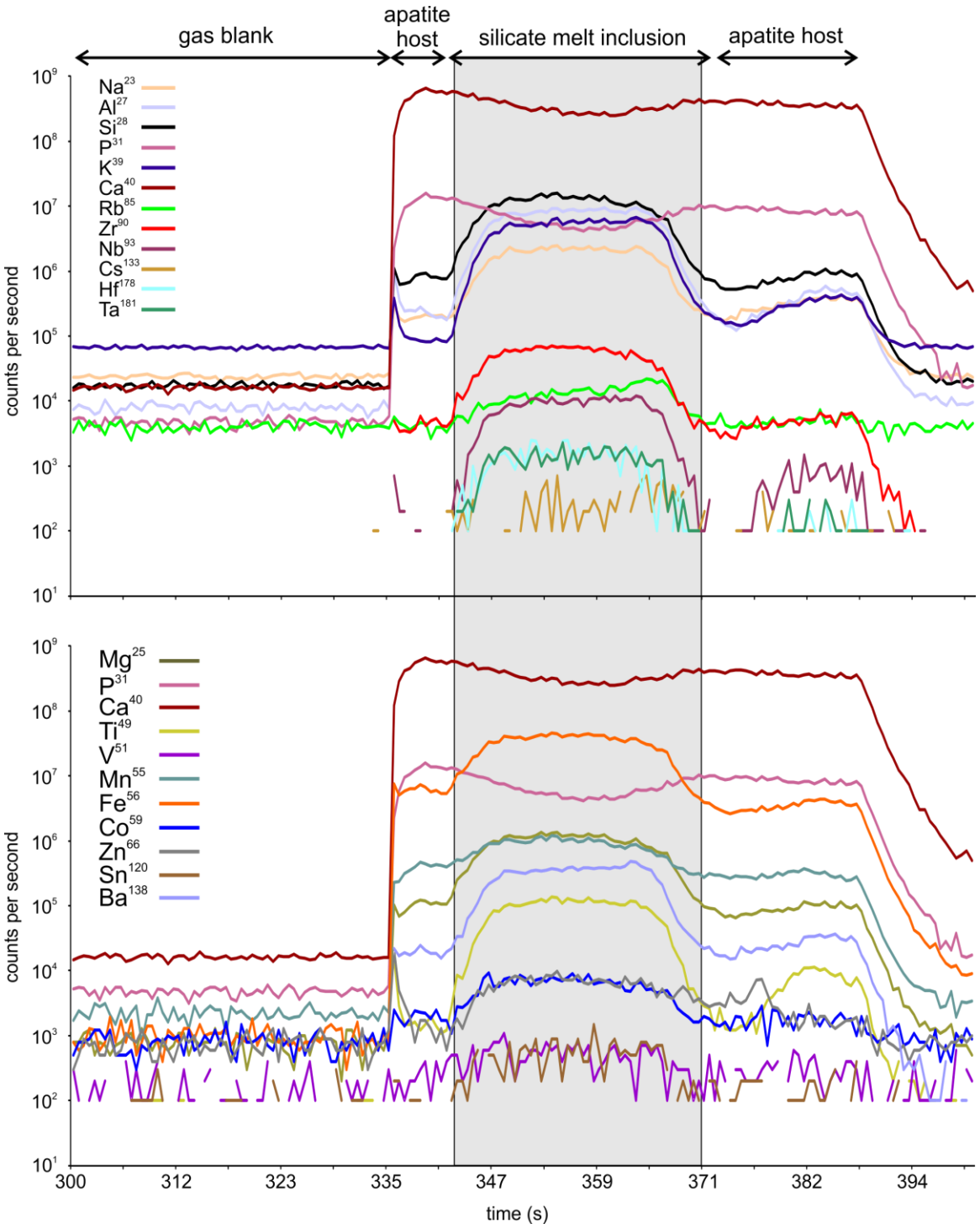

Figure 3.19: Representative LA-ICP-MS signal (signal vs. time) showing the ablation of a silicate melt inclusion in apatite. A gas blank is collected for ~35 s and then the laser is turned on. The apatite host is collected for ~ 6 s prior to the melt inclusion being encountered.

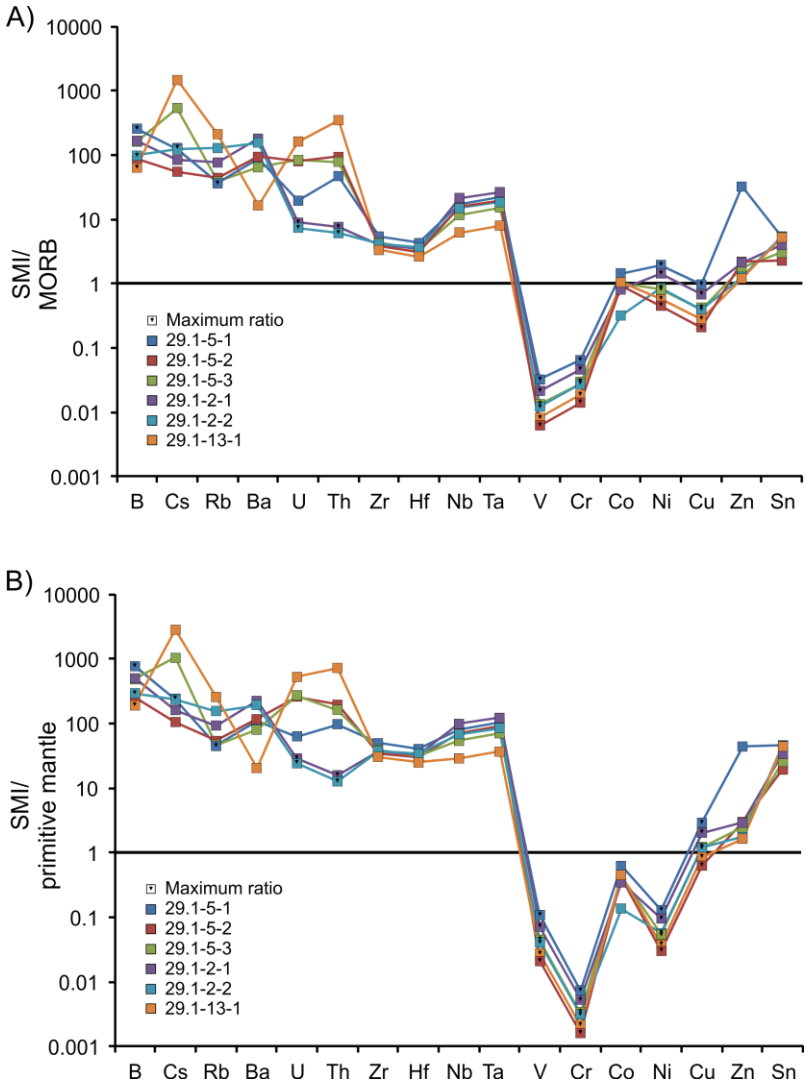

Figure 3.20 (previous page): Trace element concentrations of silicate melt inclusion compositions determined by LA-ICP-MS. A) Silicate melt trace element data normalized to MORB. Arrows pointing down in the symbols indicate that element was below detection in the silicate melt and therefore it is a maximum ratio plotted. Note that the metals (V, Cr, Ni, Cu) are all below detection limits in the silicate melt and their respective ratios are all depleted compared MORB and the detection limits for these elements were used to plot on the diagram. The high concentrations of HFSE in the melt inclusions relative to MORB, likely indicate an evolved melt was present in the CLG. B) Silicate melt trace element data normalized to primitive mantle. Arrows pointing down in the symbols indicate that element was below detection limits in the silicate melt and therefore it is a maximum ratio plotted. Maximum ratios for metals are typically below detection limits (close to 1), while HFSE are at least an order of magnitude enriched in the melts compared to primitive mantle.

Table 3.10: Silicate melt inclusion compositions determined by LA-ICP-MS using an internal standard of SiO_2

inclusion	29.1-5-1	29.1-5-2	29.1-5-3	29.1-2-1	29.1-2-2	29.1-13-1
SiO_2 (wt %)	52.2	52.2	52.2	52.2	52.2	52.2
TiO_2	1.39	1.22	1.11	1.47	1.03	0.58
Al_2O_3	18.6	13.6	11.5	14.3	14.9	16.4
FeO	38.9	23.7	32.3	22.3	10.8	18.6
MnO	0.52	0.29	0.30	0.29	0.18	0.05
MgO	12.7	12.2	13.2	10.6	2.64	8.46
Na_2O	1.56	1.09	1.11	1.75	4.97	4.64
K_2O	1.13	2.54	1.14	2.78	3.41	1.26
^{11}B (ppm)	b.d.l	78.0	147	b.d.l	b.d.l	b.d.l
^{51}V	b.d.l	b.d.l	b.d.l	b.d.l	b.d.l	b.d.l
^{52}Cr	b.d.l	b.d.l	b.d.l	b.d.l	b.d.l	b.d.l
^{59}Co	65.8	42.7	45.0	36.7	14.5	47.6
^{62}Ni	b.d.l	b.d.l	b.d.l	b.d.l	b.d.l	b.d.l
^{63}Cu	b.d.l	b.d.l	b.d.l	b.d.l	b.d.l	b.d.l
^{66}Zn	2439	166	135	161	96.9	91.3
^{75}As	b.d.l	b.d.l	b.d.l	b.d.l	b.d.l	b.d.l
^{85}Rb	b.d.l	32.47	28.4	56.5	94.6	155
^{90}Zr	524	363	414	387	397	323
^{93}Nb	53.3	47.7	35.7	65.6	45.4	19.1
^{98}Mo	b.d.l	b.d.l	b.d.l	b.d.l	1.91	1.49
^{107}Ag	b.d.l	b.d.l	b.d.l	b.d.l	b.d.l	b.d.l
^{120}Sn	6.00	2.52	3.35	4.42	5.95	5.78
^{133}Cs	b.d.l	0.50	4.92	0.76	1.11	13.38
^{138}Ba	731	777	532	1488	1291	136
^{143}Nd	207	141	b.d.l	b.d.l	b.d.l	b.d.l
^{147}Sm	60.3	40.6	b.d.l	b.d.l	b.d.l	b.d.l
^{153}Eu	10.3	9.11	b.d.l	b.d.l	b.d.l	6.70
^{169}Tm	b.d.l	0.84	b.d.l	b.d.l	b.d.l	b.d.l
^{172}Yb	b.d.l	3.08	b.d.l	b.d.l	b.d.l	b.d.l
^{178}Hf	11.5	8.39	8.99	9.41	9.66	7.08
^{181}Ta	3.86	3.39	2.63	4.56	3.17	1.37
^{182}W	b.d.l	b.d.l	b.d.l	b.d.l	b.d.l	0.81
^{208}Pb	b.d.l	3.43	3.48	b.d.l	4.36	27.2
^{209}Bi	b.d.l	b.d.l	b.d.l	b.d.l	b.d.l	b.d.l
^{232}Th	7.77	15.5	13.0	b.d.l	b.d.l	57.8
^{238}U	1.28	5.24	5.50	b.d.l	b.d.l	10.6

^{XX} represent measured isotopes and data is not only for the indicated isotope but for the element

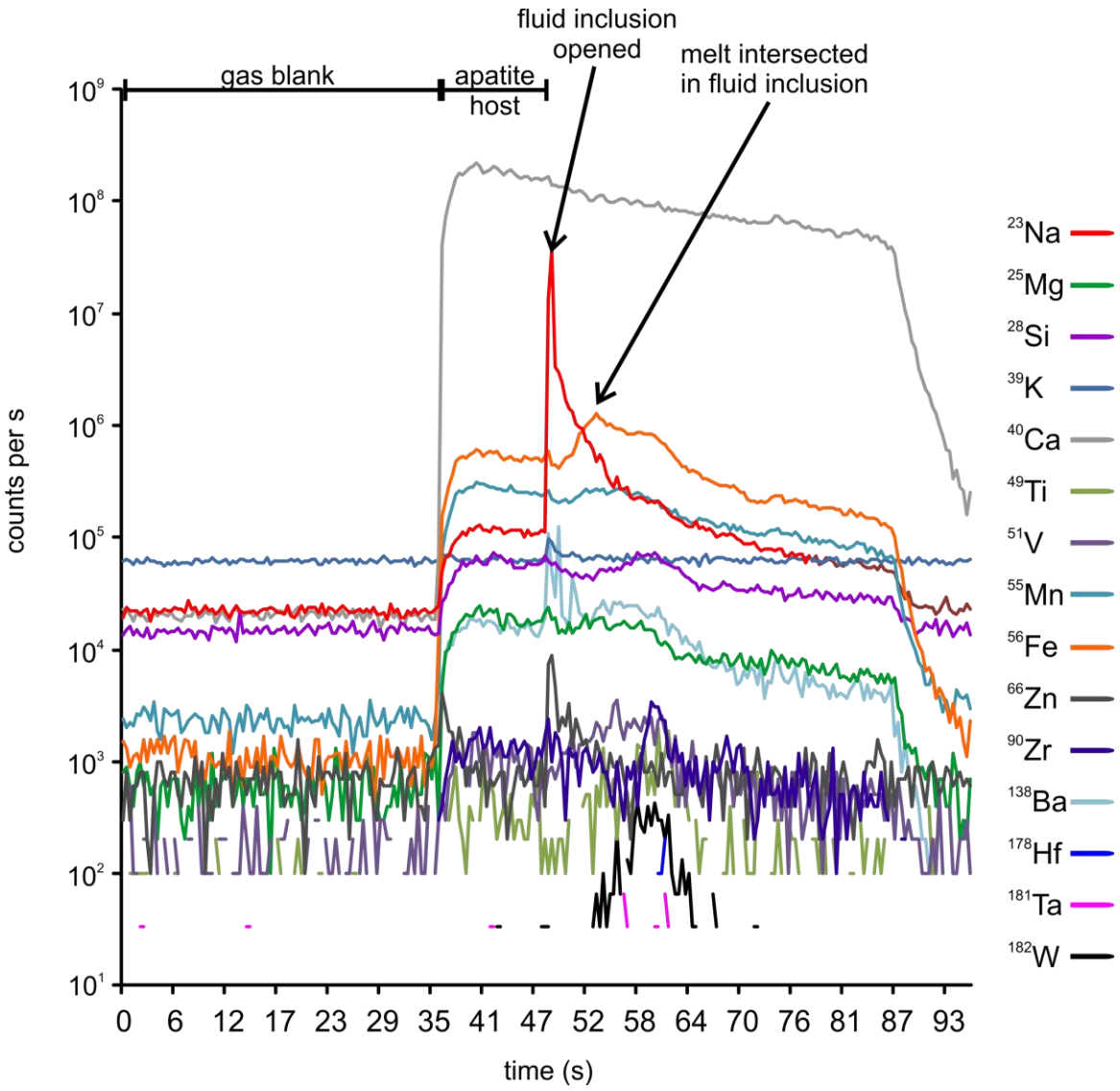

Figure 3.21: Representative LA-ICP-MS signal (signal vs. time) showing the ablation of fluid inclusions in apatite (inclusion 127-3-7-3). Calcium is shown to represent the apatite host. A gas blank is collected for ~ 60 s at which point the laser is turned on and the host apatite is collected for ~ 3 s before the fluid inclusion is encountered. Shortly after, the silicate melt in the inclusion is encountered (increased count rates for Si, Fe,Zr, W, Ta, Hf).

were also observed in the inclusions but rarely. Table 3.11 reports fluid inclusion compositional data for elements detected in inclusions as ratios relative to Na.

Semi-quantitative trace element concentrations of Cu and Co in type S3 fluid inclusions show a very weak positive trend plotted against Si (as a proxy for silicate melt) and plot in clusters when compared against Na, indicting the melt is the primary control on Cu and Co (Figure 22A,B). No correlations are observed for Ni (Figure 3.22A,B). High field strength elements (HFSE) also show a very weak correlation when plotted against Si, suggesting their concentrations are a function of the amount of melt trapped in the fluid inclusions and show no correlation to Na (Figure 22C,D). Ratios of Zr:Hf in the S3 inclusions vary between 5.9 and 168 (n=17) and Nb:Ta ratios range from 0.05 to 10.6 (n=8).

3.4 Discussion

3.4.1 Comparison to other mafic-ultramafic intrusions and the Blatchford Lake Intrusive Suite

Fluid inclusions present within the CLG share two common characteristics with inclusions described in other layered mafic-ultramafic intrusions (Table 3.1): i) they occur in abundance in evolved pegmatitic phases and within interstitial quartz and/or apatite as primary and secondary inclusions, indicating that they are present at a late magmatic stage but also persist to post-cumulus conditions, and ii) fluid inclusion assemblages preserve the trapping of immiscible carbonic-brine fluids. In comparison to the Bushveld and Stillwater complexes, there is an absence of an early high hydrosaline melt (> 80 wt % NaCl; Ballhaus and Stumpfl, 1986; Hanley et al., 2008) in the CLG. Fluid inclusions described in this study have very similar texture and composition to inclusions described

Table 3.11: Bulk trace element concentrations in fluid inclusion determined by LA-ICP-MS

Sample	^{23}Na (ppm)	^{25}Mg	^{27}Al	^{28}Si	^{31}P	^{39}K	^{40}Ca	^{49}Ti	^{51}V	^{55}Mn	^{56}Fe	^{59}Co
127-3_1_1.xl	b.d.l	4354	20.7	2427	54731	b.d.l	607985	31.6	7.16	889	7928	b.d.l
127-3_1_2.xl	15252	5122	b.d.l	665	65395	151	577099	32.9	4.93	685	8590	b.d.l
127-3_1_3.xl	b.d.l	4240	b.d.l	709	60017	69.7	599874	28.2	5.34	1180	10018	b.d.l
127-3_1_5.xl	6834	4028	b.d.l	359	71425	69.8	579158	26.6	5.08	653	6446	b.d.l
127-3_1_6.xl	10860	4537	b.d.l	974	65366	40.5	582522	27.3	5.83	752	7606	b.d.l
127-3_1_8.xl	6474	2556	15.6	9047	63437	49.9	583851	42.7	3.69	342	3710	b.d.l
127-3_1_9.xl	11120	3224	b.d.l	b.d.l	61976	65.4	591751	29.1	4.96	795	6582	b.d.l
127-3_1_10.xl	b.d.l	3882	55.8	2803	56689	b.d.l	603598	b.d.l	7.78	954	8926	b.d.l
127-3_1_11.xl	43644	2934	81.0	2107	56473	112	565249	202	18.78	645	7786	b.d.l
127-3_1_12.xl	41800	3051	b.d.l	173	62383	174	560094	30.4	4.96	1025	7745	b.d.l
127-3_1_13.xl	63694	b.d.l	b.d.l	b.d.l	67023	186	532392	28.0	6.25	b.d.l	b.d.l	b.d.l
127-3_1_14.xl	10708	b.d.l	b.d.l	b.d.l	65936	68.8	588921	25.5	b.d.l	339	b.d.l	3.47
127-3_2_3.xl	12627	b.d.l	b.d.l	354	72945	76.9	575413	30.6	2.31	1051	4641	b.d.l
127-3_5_1.xl	7473	3710	b.d.l	308	65705	39.7	587658	33.8	9.25	803	7088	3.94
127-3_5_2.xl	18832	b.d.l	b.d.l	b.d.l	69377	66.5	574927	29.2	b.d.l	b.d.l	b.d.l	b.d.l
127-3_5_3.xl	2201	4842	5141	19231	56800	59.0	522357	77.8	6.81	1495	58270	6.36
127-3_7_1.xl	1847	2138	1013	2364	68076	1926	588782	72.9	4.02	542	3121	2.02
127-3_7_2.xl	8894	b.d.l	b.d.l	b.d.l	66052	46.4	591040	31.1	3.83	b.d.l	b.d.l	b.d.l
127-3_7_3.xl	27218	2149	61.3	1115	64731	70.1	566713	120	21.5	1516	10656	b.d.l
127-3_7_5.xl	400	62097	45595	144882	12939	356	160123	90.0	56.6	1572	189712	83.1
127-3_7_6.xl	b.d.l	4189	484	2646	68343	326	566672	456	74.6	2531	25035	b.d.l
127-3_1_15.xl	18659	2862	b.d.l	b.d.l	60377	78.6	586149	32.0	2.83	964	7908	b.d.l
127-3_R_1.xl	429596	b.d.l	b.d.l	b.d.l	181688	b.d.l	b.d.l	b.d.l	b.d.l	b.d.l	b.d.l	b.d.l
127-3_R_3.xl	4004	3154	b.d.l	615	69453	105	587937	23.7	3.72	554	4148	b.d.l
127-3_R_4.xl	7173	7285	b.d.l	404	76427	b.d.l	565354	b.d.l	13.7	478	8128	b.d.l
127-3_R_5.xl	3455	445	392	3878	67395	422	586208	1408	7.56	b.d.l	5755	b.d.l
127-1_4_2.xl	200122	246	462	1263	33480	426	457743	25.7	b.d.l	1090	5514	b.d.l
127-1_a.xl	120515	4940	116	6424	37630	270	470166	55.5	34.1	1655	53433	6.33
127-1_b.xl	b.d.l	2631	585	5359	52218	b.d.l	610110	b.d.l	b.d.l	1025	6274	b.d.l
127-1EX_1_4.xl	b.d.l	3212	275	10249	17483	b.d.l	646916	b.d.l	b.d.l	1901	17883	b.d.l
127-1EX_1_5.xl	7727	1019	b.d.l	1993	47606	95.8	617199	27.6	b.d.l	2046	6312	b.d.l
127-1EX_1_6.xl	12150	1794	241	6778	40681	b.d.l	606002	300	34.6	1641	17003	b.d.l
127-1EX_1_7.xl	54916	b.d.l	b.d.l	2007	42979	b.d.l	571130	b.d.l	b.d.l	1663	16815	b.d.l
127-1EX_1_9.xl	140091	727	117	3100	25435	365	524480	b.d.l	b.d.l	1099	7055	b.d.l
127-1EX_1_10.xl	139949	3473	b.d.l	4754	35408	275	476502	233	23.1	1092	35274	7.93
127-1EX_1_11.xl	4313	938	b.d.l	b.d.l	54050	b.d.l	609097	b.d.l	14.0	1515	10185	b.d.l
127-1EX_1_12.xl	10092	6269	6103	30241	31847	8570	523511	7811	55.9	1026	54106	77.1
127-1EX_1_14.xl	70861	b.d.l	b.d.l	1897	31936	224	508468	290	95.8	1177	88094	b.d.l
127-1EX_1_16.xl	412	4583	443	18644	b.d.l	b.d.l	660751	b.d.l	b.d.l	453	19995	b.d.l
127-1EX_1_19.xl	14054	1048	88.3	1232	58654	350	565658	132	21.7	1511	37336	b.d.l
127-1EX_1_22.xl	679575	4771	2190	12730	b.d.l	b.d.l	b.d.l	b.d.l	b.d.l	4868	28403	b.d.l
127-1EX_2_2.xl	140293	3658	b.d.l	2624	58977	b.d.l	469440	b.d.l	b.d.l	237	5264	b.d.l
127-1EX_2_3.xl	63859	8410	b.d.l	1425	63097	342	521463	b.d.l	b.d.l	1595	15667	b.d.l
127-1EX_2_9.xl	2268	13999	b.d.l	4482	82581	82.6	535520	b.d.l	5.18	158	19613	b.d.l
127-1EX_2_11.xl	6277	17440	b.d.l	6375	83721	b.d.l	523530	b.d.l	b.d.l	196	18617	b.d.l
127-1EX_2_14.xl	4344	18785	4854	13052	80552	6324	515820	b.d.l	b.d.l	b.d.l	8982	b.d.l
127-1EX_2_15.xl	117601	9991	b.d.l	2339	52808	b.d.l	480166	b.d.l	b.d.l	1629	19117	b.d.l
127-1EX_2a_1.xl	48421	b.d.l	202	461	73145	549	541897	109	10.1	b.d.l	b.d.l	b.d.l
127-1EX_2a_2.xl	74927	5760	b.d.l	613	58033	b.d.l	521595	b.d.l	14.1	1589	17883	b.d.l
127-1EX_3_1.xl	11918	26753	b.d.l	22692	117618	b.d.l	335097	563	128	1649	116229	b.d.l
127-1EX_3_6.xl	35707	b.d.l	b.d.l	b.d.l	86705	b.d.l	529283	b.d.l	b.d.l	518	5086	b.d.l
127-1EX_R_3.xl	b.d.l	68412	b.d.l	36900	97182	b.d.l	b.d.l	b.d.l	b.d.l	b.d.l	452073	b.d.l
127-1EX_R_4.xl	1323	95322	8405	202129	15683	773	132210	60.9	20.4	1188	130838	20.6
127-1EX_R_5.xl	b.d.l	23329	b.d.l	11925	108853	b.d.l	392333	b.d.l	102	1213	104998	b.d.l
127-1EX_R_6.xl	294159	41017	b.d.l	19083	30419	b.d.l	b.d.l	b.d.l	b.d.l	b.d.l	329241	b.d.l
127-3_3_3.xl	702517	b.d.l	b.d.l	b.d.l	b.d.l	b.d.l	b.d.l	b.d.l	b.d.l	b.d.l	b.d.l	b.d.l
127-1EX_6_1.xl	b.d.l	18048	b.d.l	b.d.l	45171	b.d.l	555731	b.d.l	b.d.l	2912	62330	b.d.l
127-1EX_6_2.xl	b.d.l	186855	b.d.l	b.d.l	b.d.l	b.d.l	b.d.l	b.d.l	b.d.l	b.d.l	478506	b.d.l
127-1EX_6_3.xl	48487	b.d.l	b.d.l	b.d.l	53628	783	565862	b.d.l	b.d.l	620	7623	b.d.l
127-1EX_6_5.xl	17397	32422	19717	71718	b.d.l	22096	355933	13195	b.d.l	b.d.l	130097	b.d.l
127-1EX_6_6.xl	5057	7012	b.d.l	b.d.l	59022	b.d.l	591708	b.d.l	b.d.l	1420	10607	b.d.l
127-1EX_6_8.xl	1654	9181	b.d.l	4169	65403	b.d.l	566885	b.d.l	b.d.l	1258	22430	b.d.l
127-1EX_6_9.xl	2633	6010	b.d.l	14154	55469	b.d.l	584079	b.d.l	b.d.l	1174	7889	b.d.l
127-1EX_6a_3.xl	b.d.l	b.d.l	b.d.l	b.d.l	b.d.l	b.d.l	b.d.l	b.d.l	b.d.l	b.d.l	326005	b.d.l
127-1EX_8_3.xl	1361	1096	1660	7035	54227	2182	597999	1554	9.23	b.d.l	9031	40.9
127-1EX_8_6.xl	436535	b.d.l	b.d.l	b.d.l	b.d.l	b.d.l	b.d.l	b.d.l	b.d.l	b.d.l	268444	b.d.l
127-1EX_8_8.xl	b.d.l	b.d.l	b.d.l	b.d.l	b.d.l	b.d.l	524792	b.d.l	b.d.l	b.d.l	11308	b.d.l
127-1EX_8_10.xl	330631	b.d.l	b.d.l	b.d.l	b.d.l	b.d.l	b.d.l	b.d.l	b.d.l	b.d.l	425294	b.d.l
127-1EX_8_11.xl	189065	b.d.l	b.d.l	b.d.l	57918	1939	435408	b.d.l	b.d.l	b.d.l	b.d.l	b.d.l
127-1EX_8_12.xl	325550	b.d.l	b.d.l	b.d.l	b.d.l	b.d.l	b.d.l	b.d.l	b.d.l	b.d.l	152212	b.d.l
127-1EX_7_1.xl	51584	18153	14067	395111	b.d.l	12355	b.d.l	3731	b.d.l	b.d.l	5784	b.d.l
127-1EX_7_2.xl	b.d.l	3185	b.d.l	b.d.l	37551	b.d.l	480888	81.3	12.9	1857	180755	b.d.l
127-1EX_R_1.xl	710938	b.d.l	b.d.l	b.d.l	b.d.l	17912	b.d.l	b.d.l	b.d.l	b.d.l	b.d.l	b.d.l
127-1EX_R_2.xl	664173	b.d.l	b.d.l	b.d.l	b.d.l	b.d.l	b.d.l	b.d.l	b.d.l	b.d.l	b.d.l	b.d.l
127-1EX_R_4.xl	237210	49344	b.d.l	207866	b.d.l	b.d.l	b.d.l	b.d.l	b.d.l	b.d.l	103081	b.d.l

Table 3.11: Continued

^{62}Ni	^{63}Cu	^{66}Zn	^{75}As	^{90}Zr	^{93}Nb	^{107}Ag	^{120}Sn	^{133}Cs	^{138}Ba	^{178}Hf	^{181}Ta	^{182}W
b.d.l	20.5	b.d.l	3.79	3.40	b.d.l	b.d.l	b.d.l	b.d.l	11.4	b.d.l	b.d.l	b.d.l
b.d.l	b.d.l	b.d.l	b.d.l	6.96	b.d.l	b.d.l	b.d.l	b.d.l	23.6	b.d.l	b.d.l	b.d.l
20.8	21.9	b.d.l	4.81	1.12	b.d.l	b.d.l	b.d.l	b.d.l	b.d.l	0.19	b.d.l	0.26
b.d.l	25.0	b.d.l	b.d.l	6.65	b.d.l	b.d.l	b.d.l	b.d.l	28.5	b.d.l	b.d.l	0.58
b.d.l	b.d.l	b.d.l	4.65	2.83	b.d.l	b.d.l	b.d.l	b.d.l	22.3	b.d.l	b.d.l	0.26
b.d.l	b.d.l	14.0	4.16	1.80	b.d.l	b.d.l	b.d.l	b.d.l	10.5	0.11	b.d.l	0.16
b.d.l	b.d.l	b.d.l	5.76	b.d.l	b.d.l	b.d.l	b.d.l	b.d.l	24.4	b.d.l	b.d.l	b.d.l
b.d.l	32.4	b.d.l	b.d.l	8.08	b.d.l	b.d.l	b.d.l	b.d.l	11.0	b.d.l	b.d.l	b.d.l
b.d.l	b.d.l	b.d.l	2.90	3.79	0.80	b.d.l	b.d.l	b.d.l	8.29	0.22	0.075	0.35
b.d.l	32.0	b.d.l	b.d.l	19.4	b.d.l	b.d.l	b.d.l	b.d.l	41.0	0.31	b.d.l	0.45
b.d.l	b.d.l	b.d.l	b.d.l	5.45	b.d.l	b.d.l	b.d.l	b.d.l	78.0	b.d.l	0.047	b.d.l
b.d.l	b.d.l	69.1	b.d.l	b.d.l	b.d.l	b.d.l	b.d.l	b.d.l	b.d.l	b.d.l	b.d.l	0.080
b.d.l	39.4	b.d.l	b.d.l	b.d.l	b.d.l	b.d.l	b.d.l	b.d.l	b.d.l	b.d.l	b.d.l	b.d.l
b.d.l	b.d.l	b.d.l	b.d.l	14.8	b.d.l	b.d.l	b.d.l	b.d.l	b.d.l	b.d.l	b.d.l	0.59
b.d.l	20.0	b.d.l	3.30	4.07	b.d.l	b.d.l	b.d.l	b.d.l	63.5	b.d.l	b.d.l	b.d.l
b.d.l	18.5	b.d.l	b.d.l	5.30	b.d.l	b.d.l	b.d.l	b.d.l	12.5	b.d.l	b.d.l	b.d.l
b.d.l	b.d.l	b.d.l	b.d.l	7.55	0.15	0.41	b.d.l	0.046	322	0.19	0.015	0.23
b.d.l	b.d.l	11.4	b.d.l	9.05	b.d.l	b.d.l	b.d.l	b.d.l	26.7	b.d.l	b.d.l	0.22
b.d.l	40.2	46.0	b.d.l	13.4	b.d.l	b.d.l	b.d.l	b.d.l	171	0.34	b.d.l	4.31
15.8	b.d.l	85.5	b.d.l	2.39	0.38	b.d.l	0.24	0.058	7.30	b.d.l	0.12	0.03
b.d.l	b.d.l	54.8	9.47	26.6	1.58	b.d.l	b.d.l	b.d.l	155	0.68	0.16	7.51
b.d.l	29.7	9.12	b.d.l	1.60	b.d.l	b.d.l	b.d.l	b.d.l	19.4	b.d.l	b.d.l	0.38
b.d.l	b.d.l	b.d.l	b.d.l	b.d.l	b.d.l	b.d.l	b.d.l	b.d.l	b.d.l	b.d.l	b.d.l	b.d.l
b.d.l	b.d.l	b.d.l	b.d.l	4.64	b.d.l	b.d.l	b.d.l	b.d.l	42.7	0.24	b.d.l	b.d.l
b.d.l	b.d.l	b.d.l	b.d.l	13.6	b.d.l	b.d.l	b.d.l	b.d.l	b.d.l	b.d.l	b.d.l	b.d.l
26.3	50.6	60.6	b.d.l	11.4	0.65	b.d.l	1.126032	b.d.l	7.54	0.44	0.26	2.14
b.d.l	b.d.l	b.d.l	b.d.l	74.3	b.d.l	b.d.l	b.d.l	b.d.l	b.d.l	0.77	b.d.l	0.65
b.d.l	b.d.l	b.d.l	3.56	59.2	b.d.l	b.d.l	b.d.l	b.d.l	b.d.l	0.35	0.081	b.d.l
b.d.l	b.d.l	b.d.l	b.d.l	144	b.d.l	b.d.l	b.d.l	b.d.l	b.d.l	b.d.l	b.d.l	b.d.l
b.d.l	147	b.d.l	b.d.l	235	b.d.l	b.d.l	b.d.l	b.d.l	b.d.l	2.16	b.d.l	1.68
b.d.l	b.d.l	56.2	b.d.l	b.d.l	b.d.l	b.d.l	b.d.l	b.d.l	41.8	b.d.l	b.d.l	1.15
b.d.l	b.d.l	b.d.l	b.d.l	85.7	b.d.l	b.d.l	b.d.l	b.d.l	b.d.l	b.d.l	b.d.l	b.d.l
b.d.l	b.d.l	b.d.l	b.d.l	99.9	b.d.l	b.d.l	b.d.l	b.d.l	30.3	b.d.l	b.d.l	b.d.l
b.d.l	b.d.l	b.d.l	b.d.l	73.0	b.d.l	b.d.l	b.d.l	b.d.l	b.d.l	b.d.l	b.d.l	b.d.l
b.d.l	b.d.l	b.d.l	b.d.l	64.2	b.d.l	b.d.l	b.d.l	b.d.l	b.d.l	b.d.l	b.d.l	b.d.l
b.d.l	b.d.l	b.d.l	b.d.l	28.1	b.d.l	b.d.l	b.d.l	b.d.l	77.4	b.d.l	b.d.l	b.d.l
b.d.l	162	1011	334	31.4	7.07	b.d.l	20.71228	b.d.l	127	1.17	10.5	41.0
b.d.l	b.d.l	b.d.l	b.d.l	30.7	b.d.l	b.d.l	b.d.l	b.d.l	b.d.l	b.d.l	b.d.l	b.d.l
b.d.l	b.d.l	b.d.l	b.d.l	1231	b.d.l	b.d.l	b.d.l	b.d.l	b.d.l	8.57	b.d.l	1.69
b.d.l	b.d.l	b.d.l	b.d.l	15.6	b.d.l	b.d.l	b.d.l	b.d.l	97.2	b.d.l	b.d.l	1.49
b.d.l	b.d.l	b.d.l	b.d.l	b.d.l	b.d.l	b.d.l	b.d.l	b.d.l	b.d.l	b.d.l	b.d.l	b.d.l
b.d.l	b.d.l	b.d.l	b.d.l	59.5	b.d.l	b.d.l	b.d.l	b.d.l	30.7	b.d.l	b.d.l	b.d.l
b.d.l	b.d.l	b.d.l	b.d.l	b.d.l	b.d.l	b.d.l	b.d.l	b.d.l	71.8	b.d.l	b.d.l	b.d.l
b.d.l	b.d.l	b.d.l	b.d.l	43.6	b.d.l	b.d.l	b.d.l	b.d.l	85.6	0.53	b.d.l	0.99
b.d.l	b.d.l	b.d.l	b.d.l	204	b.d.l	b.d.l	b.d.l	b.d.l	120	b.d.l	b.d.l	3.61
b.d.l	b.d.l	b.d.l	b.d.l	b.d.l	b.d.l	b.d.l	b.d.l	b.d.l	469	b.d.l	b.d.l	2.86
b.d.l	b.d.l	b.d.l	b.d.l	b.d.l	b.d.l	b.d.l	b.d.l	b.d.l	96.1	b.d.l	b.d.l	b.d.l
b.d.l	26.78	1362	16.7	79.4	1.89	2.16	1.36	b.d.l	80.1	1.28	0.74	2.05
b.d.l	b.d.l	b.d.l	b.d.l	52.8	b.d.l	b.d.l	b.d.l	b.d.l	53.8	b.d.l	b.d.l	b.d.l
b.d.l	b.d.l	b.d.l	b.d.l	215	b.d.l	b.d.l	b.d.l	b.d.l	b.d.l	b.d.l	b.d.l	b.d.l
b.d.l	b.d.l	b.d.l	b.d.l	b.d.l	b.d.l	b.d.l	b.d.l	b.d.l	b.d.l	b.d.l	b.d.l	b.d.l
b.d.l	b.d.l	b.d.l	b.d.l	244	b.d.l	b.d.l	b.d.l	b.d.l	b.d.l	b.d.l	b.d.l	b.d.l
b.d.l	b.d.l	b.d.l	b.d.l	7.17	b.d.l	b.d.l	b.d.l	b.d.l	7.84	b.d.l	b.d.l	b.d.l
b.d.l	b.d.l	b.d.l	b.d.l	64.9	b.d.l	b.d.l	b.d.l	b.d.l	b.d.l	b.d.l	b.d.l	b.d.l
b.d.l	b.d.l	b.d.l	b.d.l	b.d.l	b.d.l	b.d.l	b.d.l	b.d.l	b.d.l	b.d.l	b.d.l	b.d.l
b.d.l	b.d.l	b.d.l	b.d.l	b.d.l	b.d.l	b.d.l	b.d.l	b.d.l	b.d.l	b.d.l	b.d.l	b.d.l
b.d.l	b.d.l	b.d.l	b.d.l	91.9	b.d.l	b.d.l	b.d.l	b.d.l	b.d.l	b.d.l	b.d.l	1.88
b.d.l	b.d.l	b.d.l	b.d.l	b.d.l	b.d.l	b.d.l	b.d.l	b.d.l	1969	b.d.l	b.d.l	b.d.l
b.d.l	b.d.l	b.d.l	b.d.l	143	b.d.l	b.d.l	b.d.l	b.d.l	b.d.l	b.d.l	b.d.l	b.d.l
b.d.l	b.d.l	b.d.l	958	456	b.d.l	b.d.l	b.d.l	b.d.l	b.d.l	b.d.l	36.3	77.3
b.d.l	b.d.l	b.d.l	b.d.l	26.2	b.d.l	b.d.l	b.d.l	b.d.l	26.2	b.d.l	b.d.l	b.d.l
b.d.l	b.d.l	b.d.l	b.d.l	b.d.l	b.d.l	b.d.l	b.d.l	b.d.l	b.d.l	b.d.l	b.d.l	b.d.l
b.d.l	b.d.l	b.d.l	b.d.l	248	b.d.l	b.d.l	b.d.l	b.d.l	79.3	b.d.l	b.d.l	b.d.l
b.d.l	b.d.l	b.d.l	b.d.l	b.d.l	b.d.l	b.d.l	b.d.l	b.d.l	b.d.l	b.d.l	b.d.l	b.d.l
354	56.16	314	848	8.10	3.11	b.d.l	4.08	0.068	72.3	b.d.l	66.5	59.2
b.d.l	b.d.l	b.d.l	b.d.l	b.d.l	b.d.l	b.d.l	b.d.l	b.d.l	b.d.l	b.d.l	b.d.l	b.d.l
b.d.l	b.d.l	b.d.l	b.d.l	b.d.l	b.d.l	b.d.l	b.d.l	b.d.l	b.d.l	b.d.l	b.d.l	b.d.l
b.d.l	b.d.l	b.d.l	b.d.l	b.d.l	b.d.l	b.d.l	b.d.l	b.d.l	b.d.l	b.d.l	b.d.l	b.d.l
b.d.l	b.d.l	b.d.l	b.d.l	b.d.l	b.d.l	b.d.l	b.d.l	b.d.l	98.2	b.d.l	b.d.l	b.d.l
b.d.l	b.d.l	b.d.l	b.d.l	b.d.l	b.d.l	b.d.l	b.d.l	b.d.l	b.d.l	b.d.l	b.d.l	b.d.l
b.d.l	b.d.l	b.d.l	b.d.l	b.d.l	b.d.l	b.d.l	b.d.l	b.d.l	b.d.l	b.d.l	b.d.l	b.d.l
b.d.l	b.d.l	b.d.l	b.d.l	b.d.l	b.d.l	b.d.l	b.d.l	b.d.l	b.d.l	b.d.l	b.d.l	b.d.l
b.d.l	b.d.l	b.d.l	b.d.l	b.d.l	b.d.l	b.d.l	b.d.l	b.d.l	b.d.l	b.d.l	b.d.l	b.d.l
b.d.l	b.d.l	b.d.l	b.d.l	b.d.l	b.d.l	b.d.l	b.d.l	b.d.l	b.d.l	b.d.l	b.d.l	b.d.l
b.d.l	b.d.l	b.d.l	b.d.l	b.d.l	b.d.l	b.d.l	b.d.l	b.d.l	b.d.l	b.d.l	b.d.l	b.d.l

b.d.l = below detection limits; ^{xx} represent measured isotopesand data is not only for the indicated isotope but for the element

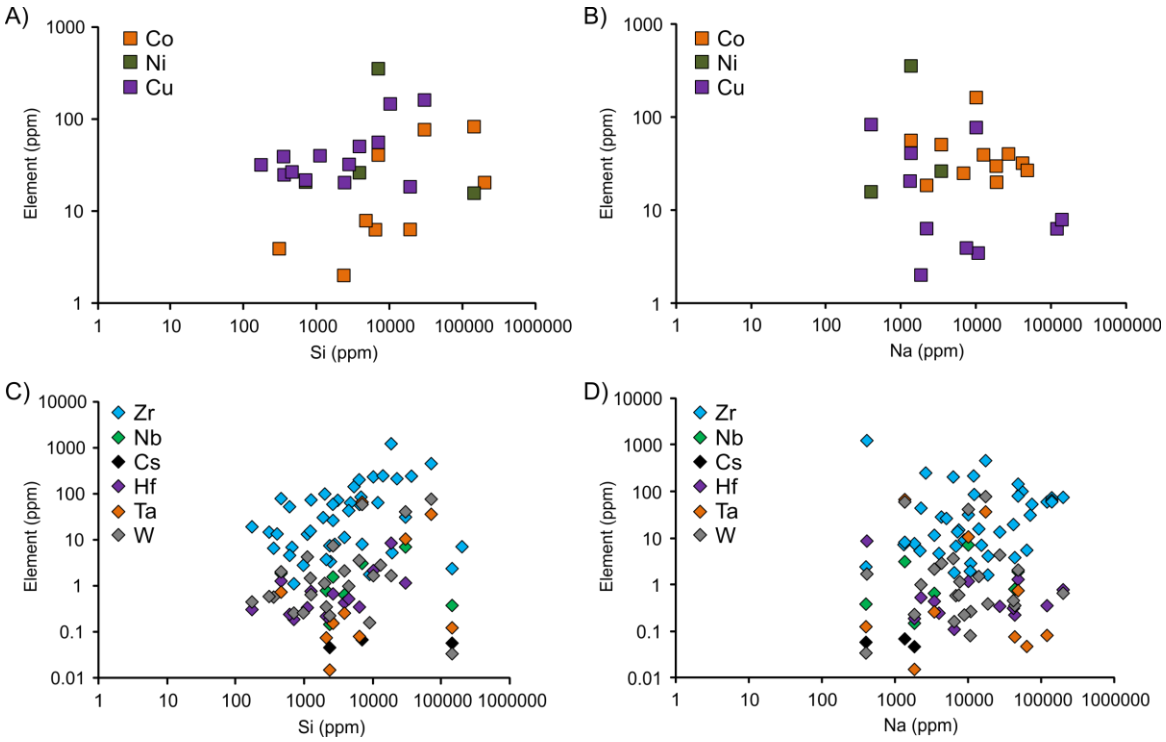

Figure 3.22: Plots of bulk trace element concentrations in type S3 fluid inclusions. A) Si vs. Co, Ni, and Cu. Note how Co and Cu have a slightly positive correlation with Si, while Ni there isno correlation. B) Na vs. Co, Ni, and Cu. Note how there are no correlations, indicating the brine does not influence these metals. C) Si vs. HFSE and Cs. Note the slightly positive correlations for all HFSE. There is no correlation for Cs. D) Si vs. HFSE and Cs. Note how there are no correlations, indicating the brine does not influence these metals. Error associated with each data point is approximately the size of the symbol for each plotted data point.

in the Bushveld, Stillwater, and Duluth Complexes where there is evidence for the trapping of two immiscible fluid phases, an aqueous brine end-member and a carbonic fluid end-member (Ballhaus and Stumpfl, 1986; Hanley et al., 2008; Gál et al., 2013). In the Stillwater Complex, Hanley et al. (2008) attributed this association to brine and carbonic fluid being sourced from different interstitial silicate liquids at different depths in the intrusion. No primary carbonic fluid inclusions were identified in the CLG as they were in the Lac des Iles and Duluth complexes (Hanley and Gladney, 2011; Gál et al., 2013) but secondary carbonic inclusions are abundant in the CLG. The similarities of volatile inclusion characteristics between large PGE sulphide mineralized layered intrusions is significant because it demonstrates that the presence of these brine-carbonic fluids in not associated with primary metal melt enrichment.

A fluid inclusion study of the T Zone that is hosted in the Thor Lake Syenite in the eastern lobe of the BLIS was conducted by Feng (2014, unpublished PhD thesis). The inclusions observed in that study were primarily aqueous inclusions with minor amounts of CO_2 and CH_4 detected by Raman spectroscopy, and showing a wide range in salinity (2-27 wt % NaCl equiv.). The general characteristics of these fluids are different from those of the CLG as the fluids observed in the CLG are much richer in carbonic phases, though they do have a similar range in salinity (9-28 wt % NaCl equiv.). Some trace elements detected (at ppm levels) in fluid inclusions from the T Zone are also detected in fluid inclusions from the CLG (K, Ti, Fe, Nb, Ta, Zr) in this study.

3.4.2 Trapping conditions for SMI and parental melt source

Silicate melt inclusions (P1) were trapped relatively early in the crystallization sequence as they are preserved in early cumulus apatite in the CLG and allow temperature

constraints for crystallization of the system to be inferred. Three lines of evidence point towards these inclusions being primary silicate melts: i) inclusions show similar bulk compositions, ii) the inclusions are mineralogically different from their host rocks (plagioclase: An_{93-98} in SMI vs. An_{37-40} in gabbro), and iii) some minerals present in the SMI are different then the minerals present in the host rock (i.e., zircon, K-feldspar). Based on SMI microthermometry, the $T_m^{liquidus}$ of the system is approximately 1164 ± 35°C based on the final melting temperature of solids in P1 inclusions hosted in early primocryst apatite. The liquidus temperature can also be approximated using the SMI major element chemistry and entering the composition into the program PELE (Boudreau, 1999). The average major element composition determined by defined area analyses of exposed P1 inclusions by using SEM-EDS was used as the melt composition for this liquidus determination instead of the LA-ICP-MS results because LA-ICP-MS analyses do not include Ca because it is present in the host (i.e., apatite). Output from PELE for the average melt inclusion composition assuming 0 wt % H_2O and 0 wt % CO_2, results in a liquidus temperature of 1179°C. This estimate is probably too high as some H_2O and CO_2 would be present in the melt (indicated by the presence of amphibole; Figure 3.8), with MORB typically containing <1 wt % H_2O (Sobolev and Chaussidon 1996; Fischer and Marty 2005; Wallace 2005) and <0.6 wt % CO_2 (Fisher and Marty 2005). Various combinations of H_2O and CO_2 contents were input into PELE to calculate a more realistic liquidus temperature. For example, results from PELE with H_2O contents of 1 wt % and CO_2 of 0.6 wt %, gave a liquidus temperature of 1156°C. A liquidus range for the CLG SMI between 1156° and 1179°C determined by PELE is consistent with $T_m^{liquidus}$ obtained by microthermometry (Figure 3.23).

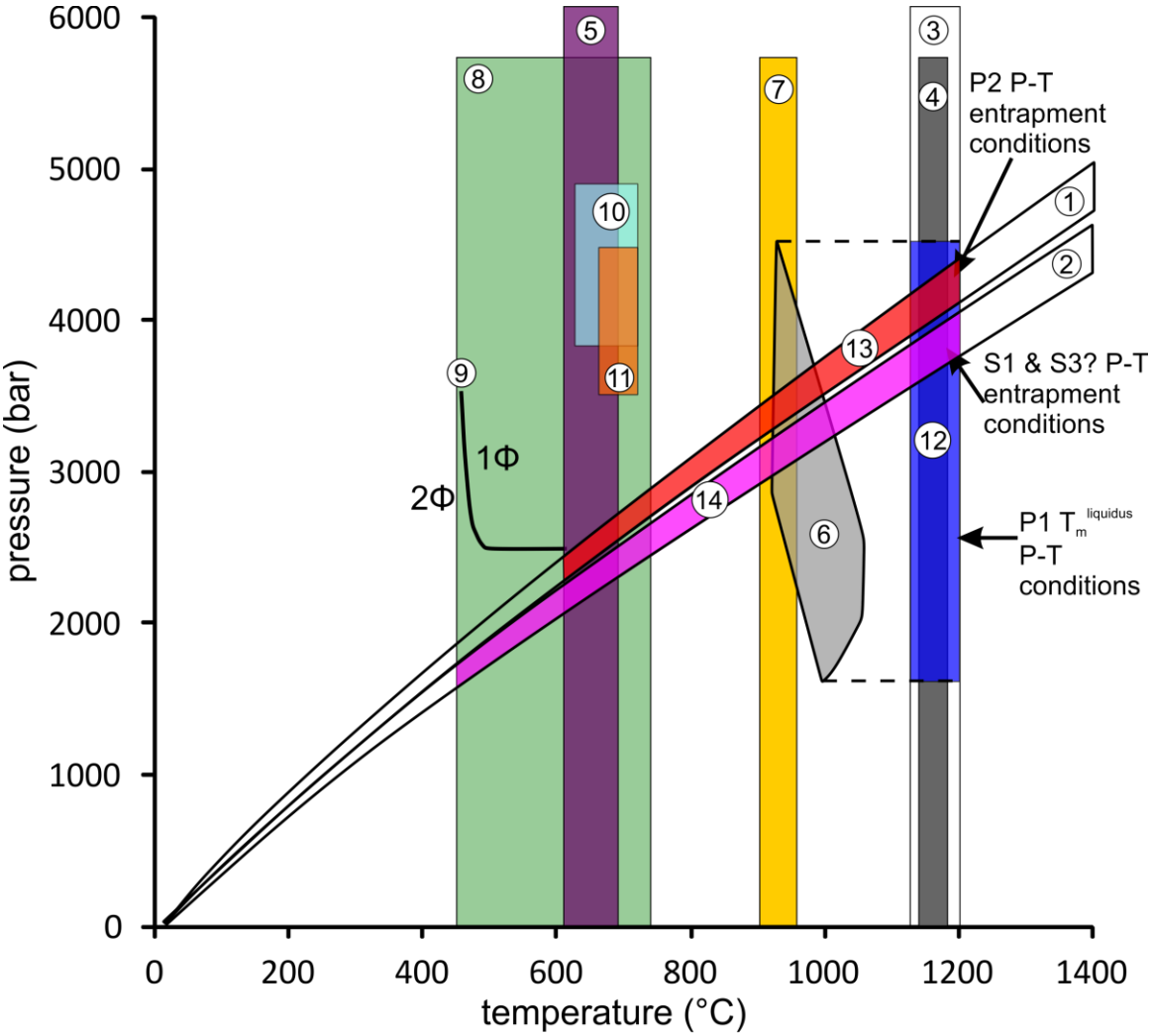

① range on type P2 carbonic component isochores
② range on type S1 fluid inclusions isochores
③ $T_m^{liquidus}$ from type P1 inclusion microthemometry
④ $T_m^{liquidus}$ calculated from PELE using Type P1 inclusion composition (0-1 wt% H_2O; 0-0.6 wt%CO_2)
⑤ final crystallization temperature based on 1st melting from P1 inclusion microthermometry
⑥ Al- and Ti-in-hornblende thermometer and barometer of Ernst and Liu (1998)
⑦ amphibole-plagioclase thermometer of Blundy and Holland (1990)
⑧ Ap-Bt thermometer (Zhu & Sverjensky, 1992)
⑨ isothermal unmixing line of a fluid with 20 wt% NaCl equiv, 20 mol % CO_2 (Schmidt & Bodnar, 2000)
⑩ P-T conditions of the Hearne Channel granite, Mumford, 2013
⑪ P-T conditions of the Whiteman quartz syenite, Mumford, 2013
⑫ estimated P-T conditions of entrapment for P1 melt inclusions
⑬ preliminary P-T constraints on P2 inclusion entrapment
⑭ P-T constraints on S1 and S3? inclusion entrapment

Figure 3.23 (previous page): Estimation of pressure and temperature trapping conditions for silicate melt and fluid inclusions in the CLG. Area 1 represents the range of isochores calculated for the carbonic component of P2 inclusions. Area 2 represents the range of isochores calculated for S1 inclusions. Area 3 is the range of $T_m^{liquidus}$ determined from microthermometry of P1 melt inclusions. Area 4 is the range of $T_m^{liquidus}$ calculated using the program PELE and the major element chemistry of P1 inclusions with variations of H_2O (0-1 wt %) and CO_2 (0-0.6 wt %) contents. Area 5 is the range of P-T conditions for the formation of amphibole base on the Al- and Ti-in-hornblende thermobarometer of Ernst and Liu (1998). Area 6 is the calculated temperature of formation of amphibole based on the plagioclase-amphibole thermometer of Blundy and Holland (1990). Area 7 is the calculated final temperature of equilibrium based on the apatite-biotite halogen exchange thermometer of Zhu and Sverjensky (1992). Line 8 is the solvus separating 1-phase (1Φ) and 2-phase (2Φ) field for an aqueous fluid with a composition of 20 wt % NaCl equiv. and 20 mol % CO_2 (Schmidt and Bodnar, 2000). Area 9 is the calculated P-T conditions of formation for the Hearne Channel granite (Mumford, 2013, unpublished PhD thesis). Area 10 is the calculated P-T conditions of formation for the Whiteman Lake quartz syenite (Mumford, 2013, unpublished PhD thesis). Area 11 is the P-T conditions of entrapment for the P1 melt inclusions, based on the $T_m^{liquidus}$ and the pressures determined from the Al- and Ti-in-hornblende thermobarometer, resulting in P-T conditions of 1135° and 1200°C and 1.6 to 4.5 kbar. Area 12 is preliminary constraint of the P-T conditions of P2 fluid inclusion entrapment based on the isochore intersections with $T_m^{liquidus}$ and the Al-in-hornblende thermometer resulting in P-T conditions of 910°-1200°C and 3.2-4.4 kbar. Area 12 is the constraint on S1 and S3 fluid inclusion entrapment based on the intersection of S1 isochores with $T_m^{liquidus}$ and the apatite-biotite thermometer, resulting in P-T conditions of 455° to 1200°C and 1.5 to 4.05 kbar. However, due to the difference in relative variability of S1 and S3 Th_{CO2} values it would suggest that the S1 isochores may not be applicable to the carbonic phase in S3 inclusions.

A rough constraint on the pressure of SMI entrapment can be approximated by the Al- and Ti-in-hornblende thermobarometer (Ernst and Liu, 1998; Figure 3.23). Titanium is accommodated increasingly in the amphibole structure as temperature increases but has a slightly negative correlation with increasing pressure. Aluminum content increases with increasing pressure (Ernst and Liu, 1998). Late cumulus amphibole phenocrysts in the CLG are Ti-rich (3.3-4.6 wt % TiO_2) and relatively Al-rich (11.6-12.3 wt % Al_2O_3), equating to T-P conditions ranging from 925° to 1060°C and 1.6 to 4.5 kbar, respectively (Figure 3.23). The pressure range obtained by this thermobarometer is similar to other pressure constraints determined for lithologies in the western portion of the BLIS (Hearne Channel granite: 3.84-4.93 kbar; Whiteman Lake quartz syenite: 3.49-4.43 kbar; Mumford, 2013, unpublished PhD Thesis; Figure 3.23) but extends to lower pressures in the CLG. Using the pressure determined from the amphibole composition and the $T_m^{liquidus}$ from microthermometry, entrapment of primary SMI is estimated between 1130° and 1200°C and 1.6 to 4.5 kbar (5.9-16.6 km depth; Figure 3.23; Table 3.12). However, caution should be taken with these pressure estimates because the amphibole analyzed is a late cumulus phase yielding lower temperatures (925°-1060°C) than the melt inclusions were likely trapped. Therefore the pressure at the time of amphibole crystallization may have been slightly different than at the time of melt entrapment.

Trace elements determined by LA-ICP-MS show that silicate melt inclusions in the CLG are enriched in HFSE and depleted in metals (Ni, Co, Cr, Cu; Figure 3.19A,B). The depletion in metals could be related either to i) S-saturation prior to the trapping of melt inclusions, leading to metal loss to a sulphide liquid, ii) the melt was derived from an initially metal-depleted, or iii) the melt was crustally contaminated.

Table 3.12: Trapping conditions estimated for fluid and melt inclusions

inclusion type	P range (kbar)	T range (°C)	basis for trapping P, T estimate
P1 (silicate melt inclusions)	1.6-4.5	1130-1200	$T_m^{liquidus}$(microthermometry) and Al- and Ti-in-hornblende T
P2 (CO_2-CH_4-H_2O-NaCl)	2.3-4.4	610-1200	intersection of carbonic-phase isochore with first melting and $T_m^{liquidus}$ of SMI
S1 & S3 (S1: CO_2-CH_4; S3: CO_2-CH_4-H_2O-NaCl)	1.5-4.05	455-1200	intersection of carbonic-phase isochore with $T_m^{liquidus}$ and Ap-Bt halogen exchange T
Whiteman Lake Quartz Syenite[1]	3.49-4.43	670-722	plagioclase-amphibole T and Al-in-hornblende P
Hearne Channel Granite[1]	3.84-4.93	645-719	plagioclase-amphibole T and Al-in-hornblende P

[1] P-T conditions from Mumford (2013, unpublished PhD thesis)

Modelling presented in Chapter 2 shows that for the sulphide mineralization present in the CLG, an already metal-depleted silicate melt was likely responsible for forming the observed marginal mineralization. As explained in Chapter 2, if a small degree of partial melting of the mantle occurs, then not all of the sulphide in the mantle may be melted and dissolved into the silicate liquid, leaving the sulphide in the upper mantle along with the Ni, Cu, and PGE that reside in that sulphide (Li et al., 2001). The low degree of partial melt for the CLG fits with the proposed evolution of the Nechalacho Layered Suite (NLS) where high concentrations of incompatible elements in the NLS would imply that only a small degree of partial melting of an upwelled mantle occurred (Sheard et al., 2012). Mumford (2013, unpublished PhD thesis) also suggests that the CLG magma was likely sourced from metasomatism of a previously depleted mantle source based on the depleted Nd isotopic signature and the high enrichment of LILE and HFSE. As well, Mumford (2013, unpublished PhD thesis) states that the most likely lithology to contaminate the BLIS was the Morose Granite and possibly lower crustal rocks of similar composition to the Kam group of the Yellowknife Greenstone Belt. Therefore, the CLG magma was formed from low degrees of partial melting that was crustal contamination, causing the enrichment in HFSE and the relatively low concentrations of chalcophile metals in the SMI (Figure 3.19A,B).

3.4.3 Trapping conditions for primary and secondary brine-carbonic fluid inclusion assemblages

Given that the apatite in mafic pegmatites is an early coarse-grained cumulate phase, P2 fluids are early with respect to pegmatite formation but are late with respect to the overall crystallization sequence of the intrusion. To constrain the trapping conditions

for immiscible fluids that are not trapped on a two-phase curve because of the variable V:L ratios of inclusions indicating they did not form by unmixing from an initial one-phase fluid, the method of intersecting isochores can be used (Roedder and Bodnar, 1980). This method involves calculating isochores for the end-member carbonic-aqueous fluids. Where the isochores intersect, the P-T conditions at which the carbonic-brine fluids were trapped can be estimated (Roedder and Bodnar, 1980). Type S3 fluid inclusions do not meet the criteria for using the method of intersecting isochores because only the carbonic end-member fluid (type S1 inclusions) is observed. Observation and microthermometric measurements of the corresponding brine end-member would be required to utilized the method of intersecting isochores. Type S3 inclusions cannot be used as the brine end-member since they are not close to suspected end-member composition (as defined by a solvus relationship in the brine-carbonic fluid system) because of their variable carbonic phase proportions. However, intersection of isochores for the carbonic end-member fluid isochores (S1 inclusions) with independent mineral thermometers give approximate P-T conditions for the trapping of the carbonic end-member and by textural association, the mixed brine-carbonic assemblages. Type P2 inclusions may also preserve the same immiscible brine-carbonic fluid assemblages based on the large variation in V_{CO2} vol %, (Figure 3.9D-G).

To calculate the isochores for the carbonic component of P2 inclusions and S1 inclusions, equations of state from Bowers and Helgeson (1983) and Bakker (1999) were used, based on a fluid composition of 98 % CO_2 and 2% CH_4. Methane was identified in the S1 inclusions based on microthermometry and Raman spectroscopy (ave 2 % ± 0.01 CH_4; n=24). The same ratio of CO_2:CH_4 ratio is characteristic of the carbonic component

in type P2 inclusions based on similar Tm_{CO2} values (-57.3° to -57.1°C). There may be a thin coating of an aqueous fluid on the inner inclusion wall of S1 inclusions that is not visually detectable but the apatite Raman peaks overlap with the peaks for H_2O, making it impossible to confirm this. For S1 inclusions, theoretical densities were calculated for a CO_2-CH_4-H_2O fluid with 93 % CO_2, 2 % CH_4, and 5 % H_2O, in order to determine the impact a small amount of H_2O would have on the inclusion density. The calculated densities were comparable to densities calculated for a H_2O-free, CO_2-CH_4 fluid (0.706-0.731 g/cc), therefore water has a negligible effect and inclusions were modeled in the CO_2-CH_4 system.

The intersection of the carbonic phase isochores in P2 inclusions with the $T_m^{liquidus}$ of P1 inclusions constrains the maximum P-T conditions of the entrapment of P2 inclusions, corresponding to 4.4 kbar and 1200°C (Figure 3.23). This would represent the maximum P-T conditions for P2 inclusions because the $T_m^{liquidus}$ for an overall melt of the CLG is likely not representative for the mafic pegmatites. Pegmatites typically crystallize from evolved melts with higher H_2O contents. With the additional H_2O, the $T_m^{liquidus}$ becomes lower. Minimum constraints for P2 inclusions may be determined by the intersection of the P2 carbonic phase isochores with the first melting temperature of SMI (which represents the final crystallization temperature of the system). This intersection results in a minimum P-T condition for the P2 carbonic phase entrapment of 2.3 kbar and 610°C. To summarize, based on the P2 isochore intersections with the first melting and $T_m^{liquidus}$ of SMI, the P-T conditions for P2 inclusion entrapment range from 610°-1200°C and 2.3-4.4 kbar (8.5-16.3 km depth; Figure 3.23; Table 3.12).

As with P2 inclusions, the intersection of S1 isochores with the $T_m^{liquidus}$ of P1 inclusions gives maximum P-T conditions of the entrapment of S1 inclusions, corresponding to 4.05 kbar and 1200°C (Figure 3.23). Again, this would be maximum entrapment conditions because of the reasons stated for the P2 inclusions above. Minimum estimates on the trapping of S1 inclusions can be constrained by the intersection of S1 isochores with the lowest temperature calculated from the apatite-biotite halogen exchange thermometer, which determines minimum conditions for fluid migration through the mafic pegmatites in the CLG, suggesting S1 fluids likely did not migrate through the pegmatites at temperatures lower than this thermometer (Zhu and Sverjensky, 1992). The minimum entrapment conditions equate to 455°C and 1.5 kbar (Figure 3.23) and the range of P-T conditions for the entrapment of S1 inclusions would be 455° to 1200°C and 1.5 to 4.05 kbar (5.6-15 km depth; Figure 3.23; Table 3.12). The large range in pressure is consistent with the variability in Th_{CO2} in S1 inclusions, which is either due to variable trapping pressure during formation of or post-entrapment modification.

As described above, S1 inclusions likely represent the carbonic end-member fluid for the mixed brine-carbonic S3 fluid inclusions and therefore the trapping conditions for S3 inclusions are likely the same as trapping conditions for S1 inclusions. However, due to the difference in relative variability of S1 Th_{CO2} (26.9-30.9°C) and S3 Th_{CO2} (-7.9-30.6°C) it would suggest that the S1 isochores may not be applicable to the carbonic phase in S3 inclusions. Variability in Th_{CO2} in S3 inclusions may indicate either differences in trapping pressure during formation of S3 inclusions or post-entrapment modification. The mode of homogenization for S1 and S3 is also different as S1

inclusions primarily homogenize to the vapor state while S3 carbonic phase primarily homogenizes to the liquid state.

3.4.4 Apatite compositional evolution-halogen and trace element geochemistry

3.4.4.1 Tracing halogen content in the melt

The evolution of volatile components during crystallization of a layered intrusion is recorded by the distribution and composition of halogen-bearing cumulus and intercumulus minerals (e.g., apatite, amphibole, micas; Boudreau et al., 1995). However, apatite is a more robust mineral for tracing halogens than amphiboles or micas because it has fewer crystal-chemical reactions possible for defining equilibrium halogen content with associated fluids or melts. Apatite also exhibits typical ideal halogen substitution behavior at magmatic temperatures (Volfinger et al., 1985; Tacker and Stormer 1989; Boudreau, 1995).

The F-rich nature of apatite in the CLG is broadly similar to other layered mafic-ultramafic intrusions such as the Skaergaard intrusion, Munni Munni Complex, Great Dyke, and in Stillwater and Bushveld Complexes above their respective major PGE reefs (Figure 3.3; Nash 1976; Boudreau, 1993; Boudreau et al., 1995; Meurer and Boudreau, 1996; Willmore et al., 2000). No Cl-rich apatite was observed in the CLG as is present in the Stillwater and Bushveld Complexes in and stratigraphically below their major PGE reef horizons (Boudreau and McCallum, 1989; Boudreau and Kruger, 1990).

As volatiles separate from a crystallizing mafic liquid, the liquid will become enriched in F compared to Cl, as F partitions into the melt relative to a volatile phase (i.e., fluid-incompatible) while Cl is compatible in a volatile phase and would fractionate into

exsolving fluid. Therefore, low Cl/F ratios in apatite can be linked directly to Cl loss during degassing and fractionation (Boudreau, 1995; Mathez and Webster, 2005). As well, no cumulus minerals sequester halogens, aside from trace amounts in mica and amphibole, thus Cl loss during degassing alone leads to decreasing Cl/F ratios in the liquid and lower Cl/F ratios in crystallizing apatite (Boudreau et al., 1995). Since apatite in the CLG is very F-rich, Cl has been lost to an exsolved volatile fluid phase prior to its crystallization or the melt simply had a low Cl/F ratio to begin with.

Comparing apatite compositions within the CLG, it is evident that the interstitial apatite in the clinopyroxenite and the gabbro with disseminated sulphides is slightly more Cl-rich than the coarse-grained apatite in pegmatites and gabbro hosting cumulus apatite (Figure 3.3). If all the apatites were formed from the same liquid, then the more Cl-rich apatite evolved from a liquid that had not yet lost as much of a Cl-rich volatile fluid phase and therefore, formed earlier than the other F-rich apatites. Alternatively, these more Cl-rich apatites could have crystallized in deeper portions of the intrusion at higher pressure where volatiles had not yet separated causing the Cl/F ratio to be higher (Boudreau et al., 1995). Within a single thin section there can be up to a 20 mol % variation in X_F (CL-07-01-29.1) and up to a 6 mol % variation in X_{Cl} (CL-07-01-95.9). Boudreau et al. (1993) has suggested these thin section variations in Cl and F mol % to, apatite being isolated from the intercumulus liquid as individual grains grew, therefore separate apatite grains in a thin section could have formed from intercumulus liquids with slightly different F/Cl ratios. However, the overall F-rich nature of all apatite in the CLG would suggest that the CLG was relatively Cl-poor and F-rich.

3.4.4.2 Trace element content of apatites in gabbro and mafic pegmatites

The REE concentration in apatite is lower in the fine- to medium-grained cumulus apatite hosting melt inclusions in a medium-grained gabbro (CL-07-01-29.1) compared to the coarse-grained apatite hosting primary and secondary fluid inclusions in mafic pegmatites (Figure 3.6A,B). These elevated levels of REE may be related to the amount of interstitial liquid the apatite has crystallized from. The finer grained apatite crystallized early relative to the other cumulus minerals in the unit, consistent with its lower REE concentrations relative to the apatite in the mafic pegmatites.

The higher concentrations of REE in apatite in the mafic pegmatites could be explained by the "trapped liquid shift effect" (Cawthorn, 2013). As melt crystallizes, incompatible elements (e.g., REE) will be concentrated into intercumulus liquid. As the cumulate column undergoes compaction, the intercumulus melt can migrate upwards and then mix with the overlying melt (Mathez, 1995). If apatite has already started to crystallize in this overlying melt, the apatite will interact with this REE-rich intercumulus liquid and the apatites REE concentrations will thereby be increased (Cawthorn, 2013). This effect agrees with the occurrence of the most REE-rich apatite occurring in the most evolved lithologies (i.e., mafic pegmatites). The intercumulus liquid will also be enriched in H_2O, which may account for their coarse-grained nature. A strong negative Eu anomaly occurring within two of the pegmatites would imply that the intercumulus liquid that may have been responsible for the "trapped liquid shift effect" was sourced from an area of the melt that had already crystallized plagioclase (Cawthorn, 2013). Compared to apatites in the mafic pegmatites, apatite in gabbro has a minor negative Eu anomaly (Figure 3.6A), suggesting that at the time of apatite crystallization, only minor plagioclase

had crystallized (Cawthorn, 2013). This would be in agreement with the observed apatite inclusions within plagioclase.

3.4.5 Brine-carbonic fluid immiscibility

The presence of type S1 inclusions trapped together in the same FIAs as type S3 inclusions showing large variations in carbonic:aqueous ratios suggests these assemblages trapped two coeval immiscible fluids. By this interpretation of the petrographic observations the fluids may represent the products of unmixing of an initially one-phase H_2O-CO_2-CH_4-NaCl fluid, to produce carbonic-dominant and brine-dominant end-member fluids. Under this scenario, end-member carbonic-dominant inclusions should have the same carbonic:aqueous ratio and brine-dominant end-member inclusions should have the same aqueous:carbonic ratio. The proportions of each end-member formed by unmixing are dictated by the starting fluid composition (Bowers and Helgeson, 1983; Duan et al., 1995; Schmidt and Bodnar, 2000; Diamond, 2003). In the mixed S1-S3 FIAs this is not the case as aqueous:carbonic ratios are highly variable because the inclusions trapped mixtures of both end-memebrs (i.e., V_{CO2} = 10-80 vol %; Figure 3.11A,B). The position of the solvus for a 20 wt % NaCl and 20 mol % CO_2 (X_{CO2} = 0.1884) one-phase aqueous-carbonic fluid is plotted on Figure 3.23. This solvus may not be applicable to the CLG because carbonic fluid appears to dominate the FIAs in terms of volumetic abundance. The position of the solvus for a one-phase fluid with much higher CO_2 concentrations is not experimentally known. While the exact location of the solvus relevant to the fluid inclusions in this study cannot be accurately plotted the experiments of Schmidt and Bodnar (2000) showed that at a constant salinity, and with increasing CO_2 content, the solvus shifts to higher P-T conditions. Therefore, we suggest the solvus for

an initial one-phase fluid, given the predominance of carbonic-dominant fluids present in the CLG, would likely be at extremely high and unrealistic P-T conditions.

It may be more appropriate to account for the variable carbonic:aqueous phase proportions in the type P2 and S3 inclusions by the heterogeneous trapping of a carbonic-dominant fluid and an brine-dominant fluid that did not unmix from an initially one-phase fluid. Rather the fluid end-members could have been sourced from two different parts of the intrusion and mingled immiscibly in common pathways. This is possible due to the differential solubility and timing of exsolution for CO_2 and H_2O-NaCl fluids from a basaltic melt. Due the low solubility of CO_2 in a melt compared to the solubility of H_2O and Cl, CO_2 should be the first volatile to exsolve (Webster, 1999; Lowenstern, 2001). It is possible that the carbonic-dominant fluid was sourced from a hotter melt (i.e., shallower stratigraphic level) that was CO_2-saturated and releasing carbonic-dominant volatiles, while at the same time a colder melt (i.e., deeper stratigraphic level) in the CLG was releasing a brine-dominant fluid having already lost CO_2 during earlier degassing (Hanley et al., 2008). These two fluids were then trapped simultaneously in the pegmatites, which would have acted as common fluid pathways for these fluids. The petrographic result would be the variable V_{CO2} vol % present in P2 and S3 inclusions and the coexistence of S1 and S3 inclusions in a given FIA (Figure 3.11I). An end-member brine-dominant fluid (with no CO_2 present) would be expected to be present in coexistence (i.e., in the same FIA) with S1 and S3 inclusions, but this end-member brine-dominant fluid (with no or minor CO_2 present) was not observed in the CLG. The process described above has been attributed to the trapped of brine-dominant and carbonic-dominant fluids in the Stillwater Complex (Hanley et al., 2008). Heterogeneous trapping

of $NaCl-H_2O-CO_2$ and $CO_2-NaCl-H_2O$ fluids has also been reported in the Bushveld Complex (Ballhaus and Stumpfl, 1986) and so appears to be a feature common to both barren and mineralized, layered mafic-ultramafic intrusions.

3.4.6 Fluid metal sources

Fluids in layered mafic-ultramafic intrusions have been suggested through field and petrographic relationships, and directly identified through microanalysis of fluid inclusions, to carry metals and sulphur, and therefore have the potential ability to impact the ore tenor in layered intrusions (Boudreau and McCallum, 1992; Meurer et al., 1999; Polovina et al., 2004; Hanley, 2006, unpublished PhD thesis; Hanley and Gladney, 2011; Gál et al., 2013; Schisa et al., 2014). Nickel (16-354 ppm), Cu (18-160 ppm), and Co (2-83 ppm) were determined by LA-ICP-MS in S3 fluid inclusions present in the CLG (Table 3.11) and are comparable in concentrations to metal contents in fluid inclusions from Ni-Cu-PGE-mineralized differentiated intrusions (Sudbury, Cu=5-1000 ppm, Hanley et al., 2005; Lac des Iles Complex: Cu and Ni = 1-100 ppm, Hanley and Gladney, 2011). The metals Co, Ni, and Cu are higher in S3 inclusions with minor melt than the primary SMI.

Compared to Ni, Cu, and Co, HFSE elements are much more abundant in S3 inclusions in the CLG (Table 3.11). A similar process to the one described above for the enrichment of trace elements in apatite in the mafic pegmatites could likely be responsible for the HFSE enrichment in type S3 fluid inclusions. As the cumulate pile crystallizes, incompatible elements and H_2O become concentrated in the intercumulus liquid but the major element composition of the intercumulous liquid may not differ significantly from the original cumulate liquid (Boudreau, 1995; Mathez, 1995). The

settling of cumulus minerals down through the cumulate column will cause the intercumulus liquid to efficently migrate upwards (e.g., Boudreau, 2016) and as pressure and/or temperature decreases, the solubility of H_2O in the interstitial melt will drop and a volatile phase will be exsolved (Mathez, 1995; Métrich and Wallace, 2005). The volatile fluid phase exsolving from this intercumulus liquid is moderately saline (~23 wt % NaCl; average salinity of the aqueous phase in type S3 inclusions) and the metals could partition into the fluid during exsolution. Zajacz et al. (2008) conducted LA-ICP-MS analysis of naturally coexisting fluid and silicate melt inclusions (of granitic composition) to determine metal fluid/melt partition coefficients ($K_D^{fluid/melt}$) and found that for Zr and Nb, $K_D^{fluid/melt}$ are < 0.1, while for Cs and W, $K_D^{fluid/melt}$ are > 1. Experimental studies have shown that Zr has a $K_D^{fluid/melt}$ between 0.2 and 4.6 and Nb has a $K_D^{fluid/melt}$ between 0.2 and 4.7 (Webster, et al., 1989). As illustrated in Figure 3.13 and 3.22, the mafic silicate melt is present in variable proportions within type S3 fluid inclusions indicating it migrated through the cumulate (mush) pile together with the immiscible brine-carbonic fluid. This melt in type S3 inclusions is highly evolved based on its enrichment in HFSE but not in terms of its major element chemistry (i.e., their mafic composition, as determined by SEM-EDS; Figure 3.13). Such a process has been described by Mathez (1995) in the Bushveld Complex, where pyroxenes in the Merensky Reef are not evolved in terms of their major element chemistry but are highly evolved in terms of their REE chemistry resulting from metasomatic enrichment by trace element enriched silicate liquid migrating up through the cumulate pile. This would indicate that as the carbonic fluid and brine exsolved and mingled in the intrusion, both of these fluid types interacted with an HFSE-enriched intercumulus liquid (sample of which is trapped in type S3

inclusions; Figure 3.22). Therefore, even at $K_D^{fluid/melt}$ near unity for HFSE, W, and Cs, the fluids would be a powerful metasomatic agent for the redistribution of these metals.

If the HFSE-enriched melt and associated fluid were externally derived, rather than internally from the CLG, a possible source would be the eastern lobe of the BLIS. In this area, the Thor Lake syenite and the NLS rocks contain Zr, Nb, and REE mineralization (Pinckston and Smith, 1995; Sheard et al., 2012; Timofeev and Williams-Jones, 2015a, 2015b; Möller and Williams-Jones, 2016). Zirconium, Nb, and REE mineralization in the NLS is thought to have formed when an alkaline, volatile rich, nepheline syenite magma was intruded into the Thor Lake Syenite. The NLS represents the most fractionated crystalization products of residual melt derived from the nepheline syenitic magmatic intrusion (Sheard et al., 2012; Möller and Williams-Jones, 2016). Möller and Williams-Jones (2016) state that a key factor for the NLS melt to sequester HFSE was its parental melt prefractionation and its exceptionally evolved, Na- and halogen-rich chemistry. The HFSE were further enriched in a final volatile stage - (H_2O, F, C) and Fe-rich, Al-depleted residual melt. If an Fe-rich, Al-depleted, HFSE-rich melt and brine from the NLS was able to channel through the mafic pegmatites of the CLG then this could be the source of melt and brine-carbonic fluid in S3 inclusions. However, SEM-EDS mapping and spot analyses of S3 inclusions show that Mg and Ti are common in the trapped melt phase in S3 inclusions and Na and K are low or absent, which is more consistent with this melt being derived from the CLG rather than from the NLS. Further work is needed to evaluate the source of this melt.

On examining the bulk rock compositions of mafic pegmatites and unaltered fine-grained gabbros in the CLG and comparing the data with rocks from Thor Lake and the

NLS, it is apparent that Thor Lake and the NLS magmas had much higher concentrations of Rb, Zr, Nb, Sn, Hf, and Ta (Figure 3.24). The mafic pegmatites in the CLG have very similar bulk trace element patterns and concentrations as SMI (P1 inclusions). Fine-grained gabbro follows the same pattern but have lower concentrations of incompatible trace elements overall (Figure 3.24). If the HFSE-enriched melt (and fluids in type P1, and S3 inclisons) were externally derived, one would expect that the trace element pattern for the pegmatites in the CLG to be similar to those for Thor Lake and NLS. Examining Nb/Ta and Zr/Hf ratios (Figure 3.25), shows that rocks of the CLG have relatively similar Nb/Ta ratios to trapped melts (P1 inclusions) wheras the rocks of the NLS, Thor Lake, and the Grace Lake granite show a much wider range in Nb/Ta ratio. Again, if the HFSE-enriched melt and fluid were externally derived, the Nb/Ta ratios of the pegmatites may be expected to have been modified by the Nb and Ta being introduced into the system from the external source. However, only Zr/Hf ratios show evidence of some modification. The similar trace element patterns and the relatively similar Nb/Ta ratios of the mafic pegmatites compared to the SMI suggest no influence from Thor Lake or the NLS. The presence of magnetite in S3 inclusions is also evidence that the HFSE-enriched melt and fluid in S3 inclusions were internally derived as the fluid could have interacted with magnetite in the mafic pegmatites or other units in the CLG and reprecipitated in fractures in apatite during melt and fluid migration.

Other elements and accidentally entrapped minerals occurring within type S3 fluid inclusions as found by LA-ICP-MS and/or SEM have a more ambiguous source. The source for As and S could be fluids interacting with the Burwash sediments as the highest natural abundances of As tend to occur in phosphatic sediments, organic-rich shales, and

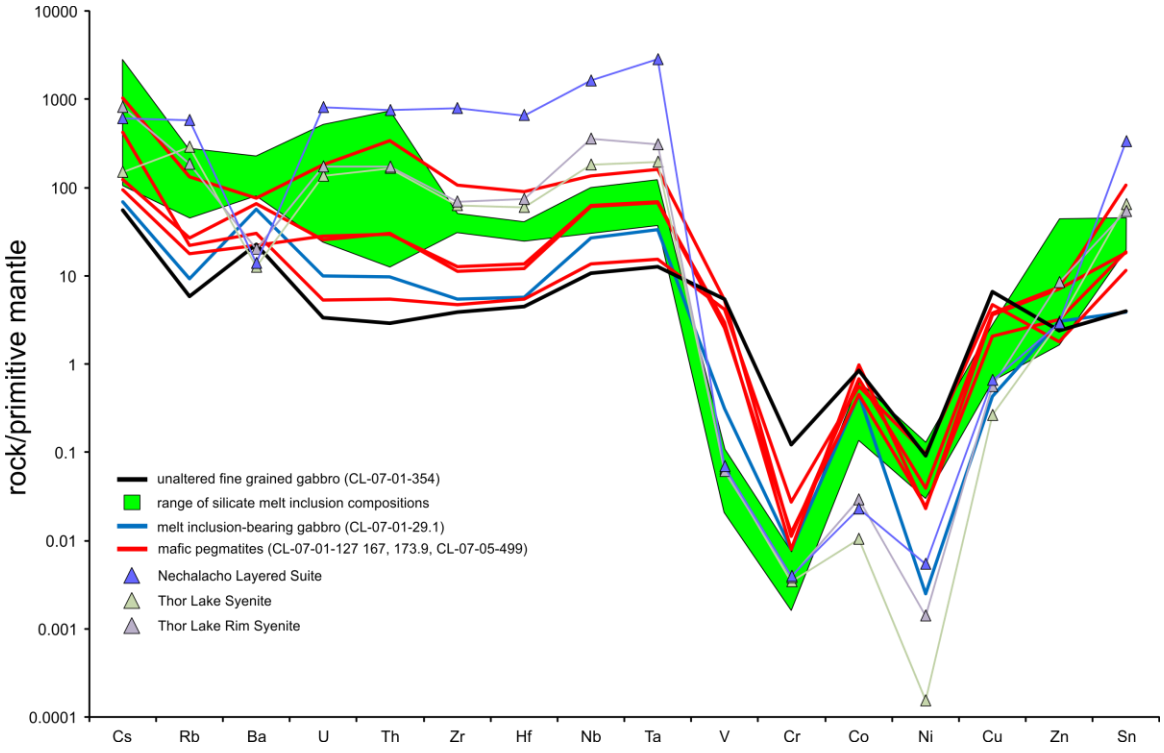

Figure 3.24: Silicate melt inclusions and rocks of the CLG compared to the Thor Lake Syenite, Thor Lake Rim Syenite, and the Nechalacho Layered Suite all normalized to primitive mantle. Note the much higher concentrations of Zr, Nb, Hf, and Ta in the Thor Lake and Nechalacho rocks compared to units in the CLG and the silicate melts. Data for Thor Lake units and Nechalacho come from Möller and Williams-Jones (2016).

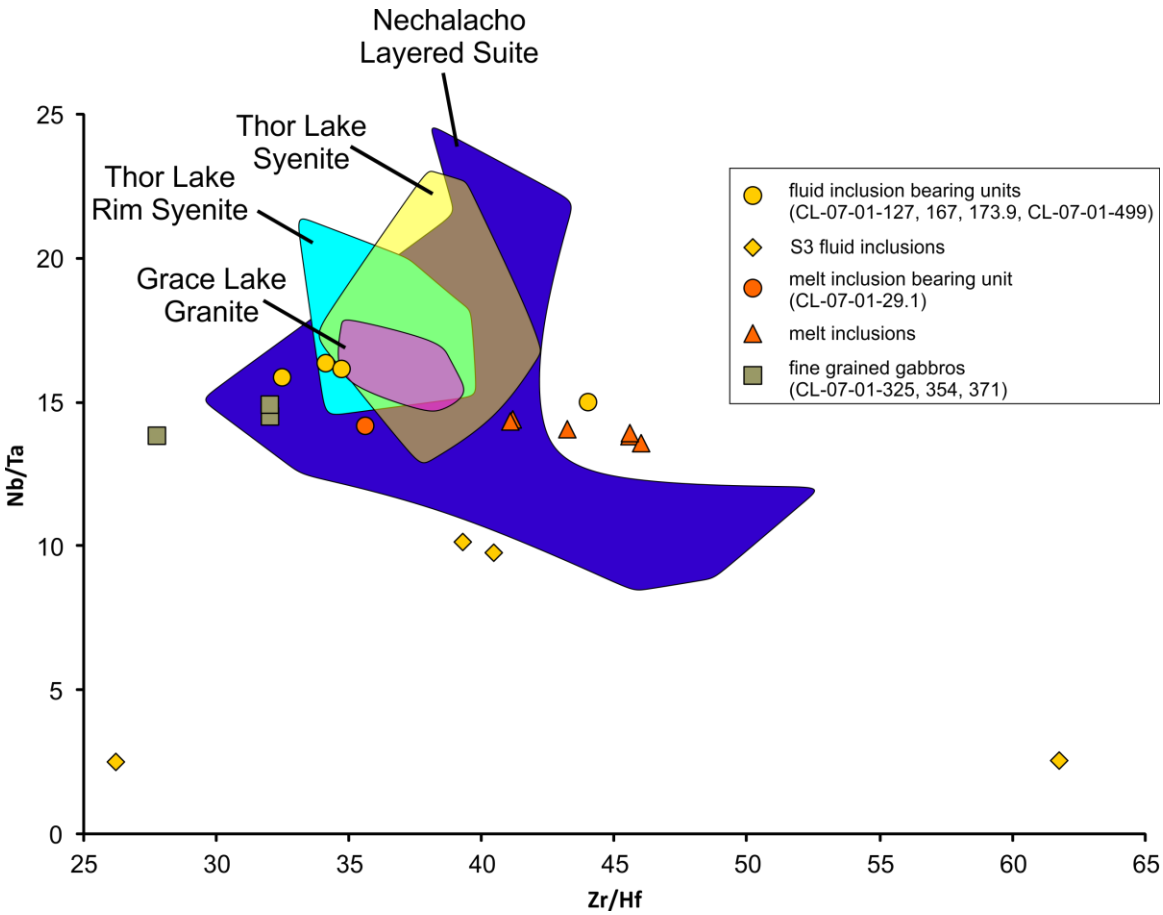

Figure 3.25: Binary plot of Zr/Hf ratio against Nb/Ta ratio of melt and fluid inclusion bearing host rocks, unaltered fine-grained gabbros of the CLG, the Grace Lake granite and units of Thor Lake and the NLS. Data for Grace Lake Granite, Thor Lake Syenite and Rim Syenite, and Nechalacho Layered Suite come from Mumford (2013, unpublished PhD thesis) and Möller and Williams-Jones (2016).

mudstones (Plant et al., 2004). Alternatively As and S could have been derived through the interaction of the fluid with existing sulphide mineralization that contains sulfarsenide minerals (gersdorffite, nickeline).

3.4.7 Source of CH_4-dominant S2 fluid inclusions

The presence of CH_4-dominant carbonic fluid inclusions within the CLG is atypical of mafic-ultramafic intrusions. One possibility for the origin of this CH_4 is the respeciation of an original CO_2-rich carbonic fluid in the presence of graphite (Cesare, 1995). This requires that the fluid inclusions trap a graphite-saturated fluid, and upon cooling and decompression, C-O-H respeciation in the inclusions can change the CO_2:CH_4 ratio internally (Morgan et al., 1993; Cesare, 1995). This depends on the initial O:H ratio of the fluid, whereby O/(O+H) ratios > 1/3, will lead to an increase in the CO_2:CH_4 ratio and O/(O+H) ratios < 1/3 will lead to a decrease in the CO_2:CH_4 ratio during cooling (Cesare, 1995). These interactions can lead to the formation of CO_2-dominant or CH_4-dominant carbonic fluid inclusions. However, graphite was not observed as a daughter or accidentally trapped phase in any fluid inclusion types from the CLG. As well, the low carbon content of the country rocks and units within the BLIS would argue that externally derived carbon did not affect fluid evolution (e.g., Lovozero, Potter et al., 2004). While graphite has been linked to the formation of CH_4 via the FT synthesis, it has not been linked to the formation of higher order hydrocarbons as detected here by GC in the CLG (Figure 3.17). The same line of evidence has been used to exclude graphite reactions for the formation of complex aliphatic hydrocarbons at Strange Lake and Lovozero (Salvi and Williams-Jones, 1997; Potter et al., 2004).

The presence of CH_4-dominant inclusions and the significant amounts of higher order hydrocarbons within them detected by GC, is explained by Fischer-Tropsch (FT) synthesis. This involves the reaction between a CO_2-dominant fluid and H_2 (produced from hydrothermal alteration reactions) to produce CH_4 and higher order hydrocarbons governed by the reactions (Potter and Konnerup-Madsen, 2003):

$$nCO + (2n+1)H_2 \rightarrow C_nH_{2n+2} + n2H_2O$$

$$nCO_2 + (3n+1)H_2 \rightarrow CH_{2n+2} + 2nH_2O$$

To catalyze the breaking of the C-O bonds, a group VIII metal in native form or as an oxide must be present (e.g., magnetite; Anderson, 1984; Salvi and Williams-Jones, 1997; Potter and Konnerup-Madsen, 2003). In order for FT reactions to proceed, H_2 must be generated. This occurs during serpentinization of olivine because Fe^{2+} will be excluded from serpentine and brucite and will be partially oxidized to Fe^{3+} and incorporated into magnetite releasing H_2 from $Fe(OH)_2$ (Sherwood-Lollar et al., 1993; Potter and Konnerup-Madsen, 2003):

$$5Mg_2SiO_{4\ (s)} + Fe_2SiO_{4\ (s)} + 9H_2O_{\ (aq)} \rightarrow 3MgSi_2O_5(OH)_{4\ (s)} + Mg(OH)_{2\ (s)} + 2Fe(OH)_{2\ (aq)}$$

$$3Fe(OH)_{2\ (aq)} \rightarrow Fe^{2+}{}_2Fe^{3+}O_{4\ (s)} + H_{2\ (aq)} + 2H_2O_{\ (aq)}$$

The formation of CH_4 in mafic and ultramafic rocks is suggested to be the result of these reactions (e.g., Abrajano et al., 1988, 1990; Kelly et al., 1996). The high modal abundances of magnetite throughout the CLG rocks could provide the catalyst for such FT reactions. However, if the parental carbonic fluid that underwent FT synthesis was sourced from within the CLG, why would only some FIAs show higher CH_4:CO_2 ratios? The CO_2-dominant, CH_4-poor FIAs may have originated earlier in the magmatic history

of the CLG when olivine was stable, while the CH_4-dominant FIAs exsolved later when olivine was altering to serpentine allowing for FT reactions to occur.

A third possibility could be an externally sourced CH_4-dominant fluid entering the CLG from the peralkaline NLS (eastern portion of the BLIS). In peralkaline systems fluid inclusions studies have shown that magmatic-hydrothermal fluids are CH_4-dominant with high concentrations of higher order hydrocarbons (C2+) (Figure 3.17; Strange Lake: Salvi and Williams-Jones, 1997; Lovozero: Potter et al., 1998, 2004). Methane and other hydrocarbons in peralkaline systems are attributed to CO_2-dominant fluids undergoing FT reactions related to the alteration of primary igneous minerals (i.e., nepheline, arfvedsonite, augite, Ti-magnetite) to minerals such as cancrinite, aegerine, biotite, magnetite, and natrolite. In the NLS, Möller and Williams-Jones (2016) report the alteration of nepheline to cancrinite, producing the H_2 needed for FT reactions to proceed as follows (Potter and Konnerup-Madsen, 2003):

$$3NaAlSiO_{4\,(s)} + Na^{+}_{(aq)} + 2H_2O_{(aq)} \rightarrow Na_4Al_3Si_3O_{12}(OH)\bullet H_2O_{(s)} + 0.5H_{2\,(aq)}$$

Magnetite and hematite are also present in the NLS representing the alteration products of aegirine and eudialyte (Möller and Williams-Jones, 2016), however only minor amounts of CO_2 and CH_4 are reported in fluid inclusions from the Thor Lake T Zone (Feng, 2014, unpublished PhD thesis).

3.4.8 Formation of calcite and monazite in fluid inclusions

Calcite has been observed in fluid inclusions in the CLG and has highly variable phase proportions suggesting accidental entrapment of a saturated mineral phase and is evidence for calcite mingling in the system at the same time as the immiscible brine-carbonic fluid inclusions (type S3; Figure 3.11A,B). As well, possible antarcticite is

observed in P2 fluid inclusions implying the fluids were Ca^{2+}-rich. The formation of calcite through the interaction with a high salinity brine and CO_2 or CH_4 can be shown through the reactions (Newton and Manning, 2002):

$$CaCl_{2\,(aq)} + H_2O_{\,(aq)} + CO_{2(g)} = CaCO_{3(s)} + 2HCl_{(aq)}$$

and

$$CaCl_{2(aq)} + CH_{4(g)} + 2O_{2(g)} = CaCO_{3(s)} + 2HCl_{(aq)} + H_2O_{(aq)}$$

The products of the reactions listed above (HCl and H_2O) may then be involved in reactions to form monazite (discussed below) that is present within the fluid inclusions.

Monazite has been observed as solid inclusions with type S3 inclusions and as solid inclusions within apatite. In natural and experimental settings, monazite is observed as either solid inclusions within or along the grain margins of fluor- and chlorapatite (Pan et al., 1993; Harlov et al., 2002a; Harlov et al., 2002b; Harlov and Förster, 2003) and all of these studies have suggested that monazite formed through fluid-rock interactions. The removal of Na and/or Si from the apatite structure will cause a charge imbalance because (Y+REE) are charge balanced through the coupled substitutions (Harlov and Förster, 2003; Harlov et al., 2005):

$$Si^{4+} + (Y+REE)^{3+} = P^{5+} + Ca^{2+}$$

and

$$Na^{+} + (Y+REE)^{3+} = 2Ca^{2+}$$

Therefore, removal of Na and/or Si will result in monazite and/or xenotime formation in fluorapatite through the reactions (Harlov and Förster, 2003):

$$[Ca_{5-2x},\ Na_x,\ (Y+REE)_x]P_3O_{12}F + x\ [2Ca^{2+} + P^{5+}]_{\,(fluid)} = Ca_5P_3O_{12}F + x(Y+REE)PO_4 + x[Na_{+}]_{\,(fluid)}$$

and

$[Ca_{5-y},\ (Y+REE)_y][P_{3-y},\ Si_y]O_{12}F + y[Ca^{2+} + 2P^{5+}]_{(fluid)} = Ca_5P_3O_{12}F + y(Y+REE)PO_4 + y[Si^{4+}]_{(fluid)}$

Experimental results by Harlov and Förster (2003) have shown for fluorapatite, monazite is formed through reactions with a H_2O, a high H_2O:CO_2, a KCl brine fluid, or a HCl solution. No monazite formed when fluorapatite was reacted with NaCl or $CaCl_2$ brine because Na^+ and Ca^{2+} can enter the fluorapatite structure and can maintain the charge balance if Na^+, Si^{4+}, or $(Y+REE)^{3+}$ be removed (Harlov and Förster, 2003, Harlov et al., 2005). Experiments of fluorapatite reacting with HCl have also been carried out and have shown monazite has formed in areas of the apatite that are depleted in (Y+REE), Si, Na, S, and Cl (Harlov et al., 2005). With the removal of Na and/or Si, this can be accompanied by the local dissolution of P in the apatite in order to form monazite (Figure 3.13C,D; Harlov et al., 2005). The products produced by the formation of calcite (i.e., HCl and/or H_2O) could then locally influence apatite dissolution-reprecipitation and form monazite within the fluid inclusions and within the host apatite.

If large scale metasomatism occurred to produce monazite present in fluid inclusions and in apatite, then one would except to see variations in the apatite trace element chemistry for elements present in monazite (Ce, La, Th, U). However, trace element chemistry for apatite is consistent between individual samples and individual spot analyses in the same grain, therefore this could imply late metasomatic processes did not alter the apatite influencing monazite precipitation. In addition, as described by Harlov and Förster (2003) and (Harlov et al. (2005), BSE images of fluid modified apatite show high contrast between metasomatically-altered and non-altered regions. Apatite in

this study did not show these large variations in composition when examined by BSE imaging suggesting late metasomatic processes did not influence monazite precipitation. Monazite present in the fluid inclusions and apatite may therefore represent accidental entrapment of saturated mineral phases.

3.5 Conclusion

This study describes a variety of fluid inclusion types preserved in coarse-grained apatite within mafic pegmatites in the CLG. The trapping of immiscible brine-carbonic fluid in primary and secondary assemblages demonstrates that the CLG was actively degassing throughout its crystallization and that fluids were sourced from different parts of the intrusion at different stages of crystallization. These brine-carbonic fluids mingled in common fluid pathways and were trapped there (i.e., mafic pegmatites). Fluids similar to those reported here and their immiscible entrapment has been documented in economic, Ni-Cu-PGE-rich layered mafic-ultramafic intrusions. Since the CLG is poorly mineralized and subeconomic, this suggests that fluids of this composition are not directly related to mineralization potential. It may be more important to have existing PGE-rich sulphides that fluids can interact with, leading to the potential remobilization of metals and reprecipitation in economically minable quantities.

Microthermometry of melt and fluid inclusions combined with independent geothermometers and barometers allows for the P-T conditions of melt and fluid entrapment to be estimated. The minimum liquidus temperature obtained from primary melt inclusions and the pressure determined from the Al- and Ti-in-hornblende geothermobarometer gives trapping conditions between 1135° and 1200°C and 1.6 to 4.5

kbar, implying the emplacement depth of the CLG is between 5.9 and 16.6 km. Primary fluid inclusions entrapment is constrained the isochore intersection by first melting and $T_m^{liquidus}$ of SMI resulting in P-T conditions of 2.3-4.4 kbar and 610°-1200°C (8.5-16.3 km depth), while S1/S3 inclusions are constrained by $T_m^{liquidus}$ and the apatite-biotite thermometer at 455° to 1200°C and 1.5 to 4.05 kbar (5.6-15 km depth). The high P-T conditions of fluid inclusion entrapment implies that the volatile activity is magmatic in origin and not related to a late hydrothermal event.

Entrapment of primary silicate melt inclusions in apatite have a relatively unevolved major element composition consistent with a gabbroic to syeno-dioritic melt, but are relatively enriched in incompatible elements (e.g., Zr, Nb, Cs, Hf, Ta) and depleted in metals (e.g., Ni, Cu, Co) suggesting this melt is likely sourced from a low degree of mantle partial melting, the melt was crustally contaminated, or sulphide saturation had occurred already causing the depletion in Ni, Cu, and Co.

Silicate melt present in S3 fluid inclusions, is the primary host for the HFSE, Cu, and Co contents. This silicate melt was likely sourced from an intercumulus liquid that was squeezed up during compaction of the cumulate pile and became highly enriched in incompatible elements. Nickel, Cu, and Co are uncommon in S3 inclusions but have higher concentrations compared to primary silicate melt inclusions and the source for these metals is currently ambiguous. This silicate melt mingled with a brine and a carbonic fluid, and all became trapped as S3 inclusions. The enrichment of incompatible elements in the intercumulus liquid can also explain the enrichment in trace elements in apatite in the mafic pegmatites over apatite in a fine- to medium-grained gabbro. As the HFSE-enriched intercumulus liquid is compressed and squeezed upwards, it interacts

with apatite already growing in the pegmatites, enriching it in incompatible elements at concentrations higher then if it only grew from its original surrounding liquid.

3.6 Acknowledgements

Financial support for this project came from the Northwest Territories Geological Survey, an NSERC DG to JH, and Nova Scotia Research and Innovation Scholarship and SEG Fellowship to KN. We would like to thank Dr. Joe Petrus for LA-ICP-MS analyses of apatite at Laurentian University, Yanan Liu for assistance with EMP analyses at the University of Toronto, Xiang Yang for SEM-EDS assistance and Mitch Kerr for GC analyses at Saint Mary's University. Scott Cairns, John Ketchum, Luke Ootes, Valerie Jackson, and Thomas Mumford are thanked for their helpful discussions about the local and regional geology of the BLIS.

3.7 References

Abrajano, T.A., Sturchio, N.C., Bohlke, J.K., Lyon, G.L., Poreda, R.J., and Stevens, C.M., 1988, Methane hydrogen gas seeps, Zambales ophiolite, Phillippines-deep or shallow origin: Chemical Geology, v. 71, p. 211-222.

Abrajano, T.A., Sturchio, N.C., Kennedy, B.M., Lyon, G.L., Muehlenbachs, K., and Bohlke, J.K., 1990, Geochemistry of reduced gas related to serpentinization of the Zambales ophiolite, Philippines: Applied Geochemistry, v. 5, p. 625-630.

Anderson, R.B., 1984, The Fischer-Tropsch synthesis: Orlando, Academic Press, Inc., 620 p.

Anderson, J.L., and Smith, D.R., 1995, The effects of temperature and fO_2 on the Al-in-hornblende barometer: American Mineralogist, v. 80, p. 549-559.

Bakker, R.J., 1999, Adaption of Bowers and Helgeson (1983) equation of state to isochore and fugacity coefficient calculation in the H_2O-CO_2-CH_4-N_2-NaCl fluid system: Chemical Geology, v. 154, p. 225-236.

Bakker, R.J., 2003, Package FLUIDS 1. Computer programs for analysis of fluid inclusion data and for modeling bulk fluid properties: Chemical Geology, v. 194, p. 3-23.

Ballhaus, C.G., and Stumpfl, E.F., 1986, Sulphide and platinum mineralization in the Merensky Reef: evidence from hydrous silicates and fluid inclusions: Contributions to Mineralogy and Petrology, v. 94, p. 193-204.

Beeskow, B., Rankin, A. H., Murphy, P. J., and Treloar, P. J., 2005, Mixed CH_4-CO_2 fluid inclusions in quartz from the South Wales Coalfield as suitable natural calibration standards for microthermometry and Raman spectroscopy: Chemical Geology, v. 223, p. 3-15.

Belousova, E., Griffin, W.L., O'Rielly, S.Y., and Fisher, N.I., 2002, Apatite as an indicator mineral for mineral exploration: trace-element compositions and their relationship to host rock type: Journal of Geochemical Exploration, v. 76, p. 45-69.

Birkett, T.C., Richardson, D.G., and Sinclair, W.D., 1994, Gravity modeling of the Blachford Lake Intrusive Suite, Northwest Territories. *In* Studies of rare-metal deposits in the Northwest Territories. *Edited by* W.D. Sinclair and D.G. Richardson. Geological Survey of Canada, p. 5-16.

Bleeker, W., and Hall, B., 2007, The Slave Craton: Geology and metallogenic evolution. *In* Mineral Deposits of Canada: A Synthesis of Major Deposit-Types, District Metallogeny, the Evolution of Geological Provinces, and Exploration Methods. *Edited by*

W.D. Goodfellow. Geological Association of Canada, Mineral Deposits Division, Special Publication, p. 849-879.

Blundy, J.D., and Holland, T.J.B., 1990, Calcic amphibole equilibria and a new amphibole-plagioclase geothermometer: Contributions to Mineralogy and Petrology, v. 104, p. 208-224.

Bodnar, R.J., and Student, J.J., 2006, Melt inclusions in plutonic rocks: petrography and microthermometry, *In* Webster, J.D., (Eds.) "Melt inclusions in plutonic rocks": Mineralogical Association of Canada Short Course, v. 36, p. 1-25.

Boudreau, A.E., 1995, Fluid evolution in layered intrusions: evidence from the chemistry of the halogen-bearing minerals. In: Magmas, fluids, and ore deposits (J.F.H. Thompson, ed.). Mineral Ass Can Short Course v. 23, p. 25-45

Boudreau, A.E., 1999, PELE - A version of the MELTS software program for the PC platform: Computers and Geosciences, v. 25, pp. 201-203.

Boudreau, A.E., 2016, Bubble migration in a compacting crystal-liquid mush: Contributions to Mineralogy and Petrology, v. 171, DOI: 10.1007/s00410-016-1237-9.

Boudreau, A.E., and McCallum, I.S., 1989, Investigations of the Stillwater Complex: Part V. Apatite as indicators of evolving fluid composition: Contributions to Mineralogy and Petrology, v. 102, p.138-153.

Boudreau, A.E., and Kruger, F.J., 1990, Variation in the composition of apatite though the Merensky Cyclic Unit in the Western Bushveld Complex: Economic Geology, v. 85, p. 737-745.

Boudreau, A.E., and McCallum, I.S., 1992, Concentration of platinum-group elements by magmatic fluids in layered intrusions: Economic Geology, v. 87, p. 1830-1848.

Boudreau, A.E., Love, C., Hoatson, D.M., 1993, Variation in the composition of apatite in the Munni Munni Complex and associated intrusions of the West Pilbara Block, Western Australia: Geochimica et Cosmochimica Acta, v. 57, p. 4467-4477.

Boudreau, A.E., Love, C., and Prendergast, M.D., 1995, Halogen geochemistry of the Great Dyke, Zimbabwe: Contributions to Mineralogy and Petrology, v. 122, p. 289-300.

Bowers, T.S., and Helgeson, H.C., 1983, Calculation of the thermodynamic and geochemical consequences of nonideal mixing in the system H_2O-CO_2-NaCl on phase relations in geologic systems: Metamorphic equilibria at high pressures and temperatures: American Mineralogist, v. 68, p. 1059-1075.

Bowring, S. A., Van Schmus, W. R., & Hoffman, P. F., 1984, U-Pb zircon ages from Authapascow Aulacogen, East Arm of Great Slave Lake, NWT, Canada: Canadian Journal of Earth Sciences, v. 21, p. 1315-1324.

Burke, E. A., 2001, Raman microspectrometry of fluid inclusions: Lithos, v. 55, p. 139-158.

Cawthorn, R.G., 2013, Rare earth element abundances in apatite in the Bushveld Complex-a consequence of the trapped liquid effect: Geology, v. 41, p. 603-606.

Cesare, B., 1995, Graphite precipitation in C-O-H fluid inclusions: closed system compositional and density changes, and thermobarometric implications: Contributions to Mineralogy and Petrology, v. 122, p. 25-33.

Chen, J., Xu, Y., and Huang, D., 2000, Geochemical characteristics and origin of natural gas in Tarim Basin, China: American Association of Petroleum Geologists Bulletin, v. 84, p. 591–606.

Darling, R.S., 1991, An extended equation to calculate NaCl contents from final clathrate melting temperatures in H_2O-CO_2-NaCl fluid inclusions: implications for P-T isochore location: Geochemica et Cosmochimica Acta, v. 55, p. 3869-3871.

Davidson, A., 1972, Granite Studies in the Slave Province. *Report of Activities*: Geological Survey of Canada, p. 109-115.

Davidson, A., 1978, The Blachford Lake Intrusive Suite: An Aphebian alkaline plutonic complex in the Slave Province, Northwest Territories. *Current Research*: Geological Survey of Canada, p. 119-127.

Davidson, A., 1981, Petrochemistry of the Blachford Lake Complex, District of Mackenzie. *Geological Survey of Canada Open File 764*, 24 p.

Davidson, A., 1982, Petrochemistry of the Blachford Lake complex near Yellowknife, Northwest Territories. In: Maurice, Y. T. (ed.) *Uranium in Granites*: Geological Survey of Canada, 71-79.

Diamond, L.W., 1992, Stability of CO_2 clathrate hydrate + CO_2 liquid + CO_2 vapour + aqueous KCl-NaCl solutions: Experimental determination and application to salinity estimates of fluid inclusions: Geochemica et Cosmochimica Acta, v. 56, p. 273-280.

Diamond, L.W., 2003, Introduction to gas-bearing, aqueous fluid inclusions, *In* Samson, I., Anderson, A., and Marshall, D., (Eds.) "Fluid Inclusions: Analysis and Interpretation": Mineralogical Association of Canada Short Course, v. 32, p. 101-158.

Duan, Z., Moller, N., and Weare, J.H., 1995, Equation of state for the NaCl-H2O-CO2 system: prediction of the phase equilibria and volumetric properties: Geochemica et Cosmochimica Acta, v. 59, p. 2869-2882.

Dubessy, J., Poty, B., and Ramboz, C., 1989, Advances in C-O-H-N-S fluid geochemistry based on micro-Raman spectrometric analysis of fluid inclusions: European Journal of Mineralogy, v. 1, p. 517-534.

Ernst, W.G., and Liu, J., 1998, Experimental phase-equilibrium study of Al- and Ti-contents of calcic amphibole in MORB-a semiquantitiative thermobarometer: American Mineralogist, v. 83, p. 952-969.

Feng, Y., 2014, Hydrothermal geochemistry and mineralizing processes in the T Zone, Thor Lake rare-element deposit, Northwest Territories, Unpublished PhD thesis, Windsor, Canada, University of Windsor, 375 p.

Fisher, T., and Marty, B., 2005, Volatile abundances in the sub-arc mantle: insights from volcanic and hydrothermal gas discharges. Journal of Volcanology and Geothermal Research v. 140, p. 205-216.

Frost, B.R. and Touret, L.R., 1989, Magmatic CO_2 and saline melts from the Sybille Monzosyenite, Laramie Anorthosite Complex, Wyoming: Contributions to Mineralogy and Petrology, v. 103, p. 178-186.

Gaetani, G.A., and Grove, T.L., 1997, Partitioning of moderately Siderophile elements among olivine, silicate melt, and sulphide melt: constraints on core formation in Earth and Mars: Geochemica et Cosmochimica Acta, v. 61, p. 1829-1846.

Gál, B., Molnar, F., Guzmics, T., Mogessie, A., Szabó, C., and Peterson, D.M., 2013, Segregation of magmatic fluids and their potential in the mobilization of platinum-group elements in the South Kawishiwi Intrusion, Duluth Complex, Minnesota-evidence from petrography, apatite geochemistry and coexisting fluid and melt inclusions: Ore Geology Reviews, v. 54, p. 59-80.

Glebovitsky, V.A., Semenov, V.S., Belyatsky, B.V., Koptev-Dvornikov, E.V., Pchelintseva, N.F., Kireev, B.S., and Koltsov, A.B., 2001, The structure of the Lukkulaisvaara Intrusion, Oulanka group, northern Karelia: petrological implications: The Canadian Mineralogist, v. 39, p. 607-637.

Guillong, M. M., Maier, D.L., Allan, M.M., Heinrich, C.A., and Yardley, B.W.D., 2008, Appendix A6: SILLS: a MATLAB based program for the reduction of laser ablation ICP-MS data of homogeneous materials and inclusions. *In* Laser Ablation ICP-MS in the Earth Sciences: Current Practices and Outstanding Issues. *Edited by* P. Sylvester. Mineralogical Association of Canada Short Course Series, v. 40.

Hammer, S., Bowring, S., Vanbreemen, O., and Parrish, R., 1992, Great Slave Lake Shear Zone, NW Canada-Mylonitic record of early Proterozoic continental convergence, collision and indentation: Journal of Petrology, v. 14, p. 757-773.

Hanley, J.J., 2006, Experimental and fluid inclusion constraints on the ore metal content and origin of volatiles associated with large Ni-Cu-PGE deposits: Unpublished PhD thesis, Toronto, Canada, University of Toronot, 285 p.

Hanley, J.J., and Gladney, E.R., 2011, The presence of carbonic-dominant volatiles during the crystallization of sulphide-bearing mafic pegmatites in the North Roby Zone, Lac des Iles Complex, Ontario: Economic Geology, v. 106, P. 33-54.

Hanley, J.J., Mungall, J.E., Pettke, T., Spooner, E.T.C., and Bray, C.J., 2005, Ore metal redistribution by hydrocarbon-brine and hydrocarbon-halide melt phases, North Range footwall of the Sudbury Igneous Complex, Ontario, Canada: Mineralium Deposita Acta, v. 40, p. 237-256.

Hanley, J.J., Mungall, J.E., Pettke, T., Spooner, E.T.C., and Bray, C.J., 2008, Fluid and halide melt inclusions of magmatic origin in the Ultramafic and Lower Banded Series, Stillwater Complex, Montana, USA: Journal of Petrology, v. 49, p. 1133-1160.

Harlov, D.E., and Förster, H-J., 2003, Fluid-induced nucleation of (Y+REE)-phosphate minerals within apatite: nature and experiment. Park II. Fluorapatite: American Mineralogist, v. 88, p. 1209-1229.

Harlov, D.E., Förster, H-J., and Nijland, T.G., 2002a, Fluid-induced nucleation of (Y+REE)-phosphate minerals within apatite: nature and experiment. Part I. Chlorapatite: American Mineralogist, v. 87, p. 245-261.

Harlov, D.E., Andersson, U.B., Förster, H-J., Nyström, J.O., Dulski, P., and Broman, C., 2002b, Apatite-monazite relations in the Kiirunavaara magnetite-apatite ore, northern Sweden: Chemical Geology, v. 191, p. 47-72.

Harlov, D.E., Wirth, R., and Förster, H-J., 2005, An experimental study of dissolution-reprecipitation in fluorapatite: fluid infiltration and the formation of apatite: Contributions to Mineralogy and Petrology, v. 150, p. 268-286.

Holloway, J.R., 1976, Fluid in the evolution of granitic magmas: consequences of finite CO_2 solubility: Geological Society of America Bulletin, v. 87, p. 1513-1518.

Hoffman, P., 1973, Evolution of an early Proterozoic continental margin – Coronation geosynclines and associated aulacogens of northwest Canadian Shield. Philosophical Transactions of the Royal Society of London a-Mathematical Physical and Engineering Sciences, v. 273, p. 547-581.

Hoffman, P.F., 1987, Continental transform tectonics-Great Slave Lake shear zone (Ca-1.9 Ga), northwest Canada: Geology, v. 15, p. 785-788.

Hollister, L.S., Grissom, G.C., Peters, E.K., Stowell, H.H., and Sisson, V.B., 1987, Confirmation of the empirical correlation of Al in hornblende with pressure of solidification of calc-alkaline plutons: American Mineralogist, v. 72, p. 231-239.

Jakobsen, J.K., Veksler, I.V., Tegner, C., and Brooks, C.K., 2011, Crystallization of the Skaergaard Intrusion from an emulsion of immiscible iron- and silica-rich liquids: evidence from melt inclusions in plagioclase: Journal of Petrology, v. 52, p. 345-373.

Kelly, D.S., and Früh-Green, G.L., 1999, Abiogenic methane in deep-seated mid-ocean ridge environments: insights from stable isotope analyses: Journal of Geophysical Research, v. 104, p. 10439-10460.

Kerr, M., Hanley, J.J., Morrison, G., Everest, J., and Bray, C., 2015, Preliminary evaluation of trace hydrocarbon speciation and abundance as an exploration tool for footwall-style sulphide ores associated with the Sudbury Igneous Complex, Ontario, Canada: Economic Geology, v. 110, p. 531-556.

Konnerup-Madsen, J., and Rose-Hansen, J., 1982, Volatiles associated with alkaline igneous rift activity: Fluid inclusions in the Ilimaussaq intrusion and the Gardar granitic complexes (South Greenland): Chemical Geology, v. 37, p. 79–93.

Konnerup-Madsen, J., Larsen, E., and Rose-Hansen, J., 1979, Hydrocarbon-rich inclusions in minerals from the alkaline Ilimaussaq intrusion, South Greenland: Bulletin de Minéralogie, v. 102, p. 642–653.

Larsen, R.B., Brooks, C.K., and Bird, D.K., 1992, Methane-bearing aqueous, saline solutions in the Skaergaard intrusion, east Greenland: Contributions to Mineralogy and Petrology, v. 112, p. 428-437.

Li, C., Maier, W.D., and de Waal, S.A., 2001, Magmatic Ni-Cu versus PGE deposits: contrasting genetic controls and exploration implications: South African Journal of Geology, v. 104, p. 309-318.

Lowenstern, J.B., 2001, Carbon dioxide in magmas and implications for hydrothermal systems: Mineralium Deposita Acta, v. 36, p. 490-502.

Marmont, C., 2006, Report on Diamond Drilling, Airborne and Ground Geophysical Surveys, Lithogeochemical Sampling and Prospecting; submitted by Kodiak Exploration, Northwest Territories Geoscience Office, Activities Report 085101, p. 123.

Marmont, C., 2007, Report on Diamond Drilling; submitted by Kodiak Exploration, Northwest Territories Geoscience Office, Activities Report 085317, p. 283.

Mathez, E.A., 1995, Magmatic metasomatism and formation of the Merensky reef, Bushveld Complex: Contributions to Mineralogy and Petrology, v. 119, p. 277-286.

Mathez, E.A., and Webster, J.A., 2005, Partitioning behavior of chlorine and fluorine in the system apatite-silicate melt-fluid: Geochimica et Cosmochimica Acta, v. 69, p. 1275-1286.

Métrich, N., and Wallace, P.J., 2008, Volatile abundances in basaltic magmas and their degassing paths tracked by melt inclusions: Reviews in Mineralogy and Petrology, v. 69, p. 363-402.

Meurer, W.P., and Boudreau, A.E., 1996, An evaluation of models of apatite compositional variability using apatite from the Middle Banded series of the Stillwater Complex Montana: Contributions to Mineralogy and Petrology, v. 125, p.225-236.

Meurer, W.P., Willmore, C.C., and Boudreau, A.E., 1999, Metal redistribution during fluid exsolution and migration in the Middle Banded series of the Stillwater Complex, Montana: Lithos, v. 47, p. 143-156.

Möller, V., and Williams-Jones, A.E., 2016, Petrogenesis of the Nechalacho Layered Suite, Canada: magmatic evolution of a REE-Nb-rich nephaline syenite intrusion: Journal of Petrology, v. 57, p. 229-276.

Morgan, G.B.VI., Chou, I-M., Pasteris, C., and Olsen, S.N., 1993, Re-equilibrium of CO2 fluid inclusions at controlled hydrogen fugacities: Journal of Metamorphic Geology, v. 11, p. 155-164.

Mumford, T.R., 2013, Petrology of the Blatchford Lake Intrusive Suite, Northwest Territories, Canada, Unpublished PhD thesis, Ottawa, Canada, Carleton University, 240 p.

Nash, W.P., 1976, Fluorine, chlorine, and OH-bearing minerals in the Skaergaard Intrusion: American Journal of Science, v. 276, p. 546-557.

Newton, R.C., and Manning, C.E., 2002, Experimental determination of calcite solubility in H_2O-NaCl solutions at deep crust/upper mantle pressures and temperatures: implications for metasomatic processes in shear zones: American Mineralogist, v. 87, p. 1401-1409.

Oakes, C.,S., Bodnar, R.J., and Simonson, J.M., 1990, The system NaCl-$CaCl_2$-H_2O: I. The ice liquidus at 1 atm pressure: Geochimica et Cosmochimica Acta, v. 54, p. 603-610.

Pan, Y.P., Fleet, M.E., and Macrae, N.D., 1993, Oriented monazite inclusions in apatite porphyroblasts from the Hemlo gold deposit, Ontario, Canada: Mineralogical Magazine, v. 57, p. 697-707.

Petersilie, I.A., and Sørensen, H., 1970, Hydrocarbon gases and bituminous substances in rocks from the Illimaussaq alkaline intrusion, South Greenland: Lithos, v. 3, p. 59–76.

Pilkington, M., Thomas, M.D, and Mumford, T.R., 2012, Geological significance of a new high resolution gravity gradiometric and magnetic survey over the Blatchford Lake Complex, Northwest Territories; Geological Survey of Canada, Open File 7084, Poster.

Pinckston, D.R., and Smith, D.G.W., 1995, Mineralogy of the Lake zone, Thor Lake rare-metals deposit, N.W.T., Canada: Canadian Journal of Earth Science, v. 32, p. 516-532.

Plant, J.A., Kinniburgh, D.G., Smedley, P.L., Fordyce, F.M., and Klinck, B.A., 2004, Arsenic and Selenium *in* Sherwood Lollar, B., Holland, H.D., and Turekian, K.K., ed., Environmental Geochemistry: Elsevier, p. 17-66.

Polovina, J.S., Hudson, D.M., Jones, R.E., 2004, Petrographic and geochemical characteristics of Postmagmatic hydrothermal alteration and mineralization in the J-M Reef, Stillwater Complex, Montana: The Canadian Mineralogist, v. 42, p. 261-277.

Potter, J., and Konnerup-Madsen, J., 2003, A review of the occurrence and origin of abiogenic hydrocarbons in igneous rocks: Geological Society of London, Special Publications, v. 214, p. 151-173.

Potter, J., Rankin, A.H., Treloar, P.J., Nivin, V.A., Ting, W., and Ni, P., 1998, A preliminary study of methane inclusions in alkaline igneous rocks of the Kola igneous province, Russia: implications for the origin of methane in igneous rocks: European Journal of Mineralogy, v. 10, p. 1167-1180.

Potter, J., Rankin, A.H., and Treloar, P.J., 2004, Abiogenic Fischer-Tropsch synthesis of hydrocarbons in alkaline igneous rocks; fluid inclusion, textural and isotopic evidence from the Lovozero complex, N.W. Russia: Lithos, v. 75, p. 311-330.

Roedder, E., and Bodnar, R. J., 1980, Geological pressure determinations from fluid inclusion studies: Annual Review of Earth and Planetary Sciences v. 8, p. 263-301.

Rosso, K.M., and Bodnar, R.J., 1995, Microthermometric and Raman spectroscopic detection limits of CO2 in fluid inclusions and the Raman spectroscopic characterization of CO_2: Geochemica et Cosmochimica Acta, v. 59, p. 3961-3975.

Salvi, S., and Williams-Jones, A.E., 1996, The role of hydrothermal processes in concentrating high-field strength elements in the Strange Lake peralkaline complex, northeastern Canada: Geochimica et Cosmochimica Acta, v. 60, p. 1917-1932.

Sakata, S., Sano, Y., Maekawa, T., and Igari, S.I., 1997, Hydrogen and carbon isotopic composition of methane as evidence for biogenic origin of natural gases from the Green Tuff Basin, Japan: Organic Geochemistry, v. 26, p. 399–407.

Salvi, S., and Williams-Jones, A.E., 1997, Fischer-Tropsch synthesis of hydrocarbons during sub-solidus alteration of the Strange Lake peralkaline granite, Quebec/Labrador, Canada: Geochimica et Cosmochimica Acta, v. 61, p. 83-99.

Schiffries, C.M., 1990, Liquid absent aqueous fluid inclusions and phase equibria in the system $CaCl_2$-NaCl-H_2O: Geochimica et Cosmochimica Acta, v. 54, p. 611-619.

Schmidt, C., and Bodnar, R.J., 2000, Synthetic fluid inclusions: XVI. PVTX properties in the system H_2O-NaCl-CO_2 at elevated temperatures, pressures, and salinities: Geochimica et Cosmochimica Acta, v. 64, p. 3853-3869.

Schisa, P., Boudreau, A., Djon, L., Tchalikian, A., and Corkery, J., 2014, The Lac des Iles palladium deposit, Ontario, Canada. Part II. Halogen variations in apatite: Mineralium Deposita, v. 50, p. 339-355.

Sheard, E.R., Williams-Jones, A.E., Heiligmann, M., Pederson, C., and Trueman, D.L., 2012, Controls on the concentration of Zirconium, Niobium, and the Rare Earth Elements in the Thor Lake rare metal deposit, Northwest Territories, Canada: Economic Geology, v. 107, p. 81-104.

Sherwood-Lollar, B., Frape, S.K., Weise, S.M., Fritz, P., Macko, S.A., and Welhan, W.A., 1993, Abiogenic methanogenesis in crystalline rocks: Geochimica et Cosmochimica Acta, v. 57, p. 5087-5097.

Sinclair, W. D., Hunt, P. A. and Birkett, T. C., 1994, U-Pb zircon and monazite ages of the Grace Lake Granite, Blatchford Lake Intrusive Suite, Slave Province, Northwest Territories. Radiogenic Age and Isotopic Studies: Report 8; Geological Survey of Canada, Current Research 1994-F, p. 15-20.

Sobolev, A.V., and Chaussidon, M., 1996, H_2O concentrations in primary melts from supra-subduction zones and mid-oceanic ridges: Implications for H_2O storage and recycling in the mantle: Earth and Planetary Science Letters, v. 137, p. 45-55.

Somarin, A.K., Kissin, S.A., Heerema, D.D., and Bihari, D.J., 2009, Hydrothermal alteration, fluid inclusion and stable isotope studies of the North Roby Zone, Lac des Iles PGE mine, Ontario, Canada: Resource Geology, v. 59, p. 107-120.

Sylvester, P. J., Cabri, L. J., Tubrett, M. N., McMahon, G., Laflamme, J. H. G., and Peregoedova, A., 2005, Synthesis and evaluation of a fused pyrrhotite standard reference material for platinum group element and gold analysis by laser ablation-ICPMS: International Platinum Symposium, Extended Abstracts, v. 10, p. 16-20.

Tacker, R.C., and Stormer, J.C., 1989, A thermodynamic model for apatite solid solutions applicable to high temperature geologic problems: American Mineralogist, v. 74, p. 877-888.

Timofeev, A., and Williams-Jones, 2015a, The origin of Niobium and Tantalum mineralization in the Nechalacho REE deposit, NWT, Canada: Economic Geology, v. 110, p. 1719-1735.

Timofeev, A., and Williams-Jones, 2015b, Controls on the distribution of Gallium in the Nechalacho REE deposit, NWT, Canada: Economic Geology, v. 110, 173-185.

Volfinger, M., Robert, J. L., Vielzeuf, D., and Neiva, A.M. R., 1985, Structural control of the chlorine content of OH-bearing silicates (micas and amphiboles): Geochimica et Cosmochimica Acta v. 49, p. 37-48.

Wallace, P., 2005, Volatiles in subduction zone magmas: concentrations and fluxes based on melt inclusion and volcanic gas data: Journal of Volcanology and Geothermal Research, v. 140, p. 217-240

Webster, J.D., Holloway, J.R., and Hervig, R.L., 1989, Partitioning of lithophile trace-elements between H_2O and H_2O+CO_2 fluids and topaz rhyolite melt: Economic Geology, v. 84, p. 116-134.

Webster, J.D., Kinzler, R.J., and Mathez, E.A., 1999, Chloride and water solubility in basalt and andesite melts and implications for magmatic degassing: Geochimica et Cosmochimica Acta, v. 63, p. 729-738.

Willmore, C.C., Boudreau, A.E., and Kruger, F.J., 2000, The halogen geochemistry of the Bushveld Complex, Republic of South Africa: Implications for chalcophile element distribution in the Lower and Critical Zones: Journal of Petrology, v. 41, p. 1517-1539.

Wopenka, B., and Pasteris, J. D., 1986, Limitations to quantitative analysis of fluid inclusions in geological samples by laser Raman microprobe spectroscopy: Applied Spectroscopy, v. 24, p. 144-151.

Wopenka, B., and Pasteris, J. D., 1987, Raman intensities and detection limits of geochemically relevant gas mixtures for a laser Raman microprobe: Analytical Chemistry, v. 59, p. 2165-2170.

Zajacz, Z., Halter, W.E., Pettke, T., and Guillong, M., 2008, Determination of fluid/melt partition coefficients by LA-ICPMS analysis of co-existing fluid and silicate melt inclusions: controls on element partitioning: Geochimica et Cosmochimica Acta, v. 72, p. 2169-2197.

Zhu, C., Sverkensky, D.A., 1992, F-Cl-OH partitioning between biotite and apatite: Geochimica et Cosmochimica Acta, v. 56, p. 3435-3467.

Chapter 4: Key conclusions and future work

4.0 Key conclusions from Chapter 2

i. Three distinct styles of sulphide mineralization are present in the Caribou Lake Gabbro: (i) disseminated sulphide mineralization, (ii) semi-massive to massive sulphide mineralization, and (iii) trace sulphide "PGE-enriched" mineralization. Two distinct sulphide mineralization events occurred within the CLG determined through modeling based on estimates of the starting silicate melt composition: (i) trace sulphide "PGE-enriched" sulphide mineralization formed through fractional crystallization of a sulphide melt derived from a S-undepleted silicate liquid under high R factors (70,000-150,000), and (ii) disseminated and semi-massive to massive sulphide mineralization also formed by fractional crystallization of a sulphide melt but was derived from a S-depleted silicate liquid and involved lower R factors ($\leq$ 3000).

ii. Sulphide melt inclusions present in the Caribou Lake Gabbro preserve the composition of the sulphide liquid at a specific stage (likely early before or slightly after MSS crystallization) in the evolution of the system. The Cu and Co concentrations in and PGE-poor nature of sulphide melt inclusions are consistent with the composition of disseminated and semi-massive to massive sulphide mineralization (when recalculated to 100 % sulphide). Sulphide melt inclusions contain a parental sulphide liquid to these mineralization styles. This would imply that sulphide melt inclusion compositions can be used as a potential tool to

determine if the initial sulphide liquid in a system is sufficiently rich in metals to produce an economic Ni-Cu-PGE deposit.

iii. Nickel concentrations in sulphide melt inclusions are lower compared to disseminated and semi-massive to massive sulphide mineralization (when recalculated to 100 % sulphide). This discrepancy in concentration can be explained by a small amount monosulphide solution was removed from the sulphide liquid by fractional crystallization, removing some Ni from the sulphide liquid.

iv. Compared to economic Ni-Cu-PGE deposits, olivine in the Caribou Lake Gabbro is depleted (≤ 1138 ppm). The presence of SUL as secondary inclusion trails in olivine, would imply that olivine was crystallizing prior to a sulphide liquid separating and therefore the segregation of a sulphide liquid may not be responsible for the Ni depletion in olivine.

v. Three explanations are proposed for subeconomic nature of Ni-Cu-PGE mineralization in the Caribou Lake Gabbro: (i) a large amount of sulphide was lost at depth as the parental silicate melt ascended to the current depth of the intrusion, (ii) low R factors likely influenced the poor metal tenors, and/or (iii) low degree of partial melting of a source region.

4.1 Key conclusions from Chapter 3

i. Entrapment of primary silicate melt inclusions within early cumulate apatite occurred between 1130° and 1200°C ($T_m^{liquidus}$ determined by microthermometry)

and 1.6 to 4.6 kbar (determined by Al- and Ti-in-hornblende geothermobarometer). Therefore the depth of emplacement of the Caribou Lake Gabbro is between 5.9 and 16.6 km, assuming a density of 2.8 g/cm^3 of the overlying material.

ii. Primary and secondary fluid inclusions preserved in early cumulus apatite in mafic pegmatites preserve the trapping of immiscible brine-carbonic fluids. This suggests the Caribou Lake Gabbro was continually loosing volatiles during it crystallization history, as the carbonic fluid would have been sourced from a shallower, hotter portion of the melt and the brine from a deeper, cooler portion of the melt. These two distinct fluids mingled in common fluid pathways (i.e., now mafic pegmatites) and became entrapped, forming P2, S1, and S3 fluid inclusions. The same types of fluids and mingling processes have been reported in (economic) Ni-Cu-PGE-bearing layered mafic-ultramafic intrusions, suggesting that fluids of this compositon are not required for mineralization. Rather, it seems necessary to have pre-existing PGE-rich sulphides that fluids can possibly interact with, remobilizing the metals and enriching magmatic sulphides further.

iii. The presence of silicate melt in type S3 fluid inclusions implies that a melt was transported with the immiscible carbonic-brine fluid. The major element chemistry of the melt in S3 inclusions is dominated by Si-Fe-Mg-Ti-Al (determined by SEM-EDS) and it is enriched in incompatible elements (determined by LA-ICP-MS). This melt likely represents an intercumulus melt that was squeezed up during compaction in the cumulate pile. As this melt percolated upwards, it becomes enriched in incompatible elements but its major

element composition remained relatively unchanged. Incompatible elements in S3 inclusions are positively correlated with Si but show no correlation with Na, indicating that the trapped melt abundance (rather than trapped brine) is the primary control on incompatible element concentration in S3 inclusions.

iv. The enrichment of incompatible elements present in S3 inclusions could indicate derivation from peralkaline, HFSE- and REE-rich Nechalacho Layered Suite in the Thor Lake syenite in the adjacent eastern portion of the Blatchford Lake Intrusive Suite. However, trace element patterns and Nb/Ta ratios in the mafic pegmatites and primary silicate melt inclusions (type P1) are similar and would suggest no external melt or fluid influence from the Thor Lake syenite or NLS.

4.2 Suggestions for Future Work

The conclusions of this work confirm speculation, based on limited drilling results, that the Caribou Lake Gabbro represents a weakly mineralized Ni-Cu-PGE layered mafic-ultramafic intrusion. The volatile activity preserved in secondary fluid inclusions appears to be associated with the intrusive phases of the eastern lobe of the Blatchford Lake Intrusive Suite. There are numerous follow-up studies that can be conducted on the Caribou Lake Gabbro to clarify the understanding of its sulphide genesis and volatile activity that was initiated through this thesis work. Below are only few suggestions of potential next steps in research:

- Obtain more detailed and concise constraints on the initial melt composition. This would involve more work on silicate melt inclusions. The inclusions would need to be homogenized on a melt inclusion microthermometry stage or in a high temperature furnace to produce glassy inclusions that could be analyzed by microbeam methods (e.g., EMP) to give a better constraint on the melt major element geochemistry. This would also allow determination of a more accurate internal standard to be used for LA-ICP-MS analyses. Analysis by EMP would also allow for determination of Cl and other elements in the melt. Homogenized melt inclusions could also be analyzed by Micro-Fourier Transform Infrared Spectrometry to determine the melts CO_2 and H_2O contents directly, that are assumed or not determined in this thesis. This would provide constraints on volatile content and crystallization depth of the melt.
- Conduct a detailed apatite halogen study throughout the intrusion to help constrain the halogen (i.e., Cl and F) evolution of the system. The results would help trace degassing events by looking for a decrease in Cl/F ratios throughout the intrusion, identifying at what stratigraphic level saline brine(s) may have exsolved from the crystallizing melt.
- Constrain the fO_2 of the mineralizing system. This could be done by examining the composition and nature of the magnetite-ilmenite composite grains present throughout the intrusion. Analysis of magnetite and ilmenite that have exsolved from an original titanomagnetite grain can place fO_2 constraints on the system provided this is due to primary exsolution and not oxidation exsolution. The

relevant oxybarometer is based on the iron redox equilbria ($6FeTiO_3$ (ilmenite) + $2Fe_3O_4$ (magnetite) = $6Fe_2TiO_4$ (ulvöspinel) + O_2) and, for given P-T-fO_2 conditions compositions of coexisting magnetite and ilmenite are unique.

- Additional fluid inclusion analyses of type 3 inclusions. The exact P-T conditions of entrapment of secondary type S3 fluids entrapment are lacking. Looking for inclusions that contain the coeval end-member brine phase of type S3 inclusions would allow for the method of intersecting isochores to be used to constraint the P-T conditions of entrapment for type S3 inclusions, assuming brine and carbonic fluids were coeval but not in equilibrium..
- Further work on the primary fluid inclusions (i.e., type P2 inclusions) present in the pegmatites to better constrain P-T conditions of volatile degassing in the intrusion. LA-ICP-MS work could also be conducted on these inclusions to determine if any metals (Ni, Cu, Co, PGE) were exsolved and extracted from the melt during the degassing event, a possible alternative to the magmatic hypotheses for low metal tenor.
- Detailed textural analyses on the trace sulphide "PGE-enriched" mineralization. More sample material would be need for this. Grain mounts could be made for a more detailed scanning for discrete PGM by MLA-SEM. Additionally, LA-ICP-MS analyses of the pyrrhotite could be completed to determine if the PGE in these samples are mostly dissolved in the structure of pyrrhotite.
- High resolution LA-ICP-MS analyses of the sulphide melt inclusions. Instead of collecting data for a large range of elements as was done in this study, a limited

element menu for enhancement of detection capabilities (i.e., Ni, Cu, Co, Fe, Pd, Pt, and Au). The dwell times for the Pd, Pt, and Au could also be increased significantly allowing for improved likelihood of detection and therefore would provide a constraint on the initial sulphide liquids PGE content.

Appendix 1: Mineralogy, geochemistry, stable isotopes, and preliminary fluid inclusion analysis of the Caribou Lake mafic-ultramafic intrusion, Northwest Territories, Canada.

Kevin Neyedley [a,+], Jacob J. Hanley [a], Hendrik Falck [b], Mostafa Fayek [c], and Ryan Sharpe [c]

[a] *Department of Geology, Saint Mary's University, 923 Robie Street, Halifax, Nova Scotia, Canada B3H 3C3*

[b] *Northwest Territories Geological Survey, 4601-B 52nd Ave, Yellowknife, NT, X1A 2R3*

[c] *Department of Geological Sciences, University of Manitoba, Winnipeg, Manitoba, Canada, R3T 2N2*

[+] Corresponding Author: kevinneyedley@gmail.com

Number of pages: 38

Number of figures: 21

Published: Northwest Territories Geoscience Office Open File 2014-08

Neyedley, K., Hanley, J., Falck, H., Fayek, M., and Sharpe, R., 2014. Mineralogy, geochemistry, stable isotopes, and preliminary fluid inclusion analysis of the Caribou Lake mafic-ultramafic intrusion, Northwest Territories, Canada. Northwest Territories Geoscience Office Open File 2014-08.

Introduction

The mafic-ultramafic Caribou Lake Intrusion (CLI), located roughly 90 km southeast of Yellowknife in the Northwest Territories, contains minor Ni-Cu-platinum group element (PGE) mineralization hosted mainly in rock units of gabbroic composition. Mineralization consists of massive to disseminated pyrrhotite with lesser amounts of chalcopyrite, pentlandite, pyrite, and sphalerite. No PGE mineral grains have been found to date, but assay results from a fine-grained gabbro with trace amounts of sulfides indicate 214 ppm Pt+Pd (Marmont, 2007). A major aspect of this project is to characterize the mineralization and its associated host rocks. Detailed core logging and sampling of a drill hole containing highly disseminated sulfide over ~10m was conducted over the summer of 2013 and two other drill holes were logged and sampled in order to examine the internal stratigraphy of the intrusion. Additional samples of massive sulfide mineralization and their associated host rocks were also collected from drill holes. Geochemical analyses of the intrusion reveal that it is tholeiitic in composition and alteration has not significantly changed the overall geochemistry of the rocks. Fluid inclusions in apatite and quartz are well preserved in various coarse grained gabbroic units and will be studied in this project.

A major question to be answered by this study is have fluids remobilized metals in the system and therefore decreased the tenor of sulfide mineralization? Whole rock geochemical results have shown that some units can be extremely enriched in vanadium (up to 2.3 wt%). Magnetite has up to 1.3 wt% vanadium and can display two styles of ilmenite exsolution: blebby texture, where ilmenite and magnetite occur as a composite grain with a grain of ilmenite on the edge of magnetite and trellis pattern exsolution, where ilmenite exsolves from titanomagnetite along the {111} plane to produce a crosshatched exsolution pattern. Questions that have arisen from the observations of high abundances of Fe-Ti oxides in the intrusion include: What was the fO_2 conditions of the intrusion, which can be constrained by reconstructing the composition of the original titanomagnetite, and is there enough magnetite with appreciable vanadium concentrations to validate further exploration in the area.

Regional Geology

The Caribou Lake mafic-ultramafic intrusion is located approximately 90km southeast of Yellowknife, Northwest Territories along the Hearne Channel, Great Slave Lake and lies at the southern margin in the Slave Province of the Canadian Shield (Figure 4.1 and Figure 4.2). The CLI comprises the western suite of the alkaline to peralkaline Blatchford Lake Intrusive Suite (BLIS), which is thought to be related to the formation of the Authapuscow Aulacogen and the associated failed rift (Bowring et al, 1984; Hoffman, 1980) that could have promoted crustal thinning, decompressional melting and served as a conduit for mantle derived magmas (Mumford, 2013). The BLIS intrudes sedimentary rocks of the Archean Yellowknife supergroup, Morose granite, and the Defeat granodiorite (Davidson, 1972, 1978). A geophysical gravity study by Birkett et al (1994) and Pilkington (2012) suggested that the BLIS is a relatively thin tabular body, approximately 1km thick with deep mafic (CLG) roots at the western contacts. The CLG also appears to extend under the Grace Lake granite for almost half of the entire complex.

The first detailed mapping of the BLIS was undertaken by Davidson (1972). His subsequent work (Davidson, 1978, 1981, 1982) identified six distinct units based on field relationships and geochronology:

1) Caribou Lake gabbro ranging to leucoferrodiorite (2184 ± 2 Ma, Mumford, 2013),
2) Whiteman Lake quartz syenite (2185 ± 2 Ma, Bowring et al, 1984),
3) Hearne Channel granite (2175 ± 5 Ma, Bowring et al, 1984),
4) Mad Lake granite (2166 ± 47 Ma, Wanless et al, 1979),
5) Grace Lake granite (2176.2 ± 1.3 Ma, Sinclair et al, 1994),
6) Thor Lake syenite (2164 ± 11 Ma, Mumford, 2013).

Based on geochemistry (Davidson, 1981), the BLIS could be broken into two distinct portions; an older sub-alkaline western lobe (Units 1-4) and a younger peralkaline eastern lobe (Units 5-6). Mumford (2013) has described units 2 to 4 as coeval multi-phase intrusives, (based on contacts and variations within the granitic intrusions), that show large scale changes from north to south; therefore, these units (2, 3, 4) are transitional and the Made Lake granite can be distributed between the northern Whiteman Lake and southern Hearne Channel, eliminating the Mad Lake granite from the intrusive suite.

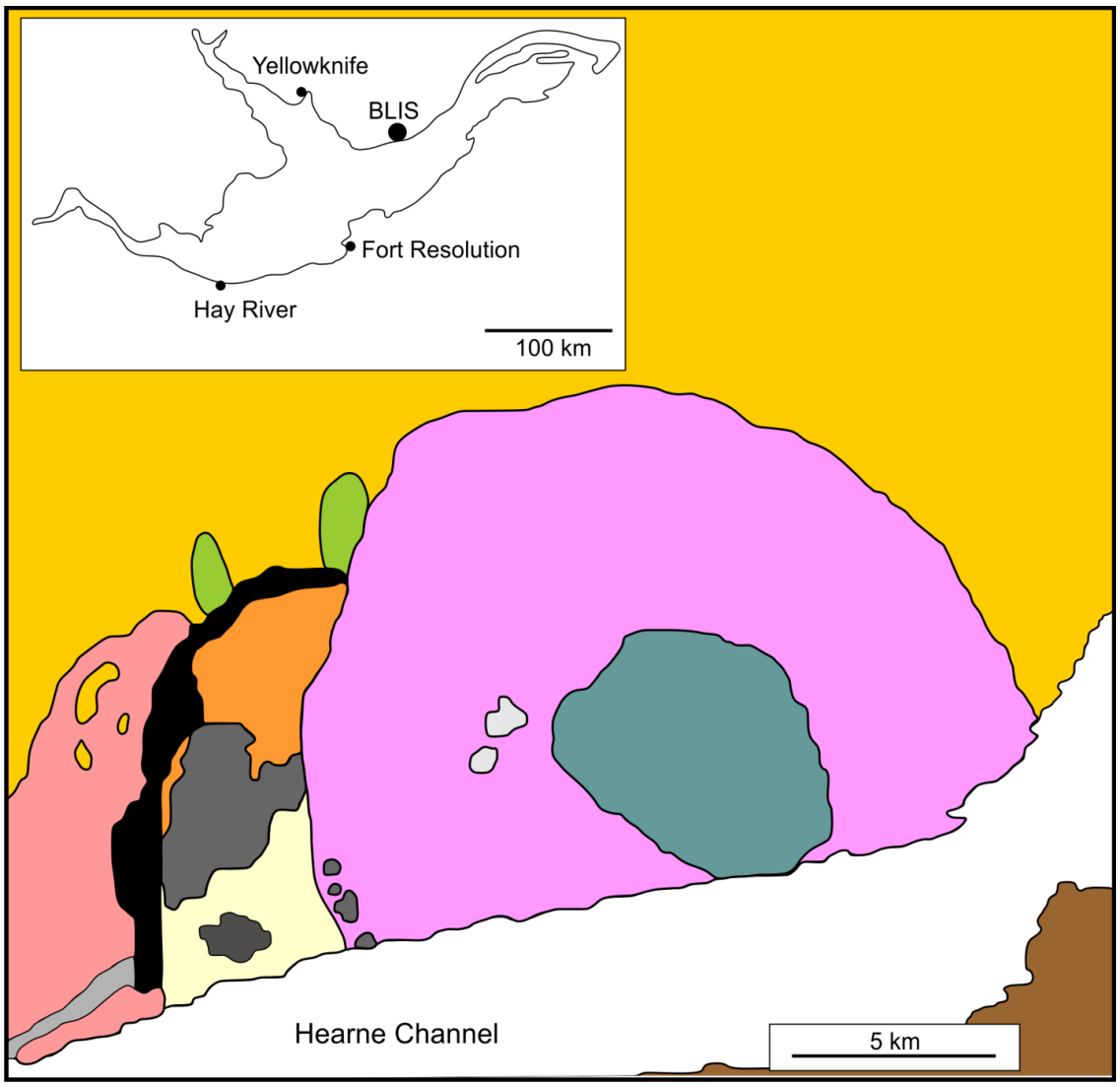

Figure 4.1: Simplified geology of the Blatchford Lake intrusive suite, modified after Davidson (1982) and Mumford (2013).

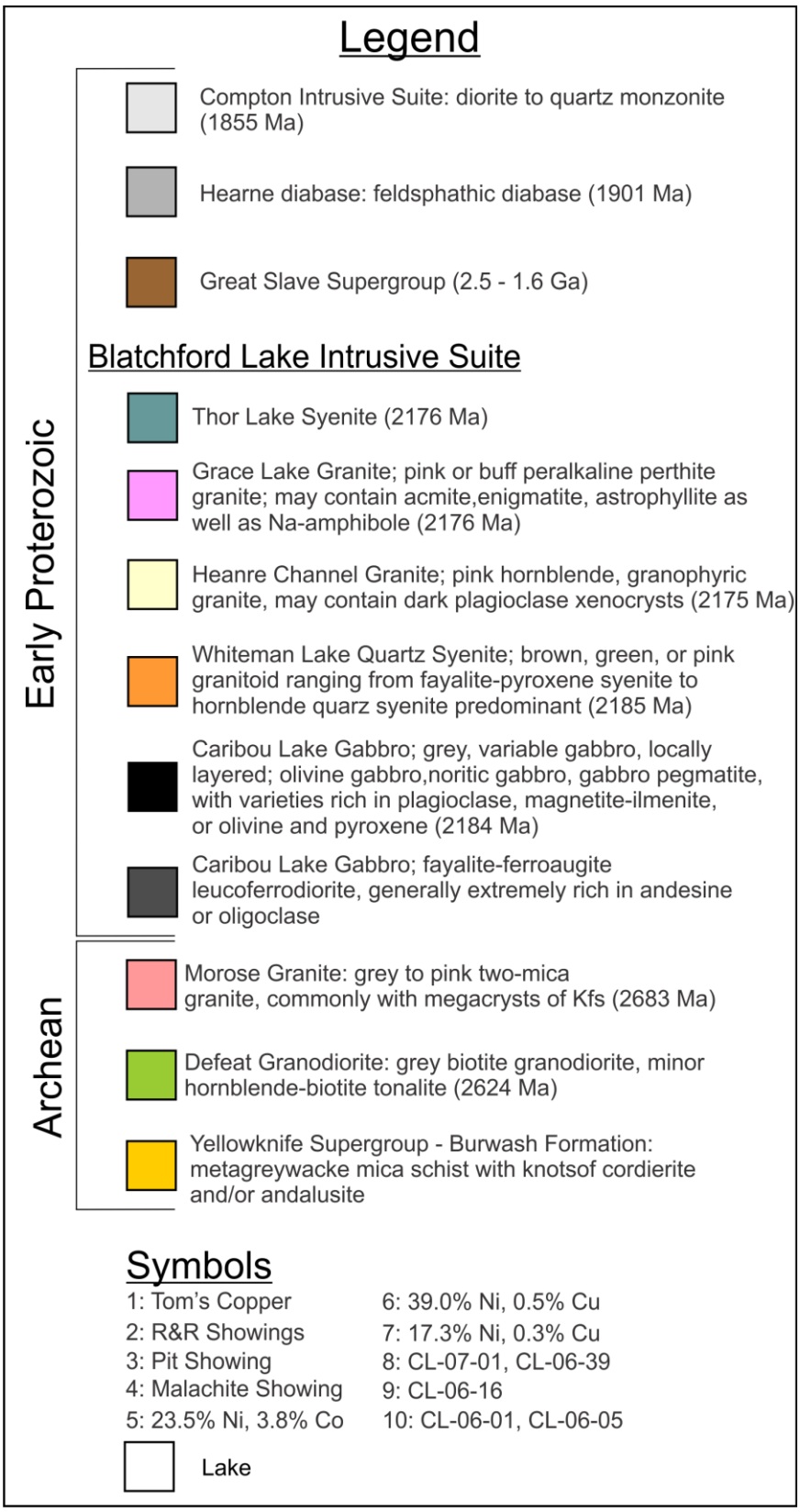

Figure 4.2: Geology legend for Figure 4.1 and Figure 4.3.

Exploration History

The Earl Jack Syndicate investigated aeromagnetic anomalies during 1963 in the Caribou Lake area. They discovered Fe-Ti occurrences with up to 15% oxide corresponding to aeromagnetic highs within an anorthositic gabbro in the higher grade zones, assays returned values of 30% Fe and 10% TiO_2. No claims were staked because zones of titanium and iron mineralization were deemed too small to be considered economic at the time (Curry et al, 1963). Shield Resources performed magnetic surveys during the 1960's and discovered sulfide occurrences associated with magnetic lows. Numerous trenches were also blasted during the time Shield held claims in the area, several of which contained niccolite hosted in carbonate veins (Curry, 1969).

Airborne magnetic and EM survey were conducted by New Caledonia Mining in 1994, also collected till samples looking for diamond indicator minerals. A few magnetic anomalies were identified, with a follow-up ground magnetic survey suggested for one of them. They also suggested that there were no significant concentrations of base metals occurring in the gabbroic units (Warman and Gelo, 1995).

In 2004 Kodiak Exploration performed reconnaissance prospecting of the Caribou Lake gabbro. They sampled previously known niccolite showings and one sample returned assay values of 38.2% Ni and 3.8% Co. One sample of gabbro within the Whiteman Lake syenite was collected and had values of 19.7% Cu and 0.3% Ni. A total of 130 samples were sent for assay analysis (Marmont, 2006). During the summer of 2005 Kodiak Exploration hired Aurora Geoscience to perform a prospecting and sampling program as well as to investigate the areas around the magnetic anomalies discovered by New Caledonia Mining. Aurora Geosciences' program resulted in 714 samples submitted for assay. Of all the 2004 and 2005 samples submitted for assay (n=844), 91 came back with values greater than 0.1% Cu and 41 with greater than 0.1% Ni. Because of the results produced during the sampling program, an airborne VTEM electromagnetic and magnetic survey over the Caribou Lake intrusion was conducted. From these surveys thirteen strong EM anomalies were identified and twelve of them occurred in the mafic-ultramafic units of the Caribou Lake intrusion (Marmont, 2006).

Kodiak's prospecting work continued into 2006 and focused on areas located around the anomalies from the EM and magnetic surveys. This program identified new

anomalies that contain modest amounts of PGE (30 ppb Pt-Pd) and one sample with Pt and Pd values of 97 and 25 ppb Pd respectively. Some mineralized carbonate veins were also found during this program, which returned assay values of 8.4% Ni and 1.25% Co (Marmont, 2006).

In 2006 Kodiak also undertook a drilling program that was designed to test the EM anomalies, explore the contact of the CLI, test the depth of surface showings, as well as to determine the stratigraphy of the CLI. The first, third and fifth drill holes produced the best results of the program, encountering massive sulfides with grades ~0.53% Ni and ~0.7% Cu (Marmont, 2006). Kodiak continued its drill program in 2007 with an additional fifteen drill holes to explore the basal contact of the CLI, re-test some VTEM anomalies and to improve their understanding of the stratigraphy. No significant sulfide intersections were encountered during the 2007 drill program (Marmont, 2007).

Study Area

The oldest part of the Blatchford Lake Intrusive Suite is the Caribou Lake gabbro (2184 ± 2 Ma, Mumford, 2013) which intrudes into the Archean sedimentary rocks of the Yellowknife Supergroup, the Morose granite, and the Defeat granodiorite (Figure 4.2 and Figure 4.3), which contain minor amounts of disseminated pyrrhotite (Davidson, 1982). Contacts between the CLI and its Archean host rocks are not commonly observed due to cover by vegetation, swamps, or lakes. Davidson (1978) described a chilled margin along the western contact and also observed progressive changes from west to east across the gabbro starting with pegmatitic patches in massive olivine gabbro along the west and north shores of Caribou and Whiteman Lakes transitioning into a massive to faintly layered noritic gabbro with plagioclase defining a weak foliation, with the most eastern portion of the gabbro identified as a leucoferrodiorite.

Drilling results in 2006 were moderately successful, with massive to heavily disseminated sulfide encountered in four drill holes approximately 3km south of Caribou Lake (Figure 4.3), including the first hole which intersected 0.53% Ni and 0.7% Cu over 3.18m (Marmont, 2006). The other intersections of massive to highly disseminated sulfide have similar Ni and Cu grades (Marmont, 2006). Sulfides are hosted by a fine to medium grained gabbro and are primarily composed of pyrrhotite with lesser amounts of

chalcopyrite and pyrite (Marmont, 2006). Drilling results in 2007 proved to be unsuccessful in the effort to find more massive sulfide intersections (Marmont, 2007).

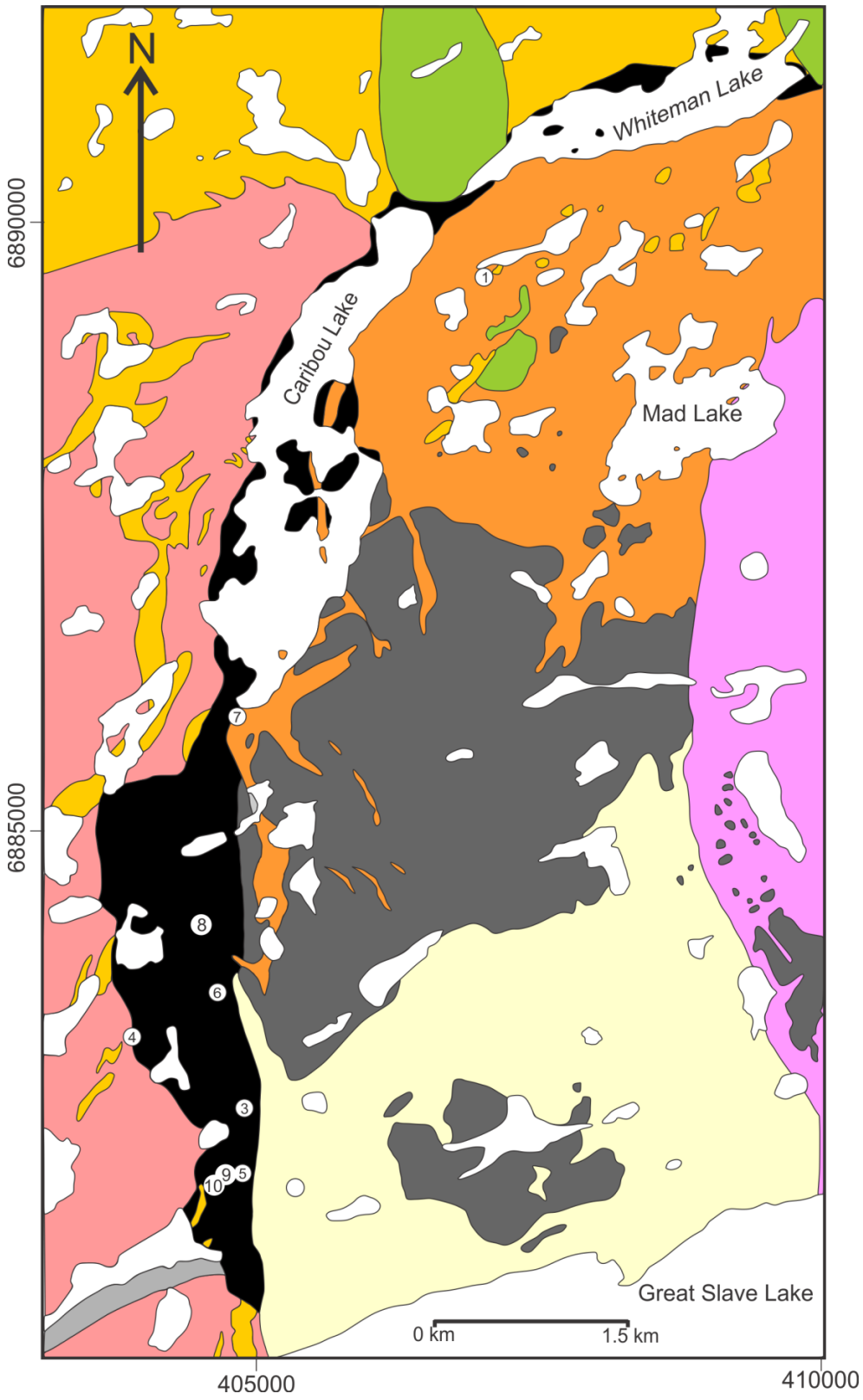

Figure 4.3: Detailed geology of the western portion of the Blatchford Lake intrusive suite, modified after Davidson (1982) and Mumford (2013).

Methodology

During the winter of 2013 a total of 29 samples were collected from Kodiak Explorations 2007 drill program by Hendrik Falck for the purpose of preliminary petrography of various units within the CLI (refer to Appendix A for sample list). During the summer of 2013, an additional 266 sample were collected from numerous drill holes from the 2006 and 2007 drill programs. Of the 266 collected only 112 were sent to Vancouver Petrographics and the Ontario Geological Survey Geolabs for whole rock and trace element analysis as well as 20 samples for Ni-sulfide fire assay for PGE contents (refer to Appendix B for sample list).

The majority of samples were collected from only three drill holes that were also descriptively logged; 1) CL-06-16 (170.7 m), 2) CL-06-39 (163.05 m), and 3) Cl-07-01(481.4 m). A total of 28 samples were sent for analysis from drill hole CL-06-16, nine of which were within a 10 m interval of heavily disseminated sulfide, the other samples represented lithology changes throughout the length of the hole. In CL-06-39, a thick ultramafic succession of approximately 50m had been intersected and represented the thickest ultramafic package encountered in drilling; a total 29 samples were shipped for analysis representing lithology changes. CL-07-01 and CL-06-39, which were drilled 200 m apart, were logged to correlate units between the two drill holes. Thirty nine samples were sent for analysis from CL-07-01, representing lithology changes throughout the length of the hole. The remaining 16 samples sent for analysis came from various drill holes representing other styles of mineralization (i.e. semi-massive to massive), host rock lithologies, and other units composing the BLIS.

The petrographic characteristics of thin sections were determined using a Nikon Eclipse H550L microscope, which has the capability to use transmitted and reflected light. The characterization of base metal sulfides and discrete mineral phases has been conducted using a LEO1450VP scanning electron microscope (SEM) at Saint Mary's University, equipped with an energy dispersive X-ray (EDS) Oxford INCA 80mm^2 silicon drift detector (SDD) capable of quantitative analysis. Measurements of all analysis were conducted at a working distance of ~20mm, with a beam current of 40uA and accelerating voltage of 25.00-30.00 kV.

Core samples were sent to the Ontario Geological Survey GeoLabs in Sudbury, Ontario for whole rock and trace element geochemistry which were determined by X-ray fluorescence spectrometry (XRF) and inductively-coupled plasma mass spectrometry (ICP-MS).

Results

Drill Hole CL-06-16

Drill hole CL-06-16 is a 170.6m long vertical drill hole that was drilled into the southern portion of the CLI (Figure 4.3). This hole was chosen for the study based on its highly disseminated sulfide mineralization. The hole is predominately composed of a gabbroic unit that varies from fine to coarse grained. Plagioclase and clinopyroxene modal proportions are relatively consistent throughout the unit, ranging from 30-50% plagioclase and 20-35% clinopyroxene. Orthopyroxene and olivine vary significantly through the gabbroic unit, ranging from 0-10% for both minerals. Alteration intensity varies throughout the gabbro as well. Short intervals of a melagabbro were observed at 34.7-36.1m in the core, which will be referred to as a clinopyroxenite. The upper and lower contacts with the surrounding gabbro are gradational. Clinopyroxenite consists of 5-10% plagioclase, 50-75% clinopyroxene, 0-15% olivine, Fe-Ti oxides 10-15%, and 3-5% pyrrhotite with trace chalcopyrite. From 51.8 m to 64.5 m, moderate to heavily disseminated sulfides occur, primarily pyrrhotite with minor amounts of chalcopyrite. A small anorthosite unit occurs at 90 metres depth within the gabbro and is only ~10 cm in length. From 87.5-88.1 m and 92.2-108.9 m alteration zones contain abundant calcite-quartz veinlets and stringers consisting of epidote, pyrite, serpentine and chlorite. Minor amounts of bleaching are present within the zone as well as minor amounts of hematite alteration. Below the alteration zone is a thick interval of quartz syenite (108.9-139.05 m) and then a plagioclase rich diabase (139.05-151.5 m). A small interval of gabbro occurs from 151.5-153.3 m. The hole ends in plagioclase rich diabase. Stratigraphic column showing variations in mineralogy and alteration is illustrated in Figures 4, 5 and 6.

Drill Hole CL-06-39

Drill hole CL-06-39 is a 163.1m long vertical drill hole that was drilled approximately 2000 m north of CL-06-16 (Figure 4.3). The significance of this hole is that it contains a ~70 m thick interval of ultramafic, the thickest ultramafic succession identified by Kodiak's drill program. The upper ~27 m of the hole is mainly composed of a gabbro with grain sizes varying from medium to coarse grained and relatively consistent modal proportions of plagioclase (45-50%), clinopyroxene (40-45%,) and Fe-Ti oxides (2-7%). A few pegmatitic gabbros were also encountered within the first 27m, one at 4.1 m and the other at 6.85 m. These pegmatites are different from the host gabbro in modal mineral abundances, with the pegmatite at 4.1m being composed of primarily of clinopyroxene (~65%) and plagioclase (~35%) and the pegmatite at 6.9m being composed of primarily of plagioclase (~65%) and clinopyroxene (30%). A small 60cm interval of dunite occurs at 20.3m within the gabbro and is strongly altered. The gabbros upper contact with the dunite is slightly chilled for 2cm downhole, where grain sizes change from <1mm at the contact to 2-8mm after the contact. A thick ultramafic interval was encountered from 27.7m to 97.45m and is primarily composed of olivine (60-90%), clinopyroxene (10-20%) and plagioclase (0-5%), varying between dunite, lherzolite and wehrlite. Rarely, plagioclase modal abundances reach ~10-15%, as such; some short intervals can be classified as troctolite (e.g. 83.9m). Iron-titanium oxides vary considerably throughout the ultramafic interval, with modal abundances ranging anywhere from trace amounts to 35% of a given interval. A short (40cm) interval of gabbro occurs within the ultramafics, with sharp contacts and abrupt changes in modal proportions, but magnetite seems to concentrate around the contacts. From 82.1-84.8m, a carbonate alteration zone is present, which occurs just before a small fault surface at 85.7m. From 97.45-118.45m is composed primarily of various types of gabbros that can be rich in plagioclase, clinopyroxene, or Fe-Ti oxides. Each type of gabbro is generally a short interval (<20cm) and contacts appear to be gradational. Rare, thin ultramafic and oxide-rich ultramafic sections are also present within this interval. Two pegmatites occur within this interval, one at 100m, which is an anorthosite and another at 103.9m, which is an olivine gabbro. A magnetite rich (~70% Fe-Ti oxides) interval also occurs at 103.7m shortly before the pegmatite. After the varied gabbro interval, a uniform gabbro occurs

until 122.95m, where an anorthosite is intersected, which appears to be highly altered. The lower contact of the anorthosite is gradational with a gabbro below at 125.9m, while the top contact of the anorthosite is sharp. The gabbro from 125.9-152.9m is similar to the uniform gabbro present above the anorthosite. At 152.9m, the lithology changes into an oxide-rich dunite, with Fe-Ti oxides composing 20-35% of the interval. This oxide-rich dunite, occurs until 156.9m where a sharp contact occurs with a gabbroic pegmatite and the pegmatite is only present for 20cm before the lithology changes back into a gabbro at 157.2m. The gabbro occurs for 3m and then the unit changes into a syenite at 160.3m, which then ends the length of the drill hole at 163.05. Stratigraphic column showing variations in mineralogy and alteration is illustrated in Figures 4.7 and 8.

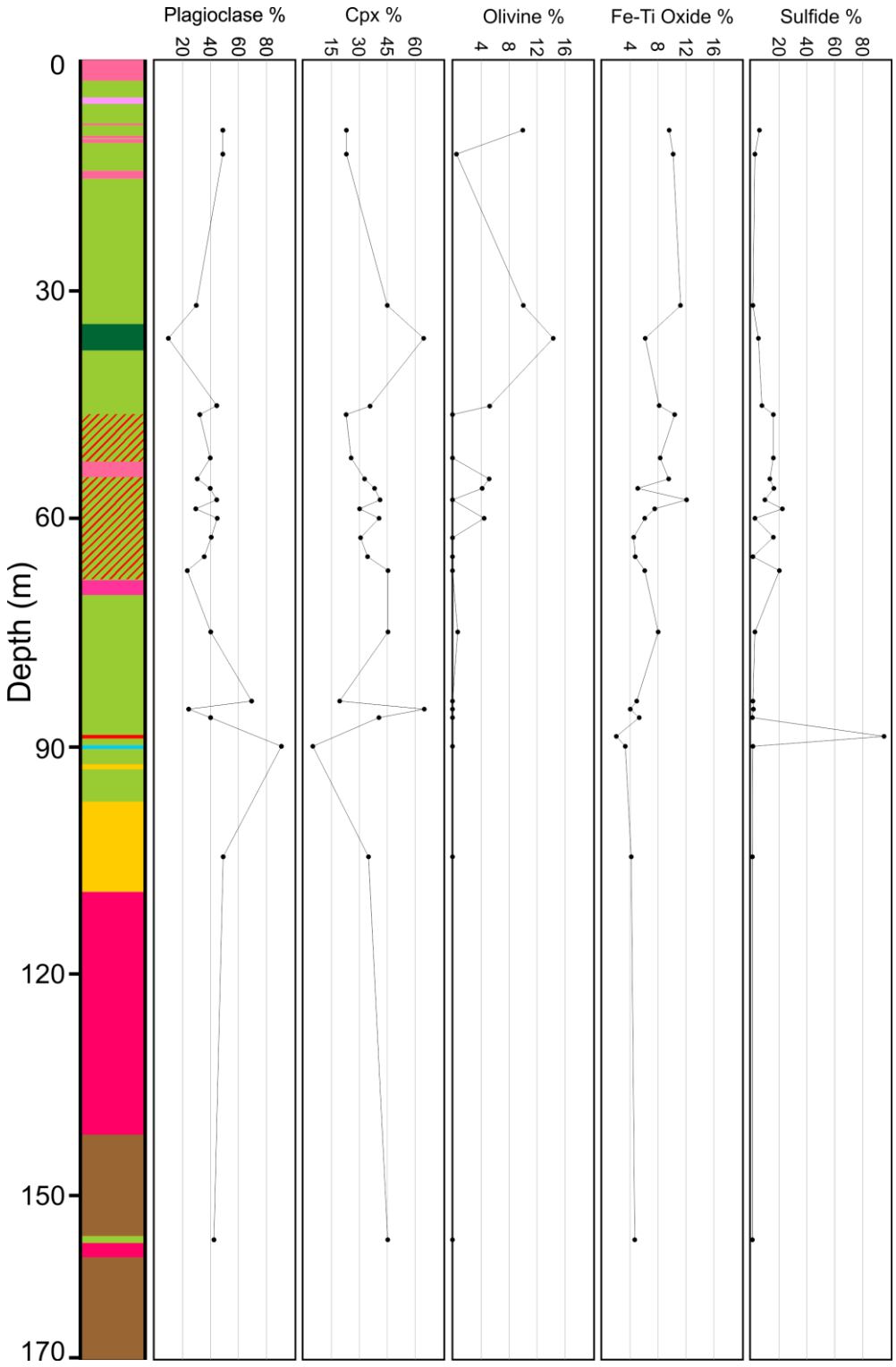

Figure 4.4: Stratigraphic column of CL-06-16 showing variations in mineral proportions.

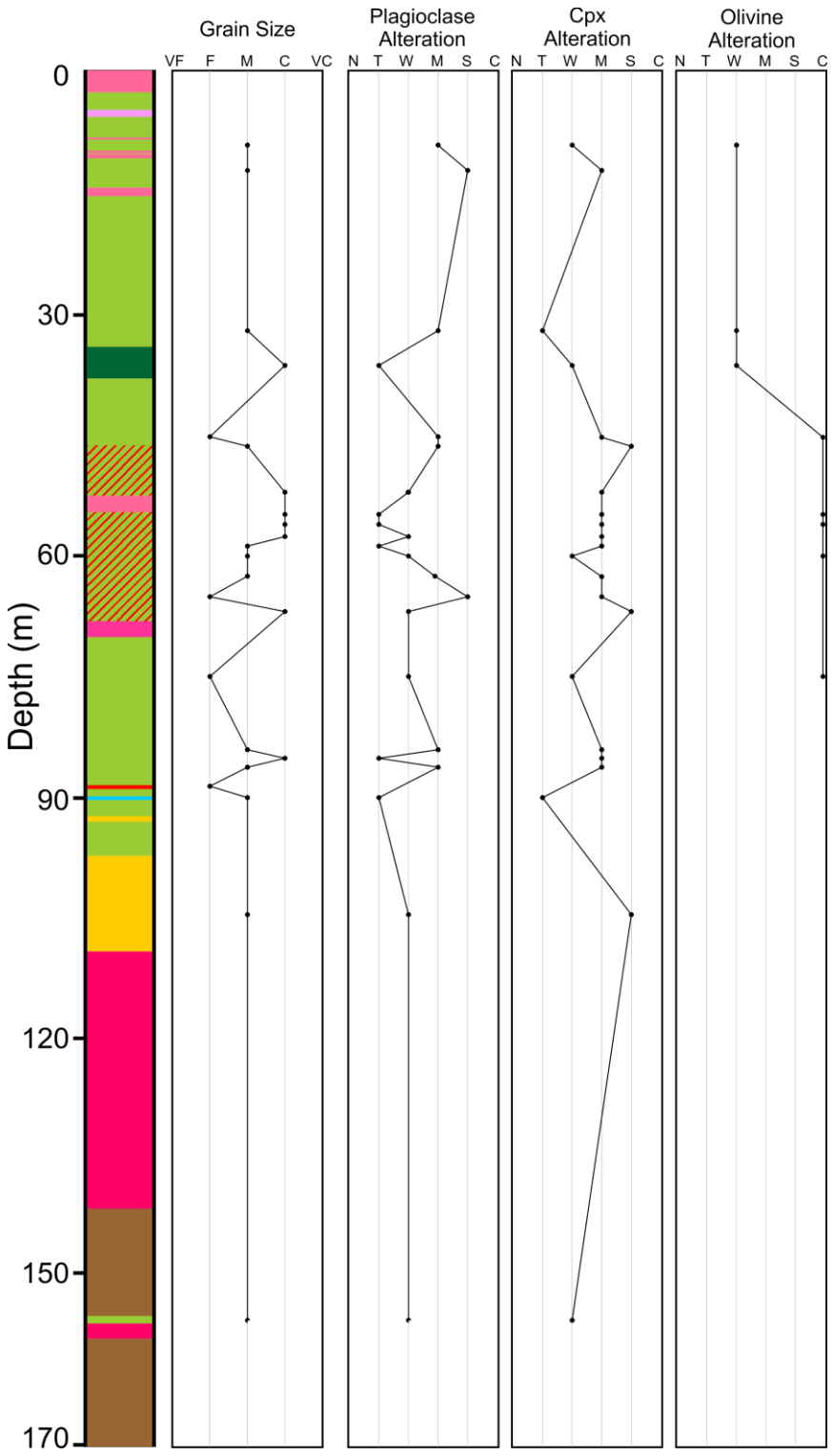

Figure 4.5: Stratigraphic column of CL-06-16 showing variations in alteration. Grain sizes: Very fine (VF) = <0.8mm; Fine (F) = 0.8-1.5; Medium (M) = 1.5-3mm; Coarse (C) 3-7mm; Very coarse = 7-12mm.

Figure 4.6: Legend for stratigraphic columns in Figures 4, 5, 7 and, 8.

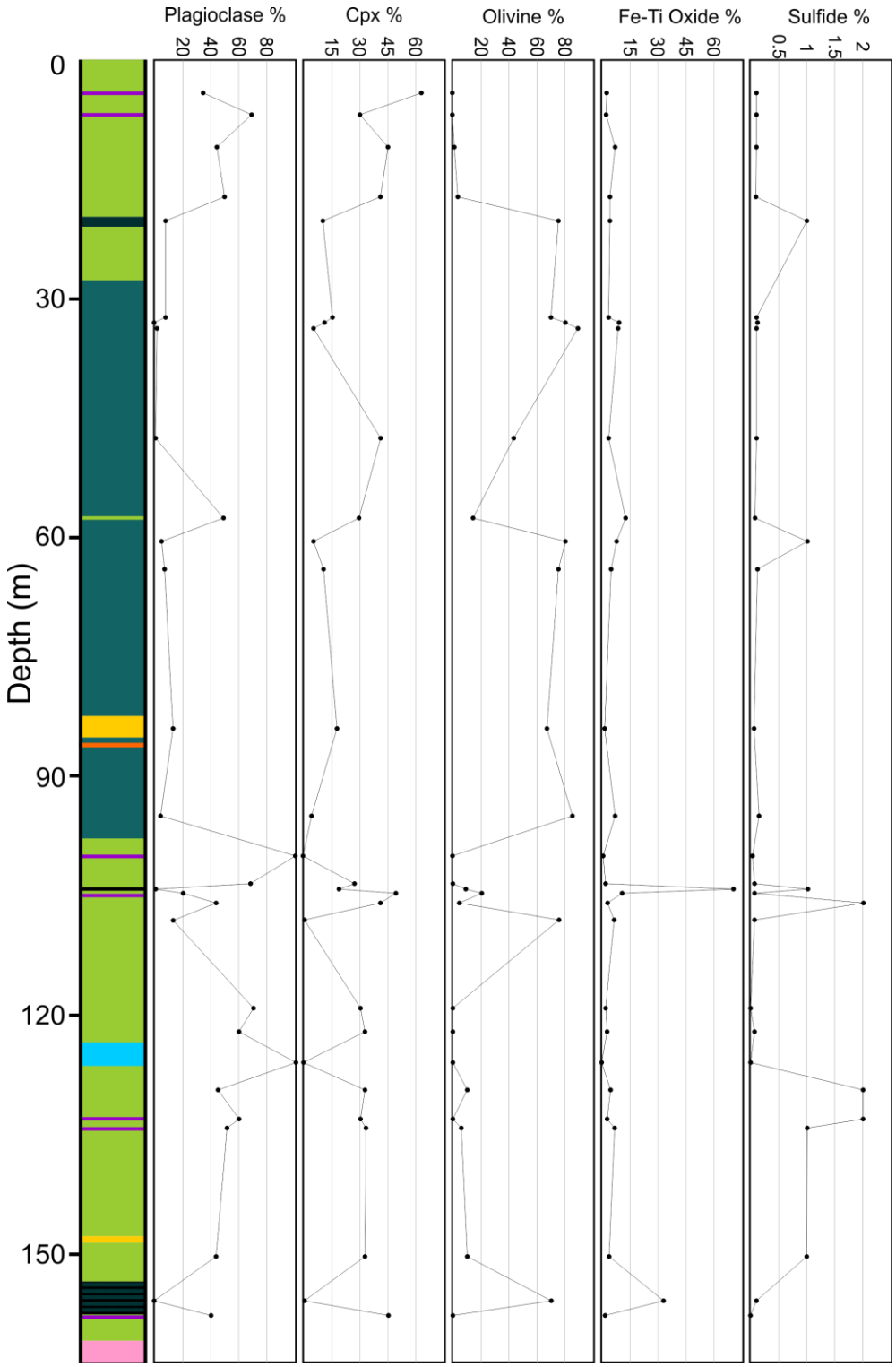

Figure 4.7: Stratigraphic column of CL-06-39 showing variations in mineral proportions.

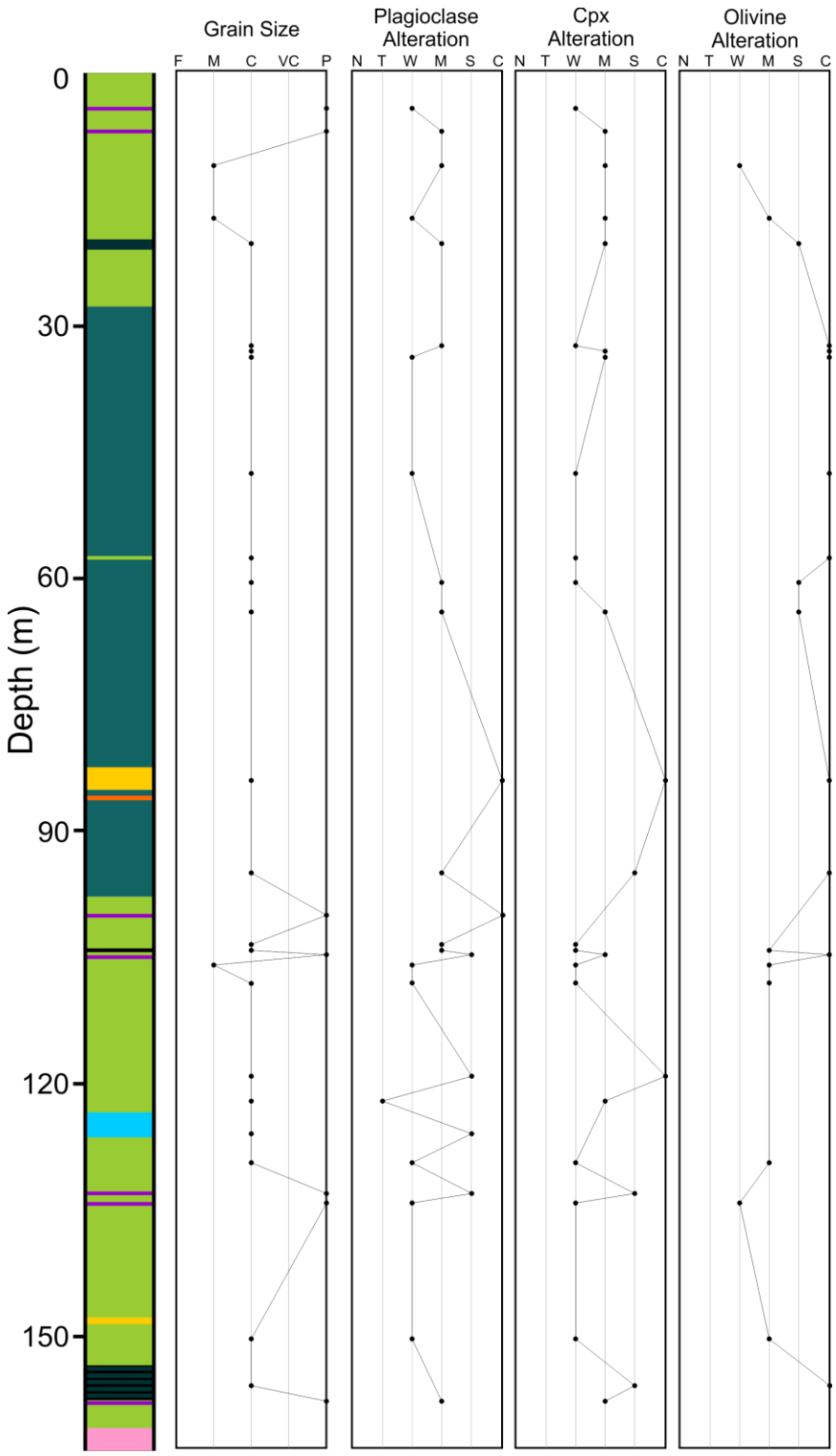

Figure 4.8: Stratigraphic column of CL-06-39 showing variations in alteration. Grain sizes: Fine (F) = 0.8-1.5; Medium (M) = 1.5-3mm; Coarse (C) 3-7mm; Very coarse = 7-12mm; Pegmatitic (P) = >12mm.

4.6.3 Petrography of CL-06-16

Gabbro

Gabbroic units in CL-06-16 are primarily composed of plagioclase (25-50%) and clinopyroxene (20-55%), with variable amounts of olivine (0-10%). Plagioclase and clinopyroxene display subophitic textures and occasionally ophitic textures are present (Figure 4.9A,B). Inclusions of plagioclase are common in pyroxene and olivine throughout the entire section (Figure 4.9C). Plagioclase grains are euhedral-subhedral and display a wide range of sizes, from 0.02-5mm. Alteration of plagioclase is also quite variable where some grains only show trace amounts of sericite alteration and others display 80% alteration (Figure 4.10). Other alterations of plagioclase are chlorite and possible epidote. In intervals with heavily disseminated sulfide, plagioclase occurs as inclusions within pyrrhotite (Figure 4.9D). Clinopyroxene ranges in size from 0.05-7mm and are subhedral-anhedral. Exsolution lamellas of ilmenite along cleavage planes are present in all clinopyroxene grains and clinopyroxene occasionally contains inclusions of magnetite and ilmenite. Alteration products of clinopyroxene include amphibole (actinolite), biotite, chlorite, serpentine, and fine grained uralitization (Figure 4.11). The majority of alteration is present along the edges of grains, and typically where amphibole is in contact with clinopyroxene, the amphibole is altered to biotite and subsequently to chlorite. Biotite is also present as fine grained alteration product in the cores of clinopyroxene. Olivine, when present, is subhedral, highly fractured and ranges in size from 0.1-2mm. Fine grained (< 0.3mm) inclusions of plagioclase and ilmenite occur in olivine implying that olivine is a late cumulus phase. Samples near the top of the hole only show weak alteration of olivine to serpentine, while further downhole, complete olivine alteration to serpentine is present (Figure 4.11). Actinolite alteration is occasionally present on the edges of serpentine as well. Fine grained pyrite, as well as magnetite, can be present along fractures in olivine. Carbonate alteration is present in the gabbro and its occurrence is very patchy and generally localized around clinopyroxene, suggesting that the carbonate is an alteration product of clinopyroxene (Figure 4.11).

Trace mineral phases that occur within gabbroic units include apatite, biotite, and amphibole. Biotite is present in three different forms; 1) corona around oxides, 2) interstitial grains to plagioclase and pyroxenes, and 3) poikilitic grains with inclusions of plagioclase and pyroxene (Figure 4.12A,B,C). Interstitial biotite grains are subhedral and

< 0.4mm. Poikilitic grains are up to 5mm and contain < 1mm inclusions of euhedral plagioclase and subhedral pyroxene. Corona textured biotite is variable in thickness and may not always form a complete rim around the oxides. Total biotite content in gabbroic units can be up to 8%, but average is ~3%. Poikilitic amphibole also occurs with similar texture and appearance as the poikilitic biotite grains (Figure 4.12D). Apatite can be present up to 1% but typically occurs in trace amounts. Apatite grains are < 1.5mm but average ~0.2mm, are euhedral-subhedral, and occur interstitially to pyroxene and plagioclase (Figure 4.12E).

Magnetite and ilmenite occur interstitially to silicates, comprising 2-12% of the gabbro and typically occur together as composite grains that are < 2.5mm. These composite grains are also found as inclusions within pyroxene and olivine. Two styles of exsolution are present within these composite grains, blebby exsolution where ilmenite exsolves to form a grain of its own on the edge of magnetite and trellis exsolution where ilmenite exsolves along a common plane (Figure 4.13 A,B). Magnetite always displays at least one style of exsolution but ilmenite can occur on its own but is not commonly observed. In sample CL-06-16-80.0, a graphic texture exists between ilmenite and feldspar, which likely indicates a eutectic crystallization of the two minerals (Figure 4.13C,D). Pyrrhotite is the dominate sulfide present within the gabbroic units comprising 1-25%. Detailed description of the disseminated sulfides is discussed below.

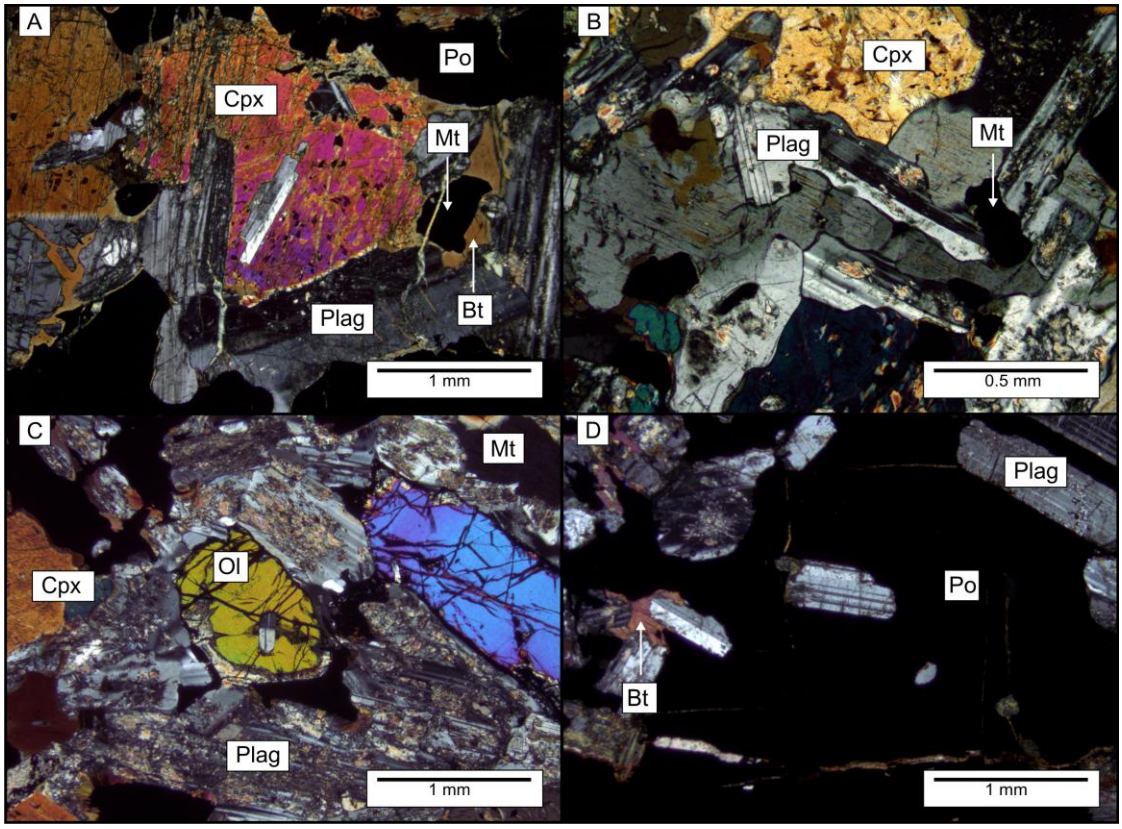

Figure 4.9: Photomicrographs showing primary textures present in gabbro units in CL-06-16. A) Subophitic texture occurring between clinopyroxene (Cpx) and plagioclase (Plag). An inclusion of Plag occurs in Cpx as well. Small grains of magnetite (Mt) occur on the edge of Cpx and have a thin corona of biotite (Bt). Sample CL-06-16-57.5. Cross polarized light (XPL). B) Subophitic texture occurring between Cpx and Plag. Interstitial Mt occurs between Plag grains. Sample CL-06-16-59.9. XPL. C) Olivine (Ol) containing an inclusion of Plag. Magnetite occurs around the edge of Ol and interstitial to Plag and Cpx. CL-06-16-8.9. XPL. D) Plagioclase inclusion within highly disseminated pyrrhotite (Po). Fine-grained Bt occurs interstitial to Plag. CL-06-16-52.5. XPL.

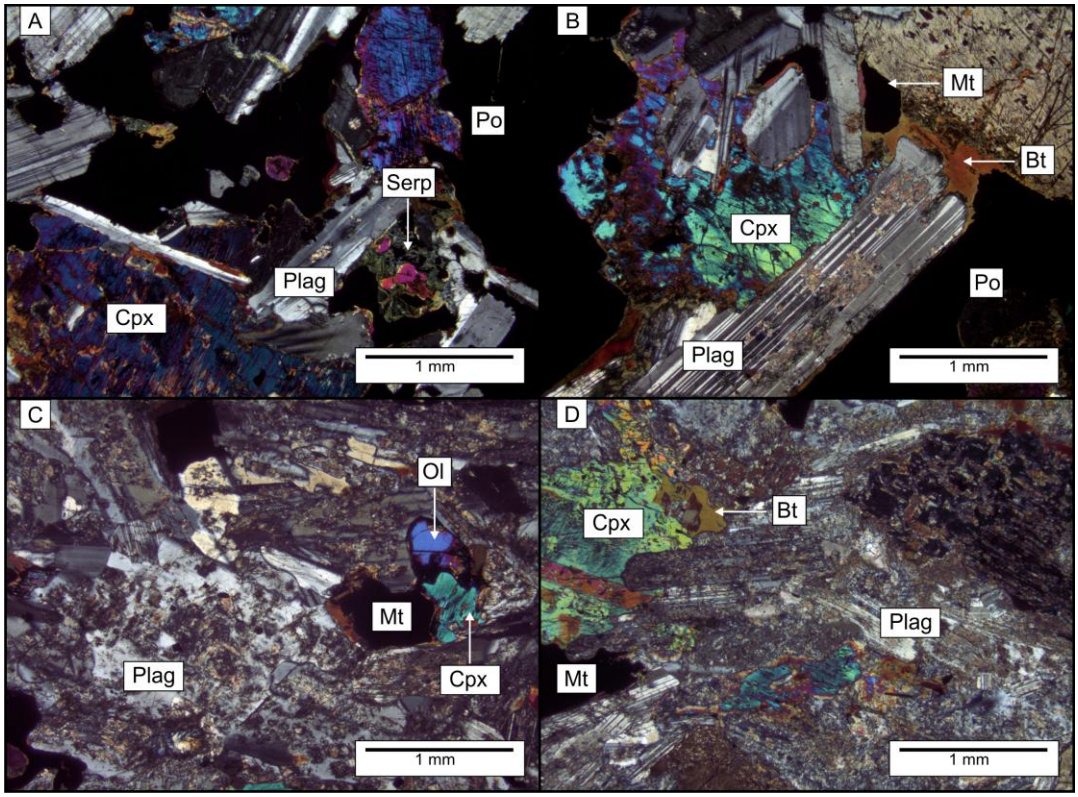

Figure 4.10: Photomicrographs showing the range of alteration intensity demonstrated by plagioclase throughout the gabbro units in CL-06-16. A) Subophitic texture between Plag and Cpx. Plagioclase shows only trace amounts of alteration. Trace amounts of serpentine (Serp) are present with remnants of Cpx at its core. CL-06-16-56.3. XPL. B) Weak alteration of plagioclase with interstitial Bt and Mt between Plag and Cpx. CL-06-116-58.6. XPL. C) Moderate alteration of Plag. CL-06-16-8.9. XPL. D) Strong alteration of Plag. CL-06-16-11.2. XPL.

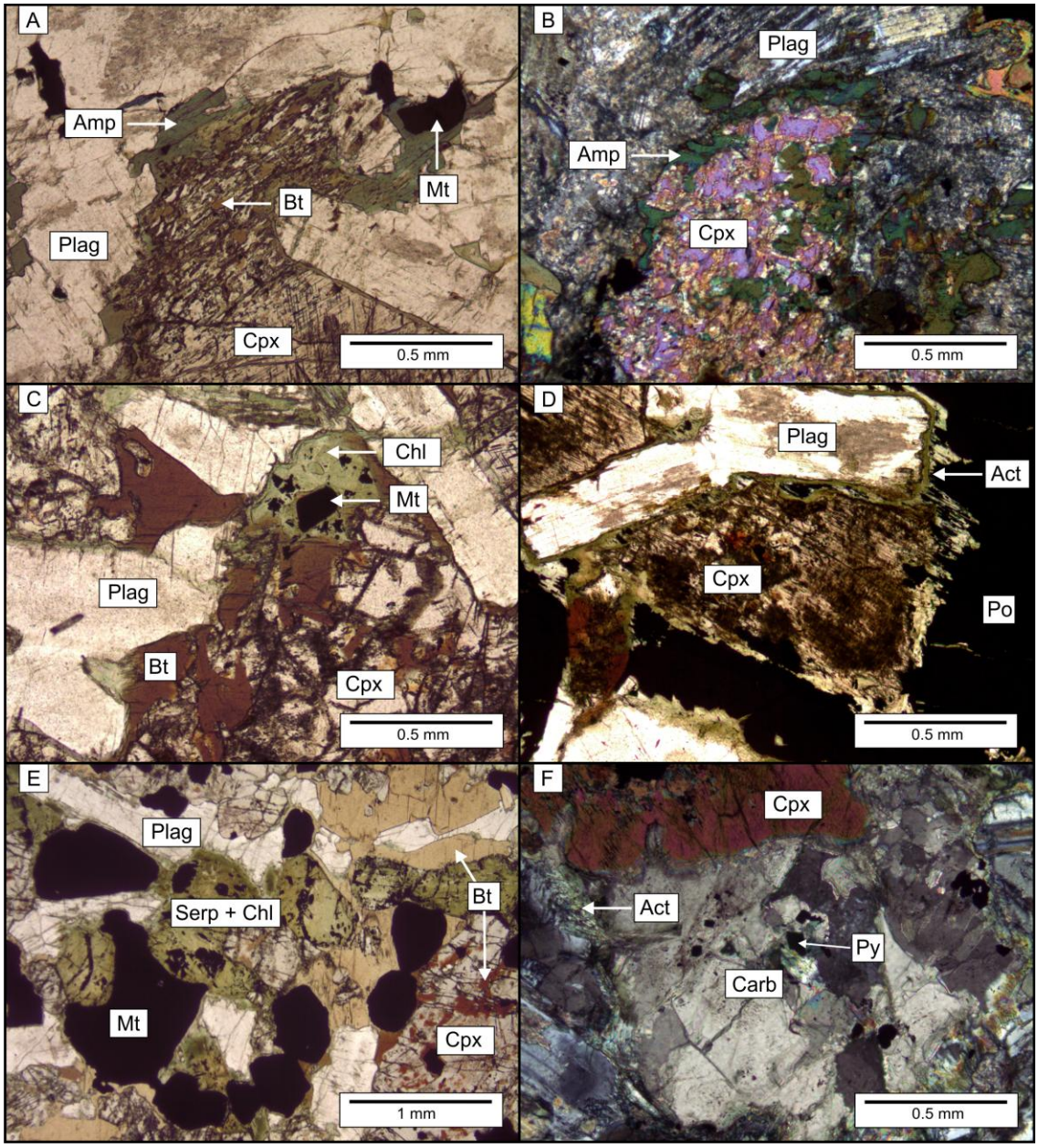
A
Amp
Bt
Mt
Plag
Cpx
0.5 mm
B
Plag
Amp
Cpx
0.5 mm
C
Chl
Mt
Plag
Bt
Cpx
0.5 mm
D
Plag
Act
Cpx
Po
0.5 mm
E
Plag
Serp + Chl
Bt
Mt
Cpx
1 mm
F
Cpx
Act
Py
Carb
0.5 mm

Figure 4.11 (previous page): Photomicrographs of alteration products of pyroxenes and olivine. A) Grain of Cpx that has an outer rim of amphibole alteration (Amp) and occurring inwards from the rim is fine grain Bt alteration. CL-06-16-52.5. Plane polarized light (PPL). B) Strong alteration of Cpx to Amp on the edge and appears to penetrate into the core of Cpx. CL-06-16-11.2. XPL. C) Moderate Bt alteration of Cpx at the core and along the rim with a patch of chlorite (Chl) with small inclusions of Mt. CL-06-16-56.3. PPL. D) Clinopyroxene and Plag have a rim of actinolite (Act) and the core has been altered to a very fine grained brown mineral (?). CL-06-16-63.8. PPL. E) Serpentine and Chl alteration olivine. CL-06016-55.0. PPL. F) Patch of carbonate (Carb) alteration next to a Cpx grain. A fine grained network of Act occurs along the rim of the Carb alt. CL-06-11.2. XPL.

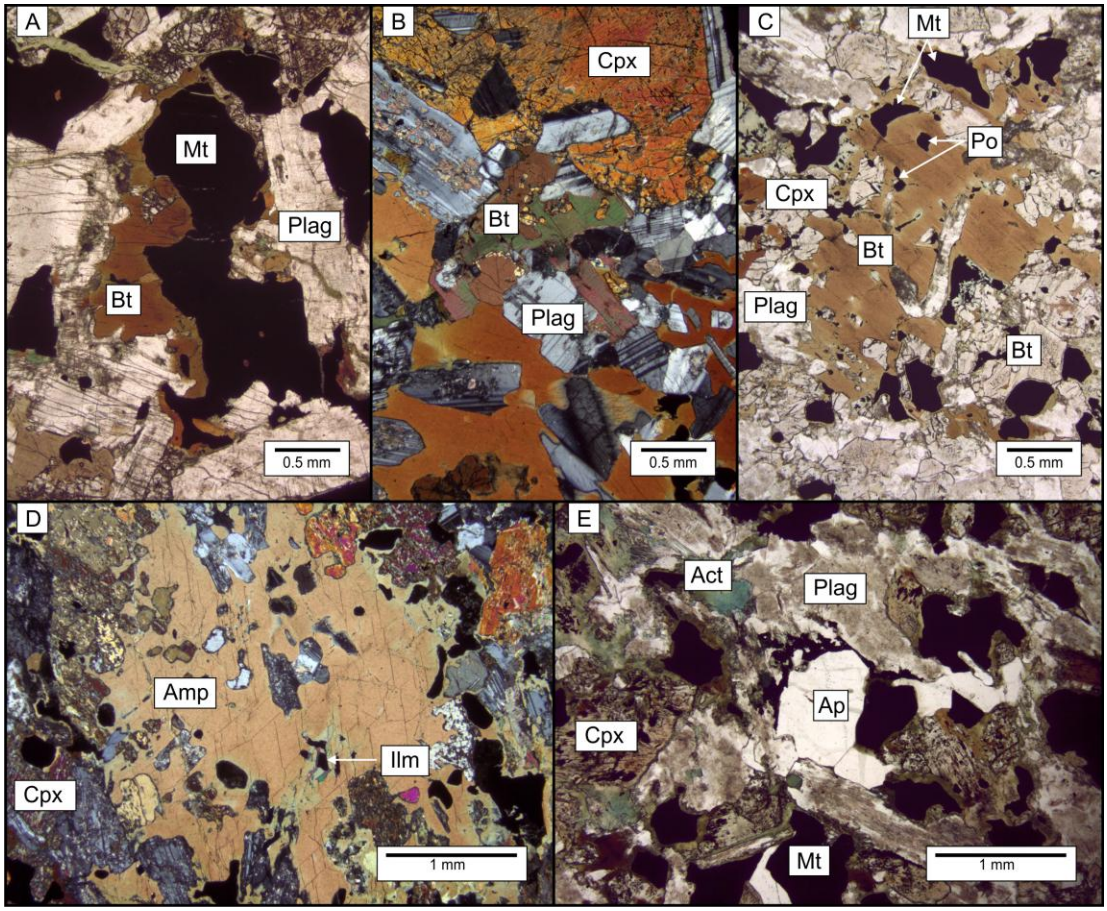

Figure 4.12: Photomicrographs of trace to minor mineral phases present in the gabbro. A) Partial Bt corona on grain of magnetite. CL-06-16-57.5. PPL. B) Interstitial Bt to plagioclase grains. CL-06-16-56.3. XPL. C) Poikilitic Bt with inclusions of Cpx, Plag, Po, and Mt. CL-06-16-47. PPL. D) Poikilitic amphibole with inclusions of Plag, ilmenite (Ilm) and Cpx. CL-06-15-52.5. XPL. E) Interstitial apatite (Ap) to plagioclase. Interstitial Mt also occurs in close proximity to Ap. CL-06-16-63.15. PPL.

Clinopyroxenite

A small interval of clinopyroxenite consists primarily of clinopyroxene (50-75%) and lesser amounts plagioclase (5-10%), and olivine (0-15%). Clinopyroxene ranges in size from 0.3-7mm and is subhedral. Alteration of clinopyroxene is generally weak and consists of biotite starting to replace the edges of grains, with small patches of biotite occurring in the cores. Very fine grained (<0.3mm) inclusions of pyrite and ilmenite occur in clinopyroxene and ilmenite exsolution occurs along cleavage planes (Figure 4.14A). Inclusions of altered olivine also occur in clinopyroxene (Figure 4.14B). Clinopyroxene and plagioclase display an ophitic texture (Figure 4.13C). Plagioclase is 0.3-5mm, subhedral, and weakly-moderately altered to sericite. Anhedral inclusions of clinopyroxene and olivine occur in plagioclase (Figure 4.14D,E). Olivine is subhedral, highly fractured and ranges in size from 0.1-2mm. Very fine grained inclusions of ilmenite (< 0.4mm) occur in olivine as well as trace amounts of pyrite. Olivine is typically relatively unaltered, but some isolated grains have been completely replaced by serpentine and chlorite (Figure 4.14B). Olivine is only present in the interval from 34.7-36.1m. Magnetite and ilmenite comprise 4-10% of the feldspathtic clinopyroxenite and are < 2.5mm in size.

Apatite is present in trace amounts up to 2% in the feldspathtic clinopyroxenite where it ranges in size from 0.05-1.5mm and is euhedral-subhedral. Apatite grains are interstitial to plagioclase and clinopyroxene, but apatite also occurs as inclusions within plagioclase suggesting it is an early phase (Figure 4.14F).

Similar to biotite in the gabbroic units, biotite in the clinopyroxenite occurs in trace amounts as coronas around oxides and as poikilitic grains with inclusions of plagioclase, oxides, and clinopyroxene. In the clinopyroxenite, magnetite, and ilmenite are commonly composite grains with two styles of exsolution. A rim of biotite is often found around these composite oxide grains. Up to 3% interstitial sulfides occur in the clinopyroxenite and predominantly consist of pyrrhotite with trace amounts of chalcopyrite, pentlandite, sphalerite, and pyrite. Sulfides are < 1.5mm with chalcopyrite occurring as very fine grained inclusions within pyrrhotite and pentlandite typically occurring as flame lamella in pyrrhotite and rare blocky form (Figure 4.13B).

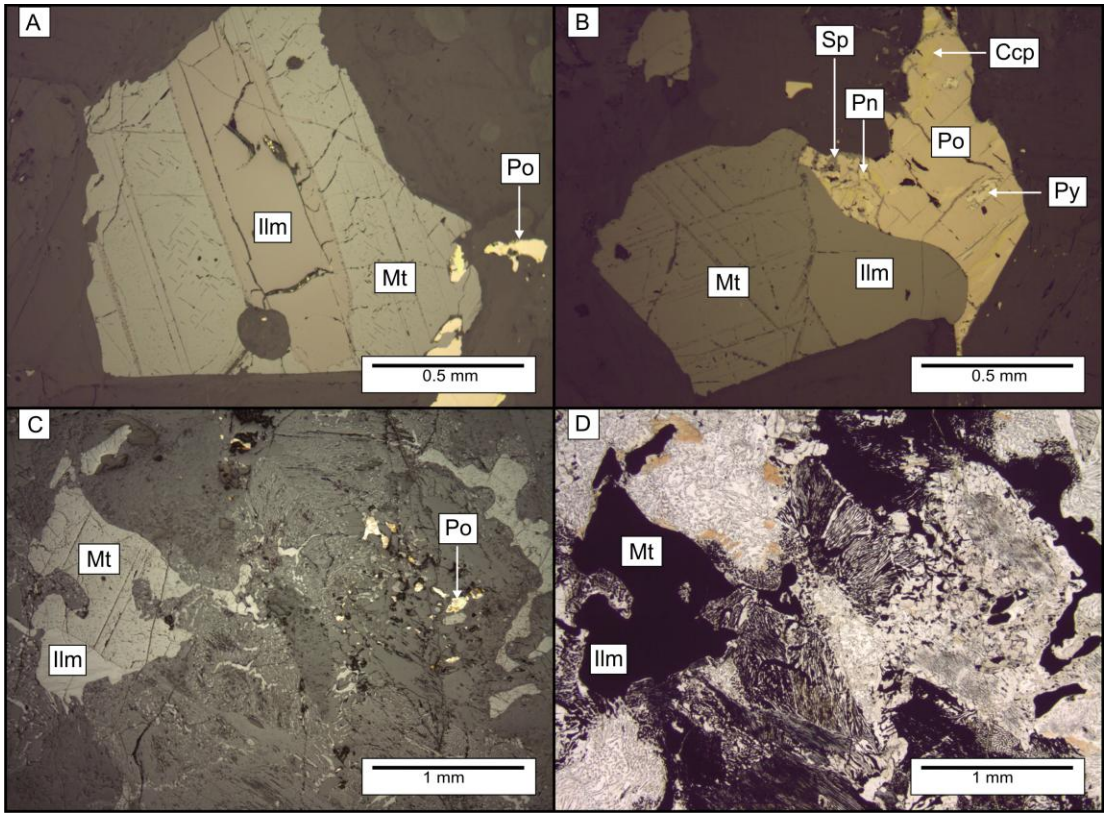

Figure 4.13: Photomicrographs of oxide and sulfide phases in the feldspathic clinopyroxenite. A) Large trellis exsolution of ilmenite (Ilm) in Mt. Fine grained Po occurs near the edge of Mt. CL-06-16-35.7. RL. B) Trellis and blebby exsolution of Ilm from Mt. Grain of Po occurs on the edge of Ilm that contains inclusions of chalcopyrite (Ccp), sphalerite (Sp), pentlandite (Pn), and Py. CL-06-16-35.7. RL. C) Graphic texture occurs between an oxide (magnetite or ilmenite?) and feldspar. Blebby ilmenite exsolution occurs in the large grain of Mt. CL-06-16-80.0. Reflected light (RL). D) Same images as A, but in PPL.

Mineralization

Sulfide mineralization occurs in two different styles: 1) fine- to coarse-grained blebby disseminations that grades into a net texture (Figure 4.15A,B), and 2) massive (Figure 4.15C). Fine to coarse grained blebby disseminated sulfides occur in a fine to medium grained gabbros. The upper contact of the mineralized interval is with a fine grained gabbro that gradational increases in sulfide percentage downhole. Initially the unit contains trace sulfides then local concentrations of patchy pyrrhotite (~20%) occur, followed by 10-15% disseminated sulfides for approximately 2m, then the gabbroic unit is crosscut by a syenite dyke. After the dyke, sulfides comprise 20-30% of the unit and form a net texture until the lower contact, which is defined by a 1cm thick band of pyrrhotite. After the pyrrhotite band, the rock is a fine grained gabbro that contains only trace amounts of sulfide. Massive sulfide mineralization has either sharp upper and lower contacts with a fine to medium grained gabbro that contain ≤ 5% fine grained disseminated sulfides or has a short interval of net-textured sulfides above hosted by a medium grained gabbro.

Massive sulfide mineralization is primarily composed of pyrrhotite (~80%), with lesser amounts of chalcopyrite (2-10%), pentlandite (trace-3%), pyrite (trace), magnetite (5%), and ilmenite (trace), and sphalerite (trace). Pyrrhotite is massive and hosts all other minerals as inclusions. Chalcopyrite primarily occurs as anhedral inclusions within pyrrhotite that are ≤ 2mm (Figure 4.16A). In one instance, chalcopyrite occurs as a 4 mm wide veinlet crosscutting pyrrhotite and seems to be associated with a 5mm wide quartz veinlet that is also crosscutting pyrrhotite. Very fine grained (< 0.05mm) inclusions of sphalerite and pyrrhotite occur in both the chalcopyrite veinlet and in the anhedral chalcopyrite inclusions hosted by pyrrhotite (Figure 4.16A,B). Pentlandite occurs as flames in pyrrhotite and in a blocky form (Figure 4.16B,C). The blocky pentlandite is ≤ 0.1mm and is generally, but not always concentrated around anhedral chalcopyrite, as well on the form of pentlandite chains. Unlike blocky pentlandite, Flame pentlandite has no strong association with chalcopyrite and is ≤ 0.02mm.

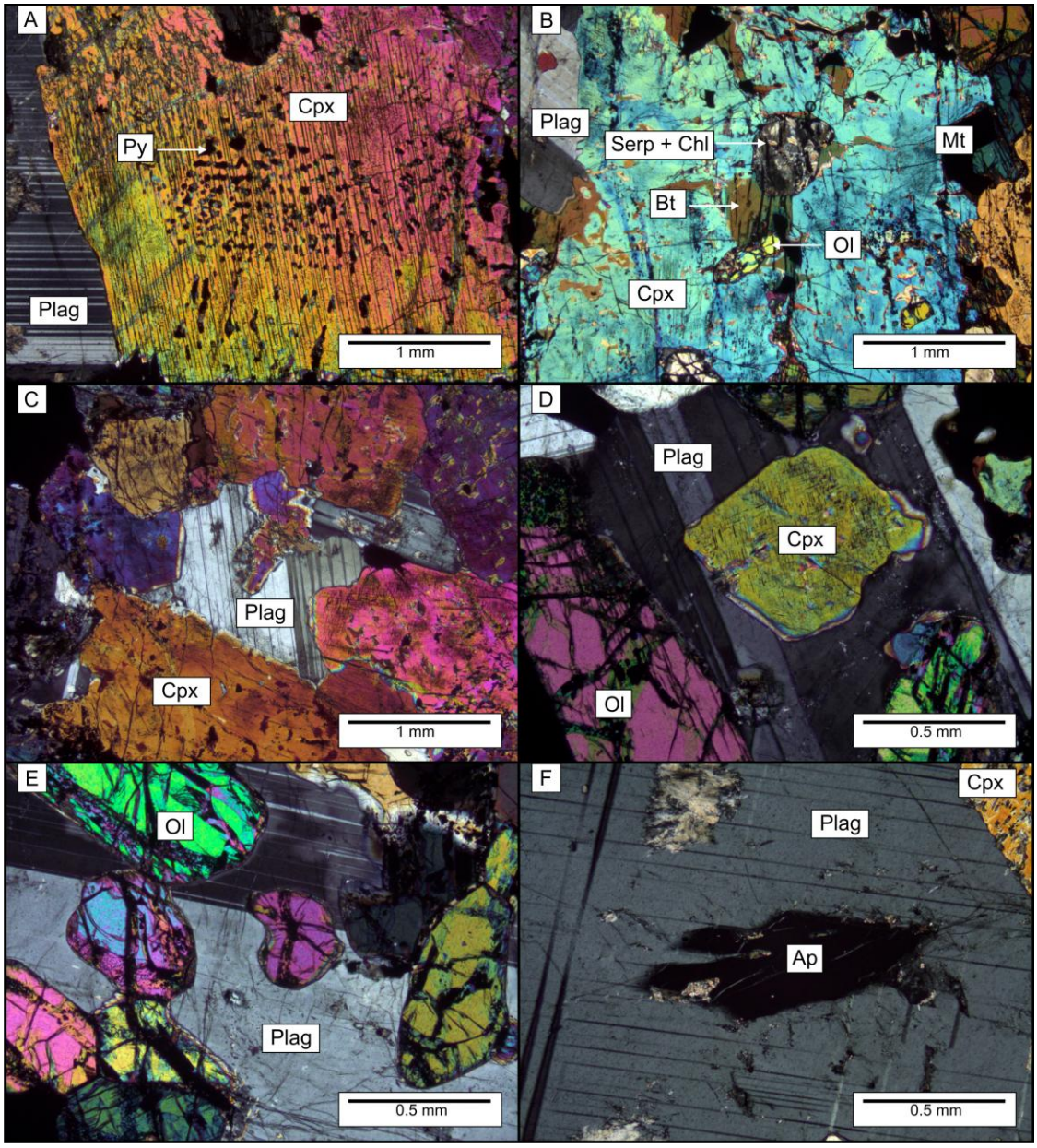
A
Cpx
Py
Plag
1 mm
B
Plag
Serp + Chl
Mt
Bt
Ol
Cpx
1 mm
C
Plag
Cpx
1 mm
D
Plag
Cpx
Ol
0.5 mm
E
Ol
Plag
0.5 mm
F
Cpx
Plag
Ap
0.5 mm

Figure 4.14 (previous page): Photomicrographs of primary textures and secondary alteration in the feldspathic clinopyroxenite. A) Fine grained inclusions of pyrite (Py) in Cpx. The Py inclusions resemble the outline of a grain and therefore Cpx may have overprinted a Py grain. CL-06-80.0. XPL. B) Large grain of Cpx that contains inclusions of non-altered Ol and Ol that has been altered to Chl and Serp. Biotite alteration is also present near the rims of Cpx and throughout the core. CL-06-16-35.7. XPL. C) Ophitic texture between Cpx and Plag. CL-06-16-35.7. XPL. D) Inclusion of Cpx within Plag. CL-06-16-35.7. XPL. E) Inclusions of Ol in Plag. CL-06-16-35.7. XPL. F) Inclusion of subhedral Ap within Plag. CL-06-16-80.0. XPL.

Geochemistry

Rocks of the CLI are of alkaline to sub-alkaline affinity and follow a tholeiitic trend (Figure 4.19). Chondrite-normalized plots of unaltered fine grained gabbros within the CLI display a negative slope, with a moderate enrichment in the light rare earth elements (LREE) over the heavy rare earth elements (HREE); (Figure 4.20A). Both the unaltered and altered fine grained both have similar LREE enriched profiles with a positive Eu anomaly (Figure 4.20A). Primitive mantle normalized plots of the unaltered fine grained gabbros show a slight enrichment in Sr and Ti, likely due to Plagioclase and ilmenite respectively (Figure 4.20B). Both altered and unaltered gabbros show depletions in Th, U, and HREE. Altered fine grained gabbros are highly enriched in Pb compared to unaltered gabbros, and show moderate enrichments in Cs and Rb, while being slightly depleted in some LREE (Figure 4.20B). Pegmatites plotted on a chondrite normalized plot also follow the same trend as unaltered fine grained gabbros, except for one sample (CL-07-05-499) (Figure 4.21A). Primitive mantle normalized plots of the pegmatites exhibit similar patterns to those of the grained gabbros (Figure 4.21B). Only a few minor enrichments, such as Pb, Rb, Ba, and Cs are noted.

Gabbroic rocks in the intrusion show similar SiO_2 contents (39-45 wt%) with each other regardless of their relative position in drill core. Typically, the gabbros with higher SiO_2 are a function of higher alteration present in the sample and Al_2O_3 also follows this trend. Magnetite and ilmenite are a direct control on the FeO and TiO_2 content of gabbros. As units with higher FeO and TiO_2 (15-18 and 2.6-4.2 wt%, respectively) contain 5-12% Fe-Ti oxides, while gabbros with lower amounts of Fe-Ti oxides (2-3%) have FeO and TiO_2 contents of ~11 and ~1.5 wt%, respectively. Ultramafic rocks (dunite, clinopyroxenite) have MgO concentrations of 13-18 wt% and highly variable FeO and TiO2 (22-51 and 2-8 wt% respectively) contents controlled by Mag and ilmenite. Vanadium concentrations are highly variable, ranging from 50 ppm up to 2.3 wt% averaging ~500 ppm. Geochemical results from the preliminary sample set collected in February 2013 are presented in Appendix C.

Nickel sulfide fire assay results of the samples collected in February 2013 returned marginal results for PGE and Au. Highest Pd and Pt concentrations, 6.72 and of 7.68 ppb respectively, occurred in a very coarse grained gabbronorite (CL-07-14-477.5).

The highest Au content was observed in a clinopyroxenite (CL-07-05-50) 21.3 ppb. Full PGE and Au results are listed in Table 1.

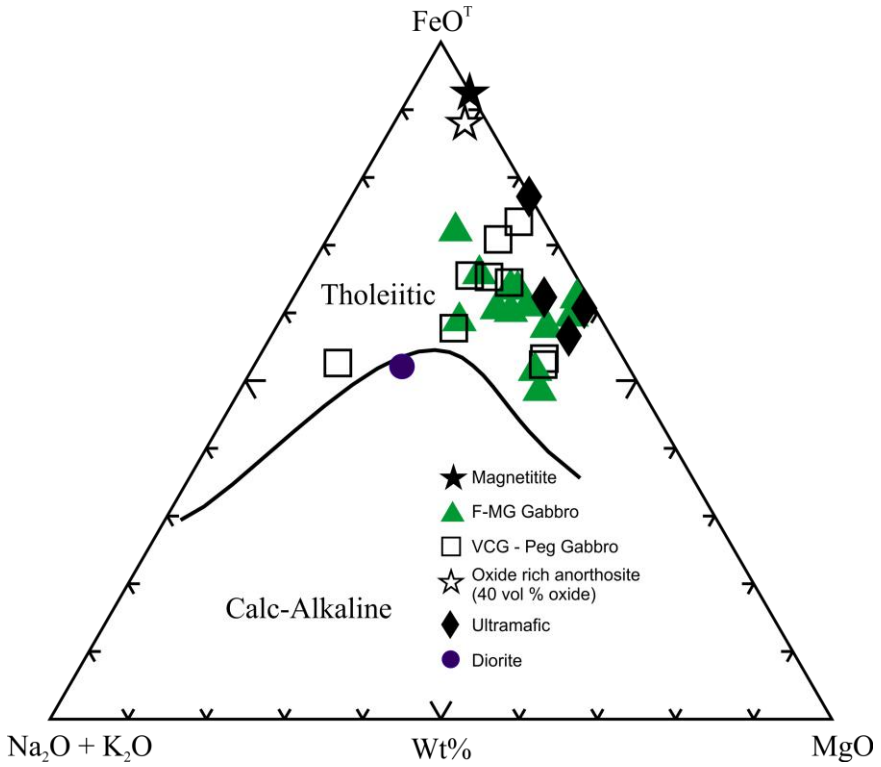

Figure 4.19: AFM diagram (after Irvine and Barager, 1971) of rocks from the Caribou Lake Intrusion show that they are of a tholeiitic composition and as the melt evolved, rocks move away from the FeO-MgO tie line. F-MG Gabbro = Fine-medium grained gabbro. VCG-pegmatitic gabbro = Very coarse grained – pegmatitic gabbro. FeO^T = total Fe.

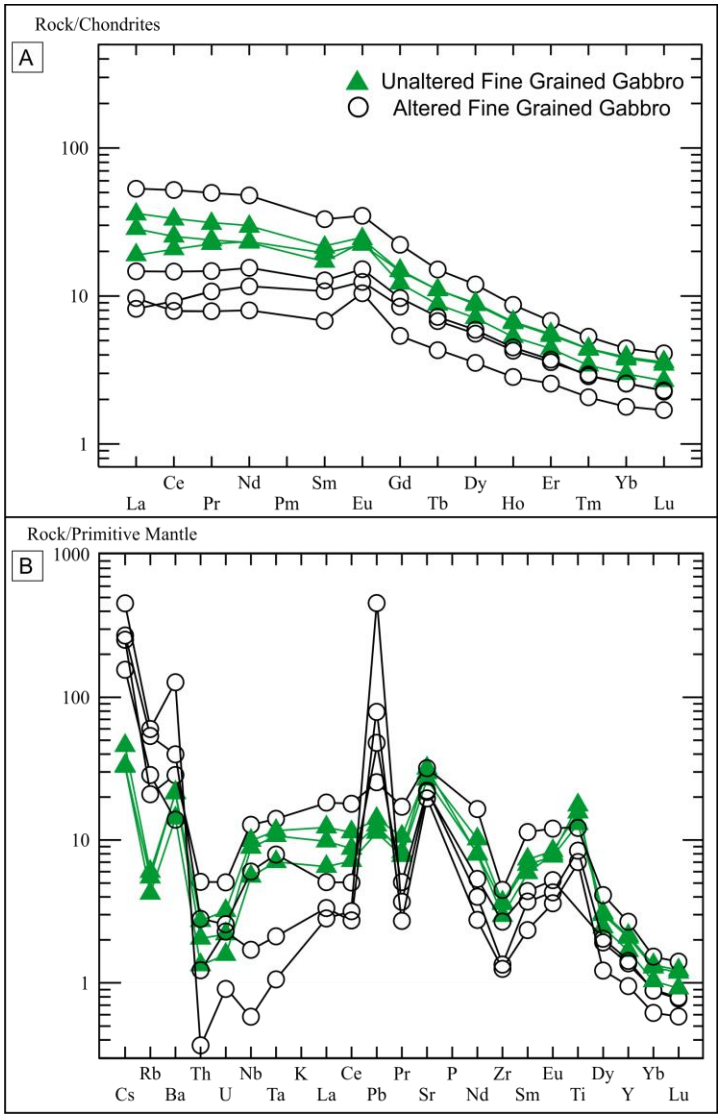

Figure 4.20: A) Chondrite normalized plot comparing unaltered and moderately to highly altered fine grained gabbros. Both show the same negative slope and a positive Eu anomaly. B) Normalized primitive mantle plot comparing same unaltered and altered fine grained gabbros as in A. Both show similar trends in trace elements, except for Pb, which is highly enriched in the altered samples. After Sun and McDonough, 1989.

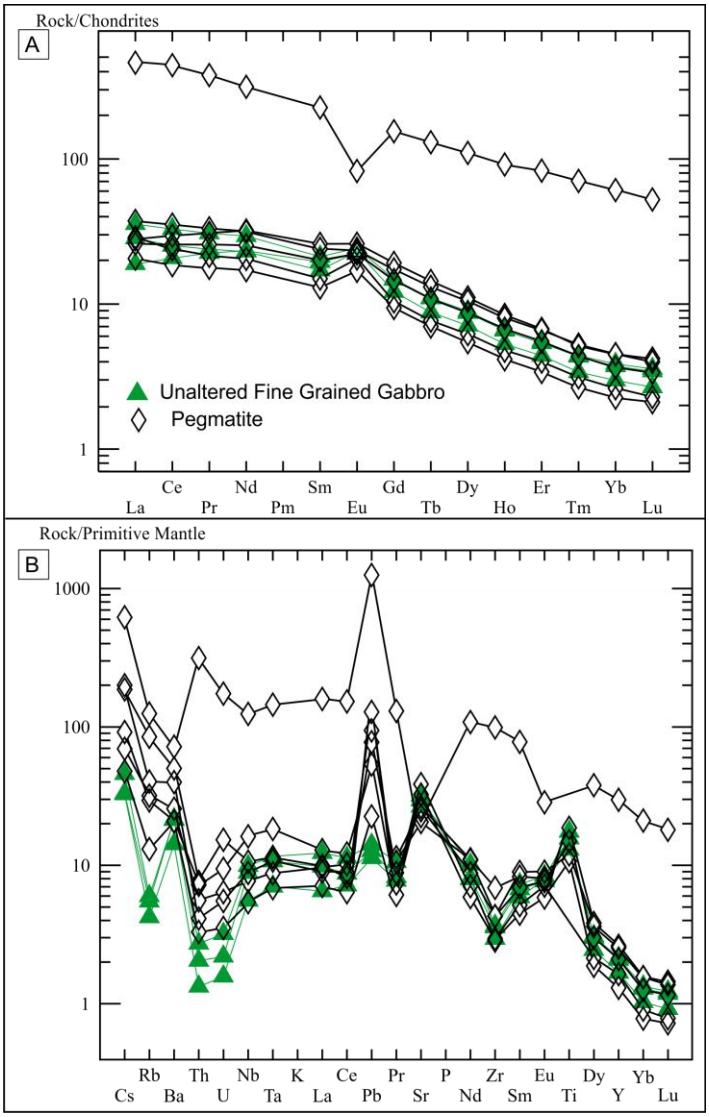

Figure 4.21: A) Chrondrite normalized plot of unaltered fine grained gabbros compared to pegmatitic gabbros. All but one sample follows the same trend as the fine grained gabbros. The outlier (CL-07-05-499) is highly enriched in all REE and exhibits a negative Eu anomaly rather than a positive anomaly. B) Normalized primitive mantle plot for same units as in A. Pegmatites have a slight enrichment in Pb compared to the unaltered gabbros. Again, the one sample is highly enriched in its trace elements compared to unaltered gabbros. After Sun and McDonough, 1989.

4.9 References

Birkett, T.C., Richardson, D.G. and Sinclair, W.D., 1994. Gravity modeling of the Blachford Lake Intrusive Suite, Northwest Territories. *In* Studies of rare-metal deposits in the Northwest Territories. *Edited by* W.D. Sinclair and D.G. Richardson. Geological Survey of Canada, p. 5-16.

Bowring, S. A., Van Schmus, W. R. & Hoffman, P. F., 1984. U-Pb zircon ages from Authapascow Aulacogen, East Arm of Great Slave Lake, NWT, Canada. Canadian Journal of Earth Sciences, v. 21, p. 1315-1324.

Crowe, D.E. and Vaughn, R.G., 1996. Characterization and use of isotopically homogeneous standards for in situ laser microprobe analysis of $^{34}S/^{32}S$ ratios. American Mineralogist, v. 81, p. 187-193.

Davidson, A., 1972. Granite Studies in the Slave Province. *Report of Activities*: Geological Survey of Canada, p. 109-115.

Davidson, A., 1978. The Blachford Lake Intrusive Suite: An Aphebian alkaline plutonic complex in the Slave Province, Northwest Territories. *Current Research*: Geological Survey of Canada, p. 119-127.

Davidson, A., 1981. Petrochemistry of the Blachford Lake Complex, District of Mackenzie. *Geological Survey of Canada Open File 764*, 24 p.

Davidson, A., 1982. Petrochemistry of the Blachford Lake complex near Yellowknife, Northwest Territories. In: Maurice, Y. T. (ed.) *Uranium in Granites*: Geological Survey of Canada, 71-79.

Curry, J.D., Lee, W.K., and Overveld, R., 1963. Earl-Jack Syndicate exploration report; submitted by Earl Jack Syndicate, Department if Indian and Northern Affairs, Activities Report 015065, 2 p.

Curry, J.D., 1969. Electromagnetic and magnetic geophysical surveys for parts of the NC claim group; submitted by Shield Resources Ltd, Department of Indian Affairs and Northern Development, Activities Report 018838, 6 p.

Gál, B., Molnár, F., Guzmics, T., Mogessie, A., Szabó, C., and Peterson, D., 2013. Segregation of magmatic fluids and their potential in the mobilization of platinum group elements in the South Kawishiwi Intrusion, Duluth Complex, Minnesota – Evidence from petrography, apatite geochemistry, and coexisting fluid and melt inclusions. Ore Geology Reviews, v. 54, p. 59-80.

Hanley, J.J., Mungall, J.E., Pettke, T., Spooner, E.T.C., and Bray, C.J., 2008. Fluid and Halide Melt Inclusions of Magmatic Origin in the Ultramafic and Lower Banded series, Stillwater Complex, Montana, USA. Journal of Petrology, v. 49, p. 1133-1160.

Hanley, J.J., and Gladney, E.R., 2011. The presence of carbonic-dominated volatiles during the crystallization of sulfide-bearing mafic pegmatites in the North Roby Zone, Lac des Iles Complex, Ontario. Economic Geology, v. 106, p.33-54.

Hoffman, P.F., 1980. Wopmay Orogen: a Wilson cycle of early Proterozoic age in 99 the Northwest of the Canadian Sheild. *In* The continental crust and its mineral deposits. *Edited by* D.W. Strangway. Geological Association of Canada, Special Paper 20, p. 523-549.

Irvine, T.N., and Baragar, W.R.A., 1971. A guide to the chemical classification of the common volcanic rocks: Canadian Journal of Earth Sciences, v. 8, p. 523-548.

Jensen M. L. and Nakai N., 1962. Sulfur isotope meteorite standards, results and recommendations. In *Biogeochemistry of Sulfur Isotopes*, NSF Symposium, p. 30-35.

Ludington, S., 1978, The biotite-apatite geothermometer revisted. American Mineralogist, v. 63, p. 551-553.

Marmont, C., 2006. Report on Diamond Drilling, Airborne and Ground Geophysical Surveys, Lithogeochemical Sampling and Prospecting; submitted by Kodiak Exploration, Northwest Territories Geoscience Office, Activities Report 085101, p. 123.

Marmont, C., 2007. Report on diamond drilling; submitted by Kodiak Exploration, Northwest Territories Geoscience Office, Activities Report 085317, p. 283.

Mumford, T., 2013. Petrology of the Blatchford Lake Intrusive Suite, Northwest Territories Canada. *Unpublished* Ph.D. thesis, Carleton University. 240 p.

Ohmoto, H., and Rye, R.O., 1979. Isotopes of sulfur and carbon, *in* Barnes, H.L., ed., Geochemistry of hydrothermal ore deposits, 2nd ed.: New York, Wiley, p. 509-567.

Pilkington, M., Thomas, M.D, and Mumford, T.R., 2012. Geological significance of a new high resolution gravity gradiometric and magnetic survey over the Blatchford Lake Complex, Northwest Territories; Geological Survey of Canada, Open File 7084, Poster.

Riciputi, L.R., Paterson, B.A. and Ripperdan, R.L., 1998. Measurement of light stable isotope ratios by SIMS: Matrix effects for oxygen, carbon, and sulfur isotopes in minerals. International Journal of Mass Spectrometry, v. 178, p. 81-112.

Ripley, R., 1990. Se/S ratios od the Virginia Formation and Cu-Ni sulfide mineralization in the Babbitt area, Duluth Complex, Minnesota. Economic Geology, v. 85, p. 1935-1940.

Ripley, E.M., and Li, C. (2003): Sulfur isotope exchange and metal enrichment in the formation of magmatic Cu-Ni-(PGE) deposits. Economic Geology, v. 98, p. 635-641.

Sinclair, W. D., Hunt, P. A. & Birkett, T. C., 1994. U-Pb zircon and monazite ages of the Grace Lake Granite, Blatchford Lake Intrusive Suite, Slave Province, Northwest Territories. *Radiogenic Age and Isotopic Studies: Report 8; Geological Survey of Canada, Current Research 1994-F*, 15-20.

Sun, S., and McDonough, W.F., 1989. Chemical and isotopic systematics of oceanic basalts: implications for mantle composition and processes. In Saunders, A.D., and Norry, M.J., (eds.) Magmatism in the Ocean Basins. Geological Society Special Publication No. 42, p. 313-345.

Toplis, M.J., and Corgne, A., 2002. An experimental study of element partitioning between magnetite, clinopyroxene, and iron-bearing silicate liquids with particular emphasis on vanadium. Contributions to Mineralogy and Petrology, v. 144, p. 22-37.

Wanless, R. K., Stevens, R. D., Lachance, G. R. & Delabio, R. N., 1979. District of Mackenzie. In: Geological Survey of Canada - Radiogenic age and isotopic studies, R. (ed.), p. 34-38.

Warman, T.A, and Gelo, K.K., 1995. Assessment report on the geological and geophysical programs conducted of the Bagpipe claims, Mackenzie Mining District, Northwest Territories; submitted by Caledonia Mining Corporation, Department of Indian and Northern Affairs, Activities Report 083658, 122 p.

Appendix 2: LA-ICP-MS run conditions

LA-ICP-MS instrument and data acquisition parameters for sulfide trace element analysis

Excimer 193-nm ArF laser RESOlution M-50	
Output Energy	100 mJ
Energy Density on sample	5 J/cm^2
Repition Rate	5 Hz
Pit Size	36, 48, or 66 μm
Ablation Cell Volume	~1.5 cm^3
Cell Gas Flow (He)	650 mL/min

Thermo X Series II quadrupole ICP-MS	
Auxiliary Gas Flow	0.8 l/min Ar
RF Power	1450 kW
Detector Mode	Dual 8 orders of magnitude linear dynamic range
Quadrupole Settline Time	Dynamically set for a minimum of 1ms

Data acquisition parameters	
Sweeps per Reading	1
Reading per Replicate	200 - 300
Replicates	1
Dwell Time per Isotope	10 ms
Points per Peak	1 per measurement
External Standard	NIST610 glass; PO724; Chalcopyrite PGE blank
Spot Size	36, 48, or 66 μm
Isotopes Analyzed for Sulfide Analyses	Si (29), S (33), Ca (43), V (51), Cr (53), Fe (57), Co (59), Ni (60), Cu (65), Zn (66), As (75), Se (82), Sr (88), Y (89), Zr (90), Ru (99), Ru (101), Rh (103), Pd (105), Pd (106), Ag (107), Pd (108), Cd (111), Sn (118), Sb (121), Te (125), Ta (181), Re (185), Os (189), Ir (193), Pt (195), Au (197), Tl (205), Pb (208), Bi (209)

LA-ICP-MS instrument and data acquisition parameters for sulfide melt inclusions

Excimer 193-nm ArF laser GeoLasPro	
Output Energy	150 mJ
Energy Density on sample	~7 -10 J/cm^2
Repition Rate	5 - 10 Hz
Pit Size	Between 16 and 90 μm
Ablation Cell Volume	~1.5 cm^3
Cell Gas Flow (He)	~1 L/min

Agilent 7500ce quadrupole ICP-MS	
Auxiliary Gas Flow	1.03 l/min Ar
RF Power	1500 V
Detector Mode	Dual 8 orders of magnitude linear dynamic range
Quadrupole Settline Time	2 ms

Data acquisition parameters	
Sweeps per Reading	1
Reading per Replicate	200 - 300
Replicates	1
Dwell Time per Isotope	10 ms, except for Pd (105), Pd (106), Pd (108), Pt (195), Au (197) had 50 ms dwell times
Points per Peak	1 per measurement
External Standard	NIST610 glass; PO724
Spot Size	Between 16 and 90 μm
Isotopes Analyzed	Na (23), Mg (25), Si (28), S (32), Ca (40), Ti (49), Fe (56), Co (59), Ni (62), Cu (63), Cu (65), Zn (66), As (75), Se (82), Pd (105), Pd (106), Ag (107), Pd (108), Cd (114), Sn (120), Sb (121), Te (125), Pt (195), Au (197), Pb (208), Bi (209)

LA-ICP-MS instrument and data acquisition parameters for silictae melt inclusions

Excimer 193-nm ArF laser GeoLasPro	
Output Energy	150 mJ
Energy Density on sample	~7 -10 J/cm^2
Repition Rate	5 - 10 Hz
Pit Size	Between 24 and 120 μm
Ablation Cell Volume	~1.5 cm^3
Cell Gas Flow (He)	~1 L/min

Agilent 7500ce quadrupole ICP-MS	
Auxiliary gas flow	1.03 L/min Ar
RF power	1500 V
Detector Mode	Dual 8 orders of magnetite linear dynamic range
Quadrupole Settline Time	2 ms

Data acquisition parameters	
Sweeps per reading	1
Reading per replicate	200 - 300
Replicates	1
Dwell time per isotope	10 ms
Points per peak	1 per measurement
External Standard	NIST610 glass
Spot Size	Between 24 and 120 μm
Isotopes Analyzed	B (11), Na (23), Mg (25), Al (27), Si (28), P (31), K (39), Ca (40), Ti (49), V (51), Cr (52), Mn (55), Fe (56), Co (59), Ni (62), Cu (63), Zn (66), As (75), Rb (85), Sr (88), Y (89), Zr (90), Nb (93), Mo (98), Ag (107), Sn (120), Sb (121), Cs (133), Ba (138), La (139), Ce (140), Pr (141), Nd (143), Sm (147), Eu (153), Gd (157), Tb (159), Dy (163), Ho (165), Er (166), Tm (169), Yb (172), Lu (175), Hf (178), Ta (181), W (182), Au (197), Pb (208), Bi (209), Th (232), U (238)

LA-ICP-MS instrument and data acquisition parameters for fluid inclusions

Excimer 193-nm ArF laser GeoLasPro	
Output Energy	150 mJ
Energy Density on sample	~7 -10 J/cm^2
Repition Rate	5 - 10 Hz
Pit Size	Between 16 and 60 μm
Ablation Cell Volume	~1.5 cm^3
Cell Gas Flow (He)	~1 L/min

Agilent 7500ce quadrupole ICP-MS	
Auxiliary gas flow	1.03 l/min Ar
RF power	1500 V
Detector Mode	Dual 8 orders of magnetite linear dynamic range
Quadrupole Settline Time	2 ms

Data acquisition parameters	
Sweeps per reading	1
Reading per replicate	200 - 300
Replicates	1
Dwell time per isotope	10 ms; except for Ni (62), As (75), Ta (181) at 30 ms
Points per peak	1 per measurement
External Standard	NIST610 glass
Spot Size	Between 16 and 60 μm
Isotopes Analyzed	Na (23), Mg (25), Al (27), Si (28), P (31), K (39), Ca (40), Ti (49), V (51), Mn (55), Fe (56), Co (59), Ni (62), Cu (63), Zn (66), As (75), Zr (90), Nb (93), Ag (107), Sn (120), Cs (133), Ba (138), La (139), Hf (178), Ta (181), W (182)

LA-ICP-MS instrument and data acquisition parameters for apatite

Excimer 193-nm ArF laser RESOlution M-50	
Output Energy	100 mJ
Energy Density on sample	5 J/cm^2
Repition Rate	5 Hz
Pit Size	66 μm
Ablation Cell Volume	~1.5 cm^3
Cell Gas Flow (He)	650 mL/min

Thermo X Series II quadrupole ICP-MS	
Auxiliary Gas Flow	0.8 L/min Ar
RF Power	1450 kW
Detector Mode	Dual 8 orders of magnitude linear dynamic range
Quadrupole Settline Time	Dynamically set for a minimum of 1ms

Data acquisition parameters	
Sweeps per Reading	1
Reading per Replicate	200 - 300
Replicates	1
Dwell Time per Isotope	10 ms
Points per Peak	1 per measurement
External Standard	NIST610 glass; Durango apatite
Spot Size	66 μm
Isotopes Analyzed for Sulfide Analyses	Na (23), Mg (24), Al (27), Si (29), P (31), K (39), Ca (43), V (51), Cr (53), Mn (55), Fe (57), Co (59), Ni (60), Cu (65), As (75), Rb (85), Sr (88), Y (89), Zr (90), Nb (93), Ag (107), Sb (121), Cs (133), La (139), Ce (140), Nd (146), Sm (147), Eu (153), Tb (159), Dy (163), Lu (175), Hf (178), Ta (181), Pb (208), Bi (209), Th (232), U (238)

Appendix 3: February 2013 sample list

Sample	Description
CL-07-01-8	Very coarse grained leucogabbro
CL-07-01-115.7	Very coarse grained gabbro, 1% Po
CL-07-01-167.8	Pegmatoidal gabbro, shows signs of fluid interactment
CL-07-01-322.4	Fine-medium grained gabbro, 1% Po, magnetite rich
CL-07-01-325.6	Fine grained gabbro
CL-07-01-354.2	Medium grained gabbro
CL-07-01-371.2	Medium grained gabbro, Tr Po, 10% Mag
CL-07-01-373	Coarse grained gabbro, shows signs of serpentinization, Tr Po
CL-07-01-380	Coarse grained gabbro, shows signs of serpentinization, Tr Po
CL-07-01-422.9	Fine grained gabbro, 1% Po, magnetite rich
CL-07-02-347	Medium grained gabbro, highly serpentinized?
CL-07-09-169	Fine-medium grained gabbro
CL-07-05-11	Medium grained gabbro, pyroxene rich
CL-07-05-14	Coarse grained gabbro, Tr Po blebs
CL-07-05-30.2	Coarse grained gabbro
CL-07-05-50	Very coarse grained gabbro, 10-15% 1-2cm blebs of Po, Cp concentrated around Po grains
CL-07-05-105	Very coarse grained leucogabbro
CL-07-05-117	Magnetite rich ultramafic rock, 1% Po
CL-07-05-142.5	Gabbro, 1% Po
CL-07-05-144	Magnetite rich ultramafic rock (pyroxenite?), 1% Po
CL-07-05-499	Very coarse grained gabbro, < 1% Po
CL-07-05-675	Magnetite rich ultramafic, Mag crystals look like a cumulate texture in areas
CL-07-07-101.1	Medium grained leucogabbro, Tr Po
CL-07-07-17	Medium-coarse grained leucogabbro, Tr Po
CL-07-07-450	Coarse grained gabbro
CL-07-07-483	Very coarse grained leucogabbro, Tr Po
CL-07-14-323.5	Very coarse grained gabbro
CL-07-14-477.5	Coarse grained gabbro, 5-10% Po, Cp concentrated on rims of Po
CL-07-15-145	Extemely coarse grained norite?

Appendix 4: Summer 2013 sample list

Sample	Description
CL-06-16-8.9	Gabbro. Grains ≤4mm. Trace pyrrhotite. 5-10% < 2mm interstitial magnetite.
CL-06-16-11.2	Gabbro. Grains ≤4mm. Trace pyrrhotite. 5-10% < 4mm interstitial magnetite.
CL-06-16-14.1	Syenite vein crosscutting gabbroic units
CL-06-16-33.7	Gabbro. Grains <2mm. Trace pyrrhotite. 5% interstitial magnetite
CL-06-16-35.7	Pyroxenite. Grains <12mm. 2% pyrrhotite. 10-15% <6mm interstitial magnetite
CL-06-16-47.0	Gabbro. Grains <3mm. 5% pyrrhotite. 5% < 3mm interstitial magnetite.
CL-06-16-47.6	Gabbro. Grains <3mm. 25% pyrrhotite. 5% < 3mm interstitial magnetite.
CL-06-16-51.2	Syenite vein crosscutting gabbroic units
CL-06-16-52.5	Gabbro with highly disseminated pyrrhotite (20-30%). Grains ≤5mm. 10% interstitial magnetite.
CL-06-16-55.0	Gabbro with highly disseminated pyrrhotite (20-30%). Grains ≤5mm. 10% interstitial magnetite.
CL-06-16-56.3	Gabbro with highly disseminated pyrrhotite (20-30%). Grains ≤5mm. 10% interstitial magnetite.
CL-06-16-57.5	Gabbro with highly disseminated pyrrhotite (20-30%). Grains ≤5mm. 10% interstitial magnetite.
CL-06-16-58.6	Gabbro with highly disseminated pyrrhotite (20-30%). Grains ≤5mm. 10% interstitial magnetite.
CL-06-16-59.9	Gabbro. Grains <2mm. 2% pyrrhotite. 5-10% interstitial <2mm magnetite.
CL-06-16-61.7	Gabbro with highly disseminated pyrrhotite (20-30%). Grains ≤5mm. 10% interstitial magnetite.
CL-06-16-63.15	Gabbro, Grains <3mm. Trace pyrrhotite. 5% <2mm interstitial magnetite
CL-06-16-63.8	Gabbro. Grains <15mm. Trace pyrrhotite. 5%, <5mm interstitial magnetite
CL-06-16-65.7	Quartz syenite vein crosscutting gabbro
CL-06-16-71.15	Gabbro. Grains <3mm. 5-10% pyrrhotite. 5%, <2mm interstitial magnetite
CL-06-16-78.75	Gabbro. Grains <15mm. Trace pyrrhotite. 5% <4mm interstitial magnetite
CL-06-16-80.0	Gabbro. Grains <15mm. Trace pyrrhotite. 5% <4mm interstitial magnetite
CL-06-16-83.5	Gabbro. Grains <2mm. Trace pyrrhotite. 5% interstitial magnetite
CL-06-16-84.6	Massive pyrrhotite
CL-06-16-90.0	Gabbro. Grains <3mm. Trace pyrrhotite. 5%, <2mm interstitial magnetite, locally rich in plagioclase
CL-06-16-103.0	Altered gabbro, bleaching and abundant epidote and chlorite stringers throughout
CL-06-16-152.45	Gabbro. Grains <1mm. Trace pyrrhotite. 5% interstitial magnetite
CL-06-16-155.6	Quartz syenite vein crosscutting gabbro
CL-06-16-170.6	Carbonate altered diabase
CL-06-39-4.1	Pegmatitic gabbro. Grains <60mm. 10% 5-20mm interstitial magnetite
CL-06-39-6.85	Pegmatitic gabbro. Plagioclase, 30%, 5-25mm. Pyroxene, 60%, 10-60mm. Magnetite, 10%, 7-12mm.
CL-06-39-10.98	Gabbro, coarse grained. Plagioclase , 30-40%, 3-7mm. Pyroxene, 40%, 4-7mm. Magnetite, interstitial, 20%, 3-6mm.
CL-06-39-17.2	Gabbro. Grains ≤3mm. Trace pyrrhotite. 5-10% < 4mm interstitial magnetite.
CL-06-39-20.35	Ultramafic. <5%, 1-3mm Plag. Highly serpentinized, formerly dunite?
CL-06-39-32.21	Feldspathic ultramafic. 10% plagioclase, <4mm. 20% interstitial magnetite, <8mm. Highly serpentinized, formerly dunite?
CL-06-39-32.82	Ultramafic. 5% plagioclase, <4mm. 20% interstitial magnetite, <8mm. Highly serpentinized, formerly dunite?
CL-06-39-33.28	Ultramafic. Trace plagioclase, <4mm. 15% interstitial magnetite, <8mm. Highly serpentinized, formerly dunite?
CL-06-39-47.36	Pegmatitic gabbro. Plagioclase, >15mm, 60%. Pyroxene, <25mm, 30%. Biotite, 5mm, 2-4%.
CL-06-39-57.38	Gabbro. Grains ≤3mm. Trace pyrrhotite. 5-10% < 4mm interstitial magnetite.
CL-06-39-60.23	Feldspathic ultramafic. 15-20% plagioclase, <5mm. 20% interstitial magnetite, <7mm. Highly serpentinized, formerly dunite?
CL-06-39-63.88	Feldspathic ultramafic. 15-20% plagioclase, <5mm. 20% interstitial magnetite, <7mm. Highly serpentinized, formerly dunite?
CL-06-39-83.9	Highly altered ultramafic. Olivine grains altered to a cream colour (?)
CL-06-39-94.95	Feldspathic ultramafic. 15-20% plagioclase, <5mm. 20% interstitial magnetite, <7mm. Highly serpentinized, formerly dunite?
CL-06-39-100.0	Pegmatitic anorthosite. Plagioclase, >30mm, 90%. Magnetite, 6-12mm, 5%. Biotite, 10mm, 2-3%.

CL-06-39-103.55	Gabbro. Grains <8mm. Magnetite, interstitial, 10%, <8mm.
CL-06-39-103.7	Feldspathic ultramafic. 15-20% plagioclase, 3-10mm. 10% interstitial magnetite, <5mm.
CL-06-39-103.91	Pegmatitic anorthosite. Plagioclase, >30mm, 90%. Magnetite, 6-12mm, 5%. Biotite, 10mm, 2-3%.
CL-06-39-105.83	Gabbro. Grains <5mm. Magnetite, interstitial, 15%, <3mm.
CL-06-39-108.0	Feldspathic ultramafic. 15-20% plagioclase, 3-10mm. 10% interstitial magnetite, <5mm.
CL-06-39-118.75	Gabbro. Grains 5-12mm. Magnetite, interstitial, 10%.
CL-06-39-122.3	Diorite. Pyroxene, 5-10%, interstitial, 2-5mm. Magnetite, interstitial, <3mm, 2%.
CL-06-39-125.0	Anorthosite. Grains 3-15mm.
CL-06-39-128.4	Gabbro. Grains <4mm. Magnetite, interstitial, 10%.
CL-06-39-132.47	Pegmatitic Gabbro. Plagioclase, 6-20mm, 40%. Pyroxene, 8-80mm, 40%. Magnetite, 4-15mm, 10%.
CL-06-39-133.4	Pegmatitic Gabbro. Plagioclase, 6-20mm, 40%. Pyroxene, 8-80mm, 40%. Magnetite, 4-15mm, 10%.
CL-06-39-150.08	Gabbro. Grains <8mm. Magnetite, interstitial, <4mm, 5-10%.
CL-06-39-154.16	Feldspathic ultramafic. Plagioclase 10-15%, 2-6mm. Magnetite, 20%, 2-5mm.
CL-06-39-156.97	Pegmatitic gabbro. Plagioclase and pyroxene, up to 5cm. Magnetite, interstitial, 5%, <5mm.
CL-07-01-9.1	Pegmatitic gabbro. Graphic texture between pyroxene and magnetite. Subophitic textures.
CL-07-01-29.1	Gabbro. Grains < 12mm. Plagioclase is altered to a cream colour rather than being white like in other units.
CL-07-01-50.2	Feldspathic ultramafic. Plagioclase, 10-15%, 1-4mm. Ophitic textures.
CL-07-01-52.3	Gabbro. Grains < 12mm. Magnetite, 2-10mm, 10-15%. Trace amounts of interstitial quartz.
CL-07-01-55.9	Gabbro. Grains < 12mm. Magnetite, 2-10mm, 10-15%. Trace amounts of interstitial quartz.
CL-07-01-67.5	Pegmatitic gabbro. Plagioclase and pyroxene, up to 5cm. Magnetite, interstitial, 20%, 2-20mm.
CL-07-01-76.9	Pegmatitic gabbro. Plagioclase and pyroxene, up to 5cm. Magnetite, interstitial, 20%, 2-20mm.
CL-07-01-79.3	Gabbro. Plagioclase and pyroxene 3-12mm. Magnetite, 2-10mm, 10-15%. 2% biotite, associated with magnetite. 2% pyrrhotite
CL-07-01-95.9	Pegmatitic gabbro. Plagioclase and pyroxene, up to 5cm. Magnetite, interstitial, 20%, 2-20mm.
CL-07-01-101	Plagioclase rich gabbro. Plagioclase, 50-60%, 3-12mm. Pyroxene, 30-35%, 2-8mm.
CL-07-01-113.8	Plagioclase rich gabbro. Plagioclase, 50-60%, 3-12mm. Pyroxene, 30-35%, 2-8mm. Trace amounts of pyrrhotite and biotite.
CL-07-01-117.2	Pyroxenite. Grains <10mm. Magnetite, 1-5mm, 20%, interstitial.
CL-07-01-124.3	Gabbro. Grains <4mm. Magnetite, interstitial, 20%.
CL-07-01-127	Pegmatitic gabbro. Plagioclase and pyroxene <70mm. Magnetite, 2-25mm, 10%. Trace apatite?
CL-07-01-128.1	Gabbro. Grains <10mm. Magnetite, interstitial, 10-20%.
CL-07-01-134.3	Pegmatitic gabbro. Plagioclase and pyroxene 10-50mm. Magnetite, 2-20mm, 20%. Trace biotite.
CL-07-01-140	Gabbro. Grains <4mm. Magnetite, interstitial, 25-30%.
CL-07-01-145.7	Pegmatitic gabbro. Plagioclase and pyroxene 10-50mm. Magnetite, 2-20mm, 20%. Trace biotite.
CL-07-01-156.3	Pegmatitic gabbro. Plagioclase and pyroxene 10-50mm. Magnetite, 2-20mm, 20%. Trace biotite.
CL-07-01-166.4	Gabbro. Grains <10mm. Magnetite, interstitial, 10-20%.
CL-07-01-171.5	Pegmatitic gabbro. Plagioclase and pyroxene 10-50mm. Magnetite, 2-20mm, 20%. Trace biotite.
CL-07-01-173.9	Pegmatitic gabbro. Plagioclase and pyroxene 10-50mm. Magnetite, 2-20mm, 20%. Trace biotite.
CL-07-01-180.1	Pegmatitic gabbro. Plagioclase and pyroxene 10-50mm. Magnetite, 2-20mm, 20%. Trace biotite.
CL-07-01-203.6	Gabbro. Grains <10mm. Magnetite, interstitial, 10-20%.
CL-07-01-222.1	Pegmatitic gabbro. Plagioclase and pyroxene 10-50mm. Magnetite, 2-20mm, 20%. Trace biotite.
CL-07-01-233	Silicified gabbro?
CL-07-01-249.9	Gabbro. Grains <8mm. Magnetite, 1-4mm, interstitial, 5-10%. Trace biotite.
CL-07-01-251.6	Granitic vein crosscutting gabbros. "sugary" appearance.
CL-07-01-271	Gabbro. Grains 3-15mm. Magnetite, 1-10mm, 15-20%.
CL-07-01-275.7	Pegmatitic gabbro. Plagioclase and pyroxene 10-50mm. Magnetite, 2-20mm, 20%. Trace biotite.
CL-07-01-277.4	Gabbro. Grains <8mm. Magnetite, 1-4mm, interstitial, 5-10%. Trace biotite. Trace quartz.
CL-07-01-287.1	Gabbro. Grains <8mm. Magnetite, 1-6mm, interstitial, 15%.

CL-07-01-308.8	Gabbro. Grains <8mm. Magnetite, 1-6mm, interstitial, 15%. Magnetite also occurs as bands across the sample.
CL-07-01-327.3	Gabbro. Grains <3mm. Magnetite, 10-15%.
CL-07-01-329	Magnetitite. 50-70% Magnetite, 1-6mm, forming a net texture.
CL-07-01-367	Magnetitite. 50-70% Magnetite, 1-6mm, forming a net texture.
CL-07-01-381.7	Pegmatitic gabbro. Plagioclase and pyroxene 8-35mm. Magnetite, 8-20mm, 10-15%. Trace biotite.
CL-07-01-411.6	Gabbro. Grains <20mm. Magnetite, 1-10mm, 15%. Trace apatite.
CL-07-01-429.8	Granitic package at bottom of hole. Quartz syenite.
CL-07-11-494.6	Morose granite. Weakly foliated. Locally megacrystic
CL-07-14-107.8	Whiteman Lake quartz syenite
CL-07-14-208.9	Whiteman Lake quartz syenite
CL-06-44-58.8	Leucoferrodiorite
CL-06-50-150	Hearne granite
GLG	Grace Lake granite
CL-06-35-56.36	Burwash sediments
CL-06-01-18.8	5-10% disseminated pyrrhotite. Hosted in 2-8mm gabbro.
CL-06-01-22.0	10-15% disseminated pyrrhotite. Pyrrhotite has been partial replaced by pyrite, 10-15%. 2% chalcopyrite. Hosted in 5-15mm gabbro.
CL-06-01-22.5	20-25% disseminated pyrrhotite. 2% chalcopyrite. Hosted in 5-15mm gabbro.
CL-06-05-75.1	10-15% disseminated pyrrhotite, <2mm. Hosted in <3mm gabbro.
CL-06-05-77.72	10-15% disseminated pyrrhotite, <2mm. Hosted in <3mm gabbro. 3mm band of chalcopyrite and pyrrhotite crosscutting gabbro.
CL-06-05-81.2	Massive Pyrrhotite. Magnetite, 10%,1-4mm. Chalcopyrite, 2%,<2mm.
CL-06-05-81.6	Massive Pyrrhotite. Magnetite, 10%,1-4mm. Chalcopyrite, 2%,<2mm. Two bands of Chalcopyrite present.
CL-07-09-57	Fine grained gabbro. Assay results from Kodiak indicate 118.4 ppb Pt + Pd
CL-07-09-60	Fine grained gabbro. Assay results from Kodiak indicate 214.1 ppb Pt + Pd

Appendix 5: CL-06-16 drill log

From	To	Lithology Description	Structure (Lwr Ctc Described)	Alterations
0.00	2.00	Qtz (5-12mm, 10%) Feld (7-15mm, 40%) Amp (3-15mm, 5-10%) Plag (5-10mm, 40%)	Sharp increase in mafic contents. From 5-10% above ctc to 30% below.	
2.00	2.60	Qtz (5-12mm, 5-10%) Feld (7-15mm, 35%) Amp (3-15mm, 10-30%) Plag (5-10mm, 35%). Amp % decreases to 10% 30cm after upr ctc and then increases to 25% 10cm above lwr ctc.	Decrease in grain size along ctc (Amp 3-5mm, feld/plag/qtz 1-4mm) chilled ctc. Also have a concentration of mafics along lwr ctc.	
2.60	4.06	Light grey gabbroic unit. Plag (intersital, 35-45%) Pyx (Seem interconnected, 40-45%) Mag (Intersital, 5%-10%). All grains <2mm. @3.75m increased % of Mag for 10 cm to 10-15%.	Sharp, 5% Po concentrated around ctc. No change in grain size observed along ctc.	
4.06	4.55	Possible intrmediate dyke? Or could just be an altered version of gabbro above. 2-3mm feld grains (40%) in groundmass along with 1-3cm feld grains (20%). Could just be plag w/ potassic alteration.	Mafic unit maybe slightly chilled, difficult to observed though. 2% Py around ctc.	
4.55	5.14	Same unit as from 2.6-4.06	Ctc core piece not present in core.	

5.14	5.50	same unit as 4.06-4.55.	Ctc core piece not present in core.	
5.50	7.90	Plag (interstial, 30-35%) Pyx (seem interconnected, 45-55%) Mag (interstial, 5-15%). All grains <3mm. Appearance of light green 1mm rectangular crystals @6.5m, alt product?	Ctc core piece not present in core.	Epd? Chl? ; White mineral; Serp
7.90	8.15	Granitic Pegmat section of grains upto2-3cm. Qtz (10-20%) Feld (45%) Amp (20%) Plag (10%)	Ctc core piece not present in core.	
8.15	9.45	Plag (interstial, 1-3mm, 30-40%) Pyx (seem interconnected, 1-4mm, 45-50%) Mag (interstitial, 5-10%, <2mm)	Sharp ctc, slight grain size change of granitic unit below from 4mm at ctc to 5-15mm after ctc, slight chilled ctc.	Serp; pot; Epd; Chl
9.45	9.75	Same unit as 7.9-8.15. Granitic Pegmat.	Band of black mineral (Amp) along ctc and 5% pot alt of mafic for 1-2cm after ctc. No chilling observed.	

9.75	9.86	Same unit as 8.15-9.45. 1-4mm gabbroic rock.	Sharp, no change in grain size in either unit. 10% pot alt of mafic above ctc for 1-2cm.	Pot
9.86	10.36	Granitic unit with similar mineral percentages from pegmatitic unit before (7.9-8.15). Grain sizes are smaller however and increase from the centre of the unit outward towards contacts. In centre grains are 1-4mm and increase outwards to 6-10mm.	Ctc core piece not present in core.	
10.36	11.67	Plag (interstial, 30-40%, 1-5mm) Pyx (seem interconected, 40-50%, 3-10mm, mainly 3-6mm grain though) Bt (trace) Mag (interstial, 5-10%, <4mm)	Gradational ctc over 10cm where grain size changes from 1-6mm down to <3mm.	Epd
11.67	13.80	Plag (Interstial, 35-45%, 1-3mm) Pyx (seem interconected, 1-3mm, 40-50%) Mag (interstial, <5%, <2mm) 5cm granitic pegmatite @12.14.	Sharp unchilled ctc	Epd
13.80	14.80	Granitic interval similar to 7.9-8.15. Amp content is apx 10% at top of unit and gradationally increases downhole to apx 20%. Grains are 0.5-2cm.	3cm concentration of Amp along ctc, after Amp is a 2mm band of <2mm plag/feld, then sharp ctc w/ mafic unit below.	

14.80	34.72	All grains are <2mm. Plag (interstial, 30-40%) Pyx (seem interconnected, 45-50%) Mag (interstial, 5-10%). @25.41-26.0 change in grain size to <4mm (same mineralogy) change is gradational over 5cm and change back into <2mm grains is also gradational over 5cm. 1cm syenitic vn @ 25.1 & 31.0.	Fracs are present above ctc in unit spaced 1cm apart and do not extend below ctc. Moving across ctc, grains size increases. Trace amts of Po are in the area of the ctc.	Epd/Chl?
34.72	36.07	Plag (interstial, 10-15%, 4-6mm) Pyx (interconnected, 70%, 4-12mm) Bt (possibly in fractures?) Mag (Interstial, 10-15%, <6mm)	Sharp ctc, no chilling or gradation in grain size/mineralogy observed.	
36.07	49.85	All grains <3mm. Plag (interstial, 40%) Pyx (seem interconnected, 50%) Mag (Interstial, 5%)	Near Ctc highlyfractured w/ serp along them. Core piece not present with actual ctc.	Chl; Epd; Serp
49.85	51.77	Syenitic unit. Feld (60%) Qtz (10-20%) Plag (10-20%) Amp (10-20%). All grains <4mm.	Ctc core piece not present in core.	Chl
51.77	59.08	Plag (interstial, 30%, <4mm) Pyx (seem interconnected, 40%, 3-5mm) Mag (interstial, <5mm, 10-15%). Gradational change to fine grained interval (<3mm grains) from 54.9-55.1. 1cm syenitic Vn @58.3m with a concentration of Amp along upr and lwr ctc w/host rock. Bottom 20cm of unit, Mag coarsens to grain sizes 4-7mm.	Gradational decrease in grain size from above to below ctc. Also have a drastic decrease in Po% from 30% down to 2-3%.	Serp; Epd; Amp/Chl

59.08	61.20	All grains <2mm. Plag (interstial, 30-40%) Pyx (seem interconnected, 50%) Mag (interstital, 5-10%)	Ctc marked by drastic increase in sulphides from 5% to 20% below.	Chl;Epd
61.20	62.15	Plag (interstial, 2-3mm, 30%) Pyx (seem interconnected, 40%, 2-4mm) Mag (Interstial, <4mm, 5-10%) Short interval of coasrening from 61.75-62.15 where grains become apx 6mm.	Ctc marked by a 1cm band of Po after which sulphides % drop to trace amounts after ctc. Grain size also decreases after ctc to <3mm.	Epd
62.15	64.55	Plag (interstial, <3mm, 30-40%) Pyx (seem interconnected, 45-50%, <3mm) Mag (interstial, 5%, <2mm) Coarse interval from 63.8-64.01 where grains are <14mm. At top and btm of coasre section there is an appearance of 4mm Po. @62.75 10cm granitic vn.	Ctc sharp, no evidence of chilling	Chl/Epd; Serp
64.55	66.39	Syenitic to granitic unit. 2-4mm grains of Feld (60%), Plag(10-15%), Qtz (10-15%), Amp (10%).	Ctc seems to be brecciated with a concentration of chl strings along and near ctc.	Qtz
66.39	68.80	Uniform unit. Plag (interstial, <2mm, 30-40%) Pyx (seem interconnected, <3mm, 45-55%) Mag (Interstital, 5-10%, <2mm).	Ctc marked by appearance of disseminated sulphides (10%)	Chl/Epd; Serp

68.80	72.00	Same mafic unit as above but contains 5-10% Po and Tr Ccp.	Ctc marked by 10cm syenitic vn and after vn have decrease in Po to Trace amounts	Chl/Epd
72.00	78.75	Same unit as 66.39-68.8m	Ctc, gradual increase in grain size over 5-10cm and separated by 4-5cm band of Po.	Chl/Epd
78.75	80.80	Plag (interstial, 4-15mm, 45%) Pyx (seem interconnected, 4-12mm, 45-50%) Mag (interstial, 5-10%, 4mm)	Ctc not in core but above ctc have qtz vnlets and fracs near base of unit for 5cm and then have abrupt change in fine grained rock below.	Chl/Epd
80.80	84.40	Plag (interstial, 30-40%, <2mm) Pyx (seem interconnected, 40-50%, <2mm) Mag(interstial, 5-10%, <2mm) Sloight coasening @ 83.8 for 5cm where grains become 4-5mm and sulphides increase to 10% and <6mm.	Ctc marked by appearance of massive sulphides	Chl; Epd
84.40	84.84	Massive sulphide. 15cm of massive Po and then transitions into a net texture (30% Po) within a mafic host rock (4-5mm grains and similar mineralogy to unit above)	Ctc marked by dissapeance of sulphides and decrease in grain size over 5cm.	

84.84	85.50	Same unit as 80.8-84.4m.	Core piece not there, but change seems to be abrupt change in grains size.	Chl/Epd
85.50	86.55	Plag (interstial, 30-40%, 2-5mm) Pyx (seem interconnected, 4-10mm, 45-55%) Mag (interstial, 5%, <3mm)	Ctc, dissapearance of dissem sulphides and decrease in grain size. Have bands of Po occurring close to lwr ctc.	Chl/Epd
86.55	87.50	All grains <2mm. Plag (interstial, 30-40%) Pyx (seem interconnected, 50%) Mag (interstital, 5-10%)	Ctc marked by appearance of carb/qtz vns	White minerl
87.50	88.13	Carb/qtz veins/Alteration zone. Entire interval looks bleached and chloritized. Unit would of likely been mafic rock present above as some primary textures are faintly visable.	Ctc, out of veining and into a <2mm mafic rock.	Serp, Chl, Pot
88.13	92.15	Plag (interstial, 35-45%, <3mm) Pyx (seem interconnected, 50-55%, <3mm). Highyl altered to serp/chl until 89.4 where slip surfaces are 10cm apart. Rock becomes more competent until end of unit with slip surfaces 30cm apart.	Ctc marked by appearance of carb/qtz vns. Have a Py/Chl; stringer along ctc.	Pot; Serp/chl

92.15	106.65	Carb/qtz veining/stringers which are spaced every 5-10cm. Alteration Zone, original host rock appears to be similar to 88.13-92.15. 92.4-93.8 and 98.0-101.9m. have a white cubic mineral (Mag alt?)occurs about 10%. @101.5 have a colour change of the unit from a slght green colour to a light grey for apx 15cm. also occurs at 102.9.	Ctc marked by an overall chnage oc colur (alteration?) to unit. Changes from a greyish/green colour to a tan colour below.	Epd, Chl, Serp, bleaching, Fe staining, Pot
106.65	108.90	Tan coloured alteration of same mafic unit above in alteration zone. Plag becomes more of a creamy colour (sericite alt?) Alteration overprints much of unit so difficult to tell mineral %. Carb/qtz strings/veinlets spaced apx 10cm apart, usually <1cm thick.	Sharp ctc w/ syentitic unit below.	Hematite, bleaching, Chl/Epd. Fe staining
108.90	139.05	Syenitic unit, possibly bleached until 118.9m. All grains are <5mm. Feld (60-70%, possible zoning of feld grains) Qtz (10-20%) green mineral (Epd?) (10%) Brown minerla (5%). Carb vnelts 3-15mm thick spaced 15cm apart. @135-136.6 have carb vnlets 4-20mm thick and highly concentrated in this interval. Possible niccolite (according to old log) in vn at 135.15. @118.7 have appearance of black intersital minerla, alt product of bt to chl?	Very sharp ctc, no chilling. Have a clay seam along ctc.	Bleaching, Chl, Epd
139.05	151.50	Diabase? 139.05-143.36, tan colour to interval. Have a gradational colour change over 10-15cm where colour changes to a dark grey. 150.6-151.5 transition back into tan colour. Magnetic.	Ctc marked by increase in grain size.	
151.50	153.30	Grain are <1mm, difficult to tell % of plag and pyx due to tan alt colour. Magnetic. Tan colour occurs for 25cm after upr ctc then turns into a grey coloured unit.	Sharp ctc w/ syentitic unit below, marked by a carb-qtz vnlet.	Epd, Hematite, bleaching?

153.30	157.90	Similar mineralogy to 108.9-139.05. Less Epd in this unit however (5%). 2cm carb vnlet @154 & 1cm vnlet @155.	Sharp ctc, no chilling observed	Chl, Epd, Sericite
157.90	161.30	Diabase, tan colour from upr ctc down to 158.6, and then changes to a grey colour. Possible visicles wfilled with feld? Qtz? 10% and 1-3mm.	Sharp ctc, no chilling observed	Epd
161.30	167.30	Possibly the same unit as above but grain sizes are somehwhat Distinguishable, <1mm. White mineral present (replacemnt mineral of Mag??) its cubic. 5% of those vesicle filled feld/qtz? 10cm carb vn @163.7. and 1-3mm carb stringers every 5-10cm. Unit coarsens @166.9 to 2-4mm grains, alterations still present.	Ctc core piece not present in core.	Bleaching? Fe staining, Hematite
167.30	170.70	Same as 158.5-161.3. grey colour. Carb vns present throughout unit. Ribbon texture of carb vns present @168.5.		Fe staining

Alt Description	Sulphides	Sulph Description	Samples
			2.15m
	Po	Interstial, 1-2%, <1mm	2.85m
	Py; Ccp	Trace for both, mainly concentrated around upr and lwr ctc.	

Epd/Chl strings spaced 20cm apart. @6.6m patchy light green alteration, epd? White mineral (clay?) occurs along fracs. @6.91 slip surface with serp and white mineral along it.	Po; Ccp; Py	Po: 2%, interstial, <2mm grains. Ccp+Py: occur along fracs w/white mineral, <1mm grains.	6.4m
Slip surface @9.1m, with serp along it. 1cm into mafic after ctc have potassic alt of plag affecting 30% of grains. Epd: stringers spaced every 15-20cm. Chl: stringers spaced every 30cm.	Po	Interstial, Tr-1%, <1mm	8.9m

5-10% pot alt 1-2cm after upr ctc and before lwr ctc.			
			10.15m
Stringers along fractures (maybe chl?) 15-20 cm spacing	Po	Interstial, closely assoc w/ Mag as 50% of Mag grains have a partial rim of Po. Po <2mm, 5%	11.2m
Stringers spaced apx 30cm apart		None	13.3m
			14.1m

Strings, spaced 25cm apart, consistent throughout unit.	Po	Trace, present around lwr ctc.	16.4m, 19.6m, 23.8m, 27.2m, 30.35m, 33.7m
	Po	2%, interstial, increased downhole towards ctc to 5-10%.	35.7m
Chl: light-medium green colur change of unit increases downhole towards lwr ctc w/ syenitic unit. Epd strings spaced 30cm apart and contain Chl in apx 50% of strings. @44.85, chl along frac surface w/ band of Po along it as well. Slip surfaces @ 42.2, 44.8, 46.1 all with serp along them.	Po	Trace in upr part of unit and increase to 5-10% in lwr part of unit after patchy and net textured intervals. @44.4, 20% net text Po. @ 47.5 30% net textured Po assoc w/ sort interval of 1cm plag/pyx grains. @47.0,48.77 patchy Po (15%) assoc w/ <2mm plag/pyx.	38.9m, 42.9m, 47.0m, 47.6m,
Strings, spaced apx 40cm apart.	Py	Trace amts along chl stringser, grains <1mm. Near upr ctc, for 10cm apx5% Py in stringers as well as 1cm clusters of VFG Py.	51.2m
Slip surfaces @55.4,56.0 with serp along them. Epd stringers 30-40cm apart. Have green alteration of 25-30% pyx grains around edges (Amp or chl)	Po; Ccp	30% Po, <10mm and Ccp 2%, <4mm. Both forming a net texture. Ccp has been observed to be tarnished to green or blue, commonly occurs on edges of Po. Sulphides can be parially to completely enclosing Mag grains. @57.35 large patch of Po 3-5cm across.	52.5m, 55.0m, 56.3m, 57.5m, 58.6m

Rare Epd stringers which only occur in upper 40cm of unit. Chl occurs with Epd stringers.	Po	2-3% interstial, increased to 5% downhole within 10cm of lwr ctc	59.9m
Strings, spaced 20-30cm apart	Po; Ccp	Net texture of Po and Ccp. Po (20-25%), <5mm. Tr-4% Ccp, <4mm, closley assoc w/ Po. Localized areas of 3cm patchy Po .	61.7m
Chl/Epd stringers spaced 20cm apart. Serp along slip surface @ 63.1.	Po	Tr, interstial, <2mm. @ 63.7 1-2cm band of Po (80% Po).	63.15m, 63.8m
Qtz stringers soaced apx 50cm apart	Py	Trace, occurs along fracs w/qtz? Strings. 1m spacing between Py bearing stringers	65.7m
Strings spaced apx 30cm apart. Slip surface @67.3 w/Serp along it.	Po	Trace, intertstial, <2mm	68.2m

Strings spaced apx 30cm apart	Po; Ccp	5-10% Po, disemminated, <1mm w/ Trace Ccp assoc w/Po	71.15m
Stringers are spaced 5-10cm apart	Po	Trace, intertstial, <2mm	75.25m
Stringers apx 30cm apart	Po	2%, intersital, < 4mm	78.75m, 80.0m
Chl/Epd strings apced 20cm apart. Chl only stringers which occur close to Chl/Epd stringers.	Po	0-4%, interstial, <2mm	83.5m
	Po	Massive and disseminated. Disseminated grains are interstial and <10mm.	84.6m

Stringers spaced 20cm apart			
Stringers spaced 20cm apart	Po	Interstial, <4mm, 2%. @ 85.75, Po increases to 10-20%. Pyx % decreases w/increased Po	85.8m
Strings of a white mineral along fractures every 10cm.	Po	Interstial, <1mm, 2%.	87.2m
After 87.9-88.0 Pot alt occurs affect Plag. Slip surfaces occur every 10cm and serp and chl are present along them.	Gn, Po, Sp	Gn: Trace, hosted in carb vn, 4mm. Sp: Trace, hosted in carb vn or along vn ctc, 1-4mm. Po: Trace, hosted in host rock and along edges of vns.	87.7m
Pot alt occurs in trace amount 50cm above lwr ctc. Serp/chl occurs along all slip faces present in unit.	Po	Trace, interstial, <1mm	90.0m

Epd & Chl stringers spaced 15cm apart. Fe staining affects Py that occurs in stringers @98.2m. Bleaching? Occurs in lwr part of unit and marks change of to unit below. Pot, trace amounts concentreated around veins. Slip surfaces throughout have serp and chl along them. **@97.5, overall change from a chl alteration ro epd alteration of host rock.**	Py; Po	Py occurs along chl/epd stringers, tr-2%, <1mm, also occur w/ qtz stringers. Slip faces also contain Py along them. Po: interstial, trace, <1mm. 92.4-93.3 2-5%. Also have Trace Po along stringers. @93.9 Po seems to form a net texture over 5cm.	93.3m, 99.0m, 102.9m
Hemaite (<5%) occurs as <2mm blebs. Bleaching? Intene and consistent throughout unit. Fe staining, throughout unit affecting stringers and host rock. Chl/Epd strings about 15cm spacing.	Py	Trace amounts present in carb/qtz stringers.	107.65m
Possible bleaching, strong until 118.9 and then decreases in intensity downhole, responsible for slight tan colour?? Chl stringers throughout 20cm spacing. Epd unifrom thoughout unit, 10%.	Py	Trace, interstial, <1mm	109.35m, 120.15m, 135.0m
			142.2m, 146.9m
Epd concentrated in first 10cm after tan colour disappears and then again 40cm before lwr ctc. Hematite is concentrated with Epd alteration. Does the tan colour reflect a bleaching alt??	Po	Tr, interstial, <1mm	152.45m

Chl/Epd Stringers, 1-2mms thick, 10-15cm spacing. Epd patchy 5%. Sericite alt in unit by appearance of creammy coloured feld grains and not affecting qtz.	Py	Trace around upr ctc and assoc w/qtz.	155.6m
Possible Epd alt occuring @162.2 until lwr ctc.			158.0m, 160.0m
Tan colour reflect bleaching? Fe staining, present throughout unit. Hematite, strings, 5-10mm thick @166.2m.			165.0m
Generally present around carb vns affecting 10-15% of vein and also affects apx 30% of qtx/feld vesicle fills.			170.6m

Appendix 6: CL-06-39 drill log

From	To	Lithology Description	Structure (lwr ctc described)	Alt's
0.00	1.50	3-4mm gabbroic rock with interstitial plag (apx 40-45%) and pyx (seem interconnected,apx 40-50%). Mag interstial (5-10%).	Core piece not there, change in grain size from ≤5mm to ≤7mm marks change	Epd/Chl
1.50	3.05	≤7mm gabbroic rock, interstital plag (40-45%), pyx (seem interconnected, 30-40%), interstital mag (5-10%, <5mm). Localized grains may be upto 2cm. @1.75m for 10cm plag and pyx upto 3cm	Ctc gradational over 10cm with grain size increasing from ≤7mm to ≤12mm. Plag % also decreases from ~40% to 30%	
3.05	3.96	5-12mm gabbroic rock with intersitial plag (5-10mm, apx 25-30%), interstital mag (3-12mm, apx 10%), pyx (seem interconnected, 5-8mm, apx 50%). Trace Bt 4-7mm (@3.2m).	Core piece not there, change in grain size from 5-12mm to 5-30mm marks change. Band of Plag occurs on finer grain side before change occurs.	
3.96	4.90	4-30mm pyx rich gabbroic rock. Plag interstitial (4-15mm, apx 30%), pyx (seem interconnected, 7-30mm, 50-60%), interstital mag (5-20mm, apx 10%). Top of unit is more pyx rich (apx 70%) and decreases downhole (apx 50%). Plag increases downhole from 15 to 30%. 5cm before contact, trace Bt present in association with Po?	Core piece not there, change in grain size from ≤30mm to ≤6mm marks change. Grain size increases to ≤15mm 10cm after ctc.	Chl/Amp?
4.90	5.60	appears to be a cyclic unit. For 10cm after top contact grain sizes are <6mm, then changes to <15mm, and 10cm before bottom contact grain sizes are <30mm. Percentages of minerals roughly the same throughout, plag apx 40%, pyx apx 40%, mag apx 10%. Grain sizes of each mineral within the cycles are plag (<6mm, 4-10mm, 7-20mm) pyx (<6mm, 5-15mm, 10-30mm) mag (<5mm, <7mm, <10mm)	Ctc abrupt change over 1cm from ≤30mm to ≤5mm. 5cm into lwr unit plag ~80&pyx~20%and then change to ~40%plag & Pyx	Chl/Amp?
5.60	8.25	4-10mm gabbroic rock with interstital plag (4-10mm, apx 40%) , pxy (seem interconnected, 5-10mm, 40-50%), interstitial mag (<5mm, apx 10%). **@6.3m** an increases in pyx % and decrease in plag % occurs (plag apx 30%, pyx apx. 50-60%, mag 10%). Grain sizes similar to above section. **@6.8m** appearance of 6cm pyx (range in grin size of px from 10-60mm, apx 60%) plag (30%, 5-25mm), Mag (7-12mm, 10%). Mag look like inclusions within pyc grains. **@7.1m** transition into finr grained unit from depth 5.6-6.3m. Gradational increase in pyx and decrease in plag downhole towatds 7.65m. **@7.65** 3cm of <3mm grains with similar as unit above. **@7.68** back into unit from 7.1-7.65m. **@7.81** Increase in grain size, same interval a 6.8-7.1m.	Ctc sharp,possibly chilled onlwr unit for 5cm (≤3mm). Chnge in unit marked by decrease in grain size from 8-30mm down to ≤7mm after chilled zone.	Chl/Amp?
8.25	9.25	Unit stsrts in grain sizes <3mm ad gradationally over 15cm grain sizes increase to <7mm. Plag (interstital, 3-7mm, 30-40%), Pyx (seem interconnected, 4-7mm, apz 40%) Mag (Interstitial, 3-6mm, apx 20%)	Ctc,Subtle change in grain size over 5cm from ≤7mm to ≤10mm	Chl/Amp?
9.25	14.93	3-10mm gabbroic rock. Plag (interstiial, 3-10mm, 35-40%) Pyx (seem interconnected, 4-10mm, 40-45%), Mag (Interstial, 4-10mm, apx 15%) Bt (closely assoc w/ mag, 2-3%)	Ctc, sharp decrease in grain size from ≤10mm down to ≤4mm. Ctc likely chilled as for 4cm after ctc grain size ≤2mm.	Chl/Amp? Epd Potassic
14.93	20.30	≤3mm gabbroic unit, that is very homogenious. Plag (interstial, 30-40%) Pyx 9seem interconnected, apx 40-50%) Mag (Interstial, 10%)	Ctc not in core, appears sharp. Change in unit from mafic to ultramafic	Chl/Epd?
20.30	20.94	Ultramafic interval. <5%, 1-3mm plag. Very dark green unit (serpentinized?) and highly magnetitc but unable to give %. Trace interstial Bt. Possible areas of cumulous olivine? (eihedral, circular and dark green) Pyx, unable to describe (too altered???)	Ctc not in core, appears sharp. Change in unit from ultramafic to mafic	
20.94	27.66	2-8mm gabbroic unit. Plag (2-6mm, interstiial, 35-40%) Pyx (seem interconnected, 3-8mm, 40-45%) Mag (interstiial, <4mm, 10%) Trace Bt. Have a concentration of mag around carb veins @21.6m (apx 20% mag)	Ctc, upr unit chilled for ~2cm(≤1mm grain size) before change of unit from mafic to ultramafic	Epd/Chl Chl/Amp?

27.66	82.10	Thick ultramafic package. Dark green pyx of oliv? (80%, 4-15mm, euhedral, likely cumulous) Mag (4-10mm, 10-20%) Plag (interstiial, <5mm, <10%) Ilmenite? (has a paler colour than mag, occurs with mag, 5%). Highly cyclic unit. **@28.73**, plag decreaes to Trace amounts, pyx apx 85%, mag 15%. **@ 28.9** Plag <10%. **@30.83** Plag trace amounts **@31.0** plag <10%. **@31.7** Plag trace. **@32.21** plag appears as a 1cm thick band and then occurs in 10% of interval. **@32.62** Plag trace-2% <3mm. **@33.65** Plag increases to 15-20% and gradually decreases to 10%until 35.0m **@35.0** Plag trace. **@35.27** Plag 15-20%. **@36.11** plag 2-3%. **@37.0** 5mm band of plag and increase of plag to 10%. **@37.85** plag <3%. **@38.15** plag 10-15%. **@38.47** Plag trace. **@38.6** plag 10-15%, <5mm. Mag 20% <5mm, Pyx or oliv? 60%, <10mm. Very homogenous until 47.41. **@47.41** pegmatoidal section of 2.5cm pyx apx 30%, >1.5cm plag apx 60%, Bt, 5mm, 2-4%. **@47.51** Back into homogenous unit from 38.6-47.41m. **@57.38** Out of ultramafic package and into 40cm of gabbroic rock. Plag (1-3cm apx 50%) Pyx (2cm, 30%) Mag(intertital, 0.5-2cm) Bt concentrated around edges of Mag. **@57.7** Back into homogenous ultramfic unit from 47.51-57.38. 67.1m have a slight decreae in dark green/black cumulous mineral from 10cm. localized (66.8, 67.2) areas of plag apx 30% and grains 1cm. 71.94-72.44, 73.44-76.28, and 77.04-78.12 plag increase to 23-30% and 4-8mm. **@81.05** Dark green/black cumulous minerals dissappear for 40cm and unit seems to become massive, mag is interstial (15%, 5-15mm), otherwise difficult to distinguish minerals. **@81.6** cumulous gains appear. some look alterd as they have a creamy light green colur to them (40-50% of grains altered) otherwise unit similar to homogenous unit aboe.	Ctc, have 1cm carb? Vnlet. Signs of alteration around 81.6 as Pyx or Oliv cumulate grains change from dark green to creamy color	Whole unit seems to be serpentinized. 35-36m may be one large slip surface w/ chl/serp along it. Other slip surfaces occur at 38.5m, 39.0m, 47.2m, 64.2m, 72.44m, 78.6m,
82.10	84.76	Alteration package. Top of unit defined by carb vnlet with brown mineral along its edges (siderite?) Original mineralogy seems to be similar to ultramfic section above. Primarily composed of darkgreen/balck oliv or pyx. These grains now have a light creamy green colour to them (3-10mm, 60-70% of unit) Interstitial mag(<10mm, 10-15%)	Ctc, 2cm carb? Vnlet. Alteration stops and move into non-altered Pyx or Oliv cumulate grains	Serp
84.76	85.70	Back into ultramafic-mafic unit from 57.5-81.05	Ctc obsurced by flt zone below	
85.70	85.80	Fault Zone. Highyl fractured and broken. Pieces seems similar to unit above.	Ctc obsurced by flt zone above	Serp
85.80	97.45	Back into ultramafic-mafic unit from 57.5-81.05. Small Carb Vn@ 86.9m 1cm thick with serp along edges. 2 1cm thick mag bad @ 90.25m. Compared to same unit above, this interval has more mag (apx 20-25%)	Ctc Core piece not there, Abrupt change in mineralogy and grain size. Move from an ultramafic into a mafic. Grain size change from ≤15mm down to ≤7mm.	Serp

97.45	118.45	<4mm gabbroic unit. Plag (Interstitial, 30-40%), Pyx (seem interconnected, 40-50%), Mag (interstial, 10-15%), Bt (trace). **@98.23** Plag(interstital, 5-10mm, 30-35%), Pyx (seem interconnected, 7-15mm, 40-50%), Oliv? (euhedral, 6-10mm, 10%) **@98.55** Plag(interstital, 3-10mm, apx20%) Pyx (apx 70%, possible oikiocryrst, cannot pick out grain edges of pyx), Mag (interstial, <5mm, 10%). **@98.70** Pyx %decreases and move into unit similar to 97.45-98.23m. **@98.85** Plag (intstitial, 4-8mm, 40%) Pyx (seem interconnected, 40-45%, 5-12mm) Mag (interstitial, <8mm, 10-15%). **@99.61** Similar interval to 98.55-98.7m. **@100.0** Plag (90%? grains >3cm? too large to tell.) Bt (3-5% 1cm grains) Mag(3-5%, 6-12mm) **@100.2** Plag(35-45%, 3-12mm) Pyx (30%, 5-7mm), Mag (Interstitial, 5%, 4-8mm) Bt (5-10%, 2-10mm). **@100.38** Similar interval to 98.85-99.61. 100.5m increase Pyx increase for 5cm. **@101.3** similar interval to 98.55-98.8 and 99.61-100. Increase in mag compared to those other intervals (15-20%). This interval looks like it may be made up of multiple small pyx grains instead of an oikiocryst, not sure though. **@101.66** similar to 98.85-99.61. 1-2% Bt present. 5cm increase of pyx at 102.3 to 70%.. **@102.62** similar to 97.45-98.23. **@102.79** similar to 101.66-102.62. **@103.06** coarsening of plag to 2-3cm grains and pyx 1-2.5cm. **@103.16** same as 98.55-98.7 **@103.55** same as 98.85-99.61, mag band at 103.7 1cm thick. **@103.74** massive mag section (70-75%, <3mm) plag (10-15%,4mm grains) pyx (10%, 5mm grains) **@103.91** plag (15% interstial, 1-3cm @104, 80%, <4cm?) Pyx (70-80% 1-5cm intrergrown w/mag) Mag (10% 1cm grains). **@104.09** Similar to 101.66-102.62. **@104.47** similar to 98.55-98.7. **@104.63** similar to 97.45-98.23. **@104.83** similar to 104.09-104.47. **@105.3** Plag (interstial, 30%, 2-4mm) Pyx (seem interconnected, 45-50%, 2-5mm), Mag (Interstial, 10-15%, <3mm). **@107.6** same as 101.03-101.66, **@108.7** same unit as 105.3-107.6. **115.5-118.45 NOT ACCESIBLE, STUCK IN CORE RACK.**	Ctc, sharp change in plag % from ~30% upto ~60%. Lwr unit may be chilled as for 2-3cm as grain sizes are ≤4mm then increase to ≤10mm.	Chl/Amp?; Serp
118.45	121.30	White grey coloured unit. Plag (seem interconnected, 5-12mm, 60%) Pyx (interestitial, 5-10mm, 25-30%) Black mineral closely assoc w/pyx Bt or Mag, <4mm, 10%. Unit not really magnetic though. Gradual coarsening of Pyx @120.6-121.3 with grains upto 15mm.	Ctc, gradational change in color from white grey to dark grey over 3-5cm	Chl/Amp?
121.30	122.95	Dark grey colured unit. Plag (seem interconnected, 85-90%? 2-12mm) Mag (<3mm, 2-3% and gradually increase in % downhole to 5-7% and <8mm) Pyx (interstial, 5-10%, 2-5mm), Tr Bt and Qtz?	Ctc, change in color from dark grey to white. Plag % also increases from ~85 to 100?	Chl/Amp?; Serp
122.95	125.93	Plag (100%?, 3-15mm) Very homogenous unit.	Ctc, color chnge from white to dark grey, and decrease plag from 100? Down to 85.	
125.93	126.30	Back into unit from 121.3-122.45	Gradational change into a more mafic unit over over 5cm. Pyx increases from ~10% to ~50%.	
126.30	132.40	Dark grey coloured unit. Plag (interstiial, 30-35%, <4mm) Pyx (seem interconnected, <4mm, 50-55%) Mag (interstial, <5mm with rare grains upto 1cm, 10%) @131.5 for 10cm coarsening of plag to grains upto 2cm w/ intersitial Po+Ccp (5%), seems like an isolated pod.	Ctc sharp, chilling occurs in top unit over 2cm with grain size decreae to ≤1mm. Black band (mag?) occurs at ctc. Grain size after ctc increase to ~2cm grains of Pyx & Plag	
132.40	132.74	Pegmatitic interval. Plag (6-20mm, 40-50%) Pyx (8-80mm, 30-40%) Bt (6-20mm, 2-5%, interstial, can occur on edges of mag) Mag (4-15mm, 5-10%, interstial, seem to contain inclusions of plag?) decrease in grain sizes downhole @132.6 where plag and pyx are <15mm	Ctc, not in core. Seems abrupt as drastic decrease in grain size from ≤15mm near lwr ctc to ≤10mm after ctc.	Chl/Amp?
132.74	133.85	Plag (interstial, 5-8mm, 40%) Pyx (seem interconnected, 45-50%, 5-10mm) Mag (interstial, 10%, 5-10mm) **@133.3** small peg pod w/ 2-3cm Bt, similar interval to 132.4-132.74.	Ctc, gradational over 5cm with increases Pyx (45 to 60%), incraed mag (10 to 20%) and decreased plag (40 to 20%).	Chl/Amp?

133.85	134.15	Plag (intersital, 25%, 2-10mm) Pyx (seem interconnected, 60%, <4mm) Mag (15-20%, <3mm) concentration of Mag in lwr 10cm and increase in grain size as well to 15mm.	Ctc, increase in mag 10cm before ctc and a band of mag at ctc but core piece dividing the two units is not there. Seems to be an abrupt decrease in Pyx % from 60 down to 40%.	Chl/Amp?
134.15	142.20	Plag (Interstial, <7mm, 30-45%) Pyx (seem interconnected, 2-8mm, 40-45%) Mag (interstial, 5-10%, <4mm) Coarsening at 141.0 for 5cm where plag is upto 15mm and pyc upto 25mm. Otherwise very homogenous unit.	Ctc, marked by qtz-carb vein and strgs. Also by appearane of beige-light green alteration to host rk.	Chl/Amp?; Serp
142.20	143.43	Mineralogy of unit in question. Plag (<5mm, ?% interstial? 30%?) Pyx may all be altered to beige light green product.	Ctc, gradational over 10cm, comes of out beige-light green alt and qtz-carb vns diminish	
143.43	143.88	Similar unit in appearance to 118.45-121.3. Plag (60-70%, 5-10mm) Pyx (15-20%, 3-10mm) Black mineral (Mag? Bt? 10-15%, <5mm) Unit not really magnetic.	Ctc, sharp, change in grain size from ≤10mm down to ≤3mm. No chilling observed.	Chl/Amp?
143.88	144.32	All grains are <3mm. Plag (interstial, 40%) Pyx (seem interconnected, 45-50%) Mag (interstial, 5-10%)	Core piece not present. Sharp change in grain size occurs from ≤3mm to ≤10mm.	Chl/Amp?
144.32	145.25	Similar to 143.43-143.88 w/2-3% Bt. @145 coarsening of plag up to 2.5cm.	Ctc, gradational over 5cm, change in grain size from ≤10mm down to ≤3mm.	Chl/Amp?; Serp
145.25	145.95	Similar to 143.88-144.32 except Plag can occur as blebs upto 10mm.	Ctc, gradational increase in grain size from ≤3mm to ≤14mm.	Serp
145.95	147.23	Plag (interstial, 4-12mm, 35-45%) Pyx (seem interconnected, 4-14mm, 45-50%) Mag (interstial, 5%, <5mm) Bt (Tace, <5mm)	Ctc, transition into alteration zone similar to alt zone above @ 142.2. Core is quarter so difficult to see actualy ctc's.	Chl
147.23	148.00	Alteration zone, similar to 142.2-143.43	Ctc core piece not present. But seems to have a carb vnlet at ctc and change in unit marked by coming out of alteration zone.	
148.00	152.90	Plag (interstial, 2-6mm, 30-40%) Pyx (seem interconnected, diffucul to tell but looks like grains are around 8mm, 50-55%) Mag (Interstial, 5-10%, <4mm)	Ctc, gradational increase in mag from ~10%above to ~20% below ctc.	Chl/Amp?; Serp
152.90	156.97	Plag (interstial, 10-15%, 4-8mm) Pyx (seem interconnected, 50-60%, 4-10mm) Mag (interstial, 20-25%, 2-5mm) Olivine? (dark green euhedral crystals, 5mm, 10%). Possible inclusions of plag within Mag???	Ctc, not in core, but drastic increase in grain size occurs from ≤10mm to ≤50mm.	Serp
156.97	157.22	Pegmatitic interval. Plag (55%, upto 5cm) Pyx (40%, upto 3.5cm) Mag (interstial, 5%, <5mm)	Ctc, sharp change in grain size from ≤50mm down to ≤8mm.	Serp
157.22	160.30	Plag (seem interconnected, 50%, 2-6mm) Pyx (seem interstial, 1-6mm, 40-45%) Mag (interstial, 1-8mm, 5-10%) Pyx may be interstial as it contains plag inclusions.	Ctc, is not magnetic within 5cm above ctc. Dark green bands occur at ctc. Change from a mafic unit to felsic units defines unit change.	Serp
160.30	163.05	Syenitic unit. Feld (60-70%) Plag (15-20%) Bt (15-20%). All grains <3mm. 5cm coarser section @160.55, grains are apx 8mm. Possible mafic fragments from unit above at 161.6-162.0, 162.2-162.3. Another coaser section w/ 10-15% mag @161.4-161.6. Over last 60cm Mag 10-15% 4-12mm and a dark green mineral present (10-15%)		Serp

Alt Description	Sulph	Sulph Description	Other	Samples
1mm stringers, apx spaced 15cm apart	None			
	Po	Trace amounts, interstitial, <2mm		2.1m
	Po	Trace amounts, interstitial, <2mm		3.22m
Green discolouration around edges of pyx apx 1mm thick Amp? Chl? Affects apx 30-40% of pyx grains within 10cm of bottom contact.		None		4.1m, 4.73m
Green discolouration around edges of pyx present throughtout unit, apx 20% of pyx affected.		None		
Green rims around pyx, affeects apx 40% of pyx grains. **@7.81** seems that green alteration around pyx has started to affect mag grains as well over 10cm length.				5.87m, 6.36m, 6.85m
Green alt around pyx, affects apx 40% of pyx grains.		None		8.68
Chl/Amp: green mineral asso c with pyx and affects apx 40-50% of pyx grains. Epd: strings, spaced apx 15cm apart and are 1-2mm thick. Potassic: plag affected around Epd stringers only		None	Banding of pyx occurs roughly every 30cm starting at 10.75m for 1m. Band of plag @10.7m.	10.98m, 14.29m
Chl/Epd?: stringers spaced 30cm apart		No sulphides observed until lwr contact where trace Po is interstial.	16.65m, multiple slip surfaces with serpentine along them.	17.2m,
Thin 1mm chl stringers throughout unit spaced 2-3cm apart	Po	2-4%, <2mm, interstial		20.35m
Epd/Chl: Stringers spaced 20cm apart Chl/Amp? Green alt around edges of pyx affecting apx 20% of pyx grains.	Po	Trace amounts, interstitial, <2mm	1cm mag seam @ 24.56. @21.6 10cm carb vein and slip surfaces, which appear highyl altered.	23.0m, 25.76m

56.39: 1cm carb? Vnlet seems to have chl along edges. 61.0: Mag vnlet 1cm thick w/ serp in centre of it? 61.8: 1cm carb vnlet w/ serp along lwr and upr contacts. 62.8: 3cm knot of Mag. 66.55: band of mag w/ creamy dark green stringer which contains mag crystals (4mm) as inclusions. 81.6: three 2 mm carb vnlets w. chl stringers along edges.	Po, Ccp	Trace amounts, interstitial, <2mm. @33.75m Po grain size increaes to <5mm and only in trace amounts over 5cm length. **@38.6** 1-2% interstital <2mm w/ trace Ccp on edges of Po. **@47.95** local increase in Po for 5cm to 15% forming a net-texture, Ccp present in cores and along rims of Po. Po grains 4-10mm, could mark change in unit? **@55.3** Po increase to 5-10% over 7cm, <5mm grains. **@71.94-72.44, 73.44-75.56** sulphides increase to 5-10% and are <1cm, Ccp occurs on edges of Po.	Cycles are determined by the appearance and dissapearance of plag. Upper and lower contacts of Peg section at 47.41 are marked by concentrations of mag over 2-4cm. Mag does not extend into pegmat section however, just in ultramafic rock. Within interval from 38.6-47.41m Pyx may be interstitial , meaning dark geen mineral would be olivine? **@57.7** abrupt change from mafic into ultramafic section, with increase of Mag (80%) around contact for 4cm	27.89m, 28.25m, 28.73m, 32.21m, 32.82m, 33.28m, 37.0m, 37.43m, 37.85m, 41.45m, 44.5m, 47.36m, 48.0m, 50.4m, 54.0m, 57.38m, 60.23m, 63.88m, 67.3m, 71.15m, 74.5m, 78.0m, 81.15m
Multiple carb vns throughout unit. Vary from 1mm - 1cm thick and occur ever 2-5cm. 2 Mag bands, 2mm thick @ 82.3. May have some chl alt within carb vnlets or ma be serp. Whole unit serpentinized.	Po; Ccp	Trace amounts of interstitial <3mm sulphides. Ccp occurs on edges of Po and appears to be hosted within carb vnlets?		83.9m
	Po; Ccp	5%, interstial, <4mm, trace Ccp on or near edges of Po		
Serpentinized.				
Some evidence of the flt zone occurs 40cm into this unit as fractures occur 5-10cm apart and have serp along them. Slip surfaces @ 90.4m, 93.9m with minor fractures and serp along them.		5%, interstial, <4mm, trace Ccp on or near edges of Po		88.63m, 92.1m, 94.95m

Slip surface @98.0m w/ serp along it. 97.45-98.23: green alteration around pyx grains affects 50% of pyx. @98.23 carb stringer 2mm thick with Chl? Along its edges. Green alteration only affects pyx around this carb stringer in the interval of 98.23-98.55. @98.7-98.85, green alteration of pyx affects 10% of pyx grains. 98.85-99.61: green alt affects 30% of pyx grains. Carb vnlet @ 99.15m for 10cm 2mm thick w/ chl/ along edges. @99.61 green alt of pyx may still be occuring in pyx interval. @100 pale green alt affecting plag? Slip surfaces @ 101.75 and 102.5, 104.83, 105.5,112.75 with serp along them. @100.2- 105.3 green alt affecting 50% of pyx grains. 105.3-118.45: green alt of pyx affects 15-20% of pyx grains. chl string 2mm thick @105.6. Carb stringer @108.5, 109.3, 117		97.45-98.23: none observed. 98.23-98.55: Trace interstial Po at top of interval and increases to 2-3% in bottom 5cm of interval, grains <10mm, tr Ccp on edges of po. 98.55 98.7: 2-3% Po, interstial, generally <3mm but is rare grain of 1cm Po, w/trace Ccp on edges. 98.85-100: Trace interstial Po, <2mm. 100-100.2: 1-2% Po 2cm w. Ccp at core and on edges. 100.2-101.3: none. 101.3-101.66: 2% interstial Po<8mm w.Ccp on edges. 101.66-118.45: Trace -2%interstitial Po, <2mm.	Cyclic unit. Top of a cycle is a <4mm gabbroic unit, then move into a 5-15mm gabbroic unit, then bottoms in a Pyx rich unit. Ctc @98.23 is sharp where grain size increases, no chilling or concentration of minerals along ctc. Ctc @ 98.55 core piece not present. Ctc @98.7 pyx % gradually decreaes over 5cm. ctc @98.85 core piece not present. Ctc @ 99.61 gradational increae in Pyx over 5cm. Ctc @ 100 abrupt change in anorthositic pegmatite. Ctc @100.2 core piece not present. ctc @100.38 decrease in Bt and increase in Pyx gradationally over 5cm. Ctc @101.3 sharp increase in pyx% over 2cm. Ctc @ 101.66: sharp decrease in pyx % and increase grain size for 5cm after ctc to 3-5cm plag/pyx and then moves into main unit. Ctc @102.62 change in grain size over 1cm to <3mm. Ctc @102.79 increase in grain size over 1cm. Ctc @103.06 increase in grain sizes. Ctc @103.16 decrease in grain sizes and increase in Pyx%. Ctc @103.55 decrease in Pyx %. Ctc @103.74 increase in mag and decrease in grain sizes. Ctc @103.91 decrease in mag %, increas in plag/pyx, and increase in grain sizes. Ctc @ 104.09 grain size decrease, pyx increase, plag decrease. Ctc @104.47 pyx %increased. Ctc @104.63 decrease in pyx. Ctc @104.83 slight increase in grain size. Ctc @105.3 decrease in grain size over 10cm. Ctc @107.6 gradational increase in Pyx over 5cm. Ctc @108.7 decrease in Pyx over 2-3cm.	98.85m, 99.7m, 100.0m, 103.55m, 103.7m, 103.91m, 105.83m, 108.0m, 111.56m
Pyx, apx 90% have some degree of alteration to a medium green colour. @119.1, 119.6, 120, 2mm carb vnlets		None		118.75m
Apx 80-90% of pyx grains altered to a green colour. @121.6 slip surface with serp along it.	Po;Ccp	Trace-2% interstial, <2mm. Ccp occurs on edges		122.3m
Carb strings apx every 30cm		None		125.03m
Carb vnlets 30cm spacing, may have chl strings along edges of vnlets	Po; Ccp	2-3% Po and 1% Ccp, both interstial and <2mm.		128.4m
5% of plag gains have a "white" centre to them, alt? zoning? Apx 60% of pyx have some degree of alt to a green colour.	Po; Ccp	Tr Po + Ccp, <1mm, interstial?	Corona texture occurs between Bt and mag	132.47m
20-30% of pyx have green alteration to them. Carb string at 133.05 w/ Py along it and chl	Py	Along carb string		132.74m, 133.4m

Carb strings at 133.9. 10% of pyx grains have green alteration.	Po	Intersitlal over last 10cm, coinciding with increased Mag contane		
134.45, 136, 138.4 10cm slip surface with serp along it. Epd strings? Spaced 30cm apart. 137.1,137.7,141.03 carb vnlet 2cm thick. Pyx altered to green colour around these vnlets. String spacing decreased to every 15cm at 140.2 until 142.2.		None		136.4m, 140.0m
Beige-light green alt affecting Pyx about 50% of unit. Thin beige strings closely assoc w/ carb vns.	Po	Trace, <2mm		142.3m
90% of pyx grains have some degree of alt to a green mineral		None		143.53m
Slight green alt to all pyx grains observed.		None		144.0m
Slip surfaces with serp along them at 144.75 & 145.3. 45-60% of pyx grains have alt of green colour to them.		None		144.42m
145.8 slip surface with serp along it		None		145.47m
rare chl? Stringers		None		146.8m
small pieces of carb vns thruout interval	Po; Ccp	1-2% Po, interstial <4mm, Trace Ccp,		147.36m
at 149.6, 150.8, 152.0 slip surfaces with serp along them. 50% of pyx have green alt to them. 2cm carb vnlet @ 149.45 and carb stringer at 152.1m.	Po	Tr-1%, intersital, <2mm		150.08n
10cm slip surface w/ serp along it @156.8	Po; Ccp	Trace-1%, interstial, <2mm, Ccp closely assoc w/Po	5cm granitic vn @153.3. Mag band at top and lwr ctc of this particular unit.	154.16m
Slip surface at upr Ctc		None		156.97m
Slip surface @ 157.7, serp along it	Po	Trace, intersitla, <2mm		157.23m, 159.6m
slip surface @161, w/ serp along it. Also around mafic fragments serp can be present.			Ctc w/ mafic fragments are sharp, no chilling observed.	162.45m

Appendix 7: CL-07-01 drill log

From	To	Lithology Description	Structure	Alt
0.00	4.50	Casing		
4.50	5.00	Plag (1-8mm, 30%, interstital) Pyx (1-10mm, 50%, interconnected) Mag (1-4mm, 10%, interstital) Bt (1-5mm, 10%) Interval highly weathered and rounded from drilling	Ctc not in core	
4.50	7.90	Dark green likely due to alteration. Plag (1-5mm, 10-15%, interstial) Pyx (1-4mm, 65%, interconnected) Mag (1-3mm, 15-20%, interstital, "net texture pattern) Every 30cm Mag strings.	Ctc not in core	Serp; Chl
7.90	8.60	Plag (4-15mm, 50-60%) Rare primary Pyx majority altered to Amp (3-15mm, 20-25%) Mag (1-8mm, 10-15%, interstial) Qtz (1-7mm, 2%, interstial) Pyx (5-10mm, 5%)	Ctc not in core	Amp; Chl
8.60	11.00	Plag (1-4cm, 40%) Pyx (majority of Pyx alterd to Amp, not altered 1-10cm, 40%)Subophitic Textures. Mag (1-5cm, interstital, 20-25%) Bt (5-20mm, 1-2%) @9.1-9.25m 80% Pyx w/ Mag inclusions forming a "graphic" texture. Mag may form rims around altered Pyx grains. Slight fining of grains from 9.3-9.4m % 10.05-10.75 where grains become <20mm.	Abrupt change in grain size to <20mm.	Amp; Chl; Serp
11.00	15.07	Plag (4-20mm, 40-50%) Pyx (5-10mm, 40%) Subophitic Textures. Mag (2-8mm, 10-15%, interstial) Bt (4-10mm, 1-2%, closely assoc w/ Mag) @11.8-12.2m increaes Mag (30%) with 2mm bands of Mag and Plag decreases to 10-15%. Mag froms a net texture in this short interval.	Sharp ctc in and out of Mag rich interval.Gradational increase in Mag % over 5cm	Chl; Amp
15.07	17.10	Similar to interval 11.8-12.2 in unit above. Mag (30%, 1-4mm, net texture) Mag band 2mm thick spaced 15-20cm apart. Possible Chl or Serp occurs along Mag bands. Plag (<10%, <5mm) Pyx (60%, 1-8mm). Short interval of gabbroic unit from above @15.36m and @ 15.61m.	Ctc, sharp change into gabbroic unit, no chilling.	Chl; Serp
17.10	22.41	Same Interval as 11.00-15.07m. Plag (4-20mm, 40-50%) Pyx (5-10mm, 40%) Subophitic Textures. Mag (2-8mm, 5-20%, interstial) Bt (4-10mm, 1-2%, closely assoc w/ Mag).	Have a concentration of Mag along ctc and unit change marked by abrupt decrease in Pyx and increase in Plag.	Chl; Amp; Serp; Carb
22.41	24.10	Plag (5-20mm, 75%) Mag (2-9mm, 10%) Bt (3-7mm, 2-3%) Likely all Pyx altered to Amp (15%, 3-8mm) Subophitic. Increase Amp downhole to 20%	Ctc abrupt increase in Pyx % and size	Amp;Chl;Carb;Pot;Serp
24.10	27.00	Plag (4-8mm, 50%) Pyx (3-10mm, 30%, interstital?) Mag (5-10mm, 15%, interstital) Bt (2-10mm, 2-3%, close assoc w/ mag) @24.9-25.1m some sort of EFG unit, diabase? Sharp ctc on ends of diabase. Pale red alt throughout diabase and multiple xcut dark strings (Chl?) @26.44Pyx and Mag decrease to 10%.	Ctc increase in Pyx and Mag %	Amp; Serp; Chl
27.00	32.84	Plag (5-12mm, 40-50%) Pyx (2-8mm, 35-40%) Mag (1-4mm, 15-20%, interstial) Bt (4-15mm, 2-3%) Qtz (Tr, 1-4mm, close assoc w/ Bt) Plag has a "creamy" color to it indicate alteration? Ser? Epd? @32m appearance of 1-4mm beige mineral, Mag alteration?	Fault gauge @ 29.95m. Ctc, sharp change into alteration zone.	Carb; Serp; Amp; Chl
32.84	42.88	Alteration Zone. Same lithology as unit above but has an intermitant "bleached" look to it until 34.3m then is completely "bleached". Brecciation textures @37.8-38.6m, 40.9-41.1m, 41.9-42.2m. Large vug of calcite and smokey qtz @37.8m. @37.8 Clasts in breccia are altered to a brick red colour and range in size from mm's - 8cm. Clasts seem to be of a mafic (gabbroic) composition and are very angular and highyl fractured. Not magnetic unit anymore.	Ctc, move out of alteration zone and into gabbroic unit from before, seem to have a concentration of hematite staining along ctc.	Carb; Hematite

42.88	44.15	Similar to 27.0-32.84m. Plag (3-10mm, 55%) Pyx (2-10mm, 35%) Mag (3-6mm, 10%, interstial) Bt (4-8mm, 2-3%) Subophitic textures.	Gradational ctc over 5cm w/ plag % decrease and increased Pyx and Mag %	Carb; Serp; Chl; Amp
44.15	46.35	Seem to be a "layered" interval with layers defined by being Plag "rich" (55%) and Plag "poor" (10-15%). Layers vary from 1cm to 40 cm thick. Plag "poor" intervals: Plag (10-15%, 1-4mm, interstial) Pyx (50-60%, 1-6mm) Ophitic textures Mag (25%, 1-3mm, interstial). Plag "rich" intervals: Plag (55%, 1-10mm) Pyx (30%, 1-6mm) Mag (10-15%, 1-4mm, interstial). @44.9 -45.1m section of <2mm grains. @45.9m Plag "rich" interval w/ increased grain sizes, Plag (4-12mm), Pyx (2-10mm) Mag (2-8mm) Tr Qtz present as well.	Ctc, Fault Zone	Chl; Amp; Serp
46.35	46.55	Fault Zone, highly fractured, gauge present		
46.55	47.40	Plag (30-35%, 4-12mm) Pyx (45-50%, 3-10mm) Mag (20%, 2-8mm, interstial) Subophitic textures. @46.7 have 60% Mag over 5cm. @ 47.15 Play increase 65%, Pyx decrease to <10%, Mag 5%. Have overal decrease in Pyx downhole.	Ctc, 10cm interval of 1-2cm Mag and 1-2cm Pyx w/ some Py then move into a FG rock.	Chl; Amp; Serp
47.40	51.80	Plag (15-20%, 1-5mm) Pyx (55%, 1-7mm) Mag (20-25%, 1-3mm, interstial) Bt (TR, <2mm, assoc w/ Mag) Ophitic textures. @48.4-48.7, anorthositic interval w/ <4cm Plag and 5-15mm Mag (10%) and an interval of 30% Mag 1-3mm. At base of anorthosite, have a 3cm Pyx grain. @48.7-51.82 Similar to unit above anorthosite, but MORE Plag (20-25%) and 2-3% Bt <2mm	Ctc, change into Pegmatitc/layered interval of units.	Amp; Chl; Serp; Carb
51.80	96.40	Layered unit of Pegmatites and Gabbro. Pegmatite: Plag (1-4cm, 40%) Pyx 1-5cm, 40%), Mag (2-20mm, 20%) Bt (Tr, <5mm). Gabbro: Plag (40-45%, 3-12mm) Pyx (4-12mm, 40%) Mag (2-10mm, 10-15%) Bt (2-3%, 2-5mm, assoc w/ Mag) Qtz (Tr, 1-4mm, interstial, Close assoc w/ Bt) Pegmatitc intervals : 51.8-52.1; 54.2-54.5; 55.75-56.08; 56.68-56.82; 57.87-58.1;58.35-58.9; 66.3-67.0; 69.65-69.9; 74.5-75.2; 76.7-78.4; 91.9-92.1; 94.8-95.1; 95.8-96.0. Within Gabbroic intervals, there can be intervals of finer grained and more Pyx (60-70%), these intervals are: 56.08-56.2; 58.9-59.1; 73-74; 75.1-76.1.	Majority of Pegmatitc ctc w/ gabbro are at 50°. Ctc, move out of Peg intervaled unit and into layered interval of Plag "rich" and Plag "poor" units	Chl; Serp; Ampl Carb;
96.40	115.70	Appear to be banded cycles w/plag rich tops and then grades to more Pyx rich bottoms. Plag "rich": Plag (50-60%, 3-12mm) Pyx (30-35%, 2-8mm) Mag (10%, 1-5mm) Nesophitic - Subophitic. Po (0-3%, <2mm, interstial) Bt (tr). Plag "poor": Plag (1-6mm, 15-20%) Pyx (60-70%, 1-8mm) Mag (10-15%, 1-4mm) Po (<3mm, 0-5%) Bt (tr). "cycles" 96.4-97.9,97.9-98.1,98.1-98.65,98.65-99.5,99.5-99.85,99.85-100.4,100.4-100.9,100.9-101.6,101.6-101.9,101.9-102.2,102.2-102.45,102.45-103.5,103.5-104.4,104.4-105.5,105.5-106.1,106.1-106.8,106.8-107.4,107.4-108.0,108.0-109.5,109.5-110.5,110.5-110.7,110.7-110.85,110.85-112.6,112.6-113.4,113.4-114.15,-114.15-114.4,114.4-114.8.	Ctc between cycles are gradational over 1-3cm and occur at apx 45°. Lwr ctc abrupt change into pegmatite	Serp;Chl;Carb
115.70	116.80	Pegmatitic interval. Plag (7-25mm, 40%) Pyx (1-4cm. 40%) Mag (2-15mm, 15%) Bt (1-5mm, 1-3%, assoc w/ mag) Po (1-7mm, 2-4%, interstial)	Sharp ctc, change in grain size and modal %	Serp;Chl
116.80	124.25	Similar type of "cycling" like before pegmatite but both types of intervals are Plag "poor". Plag "poor": Plag (10-25%, 1-8mm) Pyx (3-15mm, 50-60%) Mag (2-8mm, 20%) Olivine? (15-20%, 2-6mm, dark green, euhedral) Plag "Trace": Plag (1-2%, <2mm) Pyx (80%,3-10mm) Mag (1-5mm, 20%). Plag "poor":116.8-117.2;117.6-123.15. Plag "trace": 117.2-117.6;123.15-124.25. Pegmatite interval 121.62-122.0, Plag (>1cm, 30%) Pyx (4cm, 55%) Mag (3-20mm, 15%) Bt (10mm, 2%)	Sharp change in modal %	Amp; Chl; Serp

124.25	126.70	Overall unit is a gradational change from Pyx poor at the top and around 125m changes into Pyx rich w/ bands of Pyx poor. Pyx poor: Plag 45%, Pyx 45%, Mag 20% all <4mm subophitic textures. Pyx rich: Plag (20%, 1-6mm) Pyx (60%, 1-5mm) Ophitic textures Mag (20%, 1-5mm) Bt (tr, 1-3mm) Po (tr, <2mm). At 126.3 no Plag. Pyx 75% 1-5mm, Mag 25%, 1-4mm.	Ctc change into pegmatite	Serp; Amp
126.70	128.10	Pegmatitic interval. Plag (0.5-7cm, 45%) Pyx (1-7cm, 45%) Mag (2-25mm, 10%) Bt (tr, 5-10mm) Ap (tr, 5-10mm) Subophitic textures	Abrupt change out of pegmatitic interval	Amp; Chl
128.10	174.40	Banded gabbroic unit w/ cycles of plag rich tops and pyx ruch bottoms interuppted by several pegmatite intervals. Plag Rich: Plag (40-55%, <10mm) Pyx (35-40%, <10mm) Mag (10-20%, <10mm) Some Plag rich intervals may have grains <15mm. Plag Poor: Plag (<10%, <4mm) Pyx (60%, <4mm) Mag (30%, <5mm). Pegmatitic intervals: 131.5-132.05,132.5-138.1,139-139.15,140.7-141.5,144.5-145.8,149.3-150,153.5-153.8,156.1-157.3,167.3-167.6,173-174.4, pegmatitic intervals have similar descriptions to pegmatite @51.8. Cycles: 128.1-128.9,128.9-130.15,130.15-130.45,130.45-131.5,132.05-132.5,138.1-139,139.15-140.25,140.25-140.35,140.35-140.7,141.5-141.6,141.6-144.5,145.8-148,148-149.3,150-153,153-153.5,153.8-154.6,154.6-155,155-155.3,155.3-156.1,157.3-158.5,158.5-159.6,159.6-159.9,159.9-160.1,160.1-160.9,160.9-162.2,162.2-162.5,162.5-162.9,162.9-163.4,1634.4-163.6,163.6-164,164-164.25,164.25-164.45,164.45-165,165-165.8,165.8-166.7167.6-167.9 (all plag poor) 167.9-169.22,169.22-170.6,170.6-171.4,171.4-172.6,172.6-173.	Banding that occurs in this unit varies from 45-80, majority @ 70. Ctc occurs after a pegmatite interval. Gabbro after ctc is slightly coarser grained.	Amp; Serp; Chl
174.40	180.60	Plag (2-12mm, 45%) Pyx (3-14mm, 40%) Mag (1-6mm, 15%) Bt (Tr, 1-4mm, assoc w/ mag) 1cm plag band @ 176m. @176.7-179.0 have decrease in grain size and increase in Pyx %. Plag (1-9mm, 35-40%) Pyx (2-8mm, 45-50%) Mag (1-6mm, 15%). From 179.5-179.65 in Pyx rich again. 180.0-180.6 in a slight pegmatitic interval w. Plag and pyx upto 4cm.	CTC, move into alteration zone, sharp ctc.	Amp, Serp, Carb, Chl
180.60	184.50	Alteration Zone. Seems to be originally <10mm gabbroic rock but now has been subjected to alteration. Plenty of Chl and Carb stringers throughout and tend o occur together. Rare Pot alteration. Some areas are still magnetic but generally unit is non-magnetic. Some areas may be slightly brecciated.	Ctc, out of alteration zone	Chl, Carb, Pot
184.50	187.20	Same interval as before alteration zone (174.4-180.6) with slightly more Mag (20-25%). Pegmatite 186.4-187 w/ 30% Mag. 184.9-186.4 have the increase in Pyx %. Tr Bt in unit, 1-3mm.	CTC, move into alteration zone, sharp ctc.	
187.20	188.70	Alteration zone as 180.6-184.5. Pink calcite present.		

188.70	228.60	Same mineralogy and grain sizes as 174.4-180.6, subophitic textures. Have alternating units between Plar rich and Pyx rich units like before. Pegmatite intervals : 200-200.1, 204.6-205, 206.9-207.3, 221.9-222.4, 228-228.6. Granitic vein/veinlets: 214.7-214.8, 217.1-217.2, 221.8-221.9, 222.45-222.5, 222.8-222.87, 223.25-223.3, 223.55-223.6, 224.4-224.5. Intervals of Plag rich and Pyx rich: 188.7-189.4 Pyx, 189.4-191 Plag, 191-191.5 Pyx, 191.5-192.4 Plag, 192.4-195 Plag, 195-199.8 Plag, 199.8-200 Pyx, 200.1-201.9 Pyx, 201.9-202.2 Plag, 202.2-203.2 Pyx, 203.2-203.9 Plag, 203.9-205 Pyx, 205-205.4 Plag, 205.4-207.7 Pyx, 207.7-207.9 Plag, 207.9-208.7 Pyx, 208.7-208.9 Plag, 208.9-209.2 Pyx, 209.2-209.3 Plag, 209.3-209.4 Pyx, 209.4-214.5 Plag, 214.5-215 Pyx, 215-220.2 Plag, 220.2-221.5 Pyx, 221.5-228.6 Plag.	Ctc move into Fault zone.	Amp; Chl; Serp; Carb
228.60	231.40	Fault Zone, highly broken and fractured. Competent rock seems to be an altered gabbro. Plag (1-5mm, 40-45%) Pyx (1-5mm, 45-50%) Mag (10%, <3mm)	Ctc move out of fault zone	Serp, Chl
231.40	236.90	Seems to be a gabbro that has been "granitized" contains abundant feldspar but also still has some Pyx grains present, Mag 2-8mm, <10%. Seems to have granitic veinlets cutting through interval as well	Ctc, out of gabbro/granitic veinlets and into a gabbro, sharp ctc	Amp
236.90	250.50	Plag (1-8mm, 40-50%) Pyx (1-6mm, 35-50%) Mag (1-4mm, 5-15%) Bt (Tr, 1-3mm) Majority of Interval is: Plag (40%, 1-8mm) Pyx (50%, 1-6mm) Mag (1-3mm, 10%) Bt (Tr) but there are intervals where plag is more abundant, 240.1-240.65 Plag (85%) Pyx (tr-5%, 2-3mm) Mag (10%, 2-12mm). Carb-qtz vein @239.5, 10cm, small vug, Tr Py	Possible foliation of Plag apx 45deg.	Amp,;Chl; Serp; Carb
250.50	252.60	Sugary looking vein. Kfs and plag generally <5mm have local concentration of mafic minerals (10%, amp?) throughout.	Have increase in mafic minerals around lwr ctc (20%) but sharp change into next unit	Chl; serp
252.60	267.40	Same unit as before granitic vein. Plag (40%, 1-8mm) Pyx (1-6mm, 50%) Mag (10%, 1-3mm) Bt 9tr, 1-2mm). Pegmatitic sections, 259.6-259.8, 253.3-253.4. Possible "inclusion" of more plag rich gabbro, <10mm grains @255.5 & 262.5. @256.1 have a Chl band 5mm thick w/ concentration of <4mm Po along it. From 256-256.2 habe increased Mag (20%) and from 255.5-266 have increase in Plag (50%) 261.3-261.7 & 263-263.1 granitic vein like 250.5-252.6 w/ concentration of mafics around ctcs. Plag band 1-2cm thick @ 261.2, 262.2	Possible foliation of Plag apx 45deg. Ctc gradational increase in Mag over 20cm until move into a magnetitie (60-70% Mag)	Carb; Map; Chl
267.40	267.75	Magnetite. 60-70% Mag, <5mm. 10% Plag, <8mm, 20% Pyx, <5mm. Pyx increases to 5-15mm over final 10cm of unit.	Ctc, sudden decrease in Mag %	Amp, Chl
267.75	280.90	Plag (3-15mm, 45%) Pyx (5-15mm, 35-45%) Mag (1-10mm, 15-20%) Bt (tr, <3mm)Subophitic textures.. From 270-270.2, magnetitite unit, w/ 50-60% Mag, 1-5mm, Plag (30%, 2-12mm, surrounded by Mag) Pyx (10%, 2-8mm) After Mag interval have an anorthositic unit from 270.2-270.9 (Plag 80%, 3-12mm; Pyx 10%, 1-8mm; Mag 10%, 1-8mm; Bt Tr, 8mm) Tr amounts of qtz @ 277.5. Granitic vein @ 279m.	Ctc, sharpe change in grain size.	Amp
280.90	286.60	Plag (1-4mm, 40%) Pyx (1-6mm, 50%) Mag (1-3mm, 10%) Subophitic-ophitic textures. Anorthositic vein @ 281.1-281.25. Granitic vein @ 282.65-283.45. From 284.5-285 granitic vein w/ massive qtz @ the centre and Kfs/plag on edges, sharp ctc fragment of gabbro in portion of vein. @282-282.4 have a coarser grained interval of gabbro, grains <12mm, Bt increases 2-3%.	Possible Plag foliation @ 45deg. Ctc sharp change into Mag rich interval then into grains that are <1cm	Chl; Serp; Amp
286.60	287.80	Interval starts in Mag rich (50-60%) then grades into 10-15% Mag over 10cm. 286.6-286.7: Mag (50-60%, 1-8mm) Plag (1-6mm, 15-20%) Pyx (1-4mm, 20%). 286.7-287.6: Plag (40%, 1-12mm) Pyx (1-8mm, 45%) Mag (1-6mm, 15%) Subophitic textures. 287.6-287.8: Same as 286.6-286.7.	Ctc sudden decrease in Mag %.	Amp; Chl; Serp
287.80	302.75	Same domiant lithology as 280.9-286.6. [] of Mag @ 288.5 for 5cm. @ 295.15, 2 plag bands, Mag bands @ 297.4,301.2. From 300.4-300.8, imilar Mag rich interval as 286.6-287.8.	Ctc, change in Mag % to 30-40%	
302.75	303.00	Mag rich interval. Mag (30-40%, 1-7mm) Pyx (40%, 1-6mm) Plag (15%, 1-8mm)	[] of Mag around ctc (1cm band) then sudden decrease in Mag	Amp
303.00	305.75	Plag (1-10mm, 35-40%) Pyx (1-6mm, 50%) Mag (1-5mm,10-15%) ophitic - subophitic textures	Odd ctc as a Fg felsic vn/dyke occurs at a low angle (10) as the unit changes to a much finer grained gabbro.	Amp; Carb; Chl
305.75	307.40	Felsic dyke/vn extends from 305.75-306.33 and is 2cm wide. Gabbroic unit is same as interval 280.9-286.6.	Ctc, grad increase in grain size <1cm grains	
307.40	313.00	Alternating between <10mm grains and <5mm grains, both gabbroic units w/ several Mag rich layers. <10mm intervals: Plag (40-50%, 3-12mm) Pyx 91-8mm, 40%) Mag (2-10mm, 10-20%) Bt-Po-P(Tr). <5mm intervals: Same a s280.9-286.6. Mag bands / concentrations: 307.75, 308.85, 309.2, 309.5, 311.4, 311.8, 312.1, 312.7, 312.95	Ctc,dissappearance of consistent Mag bands	Amp
313.00	321.90	Plag (40-45%) Pyx (45-50%) Mag (10-15%) all grains <3mm. Coarse grained patches do occur in short intervals; 314.7-314.8, 315.9-316, 316.3-316.5, 316.7-316.9, 317-317.1, 318.8-318.9, 320.9-321.1, 321-321.2, 321.5-322, Coarse gained patches are: Plag (55%, 5-20mm) Pyx (30%, 3-20mm) Mag (1-10mm, 15%)	Ctc, increase in grain size	Chl; Amp

321.90	322.60	Same mineralogy as "Coarse" grained patches in unit before, local [] of Mag upto 50%.	Ctc, sharp change back into finer grained gabbro	Amp
322.60	328.90	Same interval as 313-321.9, CG patch @ 324.4, 326. Mag Band @327.2.	Ctc, abrupt increase in Mag, sharp	Chl,; Amp
328.90	329.60	Magnetite. 50-70%, 1-6mm net-textured. Difficult to tell which minerals are also there, likely Pyx or Oliv 1-8mm.	Sharp decrease in Plag	
329.60	341.40	Same as 313-321.9m. Coarse grained patches (329.7,330.9,333-333.7, 335.8,339) Mag bands (330.8,332.2-332.5) @331.5 granitic dyke/vein, similar to 251m, possible inclusion of <1mm gabbro @340m.	Ctc, sharp increase in Mag	Amp; Chl
341.40	342.00	Same type of magnetite unit as in interval, 328.9-329.6	Ctc, sharp decrease in Mag	
342.00	359.75	Same interval as 313-321.9. CG patches (344.8,346.3,347.4,350.8,356,357.3,358) Large Chl stringer that runs from 348.5-349.5 that splits the core in half, seems to have serp along it, also one at 351.3-351.7.	Ctc, sharp increase in Mag	Chl; Amp
359.75	360.40	Same type of magnetite unit as in interval, 328.9-329.6	Ctc, sharp decrease in Mag	
360.40	366.85	Unit starts in 10cm of a "CG" patch then switches to the same interval as 313-321.9. "CG" Pathces (360.9,362.2,363,364.4)	Ctc, sharp increase in Mag	Chl; Amp
366.85	367.50	Magnetite thick 4cm abnds interupter by gabbro . Very similar to other Mag intervals	Ctc, decrease in mag	
367.50	371.08	Same as 131-321.9 but w/ the "CG"Patches occurring every 20cm for 3cm. Short 5-10cm Magnetite intervals @368.7, 369. In Mag interval @369 also have 1cm Po band. Tr Bt in CG Patches.	Ctc, increase in grain size	
371.08	371.86	Magnetite as 328.9-329.6 w/short 10cm interval of gabbro at 371.7.	Ctc, decrease in mag	
371.86	372.20	CG interval similar to the patches in above units. Plag (55%, 5-20mm) Pyx (30%, 3-20mm) Mag (15%, 1-10mm) Bt (2-3%, <8mm)	Sharp ctc w/vein, slight chilling	Amp
372.20	372.50	Same type of vein/dyke as 251m, chilling observed @ upr ctc	Ctc not in core	
372.50	376.25	Pegmatite interval. Plag (upto 4.5cm, 55%) Pyx (upto 3.5cm, 30%) Mag (8-20mm, 15%) Nesophitic-subophitic. Local [] of Mag upto 40% @375.3m, granite vein @374.1-374.8, 376-376.25, Slight chilling (same veins as 251m)	Ctc, decrease in grain size after vein	Amp
376.25	384.70	After granitic vein @376-376.25 not so pegmatitic and just coarser grained. Plag (8035mm, 50%) Pyx (8-20mm, 35-40%) Mag 98-20%, 10-15%) Bt (Tr, 10mm) Local [] of Mag @ 382.4, 40%.	Ctc, sharp increase in Mag	Amp;Carb
384.70	385.05	Magnetite unit as 328.9-329.6, has local [] upto 70% Mag	Ctc, sharp decrease in Mag	
385.05	411.00	Same as 313-321.9, "FG" gabbro. Local Mag [] @386.9 (60%,5cm thick), 387.5 (40-50%,10cm), 389.4 (70%, 10cm), 390.7 (40%, 5cm), 402.7 (50%, 10cm), 403 (40%, 5cm) Also have CG patches @387, 388, 388.6, 395.8, 396.3, 399.9, 401.6, 402.9, 404.7.Mag bands @393.1,399.7. Pegmatie from 410.4-411 (Plag 5-35mm, 45%; Pyx 5-30mm, 35%; Mag 3-20mm, 20%, oliv 5%)	Ctc, sharp increase in Mag	Amp; Chl
411.00	413.70	Magnetie varies from 30-90%, lwr mag [] intervals are similar to CG patches in gabbro above. Tr Apatite @411.6 in VCG interval. 90% Mag from 412.5-413.25	Grad decrease in Mag from 413.25-413.7 down to 10-15%	Amp
413.70	424.00	Same interval as 313-321.9, CG patches @417.1,418.5,422-422.6. @417.6 have 2x2cm granitic veins. Mag bands @419, 420, 421.5, 422.6, 423.7, 423.9. Short Pegmatitic interval from 419.3-419.5.	Grad increase in plag over 5cm	Chl;Amp
424.00	424.90	Plag (60%, 1-8mm) Pyx (20-30%, 1-8mm) Mag (10-120%, 1-7mm) B (tr, <3mm) Mag Band @424.75	Sharp ctc and change into FG unit	Amp
424.90	425.80	Same as 313-321.9, inclusion of plag rich interval @425.14	Sharp ct w/ granitic unit, chilled about 50cm into granite (<5mm) then changes into <10mm grains	
425.80	481.40	Kfs (50-70%) Qtz (10-20%) Plag (10%) all <10mm. 10% mafic mineral (amp?) very homogeneous unit		

Alt Description	Sulphides	Sulph Description	Samples
	None		
Over 10cm @6.2m, 3 slip surfaces with serp along them. Whole interval seems serpentinized. Chl strings spaced every 15cm.	None		5.3
90% of Pyx altered to Amp, with Chl occurring around edges of Amp grains.	None		
50% of Pyx alterd to Amp w/ Chl concentrated around edges. Slip surface @9.13, serped	Py	1-2%, 2-12mm	9.1, 10.2
Chl strings spaced 20cm; 40% of Pyx alt to Amp	None		13
Chl stringers 20 cm apart' whole interval seems to be serpentinized.	None		15.24
Chl strings spaced 20cm; 40% of Pyx alt to Amp; long chl & carb stringer running from 17.3-17.7m, 3mm thick, carb in centre of string and chl on edges. Slip surfaces @21.36,22,19.5	None		20
Amp likely all Pyx altered to Amp; Chl conctrates around Amp rims; rare carb/chl stringers; rare Pot alt; Slip sur @22.9,23.1,23.6	None		23.7
50-60% of Pyx alt to Amp; Chl concentrated around edges of Amp; Slip sur @25.5 w/ carb and Serp along it	None		26.1
Carb stringers 15-20cm spaced after 31.0m; 60% of Pyx altered to Amp; Chl stringers 20cm spaced; Slip surfaces @28.15, 27.2, 28.6, 30.8, 31.35, 32	None		29.15
Carb strings 5-10cm apart until 38.6m then occur 50cm apart till end. Bleaching throughout unit. Hematie staing cyclic and inverse to bleaching (may just be a surface weathering feature)	None		33.9,36.5,38,40.8, 41.9,42.6

Carb stringers every 10-15cm; Chl stringers every 10cm; 80% of Pyx alt to Amp slip surfaces @43.4 43.9	None		43.5
Chl strings spaced 3-10cm apart; 20% of Pyx alt to Amp; Slip sur @44.25,44.5,44.9,45.15,46.1	Po/Py	Cluster of both occurs @ base of unit @ 45.1m, grains <2mm. Po: @45.9 2.5cm band of Po composed of <1mm grains.	44.25,44.8
Chl stringers 15cm apart; 20% of Pyx altered to Amp; Slip sur @46.7, 47, 47.1	None		46.9
80% of Pyx alt to Amp; 48.7-51.82 only 40% alt; Chl stringers 10-15cm spaced; Carb stringers spaced 50cm apart; Slip Surfaces @ 47.6, 47.8, 51.5, 51.57, 48.2, 49	Po	Tr, <2mm, interstial	50.2
Chl strings are rare at the beginning but around 57.87 start occur every 20cm; Carb veinlets occur every 1m; 40% of Pyx alt to Amp; Multiple slip surfaces (52.8, 53.1, 57.25, 57.6)	Po	Tr, <2mm, interstial, assoc w/ Mag. @69.6m 1-2% Po, 1cm grains.	52.3,55.9,56.7,61.8,67.5,71.7,76.9,79.25,89,95.9
Chl stringers rare but more common in lwr 10m of interval. Carb stringers are concentrated around 100m for 50 cm and are 5cm spaced. Slip sur @98.7,100.5,102.5,108,108.5,109,109.6,110.9,112.4,113.1,113.7,114.1	Po	Occur in both Plag "rich" and Plag "poor" intervals	100.8,101,113.8,113.9
Rare Chl stringers; Slip sur 116	Po	1-7mm, 2-4%, interstial	116.1
60% of Pyx alt to Amp; Rare Chl stringers; Slip sur @119,119,121.6	Po	Plag Poor: 0-4%, <2mm, intersital. Plag Trace: 0-3% <1mm, intersital	116.9,117.2,123.6

60% pyx alt to Amp. Slip sur @124.9,124.6,125.8	Po	125.3-126.7: tr, <2mm	124.3, 125.4
60% pyx alt to ampl; chl band 3mm thick	Po	Tr, <5mm	127
10-30% of pyx alt to amp; Chl stringers sporadic; Slip sur @ 131.5,132.4,134.7,136.8,139,139.5,140.9,141.2,142.8,143.1,150.8,149.9,150.9,151.2,156,161,163.9,164.2,	Po	0-2%, <5mm, interstial	128.1,128.4, 134.3, 139.3, 140, 145.7, 148, 149.1, 158.6, 159.4, 166.4, 166.6, 171.5
15% Pyx alt to Amp; Carb stringers 40cm apart; Rare Chl stringers; Slip sur @ 180, 178.3, 175, 175.9	None		176, 180.1
	None		181.9
	Po	Tr, 1-2mm, interstital	184.6
			187.3

10% pyx alt to Amp, Chl stringers 30cm apart; Carb stringers 40cm apart; Slip sur @189.1,192.6,195,196.8,197.2,199,201.2,202,203,207.3,208,209.7,212,205	Po	0-2%, 1-2mm, interstial.	190.3, 193, 203.6, 205.6, 214.3, 220.9, 222.1, 227.9
Chl stringers 5-10cm apart; along all fractured surfaces	None		
60-70% Pyx alt to Amp, variable alt intensity, more Amp alt around more Pot alt areas	Po	Tr, <2mm, interstial	233
20-30% pyx alt to amp; chl stringers 40 cm apart; stringers concentrated around carb vein. Slip sur @237.6,240.9,238.2,240.4,241.2,242, 244.8,247.3,250.5	Po	Tr, <2mm, interstial	239. 249.9
Abundant chl stringers, 5-10cm apart, going in all directions; slipsur @252.45	None		251.6
Carb stringers concentrated between 260-261, 20 cm spacing; Chl stringers 20cm spacing; Tr Pyx alt to Amp.	Po	Tr, <2mm, Interstial	253.8, 258.3, 265.2
20% Pyx alt to Amp; rare Chl stringers	Po	Tr, <2mm	267.4
10% Pyx alt to Amp. Slip sur @ 268, 268.6, 269, 269.9, 274	Po, Ccp	Po-Tr, <3mm; Ccp-Tr, <3mm assoc w/Po.	271, 275.7, 277.4, 280.2
Rare Chl stringers; Slip sur 285.7, 285.5, 284.6, 284.4, 283. 10-15% pyx alt to amp and increases to 30-40% from 282.-284.4	Po; Ccp	Band of Po+Ccp @ 285.2 occurring w/string of chl	281.7, 286
Rare Chl stringers; 10% Pyx alt to Amp; Slip sur @ 287	Po	Tr in non-Mag rich intervals	287.1
Slip sur @ 289, 291.5, 296, 301	None		291, 299
10% Pyx alt to Amp	Py	1-2%, cluster of <1mm grains	304.7
10-120% Pyx alt to Amp; Rar chl stringers; Slip Sur@303.4,304,304.1. Carb stringers along Slip sur	Po	Tr, <2mm	
			306.9
10-20% Pyx alt to Amp; Slip Sur @309.7-310.5, 312.6	Po,Py	Tr	308.8, 312.9
Chl stringers about 20cm apart; 10% Pyx alt to Amp; Slip Sur @ 315.3, 313.2, 319.3, 320.7	None		319.1

20% pyx alt to Amp	None		
Rare Chl stringers; Tr Pyx alt to Amp; Slip Sur @ 324.5	None		327.3
	Po	Tr, <3mm	329
Rare Chl stringers; 10% Pyx alt to Amp; Slip sur @ 336.7, 338.1, 339.2	None		333.3, 336
	Po	2%, <5mm	341.5
Chl stringers 20cm apart; 10% Pyx alt to Amp; Slip Sur @346, 346.7, 348.5, 349.5, 351.3, 353, 353.5	Po	Tr, <1mm	350.4
	Po	1-2%, <8mm	
Chl stringers 20cm apart; 10% Pyx alt to Amp; Slip Sur @366.4,363.5	Po	0-2%, <8mm, interstial, mostly in CG Patches	364.4
	Po	5%, in Mag bands, <6mm	367
Slip sur @ 368, Chl and Carb along slip sur too	None		369.3
	Po	3%, <6mm, interstit	
50% pyx alt to amp	Po	1-2%, <6mm, intersit	
	None		
30% pyx alt to amp; slip sur @372.8,374.9	None		373.2
60% Pyx alt to Amp; Rare Chl stringers; Slip sur@380	None		381.7
			384.8
10% pyx alt to amp; Chl strings 40cm apart; Slip sur @ 385.5,389.3,392,393.1,395.5,397.2,398	Po	0-2%, mainly occurs in CG patches, <8mm	388.5, 389, 390.3, 396.3, 400.4, 407.4
40% Pyx alt to Amp	Po	1-2%, <5mm scattered. 412.5-413.25 3% Po, <8mm	411.6
Chl stringers spaced 50cm apart; 10% Pyx alt to Amp; Slip sur @422.6, 420.1	Po	Tr, <3mm, intersit	415
20% pyx alt to Amp; Slip sur @424.4	Po	1-2%, <5mm assoc w/ Mag band	424.5
Slip Sur @425.4	None		
			426, 429.8, 445.1

Appendix 8: CL-06-16 thin section data

Sample Depth	Rock Type	Grain Size	
8.9	Gabbro	<2mm	m
11.2	Gabbro	<2mm	m
33.7	Clinopyroxenite	<2mm	m
35.7	Clinopyroxenite	<5mm	c
47	Gabbro	<1.5mm	f
47.6	Gabbro	<2.5	m
52.5	Gabbro	<5mm	c
55	Gabbro	<5mm	c
56.3	Gabbro	<7mm	c
57.5	Gabbro	<7mm	c
58.6	Gabbro	<3mm	m
59.9	Gabbro	<2mm	m
61.7	Gabbro	<2mm	m
63.15	Gabbro	<1mm	f
63.8	Clinopyroxenite	<5mm	c
71.15	Gabbro	<1mm	f
78.75	Massive sulfide/Plag rich Gabbro	<2mm	m
80	Clinopyroxenite	<7mm	c
83.5	Gabbro	<2mm	m
84.6	Massive sulfide	<1.5mm	f
90	Anorthosite	<2mm	m
103	Gabbro	<2.5mm	m
152.45	Gabbro	<2mm	m

Plagioclase %	Clinopyroxene %	Orhtopyroxene %	Olivine %	Fe-Ti-Oxide %
50	20	5	10	10
50	20	5	Trace	10
30	40	5	10	15
10	60	5	15	6
45	35	Trace	5	8
20	20			10
40	25	Trace		8
30	30	2	5	10
40	35	2	2	5
45	40	Trace		12
30	30	Trace		8
45	35	5	2	6
40	20	10		5
35	30	5		5
25	45			6
40	35	10	Trace	8
70	15	5		5
25	55	10		4
40	30	10		5
90	5	3		3
50	35			4
45	35	10		5

Sulfide %	Plagioclase Alteration	CPX Alteration	OPX Alteration	Olivine Alteration
4	Mod	Wk	w	Wk
2	s	Mod	m	C
Trace	Mod	Tr	t	tr
3	Tr	Wk	w	Wk
7	Mod	Mod	w	c
15	Mod	Str		
15	wk	Mod	m	
12	Tr	Mod	w	c
15	Tr	Mod	m	c
9	wk	Mod	w	
25	Tr	Mod	w	
3	wk	Wk	w	c
15	Mod	Mod	m	
Trace	s	Mod	m	
20	wk	Str		
2	wk	Wk	w	c
Trace	Mod	Mod	w	
1	wk	Mod	m	
Trace	Mod	Mod	m	
98				
Trace	Tr	Tr		
Trace	wk	Str	s	
Trace	wk	Wk	w	

Appendix 9: CL-06-39 thin section data

Sample	Rock type	Grain Size (mm)	Plagioclase %	Clinopyroxene %
CL-06-39-4.1	Gabbro	<12	35	65
CL-06-39-6.85	Gabbro	<10	70	30
CL-06-39-10.98	Gabbro	<3.5	45	45
CL-06-39-17.2	Gabbro	<3	50	40
CL-06-39-20.35	Dunite	<5	8	10
CL-06-39-32.21	Lherzolite	<5	8	15
CL-06-39-32.82	Dunite	<4	-	10
CL-06-39-33.28	Dunite	<5	t	5
CL-06-39-47.36	Lherzolite	<6	t	40
CL-06-39-57.38	oxide lherzolite	<4	-	5
CL-06-39-60.23	Dunite	<4	5	5
CL-06-39-63.88	Troctolite	<5	12	10
CL-06-39-83.9	Troctolite	<5	10-20	15-20
CL-06-39-94.95	Dunite	<5	5	5
CL-06-39-100.0	anorthosite	<15	100	-
CL-06-39-103.55	Gabbro	<4	60-70	25-30
CL-06-39-103.7	Oxide-UM	<5	t	20
CL-06-39-103.91	olivine gabbro		20	50
CL-06-39-105.83	Gabbro	<3	45	40
CL-06-39-108.0	Troctolite	>5	15-20	t
CL-06-39-118.75	Gabbro	<7	70	30
CL-06-39-122.3	Gabbro	<8	60	35
CL-06-39-125.0	anorthosite	<4	100	-
CL-06-39-128.4	Gabbro	<4	45	35
CL-06-39-132.47	Gabbro	<17	60	30
CL-06-39-133.4	Gabbro	<15	45	20
CL-06-39-150.08	Gabbro	<4	45	35
CL-06-39-154.16	Oxide dunite	<4	-	t
CL-06-39-156.97	Gabbro	<20	40	60

Olivine %	Fe-Ti-Oxide %	Sulfide %	Plagioclase Alteration	CPX Alteration	Olivine Alteration
-	t	3	w	w	-
-	t	2	w-m	w-m	-
t	t	7	m	m	w
3	t	5	w	m	m
75	1	5	m	m	s
70	t	4	m	w	c
80	t	8	-	m	c
88	t	7	m	m	c
45	t	5	w	w	c
60	t	35	-	w	c
80	1	7	m	w	s
75	t	4	m	m	s
60-70	t	t	c	c	c
85	t	7	m	s	c
-	-	-	c	-	-
-	t	2	m	w	-
10	1	70	m	w	m
20	t	10	s	m	c
5	2	5	w	w	m
75	t	7	w	w	m
-	-	2	s	c	-
-	t	4	t	m	-
-	-	t	s		-
10	2	5	w	w	m
-	1	2	s	s	
5	1	6	w	w	w
10	1	5	w	w	m
70	t	35	-	s	c
-	-	t	m	m	-

Appendix 10: CL-07-01 thin section data

Sample	Rock type	Grain Size (mm)	Plagioclase %	Clinopyroxene %	Olivine %	Fe-Ti-Oxide %
CL-07-01-8	Diorite	~5 (<8)	70	5	-	2-3(Ilm)
CL-07-01-9.1	Clinopyroxenite	<5cm	5	70	-	20 (60M/40I)
CL-07-01-29.1	Gabbro	~3(<7)	60-65	20-25	3-5	5 (60M/40I)
CL-07-01-50.2	Olivine Gabbro	~1.5 (<5)	20	55	15	10(50/50)
CL-07-01-52.3	Gabbro		50	35	Tr	15 (60I/40M)
CL-07-01-55.9	Gabbro	<25	20	60	-	15 (70I/30M)
CL-07-01-67.5	Gabbro	~5 (<10)	35	50	2-3	10 (50/50)
CL-07-01-79.3	Gabbro	<7	70	15	5	Tr
CL-07-01-95.9	Clinopyroxenite	~3 (<7)	5	75	-	15 (60I/40M)
CL-07-01-101	Olivine Gabbro	<4	45	30	10	15
CL-07-01-113.8	Olivine Gabbro	<4	50	5	30	15
CL-07-01-115.7	Gabbro	<20	75	20	-	3
CL-07-01-117.2	Dunite	<3	-	15	80	5 (50/50)
CL-07-01-124.3	Gabbro	<3	45	50	Tr	5
CL-07-01-127	Pegmatite Gabbro	< 4 cm				15
CL-07-01-128.1	Gabbro	<5 (2)	65	20-25	2	7
CL-07-01-134.3						
CL-07-01-140	Olivine CPX	<2.5 (1)	5	47	20-25	20
CL-07-01-145.7						
CL-07-01-156.3						
CL-07-01-166.4	Gabbro	<3 (1)	80	15	Tr	5
CL-07-01-167A1	Pegmatite Gabbro	< 4 cm	30	40		2
CL-07-01-167A2	Pegmatite Gabbro	< 4 cm	30	40		3
CL-07-01-167B			40-45	25-30	5	10
CL-07-01-171.5	Wehrlite	<20 (5)	10	45	40	5
CL-07-01-173.9						
CL-07-01-180.1	Gabbro	<9 (4)	25	70	-	5
CL-07-01-203.6	Gabbro	<6 (2.5)	70	25	-	3
CL-07-01-233	HBL Qtz Syenite	-	-	-	-	-
CL-07-01-249.9	Olivine Gabbro	<4 (1)	45	22	20	7
CL-07-01-251.6	HBL Qtz Syenite	-	-	-	-	-
CL-07-01-271	Gabbro	<8 (5)	85	8	4	2
CL-07-01-275.7	Gabbro	<12 (5)	65	25	5	5
CL-07-01-277.4	Gabbro	<18 (10)	75	20	-	5
CL-07-01-287.1	Gabbro	<5 (1.25)	40	45	8	5
CL-07-01-308.8	Oxide rock	<2.5 (1)	-	-	20	80
CL-07-01-322	Oxide Anorthosite	<8 (3)	60-65	-	-	30
CL-07-01-327.3	Olivine Gabbro	<2 (.7)	35	50	15	3
CL-07-01-329	Oxide Troctolite	<4 (.5)	15	2	45	35
CL-07-01-354	Gabbro		40-45	30-35	4-6	5
CL-07-01-367		<.5 (2)	7	2	18	65
CL-07-01-373	Olivine Gabbro	<15	50-55	5	10-15	15

Sulfide %		Plagioclase Alteration	CPX Alteration	Olivine Alteration	Comments
Tr		s	s	-	1% Ap, 10-15% Amp, 5% Bt
Tr		w	m	-	3% Bt, graphic Mag text; Pl inc in Mag
Tr		Tr	m	m-s	5-7% Ap, 2-3% Bt, Plag ~4mm; Cpx/Oliv ~2mm
1-2 (Po,Ccp)		Tr	w	w	Plag massive oik? Lrg Ap <5mm,1%
	1	Tr	w	m-s	
Tr		w	m-s	-	Py replace Mag; Mag str alt but only rare Py replace
3 (Po, Ccp, Pn)		m	w	w	Amp 2%
	2	m	m-s	c	
1 (Po, Ccp)		Tr	w	-	7% Bt, Tr Ap (1grain)
Tr		w	Tr	m-s	
		Tr	Tr	w	
	1	w	w	-	
1 (Po, Ccp)		-	m	C	OPX?
1 (Po, Ccp,Pn)		Tr	Tr	s	
1 (Po, Ccp, Py, Pn)		s	s		Extremely coarse grained apatite
2 (Po, Ccp, Pn, Sp)		w	w	m-s	Tr interst Ap, Plag incs in CPX
		m			
1 (Po, Pn, Ccp)		Tr	w	w	Interst Plag, "cumul" CPX Oliv, 3% Amp
		w	w		
		w			Thin Sections Does Not Represent Handsample
Tr (Po, Py, Ccp)		w	w	w	Tr Bt, 2% Amp, Tr KFS
Tr (Po, Ccp, Pn, Py)		s	s	-	Coarse grained apatite
Tr (Po, Ccp, Pn, Py)		s	s	-	
		m	m		
1 (Po, Py,Ccp,Pn)		m	w-m	m-s	Mag alt in fracs of oliv
		m	w		5% CG Ap w/incs in CPX, Mag, Bt
1 (Po,Ccp,Pn,Py)		m	w	-	Tr Ap, 2%Amp/Bt on oxides
Tr (Py,Ccp,Po,Pn)		m-s	m	-	1% interst Ap, 3% Bt, Pl inclusions in CPX, CPX interst
-		-	-	-	
1 (Po,Pn,Ccp,Py)		w	w	m-s	5% Bt/Amp halo, Tr Ap
-		-	-	-	
Tr (Po, Ccp, Py)		w	m	m	
Tr (Po, Ccp)		w	m	m	
1 (Po, Py alt)		w	s	-	
1 (po, ccp, pn, py)		w	m	m-s	
(po, Py, Ccp, Pn)		-	-	w	1% Spinel
(po, Py, Ccp, Pn)		m	-	-	5% Bt
1 (Po Pn Ccp)		Tr	w	s	
Tr (Po, Ccp)		Tr	m	m-s	Tr Bt, 1-2% Spinel, Oliv alt to act w/ mag in fracs
Tr					
Tr (Po Pn)		w	s	m-s	Spinel (3%) Amp (5%)
	2				Tr Ap

Appendix 11: February 2013 whole rock major and trace element geochemistry

Sample	CL-07-01-8	CL-07-01-115.7	CL-07-01-167.76	CL-07-01-322.4	CL-07-01-325.6
SiO_2 (wt%)	46.5	42.6	39.1	21.9	43.7
TiO_2	2.60	2.25	2.61	8.00	2.70
Al_2O_3	18.3	15.9	13.3	8.80	11.1
Fe_2O_3	11.3	13.1	18.4	44.8	16.0
MnO	0.24	0.14	0.19	0.33	0.20
MgO	3.73	8.10	8.31	4.16	8.62
CaO	7.28	13.0	10.2	6.03	13.7
Na_2O	3.88	1.71	1.86	1.15	1.73
K_2O	1.69	0.53	0.44	0.20	0.15
P_2O_5	0.25	0.063	0.35	0.089	0.042
LOI	3.3	1.40	4.15	-0.49	0.81
Ba (ppm)	524	145	199	85.2	99.3
Be	0.61	0.37	0.57	0.28	0.42
Bi	<0.15	0.15	<0.15	<0.15	<0.15
Cd	0.172	0.196	0.209	0.126	0.153
Ce	20.13	11.33	31.81	10.37	12.68
Co	21.98	65.66	59.53	137.83	65.3
Cr	17	660	71	105	486
Cs	1.77	0.377	1.995	0.204	0.258
Cu	2	363.9	142.4	92.8	92.1
Dy	1.735	1.382	3.034	1.142	2.271
Er	0.636	0.562	1.122	0.48	0.917
Eu	2.1135	0.9821	2.0192	0.7205	1.2892
Ga	21.11	21.52	22.59	34.17	18.06
Gd	2.626	1.927	4.559	1.626	3.024
Hf	1.23	1.09	1.54	2.01	1.44
Ho	0.2795	0.2351	0.4929	0.1951	0.3788
In	0.0659	0.0557	0.0775	0.1039	0.0785
La	8.57	4.87	12.56	4.27	4.47
Li	24.9	13.6	18.9	11.2	10.1
Lu	0.0625	0.0534	0.104	0.0484	0.0908
Mo	1.38	1.32	0.73	1.52	0.69
Nb	9.528	3.861	9.1	22.356	3.955
Nd	13.41	7.98	22.3	7.04	10.88
Ni	4.8	489.7	190.2	125.7	139.6
Pb	4	1.6	1.8	1.4	0.8
Pr	2.902	1.685	4.724	1.507	2.138
Rb	55.97	8.3	13.27	4.19	2.68
Sb	<0.04	<0.04	<0.04	<0.04	<0.04
Sc	10.8	26.3	13.2	18.9	40.9
Sm	2.947	1.983	5.049	1.699	2.984

Sn	10.97	0.69	1.51	0.9	0.45
Sr	1172.6	683.9	672.5	350.3	560.4
Ta	0.664	0.278	0.573	1.618	0.286
Tb	0.3288	0.2615	0.564	0.2152	0.4115
Th	0.539	0.28	0.433	0.175	0.113
Ti	16388	13909	15809	>25000	16860
Tl	0.27	0.055	0.17	0.027	0.022
Tm	0.075	0.068	0.14	0.056	0.11
U	0.12	0.074	0.11	0.059	0.033
V	74.4	376	342	1410	389
W	3.66	0.050	0.20	0.18	<0.05
Y	7.01	5.92	12.2	4.94	9.73
Yb	0.43	0.38	0.75	0.34	0.66
Zn	139	76.0	98.0	319	102
Zr	45.0	33.0	50.0	70.0	40.0

CL-07-01-354.2	CL-07-01-371.2	CL-07-01-373	CL-07-01-380	CL-07-01-422.9
41.3	41.9	36.0	39.1	38.3
3.25	3.65	6.42	4.01	4.77
12.5	13.0	11.8	16.7	16.5
20.0	19.0	29.1	19.5	22.5
0.22	0.22	0.29	0.22	0.20
7.97	7.23	8.10	5.91	4.46
10.5	10.9	5.15	7.49	6.97
2.16	2.26	2.03	2.6	2.88
0.24	0.27	0.65	0.68	0.52
0.17	0.12	0.11	0.12	0.16
0.48	0.59	-0.08	2.42	1.28
151	149	167	193	229
0.54	0.49	0.63	0.79	0.73
<0.15	<0.15	<0.15	<0.15	<0.15
0.118	0.137	0.092	0.421	0.17
20.12	15.46	13.73	13.21	21.86
88.04	72.8	104.46	73.21	101.95
321	163	57	17	227
0.262	0.361	1.031	4.597	1.31
197.2	65.7	54.5	18.6	120.4
2.208	1.805	1.1	0.769	1.493
0.89	0.729	0.49	0.317	0.602
1.4085	1.3379	0.9818	1.113	1.4591
20.55	21.29	21.66	21.66	27.48
3.055	2.496	1.531	1.192	2.248
1.28	1.03	1.62	0.84	1.25
0.371	0.2995	0.1936	0.131	0.2475
0.0694	0.069	0.0629	0.048	0.059
8.43	6.73	6.29	6.27	9.99
8.5	14.7	17.3	31.1	28.5
0.0873	0.0678	0.0583	0.0345	0.0576
0.83	0.73	1.18	0.75	0.94
7.052	6.307	17.809	7.747	8.396
13.73	10.73	7.97	7.22	12.8
179.7	88.5	40.8	20.2	107.3
1	0.9	2.3	13.3	1.6
2.922	2.269	1.854	1.726	2.945
3.48	3.81	22.65	25.98	12.32
<0.04	<0.04	<0.04	0.04	<0.04
26.1	25.5	8.8	4.6	12.2
3.249	2.61	1.733	1.398	2.563

0.52	0.43	0.95	5.27	0.54
622.7	670.1	697.7	1054.7	765.6
0.473	0.435	1.263	0.531	0.62
0.4097	0.3275	0.2015	0.1533	0.2802
0.231	0.174	1.228	0.383	0.666
20328	22753	>25000	>25000	>25000
0.02	0.018	0.14	0.44	0.049
0.11	0.087	0.064	0.039	0.072
0.067	0.046	0.54	0.09	0.16
449	430	535	361	563
0.090	0.060	0.38	0.71	0.88
9.45	7.62	5.17	3.44	6.47
0.63	0.51	0.41	0.23	0.42
131	125	206	276	181
41.0	33.0	60.0	33.0	43.0

CL-07-02-347	CL-07-03-169	CL-07-05-11	CL-07-05-14	CL-07-05-30.2	CL-07-05-50
45.4	44.2	15.3	40.0	40.1	39.3
1.47	1.79	8.00	4.32	4.21	3.53
15.0	14.9	4.83	6.46	13.0	9.10
12.8	11.7	50.9	19.9	18.4	19.9
0.14	0.14	0.36	0.26	0.18	0.18
8.15	8.34	13.5	11.1	7.96	9.21
11.7	13.0	0.58	15.0	9.67	13.9
2.31	1.73	0.050	0.63	1.77	0.72
0.44	1.12	0.030	0.44	1.26	0.90
0.013	0.0070	0.0060	0.038	0.04	0.022
1.82	2.33	3.18	1.20	2.49	1.81
96.9	889	8.30	76.7	278	119
0.34	0.6	0.08	0.76	0.72	0.4
<0.15	<0.15	<0.15	0.17	<0.15	0.29
0.118	0.351	0.06	0.394	0.236	0.381
4.85	5.63	1.41	19.92	8.94	10.65
69.43	53.11	>187	90.62	72.84	109.73
420	547	>4500	104	9	449
1.23	3.591	0.218	0.583	2.138	2.227
150.7	100.6	696.1	352.4	112.4	1005.7
0.897	1.412	0.292	3.527	1.498	1.971
0.423	0.591	0.12	1.468	0.614	0.807
0.6049	0.7214	0.1084	1.3273	0.8788	0.9386
19.85	21.55	39.75	19.73	23.43	19.46
1.104	1.74	0.358	4.428	1.989	2.625
0.48	0.74	0.59	2.45	1.07	1.58
0.1604	0.2416	0.0494	0.594	0.2539	0.3393
0.0408	0.0643	0.0827	0.1028	0.0746	0.1036
2.29	1.94	0.58	7.38	3.48	3.83
33.9	45.9	10.3	27.1	50.7	40.1
0.043	0.0584	0.0148	0.1309	0.0573	0.0776
0.33	0.35	0.56	0.6	0.47	0.59
1.213	0.412	3.545	9.632	4.282	4.187
3.73	5.42	1.16	15.62	7.23	9.02
205.4	321.2	1318	417.2	101.2	852.5
5.6	32.4	2.7	5.1	3.4	5.7
0.748	1.019	0.227	3.125	1.4	1.758
18.12	38.06	1.07	13.8	33.98	26.25
0.07	<0.04	<0.04	<0.04	<0.04	0.07
27.4	30.4	14.6	50.8	32.8	45.1
1.039	1.644	0.354	4.343	1.949	2.59

0.45	5.28	0.4	1.1	0.6	3.02
412.9	467	27.4	124.6	458.4	178.2
0.086	0.043	0.29	0.667	0.322	0.324
0.1606	0.2529	0.0519	0.638	0.2699	0.3671
0.104	0.031	<0.018	0.726	0.238	0.42
9113	10951	>25000	>25000	>25000	21710
0.13	0.27	0.086	0.11	0.15	0.23
0.053	0.075	0.016	0.18	0.073	0.099
0.048	0.019	<0.011	0.23	0.054	0.19
492	465	2190	942	983	801
0.17	0.85	<0.05	0.28	0.10	0.46
4.31	6.22	1.27	15.2	6.47	8.55
0.30	0.44	0.10	0.98	0.43	0.58
117	148	329	120	129	112
14.0	15.0	17.0	74.0	30.0	43.0

CL-07-05-105	CL-07-05-117	CL-07-05-142.8	CL-07-05-144	CL-07-05-499	CL-07-05-675
45.3	30.5	33.8	38.1	40.2	2.9
3.41	4.26	3.79	2.63	4.43	8.00
14.2	4.72	7.09	10.6	11.9	4.94
15.1	32.1	27.4	21.6	19.2	68.8
0.22	0.24	0.23	0.19	0.28	0.33
5.33	18.1	14.4	13.1	5.53	5.00
10.7	3.28	8.09	7.49	10.9	0.071
2.87	0.31	0.35	0.69	2.26	0.00
1.36	0.32	0.27	1.15	1.32	0.06
0.17	0.012	0.019	0.040	0.85	0.0050
1.28	5.15	3.25	3.21	1.26	0.04
465	52.9	53.8	163	503	3.60
0.76	1.23	0.22	0.4	17.54	0.1
<0.15	0.17	0.25	0.33	0.37	<0.15
0.135	0.07	0.253	0.279	0.548	0.032
27.01	44.04	5.44	8.32	270.96	0.74
40.72	166.57	141.21	117.26	71.69	>187
13	2949	1614	1084	29	176
1.282	1.967	2.16	4.125	4.9	0.027
10.6	317.5	773.1	900.3	113.3	10.5
2.84	3.245	1.035	1.137	27.935	0.061
1.133	1.554	0.42	0.491	13.726	0.029
2.1162	0.6674	0.4962	0.6096	4.7877	0.0687
22.58	20	19.76	19.91	23.42	49.1
4.032	4.078	1.349	1.482	31.867	0.073
2.07	6.03	0.9	1.01	25.21	0.86
0.4722	0.5795	0.1759	0.1951	5.1748	0.0099
0.0764	0.0836	0.0733	0.0635	0.1932	0.0877
11.3	18.72	2.04	3.48	109.24	0.33
27.8	16.5	60.9	68.6	25.7	1.2
0.1141	0.1578	0.0448	0.0514	1.3341	0.004
1.22	0.67	0.36	0.37	1.66	0.54
13.297	21.976	2.948	3.584	88.513	7.735
18.62	23.45	4.59	5.69	146.67	0.39
22.8	1011.7	850	790	77	298.1
5	2.1	2.3	2.9	88.8	0.7
3.941	5.83	0.875	1.227	35.933	0.095
34.19	24.09	9.49	30.65	79.16	0.65
<0.04	<0.04	<0.04	<0.04	0.08	<0.04
23.6	14.9	28.7	24.7	22.3	10.7
4.324	4.909	1.302	1.512	34.58	0.092

0.76	1.47	0.88	1.22	>14	1.21
687.3	96.6	91.3	178.4	478.2	4.9
0.89	1.326	0.219	0.264	5.892	0.66
0.5315	0.5837	0.1829	0.2022	4.8699	0.0106
0.846	3.259	0.178	0.545	26.726	0.023
21113	>25000	23320	16431	>25000	>25000
0.17	0.24	0.19	0.31	0.37	0.031
0.14	0.20	0.053	0.062	1.80	0.0037
0.26	1.10	0.038	0.20	3.65	<0.011
250	966	840	571	438	4231
0.88	0.30	0.16	1.04	3.24	0.20
12.2	15.7	4.46	5.11	135	0.27
0.81	1.19	0.30	0.37	10.4	0.025
113	175	178	125	407	396
76.0	237	24.0	30.0	1109	27.0

CL-07-07-10.1	CL-07-07-17	CL-07-07-450	CL-07-07-483	CL-07-14-323.5	CL-07-14-477.5
44.6	40.6	43.8	46.3	33.4	40.3
3.54	3.97	4.00	2.58	6.55	3.12
13.2	12.2	17.0	10.6	8.75	13.8
16.0	19.7	13.5	13.2	28.5	19.3
0.19	0.19	0.17	0.20	0.22	0.15
6.42	7.29	4.79	8.40	8.12	6.25
11.3	12.0	10.6	15.8	12.2	11.3
2.45	1.94	3.10	1.85	0.96	2.15
0.55	0.54	0.99	0.59	0.20	0.82
0.082	0.11	0.088	0.066	0.038	0.07
1.06	0.68	1.18	0.87	0.32	1.35
162	146	350	179	67.3	279
0.7	0.65	2.39	0.53	0.29	0.47
<0.15	<0.15	<0.15	<0.15	<0.15	0.35
0.153	0.192	0.152	0.17	0.248	0.496
21.31	21.59	14.63	18.06	9.37	15.73
65.21	82.24	53.52	44.16	114.19	108.27
21	53	20	56	92	122
0.829	0.725	1.473	0.549	0.388	1.581
84.8	190.3	21.1	20.2	380.4	1226.7
2.992	2.667	1.575	2.819	1.758	2.209
1.256	1.095	0.664	1.114	0.715	0.913
1.5902	1.355	1.1954	1.5099	0.9085	1.2909
21.64	23.69	22.35	16.97	25.06	23.44
4.034	3.559	2.141	3.94	2.342	2.999
1.87	2.27	1.01	1.64	1.49	1.55
0.5177	0.4526	0.2699	0.4755	0.302	0.3818
0.083	0.0874	0.0513	0.089	0.0924	0.0924
8.16	8.85	6.81	6.64	3.44	6.18
20.7	15.9	26.3	21.9	20.5	23.7
0.1241	0.1015	0.058	0.1067	0.0664	0.0855
0.82	0.83	0.64	1.04	0.74	1.83
9.523	11.528	7.562	5.483	6.085	6.287
16.33	14.72	9.56	14.98	8.22	11.85
94	187.4	13.9	47.7	299.4	906.5
3.1	3.8	6.7	5.5	2.7	9.1
3.319	3.153	2.041	2.932	1.568	2.438
17.63	18.68	53.78	20.21	6.04	25.55
<0.04	<0.04	0.05	<0.04	<0.04	0.04
24.2	28.7	17.7	39.2	34.1	25.7
4.164	3.674	2.289	3.971	2.299	3.072

0.95	1.09	3.19	0.64	0.79	2.26
600.8	527.2	814.3	433.2	306.6	558.1
0.689	0.745	0.466	0.356	0.441	0.44
0.5531	0.4916	0.2873	0.5386	0.3218	0.4052
0.585	0.614	0.645	0.475	0.203	0.35
21635	24270	>25000	15584	>25000	19397
0.15	0.10	0.24	0.086	0.041	0.27
0.15	0.13	0.080	0.13	0.082	0.11
0.27	0.20	0.32	0.13	0.05	0.12
599	758	450	316	1374	581
0.36	0.35	1.01	1.15	0.07	2.44
13.2	11.5	7.44	11.9	7.47	9.54
0.91	0.77	0.45	0.77	0.50	0.62
77.0	133	106	85.0	167	136
58.0	77.0	32.0	48.0	41.0	48.0

CL-07-15-145
48.6
1.60
20.8
9.27
0.13
1.67
8.97
4.20
1.65
0.42
2.03
661
0.99
<0.15
0.127
35.53
23.79
20
1.895
5.1
2.183
0.853
2.8451
25.07
3.544
1.45
0.3613
0.0812
15.65
26.7
0.0777
1.72
11.033
20.76
7.2
4.3
4.778
55.18
0.05
6
4.223

6.85
1321.7
0.671
0.4302
0.996
10012
0.28
0.099
0.24
50.7
1.48
9.47
0.56
80.0
57.0

Appendix 12: Summer 2013 whole rock major element geochemistry

Sample	SiO_2 (wt%)	TiO_2	Al_2O_3	Fe_2O_3	MnO	MgO	CaO	Na_2O	K_2O	Cr_2O_3	P_2O_5	BaO	LOI	Total
CL-06-16-8.9	41.7	2.84	16.3	16.0	0.14	7.43	11.1	1.89	1.07	0.01	0.032	<0.004	1.22	99.7
CL-06-16-11.2	38.7	3.82	12.6	20.2	0.17	7.56	11.5	1.93	0.73	<0.002	0.047	<0.004	1.84	99.07
CL-06-16-14.1	71.7	0.19	11.8	4.95	0.12	0.97	0.53	6.88	0.9	<0.002	0.011	<0.004	0.81	98.83
CL-06-16-33.7	40.1	3.65	13.4	18.9	0.16	7.58	12.2	1.51	0.92	0.01	0.028	<0.004	1.02	99.49
CL-06-16-35.7	40.9	2.17	5.97	21.7	0.23	14.03	12.7	0.91	0.2	0.08	0.066	<0.004	1.16	100.12
CL-06-16-47.0	38.2	4.01	11.8	23.1	0.21	7.05	10.7	1.77	0.57	0.01	0.061	<0.004	1.88	99.32
CL-06-16-51.2	74.0	0.12	11.8	3.47	0.022	1.37	0.57	4.46	2.71	<0.002	0.003	0.01	1.24	99.77
CL-06-16-63.15	41.7	3.62	13.7	18.4	0.20	6.88	11.2	2.02	0.94	<0.002	0.107	0.01	1	99.76
CL-06-65.7	74.7	0.08	12.7	2.76	0.031	1.01	0.47	6.45	0.69	<0.002	0.003	<0.004	1.02	99.91
CL-06-16-71.15	39.1	3.66	12.7	22.0	0.19	7.38	10.9	1.75	0.63	0.01	0.084	<0.004	1.16	99.64
CL-06-16-80.0	44.5	3.4	12.1	18.2	0.21	7.06	10.6	1.92	0.84	<0.002	0.164	0.01	0.48	99.59
CL-06-16-83.5	43.1	3.91	13.7	17.8	0.18	6.67	10.4	1.98	0.7	0.01	0.11	0.01	0.99	99.58
CL-06-16-90.0	50.1	2.13	16.6	14.2	0.12	3.56	6.00	3.94	0.94	0.02	0.71	0.03	1.03	99.36
CL-06-16-103.0	35.3	3.33	13.4	17.6	0.17	7.34	10.8	1.64	0.66	0.01	0.11	0.01	8.69	99.07
CL-06-16-152.45	40.4	3.18	13.0	17.1	0.15	7.65	13.2	1.31	0.89	0.01	0.037	<0.004	2.41	99.36
CL-06-16-155.6	74.0	0.13	12.0	1.4	0.041	0.85	1.45	4.1	3.17	<0.002	0.009	0.03	2.68	99.86
CL-06-16-170.6	46.9	2.07	12.3	15.5	0.14	5.05	7.18	2.29	0.43	0.01	0.20	0.01	7.57	99.68
CL-06-39-4.1	39.1	4.09	9.82	20.9	0.20	9.37	13.4	1.23	0.56		0.11		0.41	99.19
CL-06-39-6.85	40.1	3.36	11.1	17.8	0.17	9.38	14.4	1.1	0.47		0.058		0.95	98.82
CL-06-39-10.98	37.9	4.48	14.6	22.1	0.16	6.00	11.1	1.77	0.57	<0.002	0.025	<0.004	0.87	99.52
CL-06-39-17.2	41.1	6.68	12.0	17.8	0.23	6.61	11.2	2.35	0.26	<0.002	0.22	<0.004	0.27	98.74
CL-06-39-20.35	32.3	3.62	3.86	32.7	0.31	18.7	5.15	0.36	0.07	0.29	0.071	<0.004	1.54	98.95
CL-06-39-32.21	32.1	3.14	4.24	28.7	0.21	19.9	4.95	0.26	0.08	0.32	0.018	<0.004	5.39	99.33
CL-06-39-32.82	29.7	3.71	2.88	32.0	0.24	20.4	3.85	0.12	0.01	0.43	0.007	<0.004	5.36	98.77
CL-06-39-33.28	23.6	5.39	3.77	39.3	0.31	18.8	1.27	0.09	0.02	0.64	0.006	<0.004	5.38	98.61
CL-06-39-47.36	28.8	5.56	5.29	36.4	0.31	13.2	4.38	0.96	0.31		0.18		2.86	98.19
CL-06-39-57.38	34.9	4.88	9.8	26.8	0.36	10.5	5.45	1.8	0.66		0.572		3.35	98.97
CL-06-39-60.23	22.7	5.34	4.16	41.4	0.26	18.0	1.54	0.16	0.03	1.08	0.012	<0.004	4.5	99.2
CL-06-39-83.9	34.3	2.35	4.21	17.4	0.5	15.2	13.7	0.25	0.11	0.21	0.031	<0.004	10.53	98.69
CL-06-39-94.95	26.4	4.96	5.13	35.8	0.26	18.1	3.32	0.26	0.07	0.59	0.005	<0.004	4.88	99.7
CL-06-39-100.0	49.4	1.7	16.4	11.1	0.11	4.42	5.86	5.89	0.87		0.88		2.46	99.09
CL-06-39-103.55	40.4	2.8	18.4	16.2	0.14	5.86	10.2	2.09	0.6	0.19	0.10	<0.004	1.77	98.78
CL-06-39-103.91	40.0	2.49	19.1	15.5	0.13	6.06	10.6	1.57	1.43		0.059		2.29	99.22
CL-06-39-105.83	39.9	6.58	11.9	21.3	0.22	6.55	9.93	2.34	0.26	<0.002	0.077	<0.004	0.49	99.54
CL-06-39-108.0	34.6	3.42	4.97	28.4	0.24	17.6	6.83	0.6	0.09	0.36	0.051	<0.004	2.01	99.03
CL-06-39-118.75	49.7	2.36	20.3	9.4	0.10	3.46	4.75	5.44	0.76	<0.002	0.22	0.02	3.22	99.72
CL-06-39-122.3	42.7	5.09	14.9	16.7	0.20	4.26	9.58	3.3	0.75	<0.002	0.29	0.01	0.88	98.63
CL-06-39-125.0	51.7	0.58	23.5	4.58	0.057	1.47	5.53	5.76	2.29	<0.002	0.19	0.03	4.39	100.02
CL-06-39-128.4	39.4	7.06	11.0	21.3	0.24	7.32	10.3	2.07	0.2	0.01	0.074	<0.004	0.32	99.21
CL-06-39-132.47	38.7	4.49	11.8	22.1	0.19	7.02	11.9	1.78	0.83		0.16		0.83	99.68
CL-06-39-133.4	43.3	2.78	16.1	13.8	0.14	5.56	11.3	2.83	1.59		0.28		2.06	99.61
CL-06-39-150.08	40.7	7.66	11.6	19.6	0.23	7.42	10.5	2.22	0.23	<0.002	0.046	<0.004	-0.05	100.19

CL-06-39-156.97	42.0	2.11	11.8	15.4	0.16	9.48	12.8	1.85	0.52		0.061		3.06	99.17
CL-07-01-9.1	33.7	>8.00	5.06	29.7	0.48	6.51	13.0	1.11	0.29		1.406		-0.24	99.27
CL-07-01-29.1	39.3	4.55	11.0	22.5	0.33	5.11	10.6	2.69	0.43	<0.002	2.53	0.03	0.39	99.49
CL-07-01-50.2	37.2	7.3	8.73	26.3	0.34	7.14	10.3	1.81	0.2	<0.002	0.35	0.01	0.19	99.86
CL-07-01-52.3	42.2	6.2	12.8	18.0	0.23	5.58	10.4	2.7	0.35	<0.002	0.099	0.02	1.21	99.74
CL-07-01-55.9	41.7	5.35	12.5	18.5	0.25	5.81	10.4	2.74	0.37		0.087		1.55	99.18
CL-07-01-67.5	35.6	5.71	10.9	25.8	0.23	7.55	11.6	1.36	0.33		0.02		0.46	99.47
CL-07-01-67.5SP	35.5	5.87	11.0	26.0	0.23	7.49	11.5	1.38	0.33		0.02		0.53	99.85
CL-07-01-76.9	48.7	2.73	16.5	14.6	0.18	2.18	6.38	5.41	1.01		0.23		1.85	99.66
CL-07-01-79.3	44.5	1	21.9	11.0	0.10	5.2	10.5	2.65	0.61	0.01	0.11	0.02	1.77	99.35
CL-07-01-95.9	41.2	4.56	12.7	19.0	0.22	6.67	11.9	2.2	0.45		0.06		0.74	99.66
CL-07-01-101	32.7	5.65	14.2	28.8	0.19	6.15	9.11	1.41	0.26	0.02	0.039	<0.004	0.59	99.09
CL-07-01-113.8	33.3	7.38	8.87	32.5	0.34	8.12	7.90	1.63	0.19	<0.002	0.27	<0.004	-0.54	99.92
CL-07-01-117.2	26.1	5.5	3.17	37.3	0.34	18.3	3.37	0.13	0.01	0.46	0.016	<0.004	4.67	99.34
CL-07-01-124.3	41.4	4.87	12.7	19.8	0.21	6.59	12.2	2.09	0.16	<0.002	0.018	<0.004	0.18	100.09
CL-07-01-127	28.7	6.56	4.1	33.8	0.42	6.84	12.7	0.94	0.44		4.09		0.3	98.85
CL-07-01-128.1	37.4	4.52	13.2	23.7	0.21	7.54	11.3	1.46	0.2	0.01	0.033	<0.004	0.39	99.97
CL-07-01-134.3	42.2	1.69	17.8	13.9	0.16	9.06	11.3	1.73	0.5		0.053		1.05	99.35
CL-07-01-145.7	29.6	>8.00	5.93	35.6	0.37	6.93	10.5	0.94	0.14		0.16		-0.37	98.97
CL-07-01-156.3	37.8	4.87	13.2	23.5	0.25	4.93	9.90	2.43	0.4		0.21		0.99	98.5
CL-07-01-166.4	39.1	3.8	16.5	19.3	0.14	6.5	11.5	1.75	0.3	0.08	0.026	<0.004	0.77	99.71
CL-07-01-171.5	32.0	4.42	6.96	32.1	0.28	15.4	6.95	0.73	0.09		0.102		0.6	99.56
CL-07-01-173.9	39.0	4.62	10.3	24.4	0.32	4.14	11.2	3.06	0.59		1.97		0.02	99.57
CL-07-01-180.1	40.0	3.66	10.8	18.4	0.21	8.58	14.3	1.22	0.53		0.073		1.35	99.11
CL-07-01-203.6	43.2	2.91	16.6	14.6	0.13	5.57	13.5	2.02	0.58	<0.002	0.074	0.01	1.13	100.22
CL-07-01-222.1	35.7	4.96	11.8	25.0	0.17	7.06	12.3	1.31	0.51		0.043		0.6	99.43
CL-07-01-233	74.4	0.35	12.6	2.6	0.024	0.72	0.79	6.53	1.07	<0.002	0.14	0.01	0.84	100.03
CL-07-01-249.9	41.0	7.07	14.7	18.7	0.21	6.36	7.88	2.76	0.47	<0.002	0.077	<0.004	0.52	99.68
CL-07-01-251.6	76.1	0.09	12.7	1.5	0.018	0.28	0.50	4.21	4.58	0.01	0.028	0.04	0.5	100.6
CL-07-01-271	41.8	6.63	14.5	17.2	0.19	5.72	9.25	2.85	0.49		0.11		0.22	98.87
CL-07-01-275.7	43.4	6.03	13.3	15.8	0.20	6.3	10.3	2.72	0.5		0.29		0.16	99.04
CL-07-01-275.7SP	43.5	5.96	13.5	15.6	0.20	6.25	10.3	2.74	0.48		0.28		0.03	98.78
CL-07-01-277.4	46.3	4.9	14.5	14.3	0.18	5.28	9.55	3.4	0.63	<0.002	0.17	0.01	0.64	99.89
CL-07-01-287.1	43.1	3.44	12.8	17.4	0.19	7.12	12.4	2.1	0.36	0.01	0.13	0.01	0.55	99.56
CL-07-01-327.3	46.2	2.01	10.9	14.0	0.20	9.54	14.2	1.76	0.14	0.07	0.056	<0.004	0.69	99.87
CL-07-01-380	39.1	4.01	16.7	19.5	0.22	5.91	7.49	2.6	0.68		0.12		2.42	98.73
CL-07-01-381.7	43.1	2.7	18.6	16.3	0.18	6.08	7.42	3.04	0.83	<0.002	0.093	0.01	1.32	99.7
CL-07-01-429.8	73.2	0.18	13.5	1.79	0.025	0.16	0.55	4.31	5.37	<0.002	0.007	0.08	0.97	100.22

Appendix 13: Summer 2013 whole rock trace element geochemistry

Sample	Ba (ppm)	Be	Bi	Cd	Ce	Co	Cr	Cs	Cu	Dy	Er	Eu	Ga	Gd
CL-06-16-8.9	128.6	0.3	<0.47	0.23	8.09	78.38	108	1.443	305	1.071	0.455	0.785	22.19	1.488
CL-06-16-11.2	114.2	0.45	0.66	0.571	12.07	118.5	29	1.851	1172	1.699	0.68	0.91	21.93	2.251
CL-06-16-14.1	7.1	16.29	1.83	0.215	270.1	2.78	22	0.917	12.4	20.97	9.893	3.393	40.08	25.69
CL-06-16-33.7	118.2	0.4	<0.47	0.223	11.07	83.88	67	1.093	200	1.799	0.724	1.047	23.48	2.422
CL-06-16-35.7	57.1	0.48	1.08	0.78	16.16	131.3	641	0.693	979.9	2.575	1.047	1.09	14.36	3.331
CL-06-16-47.0	136.8	0.54	0.8	0.827	15.08	136	71	1.364	997.2	2.151	0.901	1.219	21.54	2.845
CL-06-16-47.6	41.6	0.24	1.35	1.078	16.77	975	58	0.718	4819	1.504	0.652	0.588	11.01	2.152
CL-06-16-51.2	57	2.62	<0.47	0.155	126.6	2.87	26	0.537	71.1	7.934	3.333	0.753	26.47	10.43
CL-06-16-52.5	132.7	0.49	0.49	0.526	14.89	276	59	1.361	4003	1.857	0.798	0.973	18.7	2.395
CL-06-55.0	77.7	0.38	0.71	0.624	14.18	281	104	1.068	3791	2.042	0.889	0.91	17.35	2.622
CL-06-16-56.3	135.6	0.64	0.74	0.475	18.48	295	51	1.102	3671	2.159	0.917	1.091	18.75	2.849
CL-06-16-57.5	94.7	0.39	0.96	0.725	13.96	421	36	0.775	5465	1.832	0.756	0.888	17.21	2.352
CL-06-16-58.6	133	0.47	0.77	0.739	13.39	256	35	0.702	3511	2.023	0.873	1.004	18.24	2.595
CL-06-16-59.9	148.3	0.46	0.75	0.818	17.01	108.8	82	0.886	863.4	2.279	0.953	1.238	21.76	3.031
CL-06-16-61.7	136.7	0.41	0.82	0.624	12.79	285	77	1.386	3177	1.921	0.829	0.965	18.65	2.496
CL-06-16-63.15	216.5	2.28	<0.47	0.456	22.26	73.52	57	1.591	188.6	2.801	1.198	1.482	25.23	3.73
CL-06-16-63.8	130.4	0.58	1.01	0.935	17.43	369	44	1.398	7206	2.29	0.998	0.958	17.46	2.937
CL-06-16-65.7	55.6	3.64	<0.47	1.334	355.3	4.19	24	0.333	50.6	14.58	8.87	1.155	30.63	17.36
CL-06-16-71.15	163.5	0.96	0.56	0.683	19.47	109.5	122	1.079	1331	2.268	0.955	1.194	23.69	3.089
CL-06-16-78.75	137.9	0.44	0.55	0.428	17.91	389	42	1.75	1944	2.32	1.035	1	16.02	2.907
CL-06-16-80.0	222.2	0.57	<0.47	0.77	21.07	67.93	15	1.308	539.4	3.385	1.543	1.31	21.56	4.254
CL-06-16-83.5	224.3	0.93	<0.47	0.263	22.39	74.8	50	1.69	314	2.746	1.155	1.488	24.4	3.683
CL-06-16-84.6	39.5	0.18	1.26	0.293	7.12	1118	13	1.485	10409	0.594	0.307	0.268	3.64	0.827
CL-06-16-90.0	350.8	1.21	<0.47	0.252	65.1	50	150	3.652	242.8	6.593	3.198	1.725	27.53	8.914
CL-06-16-103.0	154.7	1.08	<0.47	0.135	21.86	84.84	68	1.641	210	2.36	1	1.26	22.91	3.27
CL-06-16-152.45	152.7	0.56	<0.47	0.231	12.4	77.59	71	1.683	268.7	1.953	0.801	1.003	22.59	2.6
CL-06-16-155.6	280.9	3.11	<0.47	0.06	61.87	5.06	21	0.772	5.4	6.22	3.124	0.853	26.13	6.543
CL-06-16-170.6	125.8	1.44	<0.47	0.058	36.19	41.28	67	2.603	70.5	6.607	3.844	1.646	20.57	6.203
CL-06-39-4.1	117.2	0.62	<0.47	0.193	22.09	80.38	303	0.57	248	2.912	1.186	1.339	22.22	4.072
CL-06-39-6.85	83.8	0.4	<0.47	0.173	13.37	72.85	282	0.523	207.8	2.165	0.901	1.091	22.06	2.936
CL-06-39-10.98	109.8	0.3	<0.47	0.142	8.64	81.16	21	0.623	145.4	1.332	0.552	0.825	26.23	1.776
CL-06-39-17.2	148.6	0.39	<0.47	0.106	16.65	59.48	16	0.45	29.8	2.048	0.793	1.707	17.77	3.137
CL-06-39-20.35	33.1	0.22	<0.47	0.201	8.08	161.1	2065	0.588	453.7	1.15	0.474	0.612	14.61	1.642
CL-06-39-32.21	19.1	0.14	<0.47	0.064	4.14	164.7	2344	0.553	316.3	0.822	0.341	0.446	14.75	1.076
CL-06-39-32.82	3.8	0.1	<0.47	0.116	2.88	177.1	3022	0.232	407.7	0.744	0.306	0.285	15.58	0.95
CL-06-39-33.28	5.2	0.1	<0.47	0.031	1.89	>187	4366	0.308	567.7	0.412	0.169	0.184	21.09	0.55
CL-06-39-47.36	102.1	0.87	<0.47	0.232	29.2	132.8	>4500	1.114	707.3	3.059	1.345	0.991	26.39	3.919
CL-06-39-57.38	229.4	0.83	<0.47	0.694	49.04	92.97	1264	1.585	208.9	3.591	1.405	1.856	24.98	5.57
CL-06-39-60.23	12.7	0.1	0.54	0.061	2.28	>187	>4500	0.34	839.2	0.35	0.16	0.206	24.53	0.47
CL-06-39-63.88	20.5	0.14	<0.47	0.06	4.09	176.1	3468	0.465	205.8	0.673	0.288	0.335	15.81	0.867
CL-06-39-74.5	20.1	0.14	<0.47	0.089	4.26	177.1	2364	0.477	855.6	0.7	0.297	0.344	13.34	0.92
CL-06-39-83.9	11.2	12.01	1.17	0.706	59.17	114.9	1523	0.483	782.5	4.876	2.234	0.719	14.04	6.042

CL-06-39-88.63	7.7	0.14	<0.47	0.08	3.27	176.6	1940	0.368	1036	0.747	0.318	0.336	13.63	0.984
CL-06-39-94.95	17.5	0.18	<0.47	0.05	2.21	>187	4258	0.573	536.8	0.459	0.201	0.267	23.08	0.595
CL-06-39-99.7	45.2	0.24	<0.47	0.199	7.25	120.7	1255	0.517	548.8	1.46	0.594	0.714	25.37	1.959
CL-06-39-100.0	299.6	2.81	0.63	0.424	93.35	39.16	37	1.025	363	4.061	1.652	2.62	23.05	6.515
CL-06-39-103.55	146.4	0.62	<0.47	0.133	15.9	64.99	1449	0.838	219.2	1.319	0.529	1.232	26.26	1.888
CL-06-39-103.7	33.5	0.23	<0.47	0.253	7.29	170.4	>4500	0.389	711.5	1.183	0.471	0.607	33.48	1.602
CL-06-39-103.91	256	0.39	<0.47	0.156	10.59	68.38	820	0.738	318.8	1.029	0.428	0.848	25.57	1.43
CL-06-39-105.83	134.2	0.37	0.66	0.342	10.85	100.3	59	0.41	977.6	1.499	0.588	1.337	17.33	2.16
CL-06-39-108.0	43.7	0.31	<0.47	0.151	9.92	157.9	2526	0.584	436.5	1.614	0.675	0.8	16.26	2.139
CL-06-39-118.75	237.4	2.12	<0.47	0.373	19.91	17.92	25	1.514	82.1	1.484	0.668	1.308	22.22	2.075
CL-06-39-122.3	235.7	0.86	<0.47	0.477	27.29	51.56	41	3.771	147.4	2.459	0.941	1.939	23.29	3.688
CL-06-39-125.0	325	1.35	<0.47	0.03	18.02	7.3	60	0.999	6.6	1.083	0.442	1.689	23.12	1.655
CL-06-39-128.4	115.9	0.34	0.48	0.497	10.42	88.43	119	0.316	1510	1.597	0.615	1.272	16.82	2.301
CL-06-39-132.47	189.7	0.75	<0.47	0.182	25.96	74.49	106	1.252	123.5	2.323	0.963	1.109	26.08	3.342
CL-06-39-133.4	400.9	2.03	<0.47	0.315	36.74	55.92	18	3.697	282.9	3.247	1.415	1.48	23.57	4.441
CL-06-39-150.08	120.2	0.32	<0.47	0.089	8.92	78.93	97	0.526	26.7	1.369	0.532	1.194	16.72	2.043
CL-06-39-154.16	23.5	0.17	<0.47	0.099	4.1	167.5	>4500	0.899	421	0.7	0.29	0.355	23.03	0.926
CL-06-39-156.97	118.3	0.48	<0.47	0.138	16.98	52.45	182	0.963	30.5	2.924	1.196	1.41	21.6	3.989
CL-07-01-9.1	150.6	0.44	<0.47	0.219	58.61	55.95	8	0.39	13.3	5.691	2.01	3.36	19.76	9.517
CL-07-01-29.1	375.5	0.5	<0.47	0.135	92.55	47.76	21	0.323	12.9	6.417	2.231	4.831	18.78	11.74
CL-07-01-44.25	65.8	0.19	<0.47	0.147	116.5	82.34	17	0.329	16.3	8.127	2.718	4.699	11.36	14.96
CL-07-01-50.2	209.4	0.38	<0.47	0.153	24.99	73.35	21	0.233	17.5	2.671	1.008	2.143	18.22	4.269
CL-07-01-52.3	293.5	0.77	<0.47	0.105	18.11	53.21	16	0.447	14.4	2.154	0.863	2.142	19.33	3.193
CL-07-01-55.9	290.8	0.67	<0.47	0.144	18.76	49.65	13	0.691	8.5	2.24	0.867	1.996	19.93	3.188
CL-07-01-67.5	100.8	0.28	<0.47	0.229	8.25	87.25	69	0.269	107.5	1.726	0.705	0.993	25.55	2.291
CL-07-01-67.5SP	95.2	0.26	<0.47	0.214	8.23	78.76	72	0.246	76.7	1.852	0.735	1.015	25.97	2.48
CL-07-01-76.9	632	1.29	<0.47	0.25	41.46	22.58	15	3.299	15.4	3.019	1.214	3.487	27.62	4.436
CL-07-01-79.3	197.5	0.54	<0.47	0.168	15.65	76.09	110	0.626	464.5	0.933	0.397	0.96	22.16	1.363
CL-07-01-95.9	181.3	0.69	<0.47	0.151	21.41	62.41	15	0.373	77.7	2.492	0.999	1.612	21.56	3.484
CL-07-01-101	97.6	0.34	<0.47	0.172	8.05	112.2	184	0.296	340.4	0.992	0.409	0.723	29.86	1.354
CL-07-01-113.8	158.5	0.4	<0.47	0.105	21.14	104.6	32	0.183	69.2	1.929	0.73	1.452	21.57	3.045
CL-07-01-117.2	6.5	0.14	<0.47	0.097	4.76	160	3006	0.107	508.5	0.923	0.391	0.344	20.08	1.16
CL-07-01-124.3	113.1	0.3	<0.47	0.085	8.54	71.81	33	0.149	30.4	1.54	0.575	1.264	20.93	2.198
CL-07-01-127	146.7	1.18	<0.47	0.646	287.3	103.1	21	0.446	107.3	18.12	6.489	8.436	23.2	31.21
CL-07-01-128.1	92.9	0.24	<0.47	0.223	7	91.17	101	0.23	247	1.149	0.453	0.812	23.99	1.622
CL-07-01-128.4	22.6	0.12	<0.47	0.27	3.16	158.3	187	0.121	434.9	0.723	0.289	0.417	29.61	0.964
CL-07-01-134.3	102.3	0.32	<0.47	0.128	9.8	67.58	180	0.336	77.9	1.056	0.456	0.775	20.19	1.426
CL-07-01-140	60.3	0.34	<0.47	0.125	16.36	123.8	33	0.1	102.6	2.297	0.883	1.152	18.36	3.37
CL-07-01-145.7	91.2	0.32	<0.47	0.185	20.21	103.5	180	0.156	185.7	2.867	1.112	1.626	24.82	4.236
CL-07-01-156.3	237.9	1.23	<0.47	0.284	45.17	67.95	273	0.654	167	3.666	1.504	2.207	28.23	5.214
CL-07-01-159.4	4.6	0.14	<0.47	0.163	3.86	171.6	715	0.077	389.4	0.937	0.389	0.41	26.68	1.241
CL-07-01-166.4	106.2	0.3	<0.47	0.117	7.9	74.82	522	0.3	189.2	1.09	0.442	0.787	25.28	1.491
CL-07-01-171.5	58.4	0.28	<0.47	0.21	9.36	146.7	479	0.172	393.1	1.192	0.47	0.728	20.38	1.684
CL-07-01-173.9	429.2	1.21	<0.47	0.313	144.9	47.38	32	0.586	62.5	9.754	3.623	5.522	27.06	16.34

CL-07-01-180.1	114.1	0.9	<0.47	0.161	19.17	70.39	370	3.325	183.7	2.89	1.23	1.287	21.92	3.721
CL-07-01-203.6	155.5	0.46	<0.47	0.118	14.48	54.18	19	0.426	76.8	1.775	0.719	1.027	23.97	2.379
CL-07-01-222.1	119.3	0.3	<0.47	0.207	8.43	105.4	69	0.878	372.7	1.473	0.581	0.793	25.67	1.967
CL-07-01-233	90.5	2.52	<0.47	0.075	164.8	2.77	16	0.825	4.2	6.451	2.586	1.584	28.51	9.716
CL-07-01-249.9	193.1	0.36	<0.47	0.076	11.33	72.89	33	0.363	18.4	1.033	0.421	1.175	17.88	1.487
CL-07-01-251.6	316.5	4.81	<0.47	0.081	169.9	0.86	23	2.067	1.8	7.693	3.387	1.665	28.97	9.888
CL-07-01-267.4	45	0.15	<0.47	0.066	4.09	166.5	63	0.395	28.1	0.364	0.184	0.249	14.28	0.454
CL-07-01-271	223.1	0.64	<0.47	0.112	17.85	63.92	18	0.37	29.6	1.676	0.707	1.548	18.13	2.316
CL-07-01-275.7	210.3	0.74	<0.47	0.131	27.2	62.1	17	0.368	19.2	2.832	1.116	1.844	16.8	3.979
CL-07-01-275.7SF	210	0.7	<0.47	0.125	25.63	60.09	22	0.339	17.1	2.682	1.11	1.816	16.41	3.792
CL-07-01-277.4	251.9	0.96	<0.47	0.093	31.11	50.1	13	0.609	13.3	2.526	1.036	1.573	18.46	3.59
CL-07-01-287.1	191.7	0.61	<0.47	0.125	22.97	70.68	72	0.28	99.8	2.659	1.082	1.481	20.73	3.66
CL-07-01-308.8	68.6	0.2	<0.47	0.083	5.79	149.4	337	0.14	35.1	0.466	0.215	0.489	30.47	0.644
CL-07-01-327.3	96	0.4	<0.47	0.154	13.38	61.85	531	0.241	116.2	2.197	0.898	1.298	16.35	3
CL-07-01-329	31.9	0.13	<0.47	0.111	4.07	>187	699	0.055	46.8	0.323	0.156	0.244	27.2	0.431
CL-07-01-367	139.1	0.23	<0.47	0.149	12	163.5	454	0.229	342.7	0.466	0.189	0.902	37.33	0.849
CL-07-01-381.7	219.7	0.53	<0.47	0.144	14.26	62.34	10	2.692	10.3	0.826	0.353	1.124	20.02	1.216
CL-07-01-384.8	74.7	0.52	<0.47	0.187	6.73	159.1	1268	0.685	21.8	0.492	0.215	0.556	28.29	0.771
CL-07-01-411.6	97.1	0.3	<0.47	0.114	8.78	141.8	180	0.33	55	0.795	0.348	0.729	28.32	1.098
CL-07-01-429.8	732.4	3.29	<0.47	0.155	93.73	0.81	16	2.16	6.8	6.038	2.898	2.042	31.5	7.947

Hf	Ho	In	La	Li	Lu	Mo	Nb	Nd	Ni	Pb	Pr	Rb	Sb	Sc	Sm	Sn
0.93	0.183	0.055	3.43	34.7	0.046	0.66	3.652	5.88	237.9	3.5	1.22	38.14	0.04	22.9	1.515	1.04
1.48	0.284	0.095	4.96	40.1	0.069	0.92	6.432	8.74	754.6	11.3	1.825	36.02	0.05	29.9	2.27	2.47
>29	3.699	0.093	119.1	18.9	1.163	1.63	152.1	138.2	7.1	7.5	34.82	8.56	0.06	1.3	29.63	>14
1.52	0.3	0.076	4.27	32	0.071	0.57	5.122	8.83	202.1	2.3	1.781	27.07	<0.04	31.6	2.412	0.9
1.89	0.424	0.112	5.96	13.9	0.101	0.79	6.096	12.76	705.9	10.7	2.568	7.1	0.04	35.6	3.377	1.79
1.73	0.368	0.137	5.83	31.6	0.09	0.73	8.518	11.47	883.4	12	2.328	23.62	0.04	29.5	2.978	2.01
1.37	0.263	0.099	7.95	11.9	0.065	2.38	9.066	10.21	8858	12.1	2.286	8.41	<0.04	13.6	2.269	0.87
2.42	1.325	0.005	57.12	9.9	0.315	2.11	25.74	61.73	9.6	10.3	15.92	49.67	<0.04	<1.1	12.97	2.91
1.35	0.324	0.147	6.39	23.3	0.078	1.08	7.065	9.7	2516	7.8	2.109	35.17	<0.04	21.8	2.38	3.39
1.45	0.355	0.164	5.49	15.2	0.093	0.66	7.459	10.23	2526	8	2.149	11.98	<0.04	27	2.635	1.76
1.64	0.364	0.113	7.61	17.3	0.091	0.72	8.822	11.85	2678	40.4	2.609	15.27	0.04	20.5	2.819	1.43
1.42	0.315	0.124	5.49	14.2	0.079	0.83	8.549	9.7	4086	10.8	2.059	9.11	<0.04	18.4	2.396	2.01
1.53	0.349	0.127	5.33	21.3	0.084	0.64	7.132	9.73	2273	15.3	2	18.56	0.38	24.2	2.564	2.12
1.73	0.382	0.118	6.83	22.9	0.096	0.64	8.231	12.26	715.2	8.1	2.554	21.13	0.04	26.6	3.097	2.22
1.37	0.331	0.122	5.1	21.1	0.084	0.85	6.682	9.2	2904	12.9	1.918	21.85	<0.04	22.8	2.393	2.49
2.1	0.482	0.104	8.99	40.5	0.12	0.81	11.59	15.44	172.1	8.6	3.244	53.85	<0.04	28.5	3.782	7.09
1.21	0.405	0.177	7.08	19.4	0.103	1.69	7.418	11.56	3813	41.7	2.51	23.95	0.04	19.5	2.946	5.92
>29	2.899	0.028	167	8.6	1.354	9.4	35.04	138.4	6.4	88.2	40.38	6.65	0.04	<1.1	23.85	3.48
1.89	0.381	0.128	7.87	31.3	0.094	0.84	9.587	12.98	791.5	8.1	2.815	27.23	0.04	27.2	3.212	2.6
1.48	0.403	0.081	7.11	17.3	0.111	4.83	9.293	12.63	4822	12.6	2.659	25.89	0.04	20.1	3.106	1.15
2.01	0.597	0.111	7.98	22.1	0.169	0.92	9.097	16	128	4.7	3.253	35.01	<0.04	31.9	4.199	1.06
2.12	0.454	0.083	8.67	26.8	0.115	0.69	11.1	15.69	139.3	3.3	3.302	30.12	0.04	26.3	3.873	1.4
0.41	0.11	0.023	3.1	10.8	0.041	4.51	4.402	4.18	17246	11	0.947	16.83	0.04	3.9	0.89	1.34
1.15	1.174	0.081	26.14	19.6	0.361	3.36	15.16	42.54	78.3	11	9.331	47.36	0.06	19.6	9.727	2.27
2.09	0.403	0.074	9.25	31.8	0.099	1.72	10.75	14.09	183.3	15.1	3.09	27.08	0.1	27.9	3.435	0.89
1.56	0.328	0.074	4.83	25	0.075	0.49	5.114	9.7	255.8	8.1	1.959	32.02	0.05	35.2	2.59	0.95
10.95	1.16	0.054	26.02	5.6	0.338	1.95	24.59	30.99	7.4	3.6	7.905	84.9	0.13	1.3	6.913	5.62
4.33	1.326	0.097	17.21	52	0.541	1.12	7.601	20.84	34.4	7.9	4.773	11.21	0.22	46.5	5.369	1.3
2.2	0.487	0.09	8.45	10.6	0.108	1.27	8.788	16.78	346.8	2.9	3.438	14.96	<0.04	37.1	4.141	1.2
1.6	0.369	0.083	4.92	14.7	0.082	0.93	5.442	10.8	324.6	1.4	2.175	8.4	<0.04	40.8	2.882	0.94
1.04	0.224	0.067	3.48	16.3	0.053	0.46	3.587	6.54	141.2	2.4	1.338	9.25	<0.04	21.2	1.778	0.75
1.52	0.336	0.078	6.29	6.9	0.076	0.63	18.6	13.35	36.4	1.7	2.654	3.18	0.04	21.4	3.308	0.44
0.94	0.19	0.064	3.03	5.5	0.05	0.62	4.697	6.48	960.9	2.9	1.284	3.29	0.04	16.6	1.654	0.43
0.68	0.139	0.051	1.51	12.7	0.036	0.22	1.968	3.57	960.1	2.3	0.686	2.9	0.05	21.7	1.026	0.52
0.64	0.128	0.058	0.93	12.6	0.034	0.2	1.764	2.76	1101	6.1	0.52	0.8	0.07	21.8	0.856	0.39
0.48	0.065	0.068	0.7	13.7	0.019	0.19	2.208	1.67	1307	4.3	0.334	0.93	0.09	14.4	0.515	1.73
2.17	0.53	0.095	11.98	13.9	0.153	1.3	16.33	19.41	992.1	5.7	4.262	12.15	0.49	13.7	4.357	2.47
2.1	0.585	0.107	21.16	21.6	0.125	1.14	15.38	30.36	454.3	14.6	6.77	18.35	0.06	14	6.294	2.88
0.5	0.061	0.064	0.89	12.6	0.019	0.43	2.82	1.74	1380	15.3	0.35	1.05	0.07	11.2	0.451	0.63
0.6	0.118	0.05	1.54	8.5	0.031	0.52	2.181	3.28	1159	2.9	0.645	1.21	0.18	15.5	0.869	0.57
0.61	0.121	0.05	1.6	10.3	0.032	0.46	2.031	3.36	1316	4.5	0.67	1.64	0.1	19.2	0.905	0.64
1.91	0.875	0.154	30.45	24.3	0.24	1.36	19.22	27.61	893.3	45.2	7.113	4.91	0.77	22.5	6.05	12.29

0.64	0.131	0.053	1.12	5	0.034	0.33	1.746	3.17	1187	2.7	0.567	1.31	0.1	21.6	0.887	0.64
0.49	0.078	0.064	0.81	10.4	0.022	0.21	1.882	1.92	1158	11.9	0.376	2.82	0.06	18.5	0.555	1.01
1.24	0.252	0.086	2.55	11.5	0.057	0.69	3.335	6.41	744.8	3	1.185	6.46	<0.04	36.3	1.849	1.12
10.7	0.677	0.03	45	17.6	0.164	2.35	15.82	45.18	164	10.5	11.45	31.44	<0.04	3.8	8.173	3.14
1.07	0.225	0.048	7.16	25.2	0.052	0.39	4.921	9.52	373	1.7	2.141	10.45	<0.04	12.4	2.092	0.66
1.17	0.196	0.099	2.59	9.1	0.045	0.63	6.502	6.06	1087	2.6	1.202	3.75	<0.04	21.2	1.574	1.54
0.9	0.176	0.049	4.73	25	0.041	0.72	4.647	6.68	498	23.3	1.49	31.73	<0.04	14.4	1.548	0.8
1.26	0.251	0.082	4.2	5.8	0.057	0.62	14.96	8.61	747.5	2.6	1.708	3.29	<0.04	19.4	2.303	0.51
1.1	0.281	0.072	3.48	6.9	0.067	0.34	4.362	8.18	1091	2.6	1.633	2.44	<0.04	22.4	2.152	0.42
1.4	0.254	0.083	8.96	37.1	0.066	0.6	10.73	11.19	61.5	66.2	2.616	19.65	0.05	8.1	2.293	7.44
1.8	0.4	0.096	11.26	7.4	0.09	1.04	16.61	18.1	118.8	19.8	3.932	22.16	0.08	16.7	4.158	4.79
0.84	0.181	0.025	8.47	17.8	0.039	10.94	4.948	9.63	18.2	1.3	2.301	75.97	0.05	1.7	1.902	4.6
1.36	0.258	0.097	3.87	3.7	0.061	0.51	15.67	8.74	527.5	4.6	1.726	2.86	<0.04	22.1	2.365	0.8
2.77	0.395	0.082	11.23	9.4	0.086	0.93	7.796	15.74	281.3	3.5	3.566	38.48	0.26	30.9	3.555	1.3
2.72	0.566	0.066	16.13	10	0.142	1.25	22.7	21.91	212.3	5	5.03	89.89	<0.04	19.3	4.81	1.04
1.3	0.227	0.072	3.51	6	0.055	0.47	16.65	7.49	21.9	0.5	1.477	4.03	<0.04	21	2.005	4.09
0.73	0.118	0.07	1.59	15.9	0.033	0.79	3.686	3.38	1055	4.3	0.654	4.36	<0.04	15.3	0.879	1.6
1.85	0.49	0.078	6.24	31.3	0.107	0.79	3.159	14.33	121.6	2.3	2.78	16.71	<0.04	31.8	3.954	0.99
2.74	0.907	0.164	21.6	7.1	0.172	2.73	24.81	45.9	4.5	7.1	9.191	8.16	<0.04	30.9	10.42	0.56
1.6	1.018	0.083	37.15	5.1	0.17	1.82	17.73	63.45	4.9	1.1	13.36	5.59	<0.04	14.7	13.16	0.5
1.53	1.253	0.097	45.19	3.6	0.193	1.86	32.15	82.47	5.3	2.7	17.11	1.69	<0.04	15.4	16.96	0.28
1.81	0.431	0.098	9.4	4.2	0.096	1.27	22.1	18.65	7.3	0.9	3.806	2.37	<0.04	20.2	4.446	0.46
1.81	0.359	0.086	6.93	7.4	0.089	0.98	22.12	13.69	5.3	3.1	2.823	5.83	<0.04	19.5	3.357	0.46
1.99	0.364	0.089	7.51	10.2	0.088	1.19	17.9	13.91	5.5	3.6	2.8	7.11	<0.04	19.9	3.375	0.91
1.39	0.289	0.09	2.82	10.3	0.065	0.58	4.696	7.71	267	2.1	1.443	6.54	<0.04	30.6	2.26	0.83
1.44	0.313	0.09	2.79	9.2	0.068	0.52	4.021	8.1	224.8	1.8	1.512	6.59	<0.04	31.2	2.378	0.82
2.61	0.496	0.088	18.59	5.9	0.12	1.7	24.69	24.79	14.1	7	5.543	32.92	0.04	8.1	5.182	5.49
0.78	0.159	0.027	7.35	11.7	0.04	0.53	5.085	8.1	604.9	2.3	1.94	13.12	<0.04	5.7	1.574	0.48
1.99	0.411	0.076	8.68	7.2	0.093	0.8	9.75	15.2	79.8	1.5	3.173	9.38	<0.04	25	3.691	0.68
0.91	0.165	0.068	3.38	4.3	0.038	0.57	4.808	5.58	506.7	1.5	1.173	4.18	<0.04	17.7	1.439	1.02
1.5	0.309	0.076	8.58	2.7	0.068	1	12.02	14.26	94.1	0.7	3.044	2.25	<0.04	15.1	3.281	0.65
0.87	0.152	0.073	1.61	2.5	0.039	0.35	4.048	4.09	1016	1.3	0.794	0.94	<0.04	20.8	1.157	1.06
1.03	0.251	0.067	3.04	3	0.052	0.42	3.528	7.89	30.3	0.5	1.45	1.44	<0.04	23.7	2.152	0.41
3.87	2.88	0.178	117.7	4	0.477	2.8	41.59	185.8	45.6	10.3	40.86	10.72	<0.04	17.8	36.83	2.35
0.89	0.192	0.074	2.75	4.7	0.044	0.49	3.257	5.67	339.5	2.1	1.106	3.32	<0.04	23.4	1.536	0.86
0.69	0.124	0.088	1.06	2.9	0.027	0.39	2.516	3.06	616.8	1.7	0.548	1.37	<0.04	22.1	0.906	1.1
0.86	0.179	0.038	4.26	6.4	0.043	0.43	3.521	6.41	209.9	1	1.408	9.41	<0.04	15.5	1.539	0.49
1.97	0.381	0.111	5.9	2.3	0.085	1.08	19.86	13.63	51	0.5	2.592	3.42	<0.04	26.6	3.413	0.71
2.22	0.473	0.138	7.07	3.9	0.103	1.39	18.91	17.18	168.3	1	3.344	2.77	<0.04	25.1	4.354	0.67
3.41	0.616	0.116	19.46	5.7	0.152	1.23	23.56	26.94	142.4	2	6.124	13.77	<0.04	15.5	5.947	1.74
1	0.158	0.086	1.11	4.1	0.039	0.42	5.585	3.98	648.7	1.4	0.706	0.48	<0.04	22.6	1.215	1.1
0.84	0.181	0.055	3.24	9.3	0.043	0.5	3.672	5.94	313.6	1	1.216	5.76	<0.04	19.7	1.489	0.77
1.02	0.2	0.068	3.82	4.5	0.048	0.73	4.876	7.03	678.6	2.1	1.44	2.41	<0.04	19.3	1.743	1.02
3.4	1.594	0.16	60.59	6.1	0.289	2.51	39.88	94.73	47.2	1.8	20.86	16.14	0.04	15.9	19.24	2.43

2.3	0.499	0.09	7.49	16.4	0.121	1.85	13.54	14.49	319.9	3.6	3.024	30.33	<0.04	39.2	3.706	3.44
1.27	0.296	0.061	5.96	24.4	0.069	0.49	5.405	9.83	94.9	1.9	2.058	15.38	<0.04	22.2	2.423	0.84
1.26	0.25	0.078	3.22	26.6	0.055	0.68	5.077	6.81	327.6	3.7	1.364	20.91	<0.04	30.9	1.907	1.41
2.21	1.071	0.072	76.22	3.9	0.266	1.21	30.2	75.02	2.1	5.7	19.46	48.72	<0.04	2.1	12.9	5.22
1.18	0.171	0.048	4.94	21.2	0.044	0.72	17.09	7.14	18.9	0.9	1.583	10.51	<0.04	11	1.62	0.5
6.38	1.303	0.055	83.9	3.9	0.355	4.02	32.61	69.11	<1.6	14.1	19.08	163.4	0.06	1.9	12.63	2.25
1.39	0.07	0.073	1.83	9.2	0.03	0.69	29.33	2.25	31.1	1.7	0.52	5.38	<0.04	11.2	0.477	0.7
2.07	0.29	0.069	7.95	13.2	0.078	0.95	26.9	11.37	17.3	2.7	2.464	9.72	<0.04	17.8	2.585	0.62
2.32	0.474	0.077	11.32	13	0.117	0.86	34.13	18.87	15.9	2.3	4.031	9.91	<0.04	23	4.41	0.63
2.31	0.448	0.073	10.64	12.4	0.113	1.05	33.23	17.7	16.1	2.2	3.813	9.22	<0.04	22.2	4.231	0.64
1.98	0.427	0.062	13.55	10.8	0.102	0.97	17.3	17.92	9	2.6	4.14	17.07	<0.04	16.2	3.941	0.81
1.51	0.452	0.071	9.04	10	0.104	0.64	6.249	15.88	107.5	2.9	3.322	7.27	<0.04	30.2	3.751	0.66
1	0.077	0.074	2.62	6.3	0.027	0.9	11.32	3.43	121.5	0.5	0.75	2.57	<0.04	11.3	0.719	0.99
1.4	0.372	0.071	4.83	7.1	0.088	0.48	3.335	11.14	158.8	1	2.169	2.32	<0.04	45.5	2.946	0.46
1.22	0.057	0.082	1.76	4	0.025	0.87	14.07	2.42	120.2	0.4	0.558	1.21	<0.04	11	0.49	1.01
0.98	0.076	0.064	6.05	6.1	0.02	0.75	9.271	5.99	140.3	1.2	1.454	2.24	<0.04	7.9	1.055	0.78
0.8	0.138	0.034	6.68	25.3	0.037	0.6	5.882	7.38	18.7	4.8	1.771	18.41	0.04	3.8	1.382	3.33
1.05	0.086	0.074	3.07	7.8	0.026	0.65	9.604	3.95	81.3	3	0.878	3.95	<0.04	8.6	0.85	0.73
1.75	0.137	0.089	3.9	9.5	0.042	1.17	18.82	5.3	82.9	0.9	1.196	3.73	<0.04	11.3	1.2	1.04
7.69	1.084	0.055	42.63	2.4	0.332	3.15	27.78	47.29	2.5	12.3	11.68	161.8	0.04	1.1	9.4	2.37

Sr	Ta	Tb	Th	Ti	Tl	Tm	U	V	W	Y	Yb	Zn	Zr
615.2	0.257	0.204	0.189	17310	0.196	0.054	0.053	628	0.64	4.83	0.317	95	27
458.4	0.433	0.316	0.468	23548	0.248	0.087	0.151	851	0.94	7.41	0.49	159	45
35.7	9.479	3.776	28.63	969	0.025	1.352	7.079	5.2	1.42	90.34	8.357	259	1252
516.3	0.379	0.338	0.24	22580	0.192	0.088	0.065	860	0.09	7.49	0.527	103	40
205	0.406	0.459	0.453	13659	0.072	0.13	0.125	448	0.47	10.83	0.735	122	58
465.9	0.584	0.399	0.4	>25000	0.262	0.113	0.133	838	0.37	9.25	0.645	163	53
58	0.603	0.282	0.555	17380	2.276	0.079	0.166	687	0.59	6.63	0.468	176	45
34.6	1.585	1.465	26	738	0.169	0.448	3.83	4.3	0.68	30	2.558	21	72
477.9	0.477	0.337	0.48	16704	0.484	0.1	0.135	627	0.89	8.69	0.551	157	41
271.2	0.504	0.374	0.365	23192	0.559	0.113	0.11	781	0.13	8.89	0.65	222	44
473.5	0.609	0.388	0.583	16562	0.743	0.113	0.173	614	0.19	9.42	0.646	145	52
364.7	0.581	0.33	0.327	16775	0.832	0.097	0.109	677	0.13	7.68	0.563	187	45
427.7	0.5	0.368	0.422	18751	0.23	0.106	0.131	691	0.19	9.11	0.621	202	46
526.5	0.568	0.417	0.47	20277	0.221	0.118	0.171	720	0.18	9.63	0.689	136	53
419.7	0.473	0.348	0.481	18821	0.337	0.1	0.157	622	0.89	8.72	0.588	160	41
544.2	0.799	0.517	0.598	22751	0.27	0.148	0.222	691	2.3	13.05	0.872	129	69
367.7	0.509	0.409	0.45	16112	0.626	0.127	0.258	514	1.32	11.18	0.733	231	37
63.6	2.767	2.493	>109	533	0.025	1.35	21.85	2.1	1.06	84.14	8.979	397	1364
510.8	0.64	0.413	0.699	22174	0.265	0.118	0.188	807	0.41	9.93	0.676	135	62
354.3	0.68	0.415	0.736	16136	0.704	0.131	0.458	530	1.79	10.29	0.785	105	47
471.3	0.678	0.605	0.705	20929	0.148	0.196	0.425	617	1.4	15.33	1.169	136	63
563.7	0.811	0.509	0.872	24570	0.129	0.14	0.526	681	0.38	11.97	0.822	115	66
39.6	0.372	0.113	0.171	4215	1.889	0.043	0.135	86.9	2.33	3.12	0.272	127	15
434.1	1.215	1.196	1.332	13490	0.309	0.404	1.235	191.8	2.02	33.92	2.489	180	39
512.8	0.703	0.439	0.787	21364	0.215	0.122	0.223	766	1.49	10.27	0.699	80	70
419.3	0.362	0.361	0.293	20386	0.264	0.094	0.089	810	0.21	8.34	0.547	96	44
41.9	2.001	1.051	21.82	838	0.383	0.415	5.09	2.4	0.78	32.05	2.461	7	376
133.2	0.463	1.024	3.134	12348	0.058	0.547	0.55	425	0.24	36.23	3.578	77	168
347.3	0.638	0.549	0.951	24751	0.088	0.145	0.198	735.1	0.38	11.89	0.818	116	66
389.1	0.392	0.402	0.267	21026	0.116	0.107	0.078	666.8	0.09	9.2	0.608	98	46
621.5	0.268	0.249	0.19	>25000	0.092	0.067	0.048	920	<0.05	5.56	0.391	116	29
891	1.486	0.403	0.173	>25000	0.03	0.094	0.048	229.9	0.15	8.33	0.524	108	49
143.6	0.354	0.216	0.18	22400	0.053	0.058	0.048	624	0.2	4.82	0.337	196	29
69.8	0.154	0.149	0.117	19771	0.117	0.042	0.047	770	<0.05	3.49	0.246	131	19
18.7	0.142	0.132	0.041	22836	0.094	0.038	0.017	946	<0.05	3.12	0.229	190	17
17.8	0.182	0.076	0.027	>25000	0.091	0.021	0.013	1420	0.09	1.77	0.129	207	13
72.2	1.057	0.551	1.04	>25000	0.145	0.181	0.448	1078	1.55	13.19	1.076	208	77
471.2	0.999	0.699	1.041	>25000	0.208	0.165	0.409	433	0.62	14.85	0.926	266	77
56.4	0.223	0.066	0.043	>25000	0.165	0.019	0.013	1428	0.4	1.63	0.127	212	15
97.3	0.17	0.118	0.076	18212	0.089	0.038	0.016	759	<0.05	3.07	0.221	133	17
100.3	0.147	0.131	0.101	15664	0.083	0.037	0.033	579	<0.05	3.03	0.222	117	17
71	1.078	0.873	3.471	13783	0.136	0.278	0.53	492	1.54	32.3	1.632	335	57

44.7	0.145	0.136	0.076	17753	0.117	0.041	0.036	699	0.16	3.3	0.243	99	16
79	0.153	0.083	0.033	>25000	0.1	0.024	0.011	1374	0.39	2	0.151	172	13
239.9	0.256	0.269	0.128	>25000	0.065	0.072	0.039	1061	0.15	6.37	0.419	159	32
632.8	1.309	0.802	13.43	9630	0.132	0.202	4.058	83.3	3.05	19.15	1.189	146	479
837.2	0.356	0.251	0.371	18266	0.061	0.065	0.109	564	0.11	5.75	0.366	97	35
195.2	0.518	0.212	0.111	>25000	0.071	0.058	0.043	1665	0.11	5.01	0.331	267	35
785.2	0.305	0.196	0.297	15293	0.15	0.053	0.096	496.3	0.11	4.53	0.31	93	30
870.7	1.259	0.283	0.161	>25000	0.045	0.07	0.06	236.9	0.23	6.23	0.42	115	42
187.6	0.349	0.298	0.18	21698	0.074	0.082	0.097	654	0.05	7.09	0.484	158	33
1008	0.783	0.275	1.405	14385	0.11	0.079	0.543	112.4	0.91	6.94	0.451	150	53
1062	1.149	0.467	0.577	>25000	0.303	0.112	0.194	272	0.68	10.57	0.647	190	68
1301	0.369	0.206	0.662	3412	0.304	0.052	0.254	18.9	4.26	4.96	0.286	16	36
779.8	1.306	0.306	0.14	>25000	0.047	0.074	0.052	345.2	0.05	6.46	0.428	121	44
457.5	0.529	0.44	1.99	>25000	0.158	0.115	0.689	931.8	1.02	10.14	0.638	161	103
639.9	1.314	0.607	2.052	16909	0.297	0.174	0.707	397	0.74	14.98	1.021	131	104
835	1.426	0.26	0.169	>25000	0.022	0.066	0.067	331.2	0.07	5.75	0.38	105	42
49.4	0.307	0.124	0.057	>25000	0.115	0.037	0.031	1207	0.24	2.97	0.212	227	21
421.9	0.25	0.543	0.27	12361	0.071	0.142	0.095	389.2	0.19	12.18	0.793	60	52
380.6	1.721	1.145	0.621	>25000	0.12	0.23	0.142	85.1	0.26	22.5	1.261	233	91
1021	1.251	1.339	0.776	>25000	0.035	0.242	0.199	25.8	0.08	26.42	1.312	168	57
285.6	2.442	1.702	0.655	>25000	0.007	0.285	0.165	14.9	<0.05	32.68	1.481	256	55
726.1	1.668	0.529	0.323	>25000	0.008	0.12	0.077	226.3	0.06	10.84	0.701	184	60
1043	1.602	0.416	0.367	>25000	0.032	0.102	0.08	179	0.07	8.87	0.603	124	64
950	1.212	0.416	0.545	>25000	0.071	0.107	0.156	179.5	0.12	9.07	0.626	132	73
460.2	0.391	0.315	0.105	>25000	0.049	0.083	0.032	1044	<0.05	7.18	0.472	148	37
425.9	0.342	0.341	0.111	>25000	0.045	0.089	0.031	1057	<0.05	7.31	0.498	135	37
1079	1.536	0.561	1.631	17080	0.373	0.152	0.372	77.3	2	12.59	0.887	120	102
922.8	0.327	0.179	0.683	5809	0.052	0.05	0.185	165.7	0.15	4.19	0.287	54	31
662.7	0.718	0.463	0.847	>25000	0.038	0.118	0.194	374.5	0.14	10.16	0.693	106	64
571.4	0.368	0.182	0.145	>25000	0.051	0.048	0.043	1301	<0.05	4.22	0.281	164	28
606	0.886	0.37	0.469	>25000	0.008	0.084	0.097	359.1	0.07	8.11	0.493	221	50
25.4	0.322	0.163	0.068	>25000	0.08	0.048	0.018	1297	<0.05	3.93	0.277	226	25
860.5	0.286	0.29	0.056	>25000	0.006	0.068	0.017	410	<0.05	6.28	0.382	121	27
223.5	2.54	3.643	2.349	>25000	0.059	0.712	0.565	243.8	0.3	73.28	3.704	394	132
554.7	0.27	0.215	0.152	>25000	0.026	0.056	0.04	841.8	<0.05	4.9	0.308	139	24
223	0.227	0.132	0.083	>25000	0.025	0.036	0.029	1702	<0.05	3.06	0.203	229	18
682.6	0.244	0.194	0.302	9573	0.031	0.054	0.082	318.5	0.06	4.5	0.305	75	29
142.9	1.605	0.436	0.274	>25000	0.008	0.104	0.072	540	0.05	9.49	0.613	236	63
319.4	1.332	0.558	0.275	>25000	0.013	0.131	0.062	503.4	0.07	11.23	0.743	227	68
647.7	1.479	0.681	2.538	>25000	0.065	0.184	0.586	522.6	0.25	15.15	1.066	189	128
28.6	0.419	0.176	0.04	>25000	0.065	0.049	0.018	1702	<0.05	4.02	0.281	278	31
667.1	0.272	0.199	0.109	22532	0.045	0.051	0.033	786.1	<0.05	4.62	0.305	107	25
296.8	0.393	0.222	0.183	>25000	0.023	0.058	0.053	916.5	<0.05	4.9	0.329	164	31
740.6	2.466	1.954	2.378	>25000	0.079	0.413	0.516	210.8	0.35	40.15	2.199	178	118

347.8	1.135	0.524	1.64	22384	0.199	0.155	0.805	735.3	0.83	12.68	0.888	115	67
738.7	0.395	0.33	0.42	17424	0.04	0.088	0.175	568.2	0.09	7.66	0.508	83	38
435.1	0.399	0.273	0.205	>25000	0.128	0.072	0.088	997.3	0.25	6.01	0.393	126	34
117.8	1.856	1.224	13.65	1910	0.168	0.325	2.851	5.5	0.97	28.64	1.911	27	54
1065	1.455	0.198	0.283	>25000	0.028	0.053	0.086	272.1	0.06	4.34	0.31	108	42
73.4	3.601	1.401	19.46	546	0.601	0.449	5.442	2.4	1.3	35.38	2.695	26	155
182	2.627	0.065	0.179	>25000	0.033	0.027	0.106	650	0.19	1.85	0.184	232	51
910.1	1.882	0.307	0.585	>25000	0.037	0.088	0.233	296	0.42	6.93	0.538	83	77
825.6	2.309	0.53	0.738	>25000	0.037	0.141	0.276	264	0.51	11.83	0.835	71	86
809.4	2.264	0.506	0.504	>25000	0.033	0.137	0.246	257.7	0.51	11.17	0.807	68	83
942.8	1.32	0.474	2.454	>25000	0.07	0.126	0.83	202	0.94	10.97	0.745	89	72
599.3	0.446	0.49	0.467	20352	0.027	0.134	0.145	583.1	0.21	11.36	0.769	112	48
351.7	0.833	0.087	0.082	>25000	0.013	0.027	0.036	1327	<0.05	2.05	0.173	324	35
506	0.247	0.408	0.138	11750	0.022	0.112	0.038	384	<0.05	9.58	0.64	87	38
120.4	1.08	0.054	0.076	>25000	0.005	0.023	0.033	1310	0.16	1.55	0.15	353	43
486	0.809	0.099	0.367	>25000	0.018	0.022	0.059	1159	0.22	2.02	0.129	339	31
1217	0.396	0.152	0.498	15934	0.302	0.044	0.129	223.5	0.65	3.66	0.262	126	33
318.8	0.74	0.098	0.153	>25000	0.035	0.028	0.053	1221	0.25	2.35	0.165	351	43
419.8	1.31	0.149	0.222	>25000	0.012	0.046	0.058	1053	0.16	3.54	0.288	324	66
67.8	2.601	1.084	14.3	898	0.502	0.391	3.82	2.3	2.45	30.69	2.411	36	282

Appendix 14: PGE assay data

February 2013 Samples

	Au (ppb)	Ir	Pd	Pt	Rh	Ru
Detect Limit	0.22	0.01	0.12	0.17	0.02	0.08
CL-07-01-8	b.d.l	0.01	b.d.l	b.d.l	b.d.l	b.d.l
CL-07-01-115.7	1.82	0.14	1.72	1.24	0.07	0.25
CL-07-01-167.76	0.48	0.01	0.15	0.27	b.d.l	b.d.l
CL-07-01-322.4	0.76	0.01	0.15	0.23	b.d.l	b.d.l
CL-07-01-325.6	0.65	0.01	b.d.l	b.d.l	b.d.l	b.d.l
CL-07-01-354.2	1.05	0.06	1.01	0.9	0.08	0.1
CL-07-01-371.2	0.44	0.02	0.16	b.d.l	0.02	b.d.l
CL-07-01-373	0.5	0.02	0.2	b.d.l	b.d.l	b.d.l
CL-07-01-380	0.74	0.01	b.d.l	b.d.l	b.d.l	b.d.l
CL-07-01-422.9	0.41	0.11	2.22	3.72	0.13	0.21
CL-07-02-347	0.72	0.02	0.24	b.d.l	b.d.l	b.d.l
CL-07-03-169	0.93	0.13	0.77	0.69	0.07	0.24
CL-07-05-11	6.81	1.74	5.83	5.59	0.85	3.67
CL-07-05-14	4.34	0.16	0.74	0.9	0.09	0.33
CL-07-05-30.2	0.23	0.01	b.d.l	b.d.l	b.d.l	b.d.l
CL-07-05-50	21.3	1.99	5.74	1.82	1.01	3.95
CL-07-05-105	0.45	0.01	b.d.l	b.d.l	b.d.l	b.d.l
CL-07-05-117	12.5	1.3	4.98	3.02	0.64	2.49
CL-07-05-142.8	10.2	0.42	3.27	3.16	0.26	0.58
CL-07-05-144	15	0.36	3.94	3.61	0.23	0.52
CL-07-05-499	1.05	0.01	b.d.l	b.d.l	b.d.l	b.d.l
CL-07-05-675	0.63	0.03	0.26	b.d.l	0.03	0.13
CL-07-07-10.1	0.38	0.01	b.d.l	b.d.l	b.d.l	b.d.l
CL-07-07-17	0.47	0.02	0.13	b.d.l	0.02	b.d.l
CL-07-07-450	0.42	0.01	b.d.l	b.d.l	b.d.l	b.d.l
CL-07-07-483	0.4	0.01	b.d.l	b.d.l	b.d.l	b.d.l
CL-07-14-323.5	2.29	0.08	0.6	2.58	0.05	0.14
CL-07-14-477.5	15.7	0.81	6.72	7.68	0.51	1.44
CL-07-15-145	b.d.l	0.01	b.d.l	b.d.l	b.d.l	b.d.l

Summer 2013 Samples	Au (ppb)	Ir	Pd	Pt	Rh	Ru
Detect Limit	0.4	0.01	0.12	0.17	0.04	0.08
CL-06-16-47.6	13.2	0.93	9.73	4.23	1.32	1.13
CL-06-16-52.5	6.59	1.22	3.55	0.23	1.26	2.64
CL-06-55.0	9.72	0.21	4.96	0.33	0.66	0.2
CL-06-16-56.3	8.19	0.72	6.15	0.37	0.82	1.19
CL-06-16-57.5	12	0.92	7.41	b.d.l	1.14	1.67
CL-06-16-58.6	8.23	0.45	5.63	0.28	0.56	0.6
CL-06-16-59.9	4.53	0.06	1.85	0.69	0.08	b.d.l

CL-06-16-61.7	7.44	0.32	6.89	2.47	0.52	0.54
CL-06-16-63.8	9.51	0.48	8.66	0.43	0.82	0.39
CL-06-16-78.75	2.65	0.27	4.31	0.58	0.58	0.23
CL-06-16-84.6	13.3	0.27	21.6	7.7	0.97	0.09
CL-06-01-18.8	1.58	0.03	1.35	0.68	0.05	b.d.l
CL-06-01-22.0	9.48	2.74	15.5	0.3	3.25	5.56
CL-06-01-22.5	11.4	0.8	58	0.25	1.13	1.26
CL-06-05-75.1	4.43	0.11	3.14	2.75	0.16	0.16
CL-06-05-77.72	6.84	0.08	2.93	7.33	0.16	0.14
CL-06-05-81.2	16.8	1.16	12.6	8.42	2.5	1.31
CL-06-05-81.6	38.9	1.14	10.3	b.d.l	2.45	1.21
CL-07-09-57	8.91	0.07	113	29.6	3.18	0.42
CL-07-09-60	14.3	0.08	117	37.2	4.36	0.53

Appendix 15: EMP analyses

Plagioclase analyses

Sample	CL-06-16-8.9	CL-06-16-8.9	CL-06-16-8.9	CL-06-16-8.9
Point	1	2	3	4
SiO_2	52.58	51.18	52.91	51.02
TiO_2	0.12	0.06	0.08	0.08
Al_2O_3	30.90	32.33	30.59	32.21
FeO	0.85	0.23	0.14	0.16
MnO	0.02	b.d.l	b.d.l	b.d.l
MgO	0.06	0.00	0.00	0.01
CaO	12.14	14.13	12.22	14.06
Na_2O	4.43	3.58	4.52	3.33
K_2O	0.05	0.04	0.05	0.04
Total	101.13	101.52	100.49	100.90
An	60.05	68.40	59.71	69.80

CL-06-16-35.7 1	CL-06-16-35.7 2	CL-06-16-35.7 3	CL-06-16-35.7 4	CL-06-16-35.7 5
54.14	53.46	53.11	53.75	53.76
0.13	0.08	0.11	0.05	0.06
30.04	30.46	30.41	30.62	30.51
0.15	0.19	0.19	0.11	0.16
0.04	0.00	0.01	0.01	0.00
0.01	0.03	0.01	0.02	0.04
11.49	12.11	12.14	12.12	12.02
5.04	4.61	4.68	4.71	4.84
0.11	0.10	0.11	0.06	0.10
101.15	101.05	100.77	101.46	101.50
55.38	58.85	58.51	58.48	57.53

CL-06-16-35.7 6	CL-06-16-59.9 Rim-1	CL-06-16-59.9 Core-1	CL-06-16-59.9 Rim-2	CL-06-16-59.9 Core-3
53.12	54.14	54.63	54.65	52.52
0.05	0.09	0.08	0.06	0.05
30.56	29.78	29.53	29.54	30.62
0.16	0.41	0.50	0.21	0.15
0.00	0.00	0.02	b.d.l	0.02
0.01	0.02	0.13	0.04	0.01
12.26	11.13	10.80	10.83	12.41
4.64	4.88	5.29	5.33	4.35
0.08	0.12	0.18	0.09	0.07
100.89	100.55	101.16	100.72	100.19
59.09	55.35	52.45	52.59	60.94

CL-06-16-59.9 Rim-4	CL-06-16-59.9 Core-4	CL-06-16-59.9 Rim-5	CL-06-16-59.9 Core-5	CL-06-16-59.9 Rim-6
55.01	54.69	55.00	53.76	55.06
0.11	0.05	0.06	0.10	0.00
29.20	28.98	28.88	29.29	29.18
0.24	0.18	0.50	0.70	0.22
b.d.l	b.d.l	0.02	b.d.l	0.00
0.00	0.02	0.08	0.20	0.01
10.71	10.54	10.28	11.21	10.43
5.38	5.55	5.65	4.87	5.47
0.12	0.14	0.07	0.10	0.09
100.77	100.13	100.53	100.20	100.46
52.02	50.80	49.91	55.63	51.00

CL-06-16-59.9 Core-6	CL-06-16-59.9 Core-7	CL-06-16-59.9 Rim-7	CL-06-16-59.9 Core-8	CL-06-16-59.9 Rim-8
53.70	54.80	52.76	53.17	53.49
0.02	0.04	0.05	0.14	0.13
28.30	29.69	28.96	30.55	30.44
2.05	0.16	2.22	0.28	0.60
0.05	0.01	b.d.l	b.d.l	b.d.l
0.98	0.02	0.53	0.01	0.03
9.82	10.87	10.91	12.20	12.04
5.15	5.23	4.94	4.63	4.69
0.18	0.12	0.09	0.08	0.07
100.25	100.93	100.44	101.05	101.48
50.78	53.07	54.68	59.00	58.43

CL-06-16-80 Core-1	CL-06-16-80 Rim-1	CL-06-16-80 Rim-2	CL-06-16-80 Core-2	CL-06-16-80 Rim-3
57.58	57.67	57.12	56.92	57.06
0.06	0.01	0.01	0.10	b.d.l
27.25	27.19	27.52	27.47	27.47
0.19	0.30	0.20	0.32	0.22
0.00	b.d.l	0.00	b.d.l	0.00
0.01	0.02	0.02	0.02	0.00
8.74	8.64	8.88	8.97	8.98
6.41	6.39	6.45	6.29	6.09
0.39	0.33	0.35	0.34	0.38
100.62	100.53	100.56	100.39	100.15
42.01	41.95	42.36	43.21	43.91

CL-06-16-80 Core-3	CL-06-16-80 Rim-4	CL-06-16-80 Core-4	CL-06-16-80 5	CL-06-16-80 6
57.55	56.96	56.43	47.10	48.36
0.02	0.05	0.06	b.d.l	b.d.l
27.21	26.15	27.38	34.28	33.31
0.23	1.62	0.19	0.30	0.54
0.01	0.03	0.01	0.02	0.02
0.00	0.66	0.02	0.05	0.04
8.50	7.83	8.91	16.51	14.61
6.46	6.29	6.29	1.81	2.49
0.39	0.49	0.51	0.04	0.52
100.37	100.09	99.80	100.08	99.84
41.15	39.55	42.62	83.27	74.05

CL-06-16-80 7	CL-06-39-4.1 1	CL-06-39-4.1 2	CL-06-39-4.1 3	CL-06-39-4.1 4
48.63	52.35	53.23	51.80	51.50
b.d.l	0.06	0.06	0.35	0.04
33.47	30.95	30.34	30.93	31.51
0.32	0.26	0.35	0.59	0.30
0.01	0.01	0.03	b.d.l	0.00
0.04	0.02	0.08	0.08	0.05
15.34	12.90	12.31	13.11	13.53
2.56	4.09	4.41	4.03	3.79
0.07	0.16	0.16	0.26	0.24
100.42	100.79	100.96	101.14	100.94
76.45	62.98	60.09	63.27	65.46

CL-06-39-4.15	CL-06-39-20.35 Rim-1	CL-06-39-20.35 Core-1	CL-06-39-20.35 Rim-2	CL-06-39-20.35 Core-2
53.21	55.09	55.45	54.73	55.37
0.06	0.03	0.06	0.07	0.11
30.70	29.07	28.99	28.72	28.92
0.25	0.36	0.18	1.14	0.13
b.d.l	0.00	0.01	0.05	0.03
0.02	0.04	0.00	0.22	0.03
12.30	10.54	10.33	9.77	10.41
4.56	5.37	5.33	5.40	5.75
0.08	0.20	0.22	0.24	0.07
101.16	100.71	100.57	100.33	100.81
59.60	51.45	51.05	49.25	49.82

CL-06-39-20.35 Rim-3	CL-06-39-20.35 Core-3	CL-06-39-20.35 Rim-4	CL-06-39-20.35 Core-4	CL-06-39-20.35 Rim-5
54.08	53.36	53.47	50.92	54.31
0.10	0.05	0.03	0.06	0.11
29.68	30.46	30.58	32.07	30.04
0.44	0.12	0.23	0.21	0.18
0.07	0.02	0.00	0.02	0.04
0.55	0.03	0.02	0.04	0.03
11.21	12.20	12.16	14.08	11.46
4.83	4.56	4.66	3.51	4.98
0.12	0.13	0.12	0.08	0.17
101.08	100.93	101.27	100.99	101.31
55.78	59.20	58.65	68.58	55.44

CL-06-39-20.35 Core-5	CL-06-39-60.23 1	CL-06-39-60.23 2	CL-06-39-60.23 3	CL-06-39-60.23 4
53.67	51.46	51.00	53.01	50.49
0.07	0.05	0.02	0.11	0.03
30.35	31.56	31.83	30.63	32.19
0.12	0.33	0.20	0.22	0.18
0.01	0.02	0.04	0.02	0.01
0.03	0.13	0.03	0.03	b.d.l
11.85	13.21	13.69	12.34	14.18
4.81	3.83	3.71	4.49	3.49
0.15	0.08	0.10	0.15	0.06
101.06	100.66	100.61	101.00	100.63
57.15	65.28	66.74	59.81	68.95

CL-06-39-60.23 5	CL-06-39-128 Rim-1	CL-06-39-128 Core-1	CL-06-39-128 Rim-2	CL-06-39-128 Core-2
50.64	55.96	55.33	56.42	55.75
0.09	0.14	0.09	0.05	0.03
31.89	28.55	28.69	28.11	27.84
0.40	0.30	0.25	0.28	0.47
0.02	b.d.l	0.03	b.d.l	0.01
0.02	0.04	0.02	0.03	0.18
13.87	10.00	10.00	9.41	9.55
3.54	5.79	5.47	6.03	5.80
0.07	0.31	0.30	0.39	0.32
100.53	101.08	100.17	100.69	99.94
68.12	47.99	49.39	45.26	46.75

CL-06-39-128 Rim-3	CL-06-39-128 Core-3	CL-06-39-128 Rim-4	CL-06-39-128 Core-4	CL-06-39-128 Rim-5
55.58	55.86	56.37	55.68	55.76
0.04	0.07	0.07	0.07	0.02
28.30	28.40	28.19	28.58	27.95
0.26	0.20	0.31	0.16	0.35
0.02	0.02	0.04	0.01	b.d.l
0.02	0.04	0.01	0.02	0.01
10.03	9.82	9.38	10.01	9.67
5.77	5.87	5.85	5.81	5.66
0.25	0.24	0.32	0.26	0.28
100.26	100.53	100.54	100.62	99.68
48.28	47.40	46.10	48.04	47.75

CL-06-39-128 Core-5	CL-07-01-29.1 1	CL-07-01-29.1 2	CL-07-01-29.1 3	CL-07-01-29.1 4
57.51	58.86	58.04	58.12	57.99
0.07	0.13	0.11	0.03	0.07
27.33	26.69	26.83	27.02	26.83
0.19	0.21	0.13	0.14	0.19
b.d.l	b.d.l	b.d.l	0.00	0.03
0.02	0.03	0.02	b.d.l	0.02
8.72	7.73	7.97	8.19	8.27
6.25	6.88	6.74	6.67	6.55
0.32	0.47	0.50	0.45	0.44
100.39	100.97	100.34	100.62	100.40
42.71	37.28	38.39	39.38	40.04

CL-07-01-29.15	CL-07-01-29.16	CL-07-01-140 Core-1	CL-07-01-140 Rim-1	CL-07-01-140 Core-2
58.39	58.77	55.97	55.99	56.45
0.11	0.06	0.13	0.03	0.11
26.92	26.57	28.13	27.52	28.23
0.15	0.12	0.57	1.72	0.14
b.d.l	b.d.l	b.d.l	0.07	0.00
0.04	0.01	0.12	0.06	0.00
7.89	7.80	9.36	8.63	9.46
6.86	6.75	5.91	6.15	6.12
0.45	0.40	0.07	0.23	0.16
100.78	100.46	100.25	100.39	100.69
37.83	38.05	46.46	43.09	45.65

CL-07-01-140 Core-3	CL-07-01-140 Rim-3	CL-07-01-140 Rim-4	CL-07-01-140 Core-4	CL-07-01-354 Core-1
56.54	56.75	56.34	56.24	55.03
0.11	b.d.l	0.08	0.08	0.08
28.17	27.99	27.82	28.29	29.10
0.15	0.17	0.67	0.17	0.17
0.01	0.00	b.d.l	b.d.l	b.d.l
0.03	0.01	0.12	0.02	0.04
9.26	9.09	9.08	9.54	10.51
6.22	6.38	6.22	6.08	5.20
0.08	0.06	0.08	0.08	0.33
100.57	100.45	100.41	100.47	100.43
44.92	43.88	44.43	46.25	51.73

CL-07-01-354 Rim-1	CL-07-01-354 Rim-2	CL-07-01-354 Core-2	CL-07-01-354 Rim-3	CL-07-01-354 Core-3
55.69	55.56	55.34	55.12	55.39
0.08	0.03	b.d.l	0.04	0.02
28.81	28.94	29.15	28.79	29.10
0.19	0.24	0.15	0.15	0.15
0.00	0.08	0.03	0.00	b.d.l
0.02	0.02	0.04	0.02	0.04
10.18	10.45	10.49	10.45	10.40
5.67	5.33	5.35	5.43	5.67
0.31	0.33	0.29	0.29	0.30
100.95	100.97	100.81	100.29	101.04
48.89	51.01	51.12	50.67	49.50

CL-07-01-354 Rim-4	CL-07-01-354 Core-4
55.59	56.17
0.05	0.05
28.59	28.52
0.21	0.21
0.00	b.d.l
0.03	0.05
10.12	9.97
5.74	5.64
0.21	0.32
100.52	100.94
48.75	48.50

Olivine analyses

Sample	CL-06-16-8.9	CL-06-16-8.9	CL-06-16-8.9	CL-06-16-8.9
Point	1	2	3	4
SiO_2	36.19	36.45	36.30	36.01
Al_2O_3	0.00	b.d.l	b.d.l	b.d.l
FeO	35.15	34.73	35.05	36.18
MgO	28.54	29.64	28.65	27.87
MnO	0.49	0.48	0.49	0.54
CaO	0.05	0.04	0.04	0.05
NiO	0.04	0.06	0.04	0.06
TiO_2	b.d.l	0.01	0.04	b.d.l
Cr_2O_3	b.d.l	b.d.l	b.d.l	0.01
V_2O_3	b.d.l	0.01	0.01	0.01
Na_2O	-	-	-	-
K_2O	-	-	-	-
Total	100.43	101.41	100.59	100.73
Fo	58.76	59.97	58.93	57.45

CL-06-16-8.95	CL-06-16-33.71	CL-06-16-33.72	CL-06-16-33.73	CL-06-16-35.71
36.69	35.40	35.70	35.54	36.36
b.d.l	b.d.l	b.d.l	b.d.l	0.01
31.81	38.01	36.03	37.01	35.19
30.79	26.11	27.61	27.13	28.96
0.49	0.55	0.52	0.53	0.55
0.05	0.05	0.04	0.06	0.05
0.06	0.04	0.04	0.05	0.06
0.00	0.03	0.01	0.01	0.03
b.d.l	0.00	0.01	b.d.l	0.00
b.d.l	0.01	b.d.l	0.01	b.d.l
-	0.02	b.d.l	b.d.l	-
-	0.01	0.01	b.d.l	-
99.84	100.22	99.95	100.27	101.22
62.90	54.64	57.35	56.24	59.04

CL-06-16-35.7 2	CL-06-16-35.7 3	CL-06-16-35.7 4	CL-06-16-35.7 5	CL-06-16-35.7 6
36.39	36.37	36.79	36.49	36.48
0.02	b.d.l	0.00	0.01	0.01
35.02	34.93	34.53	34.86	34.83
29.11	28.84	29.22	28.94	29.10
0.54	0.53	0.50	0.53	0.48
0.04	0.06	0.04	0.03	0.03
0.07	0.06	0.05	0.04	0.08
0.02	0.02	0.02	0.03	b.d.l
b.d.l	0.02	0.01	0.01	0.01
b.d.l	0.01	b.d.l	0.00	b.d.l
-	-	-	-	-
-	-	-	-	-
101.16	100.81	101.16	100.93	101.01
59.30	59.12	59.75	59.28	59.47

CL-06-16-35.7 7	CL-06-16-35.7 8	CL-06-39-20.35 1	CL-06-39-20.35 2	CL-06-39-20.35 3
36.80	36.38	36.74	36.78	36.76
0.00	0.02	0.01	0.00	0.01
31.60	34.97	33.20	32.68	32.95
28.72	28.62	30.54	30.69	30.58
0.52	0.51	0.48	0.46	0.49
0.06	0.04	0.09	0.07	0.10
0.07	0.07	0.08	0.09	0.11
0.04	0.01	0.01	0.05	0.01
b.d.l	b.d.l	0.01	b.d.l	b.d.l
0.00	b.d.l	0.01	b.d.l	0.01
-	-	-	-	-
-	-	-	-	-
97.80	100.59	101.17	100.81	101.01
61.39	58.94	61.69	62.21	61.88

CL-06-39-20.35 4	CL-06-39-20.35 5	CL-06-39-20.35 6	CL-06-39-60.23 1	CL-06-39-60.23 2
36.64	36.66	36.66	37.39	37.51
0.00	b.d.l	0.00	0.01	b.d.l
33.13	33.44	33.29	25.07	24.62
30.38	30.12	30.28	35.64	35.92
0.54	0.48	0.48	0.37	0.33
0.09	0.12	0.08	0.09	0.09
0.09	0.08	0.09	0.15	0.14
0.03	0.07	b.d.l	0.01	0.00
b.d.l	0.01	b.d.l	0.00	0.00
0.00	0.01	b.d.l	b.d.l	0.00
-	-	-	b.d.l	0.02
-	-	-	0.00	0.01
100.90	101.00	100.87	98.70	98.63
61.58	61.17	61.44	71.31	71.86

CL-06-39-60.23 3	CL-06-39-60.23 4	CL-06-39-60.23 5	CL-06-39-103 1	CL-06-39-103 2
37.37	37.35	37.37	37.12	37.38
b.d.l	b.d.l	b.d.l	0.01	0.00
24.53	25.11	24.86	27.40	26.70
36.01	36.08	35.94	33.43	34.24
0.34	0.33	0.35	0.43	0.37
0.08	0.14	0.12	0.10	0.08
0.14	0.14	0.16	0.09	0.09
0.06	0.01	0.05	0.02	0.04
b.d.l	b.d.l	b.d.l	b.d.l	b.d.l
b.d.l	b.d.l	0.01	0.00	b.d.l
b.d.l	0.01	b.d.l	b.d.l	0.03
b.d.l	b.d.l	0.01	b.d.l	b.d.l
98.51	99.15	98.84	98.57	98.92
71.99	71.51	71.63	68.07	69.20

CL-06-39-103 3	CL-06-39-103 4	CL-06-39-103 5	CL-06-39-128 1	CL-06-39-128 2
37.53	37.11	37.37	35.28	35.50
0.01	0.02	0.01	0.02	b.d.l
26.60	27.14	26.78	39.45	38.41
34.16	33.45	33.82	24.61	24.43
0.40	0.42	0.42	0.64	0.61
0.09	0.11	0.08	0.05	0.05
0.07	0.09	0.08	0.06	0.06
0.03	0.03	0.02	0.04	b.d.l
0.01	0.00	0.00	b.d.l	b.d.l
0.00	b.d.l	0.01	b.d.l	0.00
b.d.l	b.d.l	0.01	0.01	b.d.l
b.d.l	0.00	b.d.l	0.00	0.00
98.86	98.37	98.61	100.15	99.01
69.19	68.28	68.82	52.20	52.70

CL-06-39-128 3	CL-06-39-128 4	CL-06-39-128 5	CL-06-39-128 6	CL-07-01-140 1
35.30	35.10	35.08	35.31	35.12
0.04	b.d.l	0.00	0.00	b.d.l
40.19	39.63	41.11	41.21	39.33
24.06	24.14	23.03	23.32	24.41
0.66	0.65	0.73	0.66	0.75
0.08	0.06	0.06	0.05	0.06
0.06	0.06	0.06	0.07	b.d.l
0.01	0.04	0.04	b.d.l	0.01
b.d.l	b.d.l	-0.01	b.d.l	0.00
0.01	b.d.l	b.d.l	b.d.l	0.01
0.05	b.d.l	0.03	0.00	b.d.l
0.00	b.d.l	0.00	0.00	0.00
100.45	99.65	100.13	100.61	99.65
51.15	51.60	49.48	49.78	51.99

CL-07-01-140 2	CL-07-01-140 3	CL-07-01-140 4	CL-07-01-140 5	CL-07-01-249 1
35.33	35.40	35.53	35.56	34.61
0.00	b.d.l	0.01	b.d.l	0.01
39.33	38.49	38.39	38.44	42.74
24.83	25.34	25.27	25.13	22.36
0.72	0.71	0.66	0.72	0.63
0.09	0.07	0.08	0.09	0.03
b.d.l	0.00	0.01	b.d.l	0.01
0.02	0.05	b.d.l	0.02	0.01
0.00	b.d.l	b.d.l	b.d.l	b.d.l
b.d.l	b.d.l	0.01	b.d.l	b.d.l
b.d.l	0.04	b.d.l	b.d.l	b.d.l
b.d.l	0.01	0.00	b.d.l	b.d.l
100.26	100.09	99.90	99.87	100.37
52.43	53.48	53.49	53.28	47.87

CL-07-01-249 2	CL-07-01-249 3	CL-07-01-249 4	CL-07-01-249 5	CL-07-01-249 6
34.78	34.44	34.88	34.47	34.51
0.01	0.00	0.02	b.d.l	0.00
42.25	42.81	42.00	41.77	42.41
22.64	22.37	22.24	21.92	21.80
0.61	0.62	0.65	0.59	0.60
0.04	0.07	0.04	0.06	0.06
b.d.l	0.00	0.01	b.d.l	b.d.l
b.d.l	0.01	0.02	0.01	0.02
b.d.l	0.01	0.01	b.d.l	0.00
0.01	0.01	b.d.l	0.01	b.d.l
0.00	b.d.l	0.00	b.d.l	b.d.l
b.d.l	0.00	b.d.l	0.00	0.00
100.30	100.29	99.86	98.72	99.37
48.47	47.82	48.15	47.93	47.42

CL-07-01-249 7	CL-07-01-249 8	CL-07-01-308 1	CL-07-01-308 2	CL-07-01-308 3
34.32	34.53	36.20	36.16	36.11
b.d.l	0.02	b.d.l	b.d.l	0.03
41.77	42.15	34.39	34.00	34.01
21.96	22.15	28.37	28.65	28.60
0.64	0.61	0.56	0.56	0.56
0.04	0.05	0.12	0.09	0.09
b.d.l	0.01	0.03	0.02	0.02
0.04	-0.01	0.02	0.03	0.03
0.00	b.d.l	0.00	b.d.l	0.00
b.d.l	b.d.l	b.d.l	b.d.l	0.00
b.d.l	0.04	0.06	b.d.l	b.d.l
0.01	b.d.l	0.00	b.d.l	0.00
98.71	99.52	99.72	99.47	99.41
47.97	47.96	59.03	59.55	59.51

CL-07-01-308 4	CL-07-01-308 5	CL-07-01-308 6	CL-07-01-329 1	CL-07-01-329 2
36.10	36.01	36.16	35.49	35.57
0.00	0.03	b.d.l	0.01	0.02
34.34	33.97	34.26	37.08	36.95
28.67	28.35	28.45	26.97	26.87
0.57	0.59	0.54	0.55	0.59
0.09	0.10	0.08	0.08	0.08
0.03	0.02	0.02	0.01	0.03
0.02	0.05	0.02	0.02	0.02
b.d.l	0.00	0.01	0.00	b.d.l
0.01	b.d.l	b.d.l	b.d.l	b.d.l
0.04	0.02	0.07	b.d.l	b.d.l
0.00	b.d.l	0.00	b.d.l	0.01
99.86	99.12	99.58	100.19	100.07
59.34	59.30	59.23	56.02	55.98

CL-07-01-329 3	CL-07-01-329 4	CL-07-01-329 5	CL-07-01-329 6	CL-07-01-329 7
35.45	35.38	35.53	35.73	35.61
0.02	0.02	0.01	0.04	0.01
36.52	36.67	36.41	36.11	35.76
26.84	27.34	27.05	27.46	27.84
0.60	0.63	0.55	0.54	0.56
0.09	0.07	0.07	0.07	0.08
0.01	0.02	0.01	0.03	0.01
0.05	b.d.l	0.05	0.03	0.04
0.01	0.00	0.00	0.01	0.01
0.00	0.00	0.00	0.00	b.d.l
b.d.l	0.01	0.04	0.04	0.02
0.00	0.00	b.d.l	0.00	b.d.l
99.57	100.14	99.70	100.06	99.91
56.23	56.58	56.55	57.12	57.67

CL-07-01-329 8	CL-07-01-354 1	CL-07-01-354 2	CL-07-01-354 3	CL-07-01-354 4
35.70	35.39	35.49	35.42	35.56
0.01	0.02	b.d.l	0.01	b.d.l
36.21	39.29	39.15	39.60	38.94
27.59	24.65	24.73	24.31	24.75
0.55	0.71	0.66	0.66	0.65
0.08	0.05	0.06	0.06	0.08
0.04	0.02	0.04	0.02	0.02
0.04	b.d.l	b.d.l	0.01	0.00
b.d.l	0.00	b.d.l	b.d.l	b.d.l
b.d.l	0.00	0.01	0.01	b.d.l
b.d.l	0.00	b.d.l	b.d.l	0.01
b.d.l	0.00	b.d.l	0.00	b.d.l
100.18	100.12	100.10	100.03	99.99
57.15	52.30	52.50	51.79	52.64

Clinopyroxene analyses

Sample	CL-06-16-8.9	CL-06-16-8.9	CL-06-16-8.9	CL-06-16-8.9
Point	1	2	3	4
SiO_2	49.42	49.71	48.91	49.56
TiO_2	1.67	1.68	1.80	1.67
Al_2O_3	5.04	5.13	5.82	5.20
Cr_2O_3	0.03	0.01	0.00	0.01
FeO	8.55	8.03	8.27	8.41
MnO	0.18	0.17	0.14	0.18
MgO	13.64	13.68	13.47	13.51
CaO	21.94	21.92	21.84	21.98
Na_2O	-	-	-	-
K_2O	-	-	-	-
NiO	0.01	0.00	0.02	0.00
V_2O_3	0.06	0.05	0.07	0.08
Total	100.53	100.38	100.35	100.60
Mg#	73.99	75.22	74.38	74.12

CL-06-16-8.95	CL-06-16-8.96	CL-06-16-33.71	CL-06-16-33.72	CL-06-16-33.73
49.01	45.32	48.90	49.33	48.36
2.05	3.35	1.73	1.57	1.91
6.03	3.95	5.40	4.72	5.99
0.01	0.03	0.01	0.00	0.00
8.24	14.33	7.91	7.60	7.67
0.16	0.18	0.20	0.19	0.14
13.43	13.09	13.11	13.25	12.90
21.95	19.90	22.22	22.73	22.42
-	-	0.59	0.53	0.57
-	-	0.01	0.01	0.01
0.00	0.01	0.00	0.01	b.d.l
0.07	0.11	0.08	0.04	0.08
100.94	100.28	100.15	99.98	100.03
74.40	61.97	74.71	75.66	75.00

CL-06-16-33.74	CL-06-16-33.75	CL-06-16-35.71	CL-06-16-35.72	CL-06-16-35.73
50.57	48.28	41.12	42.04	51.54
1.09	2.04	4.73	3.13	0.77
3.25	4.60	12.91	13.43	2.72
0.00	0.01	0.07	0.16	0.04
8.05	9.44	12.76	12.61	8.02
0.17	0.26	0.11	0.13	0.20
13.68	13.12	12.08	12.83	14.81
22.54	21.47	11.67	12.01	22.63
0.45	0.51	-	-	-
0.00	0.00	-	-	-
0.03	0.01	0.03	0.03	0.02
0.04	0.09	0.10	0.11	0.04
99.87	99.83	95.58	96.48	100.78
75.19	71.24	62.78	64.47	76.71

CL-06-16-80 1	CL-06-16-80 2	CL-06-16-80 3	CL-06-16-80 4	CL-06-16-80 5
51.70	51.87	50.11	52.05	51.27
0.30	0.21	1.13	0.25	0.38
1.72	1.29	1.87	1.68	2.09
0.00	-0.01	0.01	0.00	0.02
14.66	13.44	14.71	13.92	12.74
0.43	0.31	0.34	0.34	0.32
12.86	12.28	11.87	12.74	11.96
18.47	20.94	20.67	19.64	21.55
0.25	0.23	0.35	0.24	0.34
0.00	0.01	0.00	0.00	0.00
0.01	0.04	0.01	0.01	0.01
0.02	0.03	0.04	0.02	0.02
100.41	100.62	101.13	100.90	100.71
60.99	61.96	58.97	61.99	62.59

CL-06-16-80 6	CL-06-16-80 7	CL-06-39.20.35 1	CL-06-39.20.35 2	CL-06-39.20.35 3
51.91	51.39	50.14	49.80	50.13
0.30	0.22	1.54	1.64	1.56
1.70	1.62	3.90	4.22	3.90
0.01	0.00	0.11	0.12	0.11
14.79	15.73	9.08	8.79	8.85
0.42	0.43	0.18	0.18	0.18
12.93	13.32	13.60	13.36	13.60
18.87	17.20	21.72	21.56	21.96
0.30	0.24	-	-	-
0.00	0.00	-	-	-
0.01	0.00	0.03	0.02	0.01
0.04	0.03	0.04	0.07	0.05
101.26	100.16	100.35	99.76	100.35
60.90	60.16	72.73	73.05	73.25

CL-06-39.20.354	CL-06-39-60.235	CL-06-39-60.236	CL-06-39-60.237	CL-06-39-60.238
50.30	49.04	48.73	49.41	48.90
1.51	1.64	1.59	1.32	1.58
3.79	5.05	5.10	4.94	5.33
0.10	0.18	0.16	0.11	0.17
8.72	7.00	6.82	6.97	6.78
0.17	0.12	0.12	0.15	0.14
13.63	13.81	13.85	14.29	13.88
21.59	22.29	22.70	22.34	22.25
-	0.66	0.62	0.55	0.69
-	0.00	0.01	0.02	0.00
0.03	0.02	0.01	0.01	0.01
0.04	0.06	0.05	0.05	0.06
99.87	99.88	99.78	100.16	99.80
73.58	77.84	78.35	78.53	78.50

CL-06-39-103 1	CL-06-39-103 2	CL-06-39-103 3	CL-06-39-103 4	CL-06-39-103 5
49.95	49.44	49.83	49.80	49.32
1.42	1.36	1.25	1.31	1.47
5.25	5.04	5.06	5.00	5.27
0.09	0.09	0.08	0.07	0.10
7.22	7.24	7.33	7.25	7.36
0.16	0.17	0.13	0.14	0.15
13.40	13.34	13.36	13.46	13.33
23.03	23.31	22.87	23.14	23.30
0.48	0.47	0.54	0.43	0.46
0.00	0.00	0.00	0.01	0.00
0.01	0.03	0.01	0.01	0.01
0.05	0.04	0.06	0.04	0.04
101.05	100.54	100.53	100.66	100.82
76.80	76.64	76.46	76.81	76.34

CL-06-39-103 6	CL-06-39-103 7	CL-06-39-103 8	CL-06-39-128 1	CL-06-39-128 2
49.51	49.40	49.16	51.54	51.00
1.43	1.39	1.60	0.59	1.25
5.53	5.13	5.03	2.25	2.84
0.09	0.09	0.11	0.00	0.01
7.47	7.46	8.04	9.45	10.33
0.17	0.16	0.16	0.25	0.26
13.23	13.22	13.45	13.52	13.62
23.01	23.13	22.76	22.22	21.23
0.53	0.48	0.50	0.40	0.53
b.d.l	0.00	0.00	0.00	0.01
0.02	0.02	0.03	0.02	0.01
0.04	0.07	0.06	0.03	0.02
101.03	100.55	100.90	100.27	101.11
75.95	75.97	74.89	71.85	70.15

CL-06-39-128 3	CL-06-39-128 4	CL-06-39-128 5	CL-06-39-128 6	CL-06-39-128 7
50.62	50.69	51.30	50.61	51.42
1.29	1.35	0.91	1.41	1.00
3.26	3.27	2.69	3.17	2.59
0.01	0.00	0.00	0.00	b.d.l
10.13	10.13	9.55	10.25	10.16
0.29	0.30	0.26	0.27	0.24
13.10	13.05	13.35	13.09	13.45
21.47	21.35	21.92	21.48	21.65
0.50	0.48	0.45	0.48	0.53
0.00	0.00	0.01	0.01	0.00
0.00	0.00	0.02	0.01	0.01
0.02	0.03	0.02	0.03	0.00
100.71	100.66	100.48	100.80	101.05
69.75	69.66	71.37	69.48	70.24

CL-06-39-128 8	CL-07-01-9.1 1	CL-07-01-9.1 2	CL-07-01-9.1 3	CL-07-01-9.1 4
50.99	51.24	51.15	51.75	51.54
1.20	0.56	0.81	0.50	0.58
2.76	1.49	1.64	1.30	1.51
0.00	0.00	0.00	0.00	0.01
10.61	13.12	13.21	12.87	12.99
0.26	0.36	0.42	0.37	0.34
13.11	11.15	11.35	11.28	11.18
21.03	21.97	21.42	22.00	21.79
0.47	0.43	0.41	0.50	0.53
0.01	0.00	0.00	b.d.l	0.00
0.00	0.00	0.00	0.00	0.01
0.03	0.02	0.01	0.03	0.02
100.48	100.35	100.43	100.59	100.49
68.78	60.25	60.50	60.99	60.55

CL-07-01-9.15	CL-07-01-95.96	CL-07-01-95.97	CL-07-01-95.98	CL-07-01-95.99
51.45	51.43	50.42	50.52	50.65
0.79	0.26	1.36	1.00	0.82
1.72	1.86	2.98	2.67	2.53
b.d.l	0.00	b.d.l	b.d.l	0.00
12.87	9.84	10.14	9.90	10.00
0.42	0.27	0.25	0.26	0.25
11.14	13.28	13.42	13.34	13.62
21.65	22.04	21.35	21.61	21.55
0.72	0.56	0.45	0.52	0.58
0.00	0.00	0.00	0.00	0.00
b.d.l	0.01	0.00	0.00	0.00
0.01	0.02	0.04	0.01	0.03
100.74	99.57	100.40	99.82	100.06
60.67	70.65	70.22	70.62	70.82

CL-07-01-95.9 10	CL-07-01-140 1	CL-07-01-140 2	CL-07-01-140 3	CL-07-01-140 4
49.78	50.41	50.68	50.96	50.74
1.54	1.49	1.53	1.25	1.37
3.04	3.52	3.45	3.27	3.35
0.00	0.00	0.00	0.00	0.02
10.20	9.53	9.54	9.38	9.80
0.26	0.24	0.26	0.26	0.29
13.39	13.57	13.04	13.21	13.11
21.22	21.39	21.85	21.72	21.59
0.50	0.57	0.66	0.71	0.60
0.01	0.01	0.00	0.00	0.00
0.00	b.d.l	b.d.l	0.00	b.d.l
0.03	0.02	0.03	0.04	0.01
99.98	100.74	101.03	100.80	100.85
70.06	71.74	70.91	71.50	70.46

CL-07-01-140 5	CL-07-01-249 1	CL-07-01-249 2	CL-07-01-249 3	CL-07-01-249 4
50.32	50.45	44.43	49.46	50.23
1.66	1.23	0.62	1.36	1.16
3.51	3.54	6.28	3.46	3.14
0.00	0.00	b.d.l	0.01	0.01
10.01	8.83	13.20	9.69	9.20
0.25	0.25	0.17	0.22	0.24
13.35	13.07	16.02	13.21	13.33
21.39	22.21	14.11	21.60	22.06
0.60	0.48	0.26	0.50	0.45
0.00	0.00	0.02	0.00	0.00
0.00	0.00	0.00	0.00	0.00
0.04	0.03	0.04	0.04	0.03
101.13	100.10	95.13	99.55	99.84
70.39	72.51	68.40	70.86	72.10

CL-07-01-249 5	CL-07-01-249 6	CL-07-01-249 7	CL-07-01-354 1	CL-07-01-354 2
50.75	50.92	50.42	51.09	51.26
0.93	0.85	1.21	1.19	1.09
2.74	2.81	3.36	2.98	2.84
0.01	0.00	0.01	0.02	0.01
8.78	8.97	9.10	10.01	9.79
0.21	0.23	0.26	0.27	0.29
13.55	13.45	13.27	13.70	13.71
22.19	22.55	21.80	21.35	21.46
0.50	0.39	0.50	0.44	0.47
0.00	0.00	0.00	0.01	0.00
b.d.l	0.00	0.00	0.01	0.00
0.03	0.04	0.03	0.04	0.04
99.66	100.21	99.97	101.13	100.95
73.34	72.76	72.22	70.94	71.39

CL-07-01-3543	CL-07-01-3544
51.39	50.49
0.84	1.22
2.71	3.43
0.04	0.07
9.42	9.85
0.27	0.25
13.56	13.15
21.92	21.43
0.38	0.47
0.00	0.00
0.01	0.01
0.04	0.05
100.56	100.43
71.95	70.41

Amphibole analyses

Line Numbers	CL-06-16-59.9 1	CL-06-16-59.9 2	CL-06-16-59.9 3	CL-06-16-59.9 4	CL-06-16-59.9 5
SiO_2	41.65	41.27	41.20	41.28	41.26
TiO_2	4.03	4.61	4.45	4.63	4.10
Al_2O_3	11.93	12.08	12.18	11.97	12.13
Cr_2O_3	0.04	0.01	0.01	0.01	b.d.l.
FeO	14.28	14.17	14.18	14.22	14.61
MnO	0.13	0.17	0.18	0.14	0.16
MgO	11.64	11.71	11.71	11.67	11.50
CaO	11.67	11.81	11.66	11.77	11.71
Na_2O	2.61	2.51	2.70	2.41	2.54
K_2O	1.18	1.19	1.17	1.16	1.21
NiO	0.01	0.02	0.01	b.d.l.	b.d.l.
V_2O_3	0.09	0.08	0.07	0.09	0.07
F	b.d.l.	0.07	b.d.l.	0.09	0.07
Cl	0.09	0.05	0.10	0.07	0.10
O	0.01	b.d.l.	b.d.l.	b.d.l.	b.d.l.
H_2O	0.94	0.94	0.94	0.94	0.94
Total	100.22	100.65	100.52	100.38	100.31

CL-06-16-59.96	CL-06-16-59.97	CL-06-16-59.98	CL-06-16-59.99	CL-06-16-59.910
41.41	41.11	41.86	40.89	41.32
4.15	3.27	4.33	3.82	4.09
11.95	11.94	11.60	12.37	12.00
0.00	0.01	0.02	0.01	0.02
14.99	16.00	14.56	15.42	14.60
0.14	0.18	0.18	0.17	0.16
11.44	11.47	11.45	11.37	11.67
11.58	11.07	11.66	11.27	11.80
2.41	2.26	2.33	2.43	2.38
1.21	1.05	1.23	1.06	1.20
0.04	0.04	0.04	0.03	0.02
0.09	0.04	0.08	0.08	0.07
b.d.l.	0.06	0.01	0.07	0.14
0.08	0.06	0.10	0.11	0.12
b.d.l.	b.d.l.	b.d.l.	b.d.l.	b.d.l.
0.94	0.94	0.94	0.94	0.94
100.38	99.46	100.37	99.99	100.44

Biotite analyses

Sample	CL-07-01-95.9	CL-07-01-95.9	CL-07-01-95.9	CL-07-01-95.9
Point	1	2	3	4
SiO_2	36.16	36.32	36.04	36.55
TiO_2	5.64	6.25	5.69	5.27
Al_2O_3	13.41	13.51	13.55	13.68
FeO	16.98	16.71	16.76	16.02
MnO	0.10	0.06	0.05	0.05
MgO	14.29	14.45	14.74	15.18
CaO	0.02	0.04	0.04	0.04
Na_2O	0.70	0.55	0.69	0.64
K_2O	9.03	9.03	9.05	8.82
NiO	b.d.l	0.02	b.d.l	0.01
Cr_2O_3	0.01	b.d.l	0.01	b.d.l
V_2O_3	0.05	0.02	0.03	0.06
F	0.27	0.18	0.39	0.23
Cl	0.10	0.10	0.14	0.13
H_2O	3.45	3.45	3.46	3.38
Total	100.07	100.58	100.43	99.93
Total	100.22	100.70	100.62	100.06
O=F, Cl	0.14	0.10	0.20	0.13
Total -O	100.08	100.60	100.43	99.93
xCl	0.01	0.01	0.01	0.01
xF	0.03	0.02	0.05	0.03
xOH	0.96	0.97	0.94	0.96

CL-07-01-95.95	CL-07-01-29.11	CL-07-01-29.12	CL-07-01-173.91	CL-07-01-173.92
36.47	35.03	35.07	36.27	35.64
5.91	6.41	6.32	2.72	4.55
13.65	13.40	13.32	13.32	12.35
15.61	22.97	22.97	23.84	25.01
0.11	0.16	0.13	0.24	0.19
14.62	8.77	8.76	10.03	9.04
0.06	b.d.l	0.03	0.05	0.02
0.71	0.16	0.18	0.37	0.43
8.97	9.71	9.60	8.59	9.13
0.02	b.d.l	b.d.l	0.02	b.d.l
b.d.l	b.d.l	b.d.l	0.01	b.d.l
0.02	0.01	0.01	0.02	0.03
0.21	0.09	0.06	0.17	0.36
0.13	0.06	0.04	0.37	0.19
3.43	3.71	3.67	3.29	3.49
99.79	100.38	100.09	99.17	100.22
99.92	100.49	100.18	99.32	100.44
0.12	0.05	0.03	0.16	0.19
99.81	100.44	100.14	99.17	100.25
0.01	0.00	0.00	0.02	0.01
0.03	0.01	0.01	0.02	0.05
0.97	0.98	0.99	0.95	0.94

CL-07-01-173.93	CL-07-01-173.94	CL-07-01-173.95	CL-07-01-173.96	CL-07-01-173.97
36.15	35.41	35.21	35.44	34.79
4.53	4.08	4.30	4.69	4.99
12.22	12.59	11.37	11.35	11.24
24.28	24.69	29.97	29.70	30.76
0.16	0.21	0.18	0.27	0.20
9.33	8.92	5.46	5.81	5.06
0.07	0.04	0.06	0.08	0.07
0.54	0.50	0.20	0.21	0.23
9.21	9.36	8.96	9.17	8.95
0.02	b.d.l	0.03	b.d.l	0.00
0.01	0.00	b.d.l	0.05	0.01
0.03	0.05	0.00	0.01	0.03
0.11	0.27	0.03	0.02	0.19
0.23	0.33	0.58	0.54	0.53
3.52	3.58	3.43	3.51	3.43
100.32	99.80	99.64	100.70	100.27
100.42	100.01	99.79	100.83	100.47
0.10	0.19	0.14	0.13	0.20
100.32	99.82	99.64	100.70	100.27
0.02	0.02	0.04	0.04	0.04
0.01	0.03	0.00	0.00	0.02
0.97	0.94	0.96	0.96	0.94

CL-07-01-173.98
32.41
5.05
10.79
32.45
0.15
4.71
0.05
0.23
8.93
0.03
0.00
0.01
0.07
0.56
3.42
98.69
98.85
0.16
98.69
0.04
0.01
0.95

Apatite analyses

Sample	CL-06-16-59.9	CL-06-16-59.9	CL-06-16-59.9	CL-06-16-59.9
Point	1	2	3	4
CaO	54.12	53.29	54.69	54.33
P_2O_5	40.91	40.49	41.10	41.00
F	2.00	2.54	2.25	2.21
Cl	0.71	0.69	0.83	0.84
La_2O_3	0.08	0.01	b.d.l	0.02
Ce_2O_3	0.17	0.24	0.19	0.24
Nd_2O_3	b.d.l	b.d.l	0.12	b.d.l
SiO_2	0.05	0.69	0.00	0.01
MgO	0.04	0.30	0.04	0.09
FeO	0.13	0.85	0.20	0.15
MnO	0.07	0.04	0.08	0.04
Na_2O	b.d.l	b.d.l	0.00	b.d.l
K_2O	0.00	b.d.l	b.d.l	0.00
TiO_2	0.00	b.d.l	b.d.l	0.03
Al_2O_3	0.01	0.17	0.02	0.00
Total	98.29	99.32	99.52	98.96
O=F, Cl	1.00	1.23	1.14	1.12
Total -O	97.28	98.09	98.39	97.84
xCl	0.11	0.10	0.12	0.12
xF	0.55	0.70	0.62	0.61
xOH	0.34	0.20	0.26	0.27

CL-07-01-29.1 1	CL-07-01-29.1 2	CL-07-01-29.1 3	CL-07-01-29.1 4	CL-07-01-29.1 5
55.04	54.59	54.90	55.26	54.75
41.32	41.78	41.41	41.43	40.98
3.08	3.32	3.37	3.14	2.94
0.14	0.13	0.10	0.06	0.13
b.d.l	0.12	b.d.l	b.d.l	0.04
0.08	0.09	0.18	0.29	0.13
b.d.l	b.d.l	b.d.l	0.05	b.d.l
0.03	0.00	0.01	0.04	0.09
0.05	0.04	0.05	0.04	0.05
0.24	0.21	0.24	0.28	0.28
0.00	0.01	0.02	0.07	0.05
b.d.l	b.d.l	0.02	b.d.l	b.d.l
b.d.l	0.00	0.00	0.01	0.01
b.d.l	b.d.l	0.04	b.d.l	b.d.l
0.02	b.d.l	0.01	0.01	0.01
100.00	100.30	100.37	100.67	99.45
1.33	1.43	1.44	1.33	1.27
98.68	98.87	98.93	99.34	98.19
0.02	0.02	0.01	0.01	0.02
0.83	0.89	0.91	0.85	0.80
0.15	0.09	0.07	0.15	0.18

CL-07-01-29.16	CL-07-01-29.17	CL-07-01-29.18	CL-07-01-29.19	CL-07-01-29.10
54.93	54.91	54.52	54.64	54.01
41.56	41.39	41.07	41.72	40.41
3.34	3.00	3.54	3.64	2.86
0.10	0.09	0.09	0.01	0.12
b.d.l	0.08	0.13	0.02	0.08
0.14	0.17	0.19	0.25	0.09
b.d.l	0.13	b.d.l	b.d.l	b.d.l
0.04	0.00	0.07	b.d.l	0.48
0.01	0.03	0.03	b.d.l	0.17
0.17	0.18	0.30	0.25	0.78
0.06	0.03	0.04	0.01	0.04
b.d.l	b.d.l	b.d.l	b.d.l	b.d.l
b.d.l	0.00	0.01	0.00	0.01
b.d.l	0.00	0.02	b.d.l	0.01
0.03	0.02	0.01	0.03	0.05
100.38	100.03	100.02	100.58	99.11
1.43	1.28	1.51	1.54	1.23
98.95	98.75	98.51	99.04	97.87
0.01	0.01	0.01	0.00	0.02
0.90	0.81	0.96	0.98	0.78
0.09	0.17	0.03	0.02	0.20

CL-07-01-95.9 1	CL-07-01-95.9 2	CL-07-01-95.9 3	CL-07-01-95.9 4	CL-07-01-95.9 5
54.59	54.58	54.69	54.56	51.75
40.83	41.54	40.88	40.99	38.94
2.70	2.90	2.69	2.89	2.74
0.80	0.62	0.39	0.63	0.57
0.14	0.06	0.07	0.08	b.d.l
0.26	0.27	0.28	0.28	0.27
0.08	b.d.l	b.d.l	0.04	b.d.l
0.02	0.07	0.09	0.05	1.42
0.07	0.05	0.00	0.01	0.63
0.16	0.14	0.27	0.19	1.83
0.07	0.07	0.00	0.02	0.00
0.00	0.02	0.00	b.d.l	b.d.l
0.01	0.00	0.04	0.03	0.00
0.03	b.d.l	0.05	0.00	0.02
0.02	0.01	0.02	b.d.l	0.74
99.76	100.31	99.48	99.78	98.91
1.32	1.36	1.22	1.36	1.28
98.45	98.95	98.26	98.42	97.63
0.12	0.09	0.06	0.09	0.08
0.74	0.78	0.74	0.79	0.77
0.14	0.13	0.21	0.12	0.15

CL-07-01-95.96	CL-07-01-95.97	CL-07-01-95.98	CL-07-01-95.99	CL-07-01-1671
51.85	54.63	54.28	54.40	54.75
38.93	41.11	41.01	40.75	41.40
2.51	2.52	2.38	2.75	2.74
0.53	0.50	0.71	0.79	0.26
0.22	0.13	0.16	0.07	0.07
0.17	0.18	0.07	0.26	0.07
0.05	0.07	b.d.l	b.d.l	0.07
1.40	0.13	0.00	0.00	0.05
0.59	0.05	0.10	0.09	0.15
1.73	0.22	0.17	0.24	0.20
0.05	0.06	0.04	0.07	0.02
b.d.l	b.d.l	b.d.l	0.00	0.02
0.02	0.00	0.00	0.01	0.01
b.d.l	b.d.l	0.00	0.00	0.01
0.76	b.d.l	b.d.l	0.00	0.01
98.81	99.60	98.92	99.43	99.84
1.18	1.17	1.16	1.34	1.21
97.64	98.43	97.75	98.09	98.63
0.08	0.07	0.10	0.12	0.04
0.70	0.69	0.65	0.75	0.74
0.22	0.24	0.24	0.13	0.22

CL-07-01-167 2	CL-07-01-167 3	CL-07-01-167 4	CL-07-01-167 5	CL-07-01-167 6
54.20	54.89	54.90	54.68	54.65
40.94	41.23	40.77	41.07	41.12
2.89	3.06	2.90	2.72	2.67
0.27	0.27	0.25	0.25	0.25
0.05	0.11	0.03	0.14	0.10
0.16	0.25	0.24	0.37	0.19
0.03	b.d.l	0.05	b.d.l	0.04
0.31	0.02	0.04	0.03	0.01
0.19	0.10	0.08	0.07	0.09
0.42	0.22	0.15	0.16	0.13
0.08	0.10	0.07	0.06	0.08
0.03	b.d.l	0.03	0.05	0.06
0.00	0.03	0.01	0.02	0.00
b.d.l	b.d.l	0.05	b.d.l	b.d.l
0.16	0.01	b.d.l	0.03	b.d.l
99.74	100.30	99.57	99.65	99.39
1.28	1.35	1.28	1.20	1.18
98.46	98.94	98.29	98.44	98.21
0.04	0.04	0.04	0.04	0.04
0.79	0.83	0.79	0.74	0.73
0.17	0.13	0.17	0.22	0.23

CL-07-01-167 7	CL-07-01-173.9 1	CL-07-01-173.9 2	CL-07-01-173.9 3	CL-07-01-173.9 4
54.93	54.18	54.04	53.90	53.76
41.15	41.15	40.82	41.10	40.67
2.72	3.71	3.43	3.45	3.57
0.19	0.21	0.21	0.17	0.23
0.10	0.17	0.20	0.29	0.25
0.13	0.56	0.48	0.51	0.59
0.02	0.22	0.13	0.12	0.20
0.10	0.18	0.25	0.13	0.12
0.08	0.02	0.03	b.d.l	0.02
0.17	0.33	0.37	0.41	0.25
0.05	0.03	0.07	0.05	0.09
0.00	0.04	0.12	0.03	0.07
0.00	0.03	0.04	b.d.l	0.00
0.01	0.02	b.d.l	0.03	0.04
0.00	0.04	0.00	b.d.l	0.01
99.66	100.89	100.20	100.18	99.88
1.19	1.61	1.49	1.49	1.56
98.48	99.28	98.70	98.69	98.32
0.03	0.03	0.03	0.02	0.03
0.74	1.00	0.93	0.94	0.97
0.23	-0.03	0.04	0.04	0.00

CL-07-01-173.9 5	CL-07-01-173.9 6	CL-07-01-173.9 7	CL-07-01-173.9 8	CL-07-15-145 1
54.29	54.52	53.02	54.26	54.63
40.80	40.78	39.33	40.77	41.05
3.69	3.28	3.34	3.77	3.29
0.08	0.11	0.08	0.17	0.48
0.22	0.14	0.19	0.22	0.13
0.59	0.65	0.39	0.31	0.13
0.00	0.14	0.11	0.11	0.00
0.27	0.22	0.98	0.10	0.02
0.03	0.03	0.27	b.d.l	0.10
0.27	0.26	1.25	0.16	0.23
0.11	0.03	0.05	0.06	0.05
0.04	0.03	0.06	0.04	0.00
0.03	0.02	0.09	0.01	0.02
b.d.l	0.01	b.d.l	b.d.l	b.d.l
b.d.l	0.00	0.25	0.01	b.d.l
100.42	100.23	99.41	100.00	100.13
1.57	1.41	1.42	1.63	1.49
98.85	98.82	97.99	98.37	98.64
0.01	0.02	0.01	0.03	0.07
0.99	0.89	0.92	0.97	0.89
0.00	0.09	0.07	0.00	0.04

CL-07-15-145 2	CL-07-15-145 3	CL-07-15-145 4	CL-07-15-145 5	CL-07-15-145 6
54.68	54.45	54.27	54.62	54.10
41.02	40.98	40.89	40.56	41.00
2.89	3.09	3.10	3.42	2.82
0.46	0.34	0.32	0.46	0.36
0.07	0.12	0.11	0.14	0.13
0.25	0.23	0.31	0.29	0.27
b.d.l	0.06	0.10	0.00	0.02
0.04	0.05	0.05	0.09	0.02
0.06	0.01	0.00	0.03	0.01
0.23	0.12	0.06	0.12	0.10
0.07	0.11	0.08	0.07	0.08
b.d.l	0.00	0.00	0.02	0.03
0.02	b.d.l	0.03	0.01	0.02
b.d.l	0.04	0.03	b.d.l	b.d.l
b.d.l	0.00	b.d.l	0.01	0.01
99.80	99.62	99.36	99.84	98.97
1.32	1.38	1.38	1.55	1.27
98.48	98.24	97.98	98.29	97.71
0.07	0.05	0.05	0.07	0.05
0.79	0.84	0.85	0.93	0.77
0.15	0.11	0.10	0.00	0.17

Magnetite analyses

Sample	CL-06-16-8.9	CL-06-16-8.9	CL-06-16-8.9	CL-06-16-8.9	CL-06-16-8.9
Point	1	2	3	4	5
SiO_2	0.06	0.04	0.04	0.07	0.05
MgO	0.07	0.11	0.12	0.19	0.11
FeO	86.23	87.82	89.09	94.35	87.26
NiO	0.06	0.04	0.04	0.05	0.04
Cr_2O_3	0.21	0.20	0.19	0.18	0.17
TiO_2	7.39	7.79	5.83	3.64	8.18
Al_2O_3	4.24	3.74	4.21	1.43	3.09
MnO	0.22	0.19	0.18	0.09	0.23
CaO	b.d.l.	0.00	0.00	b.d.l.	0.01
V_2O_3	1.18	0.98	1.16	1.08	1.01
Total	99.66	100.90	100.87	101.07	100.16

CL-06-16-33.7 1	CL-06-16-33.7 2	CL-06-16-33.7 3	CL-06-16-33.7 4	CL-06-16-35.7 1	CL-06-16-35.7 2
0.07	0.05	0.05	0.09	0.08	0.16
0.10	0.27	0.31	0.05	0.93	0.14
88.22	80.74	89.09	83.53	88.03	87.90
0.03	0.04	0.02	0.02	0.02	0.03
0.16	0.18	0.14	0.13	1.32	2.65
7.14	9.32	7.49	12.14	4.78	4.88
3.66	1.20	2.05	3.72	4.28	3.26
0.20	0.26	0.26	0.38	0.21	0.50
0.00	0.01	0.00	0.03	b.d.l.	b.d.l.
1.11	1.05	1.12	0.86	0.91	1.91
100.63	93.10	100.43	100.95	100.55	101.43

CL-06-16-35.7 3	CL-06-16-56.3 1	CL-06-16-56.3 2	CL-06-16-56.3 3	CL-06-16-56.3 4	CL-06-16-56.3 5
0.04	0.11	0.32	1.65	1.64	0.30
0.23	0.11	0.18	0.60	0.68	0.10
90.14	96.00	93.28	91.18	92.21	93.99
0.04	0.03	0.01	0.02	0.02	0.02
1.62	0.09	0.08	0.08	0.06	0.08
5.20	1.99	3.85	2.03	3.43	3.64
2.06	1.44	1.15	2.87	2.41	1.85
0.30	0.10	0.16	0.09	0.12	0.15
0.00	b.d.l.	0.00	0.00	0.01	0.01
1.38	0.65	0.62	0.67	0.54	0.61
101.02	100.52	99.64	99.19	101.13	100.74

CL-06-05-81.6 1	CL-06-05-81.6 2	CL-06-05-81.6 3	CL-06-05-81.6 4	CL-06-05-81.6 5	CL-06-05-81.6 6
0.16	0.16	0.47	0.17	0.14	0.19
0.02	0.06	0.18	0.04	0.07	0.11
95.71	95.29	95.69	95.02	95.02	94.18
0.03	0.02	0.01	0.03	0.02	0.02
0.02	0.02	0.03	0.02	0.02	0.02
1.16	1.19	0.94	1.07	1.17	1.80
1.42	1.59	1.01	1.13	1.12	2.09
0.08	0.12	0.07	0.06	0.05	0.21
b.d.l.	0.00	0.00	b.d.l.	b.d.l.	b.d.l.
0.14	0.13	0.15	0.16	0.16	0.16
98.74	98.57	98.56	97.71	97.76	98.77

CL-06-05-81.6 7	CL-06-39-20.35 1	CL-06-39-20.35 2	CL-06-39-20.35 3	CL-06-39-20.35 4
0.14	0.04	0.04	0.06	0.04
0.07	0.43	0.46	0.27	0.33
96.37	86.76	86.87	87.09	87.60
0.03	0.07	0.04	0.09	0.06
0.01	3.27	3.89	3.17	4.03
1.33	6.19	5.88	5.85	5.13
1.42	3.09	2.65	2.94	2.56
0.13	0.37	0.43	0.35	0.31
b.d.l.	b.d.l.	0.00	0.01	b.d.l.
0.15	0.97	1.14	1.09	1.24
99.65	101.19	101.40	100.91	101.31

CL-06-39-20.35 5	CL-06-39-20.35 6	CL-06-39-60.23 1	CL-06-39-60.23 2	CL-06-39-60.23 3
0.06	0.07	0.05	0.03	0.02
0.40	0.48	1.99	1.80	2.24
86.76	84.99	77.13	79.82	76.48
0.10	0.09	0.14	0.15	0.14
3.50	3.62	3.04	2.87	3.06
6.11	7.38	13.34	10.96	13.19
3.13	3.38	3.69	2.88	3.86
0.43	0.46	0.63	0.64	0.62
b.d.l.	0.00	0.00	b.d.l.	0.01
0.97	1.08	0.61	0.60	0.60
101.44	101.56	100.55	99.61	100.13

CL-06-39-60.23 4	CL-06-39-60.23 5	CL-06-39-60.23 6	CL-06-39-103 1	CL-06-39-103 2
0.05	0.31	0.06	0.20	0.10
2.12	0.97	2.07	0.46	0.43
76.96	80.55	78.27	88.81	83.08
0.17	0.12	0.15	0.08	0.10
2.94	2.95	2.94	1.96	3.24
12.95	10.96	11.93	5.75	9.25
3.57	2.54	3.43	2.27	3.41
0.66	0.72	0.42	0.19	0.34
b.d.l.	b.d.l.	b.d.l.	0.01	b.d.l.
0.59	0.65	0.56	0.85	0.68
99.99	99.79	99.73	100.44	100.59

CL-06-39-103 3	CL-06-39-103 4	CL-06-39-103 5	CL-06-39-128 1	CL-06-39-128 2	CL-06-39-128 3
0.07	0.05	0.06	0.11	0.10	0.05
0.31	0.75	0.59	0.17	0.40	0.33
86.20	83.94	85.71	97.42	96.47	93.09
0.13	0.11	0.10	0.04	0.07	0.06
2.02	2.29	1.88	0.11	0.11	0.12
8.19	9.28	8.49	2.00	2.49	4.60
2.54	2.92	2.82	1.13	0.98	2.32
0.28	0.26	0.30	0.06	0.09	0.13
b.d.l.	b.d.l.	0.00	0.00	0.05	b.d.l.
0.80	0.74	0.80	0.77	0.70	0.93
100.49	100.26	100.68	101.76	101.34	101.51

CL-06-39-128 4	CL-06-39-128 5	CL-06-39-128 6	CL-07-01-9.1 1	CL-07-01-9.1 2	CL-07-01-9.1 3
0.26	0.11	0.10	0.09	0.10	0.12
1.00	0.40	0.42	0.10	0.07	0.21
79.79	92.68	90.46	90.69	96.19	94.70
0.04	0.06	0.07	b.d.l.	b.d.l.	b.d.l.
0.09	0.12	0.09	0.01	0.00	0.00
13.76	3.48	6.72	7.65	2.05	3.27
3.98	2.66	3.10	0.91	1.04	3.84
0.27	0.10	0.21	0.33	0.12	0.12
b.d.l.	0.03	b.d.l.	b.d.l.	0.01	0.00
0.61	0.87	0.68	0.06	0.03	0.10
99.73	100.52	101.71	99.79	99.38	102.32

CL-07-01-9.14	CL-07-01-9.15	CL-07-01-9.16	CL-07-01-9.17	CL-07-01-9.18	CL-07-01-9.19
0.11	0.11	0.09	0.08	0.10	0.13
0.33	0.08	0.09	0.21	0.19	0.02
94.02	96.89	96.09	90.58	89.52	98.01
b.d.l.	b.d.l.	0.01	0.00	0.02	0.02
0.01	0.01	b.d.l.	0.01	0.02	0.00
2.56	2.01	2.63	4.35	7.36	1.67
3.61	1.07	1.00	1.85	2.96	0.90
0.12	0.06	0.12	0.18	0.28	0.06
0.01	0.00	0.01	b.d.l.	0.00	b.d.l.
0.07	0.08	0.09	0.07	0.06	0.09
100.75	100.19	100.10	97.15	100.44	100.86

CL-07-01-9.1 10	CL-07-01-95.9 1	CL-07-01-95.9 2	CL-07-01-95.9 3	CL-07-01-95.9 4	CL-07-01-95.9 5
0.12	0.12	0.07	0.10	0.31	0.07
0.09	0.12	0.22	0.15	0.14	0.19
97.23	95.13	95.27	93.69	95.21	92.95
b.d.l.	0.02	b.d.l.	0.02	b.d.l.	0.01
0.00	0.08	0.08	0.05	0.07	0.04
1.92	2.41	2.66	3.33	2.96	4.80
0.91	1.01	1.13	1.74	0.96	1.24
0.09	0.08	0.09	0.17	0.07	0.19
0.01	0.02	0.02	0.01	0.07	b.d.l.
0.09	0.48	0.53	0.44	0.43	0.34
100.31	99.47	100.06	99.68	100.20	99.73

CL-07-01-95.96	CL-07-01-95.97	CL-07-01-140 1	CL-07-01-140 2	CL-07-01-140 3	CL-07-01-140 4
0.12	0.13	0.09	0.04	0.08	0.04
0.19	0.08	0.65	0.77	0.85	0.92
95.08	95.85	82.88	82.07	80.61	81.64
0.03	0.03	0.00	0.01	0.01	b.d.l.
0.05	0.06	0.06	0.06	0.07	0.07
2.58	1.84	13.79	13.22	14.84	14.18
1.05	0.79	3.19	3.82	3.93	3.64
0.12	0.05	0.45	0.41	0.50	0.46
0.01	b.d.l.	0.00	0.02	0.00	0.01
0.41	0.40	0.42	0.41	0.36	0.42
99.58	99.14	101.38	100.76	101.23	101.35

CL-07-01-140 5	CL-07-01-140 6	CL-07-01-140 7	CL-07-01-249 1	CL-07-01-249 2	CL-07-01-249 3
0.06	0.05	0.08	0.08	0.07	0.12
0.88	0.71	0.67	0.32	0.16	0.16
78.55	82.09	80.87	92.57	95.53	91.14
0.01	0.01	b.d.l.	0.01	b.d.l.	0.01
0.05	0.05	0.04	0.25	0.23	0.19
18.39	14.83	16.20	3.28	1.95	1.49
2.28	2.54	2.64	1.59	0.99	0.81
0.57	0.52	0.48	0.10	0.06	0.05
0.01	0.03	0.02	0.01	b.d.l.	b.d.l.
0.36	0.35	0.33	1.74	1.50	1.41
101.07	100.96	101.27	99.92	100.37	95.29

CL-07-01-249 4	CL-07-01-249 5	CL-07-01-308 1	CL-07-01-308 2	CL-07-01-308 3	CL-07-01-308 4
0.09	0.06	0.07	0.07	0.05	0.02
0.14	0.61	0.88	1.69	0.16	1.99
95.63	85.10	93.41	73.67	96.94	81.12
0.00	b.d.l.	0.06	0.03	0.02	0.02
0.21	0.27	0.17	0.19	0.22	0.20
1.63	8.05	2.98	7.30	1.36	9.13
1.23	4.23	3.60	15.90	0.83	8.42
0.03	0.32	0.13	0.29	0.06	0.41
0.01	0.00	b.d.l.	0.00	0.00	b.d.l.
1.43	1.68	0.77	0.64	0.82	0.80
100.44	100.34	101.99	99.62	100.47	101.97

CL-07-01-308 5	CL-07-01-308 6	CL-07-01-329 1	CL-07-01-329 2	CL-07-01-329 3	CL-07-01-329 4
0.06	0.06	0.09	0.07	0.08	0.08
0.56	0.18	0.11	0.45	0.15	0.58
91.40	97.67	94.86	95.14	95.47	89.86
0.02	0.01	b.d.l.	0.03	0.01	0.03
0.16	0.16	0.31	0.32	0.35	0.28
6.40	1.40	2.09	1.83	2.45	5.30
1.51	0.93	0.85	1.14	0.84	3.03
0.23	0.04	0.07	0.06	0.07	0.23
b.d.l.	0.01	b.d.l.	b.d.l.	b.d.l.	0.00
0.62	0.72	0.78	0.72	0.74	0.85
100.82	101.23	99.11	99.68	100.09	100.14

CL-07-01-329 5	CL-07-01-329 6	CL-07-01-329 7	CL-07-01-329 8	CL-07-01-329 9	CL-07-01-329 10
0.09	0.10	0.06	0.07	0.08	0.08
0.14	0.65	0.46	0.12	0.24	0.60
96.12	85.56	91.53	96.08	94.09	85.42
0.02	0.04	0.01	0.01	0.01	0.01
0.29	0.29	0.28	0.33	0.28	0.29
1.83	11.66	4.11	1.77	2.12	8.52
0.94	2.26	2.72	0.81	1.39	2.62
0.06	0.42	0.21	0.05	0.09	0.29
0.01	b.d.l.	b.d.l.	0.00	b.d.l.	0.00
0.73	0.51	0.76	0.70	0.72	0.57
100.07	101.44	100.11	99.87	99.02	98.32

CL-07-01-354 1	CL-07-01-354 2	CL-07-01-354 3	CL-07-01-354 4	CL-07-01-354 5	CL-07-01-354 6
0.05	0.11	0.06	0.06	0.11	0.09
0.21	0.27	1.31	0.66	0.09	0.14
93.50	93.07	91.86	82.34	96.51	94.41
0.03	0.04	0.03	0.01	0.03	0.03
0.87	0.69	0.83	0.56	0.62	0.54
4.11	4.12	1.53	11.90	1.51	1.97
1.29	1.86	7.27	3.07	0.92	1.16
0.11	0.14	0.08	0.44	0.03	0.11
b.d.l.	0.00	0.01	0.04	0.04	0.10
1.50	1.06	1.32	0.80	0.99	0.89
101.60	101.32	104.26	99.80	100.72	99.40

CL-07-01-354 7
0.06
0.31
94.31
0.03
0.49
2.09
2.21
0.08
0.05
0.74
100.37

Ilmenite analyses

Sample	CL-06-16-8.9	CL-06-16-8.9	CL-06-16-8.9	CL-06-16-8.9	CL-06-16-33.7
Point	1	2	3	4	1
SiO_2	0.03	b.d.l.	0.06	0.01	0.02
MgO	0.12	0.28	1.65	0.57	0.22
FeO	46.89	46.66	45.81	46.83	46.86
NiO	0.00	0.01	0.01	0.02	b.d.l.
Cr_2O_3	0.01	0.02	0.00	0.04	0.02
TiO_2	51.04	51.25	51.65	50.54	49.92
Al_2O_3	0.02	0.05	0.03	0.12	0.02
MnO	1.40	1.34	0.86	1.20	1.33
CaO	b.d.l.	0.00	0.00	b.d.l.	0.00
V_2O_3	b.d.l.	b.d.l.	b.d.l.	0.04	0.10
Total	99.46	99.56	100.05	99.36	98.43

CL-06-16-33.7 2	CL-06-16-33.7 3	CL-06-16-35.7 1	CL-06-16-35.7 2	CL-06-16-35.7 3	CL-06-16-56.3 1
0.04	b.d.l.	0.04	0.01	0.01	0.03
0.45	0.52	1.48	0.76	1.37	0.04
47.25	46.45	45.63	46.60	46.31	47.62
0.00	0.00	0.02	0.01	b.d.l.	0.00
0.02	0.02	0.09	0.13	0.07	0.02
49.90	50.54	51.42	51.00	50.96	50.92
0.06	0.01	0.05	0.02	0.02	0.03
1.16	1.34	1.15	1.27	1.32	1.52
0.00	b.d.l.	b.d.l.	0.00	0.00	b.d.l.
0.14	0.11	b.d.l.	0.05	b.d.l.	0.00
99.03	98.93	99.86	99.85	100.06	100.17

CL-06-16-56.3 2	CL-06-16-56.3 3	CL-06-16-56.3 4	CL-06-16-56.3 5	CL-06-39-20.35 1
0.37	1.83	0.01	0.16	0.01
0.18	1.33	0.06	0.08	2.02
43.34	44.90	47.02	46.89	44.95
b.d.l.	b.d.l.	0.00	b.d.l.	0.01
0.04	0.04	0.01	b.d.l.	0.05
47.05	47.09	50.68	49.87	51.90
9.28	4.40	0.24	0.65	0.02
1.62	1.69	1.72	1.68	1.01
b.d.l.	0.01	0.01	0.00	b.d.l.
b.d.l.	0.02	b.d.l.	b.d.l.	b.d.l.
101.80	101.30	99.69	99.29	99.97

CL-06-39-20.35 2	CL-06-39-20.35 3	CL-06-39-20.35 4	CL-06-39-20.35 5	CL-06-39-20.35 6
0.04	0.03	0.03	0.29	0.01
1.26	1.32	1.15	1.92	1.87
44.89	45.86	45.34	45.67	45.45
0.00	b.d.l.	0.02	0.00	0.02
0.14	0.09	0.52	0.08	0.08
51.56	51.43	50.87	51.10	51.62
0.05	0.05	1.64	0.19	0.02
2.21	0.92	1.77	0.95	0.94
0.01	b.d.l.	0.00	0.01	0.01
b.d.l.	b.d.l.	0.00	b.d.l.	b.d.l.
100.10	99.67	101.35	100.17	99.98

CL-06-39-103 1	CL-06-39-103 2	CL-06-39-103 3	CL-06-39-103 4	CL-06-39-103 5	CL-06-39-128 1
0.06	0.06	0.06	0.00	0.02	0.03
0.91	0.82	1.64	1.35	1.32	1.37
45.81	45.99	44.80	45.09	45.32	46.07
0.01	0.02	0.02	0.03	0.01	b.d.l.
0.06	0.07	0.04	0.06	0.06	0.01
50.51	50.87	51.08	51.28	50.73	51.51
0.05	0.05	0.03	0.03	0.04	0.01
1.20	1.19	1.06	1.11	1.10	0.85
b.d.l.	0.01	0.01	0.01	0.01	0.00
0.09	0.08	0.06	0.08	0.08	0.12
98.66	99.19	98.76	98.97	98.65	99.92

CL-06-39-128 2	CL-06-39-128 3	CL-06-39-128 4	CL-07-01-9.1 1	CL-07-01-9.1 2	CL-07-01-9.1 3
0.01	0.04	0.04	0.05	0.05	0.14
0.74	0.98	0.45	0.03	0.20	0.40
46.96	46.36	46.84	59.17	46.54	46.56
0.02	b.d.l.	0.01	0.02	0.00	0.00
0.01	0.00	b.d.l.	b.d.l.	b.d.l.	b.d.l.
51.35	50.96	50.59	37.00	49.94	50.15
0.03	0.04	0.28	0.26	0.03	0.11
0.90	0.96	1.25	1.54	1.76	1.55
0.03	0.00	0.00	0.01	0.02	0.03
0.09	0.09	0.10	0.05	0.06	0.07
100.05	99.32	99.52	98.07	98.57	98.98

CL-07-01-9.14	CL-07-01-9.15	CL-07-01-95.91	CL-07-01-95.92	CL-07-01-95.93	CL-07-01-95.94
b.d.l.	0.03	0.02	0.04	0.32	0.02
0.35	0.19	0.66	0.60	0.47	0.18
46.81	46.72	46.54	46.63	47.01	47.14
0.01	0.00	0.01	b.d.l.	0.01	0.00
0.00	b.d.l.	0.00	b.d.l.	b.d.l.	0.02
50.45	50.78	51.68	51.30	50.96	50.94
0.05	0.03	0.05	0.01	0.04	0.02
1.48	1.75	1.12	1.23	1.28	1.30
0.00	0.01	0.00	0.01	0.04	0.02
0.06	0.05	b.d.l.	b.d.l.	b.d.l.	b.d.l.
99.15	99.56	100.02	99.75	100.12	99.61

CL-07-01-95.95	CL-07-01-140 1	CL-07-01-140 2	CL-07-01-140 3	CL-07-01-140 4	CL-07-01-249 1
0.02	0.03	0.06	0.01	0.04	0.06
0.62	1.92	2.46	2.15	2.45	1.36
46.27	44.84	44.69	44.87	44.55	45.57
0.02	b.d.l.	0.00	0.00	b.d.l.	0.00
b.d.l.	0.00	0.02	b.d.l.	b.d.l.	0.01
50.65	51.44	51.31	51.52	51.80	50.33
0.03	0.05	0.05	0.04	0.05	0.03
1.15	0.97	0.73	1.07	0.73	0.94
0.05	0.01	b.d.l.	b.d.l.	0.00	b.d.l.
b.d.l.	0.07	0.08	0.08	0.06	0.12
98.77	99.28	99.31	99.75	99.61	98.41

CL-07-01-249 2	CL-07-01-249 3	CL-07-01-249 4	CL-07-01-249 5	CL-07-01-308 1	CL-07-01-308 2
0.01	0.02	0.05	0.67	0.01	0.01
0.83	1.57	1.76	0.82	1.88	1.61
46.17	45.38	45.68	45.80	46.01	45.66
0.01	b.d.l.	0.01	0.00	b.d.l.	b.d.l.
0.02	b.d.l.	0.00	0.01	0.02	0.01
50.86	50.19	50.58	48.68	50.62	51.67
0.02	0.03	0.02	1.26	0.06	0.04
1.11	0.66	0.61	1.23	0.85	1.12
b.d.l.	b.d.l.	b.d.l.	0.00	b.d.l.	0.01
0.11	0.14	0.11	0.08	0.11	0.08
99.11	97.98	98.77	98.32	99.60	100.14

CL-07-01-308 3	CL-07-01-308 4	CL-07-01-329 1	CL-07-01-329 2	CL-07-01-329 3	CL-07-01-329 4
0.03	0.03	0.03	0.04	0.04	0.01
1.74	1.87	0.97	1.40	1.02	1.40
45.46	45.26	45.85	45.21	45.26	44.32
0.00	0.01	0.01	b.d.l.	b.d.l.	b.d.l.
0.03	0.01	0.03	0.03	0.01	0.03
51.60	51.00	49.91	50.45	50.01	50.62
0.02	0.05	0.06	0.03	0.04	0.04
1.03	1.03	1.12	0.98	1.08	1.13
0.00	b.d.l.	0.01	b.d.l.	0.00	0.00
0.08	0.09	0.07	0.08	0.07	0.09
100.04	99.29	98.11	98.18	97.52	97.60

CL-07-01-329 5	CL-07-01-354 1	CL-07-01-354 2	CL-07-01-354 3
0.02	0.04	0.03	0.04
1.64	1.21	1.29	0.65
44.97	46.75	46.31	46.65
b.d.l.	b.d.l.	0.03	0.00
0.00	0.06	0.04	0.06
50.07	51.36	51.01	50.24
0.04	0.02	0.03	0.04
0.82	0.83	0.85	1.28
0.01	0.00	0.01	b.d.l.
0.08	0.09	b.d.l.	b.d.l.
97.57	100.33	99.59	99.01

Appendix 16: Sulfide LA-ICP-MS analyses

CL-06-16-56.3	8 - Py	11 - Py	21 - Py	23 - Py	26 - Py	5 - Pn	18 - Pn	19 - Pn	25 - Pn
Si^{29} (ppm)	b.d.l	b.d.l	b.d.l	b.d.l	b.d.l	11054.27	8696.26	39508.37	6767.54
S^{33}	198890.58	180429.20	177352.25	170140.89	162043.59	159616.21	161312.79	122542.02	128312.45
Ca^{43}	34274.51	14493.72	25969.15	15147.18	20781.63	612.29	b.d.l	b.d.l	453.49
V^{51}	b.d.l	b.d.l	b.d.l	b.d.l	b.d.l	3.12	10.83	63.94	1.15
Cr^{53}	b.d.l	b.d.l	b.d.l	b.d.l	b.d.l	b.d.l	b.d.l	b.d.l	b.d.l
Fe^{57}	534500.00	534500.00	534500.00	534500.00	534500.00	291000.00	291000.00	291000.00	291000.00
Co^{59}	454.96	781.43	314.58	473.30	1150.89	89533.90	79771.85	57205.23	51461.28
Ni^{60}	1474.70	2449.82	1200.95	1276.87	2596.23	318604.31	301380.13	260361.92	261098.20
Cu^{65}	17.14	972.19	10.82	10.31	21.57	3354.52	4386.53	5982.96	1610.15
Zn^{66}	2.42	2.40	1.18	1.33	4.29	306.76	118.01	130.79	8.23
As^{75}	1.25	0.65	0.58	b.d.l	0.97	1.54	2.18	2.75	1.15
Se^{82}	44.01	40.45	39.34	42.85	38.26	55.56	41.28	50.81	36.09
Sr^{88}	8.44	4.23	5.24	4.01	6.67	12.81	2.54	6.42	2.74
Y^{89}	3.05	0.62	1.34	1.04	1.36	0.48	0.07	1.01	0.11
Zr^{90}	0.02	0.02	b.d.l	0.01	0.05	0.11	0.14	0.29	0.13
Ru^{99}	0.00	0.00	b.d.l	0.00	0.00	0.00	0.00	0.00	0.00
Ru^{101}	b.d.l	b.d.l	b.d.l	b.d.l	b.d.l	0.00	0.00	0.00	0.12
Rh^{103}	b.d.l	b.d.l	b.d.l	0.02	b.d.l	0.32	0.15	0.31	0.08
Pd^{105}	b.d.l	b.d.l	b.d.l	b.d.l		0.66	0.27	0.23	0.21
Pd^{106}	b.d.l	b.d.l	b.d.l	b.d.l	b.d.l	0.61	0.44	0.46	0.18
Ag^{107}	0.39	2.43	0.36	0.77	1.51	168.47	138.11	88.70	79.93
Pd^{108}	b.d.l	b.d.l	b.d.l	b.d.l	b.d.l	0.68	0.38	0.38	0.28
Cd^{111}	b.d.l	b.d.l	b.d.l	b.d.l	b.d.l	2.25	0.49	0.89	b.d.l
Sn^{118}	b.d.l	0.06	b.d.l	0.08	0.29	0.09	1.26	0.38	0.36
Sb^{121}	0.67	2.29	0.94	0.61	0.71	0.56	0.12	0.07	0.07
Te^{125}	0.41	b.d.l	b.d.l	0.34	b.d.l	4.32	b.d.l	4.97	1.25
Ta^{181}	b.d.l	b.d.l	b.d.l	b.d.l	b.d.l	b.d.l	b.d.l	b.d.l	b.d.l
Re^{185}	0.13	0.38	2.19	0.49	0.19	0.13	0.07	0.18	b.d.l
Os^{189}	b.d.l	b.d.l	b.d.l	b.d.l	b.d.l	b.d.l	b.d.l	b.d.l	b.d.l
Ir^{193}	b.d.l	b.d.l	b.d.l	b.d.l	b.d.l	b.d.l	b.d.l	b.d.l	b.d.l
Pt^{195}	b.d.l	b.d.l	b.d.l	b.d.l	b.d.l	b.d.l	b.d.l	b.d.l	b.d.l
Au^{197}	b.d.l	0.05	b.d.l	b.d.l	b.d.l	0.29	11.09	0.24	0.03
Tl^{205}	0.16	0.30	0.10	0.22	0.12	93.18	9.06	67.34	109.58
Pb^{208}	212.29	243.15	120.52	138.55	155.88	15400.60	154.03	137.49	105.25
Bi^{209}	1.42	0.98	0.99	0.88	0.53	83.97	15.53	43.19	18.42

4 - Ccp	9 - Ccp	13 - Ccp	17 - Ccp	24 - Ccp	6 - Po	7 - Po	12 - Po	20 - Po	22 - Po
b.d.l	b.d.l	b.d.l	b.d.l	6243.63	b.d.l	b.d.l	b.d.l	b.d.l	b.d.l
133976.39	104126.43	122502.21	122976.86	123410.31	143497.57	140611.06	116251.19	132460.61	129571.66
b.d.l	b.d.l	b.d.l	923.54	b.d.l	291.62	b.d.l	b.d.l	b.d.l	b.d.l
b.d.l	b.d.l	b.d.l	b.d.l	6.03	0.77	0.59	b.d.l	0.38	b.d.l
b.d.l	b.d.l	b.d.l	b.d.l	b.d.l	b.d.l	b.d.l	b.d.l	b.d.l	b.d.l
314000.00	314000.00	314000.00	314000.00	314000.00	602700.00	602700.00	602700.00	602700.00	602700.00
44.20	18.39	<666.1918	36.68	31.60	694.00	421.24	751.79	656.73	758.90
399.90	1139.99	14.16	b.d.l	945.53	12417.37	9425.65	9313.54	9457.34	9111.28
374717.95	256479.43	353857.50	325818.44	340925.20	6460.43	b.d.l	7.49	b.d.l	8.43
563.90	282.14	671.53	311.85	147.21	8.80	1.80	2.10	0.68	1.27
b.d.l	0.52	b.d.l	2.34	1.57	0.92	0.60	0.78	0.83	b.d.l
42.77	31.41	36.67	33.07	37.08	44.13	39.52	37.29	42.92	37.63
0.15	0.21	0.95	0.53	1.78	0.33	0.35	0.13	0.09	0.19
0.01	b.d.l	b.d.l	0.02	0.11	0.02	b.d.l	b.d.l	b.d.l	b.d.l
0.01	b.d.l	b.d.l	0.10	0.02	0.02	b.d.l	0.02	0.03	b.d.l
0.25	0.21	0.84	0.27	0.27	0.00	0.00	0.00	0.00	0.00
0.16	0.03	b.d.l	b.d.l	0.00	0.00	0.00	0.00	0.00	0.00
15.59	10.60	16.87	14.30	15.47	0.24	b.d.l	b.d.l	0.01	b.d.l
0.00	0.00	2.61	0.00	0.00	0.00	b.d.l	b.d.l	b.d.l	b.d.l
0.12	0.08	0.33	0.11	0.06	b.d.l	b.d.l	b.d.l	b.d.l	b.d.l
20.64	24.32	20.78	20.44	24.51	3.12	0.23	0.07	0.07	0.22
0.08	0.04	b.d.l	0.11	0.06	b.d.l	b.d.l	b.d.l	b.d.l	b.d.l
3.66	1.89	4.39	1.74	1.22	b.d.l	b.d.l	b.d.l	b.d.l	b.d.l
0.07	0.45	1.23	0.80	0.23	0.12	0.18	0.22	0.32	0.12
b.d.l	b.d.l	0.05	b.d.l	0.04	b.d.l	b.d.l	b.d.l	b.d.l	b.d.l
0.74	2.11	1.26	1.68	0.88	b.d.l	0.25	b.d.l	b.d.l	b.d.l
b.d.l	b.d.l	b.d.l	b.d.l	b.d.l	b.d.l	b.d.l	b.d.l	b.d.l	b.d.l
0.15	0.11	b.d.l	b.d.l	b.d.l	0.30	0.14	0.05	0.46	0.16
b.d.l	b.d.l	b.d.l	b.d.l	b.d.l	b.d.l	b.d.l	b.d.l	b.d.l	b.d.l
b.d.l	b.d.l	b.d.l	b.d.l	b.d.l	b.d.l	b.d.l	b.d.l	b.d.l	b.d.l
b.d.l	b.d.l	b.d.l	b.d.l	b.d.l	b.d.l	b.d.l	b.d.l	b.d.l	b.d.l
b.d.l	0.10	b.d.l	b.d.l	b.d.l	b.d.l	b.d.l	b.d.l	b.d.l	b.d.l
0.53	0.64	b.d.l	0.29	2.42	2.63	0.02	b.d.l	0.01	b.d.l
24.58	23.11	4.19	8.47	18.80	60.98	4.22	0.56	1.44	2.66
4.72	10.55	1.07	1.78	1.96	2.87	1.43	0.19	0.62	1.20

CL-06-16-81.6	12 - Py	13 - Py	21 - Py	22 - Py	24 - Py	4 - Pn	5 - Pn	7 - Pn	8 - Pn
Si^{29} (ppm)	b.d.l	1907.53	b.d.l	3698.32	6744.51	6079.36	6049.21	b.d.l	b.d.l
S^{33}	207375.22	191139.69	207001.91	229981.23	244273.17	147143.41	109738.62	102235.74	166702.74
Ca^{43}	11435.94	5211.61	35028.72	16418.65	29198.73	1324.58	776.09	b.d.l	873.28
V^{51}	b.d.l	b.d.l	2.79	6.73	1.67	17.13	15.86	3.51	b.d.l
Cr^{53}	b.d.l	b.d.l	b.d.l	13.85	b.d.l	b.d.l	b.d.l	b.d.l	b.d.l
Fe^{57}	534500.00	534500.00	534500.00	534500.00	534500.00	291000.00	291000.00	291000.00	291000.00
Co^{59}	1588.80	641.44	339.16	617.25	314.50	38178.75	18773.71	22468.83	76079.14
Ni^{60}	5328.27	2317.74	991.26	719.17	1536.42	349767.21	189650.81	150535.37	370207.58
Cu^{65}	14.52	65.02	345.54	85.92	16047.70	55.07	32.04	23.82	317.21
Zn^{66}	0.80	6.56	96.99	7.05	11.45	3.96	44.51	4.59	45.66
As^{75}	2.35	1.90	30.43	11.35	18.31	8.51	2.99	4.71	2.28
Se^{82}	60.78	52.62	46.93	47.37	43.53	42.90	36.89	37.69	66.95
Sr^{88}	2.84	2.25	6.84	4.62	6.29	3.34	3.33	4.17	1.99
Y^{89}	0.40	0.53	1.75	1.35	3.63	0.22	0.17	0.15	0.17
Zr^{90}	b.d.l	0.07	0.06	0.10	b.d.l	1.45	0.73	0.10	0.33
Ru^{99}	0.00	0.00	b.d.l	0.00	0.04	0.00	0.00	0.00	0.00
Ru^{101}	b.d.l	b.d.l	b.d.l	b.d.l	b.d.l	0.00	0.00	0.00	0.00
Rh^{103}	0.04	0.02	0.02	b.d.l	0.64	b.d.l	b.d.l	0.01	0.04
Pd^{105}	b.d.l	b.d.l	b.d.l	b.d.l	0.00	b.d.l	b.d.l	0.05	0.03
Pd^{106}	b.d.l	b.d.l	b.d.l	b.d.l	b.d.l	0.13	0.05	0.11	0.15
Ag^{107}	1.56	3.40	1.06	0.65	3.00	31.09	12.78	22.74	81.37
Pd^{108}	b.d.l	0.05	b.d.l	0.05	b.d.l	b.d.l	b.d.l	0.05	0.06
Cd^{111}	b.d.l	0.58	0.39	0.21	b.d.l	b.d.l	b.d.l	b.d.l	0.35
Sn^{118}	49.00	15.75	26.33	10.29	116.38	118.53	26.05	11.49	26.95
Sb^{121}	0.43	0.31	0.26	1.54	0.51	0.33	0.21	0.10	0.35
Te^{125}	0.35	b.d.l	1.34	2.35	0.97	4.67	1.88	2.63	2.66
Ta^{181}	b.d.l	b.d.l	b.d.l	0.01	0.01	0.03	b.d.l	0.02	0.02
Re^{185}	0.18	0.06	0.06	0.06	0.13	b.d.l	0.29	0.08	0.20
Os^{189}	b.d.l	b.d.l	b.d.l	b.d.l	b.d.l	b.d.l	b.d.l	b.d.l	b.d.l
Ir^{193}	b.d.l	b.d.l	b.d.l	0.05	b.d.l	b.d.l	b.d.l	0.30	b.d.l
Pt^{195}	b.d.l	b.d.l	b.d.l	b.d.l	b.d.l	b.d.l	b.d.l	b.d.l	b.d.l
Au^{197}	0.03	b.d.l	0.05	0.06	0.71	0.08	b.d.l	0.07	0.74
Tl^{205}	0.49	0.39	0.07	0.04	0.46	21.82	17.60	16.30	12.88
Pb^{208}	199.73	248.59	142.94	122.11	204.46	115.34	61.82	114.10	182.86
Bi^{209}	0.71	1.02	4.49	4.85	3.54	13.22	9.43	15.76	24.92

9 - Ccp	10 - Ccp	19 - Ccp	23 - Ccp	26 - Ccp	6 - Po	11 - Po	17 - Po	25 - Po
b.d.l	b.d.l	6308.85	b.d.l	9797.84	b.d.l	7189.14	b.d.l	b.d.l
141709.09	136168.31	162922.95	177166.71	189994.63	163081.02	145734.81	155379.22	153795.45
830.80	1112.94	b.d.l	b.d.l	b.d.l	b.d.l	b.d.l	b.d.l	b.d.l
b.d.l	b.d.l	1.47	b.d.l	b.d.l	2.27	6.43	1.28	1.66
b.d.l	b.d.l	b.d.l	b.d.l	b.d.l	b.d.l	6.25	b.d.l	b.d.l
314000.00	314000.00	314000.00	314000.00	314000.00	602700.00	602700.00	602700.00	602700.00
13.69	2.07	78.27	0.89	3.29	574.85	469.79	532.25	264.44
909.08	25.72	315.57	14.02	50.01	8372.55	7952.05	8455.73	5987.46
396005.18	403292.63	353170.84	343591.73	402965.54	17.99	1096.08	839.20	146.94
239.20	978.25	226.63	617.46	231.98	2.66	105.14	57.99	208.58
3.89	52.90	3.44	13.44	1.97	1.83	30.08	5.23	11.75
47.37	48.89	48.69	48.56	64.44	46.58	43.92	49.40	41.92
0.50	0.65	0.78	0.65	0.53	0.56	2.92	1.49	2.12
b.d.l	b.d.l	b.d.l	b.d.l	b.d.l	b.d.l	b.d.l	0.03	b.d.l
0.05	0.07	0.14	0.14	0.11	0.09	0.14	b.d.l	0.15
0.34	0.65	b.d.l	0.41	0.83	b.d.l	0.00	b.d.l	b.d.l
b.d.l	0.63	b.d.l	b.d.l	b.d.l	b.d.l	0.00	b.d.l	b.d.l
15.54	15.28	14.49	16.28	20.23	b.d.l	b.d.l	b.d.l	b.d.l
0.00	0.00	0.00	0.00	0.00	b.d.l	b.d.l	b.d.l	b.d.l
0.09	0.13	0.07	0.10	b.d.l	b.d.l	0.08	b.d.l	b.d.l
18.09	15.93	14.70	9.76	21.32	1.29	0.45	0.77	0.64
b.d.l	b.d.l	b.d.l	0.11	b.d.l	0.07	b.d.l	b.d.l	b.d.l
1.59	4.46	0.53	2.30	2.97	b.d.l	b.d.l	b.d.l	0.68
46.98	146.31	44.44	37.01	344.61	26.41	69.66	57.23	151.32
0.19	0.13	b.d.l	0.24	b.d.l	b.d.l	0.09	0.08	0.20
2.23	b.d.l	2.15	1.65	1.35	b.d.l	b.d.l	b.d.l	b.d.l
b.d.l	b.d.l	b.d.l	b.d.l	b.d.l	b.d.l	b.d.l	b.d.l	0.02
b.d.l	b.d.l	0.41	0.18	0.42	0.21	0.30	0.24	0.38
b.d.l	b.d.l	b.d.l	b.d.l	b.d.l	b.d.l	b.d.l	b.d.l	b.d.l
b.d.l	b.d.l	b.d.l	b.d.l	b.d.l	b.d.l	0.03	0.04	0.07
b.d.l	0.36	b.d.l	0.13	b.d.l	b.d.l	b.d.l	b.d.l	0.20
0.10	0.24	b.d.l	8.64	b.d.l	b.d.l	1.30	0.04	2.44
0.38	0.07	0.20	1.00	0.39	0.05	0.67	b.d.l	b.d.l
18.08	9.25	7.15	33.68	15.21	14.57	1.93	36.86	5.55
5.24	0.94	2.05	2.73	1.72	3.99	0.56	1.19	1.23

CL-06-39-20.35	6 - Po	10 - Po	13 - Po	19 - Po	21 - Po	4 - Mrc	18 - Mrc	7 - Py	11 - Py
Si^{29} (ppm)	b.d.l	b.d.l	9087.58	b.d.l	b.d.l	14081.84	24706.89	b.d.l	5356.14
S^{33}	206624.99	211888.93	193743.04	172763.17	169879.84	261863.83	219313.51	268780.81	240183.49
Ca^{43}	b.d.l	b.d.l	b.d.l	b.d.l	b.d.l	10435.01	1308.23	23537.53	64688.80
V^{51}	b.d.l	0.71	b.d.l	b.d.l	b.d.l	b.d.l	b.d.l	b.d.l	b.d.l
Cr^{53}	b.d.l	b.d.l	b.d.l	b.d.l	b.d.l	b.d.l	b.d.l	b.d.l	b.d.l
Fe^{57}	602700.00	602700.00	602700.00	602700.00	602700.00	534500.00	534500.00	534500.00	534500.00
Co^{59}	1099.11	248.75	1499.77	109.80	242.39	674.60	400.73	2074.30	308.09
Ni^{60}	9632.42	8146.55	14017.71	8111.72	6841.48	29373.21	31891.91	9495.89	12705.39
Cu^{65}	43168.74	4.06	8277.66	249.80	4.29	82.29	95.51	36.19	788.61
Zn^{66}	18.02	3.83	1323.39	0.81	1.34	3.85	1.90	2.90	30.06
As^{75}	2.10	0.95	1.80	b.d.l	0.73	2.01	2.66	1.42	0.80
Se^{82}	45.31	58.42	63.91	54.97	43.15	69.97	68.84	62.51	65.68
Sr^{88}	2.36	0.48	1.24	0.11	0.93	5.19	17.87	9.08	14.84
Y^{89}	b.d.l	b.d.l	0.09	b.d.l	b.d.l	b.d.l	0.06	b.d.l	b.d.l
Zr^{90}	0.05	b.d.l	0.06	b.d.l	0.02	0.04	0.01	0.19	0.03
Ru^{99}	b.d.l	0.19	0.00	0.09	0.04	0.00	0.00	0.00	0.11
Ru^{101}	b.d.l	0.00	b.d.l	0.00	0.00	0.00	0.00	0.00	0.00
Rh^{103}	2.23	b.d.l	0.43	b.d.l	0.04	b.d.l	0.04	b.d.l	0.04
Pd^{105}	0.00	b.d.l	0.76	b.d.l	b.d.l	b.d.l	b.d.l	0.04	0.06
Pd^{106}	b.d.l	b.d.l	1.43	b.d.l	b.d.l	b.d.l	b.d.l	b.d.l	b.d.l
Ag^{107}	0.80	0.10	3.96	0.21	0.41	16.45	67.10	3.22	10.58
Pd^{108}	0.33	b.d.l	1.01	b.d.l	b.d.l	b.d.l	b.d.l	b.d.l	b.d.l
Cd^{111}	b.d.l	b.d.l	15.02	b.d.l	b.d.l	0.86	0.59	0.26	0.44
Sn^{118}	3.90	0.71	0.48	0.71	1.80	b.d.l	0.83	6.24	0.66
Sb^{121}	b.d.l	b.d.l	b.d.l	b.d.l	b.d.l	b.d.l	0.03	0.22	0.11
Te^{125}	b.d.l	0.64	75.08	0.45	1.43	0.96	0.63	0.49	1.73
Ta^{181}	b.d.l	b.d.l	b.d.l	b.d.l	b.d.l	b.d.l	b.d.l	0.01	b.d.l
Re^{185}	b.d.l	0.17	b.d.l	0.11	0.26	0.39	0.20	0.21	0.38
Os^{189}	b.d.l	b.d.l	b.d.l	0.08	0.08	0.16	0.08	b.d.l	0.11
Ir^{193}	b.d.l	b.d.l	b.d.l	b.d.l	b.d.l	0.03	b.d.l	0.02	b.d.l
Pt^{195}	b.d.l	b.d.l	b.d.l	b.d.l	b.d.l	b.d.l	b.d.l	b.d.l	b.d.l
Au^{197}	b.d.l	b.d.l	b.d.l	b.d.l	b.d.l	b.d.l	b.d.l	b.d.l	b.d.l
Tl^{205}	b.d.l	b.d.l	0.22	<0.012053	0.02	3.10	3.52	0.59	2.51
Pb^{208}	11.76	2.49	27.94	1.64	3.44	92.95	171.45	280.99	230.42
Bi^{209}	0.99	0.34	3.75	0.38	0.44	0.38	0.46	0.50	0.60

24 - Py	26 - Py	5 - Pn	9 - Pn	20 - Pn	23 - Pn	8 - Ccp	12 - Ccp	17 - Ccp	22 - Ccp	25 - Ccp
b.d.l	4895.44	17234.83	9112.87	b.d.l	b.d.l	4718.45	6852.19	2934.47	b.d.l	15136.01
192987.33	219684.09	241772.67	163451.82	102289.26	133104.28	116471.98	154833.48	171638.54	155657.50	173540.46
b.d.l	54279.22	b.d.l	b.d.l	649.78	b.d.l	b.d.l	b.d.l	b.d.l	b.d.l	b.d.l
b.d.l	0.79	b.d.l	b.d.l	b.d.l	b.d.l	b.d.l	b.d.l	b.d.l	b.d.l	1.32
b.d.l	b.d.l	b.d.l	b.d.l	b.d.l	b.d.l	b.d.l	b.d.l	b.d.l	b.d.l	b.d.l
534500.00	534500.00	291000.00	291000.00	291000.00	291000.00	314000.00	314000.00	314000.00	314000.00	314000.00
351.24	957.49	70496.71	42834.66	43430.43	33131.29	8.41	3.01	6.27	1.18	12.74
17607.85	8089.35	352416.59	340177.28	204321.64	281109.78	176.30	44.08	186.43	64.24	51.34
153.42	4955.45	35.48	1726.89	931.28	412.33	205177.53	335511.28	389356.32	378064.81	380240.42
3.45	491.09	4.61	96.64	10.81	3.19	2373.10	196.33	324.94	695.40	298.13
b.d.l	4.37	2.43	4.19	1.86	1.06	1.38	1.25	0.88	0.70	<1.1523
73.22	66.27	54.72	65.15	24.43	47.11	45.19	48.37	59.19	62.63	82.55
0.53	14.52	2.44	1.45	0.69	0.31	0.41	0.53	0.21	0.28	1.13
b.d.l	0.03	b.d.l	0.18	b.d.l	b.d.l	0.01	0.17	0.01	b.d.l	0.05
0.03	0.07	0.25	0.13	0.12	0.13	0.05	0.03	b.d.l	0.02	1.02
0.00	0.00	0.00	0.00	0.00	0.00	0.44	0.49	0.33	0.41	0.65
0.00	0.00	0.00	0.00	0.00	0.00	b.d.l	0.27	0.22	0.29	0.25
b.d.l	0.25	b.d.l	0.09	0.07	0.03	8.40	13.29	16.34	15.97	17.23
b.d.l	0.00	0.61	2.79	0.32	0.74	0.00	0.00	0.00	0.00	0.00
b.d.l	0.30	1.14	2.94	0.35	0.44	1.14	0.04	0.08	0.86	b.d.l
30.41	7.75	15.04	17.78	10.48	35.44	0.17	34.48	4.16	39.48	0.14
b.d.l	0.16	0.95	2.43	0.27	0.37	0.67	b.d.l	b.d.l	1.03	b.d.l
0.44	5.92	b.d.l	1.33	0.12	0.29	35.65	1.09	1.92	12.70	3.12
2.69	1.52	0.96	b.d.l	0.42	b.d.l	2.08	1.89	1.20	0.83	3.70
0.04	0.25	0.13	b.d.l	b.d.l	b.d.l	b.d.l	b.d.l	b.d.l	b.d.l	b.d.l
0.35	1.53	b.d.l	44.00	1.41	0.69	18.34	25.19	35.80	19.05	9.06
b.d.l	b.d.l	b.d.l	b.d.l	b.d.l	b.d.l	b.d.l	b.d.l	b.d.l	b.d.l	b.d.l
0.13	0.09	b.d.l	b.d.l	0.03	0.07	b.d.l	b.d.l	b.d.l	0.32	0.11
0.08	0.18	b.d.l	b.d.l	b.d.l	b.d.l	b.d.l	b.d.l	b.d.l	b.d.l	b.d.l
b.d.l	b.d.l	b.d.l	b.d.l	b.d.l	b.d.l	b.d.l	b.d.l	b.d.l	b.d.l	b.d.l
b.d.l	b.d.l	b.d.l	b.d.l	b.d.l	b.d.l	b.d.l	b.d.l	b.d.l	b.d.l	b.d.l
b.d.l	0.03	b.d.l	b.d.l	b.d.l	b.d.l	b.d.l	0.02	0.04	0.02	b.d.l
1.98	0.65	2.26	1.07	1.14	1.27	0.33	0.06	0.15	0.07	0.06
24.29	248.61	35.50	24.17	29.88	25.37	27.92	15.19	56.13	37.19	5.76
0.33	1.54	0.36	1.54	1.35	0.64	1.17	0.44	0.47	0.79	0.25

Appendix 17: LA-ICP-MS SUL analyses

Sample/ Inclusion	Na^{23} (ppm)	Mg^{25}	Si^{28}	S^{32}	Ca^{40}	Ti^{49}	Fe^{56}	Co^{59}	Ni^{62}	Cu^{65}
373_12_1	b.d.l	b.d.l	b.d.l	335000	b.d.l	317.00	623300	1538	1678	8195
373_12_2	b.d.l	b.d.l	b.d.l	364215	b.d.l	3098.26	623300	1628	1678	4463
373_12_3	3442.13	16074.34	b.d.l	314123	b.d.l	4898.80	623300	2825	3359	641
373_12_4	b.d.l	12823.89	b.d.l	290639	b.d.l	4580.83	623300	1673	1856	8289
373_12_5	b.d.l	b.d.l	b.d.l	342759	52859.31	5518.16	623300	1344	1725	6638
373_12_6	b.d.l	b.d.l	b.d.l	315689	9066.27	8627.08	623300	1541	1729	7535
373_12_7	b.d.l	b.d.l	b.d.l	302872	36329.71	1964.09	623300	1471	1481	5036
373_12_1	7269.75	b.d.l	b.d.l	336234	4731.77	4186.36	623300	1341	1299	8621
373_12_1	59467.53	b.d.l	b.d.l	327634	b.d.l	1314.66	623300	2743	<2401.6326	13872
373_12_1	15867.22	b.d.l	b.d.l	323062	b.d.l	b.d.l	623300	1413	1430	6173
373_12_1	27152.42	b.d.l	b.d.l	304136	b.d.l	2246.10	623300	1414	1470	7127
373_12_1	15237.33	b.d.l	b.d.l	327666	b.d.l	4254.22	623300	1968	1692	9781
373_12_1	10040.90	b.d.l	b.d.l	327247	1567.80	2901.28	623300	1660	1673	8933
373_12_1	19557.07	1762.85	b.d.l	384868	10456.59	3953.36	623300	1481	1774	4247
373_12_1	23362.09	b.d.l	b.d.l	394096	12170.60	4183.46	623300	1456	1589	9398
373_12_1	9752.95	b.d.l	b.d.l	287905	22285.50	3303.75	623300	1417	1515	6814
373_12_2	18826.45	b.d.l	b.d.l	278207	1254.49	2138.42	623300	1404	1504	7028
373_12_2	12670.33	b.d.l	b.d.l	315552	9971.90	2908.78	623300	1096	1569	6695
373_12_2	9173.17	b.d.l	b.d.l	293634	b.d.l	2380.64	623300	1433	1656	7586
373_12_2	19648.25	b.d.l	b.d.l	278900	5069.81	3275.00	623300	1429	1744	6903
373_12_2	18034.08	24271.53	b.d.l	222036	b.d.l	9303.32	623300	3998	5937	27165
373_12_2	26192.23	22921.35	b.d.l	238518	b.d.l	b.d.l	623300	4431	3096	10335
373_9_2	15218.46	b.d.l	b.d.l	208657	b.d.l	20789.44	623300	949	b.d.l	5127
373_9_3	<1354.7832	b.d.l	b.d.l	267185	17699.77	12695.52	623300	1079	b.d.l	5975
373_9_4	11666.81	b.d.l	b.d.l	283441	b.d.l	9223.21	623300	1379	1387	6862
373_9_5	10915.97	9622.00	b.d.l	254265	b.d.l	11795.40	623300	1412	b.d.l	5801
373_9_6	5788.60	25516.63	b.d.l	267087	b.d.l	6588.52	623300	1326	1478	6056
373_9_7	20675.11	b.d.l	b.d.l	370226	b.d.l	b.d.l	623300	2839	b.d.l	9599
373_9_8	13963.17	b.d.l	b.d.l	300697	39811.51	14532.06	623300	1906	1896	5158
127-4-1	1278.99	b.d.l	1363.00	325718	b.d.l	178.29	623300	2436	2048	6291
127-4-2	26415.95	b.d.l	b.d.l	288332	b.d.l	b.d.l	623300	2601	b.d.l	4117
127-4-3	3441.80	189450.90	312751.31	78842	b.d.l	1910.37	623300	1067	b.d.l	b.d.l
127-4-4	1335.27	b.d.l	1367.61	316749	b.d.l	177.98	623300	2441	2037	6310
127-4-5	26083.76	b.d.l	b.d.l	284172	b.d.l	b.d.l	623300	2599	b.d.l	4023
127-4-6	3245.11	193781.54	311901.81	79965	b.d.l	2046.68	623300	1130	b.d.l	b.d.l
127-4-7	b.d.l	b.d.l	b.d.l	459856	b.d.l	b.d.l	623300	2703	b.d.l	10036
127-4-8	b.d.l	10260.61	10098.74	288209	b.d.l	b.d.l	623300	2131	b.d.l	5272
127-4-9	b.d.l	b.d.l	b.d.l	264053	b.d.l	b.d.l	623300	2259	1823	4087
127-4-10	b.d.l	b.d.l	b.d.l	268930	b.d.l	b.d.l	623300	1890	b.d.l	4273
127-4-11	b.d.l	b.d.l	b.d.l	233885	b.d.l	b.d.l	623300	2164	b.d.l	4519
127-4-14	302.84	b.d.l	b.d.l	283644	b.d.l	184.28	623300	2319	1968	4886

127-4-1	n.a	7356.54	3605.32	259875	b.d.l	n.a	623300	2158	1875	4621
127-4-3	n.a	2929.00	b.d.l	310739	b.d.l	n.a	623300	1688	1822	4383
127-4-4	n.a	b.d.l	b.d.l	260219	b.d.l	n.a	623300	2568	3994	15483
127-4-5	n.a	4887.00	b.d.l	264014	b.d.l	n.a	623300	2907	b.d.l	8738
127-3-1	n.a	2564.82	4814.72	300938	b.d.l	n.a	623300	2048	2393	7913
127-3-3	n.a	2470.51	3956.40	295119	b.d.l	n.a	623300	1794	1589	<335.8374
127-3-4	n.a	b.d.l	b.d.l	283613	b.d.l	n.a	623300	1573	1438	12692
127-3-5	n.a	b.d.l	b.d.l	291342	b.d.l	n.a	623300	1860	b.d.l	5249
127-3-6	n.a	1425.43	2115.59	306254	b.d.l	n.a	623300	1660	1594	5824
127-3-7	n.a	8572.30	11997.80	289611	b.d.l	n.a	623300	2031	1809	6193
127-3-8	n.a	4246.45	6219.00	279332	b.d.l	n.a	623300	1786	b.d.l	5053
127-3-10	n.a	27014.89	29209.93	230137	b.d.l	n.a	623300	1548	b.d.l	4353
127-3-14	n.a	954.48	b.d.l	259141	b.d.l	n.a	623300	1883	1409	5536
127-3-15	n.a	b.d.l	b.d.l	b.d.l	b.d.l	n.a	623300	1932	1606	4628
127-3-16	n.a	b.d.l	b.d.l	258294	b.d.l	n.a	623300	1794	b.d.l	5385
127-3-17	n.a	b.d.l	b.d.l	268658	b.d.l	n.a	623300	1974	b.d.l	5964
127-3-18	n.a	23015.41	51703.06	237059	b.d.l	n.a	623300	1800	1429	5005
127-3-24	n.a	1166.91	1425.03	240842	b.d.l	n.a	623300	1701	1450	5214
127-3-25	n.a	b.d.l	b.d.l	260629	b.d.l	n.a	623300	1561	b.d.l	4326
127-3-26	n.a	b.d.l	b.d.l	269510	b.d.l	n.a	623300	1839	b.d.l	5750
127-3-27	n.a	b.d.l	b.d.l	294724	b.d.l	n.a	623300	2374	b.d.l	7555
373_15_1	n.a	b.d.l	b.d.l	276530	b.d.l	n.a	623300	657	1188	4541
373_15_2	n.a	b.d.l	b.d.l	261755	3033.44	n.a	623300	5543	2624	484
373-15-1	617.88	24935.03	b.d.l	317010	10434.93	201.95	623300	2905	2268	25774
373-15-3	b.d.l	25020.54	b.d.l	232070	b.d.l	211.07	623300	776	1166	5662
373-15-4	131.38	15251.43	b.d.l	205185	b.d.l	55.57	623300	488	916	10635
373-15-5	11.06	5549.59	b.d.l	260249	b.d.l	194.21	623300	1653	1461	4444

Zn^{66}	As^{75}	Se^{82}	Pd^{105}	Pd^{106}	Ag^{107}	Pd^{108}	Cd^{114}	Sn^{120}	Sb^{121}	Te^{125}	Pt^{195}
b.d.l	b.d.l	b.d.l	b.d.l	b.d.l	b.d.l	b.d.l	b.d.l	b.d.l	b.d.l	b.d.l	b.d.l
b.d.l	b.d.l	b.d.l	b.d.l	b.d.l	b.d.l	b.d.l	b.d.l	b.d.l	b.d.l	b.d.l	b.d.l
3872.73	b.d.l	b.d.l	b.d.l	b.d.l	b.d.l	b.d.l	b.d.l	b.d.l	b.d.l	b.d.l	b.d.l
447.60	b.d.l	b.d.l	b.d.l	b.d.l	17.86	b.d.l	b.d.l	b.d.l	b.d.l	b.d.l	b.d.l
b.d.l	b.d.l	b.d.l	b.d.l	b.d.l	b.d.l	b.d.l	b.d.l	b.d.l	b.d.l	b.d.l	b.d.l
b.d.l	b.d.l	b.d.l	b.d.l	b.d.l	b.d.l	b.d.l	b.d.l	b.d.l	b.d.l	b.d.l	b.d.l
b.d.l	b.d.l	b.d.l	b.d.l	b.d.l	6.90	b.d.l	b.d.l	b.d.l	b.d.l	b.d.l	b.d.l
119.09	b.d.l	b.d.l	b.d.l	b.d.l	7.75	b.d.l	b.d.l	b.d.l	b.d.l	b.d.l	b.d.l
b.d.l	b.d.l	b.d.l	b.d.l	b.d.l	b.d.l	b.d.l	b.d.l	b.d.l	b.d.l	b.d.l	b.d.l
b.d.l	b.d.l	b.d.l	b.d.l	b.d.l	b.d.l	b.d.l	b.d.l	b.d.l	b.d.l	b.d.l	b.d.l
b.d.l	b.d.l	b.d.l	b.d.l	b.d.l	9.45	b.d.l	b.d.l	b.d.l	b.d.l	b.d.l	b.d.l
149.82	b.d.l	b.d.l	b.d.l	b.d.l	7.01	b.d.l	b.d.l	b.d.l	b.d.l	b.d.l	b.d.l
100.47	b.d.l	b.d.l	b.d.l	b.d.l	7.08	b.d.l	b.d.l	b.d.l	b.d.l	b.d.l	b.d.l
b.d.l	b.d.l	b.d.l	b.d.l	b.d.l	b.d.l	b.d.l	b.d.l	b.d.l	b.d.l	b.d.l	b.d.l
b.d.l	b.d.l	b.d.l	b.d.l	b.d.l	b.d.l	b.d.l	b.d.l	b.d.l	b.d.l	b.d.l	b.d.l
b.d.l	b.d.l	b.d.l	b.d.l	b.d.l	b.d.l	b.d.l	b.d.l	b.d.l	b.d.l	b.d.l	b.d.l
b.d.l	b.d.l	b.d.l	b.d.l	b.d.l	11.06	b.d.l	b.d.l	b.d.l	b.d.l	b.d.l	b.d.l
b.d.l	b.d.l	b.d.l	b.d.l	b.d.l	b.d.l	b.d.l	b.d.l	b.d.l	b.d.l	b.d.l	b.d.l
b.d.l	b.d.l	b.d.l	b.d.l	b.d.l	8.07	b.d.l	b.d.l	b.d.l	b.d.l	b.d.l	b.d.l
180.83	b.d.l	b.d.l	b.d.l	b.d.l	7.35	b.d.l	b.d.l	b.d.l	b.d.l	b.d.l	b.d.l
b.d.l	b.d.l	b.d.l	b.d.l	b.d.l	69.87	b.d.l	b.d.l	b.d.l	b.d.l	b.d.l	b.d.l
255.77	b.d.l	b.d.l	b.d.l	b.d.l	19.17	b.d.l	b.d.l	b.d.l	b.d.l	b.d.l	b.d.l
b.d.l	b.d.l	b.d.l	b.d.l	b.d.l	b.d.l	b.d.l	b.d.l	b.d.l	b.d.l	b.d.l	b.d.l
b.d.l	b.d.l	b.d.l	b.d.l	b.d.l	b.d.l	b.d.l	b.d.l	b.d.l	b.d.l	b.d.l	b.d.l
b.d.l	b.d.l	b.d.l	b.d.l	b.d.l	b.d.l	b.d.l	b.d.l	b.d.l	b.d.l	b.d.l	b.d.l
b.d.l	b.d.l	b.d.l	b.d.l	b.d.l	b.d.l	b.d.l	b.d.l	b.d.l	b.d.l	b.d.l	b.d.l
b.d.l	b.d.l	b.d.l	b.d.l	b.d.l	b.d.l	b.d.l	b.d.l	b.d.l	b.d.l	b.d.l	b.d.l
b.d.l	b.d.l	b.d.l	b.d.l	b.d.l	b.d.l	b.d.l	b.d.l	b.d.l	b.d.l	b.d.l	b.d.l
b.d.l	b.d.l	b.d.l	b.d.l	b.d.l	b.d.l	b.d.l	b.d.l	b.d.l	b.d.l	b.d.l	b.d.l
b.d.l	b.d.l	b.d.l	b.d.l	n.a	b.d.l	b.d.l	b.d.l	b.d.l	b.d.l	b.d.l	b.d.l
b.d.l	b.d.l	b.d.l	b.d.l	n.a	b.d.l	b.d.l	b.d.l	b.d.l	b.d.l	b.d.l	b.d.l
b.d.l	b.d.l	b.d.l	b.d.l	n.a	b.d.l	b.d.l	b.d.l	b.d.l	b.d.l	b.d.l	b.d.l
b.d.l	b.d.l	b.d.l	b.d.l	n.a	b.d.l	b.d.l	b.d.l	b.d.l	b.d.l	b.d.l	b.d.l
b.d.l	b.d.l	b.d.l	b.d.l	n.a	b.d.l	b.d.l	b.d.l	b.d.l	b.d.l	b.d.l	b.d.l
b.d.l	b.d.l	b.d.l	b.d.l	n.a	b.d.l	b.d.l	b.d.l	b.d.l	b.d.l	b.d.l	b.d.l
b.d.l	b.d.l	b.d.l	b.d.l	n.a	b.d.l	b.d.l	b.d.l	b.d.l	b.d.l	b.d.l	b.d.l
b.d.l	b.d.l	b.d.l	b.d.l	n.a	b.d.l	b.d.l	b.d.l	b.d.l	b.d.l	b.d.l	b.d.l
b.d.l	b.d.l	b.d.l	b.d.l	n.a	b.d.l	b.d.l	b.d.l	b.d.l	b.d.l	b.d.l	b.d.l
b.d.l	b.d.l	b.d.l	b.d.l	n.a	b.d.l	b.d.l	b.d.l	b.d.l	b.d.l	b.d.l	b.d.l
b.d.l	b.d.l	b.d.l	b.d.l	n.a	b.d.l	b.d.l	b.d.l	b.d.l	b.d.l	b.d.l	b.d.l
b.d.l	b.d.l	b.d.l	b.d.l	n.a	b.d.l	b.d.l	b.d.l	b.d.l	b.d.l	b.d.l	b.d.l

n.a	n.a	n.a	b.d.l	b.d.l	n.a	b.d.l	b.d.l	n.a	n.a	n.a	b.d.l
n.a	n.a	n.a	b.d.l	b.d.l	n.a	b.d.l	b.d.l	n.a	n.a	n.a	b.d.l
n.a	n.a	n.a	b.d.l	b.d.l	n.a	b.d.l	b.d.l	n.a	n.a	n.a	b.d.l
n.a	n.a	n.a	b.d.l	b.d.l	n.a	b.d.l	b.d.l	n.a	n.a	n.a	b.d.l
n.a	n.a	n.a	b.d.l	b.d.l	n.a	b.d.l	b.d.l	n.a	n.a	n.a	b.d.l
n.a	n.a	n.a	b.d.l	b.d.l	n.a	b.d.l	b.d.l	n.a	n.a	n.a	b.d.l
n.a	n.a	n.a	b.d.l	b.d.l	n.a	b.d.l	b.d.l	n.a	n.a	n.a	b.d.l
n.a	n.a	n.a	b.d.l	b.d.l	n.a	b.d.l	b.d.l	n.a	n.a	n.a	b.d.l
n.a	n.a	n.a	b.d.l	b.d.l	n.a	b.d.l	b.d.l	n.a	n.a	n.a	b.d.l
n.a	n.a	n.a	b.d.l	b.d.l	n.a	b.d.l	b.d.l	n.a	n.a	n.a	b.d.l
n.a	n.a	n.a	b.d.l	b.d.l	n.a	b.d.l	b.d.l	n.a	n.a	n.a	b.d.l
n.a	n.a	n.a	b.d.l	b.d.l	n.a	b.d.l	b.d.l	n.a	n.a	n.a	b.d.l
n.a	n.a	n.a	b.d.l	b.d.l	n.a	b.d.l	b.d.l	n.a	n.a	n.a	b.d.l
n.a	n.a	n.a	b.d.l	b.d.l	n.a	b.d.l	b.d.l	n.a	n.a	n.a	b.d.l
n.a	n.a	n.a	b.d.l	b.d.l	n.a	b.d.l	b.d.l	n.a	n.a	n.a	b.d.l
n.a	n.a	n.a	b.d.l	b.d.l	n.a	b.d.l	b.d.l	n.a	n.a	n.a	b.d.l
n.a	n.a	n.a	b.d.l	b.d.l	n.a	b.d.l	b.d.l	n.a	n.a	n.a	b.d.l
n.a	n.a	n.a	b.d.l	b.d.l	n.a	b.d.l	b.d.l	n.a	n.a	n.a	b.d.l
n.a	n.a	n.a	b.d.l	b.d.l	n.a	b.d.l	b.d.l	n.a	n.a	n.a	b.d.l
n.a	n.a	n.a	b.d.l	b.d.l	n.a	b.d.l	b.d.l	n.a	n.a	n.a	b.d.l
n.a	n.a	n.a	b.d.l	b.d.l	n.a	b.d.l	b.d.l	n.a	n.a	n.a	b.d.l
n.a	n.a	n.a	b.d.l	b.d.l	n.a	b.d.l	2.09	n.a	n.a	n.a	b.d.l
n.a	n.a	n.a	b.d.l	b.d.l	n.a	b.d.l	1.52	n.a	n.a	n.a	b.d.l
788.18	b.d.l	b.d.l	b.d.l	n.a	b.d.l	b.d.l	18.24	b.d.l	b.d.l	b.d.l	b.d.l
233.25	b.d.l	17.67	b.d.l	n.a	0.79	b.d.l	6.13	0.33	b.d.l	b.d.l	b.d.l
b.d.l	b.d.l	b.d.l	b.d.l	n.a	0.78	b.d.l	b.d.l	b.d.l	b.d.l	b.d.l	b.d.l
48.70	b.d.l	20.88	b.d.l	n.a	0.74	b.d.l	2.04	b.d.l	b.d.l	b.d.l	b.d.l

Au^{197}	Pb^{208}	Bi^{209}
b.d.l	5.38	b.d.l
b.d.l	b.d.l	<6.24
b.d.l	213.53	6.91
b.d.l	421.58	b.d.l
b.d.l	b.d.l	b.d.l
b.d.l	6.90	b.d.l
b.d.l	b.d.l	1.07
b.d.l	12.51	0.88
b.d.l	b.d.l	b.d.l
b.d.l	b.d.l	b.d.l
b.d.l	10.75	b.d.l
b.d.l	6.17	b.d.l
b.d.l	4.38	1.08
b.d.l	29.22	b.d.l
b.d.l	b.d.l	b.d.l
b.d.l	7.13	b.d.l
b.d.l	11.80	b.d.l
b.d.l	b.d.l	b.d.l
b.d.l	3.99	b.d.l
b.d.l	38804.13	6.12
b.d.l	525.01	b.d.l
b.d.l	424.48	3.61
b.d.l	b.d.l	b.d.l
b.d.l	b.d.l	b.d.l
b.d.l	b.d.l	b.d.l
b.d.l	b.d.l	b.d.l
b.d.l	b.d.l	b.d.l
b.d.l	232.99	b.d.l
b.d.l	19.25	b.d.l
b.d.l	142.58	3.27
b.d.l	160.88	b.d.l
b.d.l	63.48	b.d.l
b.d.l	143.05	3.29
b.d.l	142.68	b.d.l
b.d.l	64.28	b.d.l
b.d.l	b.d.l	b.d.l
b.d.l	b.d.l	b.d.l
b.d.l	b.d.l	b.d.l
b.d.l	b.d.l	b.d.l
b.d.l	b.d.l	b.d.l
b.d.l	16.03	b.d.l

b.d.l	n.a	n.a
b.d.l	n.a	n.a
b.d.l	n.a	n.a
b.d.l	n.a	n.a
b.d.l	n.a	n.a
b.d.l	n.a	n.a
b.d.l	n.a	n.a
b.d.l	n.a	n.a
b.d.l	n.a	n.a
b.d.l	n.a	n.a
b.d.l	n.a	n.a
b.d.l	n.a	n.a
b.d.l	n.a	n.a
b.d.l	n.a	n.a
b.d.l	n.a	n.a
b.d.l	n.a	n.a
b.d.l	n.a	n.a
b.d.l	n.a	n.a
b.d.l	n.a	n.a
b.d.l	n.a	n.a
b.d.l	n.a	n.a
b.d.l	n.a	n.a
b.d.l	n.a	n.a
b.d.l	60.97	2.18
b.d.l	15.04	0.05
b.d.l	31.23	0.66
b.d.l	8.40	0.47

Appendix 18: LA-ICP-MS SMI analyses

Sample/Spot	29.1-5-1	29.1-5-2	29.1-5-3	29.1-2-1	29.1-2-2	29.1-13-1
SiO_2 (wt%)	51.85	51.85	51.85	51.85	51.85	51.85
TiO_2	1.39	1.22	1.11	1.47	1.03	0.58
Al_2O_3	18.63	13.63	11.52	14.30	14.90	16.42
FeO	38.91	23.72	32.26	22.25	10.83	18.57
MnO	0.52	0.29	0.30	0.29	0.18	0.05
MgO	12.73	12.22	13.20	10.56	2.64	8.46
CaO	b.d.l	b.d.l	b.d.l	b.d.l	b.d.l	b.d.l
Na_2O	1.56	1.09	1.11	1.75	4.97	4.64
K_2O	1.13	2.54	1.14	2.78	3.41	1.26
P_2O_5	b.d.l	b.d.l	b.d.l	b.d.l	b.d.l	b.d.l
B^{11} (ppm)	b.d.l	77.99	146.72	b.d.l	b.d.l	b.d.l
V^{51}	b.d.l	b.d.l	b.d.l	b.d.l	b.d.l	b.d.l
Cr^{52}	b.d.l	b.d.l	b.d.l	b.d.l	b.d.l	b.d.l
Co^{59}	65.76	42.72	44.95	36.66	14.46	47.63
Ni^{62}	b.d.l	b.d.l	b.d.l	b.d.l	b.d.l	b.d.l
Cu^{63}	b.d.l	b.d.l	b.d.l	b.d.l	b.d.l	b.d.l
Zn^{66}	2439.08	165.78	135.41	161.23	96.87	91.30
As^{75}	b.d.l	b.d.l	b.d.l	b.d.l	b.d.l	b.d.l
Rb^{85}	b.d.l	32.47	28.37	56.46	94.61	155.39
Sr^{88}	b.d.l	b.d.l	b.d.l	b.d.l	b.d.l	b.d.l
Y^{89}	b.d.l	b.d.l	b.d.l	b.d.l	b.d.l	b.d.l
Zr^{90}	524.04	362.79	413.85	387.40	397.08	322.66
Nb^{93}	53.29	47.70	35.67	65.63	45.44	19.08
Mo^{98}	b.d.l	b.d.l	b.d.l	b.d.l	1.91	1.49
Ag^{107}	b.d.l	b.d.l	b.d.l	b.d.l	b.d.l	b.d.l
Sn^{120}	6.00	2.52	3.35	4.42	5.95	5.78
Sb^{121}	b.d.l	b.d.l	b.d.l	b.d.l	b.d.l	b.d.l
Cs^{133}	b.d.l	0.50	4.92	0.76	1.11	13.38
Ba^{138}	731.21	776.53	532.11	1487.54	1291.29	135.76
La^{139}	b.d.l	b.d.l	b.d.l	b.d.l	b.d.l	b.d.l
Ce^{140}	b.d.l	b.d.l	b.d.l	b.d.l	b.d.l	b.d.l
Pr^{141}	b.d.l	b.d.l	b.d.l	b.d.l	b.d.l	b.d.l
Nd^{143}	207.39	141.39	b.d.l	b.d.l	b.d.l	b.d.l
Sm^{147}	60.32	40.61	b.d.l	b.d.l	b.d.l	b.d.l
Eu^{153}	10.26	9.11	b.d.l	b.d.l	b.d.l	6.70
Gd^{157}	b.d.l	b.d.l	b.d.l	b.d.l	b.d.l	b.d.l

Tb^{159}	b.d.l	b.d.l	b.d.l	b.d.l	b.d.l	b.d.l
Dy^{163}	b.d.l	b.d.l	b.d.l	b.d.l	b.d.l	b.d.l
Ho^{165}	b.d.l	b.d.l	b.d.l	b.d.l	b.d.l	b.d.l
Er^{166}	b.d.l	b.d.l	b.d.l	b.d.l	b.d.l	b.d.l
Tm^{169}	b.d.l	0.84	b.d.l	b.d.l	b.d.l	b.d.l
Yb^{172}	b.d.l	3.08	b.d.l	b.d.l	b.d.l	b.d.l
Lu^{175}	b.d.l	b.d.l	b.d.l	b.d.l	b.d.l	b.d.l
Hf^{178}	11.50	8.39	8.99	9.41	9.66	7.08
Ta^{181}	3.86	3.39	2.63	4.56	3.17	1.37
W^{182}	b.d.l	b.d.l	b.d.l	b.d.l	b.d.l	0.81
Pb^{208}	b.d.l	3.43	3.48	b.d.l	4.36	27.18
Bi^{209}	b.d.l	b.d.l	b.d.l	b.d.l	b.d.l	b.d.l
Th^{232}	7.77	15.51	12.98	b.d.l	b.d.l	57.79
U^{238}	1.28	5.24	5.50	b.d.l	b.d.l	10.64

Appendix 19: LA-ICP-MS apatite analyses

Sample	29.1	29.1	29.1	29.1	29.1	29.1	29.1	29.1	29.1	29.1
Spot	3-Ap.xl	5-Ap.xl	6-Ap.xl	7-Ap.xl	8-Ap.xl	11-Ap.xl	12-Ap.xl	13-Ap.xl	15-Ap.xl	16-Ap.xl
SiO_2 (wt%)	1.92	0.74	0.46	0.31	b.d.l	0.28	0.41	0.47	0.52	0.38
Al_2O_3	0.19	0.04	0.00	0.00	0.00	0.00	0.00	0.01	0.00	0.02
FeO	1.16	0.33	0.05	0.09	0.03	0.07	0.12	0.25	0.12	0.21
MnO	0.05	0.04	0.02	0.03	0.02	0.04	0.04	0.04	0.05	0.05
MgO	0.28	0.07	0.02	0.03	0.00	0.02	0.03	0.04	0.03	0.04
CaO	54.76	54.76	54.76	54.76	54.76	54.76	54.76	54.76	54.76	54.76
Na_2O	0.03	0.03	0.02	0.02	0.02	0.03	0.03	0.03	0.03	0.03
K_2O	0.00	0.00	0.00	b.d.l	b.d.l	b.d.l	b.d.l	b.d.l	0.00	0.00
P_2O_5	33.62	34.65	34.98	36.00	36.55	38.26	38.90	39.95	41.28	41.17
V^{51} (ppm)	0.24	0.16	0.22	b.d.l	0.19	0.17	0.23	0.25	0.24	0.17
Cr^{53}	b.d.l	b.d.l	b.d.l	1.00	b.d.l	b.d.l	1.50	b.d.l	b.d.l	b.d.l
Co^{59}	1.63	0.35	0.08	0.14	0.08	0.20	0.17	0.33	0.15	0.21
Ni^{60}	0.41	b.d.l	b.d.l	0.30	0.36	0.31	0.53	b.d.l	0.73	b.d.l
Cu^{65}	3.30	3.77	1.69	b.d.l	b.d.l	6.03	b.d.l	b.d.l	0.55	4.64
As^{75}	12.93	15.61	12.02	14.53	11.70	12.71	13.17	11.42	12.14	11.15
Rb^{85}	0.16	0.08	0.05	0.05	0.05	b.d.l	0.06	0.06	0.08	0.08
Sr^{88}	1473.59	1444.52	1439.06	1451.88	1443.15	1542.68	1565.31	1542.10	1590.52	1569.55
Y^{89}	298.38	293.39	288.37	302.53	279.84	274.31	379.51	296.65	303.52	323.57
Zr^{90}	4.27	4.24	3.82	5.19	2.76	3.97	7.13	4.44	5.01	5.26
Nb^{93}	0.04	0.02	b.d.l	0.02	0.02	0.03	0.03	0.03	0.02	0.02
Ag^{107}	0.04	0.02	0.03	0.06	b.d.l	b.d.l	b.d.l	b.d.l	b.d.l	0.01
Sb^{121}	b.d.l	b.d.l	0.02	b.d.l	b.d.l	b.d.l	b.d.l	b.d.l	0.03	b.d.l
Cs^{133}	0.05	b.d.l	b.d.l	0.01	b.d.l	0.01	b.d.l	b.d.l	b.d.l	b.d.l
La^{139}	507.14	502.53	483.01	517.65	479.73	456.04	619.41	506.27	499.63	540.64
Ce^{140}	1269.67	1260.18	1185.68	1265.47	1195.28	1162.10	1565.02	1292.51	1290.55	1385.47
Nd^{146}	839.97	824.73	792.51	834.41	781.15	759.41	1030.17	830.92	832.00	886.32
Sm^{147}	167.96	163.32	159.21	166.82	153.90	151.73	203.33	164.60	164.01	177.42
Eu^{153}	37.97	36.41	35.27	37.78	35.12	34.36	46.98	37.21	38.31	40.58
Tb^{159}	15.19	14.54	14.42	15.28	13.99	13.77	18.85	14.96	14.97	15.96
Dy^{163}	74.94	72.57	70.98	74.54	68.47	67.22	92.11	73.46	73.15	77.87
Lu^{175}	1.49	1.42	1.36	1.48	1.26	1.34	1.87	1.42	1.44	1.49
Hf^{178}	0.02	0.04	0.03	0.02	0.01	0.02	0.06	0.03	0.02	0.03
Ta^{181}	b.d.l	b.d.l	0.01	b.d.l	b.d.l	0.00	0.01	b.d.l	0.00	b.d.l
Pb^{208}	2.42	1.82	2.60	1.29	3.11	1.37	1.79	1.72	1.56	1.56
Bi^{209}	0.02	0.01	0.02	b.d.l	b.d.l	b.d.l	b.d.l	0.01	0.01	b.d.l
Th^{232}	10.13	6.83	10.67	4.57	14.11	3.99	6.77	5.40	3.06	3.47
U^{238}	2.64	2.19	2.43	1.21	3.37	1.38	1.93	1.64	0.89	1.08

127-2	127-3	127-4	127-5	127-6	127-7	127-8	127-9	127-10	127-11	127-12	127-13
3-Ap.xl	4-Ap.xl	5-Ap.xl	6-Ap.xl	7-Ap.xl	8-Ap.xl	12-Ap.xl	13-Ap.xl	14-Ap.xl	15-Ap.xl	16-Ap.xl	18-Ap.xl
0.26	0.23	0.26	0.35	b.d.l	0.34	b.d.l	0.32	0.29	b.d.l	b.d.l	0.51
0.00	0.03	0.00	0.00	0.00	b.d.l	0.00	0.01	0.00	0.00	0.00	0.10
0.09	0.16	0.10	0.07	0.08	0.05	0.06	0.13	0.08	0.09	0.07	0.32
0.06	0.07	0.07	0.06	0.06	0.05	0.06	0.06	0.07	0.07	0.07	0.07
0.03	0.05	0.04	0.02	0.03	0.01	0.02	0.04	0.03	0.04	0.03	0.18
54.72	54.72	54.72	54.72	54.72	54.72	54.72	54.72	54.72	54.72	54.72	54.72
0.08	0.07	0.06	0.08	0.08	0.08	0.06	0.05	0.04	0.04	0.04	0.04
b.d.l	0.00	0.00	b.d.l	0.00	b.d.l	b.d.l	0.00	0.00	0.00	0.00	0.00
76.65	74.98	74.61	70.77	69.25	68.96	66.15	64.52	61.36	61.80	59.79	57.94
2.54	8.74	2.94	2.69	3.33	2.45	2.99	3.05	2.82	3.06	2.66	4.77
b.d.l	b.d.l	b.d.l	b.d.l	0.88	b.d.l	b.d.l	b.d.l	1.00	b.d.l	b.d.l	b.d.l
0.49	0.39	0.15	0.12	0.13	0.11	0.13	0.15	0.30	0.81	0.10	0.62
0.38	0.63	0.39	0.87	0.55	0.51	0.34	0.39	0.67	0.33	0.37	0.68
2.37	b.d.l	b.d.l	3.49	0.13	0.32	b.d.l	b.d.l	9.33	0.13	b.d.l	2.04
19.45	18.20	16.97	20.05	18.80	17.98	14.93	13.00	18.34	10.54	9.55	12.24
0.07	0.06	0.07	0.07	0.08	0.07	0.05	0.06	0.08	0.04	0.04	0.07
1487.38	1728.68	1859.79	1276.63	1308.75	1438.77	1690.23	1761.43	1823.68	1815.52	1807.97	2004.48
499.64	485.43	459.10	530.15	508.79	524.12	421.66	394.25	301.76	277.20	259.14	361.71
6.07	6.90	6.63	6.27	5.83	5.67	6.25	5.69	5.73	5.27	4.64	6.25
0.03	0.03	0.03	0.04	0.02	0.02	0.03	0.03	0.05	0.04	0.03	0.02
0.02	0.02	b.d.l	0.08	b.d.l	b.d.l	0.02	b.d.l	0.13	b.d.l	b.d.l	b.d.l
b.d.l	b.d.l	b.d.l	0.07	0.02	0.01	0.02	b.d.l	0.08	0.01	b.d.l	0.02
b.d.l	b.d.l	b.d.l	b.d.l	b.d.l	b.d.l	b.d.l	b.d.l	0.03	b.d.l	b.d.l	b.d.l
998.44	932.62	841.70	1082.06	1039.94	1038.02	770.28	687.82	468.00	442.84	422.91	610.75
2678.49	2512.93	2298.86	2833.19	2716.70	2797.86	2010.66	1784.44	1262.72	1248.86	1173.69	1636.14
1523.87	1459.43	1352.26	1601.97	1539.06	1569.22	1170.71	1083.90	799.53	766.63	728.33	1038.63
279.86	268.73	250.99	289.53	280.30	283.71	223.01	206.25	157.89	150.01	143.63	202.51
60.82	62.27	60.01	61.36	59.90	60.70	53.62	50.86	41.20	39.49	38.04	50.98
24.23	23.28	21.86	25.81	24.84	25.00	19.82	18.66	14.06	13.43	12.69	17.79
119.86	114.32	107.26	126.62	121.55	124.30	97.45	91.15	68.71	63.49	60.76	86.19
2.40	2.16	2.05	2.65	2.49	2.55	2.06	1.90	1.33	1.20	1.10	1.48
0.05	0.05	0.04	0.06	0.04	0.03	0.05	0.04	0.05	0.03	0.04	0.04
0.01	0.00	0.00	0.00	0.01	0.01	0.00	0.00	0.01	0.00	b.d.l	0.00
4.00	2.85	3.06	3.53	3.53	4.45	4.77	4.12	3.00	2.63	3.40	1.87
0.03	b.d.l	0.12	0.03	b.d.l	0.02	0.03	0.02	0.03	0.02	0.01	0.02
6.02	6.04	5.62	5.70	5.88	6.15	5.49	5.29	3.55	3.40	3.37	5.51
1.45	1.50	1.45	1.45	1.45	1.57	1.57	1.48	0.93	0.95	0.92	1.32

127-14	167-A1	167-A2	167-A3	167-A4	167-A5	167-A6	167-A7	167-A8	167-A9	167-A10	167-A11
19-Ap.xl	3--Ap.xl	4--Ap.xl	7-Ap.xl	8-Ap.xl	9-Ap.xl	10-Ap.xl	11-Ap.xl	15-Ap.xl	16-Ap.xl	17-Ap.xl	19-Ap.xl
0.30	0.63	0.65	0.34	0.44	0.23	0.29	b.d.l	0.43	0.83	0.46	0.55
0.04	0.21	0.22	0.00	0.00	0.00	0.00	0.00	0.00	0.20	0.01	0.00
0.21	0.31	0.37	0.14	0.16	0.14	0.13	0.14	0.09	0.35	0.09	0.08
0.07	0.07	0.07	0.07	0.07	0.07	0.07	0.07	0.06	0.06	0.07	0.06
0.12	0.16	0.21	0.08	0.09	0.06	0.06	0.06	0.01	0.19	0.01	0.01
54.72	54.72	54.72	54.72	54.72	54.72	54.72	54.72	54.72	54.72	54.72	54.72
0.05	0.06	0.05	0.05	0.05	0.07	0.07	0.06	0.07	0.07	0.10	0.10
0.00	0.00	0.00	0.00	0.00	0.00	0.00	b.d.l	b.d.l	0.00	b.d.l	0.00
59.26	70.51	74.28	69.60	69.07	68.74	66.67	64.86	65.00	62.10	60.94	60.12
2.91	6.01	7.92	8.63	8.86	6.82	6.92	7.70	6.81	6.86	5.06	4.91
b.d.l	b.d.l	b.d.l	b.d.l	b.d.l	1.29	b.d.l	b.d.l	b.d.l	b.d.l	b.d.l	0.84
0.35	0.76	0.76	0.20	0.26	0.21	0.12	0.18	0.10	0.93	0.09	0.08
0.34	1.74	1.96	2.43	0.41	0.67	b.d.l	0.38	b.d.l	1.76	0.52	0.78
5.05	1.92	b.d.l	0.85	0.86	180.31	0.15	1.28	1.56	2.92	2.58	0.33
12.60	28.06	18.38	18.43	18.18	27.03	19.63	22.51	20.35	25.11	24.33	24.36
0.17	0.09	0.09	0.06	0.06	0.09	0.08	0.06	0.08	0.10	0.10	0.10
2048.48	1725.80	1759.80	1610.27	1628.86	1454.20	1411.09	1398.54	1295.98	1237.36	784.96	877.82
394.77	397.79	405.98	439.38	432.97	499.80	481.16	456.37	574.36	570.88	711.97	674.57
6.11	7.36	7.13	7.36	7.34	9.05	7.06	6.57	11.22	10.80	10.56	8.49
0.04	0.06	0.05	0.05	0.04	0.05	0.05	0.02	0.04	0.04	0.04	0.04
b.d.l	0.04	b.d.l	b.d.l	0.05	0.09	0.02	0.01	b.d.l	0.01	0.03	0.02
b.d.l	0.03	b.d.l	0.01	0.04	0.04	0.02	b.d.l	b.d.l	0.02	0.04	b.d.l
b.d.l	0.02	0.02	b.d.l	b.d.l	b.d.l	b.d.l	b.d.l	b.d.l	0.02	0.08	b.d.l
662.28	794.05	814.95	814.51	798.36	998.82	976.46	936.16	1156.47	1174.57	1443.34	1394.41
1916.29	1874.01	2064.44	1979.90	1957.77	2512.50	2443.81	2302.20	2970.92	2887.93	3520.77	3430.54
1113.05	1237.00	1274.00	1289.94	1269.13	1521.31	1474.55	1403.67	1754.46	1773.61	2153.97	2077.96
215.33	231.61	238.10	241.71	239.65	280.03	270.50	254.77	316.09	321.27	386.83	370.25
53.20	53.99	56.16	56.49	55.60	62.52	60.14	58.07	62.98	64.36	64.68	64.56
19.12	20.29	20.68	21.34	21.11	24.33	23.24	22.45	27.69	28.04	34.09	32.69
92.02	99.82	101.77	104.75	103.87	121.71	117.06	111.20	137.44	138.67	168.95	164.10
1.69	1.87	1.94	1.95	1.92	2.40	2.31	2.15	2.71	2.76	3.47	3.39
0.06	0.04	0.06	0.05	0.05	0.06	0.06	0.06	0.11	0.11	0.10	0.06
0.00	0.01	0.01	0.00	0.00	0.01	0.00	0.01	0.00	0.00	0.01	0.01
2.28	2.78	2.94	3.67	3.24	3.23	3.23	2.79	3.28	3.50	6.62	6.72
0.49	0.03	0.03	0.02	0.01	0.04	0.02	0.02	0.03	0.05	0.06	0.06
5.84	8.65	9.16	8.59	8.81	11.06	9.95	9.07	12.40	12.75	15.92	13.15
1.46	2.02	2.24	1.98	2.07	2.39	2.24	1.97	2.91	2.97	3.97	3.20

167-A12	167-A13	167-A14	173.9	173.9	173.9	173.9	173.9	173.9	173.9	173.9	173.9
20-Ap.xl	21-Ap.xl	22-Ap.xl	3-Ap.xl	4-Ap.xl	5-Ap.xl	6-Ap.xl	7-Ap.xl	8-Ap.xl	12-Ap.xl	13-Ap.xl	15-Ap.xl
0.53	0.68	0.47	0.46	b.d.l	0.28	0.38	0.37	0.35	0.35	0.22	0.30
0.07	0.14	0.03	0.02	0.00	0.00	0.04	0.00	b.d.l	0.07	0.00	0.00
0.18	0.32	0.15	0.15	0.08	0.06	0.19	0.05	0.06	0.26	0.08	0.08
0.06	0.07	0.07	0.08	0.06	0.06	0.06	0.06	0.06	0.08	0.08	0.06
0.08	0.14	0.06	0.03	0.01	0.01	0.02	0.01	0.01	0.03	0.01	0.02
54.72	54.72	54.72	54.00	54.00	54.00	54.00	54.00	54.00	54.00	54.00	54.00
0.09	0.10	0.10	0.10	0.09	0.09	0.09	0.08	0.08	0.09	0.10	0.10
0.00	0.00	b.d.l	0.00	b.d.l	0.00	0.00	0.00	0.00	0.00	0.00	b.d.l
57.20	57.66	56.21	99.68	79.30	78.63	74.21	69.39	66.45	64.64	63.34	59.56
3.53	6.01	6.73	1.78	1.62	1.66	1.73	1.65	1.57	1.66	1.68	1.46
8.52	b.d.l	b.d.l	1.14	b.d.l	b.d.l	2.12	b.d.l	b.d.l	b.d.l	b.d.l	b.d.l
0.82	0.38	0.25	0.31	0.09	0.09	0.22	0.06	b.d.l	0.39	0.17	0.15
0.78	0.83	0.55	0.61	0.33	0.37	0.59	0.31	0.55	0.54	0.46	0.41
6.32	1.12	0.50	7.32	b.d.l	b.d.l	1.42	b.d.l	0.77	1.31	0.34	0.36
28.74	21.64	26.04	28.58	25.35	22.82	25.64	23.61	24.08	21.22	22.60	20.94
0.10	0.11	0.11	0.11	0.10	0.10	0.14	0.12	0.10	0.17	0.24	0.07
1028.52	775.64	859.88	924.12	832.98	743.30	787.56	788.04	833.81	1059.47	939.53	759.63
584.90	633.50	649.99	585.01	630.64	618.04	650.30	657.12	651.68	589.59	639.61	614.40
9.75	12.49	10.60	4.57	4.03	4.14	5.83	6.21	6.05	6.89	7.80	5.33
0.04	0.07	0.05	0.03	0.03	0.02	0.05	0.03	0.03	0.03	0.03	0.02
0.07	0.01	b.d.l	0.02	b.d.l	0.03	0.02	b.d.l	b.d.l	0.01	0.02	0.11
0.04	0.01	0.11	0.04	0.02	b.d.l	0.02	b.d.l	0.01	0.03	0.02	b.d.l
b.d.l	b.d.l	0.02	b.d.l	b.d.l	b.d.l	b.d.l	b.d.l	b.d.l	0.02	b.d.l	b.d.l
1232.16	1305.94	1301.53	1264.40	1262.67	1257.90	1286.99	1284.62	1220.80	1126.11	1256.15	1138.07
2914.57	3186.90	3211.00	3676.78	3233.95	3235.40	3366.85	3300.41	3143.12	2901.98	3290.00	2928.92
1788.95	1940.27	1951.14	1802.61	1832.54	1826.99	1907.77	1905.74	1847.85	1703.66	1847.74	1680.24
320.94	350.24	350.81	320.45	327.59	325.37	344.84	347.30	337.54	312.92	333.18	307.46
57.86	65.24	68.09	52.86	49.98	48.21	58.49	59.18	60.37	59.03	59.97	47.71
28.30	30.49	31.38	27.90	29.64	29.43	31.07	31.46	30.45	27.46	29.76	28.04
141.18	151.30	155.61	139.68	147.44	146.82	153.77	157.44	153.22	134.95	148.88	140.34
2.80	3.06	3.14	3.19	3.40	3.37	3.53	3.55	3.40	2.95	3.21	3.18
0.06	0.09	0.08	0.04	0.03	0.04	0.05	0.05	0.05	0.06	0.06	0.05
0.01	0.00	0.01	0.01	0.00	0.01	0.01	0.01	0.01	0.00	0.00	0.00
10.60	9.15	8.74	4.59	4.53	6.16	4.21	4.43	5.17	6.19	7.61	2.90
0.29	0.07	0.11	0.06	0.04	0.05	0.09	0.07	0.06	0.09	0.13	0.03
20.33	12.17	11.81	10.40	14.41	15.17	12.88	15.04	14.70	10.00	13.23	6.02
4.85	2.69	2.52	3.30	3.77	4.44	3.38	3.56	3.43	2.48	3.57	1.83

173.9	173.9
16-Ap.xl	17-Ap.xl
b.d.l	0.51
0.00	0.05
0.07	0.27
0.06	0.07
0.02	0.06
54.00	54.00
0.09	0.09
b.d.l	0.00
57.54	55.40
1.74	3.40
b.d.l	b.d.l
0.11	0.39
0.42	0.60
0.37	2.41
20.70	25.16
0.10	0.13
774.69	935.56
621.02	643.38
5.87	6.98
0.03	0.04
0.01	0.05
b.d.l	0.01
b.d.l	b.d.l
1162.30	1191.17
2959.27	3127.31
1714.57	1833.02
317.56	334.43
49.17	61.61
28.58	29.45
144.59	146.71
3.23	3.16
0.06	0.05
0.01	0.01
3.30	3.25
0.02	0.10
6.94	9.06
1.92	2.17

Appendix 20: Sulphur isotope analyses

Sample	Lithology	Sulfide	Sulfide Texture/Occurrence	Generation	$\delta^{34}S$ (‰ VCDT)	Method
CL-06-16-47.6	gabbro	Py	Fracture	Secondary	0.8	C
CL-06-16-59.9	gabbro	Py	Fracture	Secondary	0.6	C
CL-06-05-77.72	gabbro	Po	Stringer	Secondary	2.5	C
CL-06-05-77.72-1	gabbro	Po	Stringer	Secondary	0.9	I
CL-06-05-77.72-2	gabbro	Po	Stringer	Secondary	0.5	I
CL-06-05-77.72-3	gabbro	Po	Stringer	Secondary	0.1	I
CL-06-05-77.72-4	gabbro	Po	Stringer	Secondary	-1.3	I
CL-06-05-77.72-5	gabbro	Po	Stringer	Secondary	0.8	I
CL-06-05-77.72-6	gabbro	Po	Stringer	Secondary	1.7	I
CL-06-05-77.72-7	gabbro	Po	Stringer	Secondary	1.2	I
CL-06-16-52.5	gabbro	Po	Disseminated	Primary	1.2	C
CL-06-16-55.0	gabbro	Po	Disseminated	Primary	1.2	C
CL-06-16-56.3	gabbro	Po	Disseminated	Primary	1.3	C
CL-06-16-57.5	gabbro	Po	Disseminated	Primary	1.3	C
CL-06-16-58.6	gabbro	Po	Disseminated	Primary	1.0	C
CL-06-16-61.7	gabbro	Po	Disseminated	Primary	1.2	C
CL-06-16-63.8	gabbro	Po	Disseminated	Primary	1.0	C
CL-06-01-22.5	gabbro	Po	Disseminated	Primary	1.4	C
CL-06-01-22	gabbro	Po	Semi-Massive	Primary	1.1	C
CL-06-16-47.6	gabbro	Po	Semi-Massive	Primary	1.2	C
CL-06-16-78.75	massive sulfide	Po	Massive	Primary	1.2	C
CL-06-16-84.6	massive sulfide	Po	Massive	Primary	1.2	C
CL-06-01-81.2	massive sulfide	Po	Massive	Primary	1.1	C
CL-06-05-81.6	massive sulfide	Po	Massive	Primary	1.3	C
CL-06-05-81.6	massive sulfide	Ccp	Disseminated	Primary	1.0	C
CL-07-01-115	gabbro	Po	Interstitial	Primary	0.0	C
CL-07-01-422.9	gabbro	Po	Interstitial	Primary	0.9	C
CL-07-05-14	gabbro	Po	Interstitial	Primary	-0.4	C
CL-07-05-50	websterite	Po	Interstitial	Primary	0.2	C
CL-07-14-323.5	gabbro	Po	Interstitial	Primary	0.3	C
C-L07-14-477.5	gabbro	Po	Interstitial	Primary	-0.1	C
CL-07-01-373	olivine gabbro	Po	Interstitial	Primary	0.9	C
CL-07-01-373-1	olivine gabbro	Po	Interstitial	Primary	1.4	I
CL-07-01-373-2	olivine gabbro	Po	Interstitial	Primary	0.7	I
CL-07-01-373-3	olivine gabbro	Po	Interstitial	Primary	0.6	I
CL-07-01-373-4	olivine gabbro	Po	Interstitial	Primary	0.5	I
CL-07-01-373-5	olivine gabbro	Po	Interstitial	Primary	0.5	I
CL-07-01-373-6	olivine gabbro	Po	Interstitial	Primary	0.6	I
CL-07-01-373-7	olivine gabbro	Po	Interstitial	Primary	1.2	I

CL-07-01-373-1	olivine gabbro	Po	Interstitial	Primary	0.6	I
CL-07-01-373-2	olivine gabbro	Po	Interstitial	Primary	0.9	I
CL-07-01-373-3	olivine gabbro	Po	Interstitial	Primary	1.1	I
CL-07-01-373-4	olivine gabbro	Po	Interstitial	Primary	0.6	I
CL-07-01-373-5	olivine gabbro	Po	Interstitial	Primary	1.0	I
CL-07-01-373-6	olivine gabbro	Po	Interstitial	Primary	0.9	I
CL-07-01-373-7	olivine gabbro	Po	Interstitial	Primary	0.9	I
CL-07-01-373-1	olivine gabbro	Po	Ilmenite hosted SUL	Primary	-0.3	I
CL-07-01-373-2	olivine gabbro	Po	Ilmenite hosted SUL	Primary	0.1	I
CL-07-01-373-3	olivine gabbro	Po	Ilmenite hosted SUL	Primary	0.2	I
CL-07-01-373-4	olivine gabbro	Po	Ilmenite hosted SUL	Primary	1.4	I
CL-07-01-373-5	olivine gabbro	Po	Ilmenite hosted SUL	Primary	-0.1	I
CL-07-01-373-6	olivine gabbro	Po	Ilmenite hosted SUL	Primary	-0.1	I
CL-07-01-373-7	olivine gabbro	Po	Ilmenite hosted SUL	Primary	0.3	I
CL-07-01-373-1	olivine gabbro	Po	Olivine hosted SUL	Primary	1.0	I
CL-07-01-373-2	olivine gabbro	Po	Olivine hosted SUL	Primary	0.4	I
CL-07-01-373-3	olivine gabbro	Po	Olivine hosted SUL	Primary	0.4	I
CL-07-01-373-4	olivine gabbro	Po	Olivine hosted SUL	Primary	0.0	I
CL-07-01-373-5	olivine gabbro	Po	Olivine hosted SUL	Primary	0.5	I
CL-07-01-373-6	olivine gabbro	Po	Olivine hosted SUL	Primary	0.1	I
CL-07-01-373-7	olivine gabbro	Po	Olivine hosted SUL	Primary	0.3	I
CL-07-01-373-8	olivine gabbro	Po	Olivine hosted SUL	Primary	-0.6	I
CL-06-16-35-1	Burwash sediments	Po	Matrix	-	-0.3	I
CL-06-16-35-2	Burwash sediments	Po	Matrix	-	-0.1	I
CL-06-16-35-3	Burwash sediments	Po	Matrix	-	0.5	I
CL-06-16-35-4	Burwash sediments	Po	Matrix	-	-0.1	I
CL-06-16-35-5	Burwash sediments	Po	Matrix	-	0.7	I
CL-06-16-35-6	Burwash sediments	Po	Matrix	-	0.2	I
CL-06-16-35-7	Burwash sediments	Po	Matrix	-	0.0	I
CL-06-16-35-8	Burwash sediments	Po	Matrix	-	0.3	I
CL-06-16-35-9	Burwash sediments	Po	Matrix	-	0.4	I
CL-06-16-35-10	Burwash sediments	Po	Matrix	-	0.8	I

Py=pyrite; Po=pyrrhotite; Ccp=chalcopyrite; SUL = sulfide melt inclusion